VIBRATION ANALYSIS OF HYBRID BEARINGS

by

Fei-Seong Chong, B.Sc.

PAGE NUMBERING AS ORIGINAL THESIS

VIBRATION ANALYSIS OF HYBRID BEARINGS

BY

F.S. CHONG

ABSTRACT

The dynamic characteristics of the oil-film within a plain line-entry (slot) hybrid journal bearing have been studied theoretically and experimentally. The study relates to the small amplitude motion of a dynamically loaded journal bearing about its static equilibrium position.

A finite-difference approximation of the lubrication equation, with provision for source flow has been presented. This equation has been solved to determine the total dimensionless static oil-film forces acting upon the journal. Also, a faster lumped parameter technique was developed as an alternative method of solution. Subsequently, two techniques were developed for the computation of the eight linearized bearing dynamic oil-film coefficients:

(i)   a perturbation technique, and

(ii) a finite disturbance technique.

Theoretical transfer functions of the bearing fluid-film were derived. Initially, the theoretical model was based on the assumption of a rigid shaft. However, experimental tests showed that shaft bending could not be eliminated from the measurements and it was therefore necessary to model this effect.

Frequency response testing was employed to identify the linear bearing dynamic performance. Sinusoidal inputs were applied to the bearing in two perpendicular directions. A Hewlett Packard HP9825A deck-top computer was used to drive the frequency response analyser and to record responses. A full scale automatic testing procedure, incorporating software and hardware interfacing was developed. The eight-bearing oil-film coeficients were then determined from the bearing frequency response functions, based on the direct method of Morton, which requires the inversion of two 4 x 4 matrices. There was poor correlation between the predicted and measured coefficients as reported by workers researching other types of bearings. Suggestions are made for the improvement of the correlation between predicted and measured coefficients.

Finally, a theoretical linearized stability analysis of rigid and flexible rotors in hybrid journal bearings has been carried out. The analysis showed that it is feasible to design the circular slot-entry bearing to match the improved stability limits offered by the non-circular bearing configurations.

A_f — Effective Friction Area

$\bar{A}_f$ — Effective Non-Dimensional Friction Area $(= \dfrac{A_f}{D^2})$

$\bar{B}$ — Dimensionless Flow Factor $(= \dfrac{\pi D}{6a})$

C — Radial Clearance

C_d — Diametral Clearance

D — Nominal Diameter of Bearing

F — Flexibility Parameter $(= \dfrac{P_s LD}{C.k})$

F_x, F_y — Fluid-film forces in X and Y directions, respectively

$\delta F_x, \delta F_y$ — Change in Fluid-Film Forces in X and Y directions, respectively

$\bar{F}_x, \bar{F}_y$ — Dimensionless fluid-film forces in X and Y directions, respectively $(= \dfrac{F_x}{P_s LD}, \quad \dfrac{F_y}{P_s LD})$

$G_{11}(s), G_{12}(s), G_{21}(s), G_{22}(s)$ — Bearing Fluid-Film Transfer Functions

H — Dimensionless Gap $(= \dfrac{h}{C})$

H_f — Friction Power at the Concentric Condition $(= \dfrac{\eta A_f U^2}{C})$

H_p — Pumping power at the concentric Condition $(= P_s q_{in})$

K — Power-ratio $(= \dfrac{H_f}{H_p}$, for concentric condition)

L — Bearing Length

N — Rotational speed (rev/sec)

N_o — Optimized rotational speed $(= S_{ho} \dfrac{P_s}{\eta} \left(\dfrac{D}{C_d}\right)^2)$

P_{ai} — Pressure at the mid-point of the ith outer land

$P_{c i}$	Pressure at the mid-point of the bearing
$P_{i,j}$	Pressure at a point in the bearing
$\bar{P}_{i,j}$	Non-dimensional pressure at a point the bearing $(= \dfrac{P_{i,j}}{P_s})$
P_s	Supply pressure
$P_x(t)$, $P_y(t)$	Excitation force in the X and Y-directions, respectively
R	Journal radius
R_{11}, R_{12}, R_{21}, R_{22}	Receptances of the bearing fluid-film
S	Sommerfeld Number $(= \dfrac{\eta\, NLD}{W} \left(\dfrac{D}{C_d}\right)^2)$
S_f	Source flow term
S_h	Sommerfeld Hybrid Parameter $(= \dfrac{\eta\, N}{P_s} \left(\dfrac{D}{C_d}\right)^2)$
S_{ho}	Optimized Sommerfeld Hubrod Parameter $(= \dfrac{1}{4\,\pi} \sqrt{\dfrac{\beta\, \bar{B}}{\bar{A}_f}})$
T	Absolute temperature
V	Bearing sliding speed or Axis parallel to the line of eccentricity
U	Axis perpendicular to the line of eccentricity
W	Bearing Load
$\bar{W}$	Fuller Number $(= \dfrac{W}{P_s\, LD})$
X	Dimensionless co-ordinate in the circumferential direction or the X-axis
Y	The Y-axis
Z	Dimensionless co-ordinate in the axial direction

a	Axial flow land width
a_s	Slot width
a_{11}, a_{12}, a_{21}, a_{22}	Stiffness coefficients
$\bar{a}_{11}$, $\bar{a}_{12}$, $\bar{a}_{21}$, $\bar{a}_{22}$	Dimensionless stiffness coefficients $(= a_{ij} \dfrac{C}{P_s LD})$
b_{11}, b_{12}, b_{21}, b_{22}	Damping coefficients
$\bar{b}_{11}$, $\bar{b}_{12}$, $\bar{b}_{21}$, $\bar{b}_{22}$	Dimensionless damping coefficients $(= b_{ij} \dfrac{\omega_o C}{P_s LD})$
e	Eccentricity
e_o	Eccentricity at the static equilibrium position
h	Film thickness
k	Stiffness of the test shaft or, half the stiffness of the single mass rotor
m	Number of grid elements along bearing length or, half the mass of the single mass rotor
m_b	Mass of the test bearing assembly
n_e	Number of grid elements around bearing
n_s	Number of slots around circumference
q_{in}, q_{out}	Volumetric flow rate into and out of the bearing
$\bar{q}_{in}$, $\bar{q}_{out}$	Dimensionless volumetric flow rate into and out of the bearing $(\bar{q}_{in,out} = \dfrac{12\,\eta}{P_s C^3} q_{in,\,out})$
s	Laplace Transform variable $(X(s) = \displaystyle\int_0^\infty \bar{x}(\tau) e^{-\sigma\tau}\, d\tau \; ; \; s = \sigma + j\Omega)$
t	Real time

$\delta u,\ \delta v$	Finite displacement in the U and V - directions, respectively
$\dot{u},\ \dot{v}$	Finite velocity in the U and V - directions, respectively
$x,\ y$	Displacement of journal centre from equilibrium position
$x_r,\ y_r$	Displacement of rotor centre from equilibrium position
y_s	Slot length
z_s	Slot thickness
$\alpha_{11},\ \alpha_{12},\ \alpha_{21},\ \alpha_{22}$	Stiffness coefficients in the U-V co-ordinate system
$\beta_{11},\ \beta_{12},\ \beta_{21},\ \beta_{22}$	Damping coefficients in the U-V co-ordinate system
β	Concentric pressure ratio $(= \dfrac{P_{i,d}}{P_s})$
γ	Angle definition
$\delta,\ \Delta$	Incremental
ε	Eccentricity-ratio $(= \dfrac{e}{C})$
η	Dynamic viscosity
θ	Angle definition
$\lambda_{i,j}$	Source factor, $\lambda_{i,j} = 1$ at the region of a source and zero elsewhere
$v\ ;\ v_{hyd.}$	Speed parameter $(= \omega \sqrt{\dfrac{m}{P_s}\dfrac{C}{LD}})\ ;\ (= \omega\sqrt{\dfrac{m\,C}{W}})$
v_s	v, at stability threshold
ρ	Mass density of lubricant
σ	Real part of root
τ	Non-dimensional time $(= \omega_o t)$
ϕ_o	Attitude angle
ψ	Bearing parameter $(= \dfrac{S}{v_{hyd.}})$

ω	Journal angular rotational speed ($= 2\pi N$ or $\omega_o \sqrt{K}$)
ω_o	Optimized journal angular rotational speed ($= 2\pi N_o$)
ω_s	Instability whirl frequency (rad/sec)
$\bar{\omega}_i$	Non-dimensional frequency corresponding to ith pair of roots ($= \dfrac{\Omega_i}{K}$ i.e. $\dfrac{\omega_s}{\omega}$)
Ωi	Optimized non-dimensional frequency corresponding to ith pair of roots ($= \dfrac{\omega_i}{\omega_o}$)
Ω_s	Ω at stability threshold
$(\ \dot{}\ )$	$\dfrac{d}{dt}$
$(\ \ddot{}\ )$	$\dfrac{d^2}{dt^2}$
$(\ ^-)$	Dimensionless parameter

Suffices

i	ith slot or grid point
j	jth slot or grid point
d	feed slot

Subscripts

o	Static equilibrium position
u	Dynamic condition denoting displacement dependent parameter in the U-direction
$\dot{u}$	Dynamic condition denoting velocity dependent parameter in the U-direction
v	Dynamic condition denoting displacement dependent parameter in the V-direction

$\dot{v}$ Dynamic condition denoting velocity
dependent parameter in the
V-direction

CONTENTS

CHAPTER 10 CONCLUSIONS AND SUGGESTIONS FOR FUTURE RESEARCH

CHAPTER 1

INTRODUCTION

1.1 Fluid-Film Lubrication - Background

Ever since the wheel was invented, mankind has been plagued with problems of bearing lubrication and shaft dynamics. Lubrication functions to enable motion between mechanical parts, whilst at the same time reducing friction and wear. The sliding surfaces are ideally separated by a film of fluid, whose thickness is several times greater than the sum of the individual surface roughnesses of the sliding components.

Such films can either be maintained from an externally pressurized supply of fluid (hydrostatic lubrication) or induced by virture of the converging gap between the bearing components and the average speed (hydrodynamic lubrication). The former type is generally required for low speed applications and the latter type for high speeds. Between these two extremes, lie the hybrid mode of lubrication, which relies on mixed modes of external pressurization and speed dependent pressurization. In large plant an external source of pressure is needed to enhance the start up performance (hydrostatic jacking) and also to ensure sufficient through-flow, where large temperature variations cannot be tolerated. Hybrid lubrication offers the possibility of improving on the zero speed characteristics of hydrostatic bearings and also on the whole range of speed characteristics of hydrodynamic bearings. This thesis is concerned with hybrid lubrication.

Bearing fluid films possess stiffness and damping properties and inertia (at high speeds), and, thus play a very important role in the dynamics of a rotor-bearing system. Usually they are the major source of damping, thereby, attenuating the dynamical forces transmitted to the pedestals, and their stiffness properties affect the critical speeds and the stability of the rotor. If the speed is sufficiently

high, the bearing fluid-film may lose its damping ability and excite
non-synchronous vibration (fractional speed whirl) of a rotor and cause
it to become unstable. This whirl motion is considerably unlike the
orbiting obtained at a rotor critical speed. It is possible to safely
pass through a rotor critical speed if the rotor and bearing damping and
balancing requirements are met, whereas the occurance of non-synchronous
precession will limit the operating speed of the rotor, and, unbalance
is of minor importance.

It is therefore necessary to have a knowledge of journal bearing
dynamics as well as static performance characteristics, when designing
a rotor bearing system.

1.2 Pressurized Bearings

1.2.1 Pressure-Fed (Forced-Feed) Hydrodynamic Bearings

Hydrodynamic bearings are widely employed in applications involving
high loads and high speeds. The pressure to support the load is gener-
ated by the rotation of the shaft, which is a distinctive feature of
all hydrodynamic bearings. The velocity induced circumferential flow
is essential to the operating principle. Some of the common types of
hydrodynamic bearings are illustrated in figure (1.1).

Hydrodynamic bearings involve some undesirable features. For
example, at zero speed, there is no load support, hence, wear occurs,
during the process of starting and stopping. Also, if the bearing
operating temperature is allowed to rise excessively, this may lead to
thermal collapse. At certain speeds and under certain conditions of
light loading, hydrodynamic bearings are very susceptible to fractional
frequency whirling. If the whirling is unstable at a particular speed,
it is impossible to continue running without causing bearing failure
or to increase the speed to achieve a stable condition.

Forced-feeding (external pressurization) is now widely employed
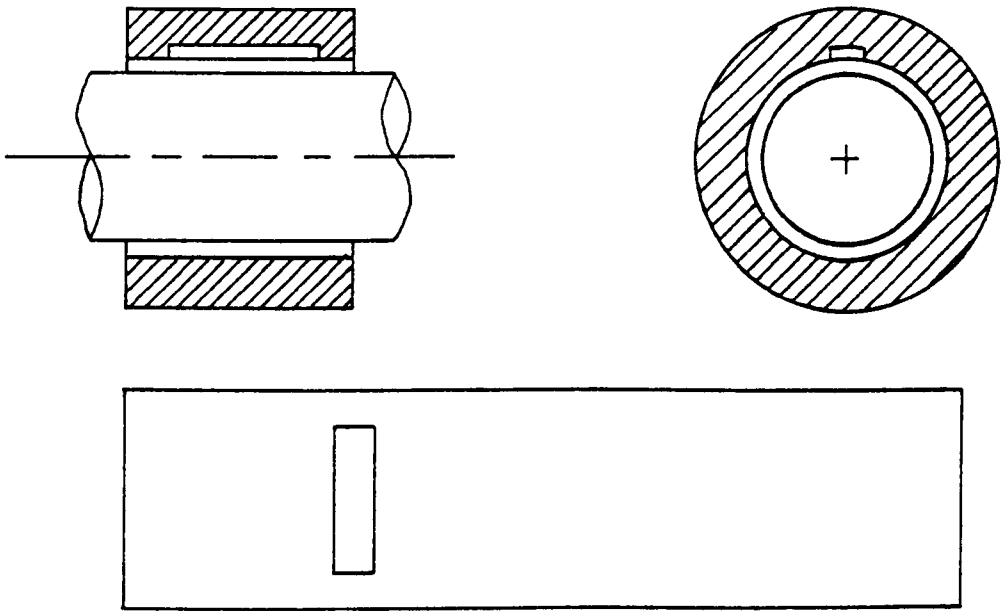
Axial Groove Bearing
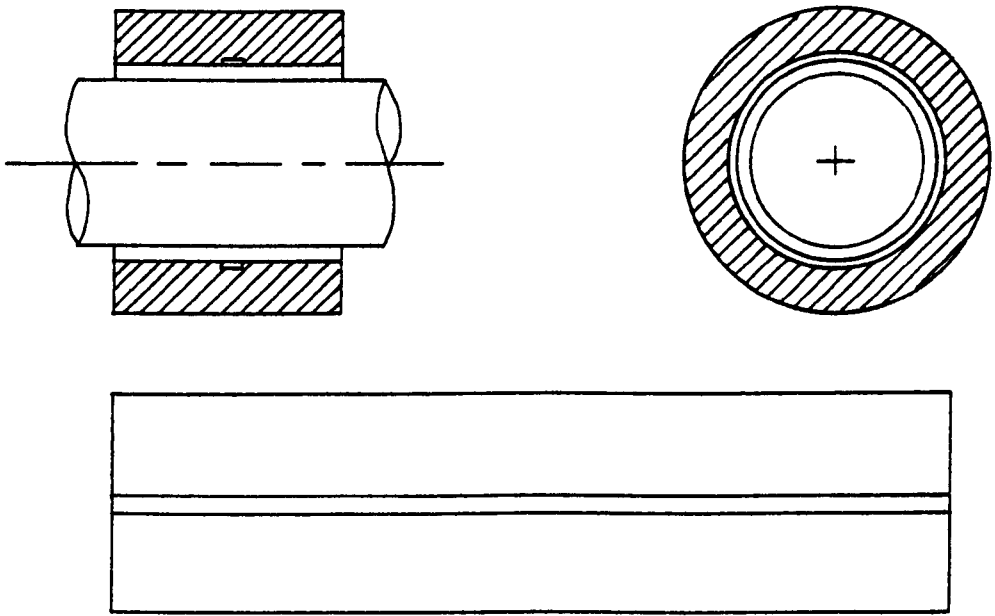
Circumferential Groove Bearing

Fig.(1.1): Common Types Of Hydrodynamic Bearings.

in hydrodynamic bearings to enhance its performance characteristics.
A rigorous analysis of forced-feed hydrodynamic journal bearings had
been conducted by Siew (5). The main advantages associated with forced
feeding are:

(1) It is possible to ensure a sufficient feed of fluid to the bearing
     to maintain the hydrodynamic oil-film, without starvation and also
     to provide cooling by convection. Over-heating and thermal dis-
     tortions may thus be avoided.

(2) By ensuring that high pressure fluid is pumped into the bearing
     (hydrostatic jacking) during starting and stopping conditions, the
     shaft can be made to float on a film of oil, thus preventing any
     wear action between the mating surfaces.

1.2.2 Hydrostatic Bearings (Externally Pressurized Bearings)

(a) Principles of Operation

Hydrostatic bearings are used to provide full fluid-film lubrication
when the relative motion of the surfaces to be separated is not large
enough to provide adequate hydrodynamic lubrication. The basic principles
of operation of a hydrostatic bearing is illustrated in figure (1.2),
and a recessed hydrostatic bearing is shown in plate (1).

Pressurized fluid at a constant supply pressure, P_s, (controlled
by a relief valve) is supplied to a number of entry ports (recesses),
via control devices of some form which act as restrictors. Except in
the case of constant volume flow, it is usual to supply hydrostatic
bearings from a constant pressure source. Basically, it involves flow
through two resistances in series, that is, the control device and the
bearing clearance.

As the fluid flows through the control device, the pressure is
reduced and arrives at the entry of the bearing at recess pressure, P_r.
The pressure further reduces as the fluid flows through the second
restriction caused by the bearing gap, its pressure reducing to atmos-
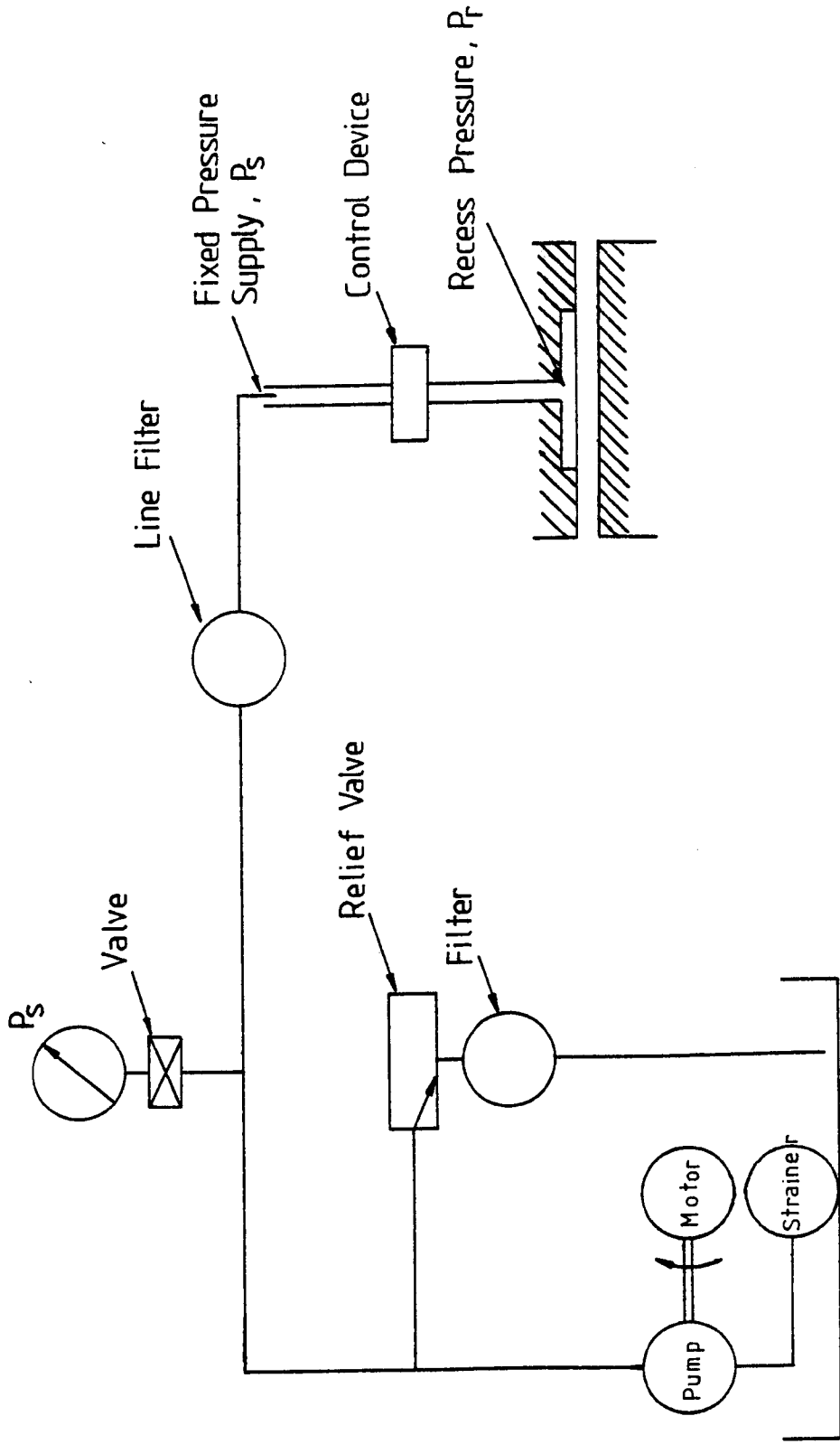
Fig.(1.2) : Basic Hydrostatic Bearing System

pheric at the outlet of the bearing.

For concentric conditions, $\varepsilon = 0$, the pressures at the recesses are equal. When the bearing is loaded, an eccentricity is caused, which leads to increased flow resistance in the low clearance (heavily loaded) side. This results in a lower flow-rate to the respective recess and, therefore, pressure in that recess is increased. Conversely, in the large clearance (unloaded) side, the recess pressure decreases. This pressure difference across the bearing load produces load capacity.

Thus, for any given loading, an eccentricity is produced for which the product of bearing pressure and projected area balances the applied load. Therefore, as a result of the pressure supply and the associated control devices, the fluid-film load support does not depend on speed. Such bearings may operate at any speed down to zero with full fluid-film separation of the surfaces, which is the principal advantages of hydrostatic bearings.

The control devices perform a major role in the operation of a hydrostatic bearing. As they function to control the flow-rate through the bearing, they also govern the bearing's oil-film stiffness. The most common forms of control devices in use are:

(i)   capillary

(ii)   pocketed orifice

(iii)   annular orifice

(iv)   slots

(v)   constant flow

(vi)   position sensing and pressure sensing values

(vii)   inherent control involving shallow recesses

(viii) porous liner.

(b) <u>Advantages and Limitations of Hydrostatic Bearings</u>

Many advantages have been claimed for hydrostatic bearings. These include:

(i)   Low friction and high stiffness at low speeds.

(ii)   Moderate temperature rise.

(iii) High precision of rotation. Because of the large clearance in hydrostatic bearings, there is an averaging effect on journal shape errors. Therefore, the running accuracy is usually very much better than the accuracy of the bearing members.

(iv)   High reliability and long life.

The following disadvantages should be considered, which may in some circumstances restrict the use of hydrostatic bearings:

(i)   High initial cost

(ii)   Auxiliary equipment such as a pump, filter, supply line, etc. is required.

(iii) The hydraulic system may be a source of external mechanical and audible vibrations.

Considering the above factors, hydrostatic bearings are thus, widely used in precision machine tools (milling, boring, grinding or turning) heavy duty grinding machines, rolling mills, etc.

1.2.3 Hybrid (Hydrostatic/Hydrodynamic) Bearings

Throughout the context of this investigation, the word 'hybrid' is used to denote the condition that both hydrostatic and hydrodynamic actions are present. Therefore the configuration of a hybrid bearing may vary between a conventional recessed hydrostatic bearing to a plain hydrodynamic bearing. An example of the former is when a hydrostatic bearing is run at speeds while forced-feeding a hydrodynamic bearing with an externally pressurised supply constitutes the latter. The only distinctive feature between them is that hybrid bearings that are hydrostatically based, have restrictors, while hybrid bearings that are hydrodynamically based usually incorporate a non-return value in the supply line as a principle of good practice (1). This discussion will be con-

fined to plain (non-recessed) hybrid bearings that are hydrostatically based, and references to other hybrid bearing configurations will only be mentioned.

There are two basic configurations of plain hybrid journal bearings the slot-entry and the hole-entry. Slot-entry bearings, which are the subject of patents taken out by C. W. Dee (2) of Aerostatic Limited, Poole, are bearing units currently available in selected size units, (see figure (1.3) and plate 2). It has the appearance of a plain hydrodynamic journal bearing, but, it has slot restrictors built into the bearing body.

The thickness of the slots is usually of the order of 12 - 50 μm. A single or double row of inlet slots may be employed depending upon the application. The slots act as laminar restrictors. Design procedures for this bearing configuration for static performance have been fully established and backed up by an extensive programme of experimental work (3). However, information on dynamic performance is still lacking. Advantages claimed by researchers of this bearing configuration are:

(i)   Slot-entry bearings are superior to the circumferential groove hydrodynamic bearings, when operating at speed, since higher loads can be supported.

(ii)   Slot-entry bearings carry loads comparable with axial groove hydrodynamic bearings, but are greatly superior for coping with rotating loads and varying directions of loading.

(iii)   Slot-entry bearings carry slightly higher loads at zero speed than four-recess hydrostatic bearings.

The second configuration of plain hybrid journal bearing is the hole-entry configuration, as illustrated in figure (1.4). The holes are disposed around two rows and can either be orifice or capillary compensated. This type of bearing has the advantage of ease of manu-facture and a further improvement over the slot-entry bearing at high
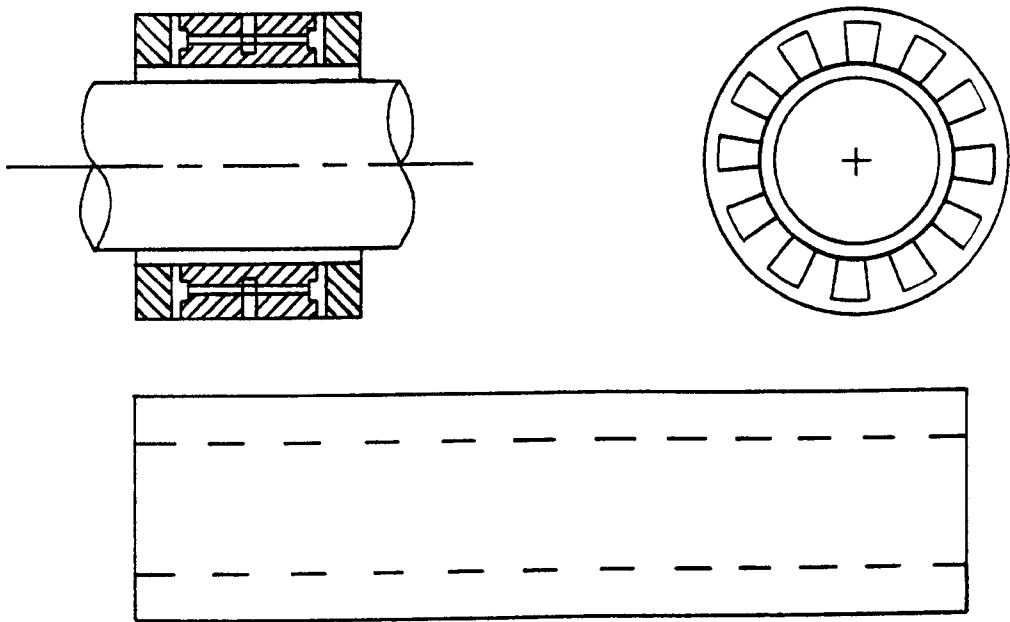
Fig.(1.3) : Plain Slot-Entry Hybrid Journal Bearing.
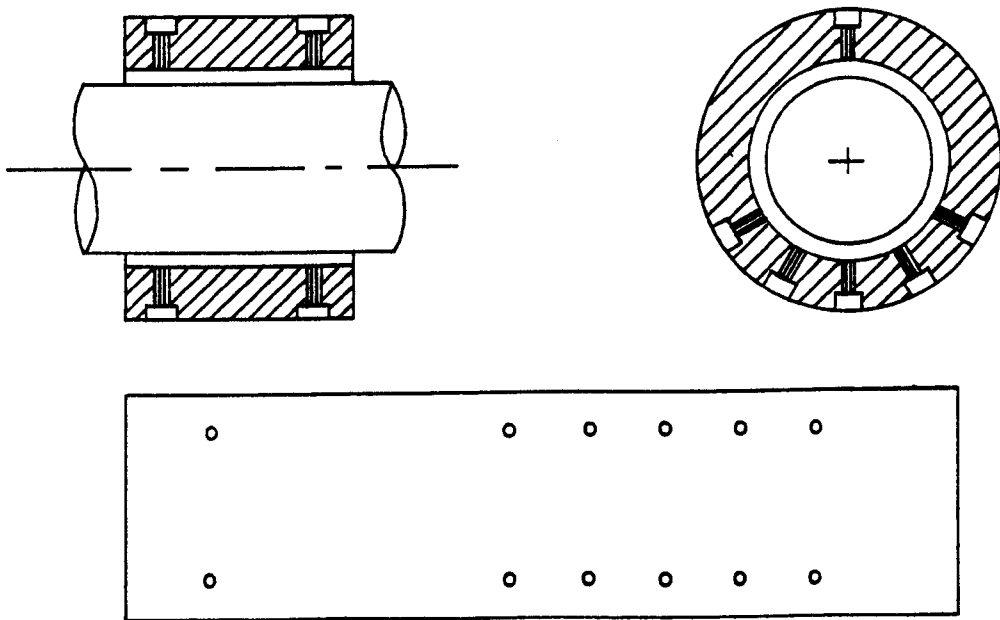
Fig.(1.4) : Asymmetric Plain Hole-Entry Hybrid Journal
Bearing.
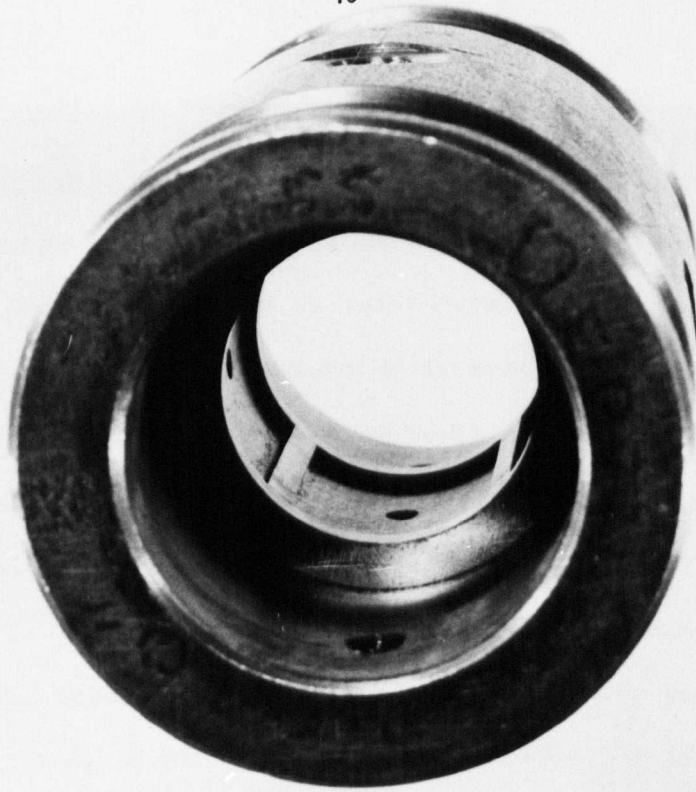
Plate (1) : Recess Hydrostatic Bearing

Plate (2) : Slot-Entry Hybrid Bearing

speeds and at very high eccentricity-ratios (6).

1.3 The Scope and Aims of The Investigation

Although there is now an availability of accurately computed data accompanying design procedures on double-entry slot hybrid journal bearings, there is still an element of uncertainty, in relation to its dynamic performance, when the bearing is called upon to operate at speeds. There is no information concerning their performance in relation to physical characteristics, like, critical speeds, instability, unbalance response, etc. To date, the only data available is that reported by Rowe et al (4), which is restricted to the concentric case, and is not presented in a convenient form, which can be directly used by rotating machinery designers or rotor-bearing dynamicists. Also, it is not known whether the slot-entry bearing is more stable than a hydrodynamic bearing or not. This thesis attempts to provide the information to bridge this gap, so that the potential advantages of the slot-entry bearing can be exploited to the fullest. Therefore the present invest-igation has been conducted with the following aims in view:

1) To compute the eight linearized dynamic coefficients for a plain hybrid journal bearing of the slot-entry configuration, and, to predict the frequency responses of the bearing fluid-film.

2) To measure, experimentally, the frequency responses of the bearing fluid-film and to determine the eight-linearized dynamic coefficients for a plain hybrid journal bearing under various operating conditions.

3) To compare the theoretical frequency responses and coefficients with those obtained experimentally.

4) To prepare and present data in a form suitable for use in a full rotor-bearing dynamic analysis.

5) To predict the stability threshold speed of rotors (rigid and flexible) operating in plain hybrid bearings and to carry out a comparison with other bearing configurations, where information
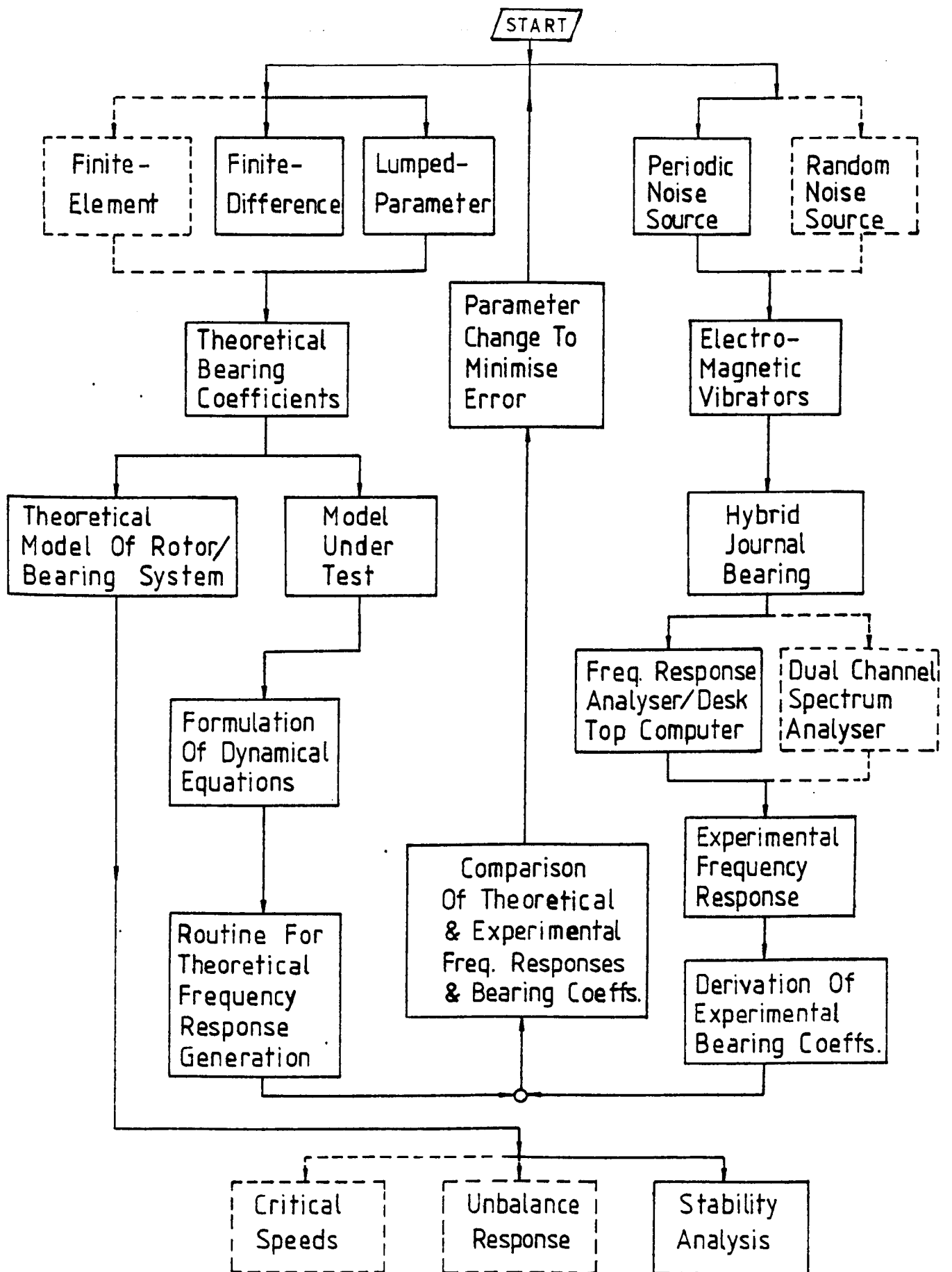
Fig.(1.5) : Programme For The Dynamic Analysis Of Hybrid Journal Bearings.

is available.

The programme for the dynamic analysis of the hybrid journal bearing is illustrated in figure (1.5).

A literature survey on fluid-film bearing research and externally pressurized bearings is detailed in Chapter 2.

As researchers of hydrostatic and hydrodynamic bearings differ in their approach to investigating the dynamic performance of bearings, a chapter on journal bearing dynamics is included in Chapter 3, so that, a better understanding and deeper appreciation of the subject can be achieved. Also, it is hoped that this may lead the way to a standard approach to dynamic analysis, so that comparison between externally pressurized and hydrodynamic bearings can be made.

Chapter 4 outlines the theoretical analysis used for carrying out performance studies of slot-entry bearings. Two models were developed; a finite-difference approximation of the Reynolds equation and a lumped parameter approach. The results (static) are discussed and compared with those of Koshal (3).

Two techniques (perturbation and finite-disturbance) are developed for the subsequent computation of the eight-linearized bearing dynamic coefficients, which define the forces for small displacements of the journal about its static equilibrium position. These are presented in Chapter 5, and the results are discussed.

Chapter 6 is a discussion of the subjects of system identification and modelling. This chapter discusses the frequency response technique, bearing fluid-film modelling and the derivation of the bearing fluid-film transfer-functions. Also, the identification of the fluid-film transfer-function and bearing coefficients from the experimental results are discussed.

The test-rig and instrumentation system used to conduct the

experimental studies are described in Chapter 7. These include the development of the software and electrical circuits for real time measurements.

The experimental procedure is discussed in Chapter 8, and the theoretical and experimental results for frequency responses and bearing coefficients are compared and discussed.

A theoretical linearized stability study of the slot-entry bearing is presented in Chapter 9.

Chapter 10 presents the conclusions and suggestions for future work.

REFERENCES

1. Fuller, D. D. 'Theory and Practice of Lubrication for Engineers', John-Wiley and Sons, New York, 1956, pp. 107 - 125.

2. Dee, C. W. and Shires G.L. 'The Current State of the Art of Fluid Bearings with Discrete Slot Inlets', Trans. ASME, Journal of Lub. Tech., Paper No. 71, 1971.

3. Koshal, D. 'The Design and Optimization of Slot Hybrid Journal Bearings', Ph.D. Thesis, Liverpool Polytechnic, 1978.

4. Rowe, W. B., Weston W. and Koshal D. 'Static and Dynamic Properties of Concentric Hydrostatic Journal Bearings', The Euromech Colloquim No. 124, Orbassano, Italy, October, 1979.

5. Siew, A. H. 'A Computational Approach to the Design and Performance Optimization of Solid and Porous Journal Bearings', Ph.D. Thesis, Cranfield Institute of Technology, 1981.

6. Rowe, W. B., Xu S. X., Chong F. S. and Weston, W. 'Hybrid Journal Bearings', Tribology International, Dec. 1982, pp. 339 - 348.

CHAPTER 2

<u>LITERATURE SURVEY</u>

2.1 <u>Fluid-Film Bearing Research</u>

Lubrication is a modern science and almost all we now consider significant has been discovered since the middle of the ninetieth century. Early research work was mainly concerned with trying out various bearing metals and lubricants to minimise friction and maximise bearing life. One of these early investigators was L. D. Girard, who, in a note to the Academy of Science Paris (1862), discussed the use of a water lubricated hydrostatic journal bearing, where frictional and wear effects could almost be eliminated. The year 1878, saw the first public demonstration of hydrostatic lubrication ('Le chemin de Fer de Glace') at the Paris Industrial Exposition. It was a heavy block on legs that glided easily on a flat surface, where the lubricant was pumped down each leg to the feet which acted as hydrostatic pads.

The breakthrough in lubrication studies came in the 1880's, where the emphasis was towards an understanding of the physical mechanism of fluid-film lubrication, rather than measurements of friction. The hydrodynamic action of the lubricant within a journal bearing was dis-covered by Beauchamp Tower (1) in 1883, and his experiments led Reynolds (2) in 1886, to work out theoretical explanations (Reynolds equation) to define the pressure distribution within the oil-film of such bearings. Petroff, who was working independently in Russia (1883) had already proposed theoretical explanations to relate friction measurements to hydrodynamic theory. Petroff's work differed in that it was based on the existence of an oil film of uniform thickness, whereas Reynold considered the more general case of films of non-uniform thickness in an eccentric bearing.

The Reynolds equation, which is a combination of the continuity
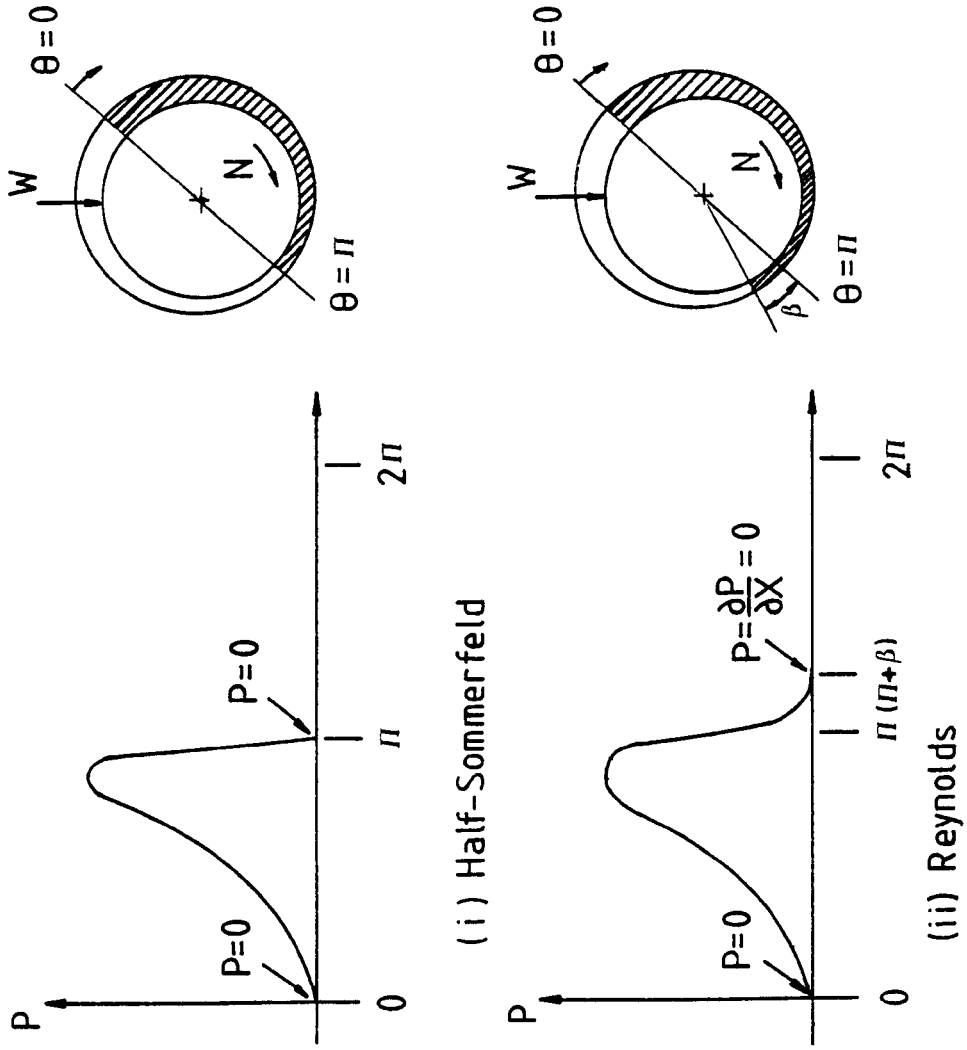
Fig.(2.1) : Boundary Conditions Of Film Pressure.

and equilibrium equations is insoluble in closed form. However, many

approximate solutions exist. Until the advent of numerical techniques

of integration, it could only be solved for the case of an infinitely

long bearing based on a substitution by Sommerfeld (3) in 1904. An

improvement of the infinitely long bearing solution was proposed by

Gumbel in 1917, who used correction factors based on the length to

diameter ratio of the bearing to correct for end leakage. Another

significant contribution in the field of analytical solutions was the

infinitely short bearing model of Dubois and Ocvirk (9) in 1952.

The boundary conditions normally used in the solution of the

Reynolds equation are the Sommerfeld (360°), the half Sommerfeld (180°)

and the Reynolds boundary conditions. These are illustrated in figure

(2.1). The Sommerfeld boundary condition is the simplest and least

realistic, at large values of eccentricity ratio and speed. It assumes

that the lubricant film extends continuously around the bearing with

no cavitation, hence negative pressures occur in the divergent zone.

Experimental studies carried out by Dyer and Reason (43) did not sub-

stantiate this theory. An improvement, is the half Sommerfeld condition

which assumes that the film starts at the point of maximum gap, extends

through 180° and terminates at the minimum gap. This is the most real-

istic boundary conditions that can normally be handled by analytical

solutions. The Reynolds condition is most commonly used by present day

investigators and is the most accurate of the three boundary conditions,

~~film breakdown)~~ though more difficult to handle. It assumes that the

film starts where the gap is at a maximum and terminates where the

pressure and the circumferential pressure gradient are simultaneously

zero. The validity of this condition has been explored by Swift (4)

and Stieber (5). When used in conjunction with an iterative tech-

nique the Reynolds condition can be easily incorporated, and by setting

all negative pressures to zero, the pressure distribution will auto-

matically take up the necessary zero gradient at the trailing end as iteration proceeds.

The film reformation boundary has been the focus of attention of several present day investigators (33, 54, 55, 61). This is based on the studies of the behaviour of film rupture in the cavitated region by Jakobsson and Floberg (12). By considering the continuity of flow, they postulated a new boundary condition governing the reformation of film pressure. This boundary condition is currently the best available, but it is difficult to incorporate in a solution. Recently several efficient algorithms for handling the Jakobsson and Floberg boundary conditions have appeared in the literature (55, 61). Another condition, which is easier to implement in a solution is to assume that film reformation occurs at a 'free' boundary $(P = \partial P/\partial x = 0)$, instead of beginning specifically at the position of maximum gap. The validity of this assumption for bearings operating at high values of eccentricity has been explored by Dyer (40).

Numerical iterative techniques are the most important means of solving the fluid lubrication problem. Among all the numerical techniques available, the relaxation approach based on successive iterations of the governing equations (a finite-difference approximation of the Reynolds equation) is the most frequently used in journal bearing analysis, since the use of direct matrix inversion is not practical. Notable among the papers on the solution of finite bearings are those by Cameron and Wood (7), Walther and Sassenfeld (8), Raimondi and Boyd (13), Heller and Shapiro (22), O'Donoghue, Rowe and Hooke (23) and many others. A method of solution of the Reynolds equation which takes advantage of the form of the boundary conditions to solve the problem exactly and accurately without requiring iteration has been presented by Castelli and Shapiro (15). Interests on this approach is growing and has been adopted by many present investigators such as

Lund et al (45) and Colsher, Anwar and Katsumata (57), although each investigator differs in the method of solving their matrix equations. The application of finite-element techniques to lubrication problems is growing rapidly and is currently the best numerical technique available. It offers a practical means of dealing with irregularities of geometric and physical properties. Notable among the papers are those by Booker and Huebner (37), Allaire, Nicholas and Gunter (44) and many others.

2.2 Hydrostatic Bearing Research

The multi-recessed type of externally pressurized bearing has been extensively studied since Fuller(6) first presented a series of articles on hydrostatic lubrication in 1947. A useful guide on the subject of hydrostatic lubrication may be seen in the work of Shaw and Macks(62).

The work of Raimondi and Boyd (10) in 1954, signifies one of the major developments in the field of hydrostatic lubrication, although their analysis is limited to thin land bearings operating at the concentric condition. They described the lumped parameter method for flows over axial and circumferential lands. The effect of hydrodynamic pressure caused by the rotation of the shaft was neglected.

Loeb (11) demonstrated that the electric analog field plotter could be used to analyse any bearing shape with reasonable accuracy. In contrast to Raimondi and Boyd's analysis, Loeb's analysis is limited to thick land bearings, also operating at the concentric condition.

Approximate expressions for the damping of a four-recess hydrostatic bearing has been derived by Mori and Yabe (14), by taking into account the effects of the axial and circumferential land squeeze films, at zero speed. The damping caused by the external restrictor was neglected.

Various refined forms of the original Raimondi and Boyd's analysis have been used by numerous workers (16, 19, 24, 25, 34) to establish the steady state behaviour of hydrostatic bearings, while the

Mori and Yabe's analysis provided the groundwork for subsequent dynamic analysis of hydrostatic bearings (27, 28   ).

Design procedures based on the thin land assumption, for a capillary compensated hydrostatic journal bearing had been presented by Cowley and Kher (16). The rotation induced flow was again neglected.

Hunt and Ahmed (19) demonstrated the importance of the rotation induced flow when analysing a six-recess capillary compensated hydrostatic bearing, but they neglected the effect of the pressure induced circumferential flow.

The subject of optimization, which has major relevance to externally pressurized bearings was put forward by Opitz (20) in 1968, although Fuller (6) was the first to perform optimization on hydrostatic bearings by varying the film thickness to minimise total power. Opitz demonstrated that choosing viscosity to minimize the total power leads to the requirement that the power-ratio, $K = 1$, while choosing the clearance leads to the requirement that $K = 3$. He further demonstrated that, if the values of K, lie between 1 and 3, the total power dissipated does not exceed the minimum value by more than 15%.

By including both pressure and rotation induced flows, Davies (25) extended the thin-land model of Raimondi and Boyd. His analysis is applicable to any number of recesses. The author further defined the concept of 'optimum speed'. This is the speed at which the ratio of the energy dissipated in shearing at the bearing lands to the total energy required for oil to flow through the concentric bearing is an optimum.

A comprehensive investigation into the design of various shapes and types of hydrostatic bearings was presented by O'Donoghue and Rowe (24, 34   ). Results were presented for thin land bearings for simplicity and thick-land bearings based on finite-difference techniques.

A solution for hydrostatic journal bearings based on accurate finite-difference techniques has been presented by Heller and Shapiro (22). Both hydrostatic and hydrodynamic effects were taken into account and the effect of cavitation was considered by substituting zero values for all negative pressures encountered during the relaxation process. Another technique, the 'cell approach', has been presented by Colsher and Anwar (57).

O'Donoghue, Rowe and Hooke (23) employed similar techniques in their analysis, and compared four different procedures for designing externally pressurized journal bearings from the point of view of cost of computing time, accuracy and ease of use. The four approaches are:

(i)   the simple concentric theory

(ii)   the lumped parameter technique

(iii) superposition of finite difference results

(iv)   full simultaneous solution by the finite difference technique with provision for cavitation.

The authors (29), further defined optimization as the process of minimizing the total power dissipation of a bearing which must fulfil certain other requirements, such as a given load on a pad which must be contained within a certain area. Design procedures for various types of hydrostatic bearings, aiming at solutions near to optimal designs have been presented by the authors (34). Rowe et al (26), introduced the optimization or speed parameter, S_{ho}, which relates design variables for a minimum power condition. The parameter S_{ho}, is the optimum value of the equivalent Sommerfeld Number for hydrostatic bearings which is termed S_h. The optimum value of S_{ho} was defined as the value of S_h corresponding to the power ratio K = 1.

At about this time, the wide applications of hydrostatic journal bearings in main-spindle assemblies of machine-tools, instigated numerous investigators of externally pressurized bearings to take into

account dynamic performance. Cowley and Kher (27) extended the model of Mori and Yabe (14) by taking into account the effect of the external restrictor. They examined the forced vibration characteristics of a flexible spindle supported in two hydrostatic bearings and represented the bearing characteristics by a one-dimensional spring and damper. The authors showed the importance of selecting the optimum bearing stiffness and damping in minimizing dynamic deflections at the spindle. Opitz et al (28) carried out a more complicated analysis than that of Cowley and Kher (27) to include the compressibility effect and an improved modelling of the damping term. The authors (27, 28) neglected the effect of shaft rotation in their theoretical analysis, although they did not observe any significant speed effects experimentally.

A closed form solution at zero shaft eccentricity, for the operation of a four recess hydrostatic journal bearing has been presented by Davies and Leonard (30). By extending a previous static analysis (25) they formulated a general unsteady-state continuity-of-flow equation for a recess in a multi-recess bearing using small perturbation analysis and applied it to an orifice-compensated bearing with four recesses at zero eccentricity. The validity of their analysis was demonstrated by the experimental confirmation of the occurrence of dynamic instability (31) and also by the experimental results (30) obtained from harmonic testing (receptances). Associated numerical solutions of the equations of motion about eccentric positions, were also adequately confirmed by Leonard and Davies (35).

Dixon and Leonard (32), extended the general analysis of Davies and Leonard (30) to include bearings with three, five and six recesses. A closed form solution was obtained for zero eccentricity. The analysis is applicable to both orifice and capillary compensated bearings. Davies (42) in extending the thin land model of (30) presented

equations of motion and expressions for receptances, for motion of the shaft about the concentric position, using signal flow graphs. His analysis can be applied to orifice, capillary or constant flow compensated bearings and any number of recesses could be accommodated.

A discussion on the mechanism of instability in hydrostatic journal bearings has been presented by Leonard and Rowe (38).

Purely experimental investigations have been reported by Patrick and Chen (21) and Ho and Chen (52), on the dynamic performance of capillary compensated hydrostatic bearings.

A system approach to the dynamic characteristics of hydrostatic bearings has been presented by Chen et al (53). Concentric dynamic force coefficients for capillary, orifice and constant flow hydrostatic bearings have been presented by Rowe (47).

Recently the finite-element technique has been adopted by Wadhwa et al (60) and many others to carry out dynamic analysis.

2.3 Hybrid Bearing Research – Slot-Entry Configuration

Approximate methods for the design of single and double-entry slot hybrid bearings have been presented by Dee and Shires (36). They derived a simplified analysis based upon axial flow modelling in the bearing clearance. A factor was introduced in the analysis to account for circumferential flow.

Stout, Porrit and Rowe (17) presented results for double slot-entry bearings at zero speed, obtained by finite-difference technique and compared them with results of Shires and Dee (18). The authors concluded that the simplified method under-estimated the bearing performance compared with finite-difference results at low eccentricities. Stout and Rowe (39) extended the work further, by presenting full design procedures for zero speed slot-entry bearings under steady loading based on their finite-difference technique.

Recently, a comprehensive investigation into the performance of slot hybrid bearings under various operating conditions of eccentricity and speed was carried out by Koshal and Rowe (45, 48). Design guides leading to optimum hybrid performance have been presented and the optimum bearing geometry was established (49). Their theoretical analysis was based on a finite-difference approximation of the class-ical Reynolds equation with provision for source flow and allowing for cavitation. More recently, Rowe et al (58) presented a theoretical analysis of hole-entry hybrid bearings. Their investigations showed that hole-entry bearings offer possible improvements over the slot configuration. Experimental work on the hole configuration has yet to be undertaken.

To date, there is no significant information on the dynamic char-acteristics of plain slot-entry hybrid bearings, except, those presented by Rowe et al (47), which is limited to the concentric condition, and, Rowe and Chong (59), where the four stiffness and four damping co-efficients are presented. The dynamic characteristics (including fluid inertia) of oil lubricated plain hybrid journal bearing of the capillary restrictor configuration had been presented by A. Ichikawa (51). Stiff-ness and damping coefficients for the recessed hybrid journal bearing had been presented by Rhode and Ezzat (41). The authors showed that the compressibility effect is significant at the high end of the fre-quency range.

Recently, Gomez (56) in his work on a heavy duty rolling mill, reported that slot-entry bearings can support any combination of static and dynamic load under constant and oscillating motion with no transient overshoot of eccentricity ratio.

2.4 Summary

Ever since the basic principle of externally pressurized lubri-cation was demonstrated to the public (1878), at the Paris Industrial

Exposition, the subject has developed and progress from crude and approximate analytical methods to accurate and realistic numerical solutions, that will handle any degree of mathematical complexity.

There is now an availability of accurately computed data and accompanying design procedures for static loads to satisfy most general requirements of externally pressurized bearings.

Attention has been increasingly focussed on design for hybrid operation. There is, therefore, an urgent need to include better and more convenient information on dynamic performance. This is necessary if progress is to be made towards overall system design of rotating machinery to include externally pressurized bearings as standard elements and to fully exploit the potential advantages offered by the hybrid mode of lubrication.

The importance of an overall rotor-bearing dynamic analysis has still to be appreciated by many designers of externally pressurized bearings.

REFERENCES

1. Tower, B. 'First Report on Friction Experiments', Proc. Inst. Mech. Engrs., Vol. 34, 1883, pp. 632 - 659.

2. Reynolds, O. 'On the Theory of Lubrication and its Application to Mr. Beuchamp Tower's Experiments, Including an Experimental Determination of the Viscosity of Olive Oil', Phil. Trans. Roy. Soc., London, Vol. 177, Pt. I. 1886, pp. 157 - 234.

3. Sommerfeld, A. 'Zur hydrodynamischen theorie der Schmiermittel-reibung', Zeitschrift fur Math. and Phys., Vol. 50, 1904, pp. 97 - 155.

4. Swift, H. W. 'The Stability of Lubricating Films In Journal Bearings', Proc. Inst. Civil Engrs., Vol. 233, 1931, pp. 267 - 322.

5. Stieber, W. 'Das Schwimmlager', Krayn, Berlin, 1933.

6. Fuller, D. D. 'Hydrostatic Lubrication', Machine Design (in 4 parts), June - Sept., 1947.

7. Cameron, A. and Wood, W.L. 'The Full Journal Bearing', Proc. Inst. Mech. Engrs., Vol. 161, 1949, pp. 59 - 72.

8. Walther, A. and Sassenfeld, H. 'Pressure Distribution and Load in a 360° Journal Bearing, for values of the character-istics, B, (ratio of diameter to length) from 0 to 8, and Eccentricity, C = 0.1 to 0.95', Dept. of Scien-tific & Ind. Research, Sponsored Research (Germany) Report No. 11, 1950, I.P.M. Report No. 8.

9. Dubois, G. B. and Ocvirk, F. W. 'Analytical derivation and experimental evaluation of Short Bearing Approximation for Full Journal Bearings', N.A.C.A. Report No. 1157, 1953.

10. Raimondi, A. A. and Boyd, J. 'An analysis of Orifice and Capillary compensated Journal Bearings', ASME-ASLE Lub. Conf., Baltimore, 1954.

11. Loeb, A. M. 'The determination of the Characteristics of Hydrostatic Bearings through the use of the Electric Analog Field Plotter', Trans. ASME, Vol. 1, No. 1, 1957.

12. Jakobsson, B. and Floberg, L. 'The Finite Journal Bearing Considering Vaporization', Trans. Chalmers Univ. Technol., Gothenburg, Sweden, 1957.

13. Raimondi, A. A. and Boyde, J. 'A Solution for the finite journal bearing and its application to analysis and design: I, II, III', Trans. ASLE, Vol. 1, 1958, pp. 159 - 209.

14. Mori, H. and Yabe, H. 'A theoretical investigation of hydrostatic bearings', Trans. Soc. Engrs., Japan, Vol. 28, No. 193, 1962, pp. 1149 - 1159.

15. Castelli, V. and Shapiro, W. 'Improved method for Numerical Solutions of the General Incompressible Fluid-Film Lubrication Problem', Jnl. of Lub. Tech., April 1967, pp. 211 - 218.

16. Kher, A. K. and Cowley, A. 'The design and performance characteristics of Capillary compensated hydrostatic journal bearings', Proc. 8th Int. M.T.D.R. Conf., 1967.

17. Stout, K. J., Porrit, T. E. and Rowe, W.B. 'The Performance of Externally Pressurized Slot Restricted Journal Bearings', 6th Int. Gas Brg. Symposium, Paper No. 7, 1967.

18. Shires, G. L. and Dee, C. W. 'Pressurized Bearings with Inlet Slots', Univ. of Southampton, Gas. Brg. Sumposium, Paper No. 7, 1967.

19. Hunt, J. B. and Ahmed, K. M. 'Load Capacity, Stiffness and Flow Characteristics of a hydrostatically lubricated six-Pocket Journal Bearing, supporting a rotating spindle', Proc. Instn. Mech. Engrs., Vol. 182, 1967/68.

20. Optiz, H. 'Pressure Pad Bearings', Proc. Instn. Mech. Engrs. Vol. 182, Part 3A, 1967 - 68, pp. 100 - 115.

21. Patrick, J. K. and Chen, N.N.S. 'Performance of a short multi-grooved capillary compensated hydrostatic journal bearing', Proc. Instn. Mech. Engrs, London, 183 (3P), 1968 - 69, pp. 107 - 115.

22. Heller, S. and Shapiro, W. 'A Numerical Solution for the Incom-pressible Hybrid Journal Bearing with Cavitation', Trans. ASME, J. Lub. Tech. Serios F, Vol. 91, 1969, pp. 508 - 516.

23. O'Donoghue, J. P., Rowe, W.B. and Hooke, J.P. 'Computer Analysis of Externally Pressurized Journal Bearings', Proc. Instn. Mech. Engrs., Vol. 184, Part 3L, 1969/70.

24. O'Donoghue, J. P. and Rowe, W.B. 'Hydrostatic Bearing Design', Tribology, Vol. 2, 1969.

25. Davies, P. B. 'A general analysis of multi-recess Hydrostatic Journal Bearings', Proc. Instn. Mech. Engrs., Vol. 184, Part 1, 1969/70.

26. O'Donoghue, J. P., Rowe, W.B. and Hooke, C.J. 'Design of hydro-static bearings using an operating parameter', Wear, 14 (1969), pp. 355 - 362.

27. Cowley, A. and Kher, A. K. 'The dynamic characteristics of a hydrostatically supported spindle bearing system', Proc. 10th Int. M.T.D.R. Conf., 1969.

28. Opitz, H., Bottcher, R. and Effenberger, W. 'Investigation in the dynamic behaviour of hydrostatic spindle-bearing systems', Proc. 10th Int. M.T.D.R. Conf., 1969.

29. Rowe, W. B., O'Donoghue, J.P. and Cameron, A. 'Optimization of externally pressurized bearings for minimum power and low temperature rise', Tribology, August, 1970, pp. 153 - 157.

30. Davies, P. B. and Leonard, R. 'The dynamic behaviour of multi-recess hydrostatic journal bearings', Proc. Instn. Mech. Engrs., Tribology Convention, 1970.

31. Davies, P. B. and Leonard, R. 'The stability of multi-recess hydrostatic journal bearings', Jnl. of Mech. Engng. Sci., 1970, 12 (2).

32. Dixon, R. S. and Leonard, R. 'Formular defining the performance of hydrostatic journal bearings incorporating 3, 4, 5 and 6 recesses', Int. J. Mach. Tool Des. Res., 1970.

33. McCallion, H., Lloyd, T. and Yousif, F.B. 'The influence of oil-supply conditions on the film extent and oil flow in journal bearings', Instn. Mech. Engrs., C55, 1971, pp. 31 - 37.

34. Rowe, W. B. and O'Donoghue, J.P. 'Design Procedures for Hydrostatic Journal Bearings', The Machinery Publishing Co. Ltd., 1971.

35. Leonard, R. and Davies, P.B. 'An experimental investigation of the dynamic behaviour of a four recessed hydrostatic journal bearing', Proc. Instn. Mech. Engrs., Joint Conf. Ext. Press. Bearings, 1971.

36. Dee, C. W. and Shires, G.L. 'The current state of the art of fluid bearings with discrete slot inlets', Trans. ASME, Jnl. Lub. Tech., Paper No. 71, 1971.

37. Booker, J.F. and Huebner, K.H. 'Application of Finite Element Methods to Lubrication: An engineering approach', Jnl. of Lub. Tech., Oct. 1972, pp. 313 - 323.

38. Leonard, R. and Rowe, W.B. 'Dynamic Force Coefficients and the Mechanism of Instability in Hydrostatic Journal Bearings', Wear, 23, 1973, pp. 277 - 282.

39. Stout, K. J. and Rowe, W.B. 'Externally Pressurized Bearings - Design for Manufacture', Trib. Int.,

    Part 1 - June 1974

    Part 2 - August 1974

    Part 3 - October 1974.

40. Dyer, D. 'Theoretical and Experimental studies of the effect of clearance and geometry in hydrodynamic journal bearings', Ph.D. Thesis, Cranfield Inst. of Tech. 1974.

41. Rhode, S. M. and Ezzat, H. A. 'On the dynamic behaviour of Hybrid Journal Bearings', GMR Research Publication, GMR - 1853, April 1975.

42. Davies, P.B. 'The dynamic behaviour of passively compensated, hydrostatic journal bearings with various numbers of recesses', Jnl. of Mech. Engng. Sci. Vol. 18, No. 6, 1976.

43. Dyer, D. and Reason, B. R. 'A study of tensile stresses in a journal bearing oil-film', Jnl. of Mech. Engng. Sci., Vol. 18, 1976, pp. 46 - 52.

44. Allaire, P. E., Nicholas, J.C. and Gunter, E.J. 'System of finite elements for Finite Bearings', Jnl. of Lub. Tech., April 1977, pp. 187 - 196.

45. Lund, J. W. and Thomsen, K.K. 'A calculation method and data for the Dynamic coefficients of Oil lubricated journal bearings', Topics in Fluid-Film Bearings and Rotor-Bearing Design and Optimisation, 1978, The Am. S. of Mech. Engrs.

46. Koshal, D. 'The Design and Optimization of Slot Hybrid Journal Bearings', Ph.D. Thesis, Liverpool Polytechnic, 1978.

47. Rowe, W. B., Weston, W. and Koshal, D. 'Static and dynamic properties of concentric hydrostatic journal bearings', The Euromech Colloquim No.124, Orbassano, Italy, Oct. 1979.

48. Rowe, W. B.   'Dyanmic and static properties of Recessed hydro-
     static journal bearings by small displacement analysis',
     Jnl. Lub. Tech., Trans. ASME, Jan. 1980, Vol. 102,
     pp. 71 - 79.

49. Koshal, D. and Rowe, W.B.   'Fluid-Film journal bearings operating
     in a Hybrid mode', 2 Parts, Trans. ASME, Jnl. of Lub.
     Tech., Aug. 1980, Vol. 103, pp. 558 - 572, (Part 1 -
     Theory, Part 2 - Expt.)

50. Rowe, W.B. and Koshal, D.   'A new basis for the optimization of
     Hybrid journal bearings', Wear, 64 (1980), pp. 115 -
     131.

51. Ichikawa, A.   'Fluid inertia effects on the dynamic characteristics
     of a plain journal bearing', Jnl. Japan Soc. of Lub.
     Engrs., Vol. 25, Part 4, 1980, pp. 261 - 268.

52. Ho, Y. S. and Chen, N.N.S.   'Dynamic characteristics of a hydro-
     static journal bearing', Wear, 63 (1980), pp. 13 - 24.

53. Chen, K. N., Yang, G.P., Wang, X and Yang, H.H.   'A system approach
     to the dynamic characteristics of hydrostatic
     bearings used on machine tools', Int. J. Mach. Tool
     Des. Res., Vol. 201, 1980, pp. 287 - 297.

54. Siew, A. H.   'A computational approach to the design and perfor-
     mance optimization of solid and porous journal
     bearings', Ph.D. Thesis, Cranfield Inst. of Tech.,
     1981.

55. Elrod, H. G.   'A cavitation algorithm', Trans. ASME, Jnl. of Lub.
     Tech., Vol. 103, July 1981, pp. 350 - 354.

56. Gomez, J.F.P. 'Oil-film bearings applied to heavy duty rolling mill drive couplings', M.Phil. Thesis, Sheffield Polytechnic, June 1982.

57. Colsher, R., Anwar, I. and Katsumata, S. 'An advanced method for predicting hybrid bearing performance', Presented at AGARD Symp. on Fluid Problems in Brgs. and Lub., Ottawa, June 1982.

58. Rowe, W. B., Xu, S.X., Chong, F.S. and Weston, W. 'Hybrid Journal Bearings', Trib. Int., Dec. 1982, pp. 339 - 348.

59. Rowe, W.B. and Chong, F.S. 'Computation of dynamic force co-efficients for hybrid (hydrostatic/hydrodynamic) bearings', Presented at the 3rd Trib. Conf., Budapest, 8 - 10 June, 1983.

60. Wadhwa, S. S., Sinhasan, R. and Singh, D.V. 'Analysis of orifice compensated externally pressurized gas bearings', Trib. Int., August 1983, pp. 203 - 211.

61. Rowe, W. B. and Chong, F.S. 'A computational algorithm for cavitating bearings - Requirement of boundary conditions which satisfy the principle of mass conservation', submitted to Trib. Int. for publication.

62. Shaw, M.C. and Macks, E.F. ' Analysis and lubrication of bearings ' (McGraw-Hill Book Co., Inc., New York).

CHAPTER 3

JOURNAL BEARING DYNAMICS

3.1 Introduction

The literature surveyed in Chapter 2 on the subject of externally pressurized bearings, revealed that most of the work on externally pressurized bearings has been concerned with static performance characteristics. Literature on the dynamic characteristics of externally pressurized journal bearings is mainly concerned with two features of dynamic performance.

(i)   Dynamic resistance to radial deflection.

(ii)   Influence of speed on stability.

In contrast to hydrodynamic bearings, hydrostatic journal bearings subject to dynamic loading, apart from being little investigated have been mainly analysed along the lines of the rotor-dynamicist or the system's approach based on closed loop control theory. The use of static stiffness and the representation of the bearing characteristics by one dimensional springs and dashpots constitute the main limitations of the work carried out by researchers of externally pressurized bearings, although reasonable agreement between theory and experiment have been reported. This is due to the fact that most of the studies carried out were concerned with predicting responses, rather than predicting any threshold of instability, or the stiffness and damping co-efficients. Holmes (27) reported that response predictions can accommodate large tolerances in the values of the co-efficients, while deduction of bearing coefficients are subjected to large errors due to ill-conditioning of the equations. However, the prediction of the threshold of instability is very sensitive to variations in the coefficient values.

Although this research is primarily concerned with the dynamic characteristics of externally pressurized bearings (hybrid lubrication),

it is nevertheless, important and informative to mention and highlight the important contributions made by the various exponents of the field of hydrodynamic lubrication and shaft dynamics. Most of the analytical developments in the field of rotor-bearing dynamics have been carried out by researchers of hydrodynamic bearings, rather than researchers of hydrostatic bearings. It is the author's opinion that a background study of this subject will contribute to a better appreciation and thorough understanding of bearing influenced rotor dynamics.

3.2 Primary Aspects of Rotor-Bearing Dynamics

A rotor is an elastic body. It is never completely rigid. There-fore, the rotor vibrates, if it is subjected to excitational forces (unbalance, etc). The state of vibration is governed by the dynamic characteristics of the whole vibrating system - rotor, bearings, bearing supports, foundation and the nature of the excitation. Rotor vibrations can generally be classified into two categories:

(i)   forced vibrations set up by external excitations

(ii)   self-excited vibrations arising from bearing fluid-film action, internal friction damping, aerodynamic or hydraulic cross-coupling forces.

The support bearings play the most vital role in influencing the vibration characteristics of the rotor - either in forced or self-excited vibrations. Under steady-state conditions, the total pressure force equals the static load acting on the bearing. If the journal is disturbed from its static-equilibrium position (due to unbalance excitation or shock loading etc.), additional pressures will be set up in the fluid-film, which act as dynamic forces on the journal in addition to the static force. The dynamic forces apart from being governed by the velocity and amplitude of the journal centre motion, do not have the same sense as the imposed force. By resolving the dynamic force into two components, δF_x and δF_y, and resolving the journal centre

motion into x and y displacements, the dynamic force components may be expressed as:

$$\delta Fx = - a_{11} x - b_{11} \dot{x} - a_{12} y - b_{12} \dot{y}$$
$$\delta Fy = - a_{21} x - b_{21} \dot{x} - a_{22} y - b_{22} \dot{y}$$

(1)

This is the basis of the linear approach to rotor-bearing dynamic analysis, that is, the formulation of a linear differential equation with constant coefficients to represent the bearing fluid-film, which is adequate for most general applications. The eight coefficients a_{ij} and b_{ij} are termed the stiffness and damping coefficients. These coefficients are calculated from lubrication theory and are properties of the particular bearing. They are functions of the bearing configuration, the lubricant properties, the rotational speed and the steady-state journal centre position. However, under certain conditions of shock and vibrations large displacements may occur and non-linearized analyses are required.

(a) Forced vibrations - This usually gives rise to problems from critical speeds and unbalance response. The bearing fluid-films have a major influence on these characteristics. They provide the major source of damping, thereby, attenuating the dynamical forces transmitted to the pedestals. Their stiffness properties affect the critical speeds and the associated mode shape (the shape of the deflected rotor at the critical speed). This phenomena can be demonstrated by two simple examples.

(i) A flexible rotor rotating in two rigid bearings

1st Critical   2nd Critical   3rd Critical
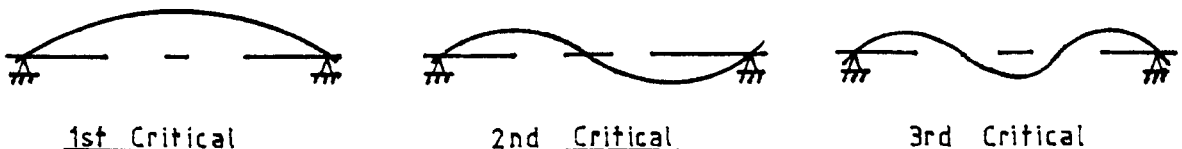
Under this condition, the shaft may behave like a simply supported

beam, with mode shapes as illustrated above.

(ii) A rigid rotor rotating in two flexible bearings.

<u>1st Critical</u>
(Translatory Whirl)

<u>2nd Critical</u>
(Conical Whirl)

<u>3rd Critical</u>
(Free-free Mode)
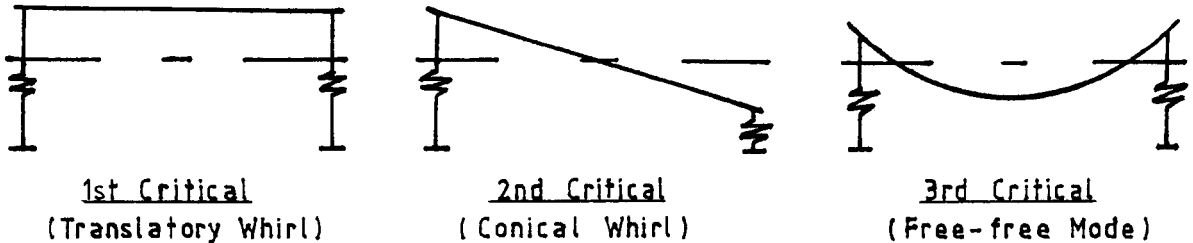
The rotor will behave like a rigid body at the 1st and 2nd critical

speeds. The rotor does not vibrate but whirls. The 3rd critical

speed may involve bending of the rotor.

(b) Self-excited vibrations - These are instabilities which will

ultimately lead to destruction of the rotor, if the whirl thres-

hold speed is exceeded. Again, the fluid-film bearings are the

most common source of instabilities. Bearing specialists have

given various names to this phenomenon, such as, half-frequency

whirl, oil-film whirl, fractional frequency whirl, non-synchronous

whirl, resonant whip or oil whip. This phenomenon refers to the

fact that at some critical frequency of rotation, the rotor may

precess about some point in the journal at a frequency not syn-

chronous with the rotation speed. A common form of whirl instab-

ility occurs at a rotation speed equal to twice the system first

critical with a precession rate equal to one half the rotor

rotation. This is usually referred to as half frequency whirl

or half speed whirl. A physical and simplified mathematical

explanation of the mechanism of whirl instability in concentric

fluid-film journal bearings has been presented by Leonard and

Rowe (18).

It is the bearing cross-coupling characteristics that produce whirl instabilities. The influence of the bearing cross-coupling characteristics (a_{12} and a_{21}) on stability is illustrated mathematically in Appendix I. The analysis shows that if the cross-coupling coefficients could be eliminated, the bearing will be inherently stable. Also, it points out the interesting phenomena that bearing asymmetry ($a_{11} \neq a_{22}$) promotes stability.

In many cases, the dynamic characteristics of the rotor bearing system can be treated as very close to linear. However, in practice non-linearity occurs at a certain amplitude of vibration, and results in interaction between forced and self-excited vibrations. Therefore, a self-excited vibration may take up the frequency of an imposed vibration or of a harmonic or subharmonic of an imposed vibration.

3.3 Review of Previous Work on Stability

The first recorded attempt to study the problem of rotor dynamics was presented by Rankine (1879), who postulated the concept of 'indifferent equilibrium', that is, the shaft is stable below its 1st critical speed, and unstable above it. Hence rotor design at that period was limited to speed regions below the 1st critical speed of the rotor. It was in 1919 that Jeffcott (1) concluded that operating above the 1st critical shaft speed is possible. This led to new concepts in rotor design and by the early 1920's, rotor design had progressed to the point that some rotors were operating in speed regions well above the 1st critical speed of the rotor. This resulted in some inexplicable phenomena, such that, some rotors were able to successfully operate in that region, while others were not. Refinement in balancing the rotors did not alleviate the problem at all. This startled many eminent investigators of that time.

Notable among them was B. L. Newkirk (2), who in 1924, carried out experimental studies to investigate this phenomenon of rotor failure

and concluded that:

1) fractional frequency whirling or fractional speed whirling always occurred at speeds above the 1st rotor critical speed, and usually the whirling frequency is equal to the 1st critical speed and was constant regardless of rotor rotational speed.

2) The onset of whirl sets in at a rotor speed roughly twice the rotor critical speed, and, if the rotor speed were increased above the speed at onset of whirl, whirl amplitudes would build up and lead to ultimate rotor failure.

3) Improvements in balancing of the rotor have no effect on the threshold speed for onset of whirl.

These conclusions clearly suggest that ideas based on 'critical speed' of the rotor were not satisfactory to explain the observed phenomena. Initially Newkirk concluded that internal frictional effects of built-up rotors were responsible, but further investigations suggested that the instability was due to the characteristics of the oil-film (3). He called this instability 'oil-whip'. He further observed that:

1) Increasing the foundation flexibility would reduce the whirl threshold speed.

2) Introducing damping into the foundation would increase the whirl threshold speed.

3) Distortion or misalignment of the bearing housing would increase stability.

At about the same period (1925), a very significant contribution to the analysis of this phenomenon of rotor failure was put forward by Stodola (4). He showed that the oil-film supporting a rigid shaft acts like a non-linear spring and postulated the concept of representing the bearing characteristics by eight Taylor expansion coefficients

(four linearized stiffness coefficients and four linearized damping
coefficients). This linearized representation of the fluid-film char-
acteristics, is widely used by present day investigators and has been
acknowledged by many to be adequate for most rotor-bearing dynamic
analysis. Hummel (5) extending the work of Stodola concluded that
rotor instability (as tested by the Routh-Hurwitz criteria) caused by
the fluid-film forces would set in at values of eccentricity-ratio
below 0.7. His analysis did not take into account squeeze film terms
in the Reynolds equation. For several years after the work of Stodola
and Hummel, little progress was made in understanding the mechanism
and characteristics of journal bearing dynamics. Research effort
during this period tended to be directed towards the development of
'anti-whirl bearings'. An attempt to explain the experimental findings
of Newkirk was conducted by Robertson (6) in 1933. His analysis was
based on a 360° non-cavitated infinitely long bearing model of Harrison
(1913), which did not allow a radial stiffness term. This led Robertson
to the startling and incorrect conclusion that instability would occur
at all speeds.

Interest in the dynamic characteristics of journal bearings in-
creased again in the mid-1940's (after World War 2) mainly due to the
economical requirements of rotating machines to run at higher speeds and
the realization of the significant role played by journal bearings in the
vibration characteristics of the rotor-bearing system. The research
tended to be split into two categories - linear and non-linear studies.
Linear analyses is concerned with the derivation and application of the
eight-linearized bearing coefficients to study the influence of the
bearings on rotor dynamic characteristics. Non-linear analyses normally involve
a time history type of approach, mainly to examine the form of instab-
ility and produce journal loci plots (transient simulation).

Stability criteria for fixed pad bearings has been presented by

Hagg (7) in 1946 based on small displacement analysis. He also showed that the frequency of whirl was infact less than half the rotor rotation frequency. Poritsky (8) in 1953, extended the work of Robertson by correctly including radial stiffness into the oil-film, and concluded that a rotor bearing system was indeed stable below twice the rotor critical speed. Poritsky also showed that increased rotor flexibility would decrease the system critical speed.

Hori (9) in 1959, carried out a combined theoretical and experimental study of oil whip. He used a long bearing model but allowed for cavitation, and concluded that in all cases, stable operation was assured for a static eccentricity-ratio greater than 0.82.

Holmes (10) in 1960, presented the oil whirl characteristics of a journal bearing (the short bearing model of Ocvirk) using a rigid rotor. A non-dimensional plot of stability was provided together with a discussion of increasing speed from zero speed to instability.

Reddi and Trumpler (11) in 1962, studied the stability of long bearings using both cavitating (180°) and non-cavitating (360°) film-models. A rigid shaft was assumed. He concluded that the non-cavitating bearing had no stable operation points, while the cavitating bearing, in fact did.

A general theoretical analysis for studying the dynamic response of rotating machinery, based on realistic boundary conditions has been presented by Lund and Sternlicht (12). The work provides a direct means of calculating the force transmitted by symmetrical two bearing rotors.

Mitchell, Holmes and Ballegooyen (13) in 1965 experimentally determined the four stiffness coefficients by applying static incremental loads to the bearing and measuring the ratios of the resulting displacements to the input forces.

A comprehensive investigation of many of the facets of turborotor

whirl and instability was presented by Gunter (14) in 1966. He extended the work of Jeffcott (1) to include the effects of bearing and support flexibility.

Glienicke (15) conducted experiments to determine the value of the bearing coefficients. He applied sinusoidal forcing to the bearing and the eight oil film coefficients were determined from amplitude and phase measurements. He pointed out that in order to achieve an accuracy of 5% in the value of the final coefficients, the measured amplitude and phase must be within ± 1% accuracy.

Using a central unbalance located on the journal, to generate the sinusoidal input forcing at the journal frequency, Holmes and Woodcock (16), determined the four damping coefficients in conjunction with the previously determined stiffness coefficients of ref. (13).

Morton (17) used a similar method to that of Glienicke's to obtain the complex form of the bearing frequency response functions at single frequency (10 Hz and 15 Hz). The bearing coefficients were calculated from these frequencies. Because of the practical difficulties of exciting a rotating shaft by an external harmonic force, Morton (20) later applied a step response technique to determine the frequency res-ponse functions from the bearing step response.

With the advent of a new generation of computers and more soph-isticated instrumentations research is now moving towards a non-linear approach and exploiting other techniques of system indentification.

More recent theoretical work has involved the application of modal methods to non-linear simulation (19, 22, etc.). As compared with finite-element or transfer-matrix simulation, modal methods have the advantage of reducing the number of equations that require integration.

Nordmann et al (23) identified the bearing coefficients using impact (pulse) testing. A Pseudo-random binary testing technique has

been used by Dogan et al (24) and Burrows and Stanway (21) for iden-
tifying the bearing coefficients. Also, the use of the fast-fourier
transform technique for identification of bearing characteristics has
been reported by Choy et al (25). These techniques will be discussed
more fully in the chapter on system identification.

3.4 Present State of the Art

The theoretical determination of bearing coefficients with constant
viscosity is now a fairly common practice. There is a need to include
factors such as geometrical imperfections, thermal and elastic distor-
tions, lubricant supply arrangements, variation of fluid properties and
more accurate boundary conditions.

There is poor correlation between experimental and theoretically
derived results, although experimental studies have not received as
much attention (28).

The representation of the bearing characteristics by the eight
linearized bearing coefficients is widely acknowledged to be adequate
for most rotor-bearing dynamic work, and, there is an urgent need to
integrate the extensive understanding of rotor dynamics and the develop-
ing studies of bearing stiffness and damping characteristics into a
single subject (26).

At present, there is still a lack of confidence in specifying the
stiffness and damping characteristics of realistic bearing configurations,
although existing procedures for the calculation of bearing character-
istics are adequate. There is a need for further well conceived and
executed experimental work that would guide the further development and
promote confidence in analytical procedures.

Two recent books published by the American Society of Mechanical
Engineers (The Lubrication Division), (29, 30) are useful guides to the
subject of rotor-bearing dynamics, while a review of this subject is well

documented in a report presented by Dowson et al (29).

.

REFERENCES

1. Jeffcott, H. H. 'The lateral vibration of loaded shafts in the neighbourhood of a whirling speed - The effect of want of balance', Phil. Mag. Series 6, Vol. 37, 1919.

2. Newkirk, B. L. 'Shaft Whipping', GEC Review, 27, 1924, pp. 169 - 178.

3. Newkirk, B. L. and Taylor, H.D. 'Shaft Whipping due to oil action in journal bearings', GEC Review, 1925.

4. Stodola, A. 'Kritische Wellenstorung Infolge der Nachgiebigkeit des Oelpolsters in Lager', Schweizerische Bauzeitung, 1925.

5. Hummel, C. 'Kritische Drehzahlen als Folge der Nachgiebigkeit des Schmiermittels im Lager', VDI Forschungsh, 1926.

6. Robertson, D. 'Whirling of a journal in a sleeve bearing', Phil. Mag. Series 7, Vol. 15, 1933, pp. 113 - 130.

7. Hagg, A. C. 'The influence of oil-film journal bearings on the stability of rotating machines', Jnl. Appl. Mech., Vol. 68, 1946.

8. Poritsky, H. 'Contribution to the theory of oil whip', Trans. ASME, August 1953, pp. 1153 - 1161.

9. Hori, Y. 'Theory of oil whip', Trans. ASME, Series E, Vol. 81, 1959.

10. Holmes, R. 'The vibration of a rigid shaft on short sleeve bearings', Jnl. of Mech. Engn. Sci., Vol. 2, No. 4, 1960.

11. Reddi, M. M. and Trumpler, P. R. 'Stability of the high speed
        journal bearing under steady load - The incompressible
        film', Trans. ASME, Jnl. Eng. Ind., Vol. 84, 1962,
        pp. 351 - 358.

12. Lund, J. W. and Sternlicht, B. 'Rotor bearing dynamics with
        emphasis on attenuation', Jnl. Basic Engng., 1962.

13. Mitchell, J. R., Holmes, R. and Van Ballegooyen, H. 'Experimental
        determination of a bearing oil-film stiffness', Proc.
        Instn. Mech. Engrs., Vol. 180, Pt 3K (1965 - 66).

14. Gunter, E. J. 'Dynamic stability of Rotor-Bearing systems',
        NASA SP-113, Office of Technology Utilization, U.S.
        Government Printing Office, 1966.

15. Glienicke, J. 'Experimental investigations of the stiffness and
        damping coefficients of turbine bearings and their
        application to instability prediction', Proc. Instn.
        Mech. Engrs., Vol. 181, Pt. 3B (1966-67).

16. Woodcock, J. S. and Holmes, R. 'Determination and application of
        the dynamic properties of a Turbo-Rotor bearing oil-
        film', Proc. Instn. Mech. Engrs., Vol. 184, Pt. 3L
        (1969-70).

17. Morton, P. G. 'Measurement of the dynamic characteristics of a
        large sleeve bearing', Trans. ASME, Jnl. Lub. Tech.,
        Vol. 93, No. 1, 1971.

18. Leonard, R. and Rowe, W.B. 'Dynamic force coefficients and the
        mechanism of instability in hydrostatic journal
        bearings', Wear, 23, 1973, pp. 277 - 282.

19. Lund, J. W. 'Modal response of a flexible rotor in fluid-film
        bearings', Jnl. of Engng. for Ind., Trans. ASME,
        Series B, Vol. 96, No. 2, May 1974, pp. 525 - 533.

20. Morton, P. G. 'The derivation of bearing characteristics by means
        of Transient Excitation applied directly to rotating
        shaft', GEC Jnl. Sci. and Tech., Vol. 42, 1975.

21. Childs, D. W. 'A Modal Transient Simulation Model for Flexible,
        Asymmetric Rotors', ASME Jnl. of Engng. for Ind.,
        1976.

22. Burrows, C. R. and Stanway, R. 'Identification of Journal Bearing
        Characteristics', Jnl. of Dyn. Syst., Meas. and Control,
        Sept. 1977, pp. 167 - 173.

23. Choy, K. C., Gunter, E. J. and Allaire, P. E. 'Fast Fourier
        Transform Analysis of Rotor-Bearing System', Presented
        at the Design Engng. Conf., Chicago, Illinois,
        Sponsored by ASME., April 17 - 20, 1978.

24. Edited by Rohde, S. M., Allaire, P. E. and Mayday, C. J.
        'Topics in Fluid-Film Bearing and Rotor-Bearing Design
        and Optimisation', Published by the Am. Soc. of Mech.
        Engrs., 1978.

25. Edited by Rohde, S. M., Maday, C. J. and Allaire, P. E.,
        'Fundamentals of the Design of Fluid-Film Bearings',
        Published by the Am. Soc. of Mech. Engrs., 1979.

26. Black, H. F. and Brown, R. D. 'Modal dynamic simulation of
        flexible shafts in hydrodynamic bearings', 2nd Int.
        Conf. on Vib. in Rotating Machinery, I.Mech.E.,
        Cambridge, Sept. 1980, pp. 109 - 113.

27. Nordmann, R. and Schollhorn, K. 'Identification of Stiffness and Damping Coefficients of Journal Bearings by means of the Impact Method', 2nd Int. Conf. on Vibs. in Rotating Machinery, I.Mech.E., Cambridge, Sept. 1980, pp. 231 - 238.

28. Dogan, I. U., Burdess, J. S. and Hewit, J.R. 'Identification of journal bearing coefficients using a Pseudo-Random Binary Sequence', 2nd Int. Conf. on Vibs. in Rotating Machinery, I.Mech.E., Cambridge, Sept. 1980, pp. 277 - 281.

29. Dowson, D. and Taylor, C. M. 'The State of knowledge in the field of bearing influenced rotor dynamic', Trib. Int., Oct. 1980, pp. 196 - 198.

30. Holmes, R. 'The measurement of oil-film stiffness and damping', Seminar on Jnl. Bearing Dynamics, Engn. Sci. Division, I.Mech.E., Nov. 1982.

31. Abdul-Wahed, N., Chaomleffel, J. P. and Nicolas, D. 'Experimental and theoretical investigation into the behavious of circular and tilting pad bearings', Presented at the 3rd. Tribology Conf., Budapest, June, 1983.

CHAPTER 4

HYBRID (HYDROSTATIC/HYDRODYNAMIC) JOURNAL BEARING ANALYSIS

4.1 Introduction

This section outlines two methods of analysing the performance of double row slot-entry hybrid journal bearings, namely, the finite difference approximation of the modified Reynolds equation and the lumped parameter method. A comparison with a previous finite difference method (8) is carried out; their relative merits are assessed and discussed with particular reference to computing accuracy at high values of eccentricity ratios.

4.2 Non-Dimensional Parameters

Some of the important non-dimensional parameters that are used in the analysis are presented below. It is usual for results to be presented in dimensionless groups so that generality and economy of presentation is achieved.

(1) __Fuller Load Parameter ($\bar{W}$)__

$$\bar{W} = \frac{W}{P_s LD}$$

This is the most generally useful load parameter for hydrostatic and hybrid modes of operation.

(2) __Dimensionless Flow-Rate ($\bar{q}in$ or $\bar{q}out$)__

$$\bar{q}in = \frac{12.\eta}{P_s C^3} qin$$

The non-dimensional term presented here, is different from that normally used for hydrodynamic bearings, where the non-dimensional term is expressed as:

$$\bar{q}in \text{ (hydrodyn.)} = \frac{qin}{RLNC}$$

Hence,

$$\bar{q}in = \bar{q}in \text{ (hydrodyn.)} \times (24.S_h{}^L/D) \qquad (4.1)$$

(3) Sommerfeld Number (S)

$$S = \frac{\eta NLD}{W}\left(\frac{D}{C_d}\right)^2$$

The Sommerfeld number, or its reciprocal, Δ, is applicable to hybrid and hydrodynamic modes of operation. It relates the load capacity to the speed, viscosity and bearing dimensions.

(4) Sommerfeld Hybrid Parameter (S_h)

$$S_h = \frac{\eta N}{P_s}\left(\frac{D}{C_d}\right)^2$$

This parameter has been called by a variety of names, including, 'The Speed Parameter', and 'The Optimization Parameter'. The variety of names reflects the importance of S_h, in specifying the hybrid mode of operation.

It may be observed that the Sommerfeld hybrid parameter is equal to the product of the Sommerfeld number and the Fuller number. It is, therefore, possible to relate and compare hybrid and hydrodynamic bearings' performance.

$$S_h = S \times \bar{\bar{W}} \tag{4.2}$$

It has also been shown that there is an optimum range for S_h to obtain maximum load and minimum power (2, 3, 4, 11). This may be demonstrated by consideration of the power ratio.

(5) Power Ratio (K)

$$K = \frac{H_f}{H_p}$$

Opitz (2) showed that choosing viscosity to minimise total power in a hybrid bearing leads to the requirement that K = 1.

By substituting the expressions for concentric friction power (H_f) and concentric pumping power (H_p) into the definition of power ratio, K, it may be shown (See Appendix II) that,

$$S_h = \frac{1}{4\pi} \sqrt{\frac{K \beta \bar{B}}{A_f}} \qquad (4.3)$$

The value of S_h when $K = 1$, that is, the minimum power value, is known as S_{ho}, 'The Optimized Speed Parameter', so that

$$S_{ho} = \frac{1}{4\pi} \sqrt{\frac{\beta \bar{B}}{A_f}} \qquad (4.4)$$

A full derivation of the optimized speed parameter, S_{ho}, is presented in Appendix II.

The value of S_{ho} may be calculated for suitable values of β, $^a/L$ and $^L/D$, and used to assist in the selection of a suitable combination of the values of η, P_s and C_d, involved in the definition of S_h, thus, ensuring the condition that $K = 1$ or any optimum value, and power dissipation is a minimum, for the chosen value of clearance or viscosity.

The optimum range for S_h can be related to an optimum range for K, in order to achieve maximum load and minimum total power. For recessed bearings, which are normally designed on the basis of zero speed load, it may be shown (4) that the optimum range for minimum power is

$$1 < K < 3 \text{ for } \frac{\text{minimum power}}{\text{zero speed load}} \qquad (4.5)$$

For non-recessed bearings, where the load is to be carried with the aid of the hybrid support mechanism, it is possible to increase K, beyond this range by minimising the ratio of load/total power (11). In this case:

$$3 < K < 9 \text{ for } \frac{\text{minimum power}}{\text{hybrid load}} \qquad (4.6)$$

Power ratio has an additional significance for maximum temperature rise, since it can be shown (See Appendix II) that,

$$\Delta T = \frac{P_s (1 + K)}{C_v \rho} \qquad (4.7)$$

Power ratio is never quoted for pressure fed hydrodynamic bearings, although it may well be relevant to design, since for any bearing shape there will be a maximum value of K, in order to avoid starvation or

excessive temperature rise.

(6)   Concentric Pressure Ratio (β)

$$\beta = \frac{P_{i,d}}{P_s}$$

The value of pressure ratio is determined by the resistance to flow in the restrictors in relation to the flow resistance in the bearing clearance. There is an optimum range for β, which may be made to correspond to the optimum ranges for K. The range is found to be (10,11):

$$0.4 < \beta < 0.7$$

4.3   Definition and Geometrical Properties of the Double Row Slot-Entry Hybrid Journal Bearing

The basic geometry and definitions of the double row slot-entry journal bearing are illustrated in figure (4.1), while figure (4.2) illustrates the co-ordinate system for load and displacement.

The direction of static load corresponds to the vertical Y co-ordinate, whereas, the V co-ordinate, at an angle ϕ_o to the vertical indicates, the line of eccentricity which corresponds to i = 1. Any other position is indicated by the angle θ, which varies from 0 to 2π.

The additional parameter, the velocity vector ė, acts at an angle α to the vertical is required for the dynamic analysis is presented in Chapter 5.

4.4   Assumptions

In the analysis of double slot-entry journal bearings operating under hybrid (hydrostatic/hydrodynamic) conditions, the following assumptions have been made:

(1)   The lubricating fluid is incompressible and its viscosity does not change with position in the bearing, that is, the fluid is isoviscous.
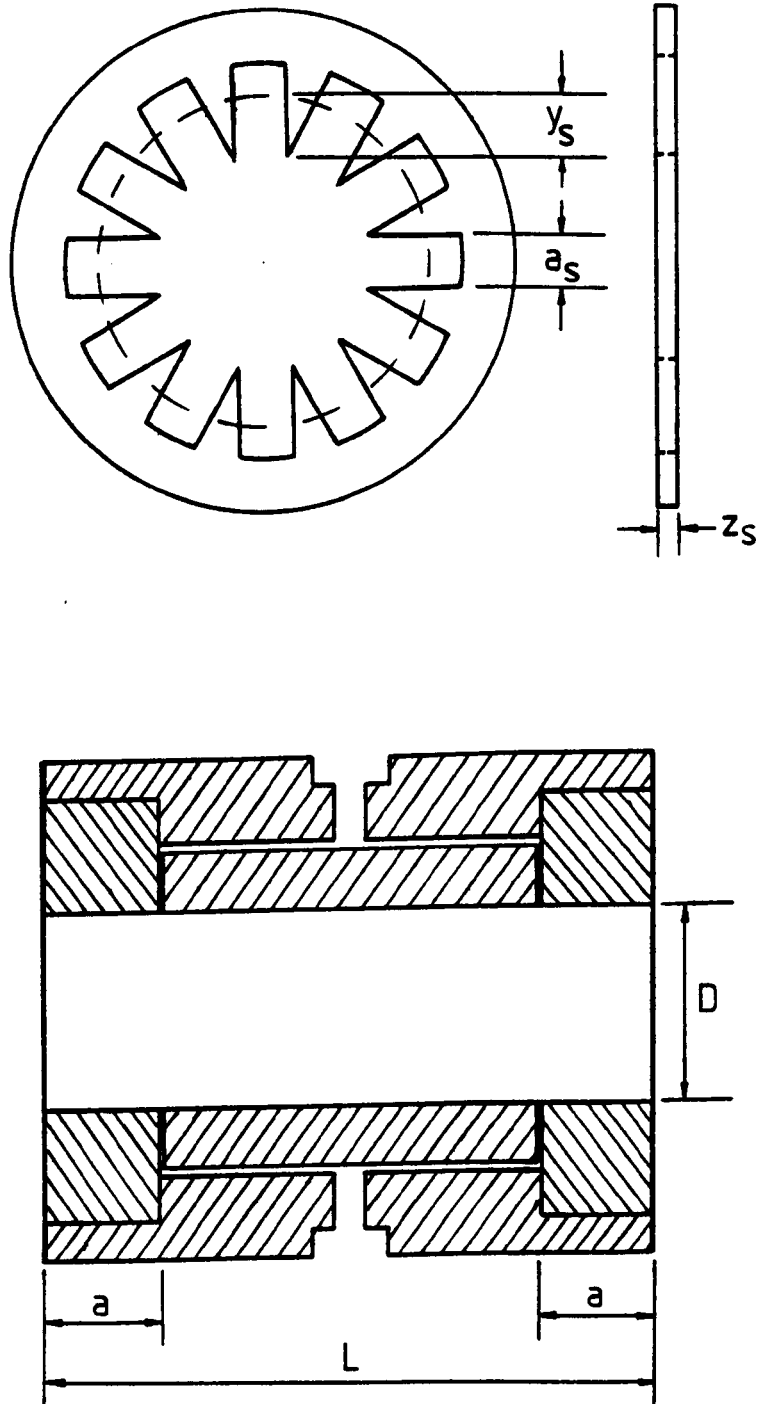
Fig.(4.1): Hybrid   Bearing   Geometry   And
          Slotted   Shim   Notation.

Fig.(4.2) : Coordinate System For Load And
Displacement.

(2)   The diametral clearance is very small compared with the diameter

so that the pressure variations across the oil film are negligible

compared with circumferential and axial variations.

(3)   Oil flow is laminar throughout the bearing system.

(4)   Inertia effects on the fluid-film may be neglected.

(5)   The curvature of the bearing surface is assumed to be negligible

as the radius of the curvature of the bearing is large in com-

parison with the fluid-film thickness.

(6)   There are no external forces acting on the fluid-film, that is,

body forces (gravitational and magnetic) are negligible.

(7)   There is no slip at the boundaries, that is, layers of fluid in

contact with the bearing surfaces have the same velocity as those

surfaces.

(8)   The slots in the bearing are equally spaced around the bearing.

(9)   Pressures at the exit from a feed slot are assumed to be constant

circumferentially.

(10)   There is no misalignment, that is, tilting of the bearing element

is neglected.

4.5   Finite Difference Approximation of the Modified Reynolds Equation

4.5.1   Introduction

The theory for the analysis os the static performanc of double slot-

entry hybrid (hydrostatic/hydrodynamic) journal bearings which is based

on a finite difference approximation of the modified form of the classical

Reynolds equation is presented in this section. This analysis differs

from a previous analysis carried out by Koshal (8), in that, circum-

ferential flow at the region of a source is not ignored. Also the pressure

field is iterated continuously from one end of the boundary to the other,

without having to miss the region of a source, where a second equation is

applied. It is found that this improved the computing accuracy.

4.5.2 Basis of Theoretical Analysis

A theoretical basis for solving the pressure fields in a double slot-entry hybrid journal bearing is the modified form of the classical Reynolds equation which has an extra term added to the usual version. The extra term has been added to make provision for source flow. A form of the modified Reynolds equation applied to a bearing with source flow is:

$$\frac{\partial}{\partial x}\left(\frac{\rho h^3}{12\eta}\frac{\partial P}{\partial x}\right) + \frac{\partial}{\partial z}\left(\frac{\rho h^3}{12\eta}\frac{\partial P}{\partial z}\right) = \frac{\partial}{\partial x}\left(\frac{\rho U h}{2}\right) + \frac{\partial}{\partial t}(\rho h) - S_f \qquad (4.8)$$

where the co-ordinates, x, refer to the circumferential direction and z, to the axial direction.

Equation (4.8) represents a general form of the lubrication equation which has special relevance to bearings incorporating source flow, including the conventional hydrostatic bearings, the hybrid bearings and the forced feed hydrodynamic bearings. The source term S_f is a general term and its evaluation is only dependent on the type of compensating device.

The film thickness h is given as:

$$h = C (1 + \varepsilon \cos \theta) \qquad (4.9)$$

At the static equilibrium position:

$$\left. \begin{array}{c} h = h_o \\[4pt] P = P_o \\[4pt] S_f = S_{fo} \end{array} \right\} \qquad (4.10)$$

Therefore equation (4.8) reduces to:

$$\frac{\partial}{\partial x}\left(h_o^3 \frac{\partial P_o}{\partial x}\right) + \frac{\partial}{\partial z}\left(h_o^3 \frac{\partial P_o}{\partial z}\right) = 6\,\eta\,U\,\frac{\partial h_o}{\partial x} - \frac{12\eta}{\rho} S_{fo} \qquad (4.11)$$

In order to generalize the equation, the following terms are non-dimensionalized:

$$P_o = \bar{P}_o \, P_s$$

$$h_o = H_o \, C$$

$$x = X \, D$$

$$z = Z \, L$$

$$(4.12)$$

Substituting equation (4.12) into equation (4.11) and rearranging terms yields:

$$\frac{\partial}{\partial X} \left(H_o^{\ 3} \frac{\partial \bar{P}_o}{\partial X} \right) + \left(\frac{D}{L} \right)^2 \frac{\partial}{\partial Z} \left(H_o^{\ 3} \frac{\partial \bar{P}_o}{\partial Z} \right) \ldots$$

$$= 24 \, \pi \, S_h \left(\frac{\partial H_o}{\partial X} \right) - \frac{12 \, \eta \, D^2}{P_s \, C^3} \frac{S_{fo}}{\rho} \qquad (4.13)$$

where $S_h = \dfrac{\eta N}{P_s} \left(\dfrac{D}{C_d} \right)^2$

4.5.3 Finite Difference Transformation

Consider now, the fluid-film to be divided into a mesh in the X and Z direction. Such a mesh is illustrated in figure (4.3). At some point in the mesh lies the integer coordinates (i, j), where i, refers to the circumferential (X) direction, and j, refers to the axial (Z) direction. If there are (m + 1) mesh points (that is, m, mesh elements), in the axial direction and, n_e, in the circumferential direction, then $1 < j < (m + 1)$ and $1 < i < n_e$. Therefore, the pitches between adjacent mesh points in the X and Z directions are respectively:

$$\Delta X = \pi / n_e$$

$$\Delta Z = 1 / m$$

$$(4.14)$$

The coordinate $i = 1$, is equivalent to $i = (n_e + 1)$, since both values correspond to $\Theta = 0$ or 2π. The coordinate $j = d$ and $(m + 1 - d)$, corresponds to the circumferential line containing the oil supply feed-slot, while, $j = 1$ and $(m + 1)$, correspond to the discharge edges of the bearing. The finite difference grid notation used in the present analysis is presented in figure (4.4). If $\Delta Z < < 1$ and $\Delta X < < \pi$, the following finite difference approximations may be made:
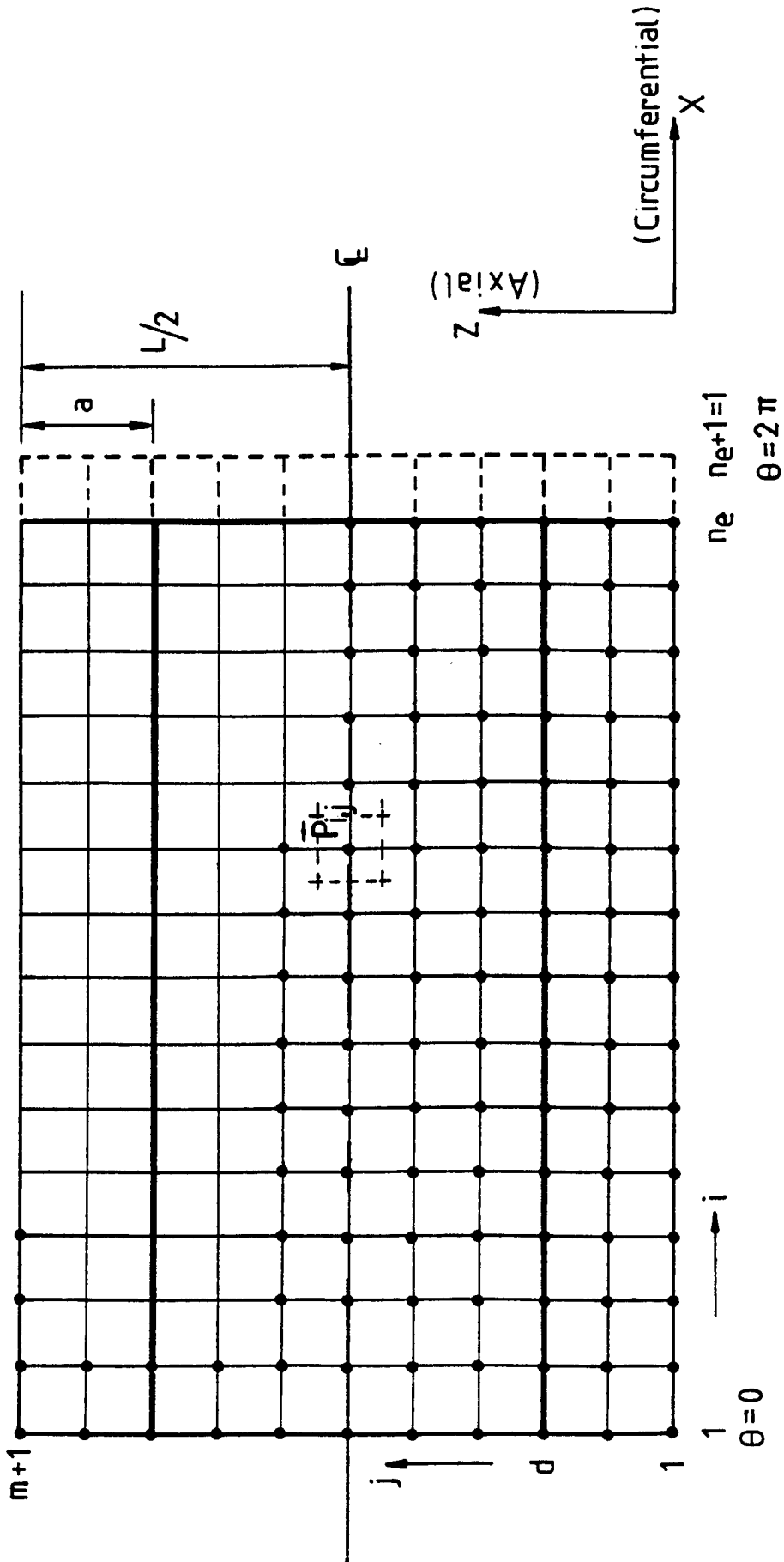
Fig.(4.3): The Finite-Difference Mesh —— Representing The Bearing Fluid-Film.
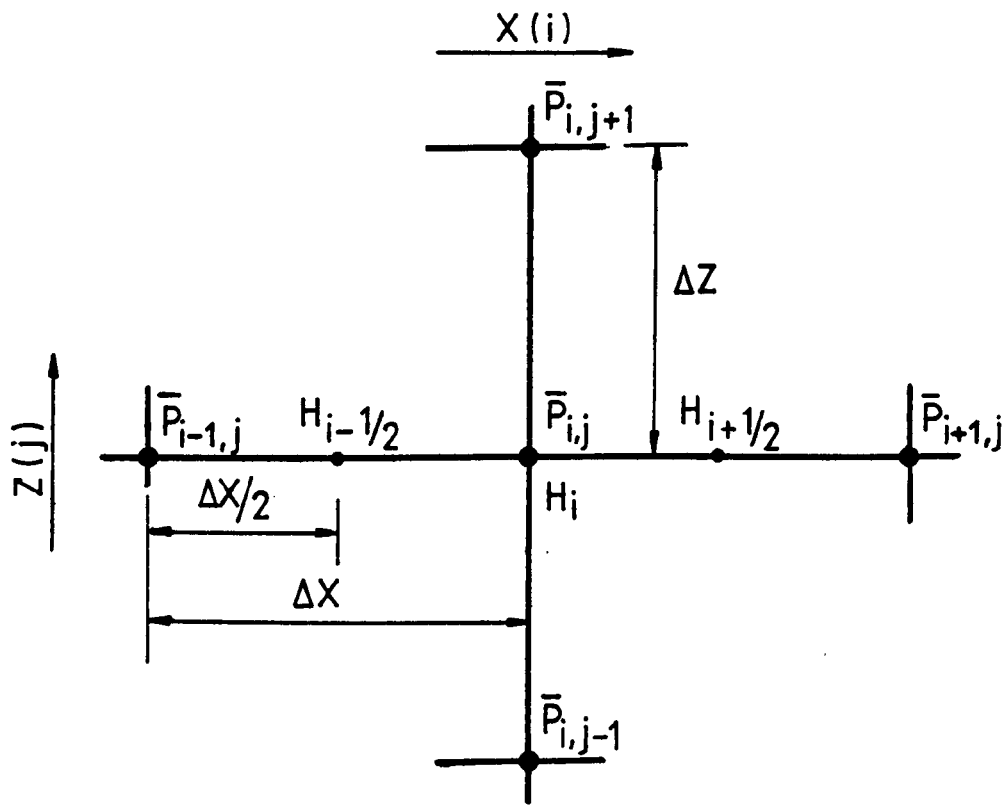
Fig.(4.4) : Finite-Difference Grid Notation.
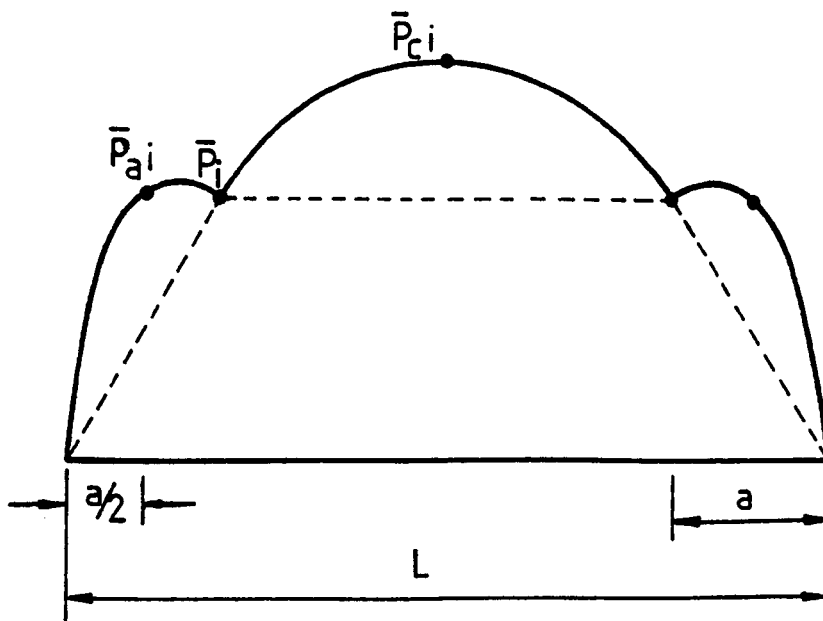
Fig.(4.5) : The Assumed Axial Pressure.

$$\left(\frac{\partial \bar{P}_o}{\partial X} \right)_{i + \frac{1}{2}, j} \doteq \left(\bar{P}_{o \, i + 1, \, j} - \bar{P}_{o \, i, \, j} \right) \Big/ \Delta X$$

$$\left. \left(\frac{\partial \bar{P}_o}{\partial X} \right)_{i - \frac{1}{2}, j} \doteq \left(\bar{P}_{o \, i, \, j} - \bar{P}_{o \, i - 1, \, j} \right) \Big/ \Delta X \right\} \quad (4.15)$$

$$\left[\frac{\partial}{\partial X} \left(H_o^3 \frac{\partial \bar{P}_o}{\partial X} \right) \right]_{i,j} \doteq \left[\left(H_o^3 \frac{\partial \bar{P}_o}{\partial X} \right)_{i + \frac{1}{2}, \, j} - \left(H_o^3 \frac{\partial \bar{P}_o}{\partial X} \right)_{i - \frac{1}{2}, \, j} \right] \Big/ \Delta X$$

$$(4.16)$$

Since, H_o is independent of Z, substituting equation (4.15) into (4.16) yields:

$$\left[\frac{\partial}{\partial X} \left(H_o^3 \frac{\partial \bar{P}_o}{\partial X} \right) \right]_{i, \, j} = \frac{1}{\Delta X^2} \left[H_o^3{}_{i + \frac{1}{2}} \bar{P}_{o \, i + \frac{1}{2}, \, j} \ldots \right.$$

$$\left. \ldots + H_o^3{}_{i - \frac{1}{2}} \bar{P}_{o \, i - \frac{1}{2}, \, j} - \left(H_o^3{}_{i + \frac{1}{2}} + H_o^3{}_{i - \frac{1}{2}} \right) \bar{P}_{o \, i,j} \right]$$

$$(4.17)$$

A similar procedure for the Z direction yields:

$$\left[\frac{\partial}{\partial Z} \left(H_o^3 \frac{\partial \bar{P}_o}{\partial Z} \right) \right]_{i,j} = \frac{1}{\Delta Z^2} \left[H_o^3{}_i \bar{P}_{o \, i, \, j + 1} + H_o^3{}_i \bar{P}_{o \, i, \, j - 1} \ldots \right.$$

$$\left. \ldots - 2 H_o^3{}_i \bar{P}_{o \, i,j} \right] \quad (4.18)$$

The term $\left(\frac{\partial H_o}{\partial X} \right)_{i, \, j}$, may be expressed as:

$$\left(\frac{\partial H_o}{\partial X} \right)_{i, \, j} = \frac{1}{\Delta X} \left(H_{o \, i + \frac{1}{2}} - H_{o \, i - \frac{1}{2}} \right) \quad (4.19)$$

or:

$$\left(\frac{\partial H_o}{\partial X} \right)_{i, \, j} = - 2 \, \epsilon \, \sin \theta_i \cdot \quad (4.20)$$

In terms of the bearing 'mesh', the angle θ_i, is given by:

$$\theta_i = 2\pi \left(\frac{i - 1}{n_e} \right) \quad (4.21)$$

Equation (4.20) was adopted for the present analysis. Substituting equations (4.17), (4.18) and (4.20) into equation (4.13) and multiplying through by $\left({}^L/D \, \Delta X \, \Delta Z \right)$, has the effect that each term of the

new equation represents a dimensionless volumetric flow-rate, where the dimensionless factor is $\frac{12\,\eta}{P_s\,C^3}$. Hence, the term $\left(\frac{12\,\eta}{P_s\,C^3}\,q_{so}\right)_{i,j}$ represents the total dimensionless source flow into one element in the region of a source. $(q_{so} = \frac{D^2\,S_{fo}}{\rho}\,\frac{L}{D}\,\Delta X\,\Delta Z)$. Furthermore, to ensure that the source term is only contributed in the region of a source, a source factor $\lambda_{i,j}$ is defined. $\lambda_{i,j} = 1$, in the region of a source and, zero elsewhere. This allows the same equation to be employed everywhere in the bearing mesh. Hence, in finite difference form equation (4.13) becomes:

$$\left[\left(\frac{L}{D}\right)\frac{\Delta Z}{\Delta X}\left(H_o^3{}_{i+\frac{1}{2}} + H_o^3{}_{i-\frac{1}{2}}\right) + \left(\frac{D}{L}\right)\frac{\Delta X}{\Delta Z}\left(2\,H_o^3{}_i\right)\,\bar{P}_{oi,j}\right]\cdots$$

$$\cdots -\left[\left(\frac{L}{D}\right)\frac{\Delta Z}{\Delta X}\left(H_o^3{}_{i+\frac{1}{2}}\right)\right]\bar{P}_{oi+1,j} - \left[\left(\frac{L}{D}\right)\frac{\Delta Z}{\Delta X}\left(H_o^3{}_{i-\frac{1}{2}}\right)\right]\bar{P}_{oi-1,j}\cdots$$

$$\cdots -\left[\left(\frac{D}{L}\right)\frac{\Delta X}{\Delta Z}\left(H_o^3{}_i\right)\right]\bar{P}_{oi,j+1} - \left[\left(\frac{D}{L}\right)\frac{\Delta X}{\Delta Z}\left(H_o^3{}_i\right)\right]\bar{P}_{oi,j-1}\cdots$$

$$= 48\,\pi\,S_h\,\varepsilon\,\text{Sin}\,\theta_i\left(\frac{L}{D}\right)\Delta X\,\Delta Z + \left(\frac{12\,\eta}{P_s\,C^3}\,q_{so}\right)_{i,j}\lambda_{i,j} \qquad (4.22)$$

It should be emphasized that equation (4.22) above, is a general finite difference lubrication equation. The usual finite difference version of the Reynolds equation, is obviously a particular form of the generalized equation, in which the factor, $\lambda_{i,j} = 0$. Any type of combination of source flows may be treated by substituting an appropriate source term in equation (4.22), in terms of the expression derived from considerations of flow continuity between the bearing and the respective compensating device.

The following section is devoted to the application of equation (4.22), to double row slot-entry hybrid bearings. This equation will be referred to as the Slot-Entry Bearing Finite Difference Equation. Any arbitrary number of elements per slot may be used, subjected to assumption (9) of Section 4.4. An expression for the source flow, in terms of the concentric pressure ratio, β, is derived by considering the flow through the slot and the concentric flow through the bearing. The full derivation is presented in Appendix III. Substituting the

expression for $\left(\frac{12 \; \eta}{P_s \; C} \; q_{so}\right)_{i,j}$ as derived in Appendix III, into equation (4.22), the following slot-entry bearing finite difference equation is formed:

$$A_{i,j} \; \bar{P}_{oi,j} \; + \; E_{i+1} \; \bar{P}_{oi+1,j} \; + \; W_{i-1} \; \bar{P}_{oi-1,j} \; + \; N_i \bar{P}_{oi,j+1} \; + \; \cdots$$

$$\cdots \; S_i \; \bar{P}_{oi,j-1} \; = \; F_{oi,j} \qquad (4.23)$$

where:

$$A_{i,j} = \left(\frac{L}{D}\right) \; \frac{\Delta Z}{\Delta X} \; (H^3_{oi+\frac{1}{2}} + H^3_{oi-\frac{1}{2}}) \; + \left(\frac{D}{L}\right) \; \frac{\Delta X}{\Delta Z} \; (2 \; H^3_{oi}) \; \cdots$$

$$\cdots \; + \; \left[\frac{\beta}{1-\beta} \; \left(\frac{\pi \; D}{a \; n_s}\right) \left(\frac{n_s}{n_e}\right)\right] \lambda_{i,j}$$

$$E_{i+1} = -\left(\frac{L}{D}\right) \; \frac{\Delta Z}{\Delta X} \; (H^3_{oi+\frac{1}{2}})$$

$$\qquad\qquad\qquad\qquad\qquad\qquad\qquad\qquad\qquad (4.24)$$

$$W_{i-1} = -\left(\frac{L}{D}\right) \; \frac{\Delta Z}{\Delta X} \; (H^3_{oi-\frac{1}{2}})$$

$$N_i = S_i = -\left(\frac{D}{L}\right) \; \frac{\Delta X}{\Delta Z} \; (H^3_{oi})$$

$$F_{oi,j} = 48 \; \pi \; S_h \; \varepsilon \; \mathrm{Sin} \; \theta_i \; \left(\frac{L}{D}\right) \; \Delta X \; \Delta Z \; \cdots$$

$$\cdots \; + \; \left[\frac{\beta}{1-\beta} \; \left(\frac{\pi \; D}{a \; n_s}\right) \left(\frac{n_s}{n_e}\right)\right] \lambda_{i,j}$$

4.5.4 Method of Solution

Since the bearing is symmetrical about its mid length, only half of the mesh in the axial direction needs to be considered, that is, $j = 1$ to $(\frac{m}{2} + 1)$. The feed slots are located at $j = d$, and the boundary discharges to atmosphere, so that the boundary conditions are:

$$\lambda_{i,j} = 1, \text{ at } j = d \text{ and zero elsewhere}$$

$$\qquad\qquad\qquad\qquad\qquad\qquad\qquad\qquad\qquad (4.25)$$

$$\bar{P}_{oi,\,1} \; (i = 1 \text{ to } n_e) = 0$$

Therefore it is only necessary to determine $\bar{P}_{oi,\,j}$, for the remaining internal 'mesh' points. Applying equation (4.23) to each of the internal 'mesh' points in turn, yields a set of (n_e x $^m/2$) simultaneous equations. Various numerical methods may be employed to solve equation (4.23). The equations may be represented in matrix form

using the i, j notation.

$$\left[W_{i-1} \text{---} S_i \text{---} A_{i,j} \text{---} E_{i+1} \text{---} N_i \text{---} \right] \left[\begin{array}{c} \bar{P}_{oi-1,\,j} \\ \bar{P}_{oi,\,j-1} \\ \bar{P}_{oi,\,j} \\ \bar{P}_{oi+1,\,j} \\ \bar{P}_{oi,\,j+1} \end{array} \right] = \left[F_{o\,i,j} \right]$$

that is, $\left[\bar{U} \right] \left[\bar{P} \right] = \left[\bar{V} \right]$

where $\bar{P}$, is the column matrix of dimension, G ($G = n_e \times {}^m/2$), which

contains the dimensionless pressures, $\bar{P}_{oi,\,j}$. Matrix $\bar{U}$ contains the

coefficients W, S, A, E and N, which is a band matrix of major dimension

G x G, and matrix $\bar{V}$, is a column matrix of dimension G, which contains

the coefficients F. A solution may then be obtained by employing the

method of direct inversion, or by the methods of elimination such as

Gaussian Elimination. However, this finite difference equation is only

equivalent to the original differential equation if ΔX and ΔZ are

infinitely small. This means that in order to achieve an accurate

solution n_e and (m + 1) must be large, the number of elements in matrix

$\bar{U}$ will be excessive and the computation time will be slow. Furthermore,

ill-conditioning effects may arise. In the present analysis, a numerical

algorithm, which is capable of fast, stable and accurate solution (an

indirect method, where the solution is approached by successive approx-

imation) as employed in the previous finite difference program was

selected.

The method selected was that of successive Relaxation, which is

essentially an extension of the Gauss-Seidel iteration technique which

does not employ a relaxation factor (6). The Relaxation factor, R,

was less than unity $(0 < R < 1.0)$, which was found to be essential for stable convergence, using the particular form of finite difference equation (4.26) below. Basically, the method involves the adjustment of the values of $\bar{P}_{oi,\,j}$, as iteration proceeds. The 'residuals', that is, the changes in the values of $\bar{P}_{oi,\,j}$, between successive iterations, therefore provide an estimate of the error. With successive iterations, the residuals should consequently converge towards zero. The finite difference equation (4.23) is rearranged, and if the number of iterations is denoted by L, the equation may be expressed as:

$$\bar{P}_{oi,\,j}^{(L)} = \frac{1}{A_{i,j}} \Big[F_{oi,j} - E_{i+1}\,\bar{P}_{oi+1,j}^{(L-1)} - W_{i-1}\,\bar{P}_{oi-1,j}^{(L-1)} - N_i\,\bar{P}_{oi,\,j+1}^{(L-1)} - S_i\,\bar{P}_{oi,\,j-1}^{(L-1)} \Big]$$

$$\ldots \text{(4.26)}$$

Equation (4.26) illustrates that, for the exact solution, the pressure at co-ordinates (i, j) are expressed in terms of the pressures at the four adjacent mesh points. (See figure (4.4)). If at the end of iteration $(L + 1)$, the pressures have the values $\bar{P}_{oi,j}^{(L+1)}$, $\bar{P}_{oi+1,j}^{(L+1)}$, etc., then the residual, $ER_{i,j}^{(L)}$, is defined as:

$$ER_{i,j}^{(L)} = \bar{P}_{oi,j}^{(L+1)} - \bar{P}_{oi,j}^{(L)} \qquad (4.27)$$

The solution may be advanced at the next iteration by setting,

$$\bar{P}_{oi,j}^{(L+1)} \begin{vmatrix} j = 2 \text{ to } (^m/2 + 1) \\ i = 1 \text{ to } n_e \end{vmatrix} = \bar{P}_{oi,j}^{(L)} + ER_{i,j}^{(L)} \qquad (4.28)$$

Equation (4.28) is in fact the Gauss-Seidel form of equation (4.23). For a stable solution, the residuals must converge towards zero and the solution would be exact. The residuals will only become zero at $L = \infty$, hence, computing time would be excessive. Therefore, some small error must be accepted. The convergence rate may be improved in the case of equation (4.25) by employing the method of successive Under-Relaxation, which introduces an 'under-relaxation factor', R, into equation (4.28), that is,

$$\bar{P}^{(L+1)}_{oi,j} \begin{vmatrix} j = 2 \text{ to } (^m\!/2 + 1) \\ i = 1 \text{ to } n_e \end{vmatrix} = \bar{P}^{(L)}_{oi,j} + R \cdot \left(ER^{(L)}_{i,j} \right) \qquad (4.29)$$

A Relaxation factor of 0.7 was used based on the criteria of stability and speed of convergence. This value was found by trial and error. Therefore, the Relaxation form of the Slot-Entry Bearing Equation may be formally written as:

$$\bar{P}^{(L+1)}_{oi,j} \begin{vmatrix} j = 2 \text{ to } (^m\!/2 + 1) \\ i = 1 \text{ to } n_e \end{vmatrix} = \bar{P}^{(L)}_{oi,j} + \frac{R}{A_i} \left[F_{oi,j} - E_{i+1} \bar{P}^{(L)}_{oi+1,j} - \ldots \right.$$

$$\ldots \left. W_{i-1} \bar{P}^{(L)}_{oi-1,j} - N_i \bar{P}^{(L)}_{oi,j+1} - S_i \bar{P}^{(L)}_{oi,j-1} - A_{i,j} \bar{P}^{(L)}_{oi,j} \right] \qquad (4.30)$$

Since, the residuals are an estimate of the error at the end of each complete iteration, the iterative procedure is repeated until the residuals have reduced to some acceptable level. Numerous 'error criteria' exist. Basically, they may be classified into two groups - the maximum or the average residual criteria. Furthermore, the 'error criteria' are more often expressed as a ratio of the residual and the dimensionless pressure. Hence, the 'error criteria' are as follows: (ACC is the maximum allowable error).

Maximum Residual	$\left\| ER^{(L)}_{max} \right\| \leqslant ACC$
Average Residual	$\left\| \displaystyle\sum_{j=2}^{(\frac{m}{2}+1)} \sum_{i=1}^{n_e} ER^{(L)}_{i,j} \right\| \leqslant ACC$
Maximum Residual Ratio	$\left\| \dfrac{ER^{(L)}_{max}}{\bar{P}_{o}^{(L)}{}_{max}} \right\| \leqslant ACC$
Average Residual Ratio	$\left\| \dfrac{\displaystyle\sum_{j=2}^{(\frac{m}{2}+1)} \sum_{i=1}^{n_e} ER^{(L)}_{i,j}}{\displaystyle\sum_{j=2}^{(\frac{m}{2}+1)} \sum_{i=1}^{n_e} \bar{P}^{(L)}_{oi,j}} \right\| \leqslant ACC$

The Average Residual criterion was selected for the present analysis. It should, however be emphasized that the solution will contain a region of sub-atmospheric pressures, and such pressures must be set to zero to take into account cavitation effects. Several boundary conditions have been postulated, as discussed in Section 2.1. The simplest condition (all negative pressures encountered in the computations are set to zero) which is capable of retaining an extremely high degree of accuracy was used in the present study. The boundary conditions are outlined in Section 4.5.5. It should be pointed out that in the approach used in most hydrodynamic bearing analyses, the negative pressures are only set to zero, when the final solution is achieved.

When the appropriate error criterion is fulfilled at iteration L_f, then

$$\bar{P}_{oi,j}^{(L_f)} \quad \left| \begin{array}{l} j = 2 \text{ to } (\frac{m}{2} + 1) \\ i = 1 \text{ to } n_e \end{array} \right. \quad \text{is the final solution,}$$

and the various bearing parameters, such as load, and flow-rate may be computed. Although it is not the primary purpose of this thesis to investigate the methods of solving the lubrication equation, it is nevertheless, useful to point out another efficient method – the column matrix approach. The method involves the rewriting of equation (4.23). The band matrix $\bar{U}$, is rearranged into a tridiagonal and two diagonal matrices. This is a direct technique and requires no iteration with a further advantage of a reduction in storage capacity. The solution is then obtained by writing a recursive relationship for the euqations. This method is probably the most advanced available for solving finite difference lubrication equation.

4.5.5 Boundary Conditions

(1) The pressure at the ends of the bearing is atmospheric

$$(\bar{P}_{oi,1} = 0).$$

(2) Pressures at the outlet of the slots are such as to retain continuity of flow, from the restrictor to the outer land.

(3) In the cavitating region, where the pressures become negative, they are set to atmospheric pressure ($\bar{P}_{oi,j} = 0$). (Note that, by incorporating an iterative procedure, the pressure distribution will automatically take up the necessary zero gradient at the trailing edge, as iteration proceeds).

4.5.6 Bearing Load

The total fluid-film force is obtained by integrating the resolved components of pressure over the whole mesh area. Several methods are available for such numerical integration, notably, the methods of Trapezoidal integration and Simpson's Rule. In the computation performed for the present investigation, it was found that, if ΔX and ΔZ, are made sufficiently small, a high accuracy is achieved by the vectorial summation of the product of pressure and elemental area.

Each elemental pressure acts on a projected area. Non-dimensionally, the projected area may be expressed as:

$$\bar{A}rea = \sin (\Delta X) . \Delta Z \qquad (4.31)$$

Whereas, in experiment, the line of load is usually predetermined, and the line of eccentricity has to be found, in analysis, the load vector has to be determined for a predetermined line of eccentricity. Therefore, it is necessary to resolve the load in the direction parallel and perpendicular to the line of eccentricity, that is, in the V and U axes, respectively.

The non-dimensional load reaction on the shaft are:

$$\bar{F}_{uo} = \bar{A}rea \sum_{i=1}^{n_e} \sum_{j=1}^{m} - \bar{P}_{oi,j} \sin \theta_i \qquad (4.32)$$

and

$$\bar{F}_{vo} = \bar{A}rea \sum_{i=1}^{n_e} \sum_{j=1}^{m} - \bar{P}_{oi,j} \cos \theta_i \qquad (4.33)$$

The resultant non-dimensional load acting on the shaft (total fluid-film force) is:

$$\bar{F}_o = (\bar{F}_{uo}^2 + \bar{F}_{vo}^2)^{\frac{1}{2}} \qquad (4.34)$$

The reaction forces may be resolved back into the X and Y co-ordinate system. Thus:

$$\bar{F}_{xo} = \bar{F}_{vo} \sin \phi_o + \bar{F}_{uo} \cos \phi_o \qquad (4.35)$$

$$\bar{F}_{yo} = \bar{F}_{vo} \cos \phi_o - \bar{F}_{vo} \sin \phi_o \qquad (4.36)$$

where:

ϕ_o, is the attitude angle at the static equilibrium position.

$$\phi_o = \tan^{-1} \left\{ \frac{\bar{F}_{uo}}{\bar{F}_{vo}} \right\} \qquad (4.37)$$

At the static equilibrium position the resultant fluid-film force $\bar{F}_o$ is equal to $\bar{F}_{yo}$ which must also be equal to the static bearing load, $\bar{W}_o$, and $\bar{F}_{xo}$ equals zero.

4.5.7 Bearing Volumetric Flow-Rate

Although, the more realistic boundary conditions, postulated by Jakobsson and Floberg (1), have not been generally implemented in the present investigation, it was nevertheless, essential to derive the expressions governing the volumetric flow rate of the bearing. Two expressions for the bearing oil flow have been derived.

(i)   Flow-rate into the bearing (The Source Flow) - qin

The total source flow through the bearing may be expressed as:

$$qin = 2 \sum_{i=1}^{n_e} qsoi$$

that is:

$$qin = \frac{a_s \, z_s^3}{y_s} \, \frac{2}{12\eta} \sum_{i=1}^{n_e} (P_s - P_{oi,d}) \qquad (4.38)$$

Non-dimensionally, equation (4.38) may be expressed as: (See Appendix III).

$$\bar{q}in = \frac{12\,\eta}{P_s\,C^3}\,qin \qquad (4.39)$$

that is:

$$\bar{q}in = 2\,\left(\frac{\beta}{1-\beta}\right)\,\left(\frac{\pi\,D}{a\,n_s}\right)\,\left(\frac{n_s}{n_e}\right)\,\sum_{i=1}^{n_e}\,(1 - \bar{P}_{oi,d}) \qquad (4.40)$$

(ii) Flow-rate out of the bearing (The Axial Flow) - qout

The flow rate from each end of the bearing is obtained by summing the flows to the edges, from the adjacent grid points.

$$qout = 2\,\frac{\Delta X}{\Delta Z}\,\frac{1}{12\eta}\,\sum_{i=1}^{n_e}\,(P_{i,2} - P_{i,1})h_{oi}^{3}$$

that is;

$$qout = \frac{2\,\pi}{12\eta}\,\frac{D}{L}\,\frac{m}{n_e}\,\sum_{i=1}^{n_e}\,P_{oi,2}\,h_{oi}^{3} \qquad (4.41)$$

Therefore, non-dimensionally equation (4.41) may be expressed as:

$$\bar{q}out = 2\pi\,\left(\frac{D}{L}\right)\,\left(\frac{m}{n_e}\right)\,\sum_{i=1}^{n_e}\,\bar{P}_{oi,2}\,H_{oi}^{3} \qquad (4.42)$$

4.5.8 The Finite Difference Computer Program

The solving of the large number of equations was carried out on the DEC-20 computing system. Two finite difference computer programs that include bearing dynamic analyses (See Chapter 5), have been written - the perturbation and the finite disturbance techniques. Therefore, the discussion presented here will only outline the section on static characteristics, which is common to both programs. Briefly, the dimensionless input variables, which are necessary to perform the analysis, are read into the program and include:

(1) Length to diameter ratio of the bearing, $(^{L}/D)$.

(2) Axial land width to bearing length ratio, $(^{a}/L)$.

(3) The relaxation factor, $(R = 0.7)$.

(4) The concentric pressure ratio, (β).

(5)   The maximum allowable residual (ACC).

(6)   The Power-ratio, (K).

(7)   The eccentricity-ratio, (ϵ)

(8)   The number of circumferential grid elements, (n_e), and

(9)   The number of axial grid, elements, (m).

The flow-chart of figure (5.3) fully illustrates the procedures involved in solving the finite difference lubrication equation. Figures (4.7a) to (4.11b) show the load-eccentricity characteristics predicted by this program. The variation of volumetric flow-rate with eccentricity is shown in figures (4.12a) and (4.12b). A full discussion of the results is presented in Section 4.7.

4.6   The Lumped Parameter Theory

4.6.1   Introduction

Present day analysis of slot hybrid journal bearings range from the simple approximate method of Dee and Shires (5) and the concentric technique of Rowe, et. al. (9), to accurate finite-difference techniques as presented by Stout and Rowe (7), Rowe and Koshal (10), Y. Pu, et. al. (12) and the present author.

The accurate method is achieved at the expense of a more rigorous mathematical analysis, that can only be solved numerically. The number of iterations required to achieve a solution depends on the number of nodal points, the initial guess and the degree of accuracy required.

From the point of view of cost of computing time, there is therefore, a need for an analysis that will allow for a reduction of the number of nodal points and yet provide a solution of reasonable accuracy. It is the aim of this section to present the results of an investigation into one such technique, which is based on a lumped parameter approach.

For
Circumferential
Flow
Calculations

For
Axial Flow
Calculations.
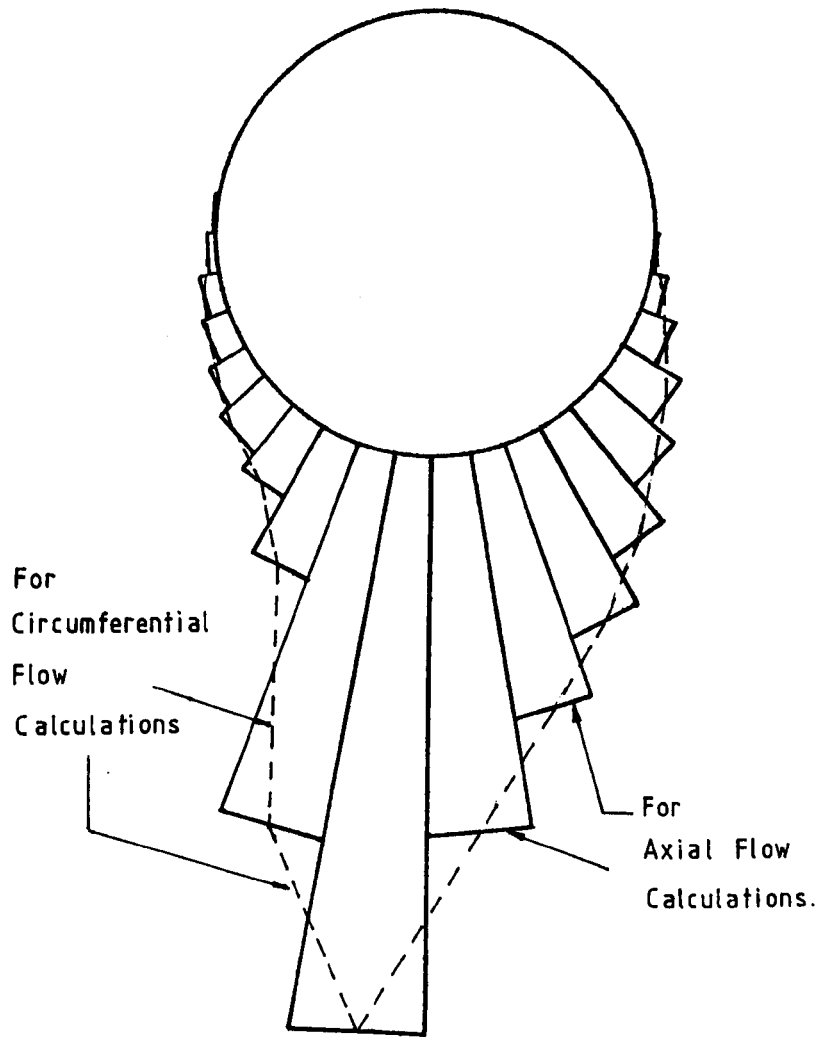
Fig. 4.5a : Circumferential Pressure Distributation
— Lumped Parameter Model

4.6.2 Assumptions

The assumptions stated in Section 4.4, together with the following assumptions were employed in the formulation of the lumped parameter technique.

(1) Although the pressures at the exit from a feed slot are assumed to be constant circumferentially, for the purpose of calculating axial flows, the circumferential pressure distribution between neighbouring regions is assumed to vary linearly for the purpose of calculating circumferential flows. (See Figure 4.5a)

(2) The axial pressure distribution between the slots and the external boundary (bearing edge) is linear for the concentric condition ($\varepsilon = 0$), and quadratic for all other values of eccentricity-ratios ($\varepsilon > 0$).

(3) The axial pressure distribution between each pair of feed-entries is linear for the concentric condition and parabolic for all other values of eccentricity-ratios. (See Figure 4.5)

4.6.3 Basis of Theoretical Analysis

The definition and geometrical properties of the double slot-entry hybrid journal bearing are as defined in Section 4.3.

The approach employed in the following analysis is akin to a "modified Ocvirk" solution. The concept of continuity of mass flow is the basis for the lumped parameter analysis. The bearing is divided into n_e sections in the circumferential direction, the width of each section, being equal to $(\pi D/n_e)$. In the axial direction, each section is divided into three control volumes, extending from the bearing edge to the centre of the bearing, as illustrated in figure (4.6b). Figure (4.6b), also, illustrates the lumped flow terms that are associated with each control volume for the ith section of the bearing. The application of the lumped parameter mesh is shown in figure (4.6a).
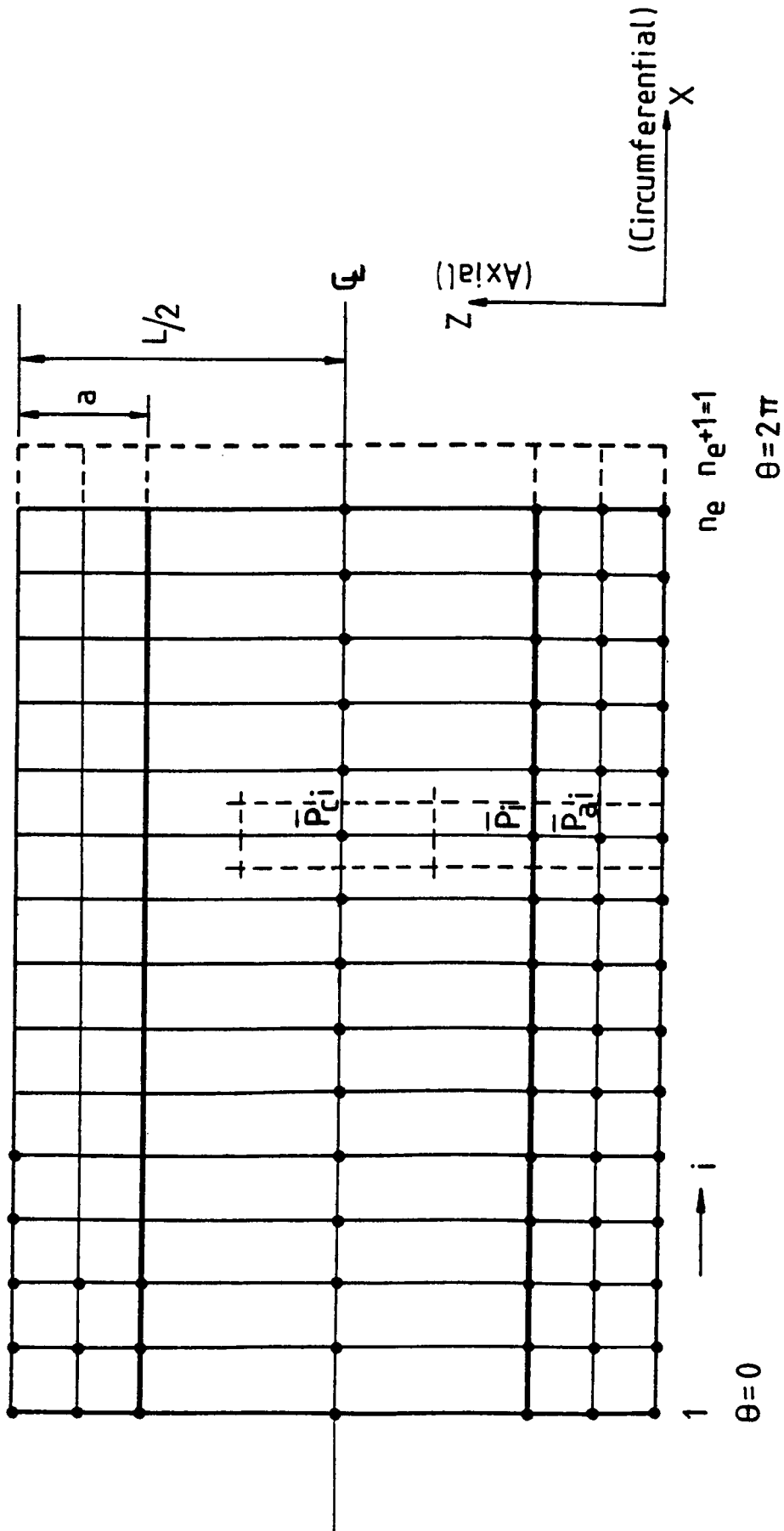
Fig.(4.6a) : The Lumped-Parameter Mesh.
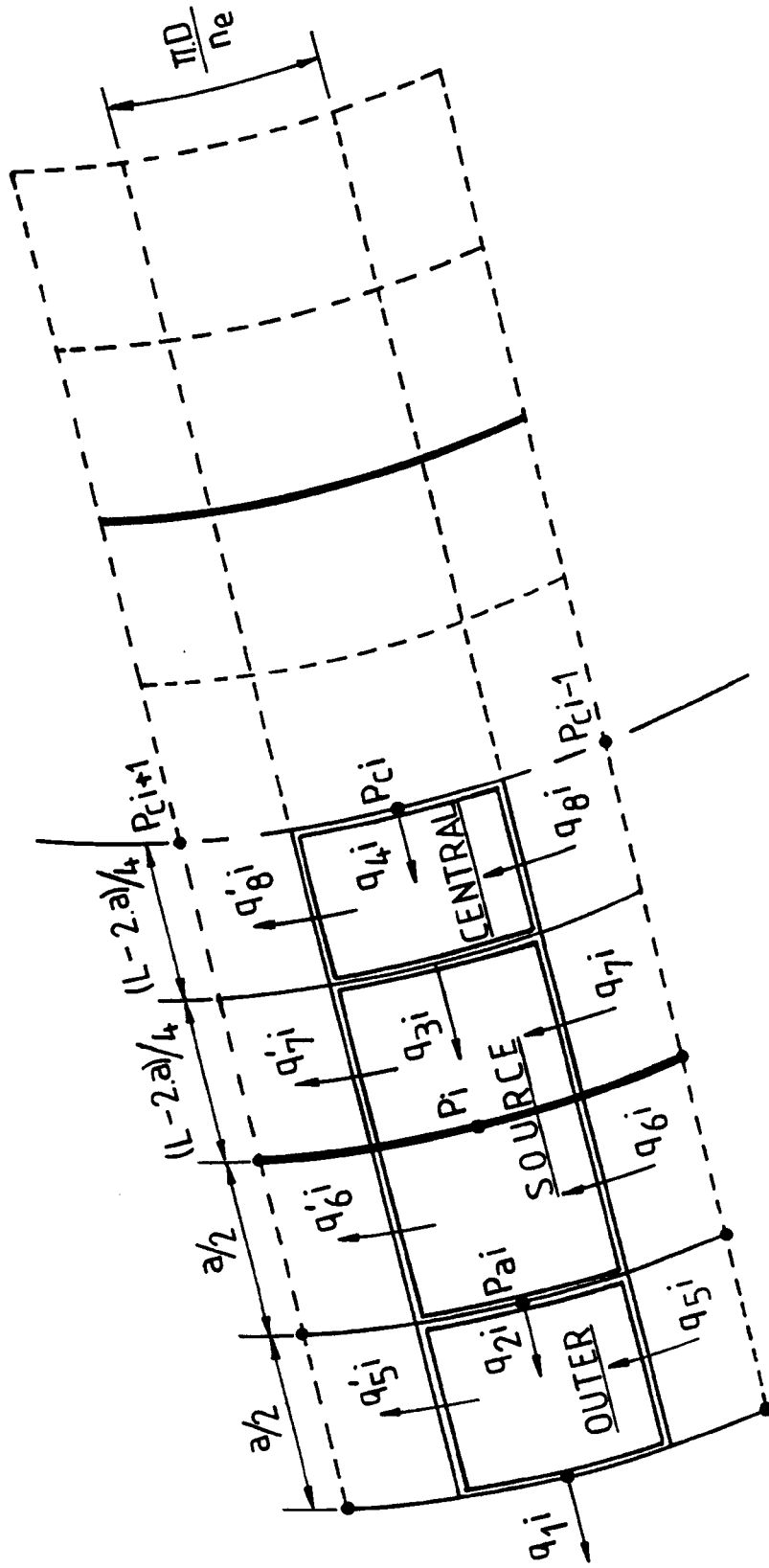
Fig.(4.6b): Figure Illustrating The Three Control Volumes And The Lumped Flow Terms.

The pressure distribution is therefore, characterised by three pressures, P_{ai}, P_i and P_{ci}. P_{ai} is the pressure at the mid-point of the ith outer land, while, P_i is the pressure at the ith feed-inlet. P_{ci} is the pressure at the mid-point of the bearing, that is the ith central land. The supply pressure being P_s. The assumed axial pressure distribution is thus illustrated in figure (4.5).

Applying the continuity of mass flow to each control volume, equations governing the pressures in the three control volumes are established, and, hence the resultant force exerted by each lumped section.

It may be noted that for a recessed bearing, a linear pressure distribution is usually assumed to occur between the recess and the bearing edge, which is reasonably accurate for values of $^a/L$ up to 0.25 (thin-land bearings). In contrast to recessed bearings, the pressure distribution across the outside edge of the plain slot-entry hybrid bearing, is considerably modified by the hydrodynamic effects. It is only for the case of pure hydrostatic operation (i.e. zero speed), that the pressure distribution can be approximated by the same linear distribution employed for recessed bearings. The theoretical model of Rowe (9), which is also akin to a modified Ocvirk solution, was employed for a concentric analysis. The model employed the superposition of parabolic variations on the linear axial pressure distribution, based on an analytical approach whereas the present numerical method allows the bearing to be analysed with varying eccentricity.

4.6.4 The Equations of Continuity of Mass Flow

In general, the mass flow of a viscous, incompressible fluid, q_i, within the bearing, may be described by the following relationship:

$$q_i = q_i^p + q_i^v + q_i^{sq} + q_{si} \qquad (4.43)$$

where: q_i^p, is the contribution due to the pressure induced flow

q_i^v, is the contribution due to the velocity induced flow

q_i^{sq}, is the contribution due to the squeeze induced flow, and

q_{si}, is the contribution due to the source flow.

At the static equilibrium condition:

$$q_i = q_{oi} = q_{oi}^p + q_{oi}^v + q_{soi} \qquad (4.44)$$

The suffix, o, is used to denote the static equilibrium condition. Equation (4.44), is the starting point for the subsequent analysis of the static characteristics of double slot-entry bearings, by the lumped parameter method.

(i) Equation of Continuity of Mass Flow Governing the ith 'OUTER' Control Volume

The full continuity equation may be expressed as:

$$q_{1oi}^p + q_{5oi}^p - q_{5oi}^p - q_{2oi}^p + q_{5oi}^v - q_{5oi}^v = 0 \qquad (4.45)$$

Writing down the non-dimensional expressions for the q_i, terms as derived in Appendix IV, yields:

$$(4 \bar{P}_{aoi} - \bar{P}_{oi})(\frac{\pi D}{a n_e}) H_{oi}^3 + \left[(\frac{2}{3} \bar{P}_{aoi} - \frac{1}{12} \bar{P}_{oi}) \cdots \right.$$

$$\cdots -(\frac{2}{3} \bar{P}_{aoi+1} - \frac{1}{12} \bar{P}_{oi+1})\right] \frac{1}{2} (\frac{a n_e}{\pi D}) H_{oi+\frac{1}{2}}^3 \cdots$$

$$\cdots -\left[(\frac{2}{3} \bar{P}_{aoi-1} - \frac{1}{12} \bar{P}_{oi-1}) - (\frac{2}{3} \bar{P}_{aoi} - \frac{1}{12} \bar{P}_{oi})\right] \frac{1}{2} (\frac{a n_e}{\pi D}) H_{oi-\frac{1}{2}}^3 \cdots$$

$$\cdots - \bar{P}_{oi} (\frac{\pi D}{a n_e}) H_{oi}^3 + 12 \pi S_h (\frac{a}{L}) (\frac{L}{D}) H_{oi+\frac{1}{2}} \cdots$$

$$\cdots - 12 \pi S_h (\frac{a}{L})(\frac{L}{D}) H_{oi-\frac{1}{2}} = 0 \qquad (4.46)$$

Rearranging and simplifying equation (4.46) yields:

$$\bar{P}_{aoi} \left[4 (\frac{\pi D}{a n_e}) H_{oi}^3 + \frac{1}{3} (\frac{a n_e}{\pi D}) (H_{oi+\frac{1}{2}}^3 + H_{oi-\frac{1}{2}}^3)\right]$$

$$= \bar{P}_{oi} \left[2 (\frac{\pi D}{a n_e}) H_{oi}^3 + \frac{1}{24} (\frac{a n_e}{\pi D})(H_{oi+\frac{1}{2}}^3 + H_{oi-\frac{1}{2}}^3)\right] \cdots$$

$$\cdots - \bar{P}_{oi+1} \left[\frac{1}{24} (\frac{a n_e}{\pi D}) H_{oi+\frac{1}{2}}^3\right] - \bar{P}_{oi-1} \left[\frac{1}{24} (\frac{a n_e}{\pi D}) H_{oi-\frac{1}{2}}^3\right] \cdots$$

$$\ldots + \bar{P}_{aoi + 1} \left[\frac{1}{3} \left(\frac{a \, n_e}{\pi \, D} \right) H^3_{oi + \frac{1}{2}} \right] + \bar{P}_{aoi - 1} \left[\frac{1}{3} \left(\frac{a \, n_e}{\pi \, D} \right) H^3_{oi - \frac{1}{2}} \right] \ldots$$

$$\ldots - 12 \, \pi \, S_h \left(\frac{a}{L} \right)\left(\frac{L}{D} \right) \left(H_{oi + \frac{1}{2}} - H_{oi - \frac{1}{2}} \right) \tag{4.47}$$

It is now possible to write equation (4.47) in a form which allows the pressures within the boundary of control volume 'OUTER', to be specified at every lumped point in the field. Thus, equation (4.47) reduces to:

$$\bar{P}_{aoi} = \left[\bar{P}_{oi} \left[2 \left(\frac{1}{A} \right) H^3_{oi} + \frac{1}{24} \, A \left(H^3_{oi + \frac{1}{2}} + H^3_{oi - \frac{1}{2}} \right) \right] \ldots$$

$$\ldots - \bar{P}_{oi + 1} \left(\frac{1}{24} \, A \, H^3_{oi + \frac{1}{2}} \right) - \bar{P}_{oi - 1} \left(\frac{1}{24} \, A \, H^3_{oi - \frac{1}{2}} \right) \ldots$$

$$\ldots + \bar{P}_{aoi + 1} \left(\frac{1}{3} \, A \, H^3_{oi + \frac{1}{2}} \right) + \bar{P}_{aoi - 1} \left(\frac{1}{3} \, A \, H^3_{oi - \frac{1}{2}} \right) \ldots$$

$$\ldots - 12 \, \pi \, S_h \left(\frac{a}{L} \right)\left(\frac{L}{D} \right)\left(H_{oi + \frac{1}{2}} - H_{oi - \frac{1}{2}} \right) \Big] \Big/ \ldots$$

$$\ldots \left[4 \left(\frac{1}{A} \right) H^3_{oi} + \frac{1}{3} \, A \left(H^3_{oi + \frac{1}{2}} + H^3_{oi - \frac{1}{2}} \right) \right] \tag{4.48}$$

where: $A = \left(\frac{a \, n_e}{\pi \, D} \right) = \left(\frac{a}{L} \right)\left(\frac{L}{D} \right)\left(\frac{n_e}{\pi} \right)$

(ii) **Equation of Continuity of Mass Flow Governing the ith 'SOURCE' Control Volume**

The full continuity equation maybe expressed as:

$$q^P_{2oi} + q^{,P}_{6oi} + q^{,P}_{7oi} - q^P_{6oi} - q^P_{7oi} - q^P_{3oi} \ldots$$

$$\ldots - q_{soi} + q^{,V}_{6oi} + q^{,V}_{7oi} - q^V_{6oi} - q^V_{7oi} = 0 \tag{4.49}$$

Again, writing down the non-dimensional expressions for the q_i terms as derived in Appendix IV, and the q_{soi} term as derived in Appendix V yields:

$$\bar{P}_{oi} \left(\frac{1}{A} \right) H^3_{oi} + \left[\left(\frac{5}{12} \, \bar{P}_{oi} + \frac{2}{3} \, \bar{P}_{aoi} \right) - \left(\frac{5}{12} \, \bar{P}_{oi+1} + \frac{2}{3} \, \bar{P}_{aoi+1} \right) \right]$$

$$\ldots \tfrac{1}{2} \, A \, H^3_{oi+\frac{1}{2}} + \left[\left(\frac{1}{4} \, \bar{P}_{coi} + \frac{3}{4} \, \bar{P}_{oi} \right) - \left(\frac{1}{4} \, \bar{P}_{coi+1} + \frac{3}{4} \, \bar{P}_{oi+1} \right) \right]$$

$$\ldots \frac{1}{4} \, B \, H^3_{oi+\frac{1}{2}} - \left[\left(\frac{5}{12} \, \bar{P}_{oi-1} + \frac{2}{3} \, \bar{P}_{aoi-1} \right) - \left(\frac{5}{12} \, \bar{P}_{oi} + \frac{2}{3} \, \bar{P}_{aoi} \right) \right] \ldots$$

$$\ldots \tfrac{1}{2} \, A \, H_{oi-\frac{1}{2}}^3 - \left[\left(\tfrac{1}{4} \bar{P}_{coi-1} + \tfrac{3}{4} \bar{P}_{oi-1} \right) - \left(\tfrac{1}{4} \bar{P}_{coi} + \tfrac{3}{4} \bar{P}_{oi} \right) \right] \ldots$$

$$\ldots \tfrac{1}{4} \, B \, H_{oi-\frac{1}{2}}^3 - 2 \, (\bar{P}_{coi} - \bar{P}_{oi}) \left(\tfrac{1}{B} \right) H_{oi}^3 \ldots$$

$$\ldots - (1 - \bar{P}_{oi}) \left(\tfrac{1}{A} \right) \left(\tfrac{\beta}{1 - \beta} \right) \left(\tfrac{n_s}{n_e} \right) + 12 \, \pi \, S_h \left(\tfrac{a}{L} \right) \left(\tfrac{L}{D} \right) H_{oi+\frac{1}{2}} \ldots$$

$$\ldots + 6 \, \pi \, S_h \left(1 - \tfrac{2a}{L} \right) \left(\tfrac{L}{D} \right) H_{oi+\frac{1}{2}} - 12 \, \pi \, S_h \left(\tfrac{a}{L} \right) \left(\tfrac{L}{D} \right) H_{oi-\frac{1}{2}} \ldots$$

$$\ldots - 6 \, \pi \, S_h \left(1 - \tfrac{2a}{L} \right) \left(\tfrac{L}{D} \right) H_{oi-\frac{1}{2}} = 0 \tag{4.50}$$

where: $B = \left(1 - \tfrac{2a}{L} \right) \left(\tfrac{L}{D} \right) \left(\tfrac{n_e}{\pi} \right)$

Rearranging and simplifying equation (4.50) yields:

$$\bar{P}_{oi} \left[\left(\tfrac{1}{A} \right) H_{oi}^3 + \tfrac{5}{24} A \, H_{oi+\frac{1}{2}}^3 + \tfrac{5}{24} A \, H_{oi-\frac{1}{2}}^3 \ldots \right.$$

$$\ldots + \tfrac{3}{16} B \, H_{oi+\frac{1}{2}}^3 + \tfrac{3}{16} B \, H_{oi-\frac{1}{2}}^3 + 2 \left(\tfrac{1}{B} \right) H_{oi}^3 + AZY \left(\tfrac{n_s}{n_e} \right) \bigg]$$

$$= \bar{P}_{oi+1} \left(\tfrac{5}{24} A \, H_{oi+\frac{1}{2}}^3 + \tfrac{3}{16} B \, H_{oi+\frac{1}{2}}^3 \right) \ldots$$

$$\ldots + \bar{P}_{oi-1} \left(\tfrac{5}{24} A \, H_{oi-\frac{1}{2}}^3 + \tfrac{3}{16} B \, H_{oi-\frac{1}{2}}^3 \right) \ldots$$

$$\ldots - \bar{P}_{aoi} \left(\tfrac{1}{3} A \, H_{oi+\frac{1}{2}}^3 + \tfrac{1}{3} A \, H_{oi-\frac{1}{2}}^3 \right) \ldots$$

$$\ldots + \bar{P}_{aoi+1} \left(\tfrac{1}{3} A \, H_{oi+\frac{1}{2}}^3 \right) + \bar{P}_{aoi-1} \left(\tfrac{1}{3} A \, H_{oi-\frac{1}{2}}^3 \right) \ldots$$

$$\ldots + \bar{P}_{coi} \left[2 \left(\tfrac{1}{B} \right) H_{oi}^3 - \tfrac{1}{16} B \, H_{oi+\frac{1}{2}}^3 - \tfrac{1}{16} B \, H_{oi-\frac{1}{2}}^3 \right] \ldots$$

$$\ldots + \bar{P}_{coi+1} \left(\tfrac{1}{16} B \, H_{oi+\frac{1}{2}}^3 \right) + P_{coi-1} \left(\tfrac{1}{16} B \, H_{oi-\frac{1}{2}}^3 \right) \ldots$$

$$\ldots - 12 \, \pi \, S_h \left(\tfrac{a}{L} \right) \left(\tfrac{L}{D} \right) \left(H_{oi+\frac{1}{2}} - H_{oi-\frac{1}{2}} \right) \ldots$$

$$\ldots 6 \, \pi \, S_h \left(1 - \tfrac{2a}{L} \right) \left(\tfrac{L}{D} \right) \left(H_{oi+\frac{1}{2}} - H_{oi-\frac{1}{2}} \right) \ldots$$

$$\ldots + AZY \left(\tfrac{n_s}{n_e} \right) = 0 \tag{4.51}$$

Therefore, the expression, which allows the pressures within the boundary of the source region, P_{oi}, to be specified at every lumped

point in the field may be expressed as:

$$\bar{P}_{oi} = \left[\bar{P}_{oi+1} \left(\frac{5}{24} A + \frac{3}{16} B \right) H^3_{oi+\frac{1}{2}} \; \ldots \right.$$

$$\ldots + \bar{P}_{oi-1} \left(\frac{5}{24} A + \frac{3}{16} B \right) H^3_{oi-\frac{1}{2}} - \bar{P}_{aoi} \left(H^3_{oi+\frac{1}{2}} + H^3_{oi-\frac{1}{2}} \right) \frac{1}{3} A \; \ldots$$

$$\ldots + \bar{P}_{aoi+1} \left(\frac{1}{3} A \; H^3_{oi+\frac{1}{2}} \right) + \bar{P}_{aoi-1} \left(\frac{1}{3} A \; H^3_{oi-\frac{1}{2}} \right) \ldots$$

$$\ldots + \bar{P}_{coi} \left[2 \left(\frac{1}{B} \right) H^3_{oi} - \left(H^3_{oi+\frac{1}{2}} + H^3_{oi-\frac{1}{2}} \right) \frac{1}{16} B \right] \ldots$$

$$\ldots + \bar{P}_{coi+1} \left(\frac{1}{16} B \; H^3_{oi+\frac{1}{2}} \right) + \bar{P}_{coi-1} \left(\frac{1}{16} B \; H^3_{oi-\frac{1}{2}} \right) \ldots$$

$$\ldots - 12 \; \pi \; S_h \left(\frac{a}{L} \right) \left(\frac{L}{D} \right) \left(H_{oi+\frac{1}{2}} - H_{oi-\frac{1}{2}} \right) \ldots$$

$$\ldots - 6 \; \pi \; S_h \left(1 - \frac{2a}{L} \right) \left(\frac{L}{D} \right) \left(H_{oi+\frac{1}{2}} - H_{oi-\frac{1}{2}} \right) \ldots$$

$$\ldots + AZY \left(\frac{n_s}{n_e} \right) \left. \right] \Big/ \ldots$$

$$\ldots \left[\left(\frac{1}{A} + 2 \left(\frac{1}{B} \right) \right) H^3_{oi} + \left(\frac{5}{24} A + \frac{3}{16} B \right) H^3_{oi+\frac{1}{2}} \; \ldots \right.$$

$$\ldots + \left(\frac{5}{24} A + \frac{3}{16} B \right) H^3_{oi-\frac{1}{2}} + AZY \left(\frac{n_s}{n_e} \right) \right] \tag{4.52}$$

(iii) **Equation of Continuity of Mass Flow Governing the ith 'CENTRAL'**
   Control Volume

The full continuity equation may be expressed as:

$$q^p_{3oi} + q'^p_{8oi} - q^p_{4oi} - q^p_{8oi} + q'^v_{8oi} - q^v_{8oi} = 0 \tag{4.53}$$

Applying the non-dimensional expressions for the q_i, terms, as derived in Appendix IV, yields:

$$2 \left(\bar{P}_{coi} - \bar{P}_{oi} \right) \left(\frac{1}{B} \right) H^3_{oi} + \left[\left(\frac{1}{12} \bar{P}_{oi} + \frac{11}{12} \bar{P}_{coi} \right) \; \ldots \right.$$

$$\ldots - \left(\frac{1}{12} \bar{P}_{oi+1} + \frac{11}{12} \bar{P}_{coi+1} \right) \right] \frac{1}{4} B \; H^3_{oi+\frac{1}{2}} - 0 \; \ldots$$

$$\ldots - \left[\left(\frac{1}{12} \bar{P}_{oi-1} + \frac{11}{12} \bar{P}_{coi-1} \right) - \left(\frac{1}{12} \bar{P}_{oi} + \frac{11}{12} \bar{P}_{coi} \right) \right] \frac{1}{4} B \; H^3_{oi-\frac{1}{2}} \; \ldots$$

$$\ldots + 6 \; \pi \; S_h \left(1 - \frac{2a}{L} \right) \left(\frac{L}{D} \right) \left(H_{oi+\frac{1}{2}} - H_{oi-\frac{1}{2}} \right) = 0 \tag{4.54}$$

Rearranging and simplifying equation (4.54) yields:

$$\bar{P}_{coi} \left[2\left(\frac{1}{B}\right) H^3_{oi} + \frac{11}{48} B\, H^3_{oi+\frac{1}{2}} + \frac{11}{48} B\, H^3_{oi-\frac{1}{2}} \right]$$

$$\ldots = \bar{P}_{coi+1} \left(\frac{11}{48} B\, H^3_{oi+\frac{1}{2}} \right) + \bar{P}_{coi-1} \left(\frac{11}{48} B\, H^3_{oi-\frac{1}{2}} \right) \ldots$$

$$\ldots + \bar{P}_{oi} \left[2\left(\frac{1}{B}\right) H^3_{oi} - \frac{1}{48} B\, H^3_{oi+\frac{1}{2}} - \frac{1}{48} B\, H^3_{oi-\frac{1}{2}} \right] \ldots$$

$$\ldots + \bar{P}_{oi+1} \left(\frac{1}{48} B\, H^3_{oi+\frac{1}{2}} \right) + \bar{P}_{oi-1} \left(\frac{1}{48} B\, H^3_{oi-\frac{1}{2}} \right) \ldots$$

$$\ldots - 6\,\pi\, S_h \left(1 - \frac{2a}{L} \right)\left(\frac{L}{D}\right)\left(H_{oi+\frac{1}{2}} - H_{oi-\frac{1}{2}} \right) \qquad (4.55)$$

Thus, the expression which allows the pressures, P_{coi}, to be specified at every lumped point in the field, may be expressed as:

$$\bar{P}_{coi} = \left[\bar{P}_{coi+1} \left(\frac{11}{48} B\, H^3_{oi+\frac{1}{2}} \right) + \bar{P}_{coi-1} \left(\frac{11}{48} B\, H^3_{oi-\frac{1}{2}} \right) \ldots \right.$$

$$\ldots + \bar{P}_{oi} \left[2\left(\frac{1}{B}\right) H^3_{oi} - \left(H^3_{oi+\frac{1}{2}} + H^3_{oi-\frac{1}{2}} \right) \frac{1}{48} B \right] \ldots$$

$$\ldots + \bar{P}_{oi+1} \left(\frac{1}{48} B\, H^3_{oi+\frac{1}{2}} \right) + \bar{P}_{oi-1} \left(\frac{1}{48} B\, H^3_{oi-\frac{1}{2}} \right) \ldots$$

$$\left. \ldots - 6\,\pi\, S_h \left(1 - \frac{2a}{L} \right)\left(\frac{L}{D}\right)\left(H_{oi+\frac{1}{2}} - H_{oi-\frac{1}{2}} \right) \right] \Big/ \ldots$$

$$\ldots \left[2\left(\frac{1}{B}\right) H^3_{oi} + \left(H^3_{oi+\frac{1}{2}} + H^3_{oi-\frac{1}{2}} \right) \frac{11}{48} B \right] \qquad (4.56)$$

4.6.5 Method of Solution

The pressure equations given in section 4.6.4 governing every lumped point in the field represent a set of simultaneous equations. The iteration procedure, based upon successive under-relaxation, as described in Section 4.5.4, is employed to solve equations (4.48), (4.52) and (4.56).

4.6.6 Boundary Conditions

The boundary conditions used in this analysis are the same as described in Section 4.5.5.

4.6.7 Bearing Load

The non-dimensional load reaction on the shaft resolved in the U-axis may be expressed as:

$$\bar{F}_{uo} = \sum_{i=1}^{n_e} - \bar{W}_i \sin \theta i \qquad (4.57)$$

The non-dimensional load reaction on the shaft resolved in the V-axis may be expressed as:

$$\bar{F}_{vo} = \sum_{i=1}^{n_e} - \bar{W}_i \cos \theta i \qquad (4.58)$$

where: $\bar{W}_i = 2 \left(\frac{1}{6} \bar{P}_{oi} + \frac{2}{3} \bar{P}_{aoi} \right) \left(\bar{AR}_o \right) + \bar{P}_{oi} \left(\bar{AR}_c \right) \dots$

$$\dots + \frac{2}{3} \left(\bar{P}_{coi} - \bar{P}_{oi} \right) \left(\bar{AR}_c \right)$$

$$\bar{AR}_o = \left(\frac{a}{L} \right) \sin \left(\frac{\pi}{n_e} \right)$$

$$\bar{AR}_c = \left(1 - \frac{2a}{L} \right) \sin \left(\frac{\pi}{n_e} \right)$$

Hence, the resultant non-dimensional load, $\bar{F}_o$, and the attitude angle, ϕ_o, may be obtained, as outlined in Section 4.5.6.

4.6.8 Bearing Volumetric Flow-Rate

Two expressions governing the bearing oil flow are derived.

(i) Flow-rate into the bearing (The Source Flow) $-q_{in}$

The total source flow through the bearing may be expressed by equation (4.40) as derived in Section 4.5.6, replacing $P_{oi,d}$ by, P_{oi}.

In non-dimensional form:

$$\bar{q}_{in} = 2 \left(\frac{\beta}{1 - \beta} \right) \left(\frac{\pi \, D}{a \, n_s} \right) \left(\frac{n_s}{n_e} \right) \sum_{i=1}^{n_e} \left(1 - \bar{P}_{oi} \right) \qquad (4.59)$$

(ii) Flow-rate out of the bearing (The Axial Flow) $-q_{out}$

The flow-rate from each end of the bearing, for each lumped section is obtained from consideration of the expression governing the variation of the axial pressure along the outer land (See Appendix V).

The total flow-rate out of the bearing may be expressed as:

$$q_{out} = 2 \sum_{i=1}^{n_e} - \left. \frac{dP}{dx} \right|_{x=a} \frac{\Delta X}{12\eta} h_{oi}^3$$

Substituting the expression for $\left. \frac{dP}{dx} \right|_{x=a}$, given in equation (AV - 8) yields:

$$q_{out} = 2 \frac{\Delta X}{12\eta} \frac{1}{a} \sum_{i=1}^{n_e} \left(4 P_{aoi} - P_{oi} \right) h_{oi}^3$$

that is:

$$q_{out} = \frac{2}{12\eta} \left(\frac{\pi}{n_e} \right) \left(\frac{D}{L} \right) \left(\frac{L}{a} \right) \sum_{i=1}^{n_e} \left(4 P_{aoi} - P_{oi} \right) h_{oi}^3 \qquad (4.60)$$

Or in non-dimensional form:

$$\bar{q}_{out} = 2 \left(\frac{\pi}{n_e} \right) \left(\frac{D}{L} \right) \left(\frac{L}{a} \right) \sum_{i=1}^{n_e} \left(4 \bar{P}_{aoi} - \bar{P}_{oi} \right) H_{oi}^3 \qquad (4.61)$$

4.6.9 The Lumped Parameter Computer Program

A lumped parameter computer program that includes bearing dynamic analysis (the finite-disturbance technique) has been written. (See Chapter 5). The input variables for this program are similar to the finite difference program described in Section 4.5.7, except that the number of axial grid elements (m), is not required.

4.7 Discussions and Conclusions

For the program to be certified as reliable and accurate, it must first be tested for a wide range of operating parameters, and a comparison with other predictions or any published results (theoretical and experimental) carried out. Results are therefore, presented for a wide range of bearing operating parameters, such as various values of concentric pressure-ratio, (β), bearing length to diameter-ratio, (L/D), axial-length width to bearing length ration, (a/L), and power-ratio, (K), where the value of K spans from zero up to 119. A comparison with a previous finite difference program (8) was carried out. The previous

finite difference program did not take into account the circumferential

flows at the source (feed-slots) and the equation was not presented in a

general form. Two equations were required - one for the source region

and one elsewhere. The results were also compared with those obtained

experimentally. The experimental results being obtained from reference

(8).

Let us first consider the effect of varying the number of circum-

ferential grid elements on the slot entry bearing, finite difference

static characteristics. This is illustrated in table 4.1, below, where

the results are obtained from the present finite difference program.

Table 4.1: Effect of the number of circumferential grid elements on

the static characteristic ($^{a}/L$ = 0.1, $^{L}/D$ = 1.0, β = 0.17,

K = 60.7)

	$\bar{W}$				ϕ^{o}			
ε \ n_{e}	12	24	36	48	12	24	36	48
0.1	0.346	0.347	0.348	0.348	81.07	80.96	80.99	81.01
0.2	0.619	0.620	0.620	0.621	75.71	75.71	75.54	75.55
0.3	0.932	0.928	0.929	0.929	69.79	70.21	70.20	70.20
0.4	1.315	1.308	1.307	1.307	64.09	64.64	64.70	64.70
0.5	1.817	1.804	1.803	1.803	58.51	59.21	59.31	59.32
0.6	2.518	2.499	2.510	2.514	52.91	53.90	53.59	53.49
0.7	2.588	3.631	3.656	3.648	47.19	47.54	47.10	47.24
0.8	5.441	5.943	5.915	5.955	41.11	39.23	39.55	39.29
0.9	9.226	13.007	13.273	12.247	34.57	28.44	28.42	28.58

Although the results were computed, for a bearing with 12 slots

per row, it is observed that using 12 circumferential grid elements, is

not sufficient to predict the static characteristic adequately. For

eccentricity-ratios greater than 0.6, it is essential to increase the

number of circumferential grid elements to ensure accuracy in the com-

puted results. Using 36 circumferential grid elements, seems to be ideal
for this purpose, as increasing the circumferential grid elements to 48
or more, give almost identical results to that of 36. It should be noted
that varying the number of axial grid elements also produces discrep-
ancies in the computed results, although, this effect is not as sens-
itive as circumferential variations. In the present analysis, the
number of axial grid elements used was 20, and was found to be adequate,
for providing sufficient accuracy in the computed results.

Figures (4.7a) to (4.11b) provide a comparison of the predicted
results with previous work. The bearing's static characteristics at
low K values, that is, at K = 0 and 1, are presented in figure (4.7a).
It can be observed that, at K = 0, and for $\varepsilon < 0.6$, the present finite
difference and lumped parameter programs predict the same characteristics
as the previous finite difference program of reference (8). For
$\varepsilon > 0.6$, an improvement over the previous program was obtained, although
discrepancies between the experimental results still exist around this
region. Thus, highlighting the inadequacy of the present analysis to
cater for heavily loaded bearings, where elasticity and variable vis-
cosity effects have to be considered. Figure (4.7a), also illustrates
the good agreement between the three predicted results of dimensionless
load, at K = 1. Reasonable agreement between the three predicted results
of attitude angle can also be observed in figure (4.7b). The figure
shows the slight improvement of attitude angle obtained by the present
programs at higher values of eccentricity-ratio.

The static characteristics at moderate values of K (K = 7.48 and
10.9), are presented in figures (4.8a) to (4.9b). In general, there
is good agreement between the three sets of computed results. There
is better agreement between the experimentally determined attitude
angle and the results predicted by the present programs. (See Figures
(4.2b) and (4.3b)). Also, at high values of eccentricity-ratio, the

results of dimensionless load, predicted by the present programs correlate better with the experimental results, when compared with the previous program.

Figures (4.10a) to (4.11b) illustrate the static characteristics at high values of K. (K = 60.7 and 119). The same phenomena as described above can be observed here

Dimensionless flow-rates for two values of K, (K = 10.9 and 60.7) are presented in figures (4.12a) and (4.12b). It is interesting to note the discrepancies between $\bar{q}_{in}$ and $\bar{q}_{out}$, thus, demonstrating that the principle of mass conservation have been violated, and draws attention to the inadequacy of the boundary conditions employed in the present analysis. The boundary conditions employed do not take proper account of mass conservation within the cavitated region. Since then, an efficient finite difference program, employing the Jakobsson and Floberg boundary conditions (1) have been developed. It can be observed that there is better agreement between $\bar{q}_{in}$ and $\bar{q}_{out}$, although the accuracy of this prediction, has yet to be compared with the experimental findings.

The procedure for implementing the Jakobsson-Floberg boundary condition, which automatically ensures that the requirement of mass conservation is satisfied throughout the bearing is presented in reference (13). In order to keep within the aims of the present investigation and due to the constraint on time, the implementation of the Jakobsson and Floberg boundary condition for dynamic analysis has been set aside for future work.

The general conclusions from the investigation of the static hybrid bearing performance are:

1) Two computer programs for predicting the static characteristics of slot-entry bearings, have been successfully developed.

2) The accuracy and reliability of these two programs have been rigorously tested, with results obtained from previous work.

3) In terms of computing time, the lumped parameter program, is far superior to its finite-difference counterpart, although, in terms of accuracy, there is little to choose between the two. The lumped parameter program computes approximately nine times faster than the finite-difference program. For a typical computer run, (say, $^a/L = 0.25$, $^L/D = 0.83$, $\beta = 0.38$ and $K = 10.9$), the finite difference program uses 660.05 seconds of C.P.U. time, while the lumped-parameter program uses 74.69 seconds.

4) In order to achieve sufficient accuracy in the computed results for eccentricity-ratios greater than 0.6, the number of circumferential grid elements should be increased to 24, although the inadequacy of the present analysis to cater for heavily loaded bearings should be noted.

5) The studies carried out by employing the Jakobsson and Floberg boundary conditions, suggest that the present boundary condition is inadequate in predicting the bearing flow-rate, although, in the absence of an appropriate boundary condition, the bearing in-flow would represent a reasonable estimate. The out-flow (side-leakage) should never be used as it greatly over-estimates the flow.

6) The results predicted by the present boundary condition, for bearings operating at high values of K (K > 60) and low values of concentric pressure-ration, β, ($\beta < 0.3$) should be treated with caution. When using the Jakobsson and Floberg boundary conditions the results suggest that the bearing is badly starved and that the present boundary condition over-estimates the

static load and attitude angle, especially at high values of eccentricity-ratio.

Fig.(4.7a) : Variation Of Load Parameter With Eccentricity-
Ratio. (K = 0.0 and 1.0)

Fig.(4.7b): Variation Of Attitude Angle With Eccentricity-
Ratio. (K = 1.0)

$a/L = 0.1$
$L/D = 1.0$
$B = 0.63$
$S_{ho} = 0.082$

Theory

Finite Difference(New)
Finite Difference(Old)
Lumped Parameter

Experiment

K = 0.0
K = 1.0

Fig.(4.8a): Variation Of Load Parameter With Eccentricity-
Ratio. (K = 7.48)

$$\frac{W}{P_S L D}$$

a/L = 0.1
L/D = 1.0
β = 0.63
Sho = 0.082

ε

Fig.(4.8b): Variation Of Attitude Angle With Eccentricity-
Ratio. (K = 7.48)

ϕ (Deg.)

ε
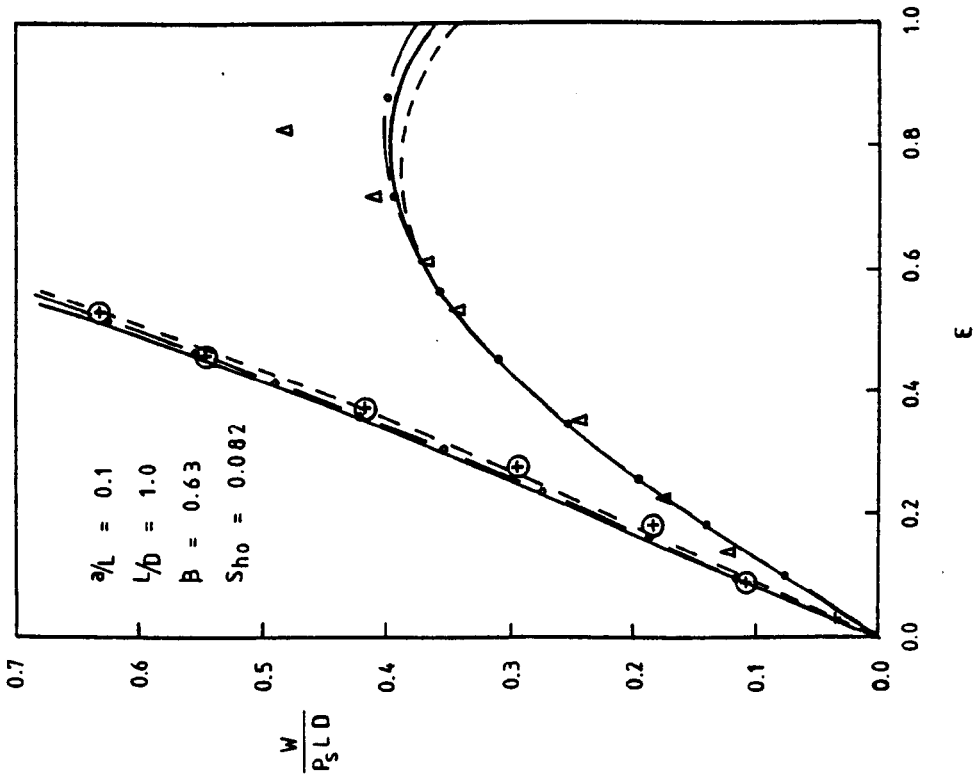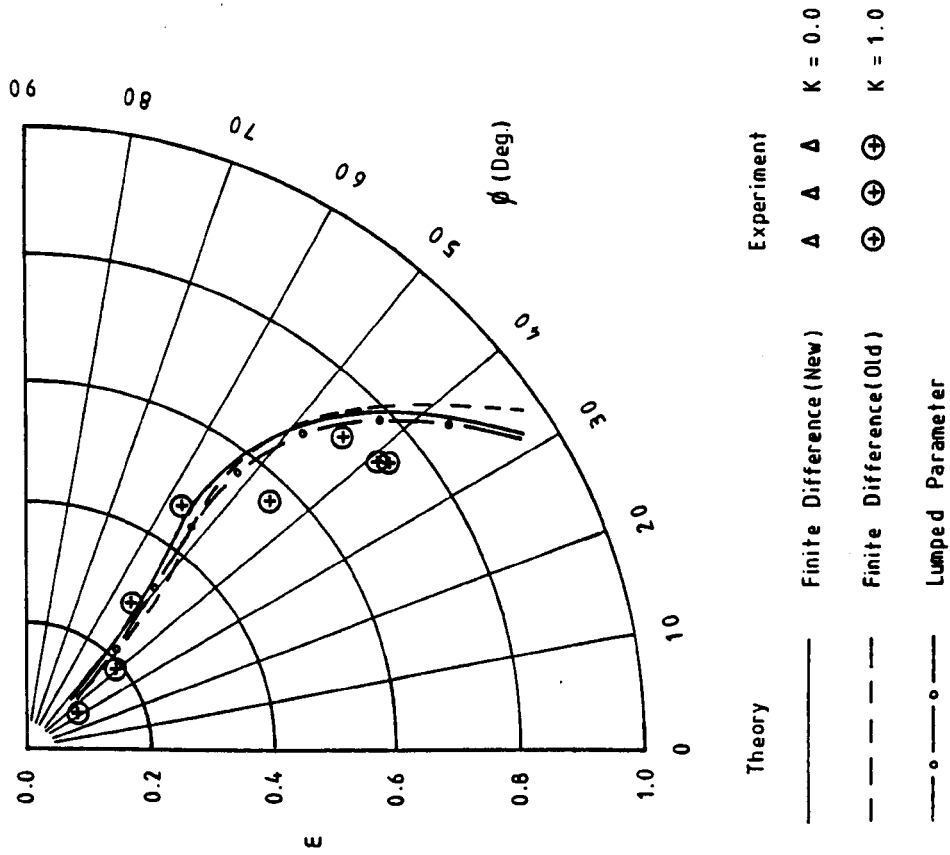
Theory

Experiment

—————— Finite Difference (New)

– – – – – Finite Difference (Old)

——o——o—— Lumped Parameter

⊕ ⊕ ⊕ K = 7.48
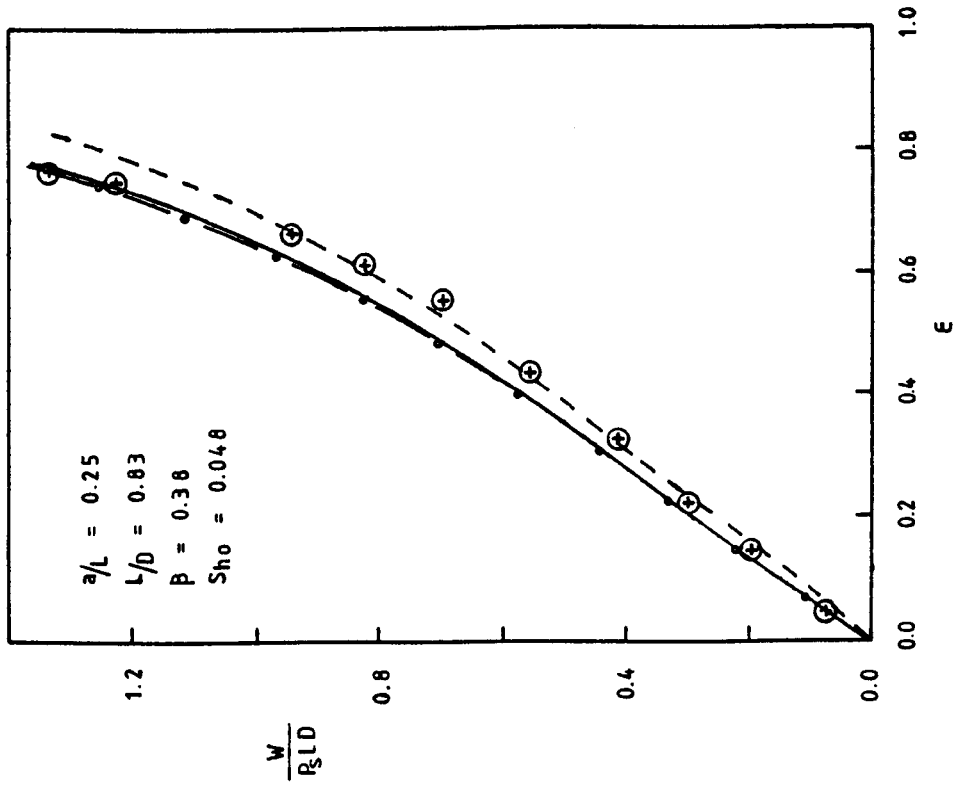
Fig(4.9b) : Variation Of Attitude Angle With Eccentricity-
Ratio. (K = 10.9)

Fig(4.9a) : Variation Of Load Parameter With Eccentricity-
Ratio. (K = 10.9)

ϕ (Deg.)

Experiment

⊕ ⊕ ⊕ K = 10.9

Theory

—————— Finite Difference (New)

— — — — Finite Difference (Old)

——o——o—— Lumped Parameter

a/L = 0.25
L/D = 0.83
P̄ = 0.38
Sho = 0.048

$\frac{W}{P_s LD}$

ε

ε

Fig.(4.10b): Variation Of Attitude Angle With Eccentricity-
Ratio. (K = 60.7)

Fig.(4.10a): Variation Of Load Parameter With Eccentricity-
Ratio. (K = 60.7)
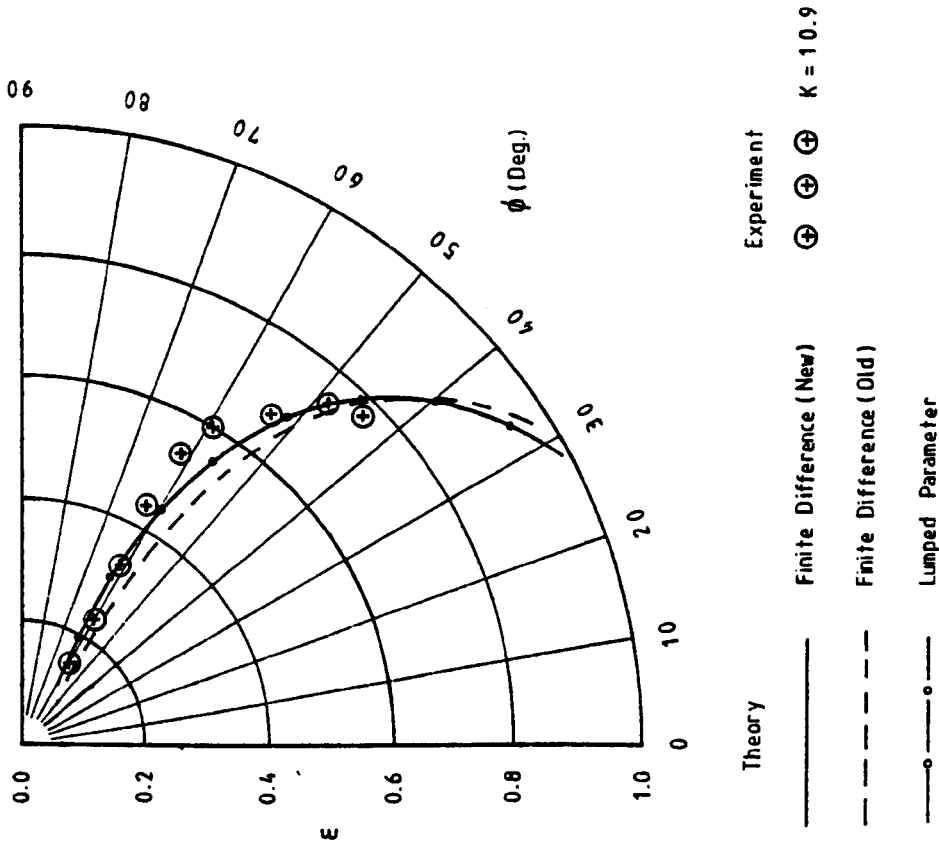
Fig.(4.11a): Variation Of Load Parameter With Eccentricity-
Ratio. (K = 119)

$\dfrac{W}{P_s LD}$

ε

a/L = 0.1
L/D = 1.0
β = 0.19
Sho = 0.045
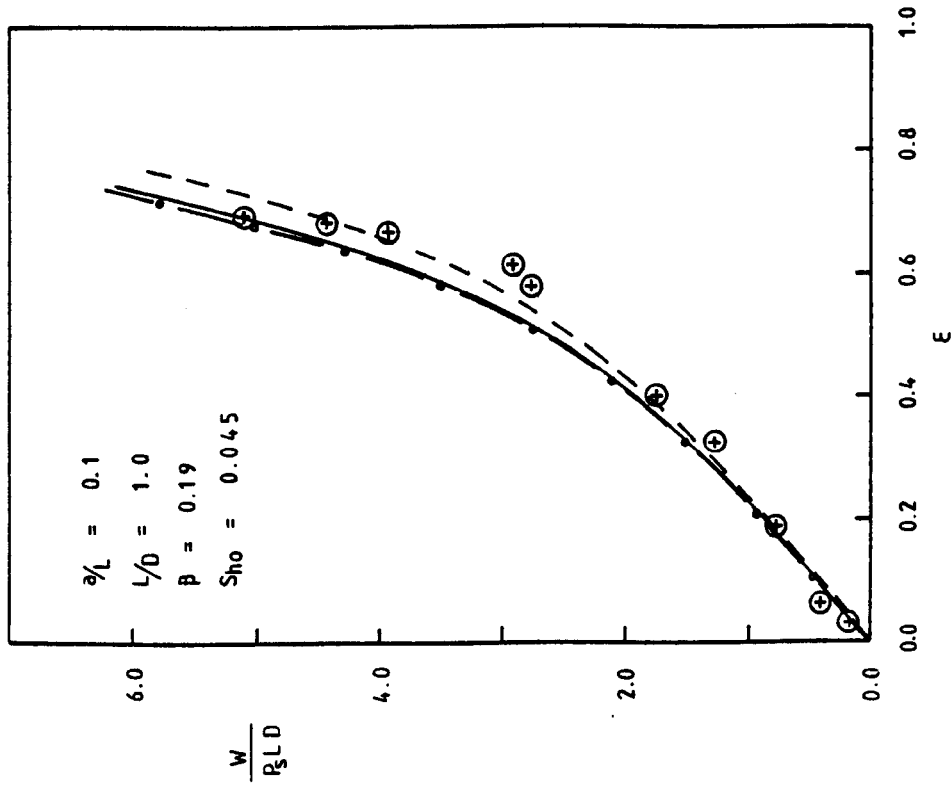
Fig.(4.11b) : Variation Of Attitude Angle With Eccentricity-
Ratio. (K = 119)

∅ (Deg.)

ε

Theory

——————— Finite Difference (New)

– – – – – – Finite Difference (Old)

——o—— Lumped Parameter
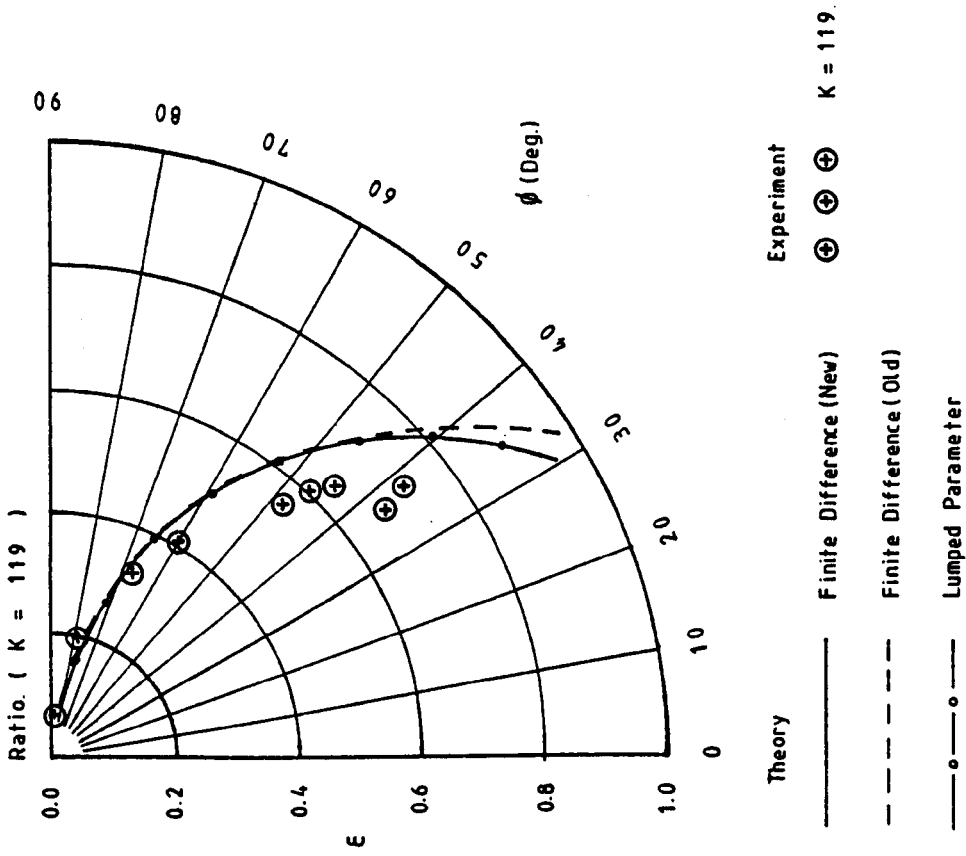
Experiment

⊕ ⊕ ⊕   K = 119

Fig.(4.12a): Variation Of Dimensionless Flow-Rate With Eccentricity-Ratio. (K = 10.9)

$a/L = 0.25$
$L/D = 0.83$
$\beta = 0.38$
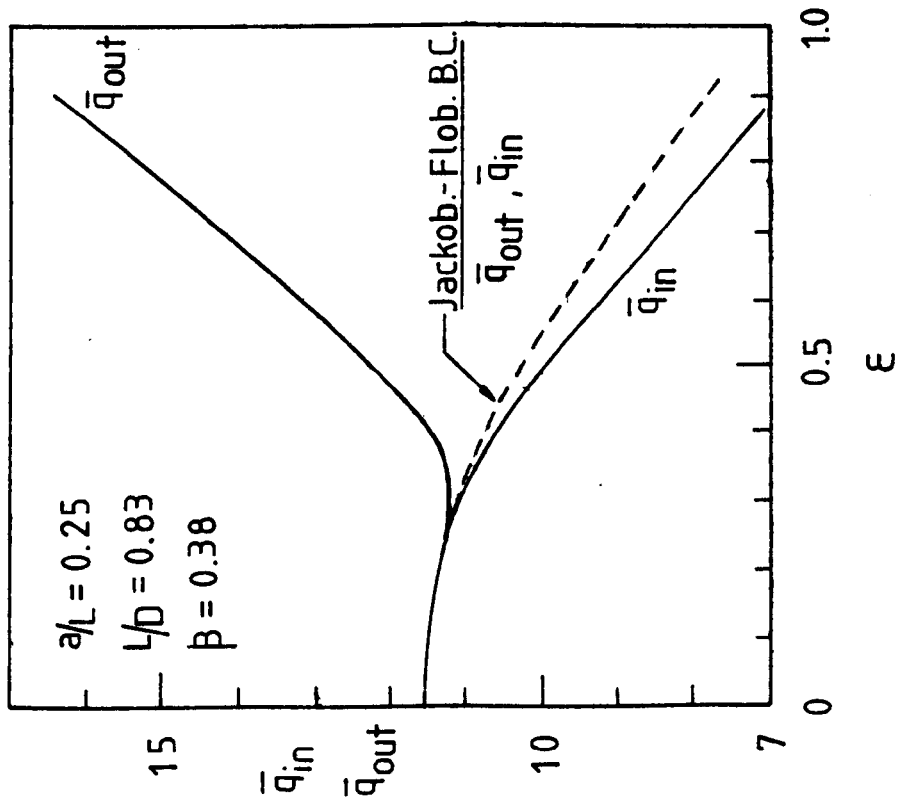
Fig.(4.12b): Variation Of Dimensionless Flow-Rate With Eccentricity-Ratio. (K = 60.7)

$a/L = 0.1$
$L/D = 1.0$
$\beta = 0.17$
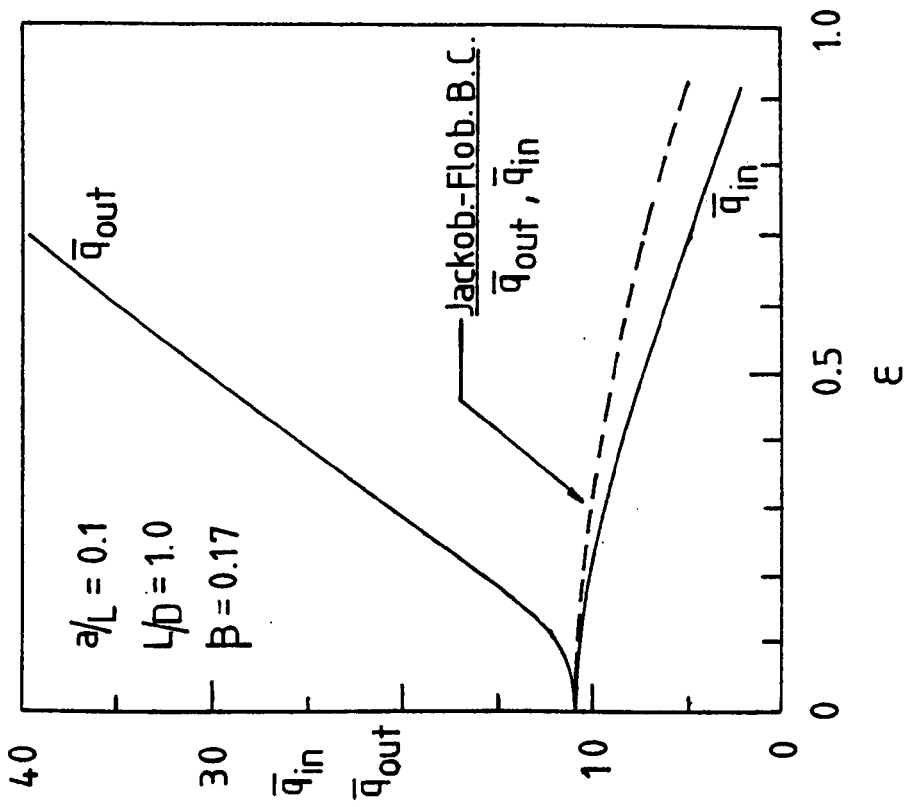
REFERENCES

1. Jakobsson, B. and Floberg, L. 'The finite journal bearing considering vaporization', Trans. Chalmers Univ. Technol., Gothenburg, Sweden, 1957.

2. Opitz, H. 'Pressure Pad Bearing', Proc. Instn. Mech. Engrs., Vol. 182, Part 3A, 1967-68, pp 100-115.

3. O'Donoghue, J.P., Rowe, W.B. and Hooke, C.J. 'Design of hydrostatic bearings using an operating parameter', Wear, 14 (1969), pp. 355-362.

4. Rowe, W.B., O'Donoghue, J.P. and Cameron, A. 'Optimization of externally pressurized bearings for minimum power and low temperature rise', Tribology, Aug. 1970, pp. 153-157.

5. Dee, C.W. and Shires, G.L. 'The current state of the art of fluid bearings with discrete slot inlets', Jnl. of Lub. Tech., Trans. ASME, Paper No. 71, 1971.

6. Williams, P.W. 'Numerical Computations', Thomas Nelson and Sons Ltd., 1972.

7. Stout, K.J. and Rowe, W.B. 'Externally pressurized Bearings - Design for manufacture', Tribology International,
   Part 1 - June 1974
   Part 2 - Aug. 1974
   Part 3 - Oct. 1974

8. Koshal, D. 'The design and optimization of slot hybrid journal bearings', Ph.D. Thesis, Liverpool Poly., 1978.

9.   Rowe, W.B., Weston, W. and Koshal, D.   'Static and dynamic properties of concentric hydrostatic journal bearings', The Euromech Colloquim No. 124, Orbassano, Italy, Oct. 1979.

10. Koshal, D. and Rowe, W.B.   'Fluid-film journal bearings operating in a hybrid mode', Jnl. of Lub. Tech., Trans, ASME, Vol. 103, Aug. 1980, pp. 558-572.

11. Rowe, W.B. and Koshal, D.   'A new basis for the optimization of hybrid journal bearings', Wear, 64 (1980), pp. 115-131.

12. Pu, Y., Li, W.L. and Qi, S.Z.   'Study on calculation and experiment of load capacity of slot fed fluid bearings', Mech. Eng. Dept. Report., Tianjin Univ., China, 1982.

13. Rowe, W.B. and Chong, F.S.   'A computational algorithm for cavitating bearings - Requirement of boundary conditions which satisfy the principle of mass conservation', Tribology International, Vol. 17, No. 5, Oct. 1984, pp. 243-250.

CHAPTER 5

DERIVATION OF THE EIGHT LINEARIZED BEARING DYNAMIC COEFFICIENTS

5.1 Introduction

Bearing dynamic coefficients of the equations of motion must be evaluated before bearing responses, bearing stability or critical speeds can be investigated. Bearing dynamic analysis may be either primarily concerned with:

(1) defining the bearing reaction vector as a function of the journal centre's displacement and velocity vectors, or

(2) defining the velocity vector of the bearing as a function of its load and displacement vectors.

The latter description is particularly useful for some situations in which the load applied to the bearing is a complex function of time, such as, in bearings of internal combustion engines. The mobility method of Booker (3) and the Impulse method of Block (7) are based on this approach. The former description is the classical approach usually employed for situations in which the forces on the rotor are simple functions of time. This chapter and the subsequent chapters of this thesis, are devoted to the derivation of bearing coefficients and their application to analysis of bearing performance by the classical linear analysis approach.

The amplitude and velocity of the journal centre motion are highly non-linear functions of the bearing reaction forces. In most practical situations, however, it is sufficiently accurate to perform a linear analysis, for small displacements from the steady-state position (9, 15, 16). Non-linear analysis is required for transient rotor-bearing dynamic studies involving large excursions, whilst, linearized bearing dynamic coefficients are sufficient for small amplitude synchronous rotor-response, critical speeds or stability studies. Linear analysis

offers several advantages:

(1) a rotor-bearing dynamic analysis, which is independent of any
     particular rotor design, may be carried out, and

(2) using superposition, parametric studies of the linear rotor-
     bearing system may be carried out.

5.2 The Linearized Bearing Dynamic Coefficients

In the dynamic analysis of rotating machines, the bearing dynamic
characteristics may be derived, in terms of the forces developed in
the bearing due to translational, axial and torsional motions imposed
on the journal. The starting point for the linear analysis is, there-
fore, the linearization of these forces based on small perturbations
about the equilibrium position. The forces may be represented by their
first order Taylor series expansion. This gives a set of 32 linearized
bearing coefficients. In most practical cases, the degrees of freedom
associated with the axial and torsional motions, may be ignored, com-
pared with the translational motion. This yields a set of 8 linearized
coefficients, that is, 4 stiffness (displacement dependent) and 4 damp-
ing (velocity dependent) coefficients. The representation of the
bearing characteristics by 8 linearized bearing dynamic coefficients,
is most commonly accepted in the field of rotor-bearing dynamic analysis.

By retaining the second order terms in the Taylor series expansion,
Bannister (10) obtained 28 linearized coefficients. These gave better
correlation with the experimental results for synchronous forcing, than
the usual 8 coefficients. However, the use of 28 coefficients is some-
what unwieldy and unlikely to find favour amongst rotor-bearing dynamicists.

The Reynolds equation is a laminar, thin film lubrication equation,
that ignores the inertia forces in the fluid-film. In reducing the
Navier-Stokes equations to the Reynolds equation, the Reynolds number
is assumed to be very much less than unity. Although, the transition

to either Taylor Vortex flow or to turbulent flow occurs at a
Reynolds number of approximately 1000 to 1500, there is an intermediate
laminar flow range, where the Reynolds number value is of the order of
100's. Under this condition, inertia effects may be considerable.
Several investigators (2, 6, 14) have examined this problem and
derived 12 linearized coefficients, that is, 4 stiffness, 4 damping and
4 inertia (acceleration dependent) coefficients. The inertia coefficients
were found to be significant for small, short rotors, as the inertia
effects represent an added mass of several times that of the journal
itself. Failure to include the inertia coefficients in the theoretical
calculations of the 'critical journal mass' (a stability parameter
which gives a quantitative indication of a threshold speed beyond which
the bearing is unstable) would result in an over-estimation of the
actual 'critical journal mass'.

Other investigators (4,5,8,11, 12,13), though less numerous, have
devoted their attention to modelling for bearing operating conditions,
including the influence of thermal effects (variable viscosity), com-
pressibility, shaft-misalignment or non-laminar lubricant flow. The
majority of these investigators have adopted the use of 8 linearized
coefficients, (4,8, 11, 12, 13), while a few have adopted the use of 12
coefficients (5, 17).

A representation of the bearing fluid-film by the 8 linearized
bearing dynamic coefficients is illustrated in figure (5.1). Figure
(5.2) illustrates the coordinate system for load and displacement. The
fixed X - Y set of coordinates are such that Y is in the direction of
the static load, $W_{y(static)}$. The moving U - V set of coordinates are
such that V, is in the direction of the eccentricity vector and U is in
the direction perpendicular to the eccentricity vector. The U - V co-
ordinates coincide with the X - Y coordinates, when $\phi_o = 0$. The
relationship between the fixed X - Y and the moving coordinate system

Fig.5.2: Coordinate System For Load And Displacement.
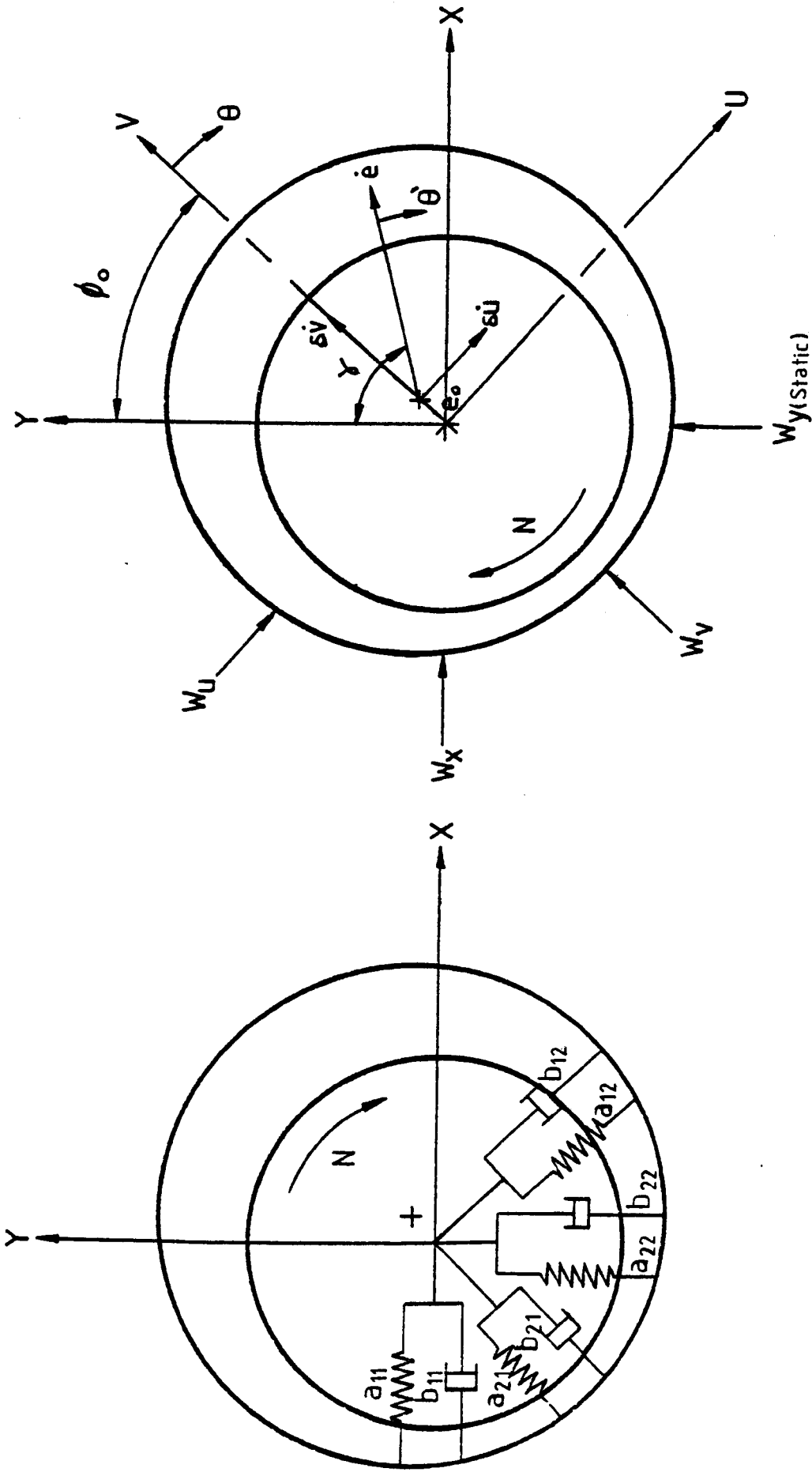
Fig.5.1: Representation Of The Bearing Fluid-Film
By Eight Linearized Coefficients.

may be written as:

$$
\begin{bmatrix} x \\ \\ y \end{bmatrix} = \begin{bmatrix} \cos \phi_o & \sin \phi_o \\ \\ -\sin \phi_o & \cos \phi_o \end{bmatrix} \begin{bmatrix} u \\ \\ v \end{bmatrix}
$$

$$
\begin{bmatrix} u \\ \\ v \end{bmatrix} = \begin{bmatrix} \cos \phi_o & -\sin \phi_o \\ \\ \sin \phi_o & \cos \phi_o \end{bmatrix} \begin{bmatrix} x \\ \\ y \end{bmatrix}
$$

(5.1)

For purely translational motions, the bearing reaction forces may be expressed as:

$$
\begin{aligned}
F_x &= F_x \ (x, y, \dot{x}, \dot{y}) \\
F_y &= F_y \ (x, y, \dot{x}, \dot{y})
\end{aligned}
$$

(5.2)

where:

x and y are the displacements of the journal centre,

$\dot{x}$ and $\dot{y}$ are the velocities of the journal centre.

At the static equilibrium position (x_o, y_o), the static bearing load, $W_{y(static)}$, is opposed by an equal and opposite force, F_{yo}, representing the integrated pressures in the fluid-film, such that:

$$
\begin{aligned}
W_{y(static)} &= -F_{yo} \\
W_{x(static)} &= -F_{xo} = 0
\end{aligned}
$$

(5.3)

The sign convention used is that, a force, such as W_y, is taken to be positive, if it acts in the same direction as Y.

Under dynamic conditions due to small perturbations of the journal centre, additional pressures are set up in the fluid-film, resulting in an increase of the fluid-film forces:

$$
\begin{aligned}
F_x &= F_{xo} + \delta F_x \\
F_y &= F_{yo} + \delta F_y
\end{aligned}
$$

(5.4)

A first order perturbation of equation (5.2) yields:

$$F_x = F_{xo} + \left(\frac{\partial F_x}{\partial x}\right)_o \delta x + \left(\frac{\partial F_x}{\partial y}\right)_o \delta y + \left(\frac{\partial F_x}{\partial \dot{x}}\right)_o \delta \dot{x} + \left(\frac{\partial F_x}{\partial \dot{y}}\right)_o \delta \dot{y}$$

(5.5)

$$F_y = F_{yo} + \left(\frac{\partial F_y}{\partial x}\right)_o \delta x + \left(\frac{\partial F_y}{\partial y}\right)_o \delta y + \left(\frac{\partial F_y}{\partial \dot{x}}\right)_o \delta \dot{x} + \left(\frac{\partial F_y}{\partial \dot{y}}\right)_o \delta \dot{y}$$

Hence, the equations of motion governing the relationship between small displacements from the equilibrium position and small disturbing forces giving rise to the displacement in the X and Y directions may be expressed as:

$$\begin{bmatrix} \delta F_x \\ \\ \delta F_y \end{bmatrix} = \begin{bmatrix} \left(\frac{\partial F_x}{\partial x}\right)_o & \left(\frac{\partial F_x}{\partial y}\right)_o \\ \\ \left(\frac{\partial F_y}{\partial x}\right)_o & \left(\frac{\partial F_y}{\partial y}\right)_o \end{bmatrix} \begin{bmatrix} \delta x \\ \\ \delta y \end{bmatrix} + \begin{bmatrix} \left(\frac{\partial F_x}{\partial \dot{x}}\right)_o & \left(\frac{\partial F_x}{\partial \dot{y}}\right)_o \\ \\ \left(\frac{\partial F_y}{\partial \dot{x}}\right)_o & \left(\frac{\partial F_y}{\partial \dot{y}}\right)_o \end{bmatrix} \begin{bmatrix} \delta \dot{x} \\ \\ \delta \dot{y} \end{bmatrix}$$

(5.6)

The subscript 'o' denotes that the derivatives are to be evaluated at the static equilibrium position. For convenience of representation, the partial derivatives may be written as:

$$\begin{bmatrix} \delta F_x \\ \\ \delta F_y \end{bmatrix} = \begin{bmatrix} -a_{11} & -a_{12} \\ \\ -a_{21} & -a_{22} \end{bmatrix} \begin{bmatrix} \delta x \\ \\ \delta y \end{bmatrix} + \begin{bmatrix} -b_{11} & -b_{12} \\ \\ -b_{21} & -b_{22} \end{bmatrix} \begin{bmatrix} \delta \dot{x} \\ \\ \delta \dot{y} \end{bmatrix}$$

(5.7)

The minus signs are due to the convention of W_x and W_y being positive in the same direction as X and Y respectively. The a's are the stiffness coefficients and the b's are the damping coefficients. The first index denotes the force direction and the second index denotes the displacement direction. The next requirement is concerned with the evaluation of these forces from lubrication theory, which will then lead to the evaluation of the 8 coefficients.

It should be noted that the coefficients are not only functions of the bearing type and bearing geometry, but also functions of the steady state journal position and the operating parameters such as speed, load and lubricant viscosity. Therefore, each operating point of the journal centre locus corresponds to different values of the eight coefficients.

Although the 8 linearized bearing dynamic coefficients have proved extremely useful in rotor-bearing dynamic analysis it is appropriate to mention the limitation of this approach. This method of rotor-dynamic analysis is limited by the lack of confidence in specifying the values of these coefficients. This is due in part to the use of specific assumptions, which are common in most bearing analysis, and in part, to the difficulties associated with their experimental determination. Until the present time, reports of theoretical studies far outnumber these from experimental investigations. Some factors that influence the accuracy of the linearized coefficients include:

(1) Thermal and elastic deformations which are usually not accounted for. Lund (15) pointed out that the errors, introduced by using the linearized coefficients are normally considerably smaller than those caused by the contributions from thermal and elastic deformations.

(2) The basic bearing analysis usually assumes constant lubricant viscosity and only accounts incompletely for film rupture.

There is a need for more accurate boundary conditions and to account for variations of fluid properties.

(3) Misalignment is usually neglected. Boncompain and Frene (13) have shown that some of the coefficients (a_{11}, b_{12} and b_{21}) were significantly affected compared to the well aligned case.

(3) The flow is usually assumed to be laminar. It has been shown that, for a given Sommerfeld number, the values of the 8 co-

efficients can vary substantially from the laminar flow values, particularly at high Reynolds number (17).

(5) The entry-ports, restrictors and feed-pressures are usually not adequately accounted for.

This thesis is concerned with the derivation of the 8 linearized bearing dynamic coefficients, subject to the assumptions stated in Section 5.4. It is hoped that this analysis will serve as a first step in a more comprehensive study of the subject of rotor-bearing dynamics involving externally pressurized bearings. In the subsequent sections of this chapter, the techniques developed for deriving the 8 linearized bearing dynamic coefficients of the slot-hybrid journal bearing are presented. A review of the analytical methods in bearing coefficients evaluation is included in Appendix VI.

5.3 The Dimensionless Coefficients

$$\bar{a}_{ij} = a_{ij} \ \frac{C}{P_s \, LD}$$

$$\bar{b}_{ij} = b_{ij} \ \frac{\omega_o \, C}{P_s \, LD}$$

This is the dimensionless form of the stiffness coefficients $(\bar{a}_{ij})$ and damping coefficients $(\bar{b}_{ij})$, used in hydrostatic and hybrid bearing analysis. In the hydrodynamic mode of lubrication, the dimensionless stiffness coefficients are normally presented as $\bar{a}_{ij} = a_{ij} \ \dfrac{C}{W}$

As the performance characteristics of hydrostatic and hybrid bearings are defined, even at zero speeds, it is, appropriate to make the dimensionless damping coefficients, independent of the journal rotational speed. Hence, an optimized angular rotational speed, ω_o, (the angular rotational speed at $S_h = S_{ho}$, that is, K = 1) is defined. For hydrodynamic bearings, the non-dimensional damping coefficients are usually expressed as, $\bar{b}_{ij} = b_{ij} \ \dfrac{\omega \, C}{W}$.

5.4 Assumptions

The assumptions stated in Section 4.4 together with the following assumption were employed in the derivation of the linearized bearing dynamic coefficients.

(1) The disturbing forces are sufficiently large to perturb the bearing from its steady-state position, and yet small enough to allow linearization to be observed.

5.5 Techniques Developed During the Present Investigation

Two methods of predicting the 8 linearized bearing dynamic coefficients of the double-entry slot hybrid journal bearing were developed during this investigation, namely:

(1) A Perturbation technique, and

(2) A Finite Disturbance technique.

The finite difference computer program developed in Chapter 4, was extended to produce the 8 bearing dynamic coefficients by either the perturbation or finite disturbance techniques. An extension of the lumped parameter program to produce the 8 bearing dynamic coefficients was also carried out, by employing the finite disturbance technique. A method for evaluating the stiffness coefficients from static loading characteristics is also presented. The present investigation, therefore, results in the development of three computer programs, each capable of providing information on both the static and the dynamic (8 bearing dynamic coefficients) characteristics. The three programs are:

(1) Perturbed finite difference program,

(2) Finite disturbance finite difference program, and

(3) Finite disturbance lumped parameter program.

5.6 The Perturbation Technique

The perturbation technique (small amplitude motion approach - see

Appendix VI) originally developed by Lund (15) for the analysis of hydrodynamic bearings, was extended to include hybrid bearing analysis. Generality of presentation was observed, so that this technique may be used for analysing any type of fluid-film bearings, such as, hydrostatic, hybrid or hydrodynamic bearings, although the emphasis is on the double-entry slot hybrid bearing.

5.6.1 Formulation of the Perturbed Lubrication Equations

A form of the dynamic state lubrication equation applied to a bearing with source flow (see Section 4.5.2) is:

$$\frac{\partial}{\partial x}\left(h^3 \frac{\partial P}{\partial x}\right) + \frac{\partial}{\partial z}\left(h^3 \frac{\partial P}{\partial z}\right) = 6\eta\, U\frac{\partial h}{\partial x} + 12\eta\, \frac{\partial h}{\partial t} - \frac{12\eta}{\rho} S_f$$

$$\ldots (5.8)$$

Let the small clearance perturbation be denoted by δh. Thus under dynamic conditions the film-thickness, h, may be expressed as:

$$h = h_o + \delta h \qquad (5.9)$$

The variation in the film-thickness, δh is associated with a perturbation in the film pressure:

$$P = P_o + \delta P \qquad (5.10)$$

together with a perturbation in the source flow:

$$S_f = S_{fo} + \delta S_f \qquad (5.11)$$

Substituting equations (5.9), (5.10) and (5.11) into the lubrication equation results in:

$$\frac{\partial}{\partial x}\left((h_o + \delta h)^3 \frac{\partial(P_o + \delta P)}{\partial x}\right) + \frac{\partial}{\partial z}\left((h_o + \delta h)^3 \frac{\partial(P_o + \delta P)}{\partial z}\right) = \cdots$$

$$\ldots\; 6\eta\, U\, \frac{\partial(h_o + \delta h)}{\partial x} + 12\eta\, \frac{\partial(h_o + \delta h)}{\partial t} - \frac{12\eta}{\rho}(S_{fo} + \delta S_f) \qquad (5.12)$$

By considering terms of zero and first order only, equation (5.12) may be expressed as:

$$\frac{\partial}{\partial x}\left(h_o{}^3 \frac{\partial P_o}{\partial x}\right) + \frac{\partial}{\partial z}\left(h_o{}^3 \frac{\partial P_o}{\partial z}\right) = 6\eta\, U\, \frac{\partial h_o}{\partial x} - \frac{12\eta}{\rho} S_{fo} \qquad (5.13)$$

and,

$$\frac{\partial}{\partial x}\left(h_o{}^3 \frac{\partial \delta P}{\partial x}\right) + \frac{\partial}{\partial z}\left(h_o{}^3 \frac{\partial \delta P}{\partial z}\right) = 6\eta \; U \frac{\partial \delta h}{\partial x} \quad \ldots$$

$$\ldots \; - \frac{3}{h_o} \; \delta h \; 6\eta \; U \frac{\partial h_o}{\partial x} - 3 \, h_o{}^3 \frac{\partial P_o}{\partial x} \; \frac{\partial}{\partial x}\left(\frac{\delta h}{h_o}\right) \quad \ldots$$

$$\ldots \; + \frac{\partial(\delta h)}{\partial t} 12\eta + \frac{3}{h_o}\; \delta h \left(\frac{12\eta}{\rho}\; S_{fo}\right) - \frac{12\eta}{\rho}\; \delta S_f \tag{5.14}$$

The first equation (equation 5.13) gives the static equilibrium

solution, which has been dealt with in Chapter 4. Equation (5.14)

provides the solution for the dynamic conditions. This equation is the

perturbed form of the lubrication equation, which has special relevance

for bearings incorporating source flows. In bearing computational

analysis, it is appropriate to work with moving U-V coordinates,

aligned with the eccentricity vector.

The dynamic pressure is governed by the excursions (δu, δv, $\delta \dot{u}$

and $\delta \dot{v}$) of the journal or bearing centre. It may be expressed as:

$$\delta P = P_u \; \delta u + P_v \; \delta v + P_{\dot{u}} \; \delta \dot{u} + P_{\dot{v}} \; \delta \dot{v} \tag{5.15a}$$

Similarly, δh, may be expressed as:

$$\delta h = \delta u \, \cos \, \theta + \delta v \, \sin \, \theta \tag{5.15b}$$

By substituting the expressions for δP and δh, into equation (5.14),

the following equation is obtained:

$$\left[\frac{\partial}{\partial x}\left(h_o{}^3 \frac{\partial P_u}{\partial x}\right) + \frac{\partial}{\partial z}\left(h_o{}^3 \frac{\partial P_u}{\partial z}\right)\right]\delta u + \left[\frac{\partial}{\partial x}\left(h_o{}^3 \frac{\partial P_v}{\partial x}\right) + \frac{\partial}{\partial z}\left(h_o{}^3 \frac{\partial P_v}{\partial z}\right)\right]\delta v \; \ldots$$

$$\ldots \; + \left[\frac{\partial}{\partial x}\left(h_o{}^3 \frac{\partial P_{\dot{u}}}{\partial x}\right) + \frac{\partial}{\partial z}\left(h_o{}^3 \frac{\partial P_{\dot{u}}}{\partial z}\right)\right]\delta \dot{u} + \left[\frac{\partial}{\partial x}\left(h_o{}^3 \frac{\partial P_{\dot{v}}}{\partial x}\right) + \frac{\partial}{\partial z}\left(h_o{}^3 \frac{\partial P_{\dot{v}}}{\partial z}\right)\right]\delta \dot{v} \; \ldots$$

$$\ldots \; = 6\eta \; U \frac{\partial}{\partial x}(\delta u \, \sin\theta + \delta v \, \cos\theta) - \frac{3}{h_o} 6\eta \; U \frac{\partial h_o}{\partial x}(\delta u \, \sin\theta + \delta v \, \cos\theta) \; \ldots$$

$$\ldots \; - 3 \, h_o{}^3 \frac{\partial P_o}{\partial x} \; \frac{\partial}{\partial x}\left(\frac{\delta u \, \sin\theta + \delta v \, \cos\theta}{h_o}\right) + 12\eta \frac{\partial}{\partial t}(\delta u \, \sin\theta + \delta v \, \cos\theta) \; \ldots$$

$$\ldots \; + \frac{3}{h_o}\left(\frac{12\eta}{\rho}\; S_{fo}\right)(\delta u \, \sin\theta + \delta v \, \cos\theta) - \frac{12\eta}{\rho}\; \delta S_f \tag{5.16}$$

In order to generalize the equation, the following terms are non-

dimensionalised:

$$\delta u = \delta \bar{u} \; C \qquad ; \qquad \delta v = \delta \bar{v} \; C$$

$$\delta \dot{u} = \delta \bar{\dot{u}} \; \omega_o \; C \; ; \qquad \delta \dot{v} = \delta \bar{\dot{v}} \; \omega_o \; C$$

$$h_o = H_o \; C \qquad ; \qquad x = XD$$

$$z = ZL \qquad ; \qquad t = {}^{\tau}\!/\!_{\omega_o}$$

$$P_o = \bar{P}_o \; P_s \qquad ; \qquad P_u = \bar{P}_u \; \frac{P_s}{C}$$

$$P_v = \bar{P}_v \; \frac{P_s}{C} \qquad ; \qquad P_{\dot{u}} = \bar{P}_{\dot{u}} \; \frac{P_s}{\omega_o \; C}$$

$$P_{\dot{v}} = \bar{P}_{\dot{v}} \; \frac{P_s}{\omega_o \; C} \quad ;$$

(5.17)

Substituting equation (5.17) into equation (5.16) and multiplying through by $\dfrac{D^2}{C \; P_s}$, and simplifying, results in equation 5.18

$$\left[\frac{\partial}{\partial X} \left(H_o{}^3 \; \frac{\partial \bar{P}_u}{\partial X} \right) + \frac{\partial}{\partial Z} \left(H_o{}^3 \; \frac{\partial \bar{P}_u}{\partial Z} \right) \left(\frac{D}{L} \right)^2 \right] \delta \bar{u} \; \ldots$$

$$\ldots + \left[\frac{\partial}{\partial X} \left(H_o{}^3 \; \frac{\partial \bar{P}_v}{\partial X} \right) + \frac{\partial}{\partial Z} \left(H_o{}^3 \; \frac{\partial \bar{P}_v}{\partial Z} \right) \left(\frac{D}{L} \right)^2 \right] \delta \bar{v} \; \ldots$$

$$\ldots + \left[\frac{\partial}{\partial X} \left(H_o{}^3 \; \frac{\partial \bar{P}_{\dot{u}}}{\partial X} \right) + \frac{\partial}{\partial Z} \left(H_o{}^3 \; \frac{\partial \bar{P}_{\dot{u}}}{\partial Z} \right) \left(\frac{D}{L} \right)^2 \right] \delta \bar{\dot{u}}$$

$$\ldots + \left[\frac{\partial}{\partial X} \left(H_o{}^3 \; \frac{\partial \bar{P}_{\dot{v}}}{\partial X} \right) + \frac{\partial}{\partial Z} \left(H_o{}^3 \; \frac{\partial \bar{P}_{\dot{v}}}{\partial Z} \right) \left(\frac{D}{L} \right)^2 \right] \delta \bar{\dot{v}}$$

$$\ldots = \left[48 \; \pi \; S_h \left(\frac{3}{H_o} \; \varepsilon \; \sin\theta \; \sin\theta \; + \; \cos\theta \right) \ldots \right.$$

$$\ldots - 6 \; H_o \; \frac{\partial \bar{P}_o}{\partial X} \left(H_o \; \cos\theta + \varepsilon \; \sin\theta \; \sin\theta \right) \ldots$$

$$\ldots + \frac{3}{H_o} \left(\frac{12\eta}{P_s \; C} \; q_{so} \left(\frac{D}{L} \right) \; \frac{1}{\Delta X \; \Delta Z} \right) \sin\theta \; \right] \delta \bar{u} \; \ldots$$

$$\ldots + \left[48 \; \pi \; S_h \left(\frac{3}{H_o} \; \varepsilon \; \sin\theta \; \cos\theta \; - \; \sin\theta \right) \ldots \right.$$

$$\ldots + 6 \; H_o \; \frac{\partial \bar{P}_o}{\partial X} \left(H_o \; \sin\theta - \varepsilon \; \sin\theta \; \cos\theta \right) \; \ldots$$

(5.18)

$$\cdots + \frac{3}{H_o} \left(\frac{12 \; \eta}{P_s \; C} \; q_{so} \left(\frac{D}{L} \right) \; \frac{1}{\Delta X \; \Delta Z} \right) \cos\theta \; \right] \; \delta\bar{v} \cdots$$

$$\cdots + \left[48 \; (2 \; \pi \; S_{ho}) \; \sin\theta \; \right] \delta\bar{u} \cdots$$

$$\cdots + \left[48 \; (2 \; \pi \; S_{ho}) \; \cos\theta \; \right] \delta\bar{v} \cdots$$

$$\cdots - \left(\frac{12\eta}{P_s \; C} \; \delta_{qs} \left(\frac{D}{L} \right) \; \frac{1}{\Delta X \; \Delta Z} \right).$$

Equation (5.18) represents a general form of the non-dimensional per-turbed lubrication equation. This equation is the starting point for the dynamic analysis of any specific bearing type. Any type of source flows may be treated by substituting the appropriate source terms in equation (5.18).

The following section is devoted to the application of equation (5.18) to double row slot-entry hybrid bearings. The first require-ment is to derive expressions of the source flows, q_{so} and δ_{qs}. A full derivation is presented in Appendix III. Substituting the expressions for source flows as derived in Appendix III, into equation (5.18) and rearranging terms results in the formation of four sets of partial differential equations, where the left hand side of the equations are all identical, and similar in form to equation (5.13), the steady state equation. It is more convenient to express this set of equations in matrix form. Therefore, the static and dynamic equations may be expressed as:

$$
\left[\frac{\partial}{\partial X}\left(H_o^{\;3}\frac{\partial}{\partial X}\right) + \left(\frac{D}{L}\right)^2\frac{\partial}{\partial Z}\left(H_o^{\;3}\frac{\partial}{\partial Z}\right) - \left(\frac{\pi\,D}{a\,n_s}\right)\left(\frac{n_s}{n_e}\right)\left(\frac{\beta}{1-\beta}\right)\left(\frac{D}{L}\right)\frac{1}{\Delta X\,\Delta Z} \right]
\left[\begin{array}{c} \bar{P}_o \\[4pt] \bar{P}_u \\[4pt] \bar{P}_v \\[4pt] \bar{P}_{\dot u} \\[4pt] \bar{P}_{\dot v} \end{array}\right] =
$$

$$
\left[
\begin{array}{l}
24\,\pi\,S_h\dfrac{\partial H_o}{\partial X} \; - \left(\dfrac{\pi D}{a\,n_s}\right)\left(\dfrac{n_s}{n_e}\right)\left(\dfrac{\beta}{1-\beta}\right)\left(\dfrac{D}{L}\right)\dfrac{1}{\Delta X\,\Delta Z}\;. \\[16pt]
48\,\pi\,S_h\left(\dfrac{3}{H_o}\,\varepsilon\,\sin\theta\;\sin\theta+\cos\theta\right) - 6H_o\dfrac{\partial\bar{P}_o}{\partial X}\left(H_o\cos\theta+\varepsilon\sin\theta\sin\theta\right)\ldots \\[16pt]
\ldots\; + \dfrac{3}{H_o}\,(1-\bar{P}_o)\left(\dfrac{\pi\,D}{a\,n_s}\right)\left(\dfrac{n_s}{n_e}\right)\left(\dfrac{\beta}{1-\beta}\right)\left(\dfrac{D}{L}\right)\dfrac{\sin\theta}{\Delta X\,\Delta Z}\;. \\[16pt]
48\,\pi\,S_h\left(\dfrac{3}{H_o}\,\varepsilon\sin\theta\;\cos\theta-\sin\theta\right) + 6H_o\dfrac{\partial\bar{P}_o}{\partial X}\left(H_o\sin\theta-\varepsilon\sin\theta\cos\theta\right)\ldots \\[16pt]
\ldots\; + \dfrac{3}{H_o}\,(1-\bar{P}_o)\left(\dfrac{\pi\,D}{a\,n_s}\right)\left(\dfrac{n_s}{n_e}\right)\left(\dfrac{\beta}{1-\beta}\right)\left(\dfrac{D}{L}\right)\dfrac{\cos\theta}{\Delta X\,\Delta Z}\;. \\[16pt]
48\,(2\,\pi\,S_{ho})\,\sin\theta\;. \\[10pt]
48\,(2\,\pi\,S_{ho})\,\cos\theta\;.
\end{array}
\right]
\tag{5.19}
$$

The first equation gives the static equilibrium solution, which has been dealt with in Chapter 4. The remaining four equations, give the solution for the dynamic pressures, which can be integrated to obtain the stiffness and damping coefficients. A full derivation of equations (5.19) is presented in Appendix VII. Equations (5.19) are readily solved numerically as finite difference equations.

5.6.2 Finite Difference Transformation

The finite difference form of equations (5.19) may be expressed as:

$$
\left[\; A_{i,j} \;\right]
\begin{bmatrix}
\bar{P}_{oi,j} \\
\bar{P}_{ui,j} \\
\bar{P}_{vi,j} \\
\bar{P}_{\dot{u}i,j} \\
\bar{P}_{\dot{v}i,j}
\end{bmatrix}
+
\left[\; E_{i+1} \;\right]
\begin{bmatrix}
\bar{P}_{oi+1,j} \\
\bar{P}_{ui+1,j} \\
\bar{P}_{vi+1,j} \\
\bar{P}_{\dot{u}i+1,j} \\
\bar{P}_{\dot{v}i+1,j}
\end{bmatrix}
+
\left[\; W_{i-1} \;\right]
\begin{bmatrix}
\bar{P}_{oi-1,j} \\
\bar{P}_{ui-1,j} \\
\bar{P}_{vi-1,j} \\
\bar{P}_{\dot{u}i-1,j} \\
\bar{P}_{\dot{v}i-1,j}
\end{bmatrix}
\cdots
$$

$$
\cdots +
\left[\; N_{i} \;\right]
\begin{bmatrix}
\bar{P}_{oi,j+1} \\
\bar{P}_{ui,j+1} \\
\bar{P}_{vi,j+1} \\
\bar{P}_{\dot{u}i,j+1} \\
\bar{P}_{\dot{v}i,j+1}
\end{bmatrix}
+
\left[\; S_{i} \;\right]
\begin{bmatrix}
\bar{P}_{oi,j-1} \\
\bar{P}_{ui,j-1} \\
\bar{P}_{vi,j-1} \\
\bar{P}_{\dot{u}i,j-1} \\
\bar{P}_{\dot{v}i,j-1}
\end{bmatrix}
=
\begin{bmatrix}
F_{oi,j} \\
F_{ui,j} \\
F_{vi,j} \\
F_{\dot{u}i,j} \\
F_{\dot{v}i,j}
\end{bmatrix}
\quad \ldots (5.20)
$$

where:

$$
A_{i,j} = \left(\frac{L}{D}\right) \frac{\Delta Z}{\Delta X} \left(H^3_{oi+\frac{1}{2}} + H^3_{oi-\frac{1}{2}} \right) + \left(\frac{D}{L}\right) \frac{\Delta X}{\Delta Z} \left(2.H^3_{oi} \right) \cdots
$$

$$
\cdots + \frac{\beta}{1-\beta} \left(\frac{\pi\, D}{a\, n_s} \right)\left(\frac{n_s}{n_e} \right) \lambda i,j .
$$

$$
E_{i+1} = -\left(\frac{L}{D}\right) \frac{\Delta Z}{\Delta X} \left(H^3_{oi+\frac{1}{2}} \right)
$$

$$
W_{i-1} = -\left(\frac{L}{D}\right) \frac{\Delta Z}{\Delta X} \left(H^3_{oi-\frac{1}{2}} \right)
$$

$$
N_{i} = S_{i} = -\left(\frac{D}{L}\right) \frac{\Delta X}{\Delta Z} \left(H^3_{oi} \right)
$$

$$
F_{oi,j} = 48\, \pi\, S_h\, \varepsilon\, \sin\theta i \left(\frac{L}{D}\right) \Delta X . \Delta Z \cdots
$$

$$
\cdots + \left(\frac{\beta}{1-\beta}\right)\left(\frac{\pi\, D}{a\, n_s} \right)\left(\frac{n_s}{n_e} \right) \lambda i,j
$$

$$F_{ui,j} = 48 \pi S_h \left(\frac{3}{H_{oi}} \varepsilon \sin\theta_i \sin\theta_i + \cos\theta_i \right) \left(\frac{L}{D} \right) \Delta X \Delta Z \ldots$$

$$\ldots + 3 H_{oi} \left(\bar{P}_{oi-1,j} - \bar{P}_{oi+1,j} \right) \left(H_{oi} \cos\theta_i + \varepsilon \sin\theta_i \sin\theta_i \right) \left(\frac{L}{D} \right) \Delta Z \ldots$$

$$\ldots + \frac{3}{H_{oi}} \left(1 - \bar{P}_{oi,j} \right) \left(\frac{\pi D}{a n_s} \right) \left(\frac{n_s}{n_e} \right) \left(\frac{\beta}{1-\beta} \right) \sin\theta_i \ \lambda_{i,j}.$$

$$F_{vi,j} = 48 \pi S_h \left(\frac{3}{H_{oi}} \varepsilon \sin\theta_i \cos\theta_i - \sin\theta_i \right) \left(\frac{L}{D} \right) \Delta X \Delta Z \ldots$$

$$\ldots + 3 H_{oi} \left(\bar{P}_{oi-1,j} - \bar{P}_{oi+1,j} \right) \left(H_{oi} \sin\theta_i - \varepsilon \sin\theta_i \cos\theta_i \right) \left(\frac{L}{D} \right) \Delta Z \ldots$$

$$\ldots + \frac{3}{H_{oi}} \left(1 - \bar{P}_{oi,j} \right) \left(\frac{\pi D}{a n_s} \right) \left(\frac{n_s}{n_e} \right) \left(\frac{\beta}{1-\beta} \right) \cos\theta_i \ \lambda_{i,j}.$$

$$F_{\dot{u}i,j} = 48 \left(2 \pi S_{ho} \right) \left(\frac{L}{D} \right) \Delta X \Delta Z \sin\theta_i.$$

$$F_{\dot{v}i,j} = 48 \left(2 \pi S_{ho} \right) \left(\frac{L}{D} \right) \Delta X \Delta Z \cos\theta_i.$$

$$(5.21)$$

In short notation, equations (5.20) may be written as:

$$A_{i,j} \ \bar{P}_{zi,j} \Big|_{z = o,u,v,\dot{u},\dot{v}} + E_{i+1} \ \bar{P}_{zi+1,j} \Big|_{z = o,u,v,\dot{u},\dot{v}} \ldots$$

$$\ldots + W_{i-1} \ \bar{P}_{zi-1,j} \Big|_{z=o,u,v,\dot{u},\dot{v}} + N_i \ \bar{P}_{zi,j+1} \Big|_{z = o,u,v,\dot{u},\dot{v}} \ldots$$

$$\ldots + S_i \ \bar{P}_{zi,j-1} \Big|_{z = o,u,v,\dot{u},\dot{v}} = F_{zi,j} \Big|_{z = o,u,v,\dot{u},\dot{v}} \ldots$$

$$(5.22)$$

Equations (5.22) are known as the steady and dynamic states slot-entry bearing finite difference equation.

5.6.3 Method of Solution

Equations (5.22) are in the same form as equation (4.23) of Chapter 4. At z = 'o', the steady state condition, equation (5.22) is, in fact, the exact equivalence of equation (4.23), the solution of which was discussed previously in Section 4.5.5. It is now necessary to solve for __five__ sets of equations instead of one, that is, one set

of equations (z = 'o') to determine the steady state characteristics, and another four sets of equations (z = u,v,$\dot{u}$,$\dot{v}$) to determine the stiffness and damping characteristics. Although, numerous numerical iterative and matrix techniques are available for the solution of equations such as equations (5.22), the successive relaxation method described in Section 4.5.4 was selected. The relaxation form of the equations for slot-entry bearings may be expressed as:

$$\left\{ \bar{P}_{zi,j}^{(L+1)} \left| \begin{array}{l} j = 2 \text{ to } (^{m}/2 + 1) \\ i = 1 \text{ to } n_e \end{array} \right\} \right|_{z = o,u,v,\dot{u},\dot{v}} = \bar{P}_{zi,j}^{(L)} + \frac{R}{A_i} \Big[F_{ij} \cdots$$

$$\cdots - E_{i+1} \bar{P}_{zi+1,j}^{(L)} - W_{i-1} \bar{P}_{zi-1,j}^{(L)} - N_i \bar{P}_{zi,j+1}^{(L)} \cdots$$

$$\cdots - S_i \bar{P}_{zi,j-1}^{(L)} - A_{ij} \bar{P}_{zi,j}^{(L)} \Big] \tag{5.23}$$

where:

R, is the relaxation factor, (R = 0.7), and

L, denotes the number of iterations.

Therefore, the dynamic solution requires that the procedures as described in Section 4.5.4 be repeated for a total of _five_ cycles.

Due to the fact that the operator (the left hand side of the equations) is common to all the five equations, the column matrix method (15) may be more efficient than the present method of successive relaxation, although it has not yet been implemented (see equation (5.19)).

5.6.4 Boundary Conditions

The boundary conditions stated in Section 4.5.5., together with the following conditions are employed for the dynamic analysis.

(1) For analytical convenience, the disturbing forces are not severe enough to cause variations in the cavitation boundaries, that is, regions that were cavitating in the static equilibrium condition, remain cavitating under

dynamic conditions without expansion or contraction in area.

(2) Under dynamic conditions, the dynamic pressures at the full-film regions may be either positive or negative in value. A negative value signifies that the dynamic pressure is less than its steady-state value, whilst, a positive value signifies that the dynamic pressure is greater than the corresponding steady-state value.

5.6.5 Bearing Coefficients Evaluation

It is convenient to resolve the reaction forces in the direction parallel and perpendicular to the line of eccentricity, that is, the V and U axes, respectively. The non-dimensional reaction forces expressed in the U - V coordinate system are as follows:

$$
\begin{bmatrix} \delta \bar{F}_u \\ \\ \delta \bar{F}_v \end{bmatrix} = \begin{bmatrix} \bar{\alpha}_{11} & \bar{\alpha}_{12} \\ \\ \bar{\alpha}_{21} & \bar{\alpha}_{22} \end{bmatrix} \begin{bmatrix} \delta \bar{u} \\ \\ \delta \bar{v} \end{bmatrix} + \begin{bmatrix} \bar{\beta}_{11} & \bar{\beta}_{12} \\ \\ \bar{\beta}_{21} & \bar{\beta}_{22} \end{bmatrix} \begin{bmatrix} \delta \dot{\bar{u}} \\ \\ \delta \dot{\bar{v}} \end{bmatrix} \qquad (5.24)
$$

$\bar{\alpha}_{i,j}$ are the displacement dependent terms, while, the velocity dependent terms are expressed by $\bar{\beta}_{ij}$, that is, the stiffness and damping co-efficients, respectively, expressed in the U - V coordinate system. These coefficients are evaluated by integrating the resolved components of the dynamic pressures over the whole mesh area:

$$
\begin{bmatrix} \bar{\alpha}_{11} \\ \\ \bar{\alpha}_{21} \end{bmatrix} = \overline{Area} \sum_{i=1}^{n_e} \sum_{j=1}^{m} - \bar{P}_{ui,j} \begin{bmatrix} \sin\theta_i \\ \\ \cos\theta_i \end{bmatrix}
$$

$$
\begin{bmatrix} \bar{\alpha}_{12} \\ \\ \bar{\alpha}_{22} \end{bmatrix} = \overline{Area} \sum_{i=1}^{n_e} \sum_{j=1}^{m} - \bar{P}_{vi,j} \begin{bmatrix} \sin\theta_i \\ \\ \cos\theta_i \end{bmatrix} \qquad \Bigg\} \quad (5.25)
$$

$$
\begin{bmatrix} \bar{\beta}_{11} \\ \\ \bar{\beta}_{21} \end{bmatrix} = \overline{Area} \sum_{i=1}^{n_e} \sum_{j=1}^{m} - \bar{P}_{\dot{u}i,j} \begin{bmatrix} \sin\theta_i \\ \\ \cos\theta_i \end{bmatrix}
$$

and,

$$\begin{bmatrix} \bar{\beta}_{12} \\ \\ \bar{\beta}_{22} \end{bmatrix} = \bar{\text{Area}} \sum_{i=1}^{n_e} \sum_{j=1}^{m} -\bar{P}_{vi,j} \begin{bmatrix} \sin\theta_i \\ \\ \cos\theta_i \end{bmatrix} \qquad (5.26)$$

Then utilizing the transformation given by equation (5.1):

$$\begin{bmatrix} \delta\bar{F}_x \\ \\ \delta\bar{F}_y \end{bmatrix} = \begin{bmatrix} \cos\phi_o & \sin\phi_o \\ \\ -\sin\phi_o & \cos\phi_o \end{bmatrix} \begin{bmatrix} \delta\bar{F}_u \\ \\ \delta\bar{F}_v \end{bmatrix} \qquad (5.27)$$

By substituting equation (5.24) into equation (5.27) and utilizing the relationship developed in equation (5.1), the following equations are obtained:

$$\begin{bmatrix} \delta\bar{F}_x \\ \\ \delta\bar{F}_y \end{bmatrix} = \begin{bmatrix} \cos\phi_o & \sin\phi_o \\ \\ -\sin\phi_o & \cos\phi_o \end{bmatrix} \begin{bmatrix} \bar{\alpha}_{11} & \bar{\alpha}_{12} \\ \\ \bar{\alpha}_{21} & \bar{\alpha}_{22} \end{bmatrix} \begin{bmatrix} \cos\phi_o & -\sin\phi_o \\ \\ \sin\phi_o & \cos\phi_o \end{bmatrix} \begin{bmatrix} \delta\bar{x} \\ \\ \delta\bar{y} \end{bmatrix} \cdots$$

$$\cdots + \begin{bmatrix} \cos\phi_o & \sin\phi_o \\ \\ -\sin\phi_o & \cos\phi_o \end{bmatrix} \begin{bmatrix} \bar{\beta}_{11} & \bar{\beta}_{12} \\ \\ \bar{\beta}_{21} & \bar{\beta}_{22} \end{bmatrix} \begin{bmatrix} \cos\phi_o & -\sin\phi_o \\ \\ \sin\phi_o & \cos\phi_o \end{bmatrix} \begin{bmatrix} \dot{\bar{x}} \\ \\ \delta\dot{\bar{y}} \end{bmatrix}$$

$$(5.28)$$

Equation (5.28) is now in a similar form to equation (5.7), that is:

$$\begin{bmatrix} \delta\bar{F}_x \\ \\ \delta\bar{F}_y \end{bmatrix} = \begin{bmatrix} \bar{a}_{11} & \bar{a}_{12} \\ \\ \bar{a}_{21} & \bar{a}_{22} \end{bmatrix} \begin{bmatrix} \delta\bar{x} \\ \\ \delta\bar{y} \end{bmatrix} + \begin{bmatrix} \bar{b}_{11} & \bar{b}_{12} \\ \\ \bar{b}_{21} & \bar{b}_{22} \end{bmatrix} \begin{bmatrix} \delta\dot{\bar{x}} \\ \\ \delta\dot{\bar{y}} \end{bmatrix}$$

Hence, the $\bar{a}_{ij}$ coefficients are given by:

$$\begin{bmatrix} \bar{a}_{11} & \bar{a}_{12} \\ \\ \bar{a}_{21} & \bar{a}_{22} \end{bmatrix} = \begin{bmatrix} (S_{11}\cos\phi_o + S_{12}\sin\phi_o) & (-S_{11}\sin\phi_o + S_{12}\cos\phi_o) \\ \\ (S_{21}\cos\phi_o + S_{22}\sin\phi_o) & (-S_{21}\sin\phi_o + S_{22}\cos\phi_o) \end{bmatrix}$$

$$(5.29)$$

where:

$$
\begin{bmatrix} S_{11} & S_{12} \\ \\ S_{21} & S_{22} \end{bmatrix} = \begin{bmatrix} (\cos\phi_o\ \bar{a}_{11} + \sin\phi_o\ \bar{a}_{21}) & (\cos\phi_o\ \bar{a}_{12} + \sin\phi_o\ \bar{a}_{22}) \\ \\ (-\sin\phi_o\ \bar{a}_{11} + \cos\phi_o\ \bar{a}_{21}) & (-\sin\phi_o\ \bar{a}_{12} + \cos\phi_o\ \bar{a}_{22}) \end{bmatrix}
$$

Similarly, $\bar{b}_{ij}$ coefficients are given by:

$$
\begin{bmatrix} \bar{b}_{11} & \bar{b}_{12} \\ \\ \bar{b}_{21} & \bar{b}_{22} \end{bmatrix} = \begin{bmatrix} (D_{11}\cos\phi_o + D_{12}\sin\phi_o) & (-D_{11}\sin\phi_o + D_{12}\cos\phi_o) \\ \\ (D_{21}\cos\phi_o + D_{22}\sin\phi_o) & (-D_{21}\sin\phi_o + D_{22}\cos\phi_o) \end{bmatrix}
$$

$$\dots \ (5.30)$$

where:

$$
\begin{bmatrix} D_{11} & D_{12} \\ \\ D_{21} & D_{22} \end{bmatrix} = \begin{bmatrix} (\cos\phi_o\ \bar{\beta}_{11} + \sin\phi_o\ \bar{\beta}_{21}) & (\cos\phi_o\ \bar{\beta}_{12} + \sin\phi_o\ \bar{\beta}_{22}) \\ \\ (-\sin\phi_o\ \bar{\beta}_{11} + \cos\phi_o\ \bar{\beta}_{21}) & (-\sin\phi_o\ \bar{\beta}_{12} + \cos\phi_o\ \bar{\beta}_{22}) \end{bmatrix}
$$

5.6.6 The Perturbed Finite Difference Computer Program (PFD.FOR)

The perturbed finite difference computer program (PFD.FOR), may be used to perform the following analysis:

(1) static analysis

(2) dynamic analysis, that is, the 8 linearized bearing dynamic

   coefficients.

In addition to the dimensionless input variables, stated in Section 4.5.8, the following input variables are also required:

(1) the maximum allowable residual for the dynamic conditions (ACC1)

(2) the relaxation factor for the dynamic conditions $(R1 = 0.7)$, and

(3) whether a static or dynamic analysis is required (DS).

The procedures involved in solving these five sets of finite difference lubrication equations are fully illustrated in the algorithm of figure (5.3). Figures (5.8a) to (5.16b) show the non-dimensional stiffness and damping coefficients predicted in this program. A discussion of the results is presented in Section 5.8.
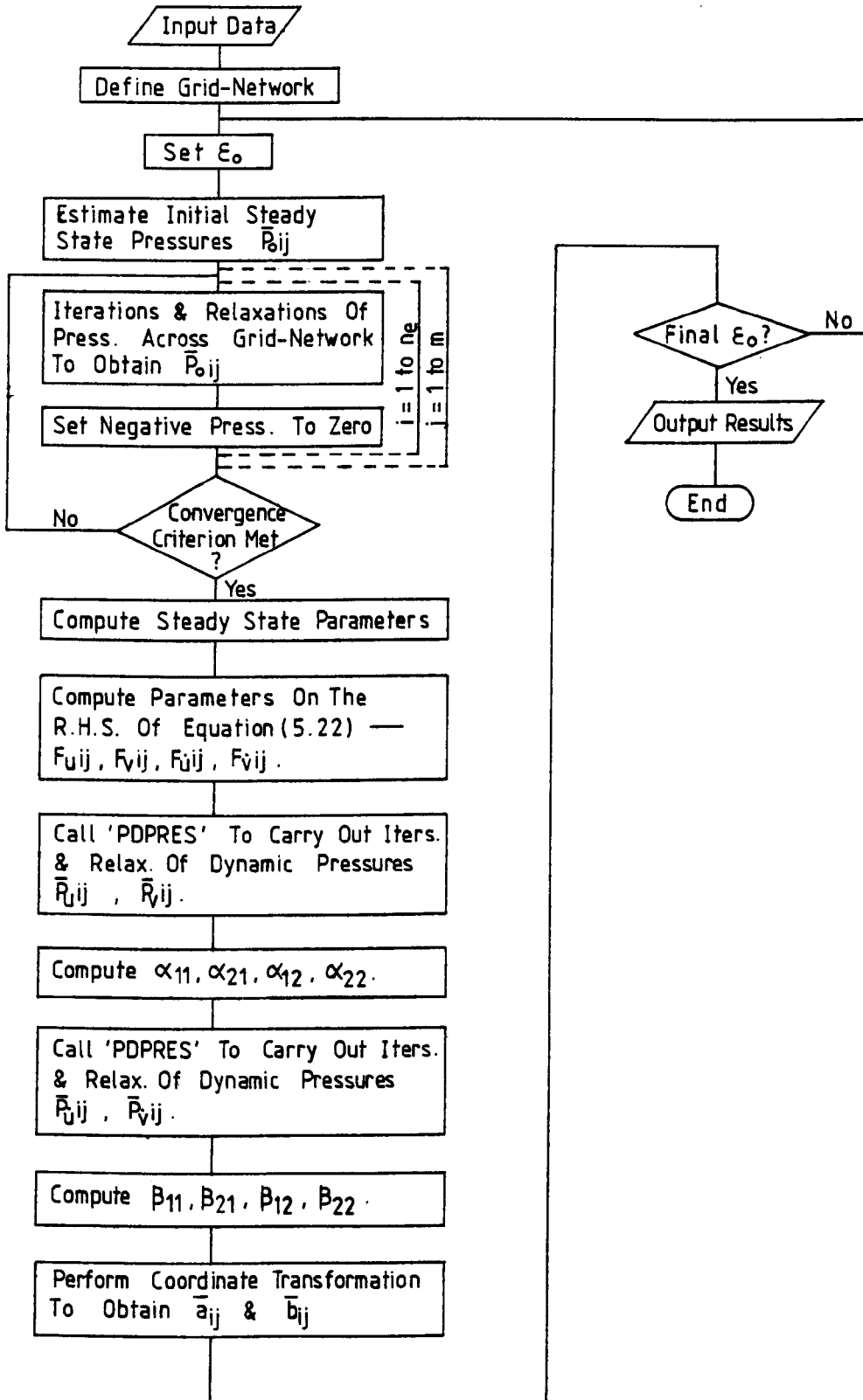
Fig. (5.3): Algorithm For Computing The Bearing Dynamic
Coefficients By The Perturbation Technique
— Program (PFD.FOR)

5.7 The Finite Disturbance Technique (See Appendix VI)

As with the Perturbation Technique, generality of presentation was observed, although attention was focussed on the double-entry slot hybrid journal bearing.

5.7.1 Formulation of the Finite Disturbance Technique

A form of the dynamic state generalized lubrication equation (Equation 5.8) has been presented in Section 5.6.1. Non-dimensionally equation (5.8) may be expressed as:

$$\frac{\partial}{\partial X} \left(H^3 \frac{\partial \bar{P}}{\partial X} \right) + \frac{\partial}{\partial Z} \left(H^3 \frac{\partial \bar{P}}{\partial Z} \right) = 24 \pi S_h \frac{\partial H}{\partial X} \ldots$$

$$\ldots + 48 \pi S_s \omega_o \frac{\partial H}{\partial \tau} \left(\frac{1}{\dot{\epsilon}} \right) - \frac{12 \eta D^2}{P_s C^3} \frac{S_f}{\rho} \ldots \tag{5.31}$$

where:

$$S_h = \frac{\eta N}{P_s} \left(\frac{D}{C_d} \right)^2$$

$$S_s = \frac{\eta \dot{\epsilon}}{P_s} \left(\frac{D}{C_d} \right)^2 \qquad \left.\begin{array}{c} \\ \\ \\ \end{array}\right\} \tag{5.32}$$

$$\tau = \omega_o t$$

The present analysis is carried out in the U - V coordinate system, that is, finite values of displacements (δu, δv) and velocities (u̇, v̇) are applied to the bearing centre (or the journal centre), in the directions perpendicular to and along the line of the corresponding steady-state eccentricity. Therefore, it is necessary to express $\frac{\partial H}{\partial \tau}$, in terms of the magnitude and direction of the dimensionless velocity of the dynamic bearing centre (or dynamic journal centre). This is illustrated in figure (5.2), where the velocity vector, $\dot{e}$, is acting at an angle, γ, to the vertical Y-axis. Non-dimensionally, the local film thickness, H, is expressed as:

$$H = 1 + \epsilon \cos\theta$$

$$\left. \frac{\partial H}{\partial \tau} \right|_{\theta = constant} = \frac{\dot{\epsilon}}{\omega_o} \cos (\theta - (\gamma - \phi_o))$$

that is,

$$\frac{\partial H}{\partial \tau} = \frac{\dot{\varepsilon}}{\omega_o} \cos\theta' \qquad (5.33)$$

where:

$$\theta' = \theta - (\gamma - \phi_o) \qquad (5.34)$$

γ, denotes the direction of the velocity vector,

measured from the vertical Y-axis.

ϕ_o, is the steady-state attitude angle.

Referring to figure (5.2), it can be seen that, if $\gamma - \phi_o = 0$, the

velocity vector will be directed along the V-direction, and, if

$\gamma - \phi_o = \pi/2$, the velocity vector will act in the U-direction.

Therefore, the finite disturbance form of the non-dimensional

generalized lubrication equation may be expressed as:

$$\frac{\partial}{\partial X}\left(H^3 \frac{\partial \bar{P}}{\partial X} \right) + \frac{\partial}{\partial Z}\left(H^3 \frac{\partial \bar{P}}{\partial Z} \right) = 24 \pi S_h \frac{\partial H}{\partial X} \dots$$

$$\dots + 48 S_s \cos\theta' - \frac{12 \eta D^2}{P_s C^3} \frac{S_f}{\rho} \qquad (5.35)$$

The dynamic conditions arising from the finite displacements

(δu, δv) and finite velocities ($\dot{u}$, $\dot{v}$) are illustrated in figures

(5.4) and (5.5) respectively. If such dynamic conditions occur, then

the bearing reaction forces, $\delta \bar{F}_u$ and $\delta \bar{F}_v$, may be expressed in terms of

the linearized bearing coefficients, as follows:

$$\begin{bmatrix} \delta\bar{F}_u \\ \\ \delta\bar{F}_v \end{bmatrix} = \begin{bmatrix} \bar{\alpha}_{11} & \bar{\alpha}_{12} \\ \\ \bar{\alpha}_{21} & \bar{\alpha}_{22} \end{bmatrix} \begin{bmatrix} \delta\bar{u} \\ \\ \delta\bar{v} \end{bmatrix} + \begin{bmatrix} \bar{\beta}_{11} & \bar{\beta}_{12} \\ \\ \bar{\beta}_{21} & \bar{\beta}_{22} \end{bmatrix} \begin{bmatrix} \dot{\bar{u}} \\ \\ \dot{\bar{v}} \end{bmatrix} \qquad (5.36)$$

It can be seen that the above equations have the same form as those of

equations (5.24). The $\bar{\alpha}_{ij}$ terms, are the stiffness coefficients expressed

in the U - V coordinate system, and the $\bar{\beta}_{ij}$ terms, are the damping co-

efficients.
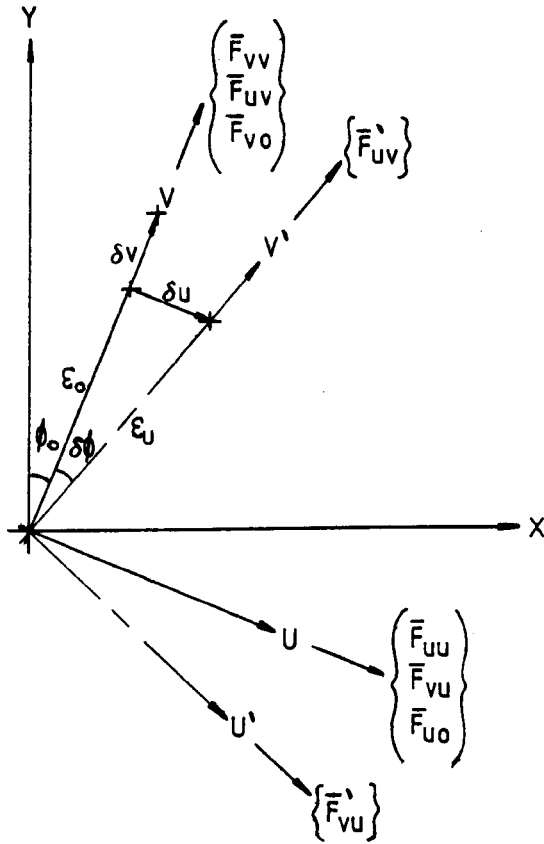
Fig. 5.4 : Finite Disturbance —— Stiffness
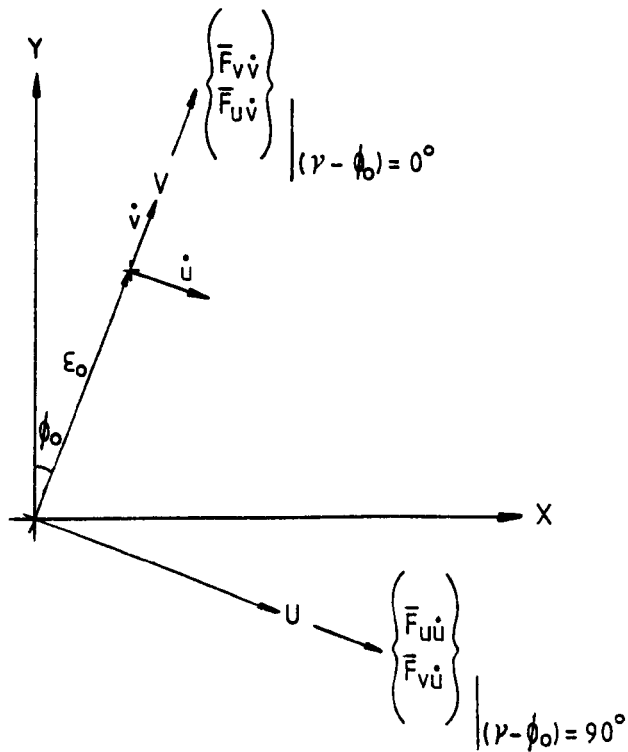
Fig.5.5 : Finite Disturbance —— Damping

5.7.1.1 Stiffness Coefficients

Consider figure (5.4). The equilibrium position of the bearing is defined by the eccentricity-ratio, ε_o, and the attitude angle ϕ_o. At this position, the total fluid-film forces expressed in the $U - V$ coordinate system are F_{uo} and F_{vo}. When the bearing centre is displaced to some position (ε_v, ϕ_o) by an amount $\delta\bar{v}$, and held there ($\delta\bar{u} = \bar{u} = \bar{v} = o$), the dimensionless bearing reaction forces trying to restore the bearing to the original position (ε_o, ϕ_o), may be written in terms of the displacement coefficients as:

$$\begin{bmatrix} \delta\bar{F}_{uv} \\ \\ \delta\bar{F}_{vv} \end{bmatrix} = \begin{bmatrix} \bar{\alpha}_{11} & \bar{\alpha}_{12} \\ \\ \bar{\alpha}_{21} & \bar{\alpha}_{22} \end{bmatrix} \begin{bmatrix} 0 \\ \\ \delta\bar{v} \end{bmatrix} \qquad (5.37)$$

from which,

$$\left.\begin{aligned} \bar{\alpha}_{12} &= \frac{\delta\bar{F}_{uv}}{\delta\bar{v}} \\ \\ \bar{\alpha}_{22} &= \frac{\delta\bar{F}_{vv}}{\delta\bar{v}} \end{aligned}\right\} \qquad (5.38)$$

where:

$$\left.\begin{aligned} \delta\bar{F}_{uv} &= \bar{F}_{uv}\Big|_{\varepsilon_v} - \bar{F}_{uo}\Big|_{\varepsilon_o} \\ \\ \delta\bar{F}_{vv} &= \bar{F}_{vv}\Big|_{\varepsilon_v} - \bar{F}_{uo}\Big|_{\varepsilon_o} \end{aligned}\right\} \qquad (5.39)$$

$$\varepsilon_v = \varepsilon_o + \delta\bar{v} \qquad (5.40)$$

By similar argument for the U-direction, let the bearing be displaced from the static equilibrium position ε_o, ϕ_o, by an amount, $\delta\bar{u}$, to a new position ε_u, $\phi_o + \delta\phi$, with $\delta\bar{v} = \bar{u} = \bar{v} = o$.

$$\begin{bmatrix} \delta\bar{F}_{uu} \\ \\ \delta\bar{F}_{vu} \end{bmatrix} = \begin{bmatrix} \bar{\alpha}_{11} & \bar{\alpha}_{12} \\ \\ \bar{\alpha}_{21} & \bar{\alpha}_{22} \end{bmatrix} \begin{bmatrix} \delta\bar{u} \\ \\ 0 \end{bmatrix} \qquad (5.41)$$

from which,

$$\bar{\alpha}_{11} = \frac{\delta \bar{F}_{uu}}{\delta \bar{u}}$$

$$\bar{\alpha}_{21} = \frac{\delta \bar{F}_{vu}}{\delta \bar{u}}$$

$$\left.\begin{array}{c} \\ \\ \\ \\ \\ \end{array}\right\} \quad (5.42)$$

where:

$$\delta \bar{F}_{uu} = \bar{F}_{uu}\bigg|_{\varepsilon_u} - \bar{F}_{uo}\bigg|_{\varepsilon_o}$$

$$\delta \bar{F}_{vu} = \bar{F}_{vu}\bigg|_{\varepsilon_u} - \bar{F}_{vo}\bigg|_{\varepsilon_o}$$

$$\left.\begin{array}{c} \\ \\ \\ \\ \end{array}\right\} \quad (5.43)$$

As the eccentricity vector, ε_u, is shifted by an angle, $\delta\phi$, relative to the V-axis, a coordinate transformation is required, to obtain the fluid-film forces $\bar{F}_{uu}$ and $\bar{F}_{vu}$, that is:

$$\begin{bmatrix} F_{uu} \\ \\ F_{vu} \end{bmatrix} = \begin{bmatrix} \cos\delta\phi & \sin\delta\phi \\ \\ -\sin\delta\phi & \cos\delta\phi \end{bmatrix} \begin{bmatrix} \bar{F}'_{uu} \\ \\ \bar{F}'_{vu} \end{bmatrix} \qquad (5.44)$$

where:

$\bar{F}'_{uu}$, is the total dimensionless fluid film force resolved

in the direction perpendicular to the vector ε_u.

$\bar{F}'_{vu}$, is the total dimensionless fluid film force resolved

in the direction parallel to the vector ε_u.

Furthermore, by reference to figure (5.3a), the following trigono-metrical relationships may be written for ε_u and $\delta\phi$:

$$\varepsilon_u = (\varepsilon_o^2 + \delta\bar{u}^2)^{\frac{1}{2}} \qquad (5.45)$$

$$\delta\phi = \tan^{-1}\left(\frac{\delta\bar{u}}{\varepsilon_o}\right) \qquad (5.46)$$

Although it is essential to compute the coefficients for both positive and negative values of $\delta\bar{u}$ and $\delta\bar{v}$ and then to take the averaged values, the present analysis showed that accurate results may be obtained by computing for several positive values of $\delta\bar{u}$ and $\delta\bar{v}$. The co-efficients

are then determined by performing a linear regression of the incremental fluid-film forces on the finite displacements, that is, the principle of least squares is used. Consider the figure below:
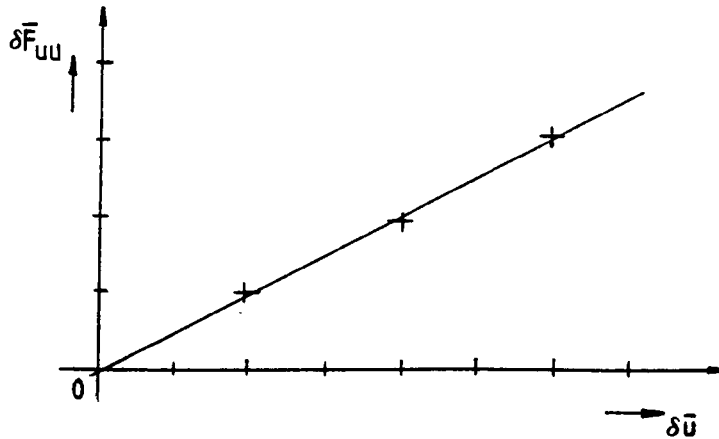
Graph showing the variation of $\delta\bar{F}_{uu}$ with $\delta\bar{u}$

The equation of a straight line may be used to represent the data, that is:

$$(\delta\bar{F}_{uui})_c \Bigg|_{i=1}^{n_c} = \bar{\alpha}_{11} \; \delta u_i \Bigg|_{i=1}^{n_c} + \; a_o \qquad (5.47)$$

where:

$\bar{\alpha}_{11}$, represents the gradient of the straight line, and, hence the stiffness coefficient.

a_o, is the intercept on the vertical axis, which equals zero.

n_c, is the total number of data points.

$(\delta\bar{F}_{uui})c$, is the value of the incremental fluid-film force derived from equation (5.47).

Applying the principle of least squares:

$$\sum_{i=1}^{n_c} (\delta\bar{F}_{uui} - (\delta\bar{F}_{uui})_c)^2 = E \qquad (5.48)$$

Equation (5.48) may be rewritten as:

$$E = \sum_{i=1}^{n_c} (\delta F_{uui} - \bar{\alpha}_{11} \, \delta \bar{u}i - a_o)^2 \qquad (5.49)$$

The next procedure is to minimize E, that is, minimize the sum of the squares of the deviations of the $\delta \bar{F}_{uui}$ values. Thus:

$$\frac{\partial E}{\partial a_o} = \sum_{i=1}^{n_c} -2 \, (\delta \bar{F}_{uui} - \bar{\alpha}_{11} \, \delta \bar{u}_i - a_o) = o$$

$$\frac{\partial E}{\partial (\bar{\alpha}_{11})} = \sum_{i=1}^{n_c} 2 \, (\delta \bar{F}_{uui} - \bar{\alpha}_{11} \, \delta \bar{u}_i - a_o)(-\delta \bar{u}_i) = o$$

The above equations may be rearranged as:

$$\left. \begin{array}{l} n_c \, a_o + \left(\sum\limits_{i=1}^{n_c} \delta \bar{u}_i \right) \bar{\alpha}_{11} = \left(\sum\limits_{i=1}^{n_c} \delta \bar{F}_{uui} \right) \\[2em] \left(\sum\limits_{i=1}^{n_c} \delta \bar{u}_i \right) a_o + \left(\sum\limits_{i=1}^{n_c} \delta \bar{u}_i^2 \right) \bar{\alpha}_{11} = \left(\sum\limits_{i=1}^{n_c} \delta \bar{u}_i \, \delta \bar{F}_{uui} \right) \end{array} \right\} \qquad (5.50)$$

Hence, equations (5.50) may be solved to obtain expressions for $\bar{\alpha}_{11}$.

$$\bar{\alpha}_{11} = \frac{n_c \left(\sum\limits_{i=1}^{n_c} \delta \bar{u}_i \, \delta \bar{F}_{uui} \right) - \left(\sum\limits_{i=1}^{n_c} \delta \bar{u}_i \, \sum\limits_{i=1}^{n_c} \delta \bar{F}_{uui} \right)}{n_c \left(\sum\limits_{i=1}^{n_c} \delta \bar{u}_i^2 \right) - \left(\sum\limits_{i=1}^{n_c} \delta \bar{u}_i \right)^2} \qquad (5.51)$$

Analogously, the remaining three coefficients $\bar{\alpha}_{12}$, $\bar{\alpha}_{21}$, $\bar{\alpha}_{22}$ may be arrived at in a similar manner. By substituting for the appropriate incremental force and displacement terms in equation (5.51), the corresponding $\bar{\alpha}_{i,j}$ coefficients are determined. The stiffness coefficients, $\bar{a}_{ij}$ may then be obtained using equation (5.29).

Briefly, the computational procedure may be summarised as follows:

(a) Select a position, ε_o, on the static load locus and compute the

static values, $\bar{F}_{uo}$, $\bar{F}_{vo}$ and ϕ_o.

(b) Choose small values of $\delta\bar{u}$ and $\delta\bar{v}$, and hence, calculate ε_u, ε_v and $\delta\phi$ from equations (5.45), (5.40) and (5.46) respectively.

(c) Compute the total fluid-film forces $\bar{F}_{uv}$, $\bar{F}_{vv}$ and $\bar{F}'_{uu}$, $\bar{F}'_{vu}$ for the eccentricity-ratios ε_v and ε_u, respectively.

(d) Perform a coordinate transformation using equations (5.44) to obtain the fluid-film forces $\bar{F}_{uu}$ and $\bar{F}_{vu}$.

(e) Calculate the four incremental fluid-film forces $\delta\bar{F}_{uv}$, $\delta\bar{F}_{vv}$ and $\delta\bar{F}_{uu}$, $\delta\bar{F}_{vu}$ from equations (5.39) and (5.43).

(f) Increase the values of $\delta\bar{u}$ and $\delta\bar{v}$, and repeat the procedures outlined in steps (b) to (e), until a minimum of three sets of incremental fluid-film forces are obtained.

(g) Calculate the $\bar{\alpha}_{i,j}$ coefficients using equation (5.51).

(h) Determine the stiffness coefficients, $\bar{a}_{i,j}$, using equation (5.29).

5.7.1.2 Damping Coefficients

Consider figure (5.5). Assume that the bearing is now operating at the steady-state position, (ε_o, ϕ_o), an instantaneous velocity of magnitude $\bar{v}$, is applied to the bearing centre in the V-direction ($\delta u = \delta v = \bar{\dot{u}} = o$; $\bar{\dot{v}} \neq o$). The fluid film forces are:

$$\begin{bmatrix} \delta\bar{F}_{u\dot{v}} \\ \\ \delta\bar{F}_{v\dot{v}} \end{bmatrix} = \begin{bmatrix} \bar{\beta}_{11} & \bar{\beta}_{12} \\ \\ \bar{\beta}_{21} & \bar{\beta}_{22} \end{bmatrix} \begin{bmatrix} 0 \\ \\ \bar{\dot{v}} \end{bmatrix} \qquad (5.52)$$

from which,

$$\bar{\beta}_{12} = \frac{\delta\bar{F}_{u\dot{v}}}{\bar{\dot{v}}}$$

$$\left.\begin{array}{c} \\ \\ \\ \\ \end{array}\right\} \qquad (5.53)$$

$$\bar{\beta}_{22} = \frac{\delta\bar{F}_{v\dot{v}}}{\bar{\dot{v}}}$$

where:

$$\delta \bar{F}_{u\dot{v}} = \bar{F}_{u\dot{v}}\bigg|_{(\gamma-\phi_o)=o} - \bar{F}_{uo}\bigg|_{\varepsilon_o}$$

$$\delta \bar{F}_{v\dot{v}} = \bar{F}_{v\dot{v}}\bigg|_{(\gamma-\phi_o)=o} - \bar{F}_{vo}\bigg|_{\varepsilon_o} \quad \Biggr\} \quad (5.54)$$

Similarly, for $\bar{u}$ applied along the U-axis ($\delta\bar{u} = \delta\bar{v} = \bar{v} = o$; $\bar{u} \neq o$):

$$\begin{bmatrix} \delta F_{u\dot{u}} \\ \delta F_{v\dot{u}} \end{bmatrix} = \begin{bmatrix} \bar{\beta}_{11} & \bar{\beta}_{12} \\ \bar{\beta}_{21} & \bar{\beta}_{22} \end{bmatrix} \begin{bmatrix} \bar{u} \\ 0 \end{bmatrix} \qquad (5.55)$$

from which,

$$\bar{\beta}_{11} = \frac{\delta\bar{F}_{u\dot{u}}}{\bar{u}}$$

$$\bar{\beta}_{21} = \frac{\delta\bar{F}_{v\dot{u}}}{\bar{u}} \quad \Biggr\} \quad (5.56)$$

where:

$$\delta\bar{F}_{u\dot{u}} = \bar{F}_{u\dot{u}}\bigg|_{(\gamma-\phi_o)=\frac{\pi}{2}} - \bar{F}_{uo}\bigg|_{\varepsilon_o}$$

$$\delta\bar{F}_{v\dot{u}} = \bar{F}_{v\dot{u}}\bigg|_{(\gamma-\phi_o)=\frac{\pi}{2}} - \bar{F}_{vo}\bigg|_{\varepsilon_o} \quad \Biggr\} \quad (5.57)$$

It is more convenient to express the dimensionless velocity vectors $(\bar{u}, \bar{v})$, in terms of the non-dimensional parameter, S_s, which is the squeeze parameter, $\left(S_s = \frac{\eta\dot{\varepsilon}}{P_s}\left(\frac{D}{C_d}\right)^2\right)$, and the optimized speed parameter, S_{ho}.

Hence,

$$\frac{S_s}{S_{ho}} = \frac{\dfrac{\eta\dot{\varepsilon}}{P_s}\left(\dfrac{D}{C_d}\right)^2}{\dfrac{\eta N_o}{P_s}\left(\dfrac{D}{C_d}\right)^2}$$

from which,

$$\dot{\varepsilon} = \frac{N_o S_s}{S_{ho}}$$

$$= \frac{\omega_o \, S_s}{2 \, \pi \, S_{ho}}$$

or,

$$\bar{\varepsilon} = \frac{S_s}{2 \, \pi \, S_{ho}}$$

where:

$$\bar{\varepsilon} = \frac{\dot{e}}{\omega_o \, C}$$

Thus, the dimensionless velocity vectors, $(\bar{u}, \bar{v})$ may be expressed as:

$$\bar{u} = \bar{v} = \frac{S_s}{2 \, \pi \, S_{ho}} \qquad (5.58)$$

Therefore, instead of specifying the values of $\bar{u}$, $\bar{v}$ directly, the velocity vectors $(\bar{u}, \bar{v})$, are derived from equation (5.58) for a given value of S_s. Again, computations were carried out for several positive values of $\bar{u}$, $\bar{v}$ and the linear least squares fitting technique as outlined in Section 5.7.1.1, was used to determine the $\bar{\beta}_{ij}$ coefficients. A coordinate transformation to the conventional X - Y coordinate system, using equation (5.30) will produce the $\bar{b}_{ij}$, coefficients. Thus, the computational procedure may be summarised as:

(a) Select a value of ε_o, on the static load locus and compute $\bar{F}_{uo}$, $\bar{F}_{vo}$ and ϕ_o.

(b) Define direction of velocity vector (i.e. $\gamma - \phi_o = 0$ or $\frac{\pi}{2}$) and choose small values of S_s for the respective direction.

(c) Calculate the dimensionless velocities $(\bar{u}, \bar{v})$ using equation (5.58), for the directions $(\gamma - \phi_o) = \frac{\pi}{2}$ and $(\gamma - \phi_o) = 0$, respectively.

(d) Compute the film forces $\bar{F}_{u\dot{v}}\Big|_{(\gamma-\phi_o) \, = \, 0}$, $\bar{F}_{v\dot{v}}\Big|_{(\gamma-\phi_o) \, = \, 0}$ and $\bar{F}_{u\dot{u}}\Big|_{(\gamma-\phi_o) \, = \, \frac{\pi}{2}}$, $\bar{F}_{v\dot{u}}\Big|_{(\gamma-\phi_o) \, = \, \frac{\pi}{2}}$ for the eccentricity-ratio, ε_o, and setting $(\gamma - \phi_o) = 0$ and $(\gamma - \phi_o) = \frac{\pi}{2}$ respectively.

(e)   Calculate the four incremental film-forces $\delta \bar{F}_{u\dot{v}}\Big|_{(\gamma-\phi_o)\ =\ o}$,

$\delta \bar{F}_{v\dot{v}}\Big|_{(\gamma-\phi_o)\ =\ o}$ and $\delta \bar{F}_{u\dot{u}}\Big|_{(\gamma-\phi_o)\ =\ \frac{\pi}{2}}$, $\delta \bar{F}_{v\dot{u}}\Big|_{(\gamma-\phi_o)\ =\ \frac{\pi}{2}}$ from

equations (5.54) and (5.57).

(f)   Increase the values of S_s, and repeat the procedures outlined in

steps (b) to (e), until a minimum of three sets of incremental

film forces are obtained.

(g)   Calculate the $\bar{\beta}_{ij}$, coefficients using equation (5.51).

(h)   The damping coefficients, $\bar{b}_{i.j}$, may then be determined using

equations (5.30).

5.7.1.3   Stiffness Coefficients - Static Load Locus Method

Consider the figure below, where the equilibrium position of the

bearing is defined by the eccentricity-ratio, ε_o, and attitude angle,

ϕ_o. Under this condition, the fluid-film forces resolved in the U - V

coordinate system are given by $\bar{F}_{uo}$ and $\bar{F}_{vo}$.
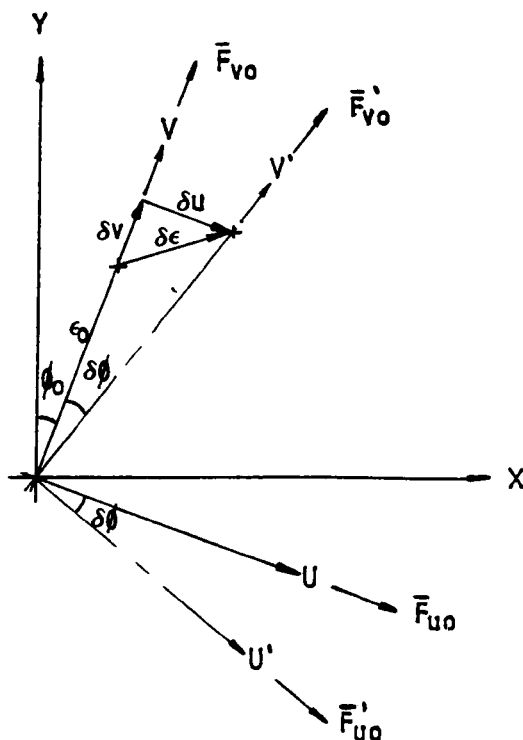
Figure illustrating the coordinate system for load and displacement

The fluid-film forces are governed by the magnitude and direction of the eccentricity vector, ε and ϕ, respectively. Hence,

$$\left.\begin{array}{l} \bar{F}_{uo} = \bar{F}_{uo} \ (\varepsilon, \ \phi) \\[12pt] \bar{F}_{vo} = \bar{F}_{vo} \ (\varepsilon, \ \phi) \end{array}\right\} \qquad (5.59)$$

From the calculus of small variations, the change in fluid-film forces, due to a small change in eccentricity-ratio, $\delta\varepsilon$, and a corresponding variation of the attitude angle, by a small amount, $\delta\phi$, may be expressed as:

$$\begin{bmatrix} \delta\bar{F}_{uo} \\[12pt] \delta\bar{F}_{vo} \end{bmatrix} = \begin{bmatrix} \dfrac{\partial\bar{F}_{uo}}{\partial\varepsilon} & \dfrac{\partial\bar{F}_{uo}}{\partial\phi} \\[16pt] \dfrac{\partial\bar{F}_{vo}}{\partial\varepsilon} & \dfrac{\partial\bar{F}_{vo}}{\partial\phi} \end{bmatrix} \begin{bmatrix} \delta\varepsilon \\[12pt] \delta\phi \end{bmatrix} \qquad (5.60)$$

where:

    ε, is the steady-state eccentricity-ratio, i.e. $\varepsilon = \varepsilon_o$.

    ϕ, is the steady-state attitude angle, i.e. $\phi = \phi_o$.

If $\delta\varepsilon << 0$ and $\delta\phi << 0$, then:

$$\left.\begin{array}{l} \delta\bar{v} = \delta\varepsilon \\[12pt] \delta\bar{u} = \varepsilon \ \delta \ \phi \end{array}\right\} \qquad (5.61)$$

The static equilibrium fluid-film forces, $\bar{F}_{uo}$ and $\bar{F}_{vo}$, may be expressed in relation to their resolved components in the U' - V' coordinate system, as:

$$\begin{bmatrix} \bar{F}'_{uo} \\[12pt] \bar{F}'_{vo} \end{bmatrix} = \begin{bmatrix} \cos\delta\phi & -\sin\delta\phi \\[12pt] \sin\delta\phi & \cos\delta\phi \end{bmatrix} \begin{bmatrix} \bar{F}_{uo} \\[12pt] \bar{F}_{vo} \end{bmatrix} \qquad (5.62)$$

where:

    $\bar{F}'_{uo}$, is the steady-state film force resolved along the U'-axis.

    $\bar{F}'_{vo}$, is the steady-state film force resolved along the V'-axis.

Again, if $\delta \phi < < 0$; equation (5.63) may be rewritten as:

$$
\begin{bmatrix} \bar{F}'_{uo} \\ \\ \bar{F}'_{vo} \end{bmatrix} = \begin{bmatrix} 1 & -\delta\phi \\ \\ \delta\phi & 1 \end{bmatrix} \begin{bmatrix} \bar{F}_{uo} \\ \\ \bar{F}_{vo} \end{bmatrix}
$$

(5.63)

Equations (5.63) may be rewritten as:

$$
\delta\phi \, \bar{F}_{vo} = \bar{F}_{uo} - \bar{F}'_{uo}
$$

and,

$$
-\delta\phi \, \bar{F}_{uo} = \bar{F}_{vo} - \bar{F}'_{vo}
$$

Hence, the above equations may be expressed as:

$$
\delta\phi \, \bar{F}_{vo} = \delta\bar{F}_{uo}
$$

and,

$$
-\delta\phi \, \bar{F}_{uo} = \delta\bar{F}_{vo}
$$

Thus:

$$
\left. \frac{\delta\bar{F}_{uo}}{\delta\phi} \right|_{\phi \to o} = \frac{\partial\bar{F}_{uo}}{\partial\phi} = \bar{F}_{vo}
$$

and

$$
\left. \frac{\delta\bar{F}_{vo}}{\delta\phi} \right|_{\phi \to o} = \frac{\partial\bar{F}_{vo}}{\partial\phi} = - \bar{F}_{uo}
$$

(5.64)

It is now possible to rewrite equation (5.60) using the expressions defined in equations (5.61) and (5.64).

$$
\begin{bmatrix} \delta\bar{F}_{uo} \\ \\ \delta\bar{F}_{vo} \end{bmatrix} = \begin{bmatrix} \dfrac{\bar{F}_{vo}}{\epsilon} & \dfrac{\partial\bar{F}_{uo}}{\partial\epsilon} \\ \\ \dfrac{-\bar{F}_{uo}}{\epsilon} & \dfrac{\partial\bar{F}_{vo}}{\partial\epsilon} \end{bmatrix} \begin{bmatrix} \delta\bar{u} \\ \\ \delta\bar{v} \end{bmatrix}
$$

(5.65)

Equations (5.65) are now in a similar form to equations (5.37) and (5.41), and may be expressed in terms of the $\bar{\alpha}_{ij}$ coefficients, as:

$$
\begin{bmatrix} \bar{\alpha}_{11} & \bar{\alpha}_{12} \\ \\ \bar{\alpha}_{21} & \bar{\alpha}_{22} \end{bmatrix} = \begin{bmatrix} \dfrac{\bar{F}_{vo}}{\varepsilon} & \dfrac{\partial \bar{F}_{uo}}{\partial \varepsilon} \\ \\ \dfrac{-\bar{F}_{uo}}{\varepsilon} & \dfrac{\partial \bar{F}_{vo}}{\partial \varepsilon} \end{bmatrix} \qquad (5.66)
$$

It can be seen from equation (5.66) that the $\bar{\alpha}_{ij}$ terms, are determined purely from static loading characteristics. A polynomial least square curve-fitting routine adapted from reference (1), was written, to provide analytical expressions governing the static load and the eccentricity-ratio, so that the derivatives may be evaluated more accurately. A coordinate transformation may then be carried out, using equation (5.29), to determine the stiffness coefficients, $\bar{a}_{ij}$, in the conventional X - Y coordinate system.

5.7.2 Finite Difference Transformation

By following the arguments outlined in Section 4.5.3, the finite difference form of equation (5.35) for the finite disturbance case may be expressed as:

$$
A_{i,j}\,\bar{P}_{i,j} + E_{i+1}\,\bar{P}_{i+1,j} + W_{i-1,}\,\bar{P}_{i-1,j} \cdots
$$

$$
\cdots + N_i\,\bar{P}_{i,j+1} + S_i\,\bar{P}_{i,j-1} = F_{i,j} \qquad (5.67)
$$

where:

$$
A_{i,j} = \left(\frac{L}{D}\right)\frac{\Delta Z}{\Delta X}\,(H^3_{i+\frac{1}{2}} + H^3_{i-\frac{1}{2}}) + \left(\frac{D}{L}\right)\frac{\Delta X}{\Delta Z}\,(2\,H^3_i) \cdots
$$

$$
\cdots + \frac{\beta}{1-\beta}\left(\frac{\pi\,D}{a\,n_s}\right)\left(\frac{n_s}{n_e}\right)\lambda_{i,j}
$$

$$
E_{i+1} = -\left(\frac{L}{D}\right)\frac{\Delta Z}{\Delta X}\,(H^3_{i+\frac{1}{2}})
$$

$$
W_{i-1} = -\left(\frac{L}{D}\right)\frac{\Delta Z}{\Delta X}\,(H^3_{i-\frac{1}{2}})
$$

$$
N_i = S_i = -\left(\frac{D}{L}\right)\frac{\Delta X}{\Delta Z}\,(H_i{}^3), \text{ and}
$$

$$(5.68)$$

$$F_{i,j} = 48 \pi S_h \quad \sin\theta_i \left(\frac{L}{D}\right) \Delta X \, \Delta Z \, \ldots$$

$$\ldots + 48 S_s \cos\theta_i' + \frac{\beta}{1-\beta} \left(\frac{\pi D}{a \, n_s}\right)\left(\frac{n_s}{n_e}\right) \lambda_{i,j}$$

5.7.2.1 Method of Solution

The method of successive relaxation as outlined in Section 4.5.4 was employed to solve equation (5.68). Based upon the criteria of stability and speed of convergence, a relaxation factor, R1 = 0.7, (determined by trial and error) was used. Therefore, the relaxation form of the Slot-Entry Bearing Finite Disturbance Equation may be formally written as:

$$\bar{P}_{i,j}^{(L+1)} \left|\begin{array}{l} j=2 \text{ to } (^m/2 + 1) \\ \\ i=1 \text{ to } n_e \end{array}\right. = \bar{P}_{i,j}^{(L)} + \frac{R}{A_{i,j}} \left[F_{i,j} \; \ldots\right.$$

$$\ldots - E_{i+1} \bar{P}_{i+1,j}^{(L)} - W_{i-1} \bar{P}_{i-1,j}^{(L)} - N_i \bar{P}_{i,j+1}^{(L)} \; \ldots$$

$$\ldots - S_i \bar{P}_{i,j-1}^{(L)} - A_{i,j} \bar{P}_{i,j}^{(L)} \left.\right] \tag{5.69}$$

A solution pertaining to the steady-state condition is first obtained, and then equation (5.69) is repeatedly solved for finite values of velocities (S_s) and finite values of displacements, as described in Sections (5.7.1.1) and (5.7.1.2), respectively.

5.7.2.2 Boundary Conditions

The boundary conditions stated in Section 4.5.5, together with the following conditions, are employed for the dynamic analysis:

(1) Expansion or contraction of the areas of the cavitating regions
     do not occur as a result of the dynamic forces.

(2) The presence of negative pressures at the full-film regions
     signify that the linear range is violated. Hence, the computation
     is terminated and rejected, once a negative pressure is en-

countered at the full-film region.

5.7.2.3 The Finite Disturbance Finite Difference Computer Program (FFD.FOR)

The program (FFD.FOR) may be used for:

(1) static analysis, or

(2) dynamic analysis (the 8 linearized bearing dynamic coefficients), when used in conjunction with program BCOEF.FOR.

The following input variables in combination with those mentioned in Section 4.5.8 are required to perform the dynamic analysis:

(1) the magnitudes of the displacement vectors in the V and U-direction, (DEV) and (DEU) respectively.

(2) the magnitudes of the velocity vectors in the V and U-direction, (DSV) and DSU), respectively.

(3) the total number of finite disturbances required, (IMAX).

(4) the relaxation factor at the dynamic conditions, ($R1 = 0.7$).

(5) the maximum allowable residual at the dynamic conditions, (ACCI), and

(6) whether a static or dynamic analysis is required, (DS).

Programme FFD.FOR, will set up the calculations of the static and dynamic pressures. From these calculations, the static and dynamic loads, and hence, the bearing coefficients, expressed in the U - V coordinate system are determined. The procedures involved are fully illustrated in the algorithm of figure (5.6).

A second program BCOEF.FOR, is used to perform the calculations for the stiffness coefficients, based on the static results of program FFD.FOR, and to carry out the coordinate transformations, so that the bearing coefficients are expressed in the conventional X - Y coordinate system. The procedures are illustrated in the algorithm
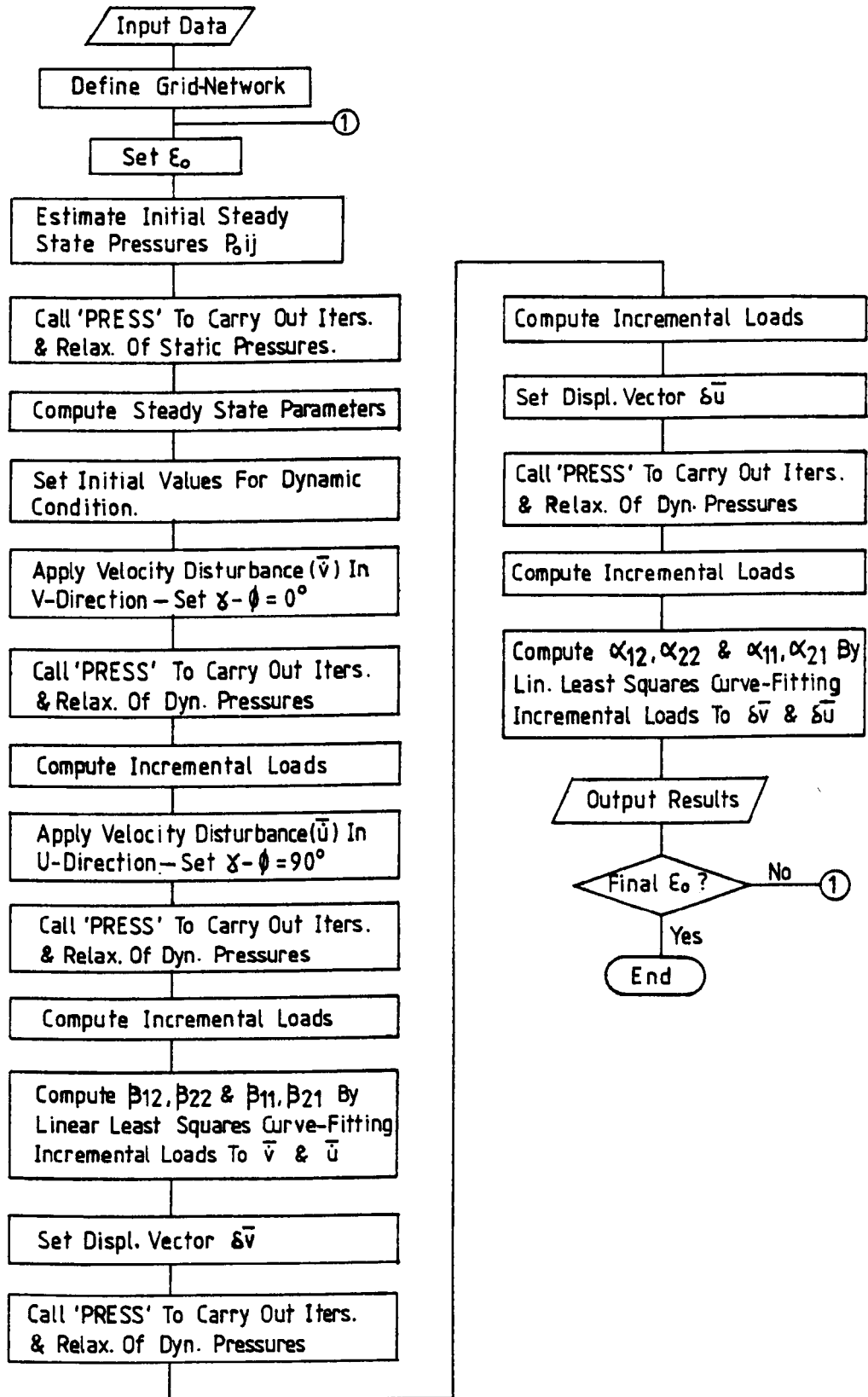
Fig.(5.6) : Algorithm For Computing The Bearing Dynamic
Coefficients By The Finite Disturbance Technique
— Program (FFD.FOR)
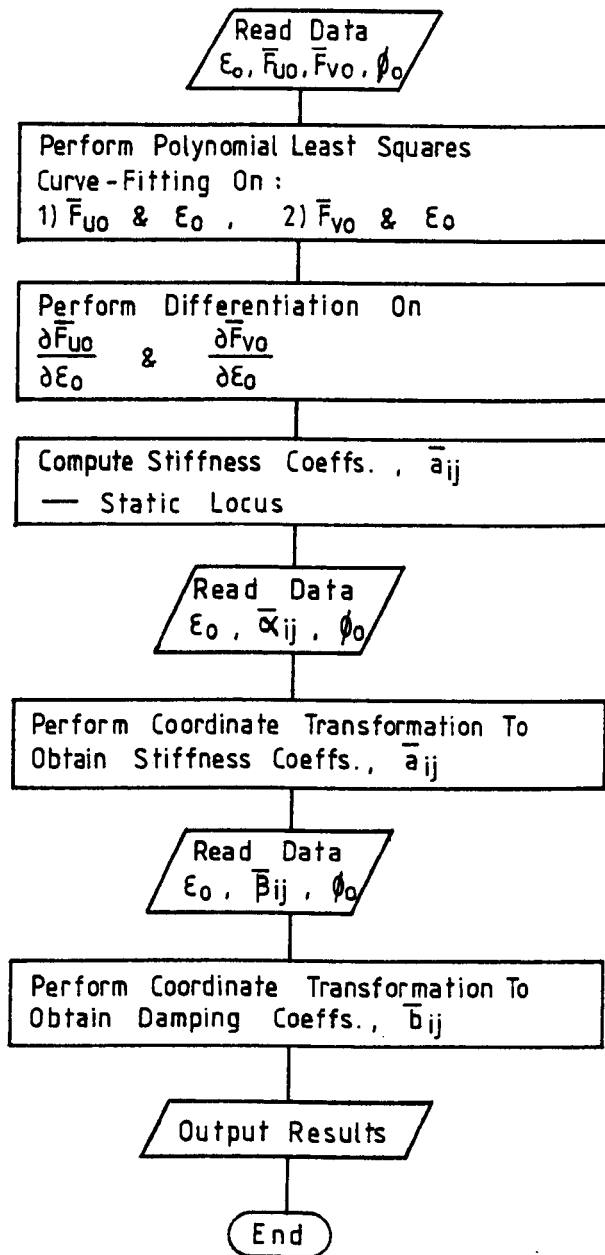
Fig.(5.7): Algorithm For Program BCOEF.FOR

of figure (5.7). The dimensionless stiffness and damping coefficients predicted by this program, are presented in figures (5.8a) to (5.16b). A discussion of the results is presented in Section 5.8.

5.7.3 Lumped Parameter Method

The basis of the lumped parameter technique has been fully discussed in Section 4.6. By referring to Section 4.6, it is, therefore, possible to write down the dynamic-state lumped parameter equations directly, as:

(i) **The Dynamic-State Equation of Continuity of Mass Flow Governing The ith 'OUTER' Control Volume**

The full continuity equation may be expressed as (see figure 4.6b):

$$q_{1i}^{p} + q_{5i}^{'p} - q_{5i}^{p} - q_{2i}^{p} + q_{5i}^{'v} - q_{5i}^{v} + q_{5i}^{sq} = 0 \qquad (5.70)$$

Writing down the non-dimensional expressions for the q_i, terms as derived in Appendix IV and rearranging and simplifying yields:

$$\bar{P}_{ai} = \Bigg[\bar{P}_i \Big[2 \left(\frac{1}{A}\right) H_i^3 + \frac{1}{24} A \left(H_{i+\frac{1}{2}}^3 + H_{i-\frac{1}{2}}^3 \right) \Big] \cdots$$

$$\cdots - \bar{P}_{i+1} \left(\frac{1}{24} A H_{i+\frac{1}{2}}^3 \right) - \bar{P}_{i-1} \left(\frac{1}{24} A H_{i-\frac{1}{2}}^3 \right) \cdots$$

$$\cdots + \bar{P}_{ai+1} \left(\frac{1}{3} A H_{i+\frac{1}{2}}^3 \right) + \bar{P}_{ai-1} \left(\frac{1}{3} A H_{i-\frac{1}{2}}^3 \right) \cdots$$

$$\cdots - 12 \pi S_h \left(\frac{a}{L}\right)\left(\frac{L}{D}\right) (H_{i+\frac{1}{2}} - H_{i-\frac{1}{2}}) \cdots$$

$$\cdots + 24 S_s \left(\frac{a}{L}\right)\left(\frac{L}{D}\right) \sin\left(\frac{\pi}{n_e}\right) \cos\theta'_i \Bigg] \Bigg/ \cdots$$

$$\cdots \left[4 \left(\frac{1}{A}\right) H_i^3 + \frac{1}{3} A \left(H_{i+\frac{1}{2}}^3 + H_{i-\frac{1}{2}}^3 \right) \right] \qquad (5.71)$$

(ii) **The Dynamic-State Equation of Mass Flow Governing the ith 'SOURCE' Control Volume (See figure 4.6b)**

The full continuity equation is expressed as:

$$q_{2i}^{p} + q_{6i}^{'p} + q_{7i}^{'p} - q_{6i}^{p} - q_{7i}^{p} - q_{3i}^{p} \cdots$$

$$\cdots - q_{si}^{s} + q_{6i}^{'v} + q_{7i}^{'v} - q_{6i}^{v} - q_{7i}^{v} \cdots$$

$$\cdots + q_{6i}^{sq} + q_{7i}^{sq} = 0 \qquad (5.72)$$

Again, writing down the non-dimensional expressions for the q_i terms as derived in Appendix IV, and the q_{si} term of Appendix V and re-arranging and simplifying, yields:

$$\bar{P}_i = \left[\; \bar{P}_{i+1} \left(\frac{5}{24} \; A + \frac{3}{16} \; B \right) H_{i+\frac{1}{2}}^3 \; \cdots \right.$$

$$\cdots + \bar{P}_{i-1} \left(\frac{5}{24} \; A + \frac{3}{16} \; B \right) H_{i-\frac{1}{2}}^3 - \bar{P}_{ai} \left(H_{i+\frac{1}{2}}^3 + H_{i-\frac{1}{2}}^3 \right) \frac{1}{3} \; A \; \cdots$$

$$\cdots + \bar{P}_{ai+1} \left(\frac{1}{3} \; A \; H_{i+\frac{1}{2}}^3 \right) + \bar{P}_{ai-1} \left(\frac{1}{3} \; A \; H_{i-\frac{1}{2}}^3 \right) \cdots$$

$$\cdots + \bar{P}_{ci} \left(2 \left(\frac{1}{B} \right) H_i^3 - \left(H_{i+\frac{1}{2}}^3 + H_{i-\frac{1}{2}}^3 \right) \frac{1}{16} \; B \right) \cdots$$

$$\cdots + \bar{P}_{ci+1} \left(\frac{1}{16} \; B \; H_{i+\frac{1}{2}}^3 \right) + \bar{P}_{ci-1} \left(\frac{1}{16} \; B \; H_{i-\frac{1}{2}}^3 \right) \cdots$$

$$\cdots - 12 \; \pi \; S_h \left(\frac{a}{L} \right) \left(\frac{L}{D} \right) \left(H_{i+\frac{1}{2}} - H_{i-\frac{1}{2}} \right) \cdots$$

$$\cdots - 6 \; \pi \; S_h \left(1 - \frac{2 \; a}{L} \right) \left(\frac{L}{D} \right) \left(H_{i+\frac{1}{2}} - H_{i-\frac{1}{2}} \right) \cdots$$

$$\cdots + 24 \; S_s \left(\frac{a}{L} \right) \left(\frac{L}{D} \right) \sin \left(\frac{\pi}{n_e} \right) \cos\theta'_i \; \cdots$$

$$\cdots + 12 \; S_s \left(1 - \frac{2 \; a}{L} \right) \left(\frac{L}{D} \right) \sin \left(\frac{\pi}{n_e} \right) \cos\theta'_i \; \cdots$$

$$\cdots + AZY \left(\frac{n_s}{n_e} \right) \; \right] \Big/ \; \cdots$$

$$\cdots \left[\left(\frac{1}{A} + 2 \left(\frac{1}{B} \right) \right) H_i^3 + \left(\frac{5}{24} \; A + \frac{3}{16} \; B \right) H_{i+\frac{1}{2}}^3 \; \cdots \right.$$

$$\cdots + \left(\frac{5}{24} \; A + \frac{3}{16} \; B \right) H_{i-\frac{1}{2}}^3 + AZY \left(\frac{n_s}{n_e} \right) \; \right] \qquad (5.73)$$

(iii) **The Dynamic-State Equation of Continuity of Mass Flow Governing The ith 'CENTRAL' Control Volume** (see figure 4.6b)

The full continuity equation may be expressed as:

$$q_{31}^p + q_{8i}^{'p} - q_{4i}^p - q_{8i}^p + q_{8i}^{'v} - q_{8i}^v \; \cdots$$

$$\cdots + q_{8i}^{sq} = 0 \qquad (5.74)$$

Again, substituting for the appropriate terms of q_i, as derived in Appendix IV, and, rearranging and simplifying, yields:

$$
\begin{aligned}
\bar{P}_{ci} = \Bigg[& \bar{P}_{ci+1}\left(\frac{11}{48}\ B\ H^3_{i+\frac{1}{2}}\right) + \bar{P}_{ci-1}\left(\frac{11}{48}\ B\ H^3_{i-\frac{1}{2}}\right) \ldots \\
& \ldots + \bar{P}_i\left(2\left(\frac{1}{B}\right)H^3_i - \left(H^3_{i+\frac{1}{2}} + H^3_{i-\frac{1}{2}}\right)\frac{1}{48}\ B\right) \ldots \\
& \ldots + \bar{P}_{i+1}\left(\frac{1}{48}\ B\ H^3_{i+\frac{1}{2}}\right) + \bar{P}_{i-1}\left(\frac{1}{48}\ B\ H^3_{i-\frac{1}{2}}\right) \ldots \\
& \ldots - 6\ \pi\ S_h\left(1 - \frac{2\ a}{L}\right)\left(\frac{L}{D}\right)\left(H_{i+\frac{1}{2}} - H_{i-\frac{1}{2}}\right) \ldots \\
& \ldots + 12\ S_s\left(1 - \frac{2\ a}{L}\right)\left(\frac{L}{D}\right)\sin\left(\frac{\pi}{n_e}\right)\cos\theta'_i\ \Bigg] \Bigg/ \ldots \\
& \ldots \left[2\left(\frac{1}{B}\right)H^3_i + \left(H^3_{i+\frac{1}{2}} + H^3_{i-\frac{1}{2}}\right)\frac{11}{48}\ B\right]
\end{aligned}
\tag{5.75}
$$

5.7.3.1 Method of Solution

The method of successive relaxation (R1 = 0.7) was employed to solve equations (5.71), (5.73) and (5.75), in accordance with the procedures described in Section 5.7.2.1.

5.7.3.2 Boundary Conditions

The boundary conditions are as described in Section 5.7.2.2.

5.7.3.3 The Finite Disturbance Lumped Parameter Computer Program (FLP.FOR)

The finite disturbance lumped parameter computer program is similar in structure to that of program FFD.FOR, described in Section 5.7.2.3. Hence, both static and dynamic (in conjunction with program BCOEF.FOR) analyses may be carried out. The input variables that are required to perform the analysis are as described in Section 5.7.2.3. A comparison of the non-dimensional stiffness and damping coefficients predicted by this program and the perturbed finite difference program are presented in Tables 5.2a and 5.2b, respectively. The results are discussed in Section 5.8.

5.8 Discussions and Conclusions

The requirements of accuracy and reliability are highly desirable features of any computational model. Economic considerations, dictate that these requirements be achieved at the minimum of computing time, however, it should be appreciated that accuracy and minimum computational time conflict with each other, and a compromise between the two is therefore required. In order to ascertain whether such requirements are adequately met, results are computed for a wide range of bearing operating parameters (such as, various values of $^a/L$, $^L/D$, β and K) and compared with other computational models. Prior to this investigation, information on the stiffness and damping coefficients of the slot-entry bearing configuration were not available in the bearing literature, hence, comparisons with other independent investigators cannot be carried out. Therefore three computational models as described in this chapter, were developed to provide a basis for determining the order of accuracy of the predicted stiffness and damping coefficients. Comparisons with the experimentally determined coefficients were not carried out at this stage. Nevertheless, it is important to spell out the following points:

(1) It will be shown that the variability in the computed coefficients is very small compared to the scatter which is found in experimentally determined values. However, as reported by Holmes (18), the variability is not reflected to the same extent in the responses predicted from the coefficients and thus the accuracy of the computed coefficients is sufficiently accurate for that purpose.

(2) The results of the dynamic analysis can only be as accurate as the static analysis permits. Therefore, every effort should be devoted to ensure the accuracy and reliability of the static analysis, before embarking upon the dynamic solution. Further-

more, equations (5.29) and (5.30) illustrate another feature concerning the importance of an accurate static solution. The accuracy of the bearing coefficients is clearly dependent on the accuracy of ϕ_o, the attitude angle.

Due to the stringent condition placed upon accuracy, this investigation showed that for the perturbed finite difference solution, the maximum allowable residuals (ACC and ACCI), have to be limited to 10^{-7}. The investigation also showed that finite disturbance analyses require a more stringent condition to be placed upon accuracy. In this case, the maximum allowable residuals (ACC and ACCI) were found to be 10^{-8}.

The effect of the variations of the number of grid elements (circumferential and axial) on the accuracy of the computed results was carried out. Tables (5.1a, 5.1b) and (5.2a, 5.2b), show the variations of the number of circumferential grid elements on the dimensionless stiffness and damping coefficients, respectively. The perturbed finite difference (PFD.FOR) program was employed in this investigation. It can be observed that using 12 circumferential grid elements, is not sufficient to predict the dynamic characteristics adequately. The results presented in tables (5.1a) to (5.2b) showed that the use of 36 circumferential grid elements may be adequate for low values of eccentricity-ratios, that is, $\varepsilon \leqslant 0.5$. For $\varepsilon \geqslant 0.6$, it is necessary to increase the number of circumferential grid elements to 96, in order to achieve the required accuracy. It can be observed that this follow a similar pattern to that of the static analysis. In the present analysis, the number of axial grid elements employed was 20, and was found to be sufficient for the required accuracy.

A comparison of the perturbed finite difference and finite disturbance finite difference solutions are presented in figures (5.8a)

to (5.16b). Figures (5.8a) to (5.10b), show the stiffness and damping coefficients for a bearing of $^a/L$ = 0.25, $^L/D$ = 1.0 and β = 0.5, at various values of K. It can be seen that there is good agreement between the perturbation and the finite disturbance techniques. As the value of K increases, the difference in the values of $\bar{a}_{12}$ and $\bar{a}_{21}$ coefficients becomes more significant, accompanied by a reduction in damping. This would imply that instability would set in at high K values as instability arises from a large difference between $\bar{a}_{12}$ and $\bar{a}_{21}$. However, it should be pointed out that instability can only be predicted when the actual rotor/bearing system is known. Figures (5.11a) to (5.12b) show the eight coefficients for a bearing of $^L/D$ = 1.0, β = 0.5, and K = 3, at various values of $^a/L$. Again, good correlation between the two techniques is observed. Reducing $^a/L$ to 0.1 has the effect of increasing the damping values. The stiffness and damping coefficients for a bearing of $^a/L$ = 0.25, K = 3 and β = 0.5, at various values of $^L/D$ are illustrated in figures (5.13a) to (5.14b). The figures show that there is good agreement between the two techniques. It can be deduced that a bearing with $^L/D$ = 2.0, would exhibit greater instability that $^L/D$ = 0.5, as the difference in the values of the $\bar{a}_{12}$ and $\bar{a}_{21}$ coefficients are more pronounced for $^L/D$ = 2.0. Also, the damping is reduced as compared with $^L/D$ = 0.5.

Figures (5.15a) to (5.16b) show the stiffness and damping co-efficients for a bearing of $^L/D$ = 1.0, $^a/L$ = 0.25 and K = 3.0, at various values of β. Again, good agreement between the perturbation and finite disturbance techniques is observed. It is seen that a low value of concentric pressure-ratio, β = 0.1, has the effect of reducing the difference between the $\bar{a}_{12}$ and $\bar{a}_{21}$ coefficients, and increasing the values of the damping coefficients. This would indicate that a low value of pressure-ratio is a prerequisite for stability, in contrast to the steady-state condition, where a pressure-ratio,

β = 0.5 was required to ensure optimum static characteristics. This further highlights the concern as to whether the dynamic conditions are governed by the same optimized parameter values as the static condition. This subject is dealt with in Chapter 9.

Within the range of the bearing operating parameters being tested, the finite disturbance technique has proved to be as accurate as the perturbation technique. In terms of computing time, the perturbation technique is preferred. The same set of results may be obtained at a computing time of approximately 0.8 times that of the finite disturbance technique. However, the main advantage of the finite disturbance technique, is the simplicity involved in the formulation of the dynamic state lubrication equation, as it required no rigorous mathematical derivation. Hence, an existing static solution may be easily extended to provide calculations for the stiffness and damping coefficients. Also, by the respecification of the boundary conditions, the finite disturbance technique may be used to perform a non-linear analysis. The main drawback of this technique is the difficulty in specifying the values of the finite displacements and velocities. A value which is too large would invalidate the linear analysis, whilst, too small a value may not be sufficient to effect any changes in the fluid-film, and may lead to inaccuracies in computing. Hence, a great deal of effort is required to ensure that the appropriate values are selected. This is where the perturbation technique is better, as it does not require such specifications. The values employed for the present finite disturbance analyses are as follows:

	$\delta\bar{u}$	$\delta\bar{v}$	$S_s\big\vert\gamma-\phi_o=0$	$S_s\big\vert\gamma-\phi_o=\pi/2$
Non-cavitating Bearing	1.0×10^{-3}	1.0×10^{-3}	5.0×10^{-3}	5.0×10^{-3}
Cavitating Bearing	1.0×10^{-3}	5.0×10^{-6}	1.0×10^{-4}	1.0×10^{-4}

The disadvantage of the perturbation technique lies in the procedures that are involved in formulating the perturbed lubrication equation, where a rigorous mathematical derivation is involved. In view of the dependence of the finite disturbance results on the specified values of displacements and velocities, and in order to ensure confidence in the computed results, the finite disturbance results should be checked against another independent source, such as the perturbation results. In the present investigation, the incorporation of a linear regression of the incremental fluid-film forces on the displacements or velocities, has helped to promote the accuracy of the finite disturbance analysis.

A comparison of the perturbed finite difference and the finite disturbance lumped parameter results, for a bearing of $^a/L = 0.25$, $^L/D = 1.0$, $\beta = 0.5$ and $K = 30$, is illustrated in Tables 5.3a and 5.3b. There is good agreement between the two models. However, in terms of computing time, the lumped parameter program is four times as fast as the perturbed finite difference program. To compute the results of Tables 5.3a and 5.3b, the lumped parameter program uses 45.99 minutes of C.P.U. time, whilst the perturbed finite difference program uses 3 hours and 8.85 minutes of C.P.U. time. It was found that there was poor correlation between the lumped parameter and the finite difference models, as $^a/L$ approaches 0.5, that is, a single row slot-entry bearing. A comparison of the steady state circumferential pressures predicted by these two models for a bearing of $^a/L = 0.4$, $K = 3.0$, $^L/D = 1.0$ and $\beta = 0.5$, at $\varepsilon = 0.9$, is illustrated in figure (5.17a), while, the axial pressure distribution is illustrated in figure (5.17b). Figures (5.17a) and (5.17b) show that the poor correlation may be attributed to the validity of the assumption of a quadratic pressure profile as $^a/L$ approaches 0.5. Figure (5.17b) suggests that a parabolic pressure profile is more appropriate. Therefore, the lumped parameter results

for $^a/L > 0.4$, should be treated with caution.

A comparison of the stiffness coefficients predicted from static loading characteristics (static load locus) and the perturbation technique is illustrated in table 5.4. It can be observed that there is reasonable agreement between the two techniques up to $\varepsilon = 0.8$. As the polynomial least square fitting criterion was employed in the static load locus analysis, the computed coefficients may be affected by the degree of the polynomial.

The general conclusions of this chapter may be summarised as:

(1) An overall view of the fundamentals of bearing dynamic analysis has been presented, with the aim of providing the basis for the coherent working understanding, necessary for the application of the most appropriate techniques for problem-solving.

(2) Three computer programs for performing the static and dynamic analysis of double row slot-entry hybrid bearings, have been successfully developed.

(3) The accuracy and reliability of these three programs have been rigorously tested and they serve to provide a cross-check on the reasonableness of the results, and, thus have proved to be valuable in refining the computations.

(4) The analysis has shown that the finite disturbance technique is as accurate as the perturbation technique.

(5) The imposition of a more stringent condition on accuracy and the incorporation of a linear least square criterion in the computation, have helped in refining the accuracy of the finite disturbance technique.

(6) Although the lumped parameter program has proved to be highly efficient in terms of computing time, the present investigation

showed that for values of $^a/L \geqslant 0.4$, the lumped parameter pre-
dictions should be treated with caution, as it tends to under-
estimate the pressures at the outer land.

(7) The inadequacy of the present analysis to cater for heavily
loaded bearings and to take proper account of mass conservation
within the cavitated regions, should be duly noted. Hence, the
results for bearings operating at high values of eccentricity-
ratios, or high values of power-ratios, K (K > 60) or low values
of concentric pressure-ratios, β ($\beta \leqslant 0.3$), should be treated
with caution.

Table 5.1a: Variation of Stiffness Coefficients with Number of Circumferential Grid Elements

$(^a/L = 0.25;\ ^L/D = 1.0,\ \beta = 0.5;\ K = 3)$

ω \ ne	$\bar{a}_{11}$						$\bar{a}_{22}$					
	12	36	60	96	120	132	12	36	60	96	120	132
0	0.7128	0.7197	0.7200	0.7202	0.7202	0.7202	0.7128	0.7197	0.7200	0.7202	0.7202	0.7202
0.1	0.7071	0.7125	0.7129	0.7130	0.7131	0.7131	0.7150	0.7187	0.7191	0.7192	0.7192	0.7192
0.2	0.6831	0.6893	0.6899	0.6901	0.6901	0.6902	0.7139	0.7159	0.7161	0.7162	0.7162	0.7162
0.3	0.6372	0.6453	0.6461	0.6463	0.6464	0.6465	0.7130	0.7122	0.7122	0.7122	0.7122	0.7122
0.4	0.5579	0.5710	0.5722	0.5725	0.5727	0.5727	0.7138	0.7122	0.7117	0.7115	0.7115	0.7115
0.5	0.4311	0.4500	0.4517	0.4522	0.4524	0.4525	0.7452	0.7299	0.7286	0.7281	0.7280	0.7280
0.6	0.7484	0.7644	0.7506	0.7493	0.7523	0.7490	0.8550	0.7981	0.7810	0.7801	0.7846	0.7840
0.7	1.1913	1.1261	1.1179	1.1172	1.1208	1.1248	1.2549	1.3078	1.2652	1.2641	1.2806	1.2803
0.8	2.2639	2.1544	2.1702	2.1606	2.16452	2.1729	2.4371	3.3289	3.3567	3.4947	3.4823	3.4652
0.9	7.8470	6.0183	5.9393	5.9911	5.9949	5.9960	5.5863	23.6983	22.6215	22.6867	22.6867	22.6394

Table 5.1b: Variation of Stiffness Coefficients with Number of Circumferential Grid Elements

$$(a/L = 0.25; \quad L/D = 1.0; \quad \beta = 0.5; \quad K = 3)$$

ε \ n_e	$\bar{a}_{12}$						$\bar{a}_{24}$					
	12	36	60	96	120	132	12	36	60	96	120	132
0	-0.7250	-0.7316	-0.7320	-0.7321	-0.7321	-0.7321	0.7250	0.7316	0.7320	0.7321	0.7321	0.7321
0.1	-0.7348	-0.7396	-0.7400	-0.7401	-0.7401	-0.7401	0.7311	0.7357	0.7360	0.7361	0.7362	0.7362
0.2	-0.7587	-0.7645	-0.7650	-0.7651	-0.7652	-0.7652	0.7439	0.7439	0.7488	0.7489	0.7489	0.7489
0.3	-0.8031	-0.8098	-0.8105	-0.8106	-0.8107	-0.8108	0.7701	0.7733	0.7734	0.7735	0.7735	0.7735
0.4	-0.8722	-0.8816	-0.8825	-0.8828	-0.8829	-0.8830	0.8174	0.8195	0.8195	0.8195	0.8194	0.8194
0.5	-0.9726	-0.9896	-0.9912	-0.9916	-0.9919	-0.9920	0.9148	0.9141	0.9136	0.9136	0.9134	0.9134
0.6	-0.6764	-0.7499	-0.7880	-0.7905	-0.7801	-0.7834	1.0692	1.0113	1.0091	1.0078	1.0133	1.0148
0.7	-0.5871	-0.5168	-0.5903	-0.5788	-0.5532	-0.5514	1.5283	1.5373	1.5290	1.5272	1.5308	1.5323
0.8	-0.7192	0.0395	0.0778	0.2286	0.2153	0.2002	3.2410	3.4226	3.4317	3.4167	3.4238	3.4307
0.9	-2.6191	5.2977	4.7327	4.7780	4.7532	4.7477	11.9573	14.2336	13.9959	14.0598	14.0607	14.0649

Table 5.2a: Variation of Damping Coefficients with Number of Circumferential Grid Elements

$$(^a/L = 0.25; \ ^L/D = 1.0; \ \beta = 0.5; \ K = 3.0)$$

ε	$\bar{b}_{11}$						$\bar{b}_{22}$					
n_e	12	36	60	96	120	132	12	36	60	96	120	132
0	0.8360	0.8448	0.8452	0.8454	0.8454	0.8454	0.8360	0.8448	0.8452	0.8454	0.8454	0.8454
0.1	0.8468	0.8532	0.8537	0.8538	0.8538	0.8538	0.8482	0.8530	0.8534	0.8536	0.8536	0.8536
0.2	0.8742	0.8801	0.8806	0.8807	0.8807	0.8807	0.8732	0.8783	0.8788	0.8789	0.8790	0.8790
0.3	0.9241	0.9314	0.9319	0.9321	0.9321	0.9321	0.9174	0.9233	0.9238	0.9240	0.9241	0.9241
0.4	1.0118	1.0217	1.0223	1.0226	1.0225	1.0225	0.9859	0.9936	0.9943	0.9945	0.9947	0.9947
0.5	1.1733	1.1869	1.1877	1.1881	1.1880	1.1880	1.0913	1.1018	1.1028	1.1030	1.1032	1.1033
0.6	0.9404	0.9870	1.0197	1.0219	1.0132	1.0167	1.2390	1.2346	1.2456	1.2452	1.2472	1.2492
0.7	1.0632	1.0262	1.0841	1.0741	1.0526	1.0514	1.6352	1.6242	1.6517	1.6467	1.6401	1.6410
0.8	1.8754	1.4349	1.4046	1.2828	1.2940	1.3107	3.1564	3.0036	2.9986	2.9051	2.9193	2.9341
0.9	6.0831	1.8466	2.0618	2.0554	2.0706	2.0690	12.2730	10.0967	10.5253	10.5781	10.6057	10.6156

Table 5.2b: Variation of Damping Coefficients with Number of Circumferential Grid Elements

$(^a/L = 0.25; {}^L/D = 1.0; \beta = 0.5; K = 3)$

$$\bar{b}_{12} = \bar{b}_{21}$$

n_e / ε	12	36	60	96	120	132
0	0	0	0	0	0	0
0.1	0.0048	0.0049	0.0049	0.0049	0.0049	0.0049
0.2	0.0198	0.0202	0.0203	0.0203	0.0203	0.0203
0.3	0.0489	0.0491	0.0492	0.0492	0.0492	0.0492
0.4	0.0971	0.0985	0.0987	0.0988	0.0988	0.0988
0.5	0.1812	0.1849	0.1853	0.1854	0.1855	0.1855
0.6	0.3614	0.4060	0.4179	0.4184	0.4129	0.4127
0.7	0.7082	0.6465	0.6846	0.6775	0.6635	0.6640
0.8	1.7149	1.3718	1.3483	1.2392	1.2490	1.2661
0.9	7.6420	3.2026	2.5166	3.5179	3.5382	3.5388

Table 5.3a: A Comparison of the Perturbed Finite Difference and the Finite Disturbance Lumped Parameter Results (Stiffness Coefficients)

$(a/L = 0.25;\ L/D = 1.0;\ \beta = 0.5;\ K = 30)$

ϵ	FINITE DIFFERENCE (PERTURBATION)				LUMPED PARAMETER (FINITE DISTURBANCE)			
	$\bar{a}_{11}$	$\bar{a}_{12}$	$\bar{a}_{21}$	$\bar{a}_{22}$	$\bar{a}_{11}$	$\bar{a}_{12}$	$\bar{a}_{21}$	$\bar{a}_{22}$
0	0.7202	-2.3151	2.3151	0.7202	0.7186	-2.3259	2.3254	0.7187
0.1	0.7090	-2.3274	2.3409	0.7232	0.7071	-2.3388	2.3533	0.7226
0.2	0.6737	-2.3653	2.4226	0.7326	0.6715	-2.3770	2.4370	0.7322
0.3	1.1025	-2.0676	1.7391	0.6131	0.9710	-2.1196	1.6951	0.5890
0.4	1.3263	-1.8272	1.8142	0.7513	1.1440	-1.9347	1.8130	0.7431
0.5	1.6393	-1.6182	2.1300	1.0452	1.5126	-1.7313	2.0884	1.0079
0.6	2.1883	-1.4000	2.8859	1.6792	2.0536	-1.4808	2.8140	1.6339
0.7	3.4257	-0.7889	4.7826	3.4621	3.2529	-0.8523	4.6880	3.4276
0.8	6.4966	1.4351	10.9073	10.9325	6.2334	1.3896	10.6214	10.7727
0.9	16.4094	13.7993	42.4784	73.8778	16.0448	13.5239	41.4027	71.7381

Table 5.3b: A Comparison of the Perturbed Finite Difference and the Finite

Disturbance Lumped Parameter Results (Damping Coefficients)

($^a/L = 0.25$; $^L/D = 1.0$; $\beta = 0.5$; K = 30)

ϵ	FINITE DIFFERENCE (PERTURBATION)			LUMPED PARAMETER (FINITE DISTURBANCE)		
	$\bar{b}_{11}$	$\bar{b}_{12} = \bar{b}_{21}$	$\bar{b}_{22}$	$\bar{b}_{11}$	$\bar{b}_{12} = \bar{b}_{21}$	$\bar{b}_{22}$
0	0.8454	0	0.8454	0.8500	0	0.8500
0.1	0.8577	.0.0027	0.8487	0.8625	0.0028	0.8543
0.2	0.8967	0.0112	0.8629	0.9021	0.0114	0.8677
0.3	0.7902	0.1559	0.6331	0.7817	0.1583	0.6444
0.4	0.7256	0.2145	0.6587	0.7440	0.2089	0.6774
0.5	0.6990	0.2817	0.7512	0.7067	0.2803	0.7507
0.6	0.7413	0.3906	0.9448	0.7501	0.3986	0.9373
0.7	0.8477	0.6164	1.3819	0.8519	0.6130	1.3708
0.8	1.1082	1.1702	2.7665	1.0857	1.1340	2.6941
0.9	1.7262	3.1444	10.5704	1.7837	3.225	10.5241

Table 5.4: A Comparison of the Stiffness Coefficients Predicted from

The Static Load Locus Method and the Perturbation Method

$(^a/L = 0.25; \ ^L/D = 0.5; \ \beta = 0.5; \ K = 3.0)$

ϵ	FINITE DIFFERENCE (STATIC LOAD LOCUS)				FINITE DIFFERENCE (PERTURBATION)			
	$\bar{a}_{11}$	$\bar{a}_{12}$	$\bar{a}_{21}$	$\bar{a}_{22}$	$\bar{a}_{11}$	$\bar{a}_{12}$	$\bar{a}_{21}$	$\bar{a}_{22}$
0	0.8347	-0.4138	0.4138	0.8347	0.8273	-0.4226	0.4226	0.8273
0.1	0.8266	-0.4317	0.4211	0.8345	0.8222	-0.4303	0.4234	0.8232
0.2	0.8075	-0.4694	0.4338	0.8227	0.8057	-0.4548	0.4257	0.8109
0.3	0.7811	-0.5057	0.4381	0.7888	0.7742	-0.5000	0.4300	0.7901
0.4	0.7348	-0.5604	0.4422	0.7509	0.7206	-0.5737	0.4395	0.7649
0.5	0.6331	-0.6930	0.4760	0.7390	0.6301	-0.6903	0.4659	0.7507
0.6	0.4636	-0.8992	0.5690	0.7639	0.4685	-0.8791	0.5483	0.7887
0.7	0.4514	-0.9029	0.8394	1.0202	0.5238	-0.7984	0.9462	1.1907
0.8	1.5285	0.0896	2.6777	3.1669	1.2432	-0.2870	2.4103	2.9811
0.9	3.5341	1.9777	9.6919	17.0445	4.5165	3.9471	12.1912	21.4453
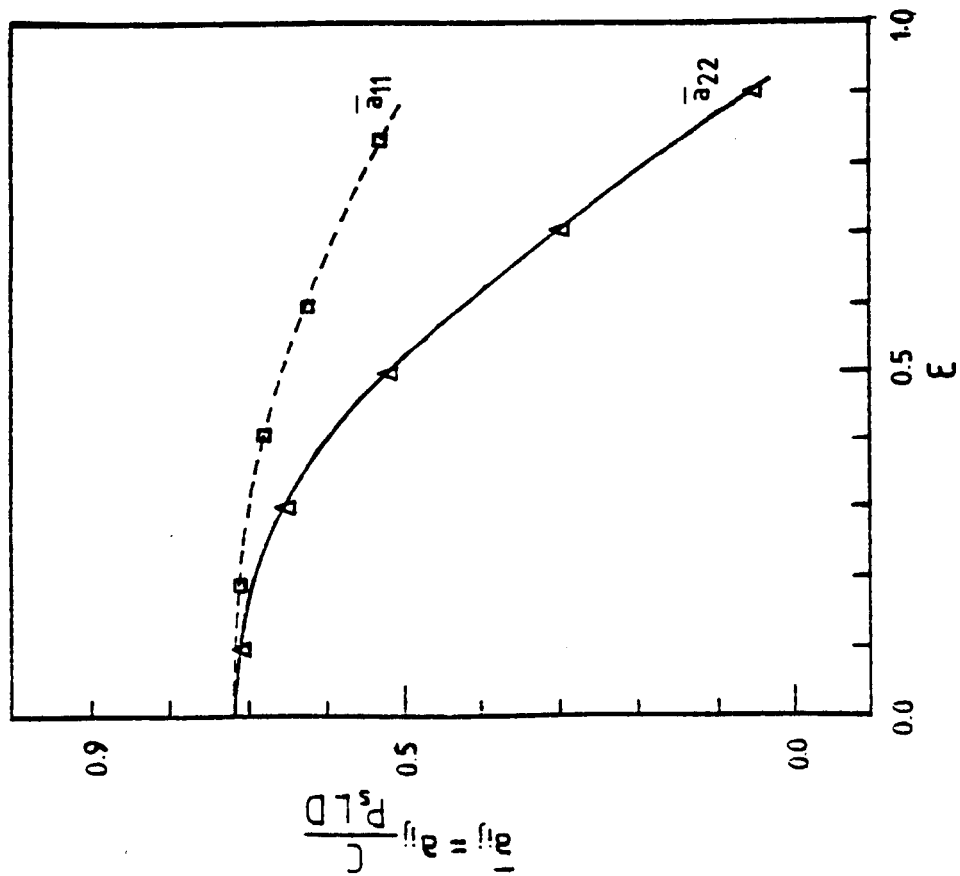
Fig.5.8b: Variation Of Dimensionless Damping Coeffs.
With Eccentricity-Ratio. ($S_{ho} = 0.046$; $K = 0.0$)

$$\bar{b}_{ij} = b_{ij} \frac{W_o C}{P_s L D}$$
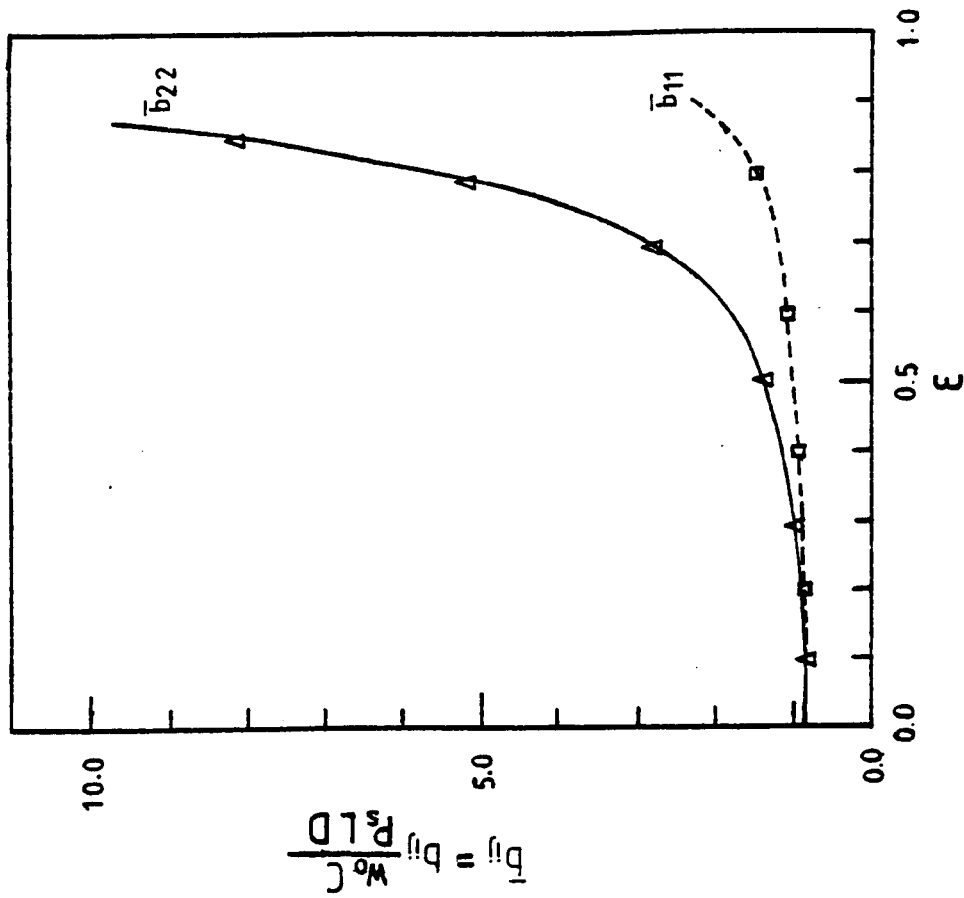
Lines —— Perturbation Results

Symbols—Finite Disturb. Results

Fig. 5.8a: Variation Of Dimensionless Stiffness Coeffs.
With Eccentricity-Ratio. ($S_{ho} = 0.046$; $K = 0.0$)

$$\bar{a}_{ij} = a_{ij} \frac{C}{P_s L D}$$

$a/L = 0.25$, $L/D = 1.0$, $\beta = 0.5$

Fig.5.9a: Variation Of Dimensionless Stiffness Coeffs.
With Eccentricity-Ratio. (S_{ho} = 0.046 ; K = 3.0)

Fig.5.9b: Variation Of Dimensionless Damping Coeffs.
With Eccentricity-Ratio. (S_{ho} = 0.046 ; K = 3.0)

a/L = 0.25 , L/D =1.0 , B =0.5
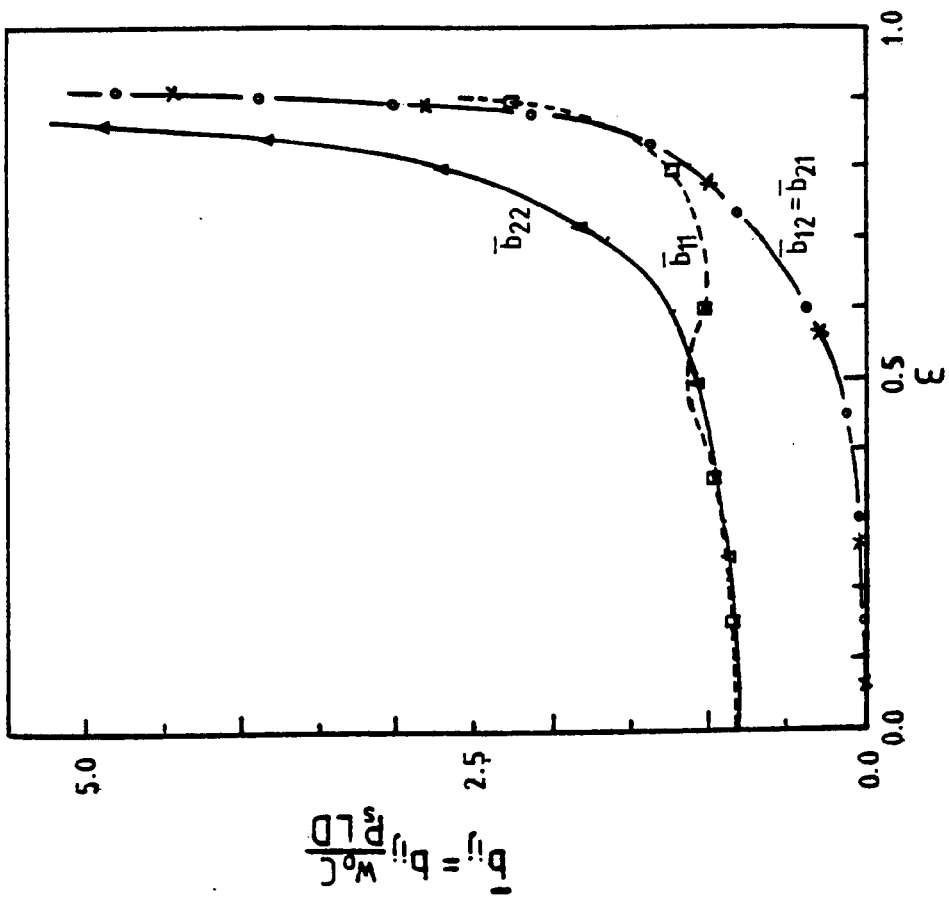
Lines —— Perturb. Results

Symbols —— Finite Disturb. Results

Fig.5.10a : Variation Of Dimensionless Stiffness Coeffs.
With Eccentricity-Ratio. ($S_{ho} = 0.046$; $K = 30.0$)

Fig.5.10b : Variation Of Dimensionless Damping Coeffs.
With Eccentricity-Ratio. ($S_{ho} = 0.046$; $K = 30.0$)

$\bar{a}_{ij} = a_{ij} \dfrac{C}{R_s L D}$

$\bar{b}_{ij} = b_{ij} \dfrac{w_o C}{R_s L D}$
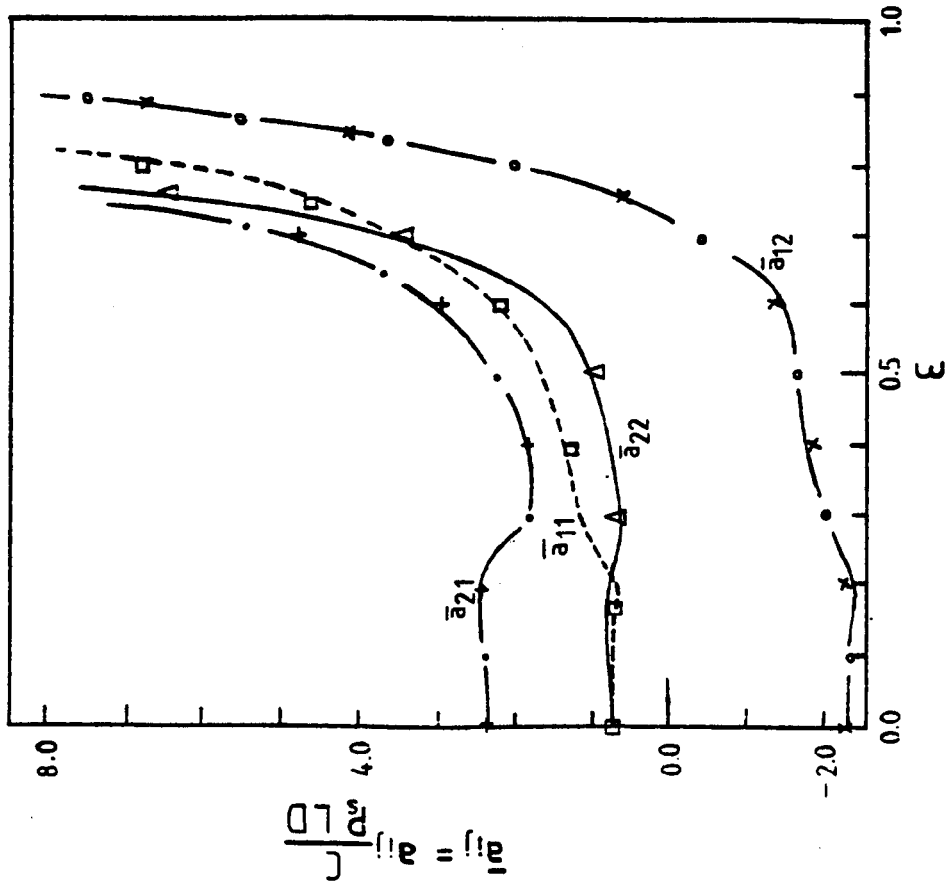
$a/L = 0.25$, $L/D = 1.0$, $\beta = 0.5$

Lines —— Perturb. Results

Symbols —— Finite Disturb. Results

155
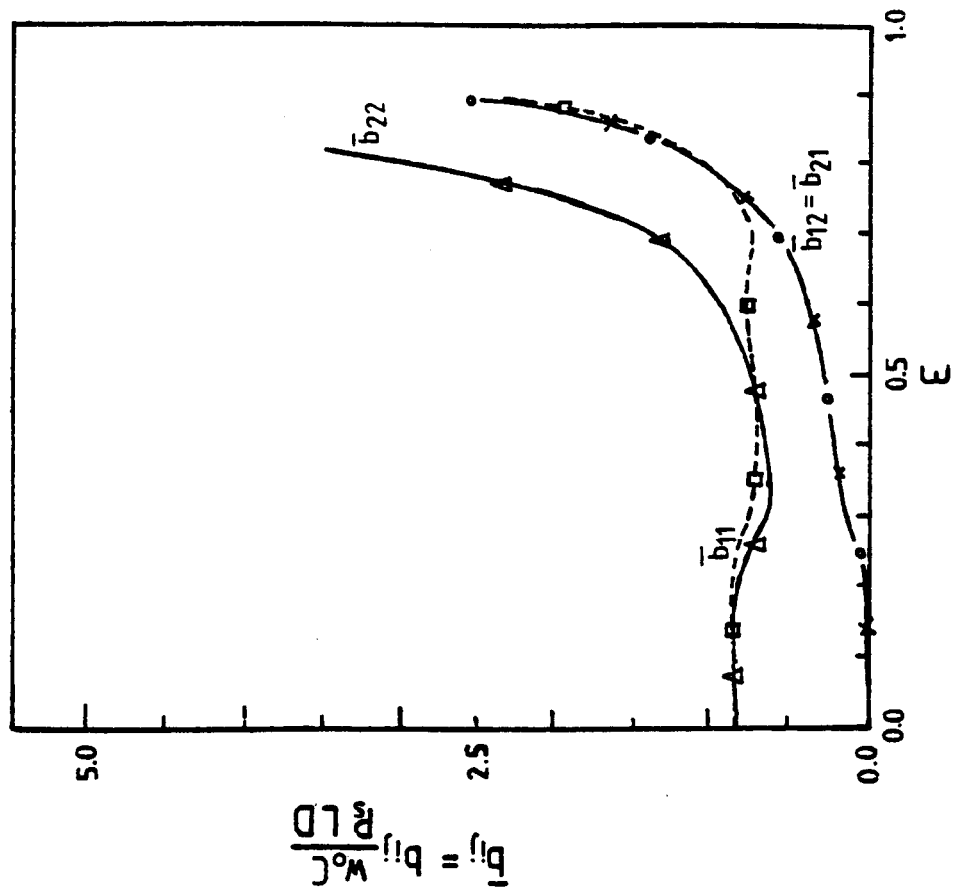
Fig.5.11a : Variation Of Dimensionless Stiffness Coeffs. With Eccentricity-Ratio. ($S_{ho} = 0.073$; $K = 3.0$)

Fig.5.11b: Variation Of Dimensionless Damping Coeffs. With Eccentricity-Ratio. ($S_{ho} = 0.073$; $K = 3.0$)

$\bar{a}_{ij} = a_{ij} \dfrac{C}{_sP\ LD}$

$\bar{b}_{ij} = b_{ij} \dfrac{W_oC}{_sP\ LD}$

Lines —— Perturb. Results

Symbols —— Finite Disturb. Results

$a/L = 0.1$, $L/D = 1.0$, $\beta = 0.5$

156
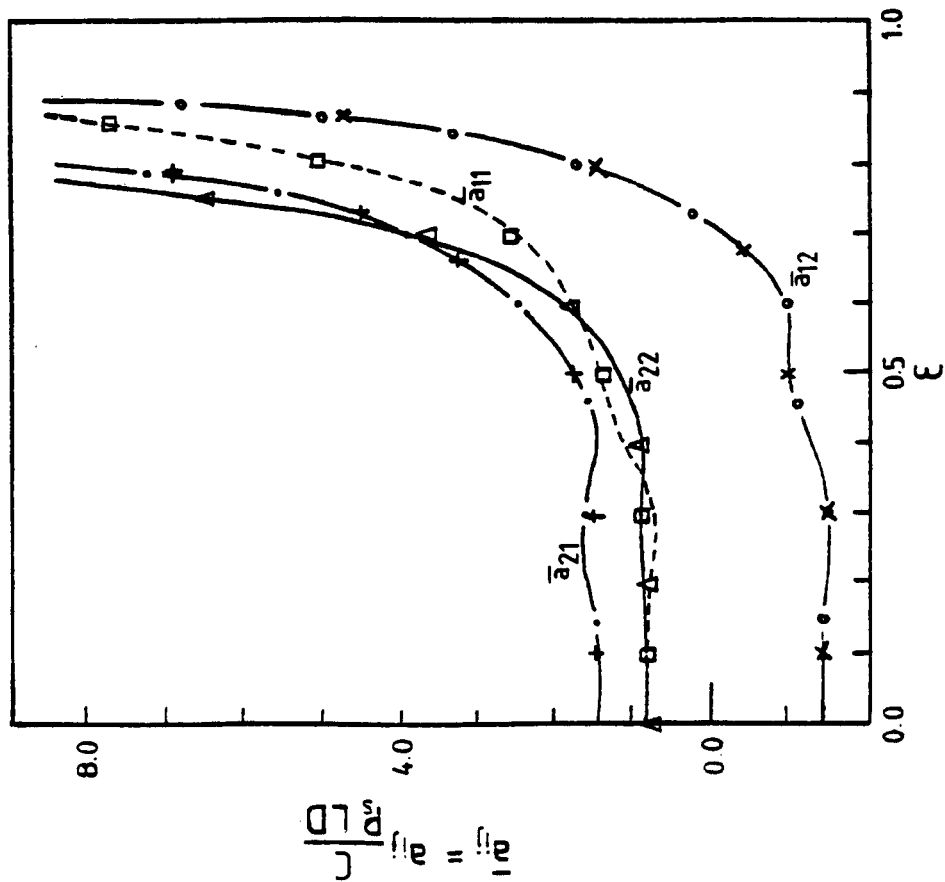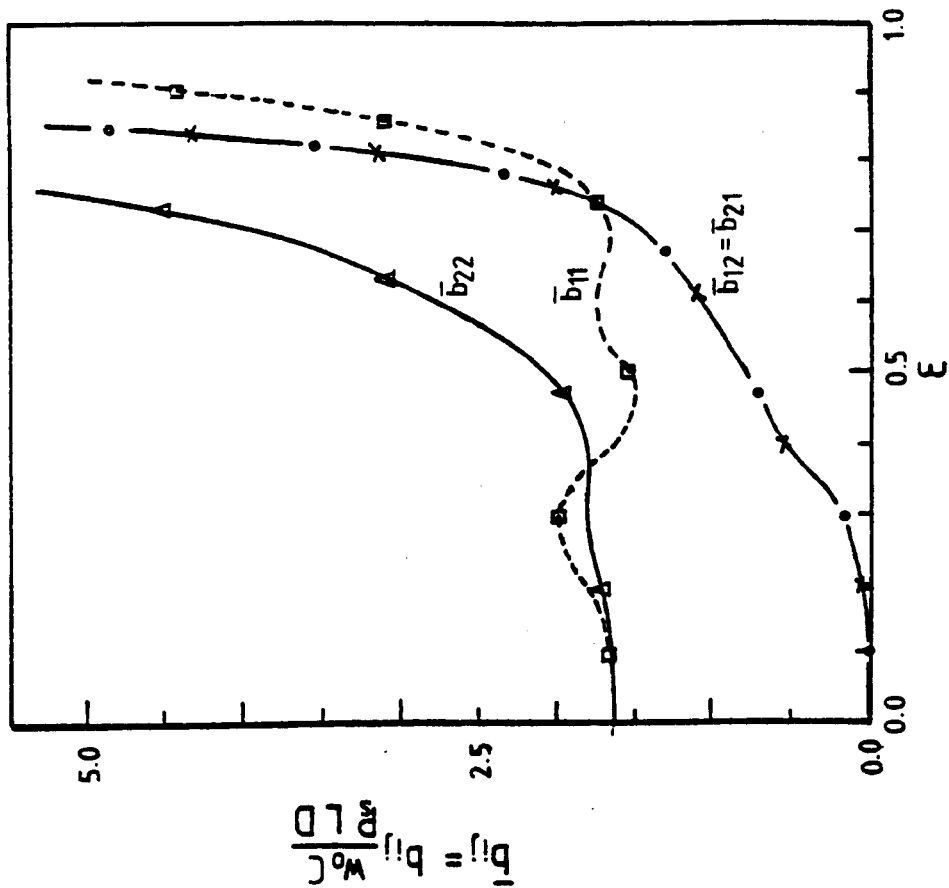
Fig.5.12a: Variation Of Dimensionless Stiffness Coeffs.
With Eccentricity-Ratio. (S_{ho} = 0.036 ; K = 3.0)
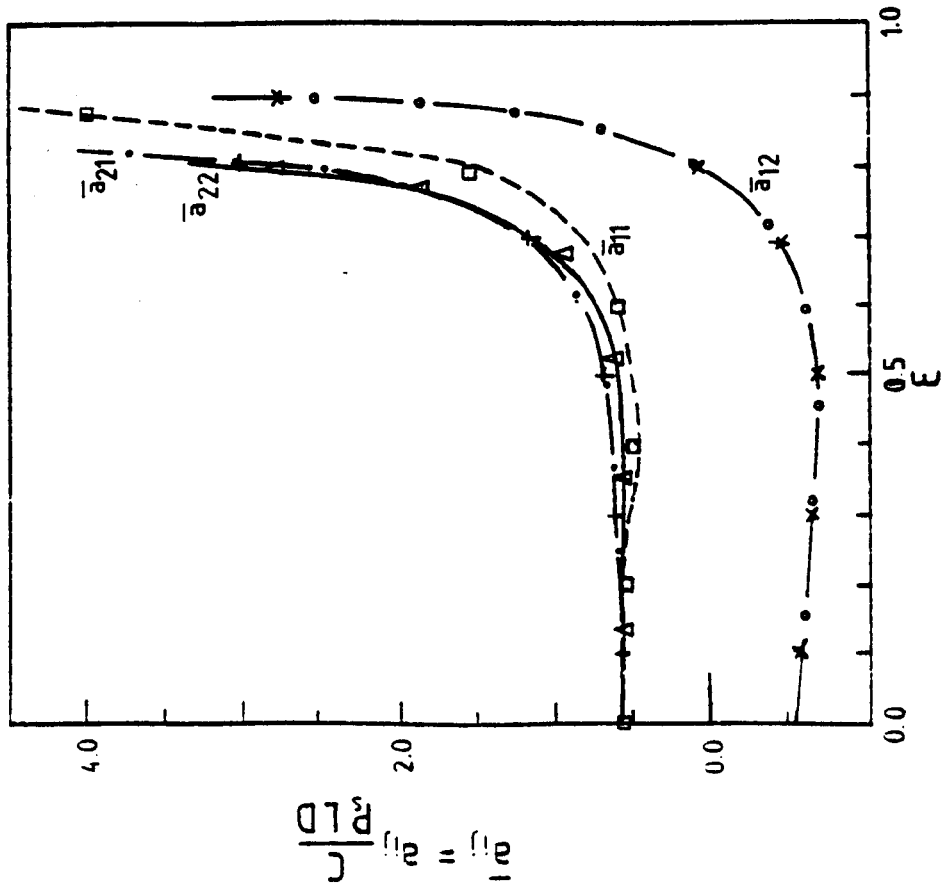
Fig.5.12b: Variation Of Dimensionless Damping Coeffs.
With Eccentricity-Ratio. (S_{ho} = 0.036 ; K = 3.0)

a/L = 0.4 , L/D = 1.0 , β = 0.5
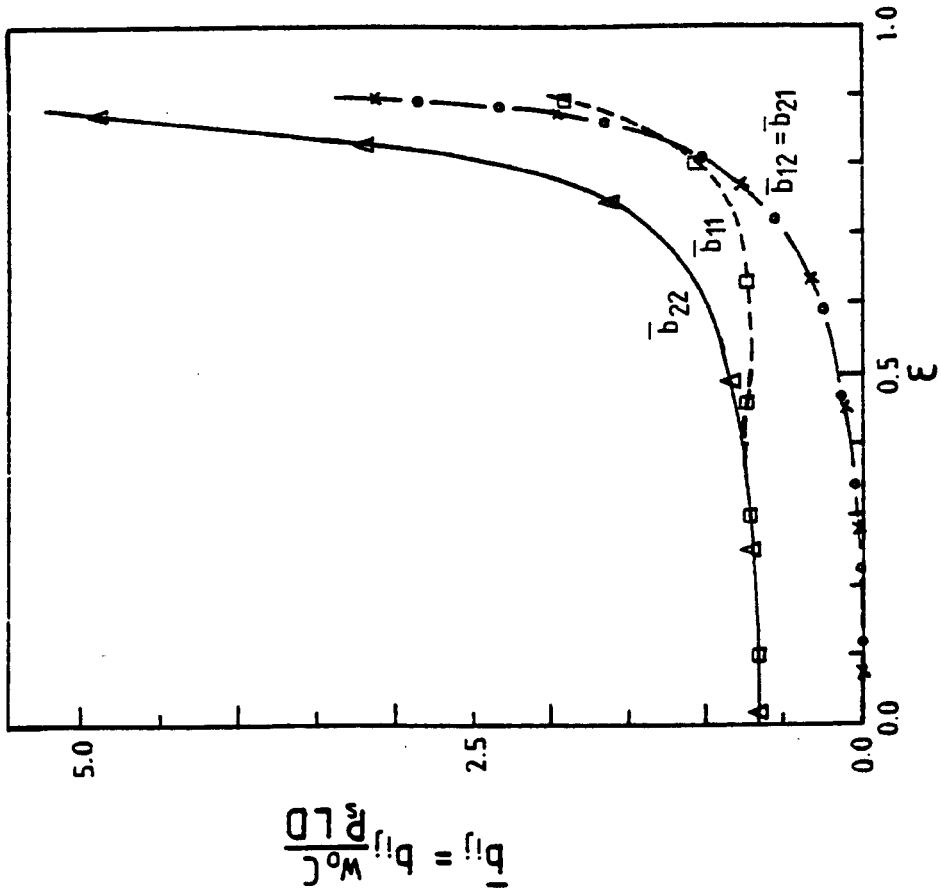
Lines —— Perturb. Results

Symbols —— Finite Disturb. Results

Fig.5.13a:Variation Of Dimensionless Stiffness Coeffs.
With Eccentricity-Ratio. (S_{ho} = 0.092 ; K=3.0)
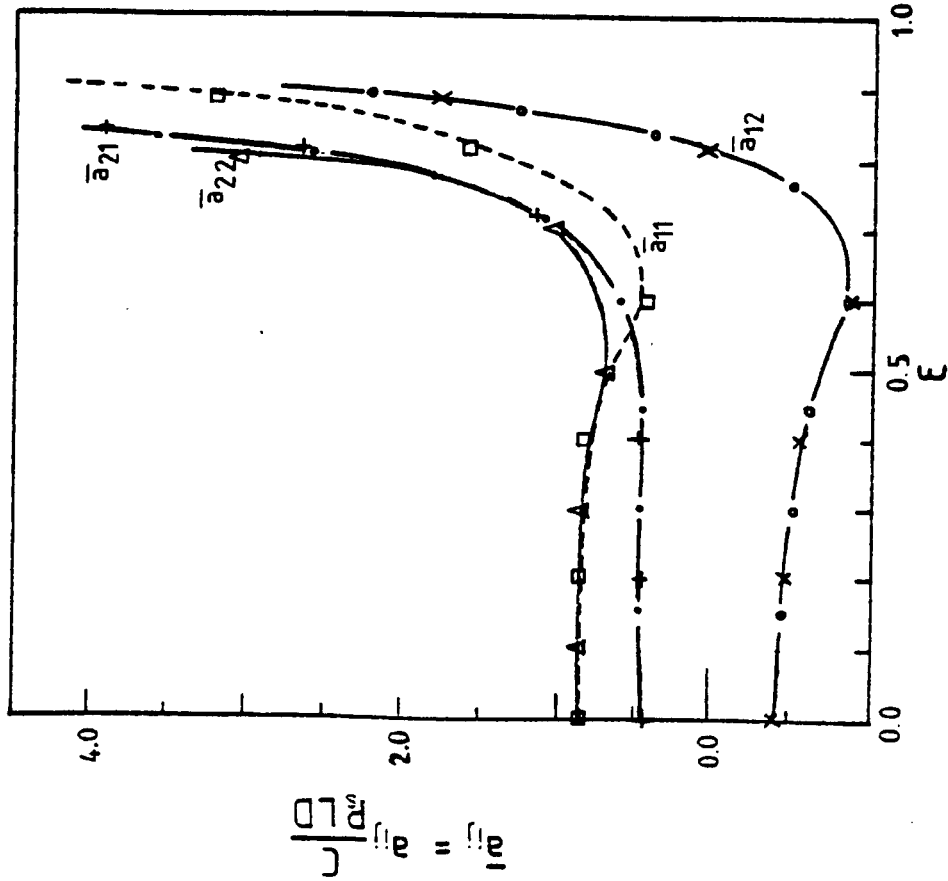
Fig.5.13b:Variation Of Dimensionless Damping Coeffs.
With Eccentricity-Ratio. (S_{ho} = 0.092 ; K = 3.0)

$$\bar{a}_{ij} = a_{ij} \frac{C}{\beta LD}$$

$$\bar{b}_{ij} = b_{ij} \frac{W_o C}{\beta LD}$$

a/L= 0.25 , L/D = 0.5 , β=0.5

Lines —— Perturb. Results

Symbols —— Finite Disturb. Results

Fig.5.14b: Variation Of Dimensionless Damping Coeffs.
With Eccentricity-Ratio.(S_{ho} = 0.023 ; K = 3.0)

$$\bar{b}_{ij} = b_{ij} \frac{W_o C}{R L D}$$

$\bar{b}_{22}$

$\bar{b}_{11}$

$\bar{b}_{12} = \bar{b}_{21}$
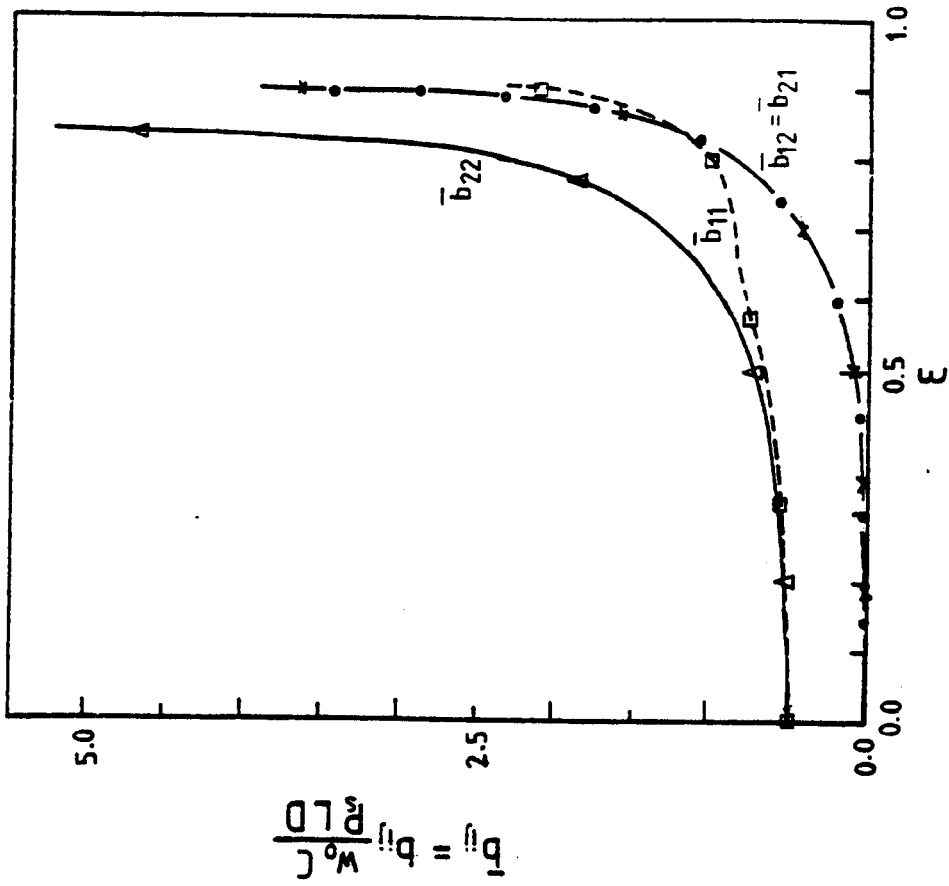
Lines —— Perturb. Results

Symbols —— Finite Disturb. Results

Fig.5.14a: Variation Of Dimensionless Stiffness Coeffs.
With Eccentricity-Ratio.(S_{ho} = 0.023 ; K = 3.0)

$$\bar{a}_{ij} = a_{ij} \frac{C}{R L D}$$

$\bar{a}_{21}$

$\bar{a}_{11}$

$\bar{a}_{22}$

$\bar{a}_{12}$

a/L = 0.25 , L/D = 2.0 , β = 0.5

Fig.5.15b: Variation Of Dimensionless Damping Coeffs. With Eccentricity-Ratio.(S_{ho}=0.021 , K=3.0)

$\bar{b}_{ij} = b_{ij} \dfrac{W_o C}{P L D}$
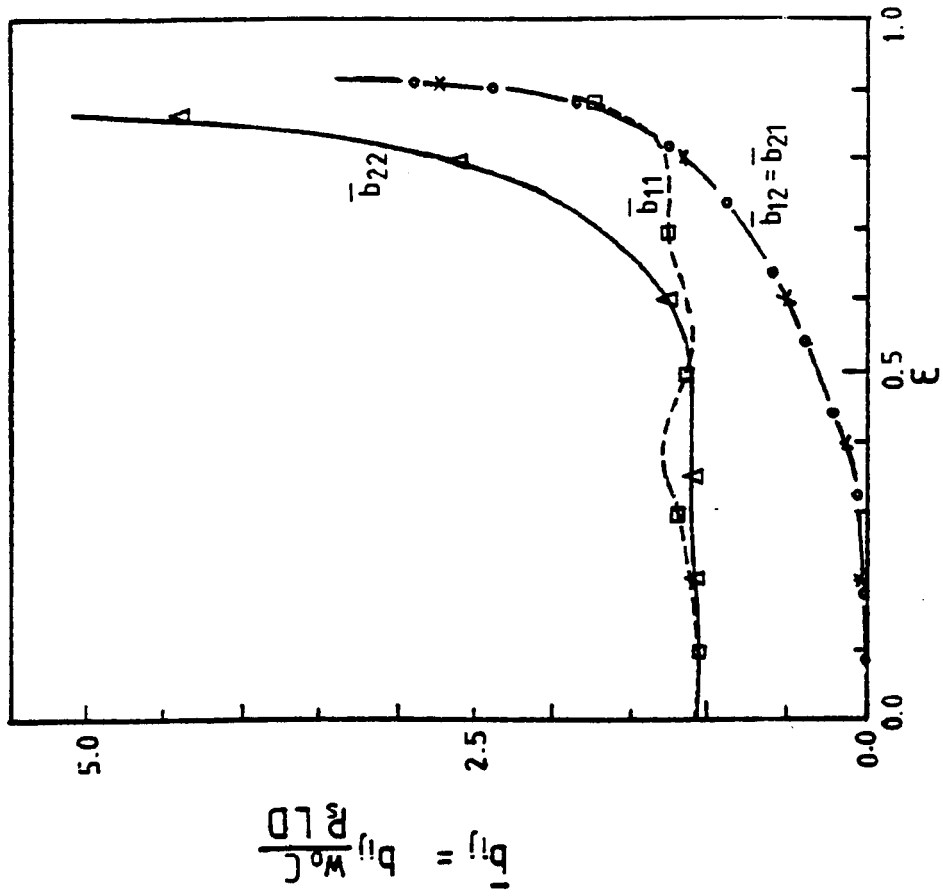
Fig.5.15a: Variation Of Dimensionless Stiffness Coeffs. With Eccentricity-Ratio.(S_{ho}=0.021 , K=3.0)

$\bar{a}_{ij} = a_{ij} \dfrac{C}{P_s L D}$

Lines ——— Perturb. Results

Symbols ——— Finite Disturb. Results

$a/L = 0.25$, $Y_D = 1.0$, $B = 0.1$

Fig.5.16b: Variation Of Dimensionless Damping Coeffs. With Eccentricity-Ratio.(S_{ho}=0.062 ; K=3.0)

$$\bar{b}_{ij} = b_{ij}\frac{w_o C}{P_s L D}$$

Fig.5.16a: Variation Of Dimensionless Stiffness Coeffs. With Eccentricity-Ratio.(S_{ho}=0.062 ; K=3.0)

$$\bar{a}_{ij} = a_{ij}\frac{C}{P_s L D}$$

Lines —— Perturb. Results

Symbols —— Finite Disturb. Results

a_L = 0.25 , L_D = 1.0 , β = 0.9
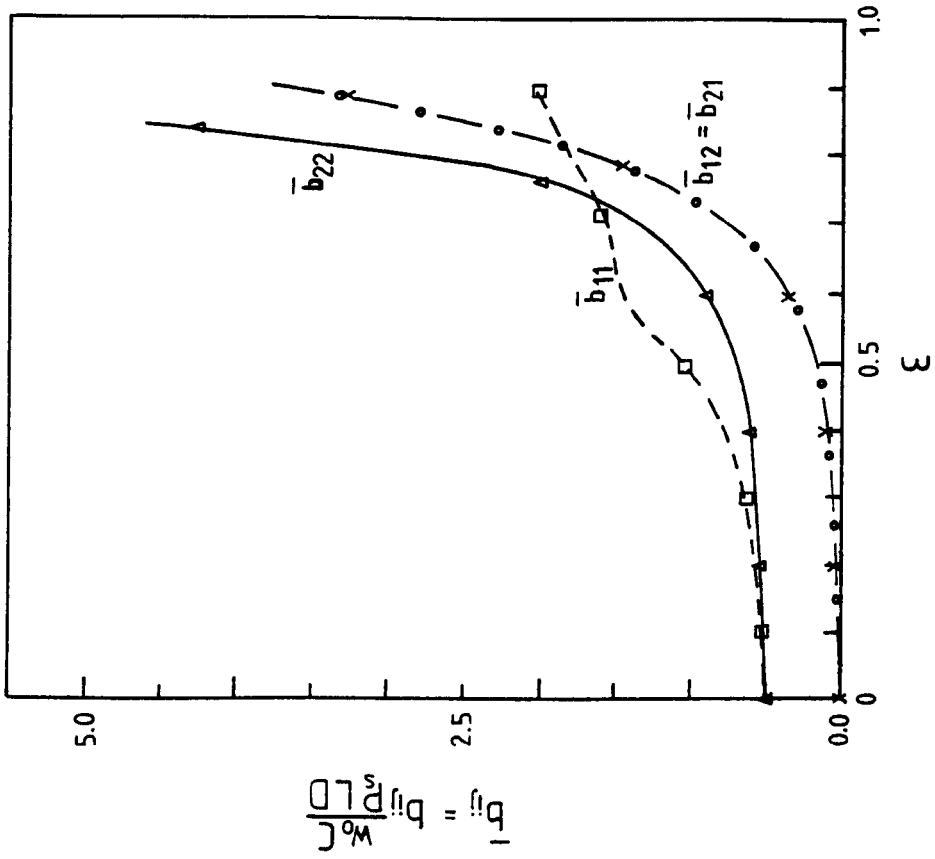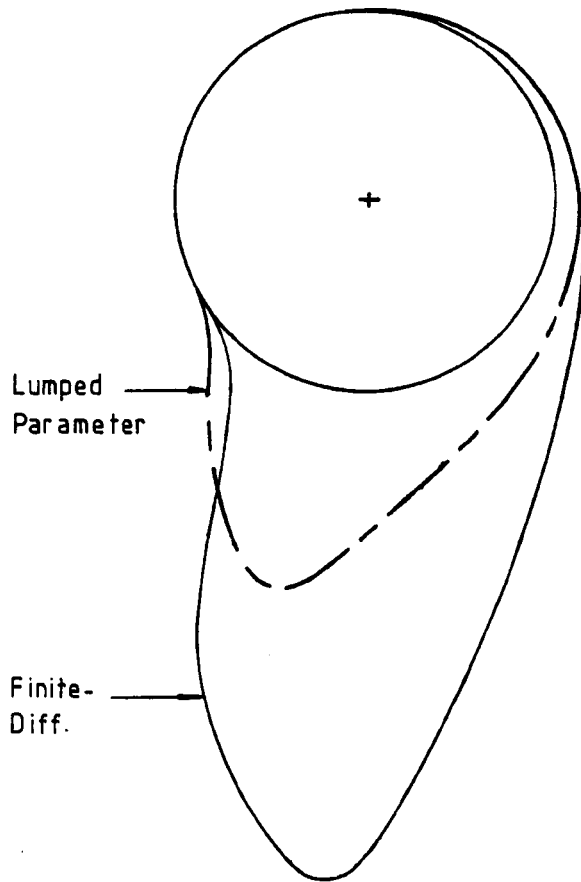
Fig. 5.17a : Circumferential Pressure At Outer Land.
$(\text{a}/_L = 0.4, \text{L}/_D = 1.0, \beta = 0.5, K = 3.0, \epsilon = 0.9)$
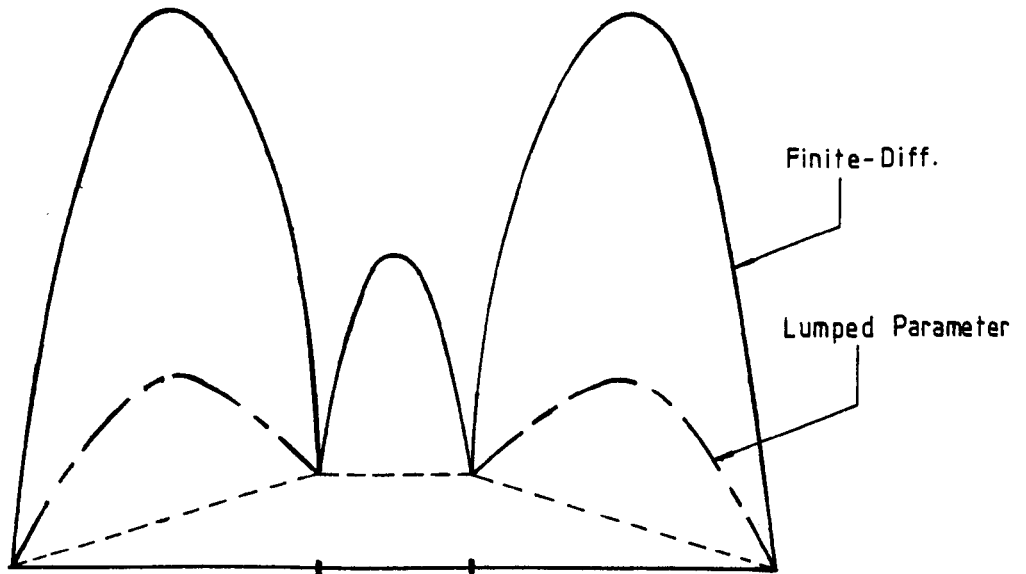
Fig. 5.17b : Axial Pressure — Heavily Loaded Side.

REFERENCES

1. Hamming, R.W. 'Numerical Methods for Scientists and Engineers',
    1st Ed., McGraw-Hill, N.Y., 1962.

2. Smith, D.M. 'Journal bearing dynamic characteristics - Effect of
    inertia of lubricant', Proced. Instn. of Mech.
    Engrs., Vol. 179, Pt. 3J, 1965, pp. 37-44.

3. Booker, J.F. 'Dynamically loaded journal bearings: Mobility
    method of solution', Jnl. of Basic Engrng.,
    Sept. 1965, pp. 537-546.

4. Heller, S. 'Static and dynamic performance of externally
    pressurized fluid film journal bearings in the
    turbulent regime', Jnl. of Lub. Tech., Trans,
    ASME, July, 1974, pp. 381-390.

5. Walton, M.H. 'Investigation of static and dynamic characteristics
    of circular journal bearings in superlaminar
    regimes', Ph.D. Thesis, Dept. of Mech. Eng.,
    Herriot-Watt Univ., Jan. 1975.

6. Reinhardt, E. and Lund, J.W. 'The influence of fluid inertia on
    the dynamic properties of journal bearings',
    Jnl. of Lub. Tech., Trans. ASME, April, 1975,
    pp. 159-167.

7. Block, H. 'Full journal bearings under dynamic duty: Impulse
    method of solution and flapping action', Jnl.
    of Lub. Tech., Trans. ASME, April 1975, pp.
    168-179.

163

8.   Rohde, S.M. and Ezzat, H.A.   'On the dynamic behaviour of hybrid journal bearings', GMR Research Publication - GMR 1853, April, 1975.

9.   Jain, P.C. and Srinivasan, V.   'A review of self-excited vibrations in oil film journal bearings', Wear, 31 (1975), pp. 219-225.

10. Bannister, R.H.   'A theoretical and experimental investigation illustrating the influence of non-linearity and misalignment on the 8-oil film coefficients', Vib. in Rot. M/ry., I.Mech.E. Conf., Cambridge, Sept. 1976.

11. Parkins, D.W.   'Theoretical and experimental determination of the dynamic characteristics of a hydrodynamic journal bearing', Jnl. of Lub. Tech., Trans. ASME, April 1979, pp. 129-139.

12. Craighead, I.A., Dowson, D., Sharp, R.S. and Taylor, C.M. 'The influence of thermal effects and shaft mis-alignment on the dynamic behaviour of fluid-film bearings', Proceds. of the 6th Leeds-Lyon Symp. on Trib., Sept. 1979, pp. 47-55.

13. Boncompain, R. and Frene, J.   'Thermohydrodynamic analysis of a finite journal bearing static and dynamic characteristics', Proceds. of the 6th Leeds-Lyon Symp. on Trib., Sept. 1979, pp. 33-44.

14. Ichikawa, A.   'Fluid inertia effects on the dynamic characteristics of a hybrid plain journal bearing', Jnl. Japan Soc. of Lub. Engrs., Vol. 25, Part

4, 1980, pp. 261-268.

15. Lund, J.W. 'Review of analytical methods in rotor-bearing dynamics', Tribology Int., Oct. 1980, pp. 233-236.

16. Dowson, D. and Taylor, C.M. 'The state of knowledge in the field of bearing influenced rotor dynamics', Tribology Int., Oct. 1980, pp. 196-198.

17. Glienicke, D., Han, C. and Leonhard, M. 'Practical determination and use of bearing dynamic coefficients', Tribology Int., Dec. 1980, pp. 297-309.

18. Holmes, R. 'The measurement of oil film stiffness and damping', Seminar on Journal Bearing Dynamics, I.Mech.E., Stafford, Nov. 1982.

CHAPTER 6

MODELLING AND IDENTIFICATION ANALYSIS

6.1 Introduction

In this chapter, some of the important aspects of identification are briefly discussed, followed by a review of the techniques employed in the identification of bearing fluid-film characteristics. The chapter covers, the derivation of the expressions for the bearing fluid-film transfer function, the identification analysis leading to the determination of these models from the overall system and the procedure for estimating the bearing coefficients from experimental results.

6.2 Identification Analysis

Identification or system modelling is concerned with:

(1) the determination of a mathematical model to describe the input (forcing function) and output (response) relationship of the dynamic system, through some form of difference (discrete time system) or differential (continuous time system) equations, and

(2) the experimental testing of the actual system to obtain information about the system's input-output relationship.

There are a number of techniques available for system identification. These techniques may be based on analysis in the time domain or frequency domain. Examples of techniques using the analysis in the time domain are the transient response techniques (step and impulse), model reference (Z - transform modelling) and correlation techniques. The frequency response (sinusoidal testing) and the spectral analysis techniques, are examples of techniques using analysis in the frequency domain.

The transient response and frequency response techniques are classical methods of analyses. Such methods of analyses are based on

transfer function representations and are associated with deterministic forcing functions. The frequency response method is the most widely used technique. It is simple to apply and provides reliable results. This investigation is concerned with the application of the frequency response method for identifying the slot-entry bearing oil-film characteristics. The background theory on the frequency response method is outlined in Appendix VIII.

The correlation and spectral analysis methods are statistical methods of identification and are associated with broad band or parallel frequency excitations. Such methods of analysis are involved with non-deterministic forcing functions. Some of the common forms of broad band signals are the pseudo random binary sequency (PRBS) signals and white noise. These methods are idealy suited for on-line testing of the system transfer function or for a noisy environment. By application of the appropriate statistical procedure of identification (correlation or spectral analysis), the effect of the inherent noise can be largely eliminated and the response characteristics may be accurately determined. It is beyond the scope of this thesis to discuss the background theory governing the correlation and spectral analysis methods, when excellent references on this subject are available (6, 7 and 9).

The correlation and spectral analysis methods may be viewed as the identification techniques that are at the interface between classical and modern control. In modern control, the models used to describe the system are parametric, in terms of state equations. Such methods of analysis are based on the use of estimation and optimization theory. In contrast to the methods mentioned above, in which the system parameters have to be inferred from the measured waveform, modern parametric methods produce a direct estimate of the system parameters.

6.3 Review of Previous Work on Identification of Bearing Fluid-Film Characteristics

There have been numerous reports on the application of identification techniques for estimating linearized oil-film coefficients. In some cases, the stiffness coefficients may be determined from static measurements (1, 4) which do not require the use of such identification techniques. Static measurements of the stiffness coefficients may be achieved by adopting the 'force' or the 'displacement' method. The 'force' method consists of applying a force in two directions in turn and each time measuring the resulting deflections in two orthorgonal directions (1). In the 'displacement' method, a controlled displacement is applied in two directions in turn, and each time the resulting forces along and normal to the displacements are measured (4).

A range of identification techniques have been employed for estimating the bearing oil-film characteristics. They may be classified in terms of the type of excitation.

a)   Harmonic Forcing

The technique of exciting the bearing sinusoidally (frequency response method) constitutes one of the most widely used method in the identification of bearing oil-film characteristics. Sinusoidal excitations may be generated by unbalance in the shaft or via vibrators. Published work relating to this subject dates from Glienicke (2), who excited the bearing at a frequency synchronous with the rotational frequency, via two vibrators. The eight coefficients were determined directly from the frequency response data. The measurements of the vibration amplitudes and phase angles of the resulting motion in the two directions, provided the necessary 8 equations for the solution of the coefficients (2 sets of 4 equations). Glienicke indicated that an accuracy of ± 1% in amplitude and ± 1 degree in phase was necessary to obtain an accuracy of ± 5% in the final coefficients. Morton (5) used

a similar method to that of Glienicke on a large scale test-rig, but excited the bearing at a frequency (10 Hz and 15 Hz) non-cynchronous with the running frequency. This work is particularly relevant to the author's investigation. The stiffness and damping coefficients were calculated from the frequency response functions. Poor correlation between the experimental and theoretical coefficients were observed. The application of the sinusoidal testing method to a large scale test-rig has also been reported by Hisa et. al. (17).

Woodcock and Holmes (4) determined the stiffness coefficients (static measurements) from one rig and damping coefficients from another, where a central unbalance located on the journal was used to generate the sinusoidal excitation at the journal frequency. The journal response (amplitude and phase) together with the previously determined stiffness coefficients were used to obtain the damping co-efficients. This necessitates the solution of 2 sets of simultaneous equations, having 2 equations in each set, in contrast to the methods of Morton (5) and Glienicke (2), which requires the solution of 2 sets of 4 equations. They indicated that a phase error of ± 1 degree would produce a ± 2% error in the damping coefficients.

Some of the limitations of sinusoidal testing are:

(i)   the test frequencies selected may not excite the system in a manner such that all the system modes are excited, although this limitation may be overcome by introducing broad-band excitation.

(ii)   frequency response testing over a wide frequency spectrum is a time consuming process, hence the accuracy may be affected by parameter drift.

(iii) the presence of noise, generated by surface roughness, lack of journal circularity, and instrumentation, may lead to the problem

of signal corruption.

(iv)   the difficulty of obtaining accurate measurements of the phase

angle, though this may be overcome by modern equipment.

b)   Step Forcing

A different method of obtaining relative motion between journal

and bearing was reported by Morton (8), which allows a step change in

force to be applied to a rotating shaft. Using Fourier transformation

Morton obtained the complex form of the frequency response functions

from the transient data. The coefficients were then determined at

single frequencies. Low pass filters were used to filter some of the

high frequency noise. The synchronous frequency signals generated

by the residual out-of-balance and machining imperfections were re-

moved from the step response manually. The resulting estimated co-

efficients exhibited considerable experimental scatter, especially the

cross-damping terms which were poorly defined. Morton attributed this

to ill-conditioning of the receptance matrix.

The disadvantages associated with step forcing are:

(i)   a step function is band limited and may only be capable of weakly

exciting certain system modes.

(ii)   the transient signals are highly sensitive to corruption by noise.

c)   Broad-Band Excitation

In recent years there has been a dramatic increase in the use of

multi-frequency test signals in the identification of bearing oil-

film characteristics. Dogan, Burdess and Hewit (15) have reported a

frequency-domain technique for estimating the bearing oil-film co-

efficients using PRBS test signals. The bearing coefficients were

determined by fitting transfer functions to the experimental results.

The identification of the bearing oil-film coefficients by means of

the impact method was reported by Nordmann and Schollhorn (16). The

rotor was excited by a hammer (pulse testing). By Fourier transform-
ation, the signals from the time domain were transformed to the fre-
quency domain, and the complex frequency response functions were det-
ermined. Analytical frequency response functions were then fitted to
the measured functions based on the principle of least squares. The
stiffness and damping coefficients were then determined by an intera-
tive fitting process. Burrows and Stanway (10) have proposed the use
of PRBS signals in the time-domain, with a multiple regression analysis
for estimating the coefficients and applied the method to squeeze film
dampers (11, 12, 13). Their approach involved the digital processing
of the sampled displacement and disturbing forces, thus producing direct
estimates of the coefficients. Although time-domain estimation based
on multi-frequency test signals and a least squares estimator is
ideally superior to the classical approaches, in practice, measurement
noise and the transformation from continuous to discrete time in the
numerical process tend to cause large errors in the coefficient est-
imated (14). In order to reduce the effect of noise on the estimates,
Sahinkaya and Burrows (23) have presented a technique which employed
a Kalman filter together with a sequential least-square estimator.

PRBS and SPHS (Schroeder-phased harmonic signals) testing of
squeeze-film bearings in the frequency domain, have been reported by
Burrows et. al. (18) and later, Burrows and Sahinkaya (19) presented
a frequency domain algorithm which produces estimates for the co-
efficients directly from the test data, without recourse to curve-
fitting. Recently, they developed a similar algorithm in the time-
domain, but, instead of a multi-frequency test signal, the rotor's
synchronous (unbalance) response was used as the test signal (22).

Although reasonable accuracy in the coefficient estimates have
been reported by most of the investigators, it should be noted that
the majority of the investigations were carried out under 'controlled'

conditions and limited to simple bearing models, such as squeeze-film dampers. Hence, contributing to the difficulty in comparing the reliability of the identification techniques developed in the field of modern control, with the classical methods. However, in view of the limitation (large scatter in the coefficients and time consuming) offered by the classical methods, there is reason to believe that modern control will play a major role in the identification of bearing oil-film characteristics.

d)   Indirect Approach

An indirect approach to coefficient determination has been reported by Orcutt and Arwas (3). They measured journal orbits produced by a synchronous unbalanced rotation. Displacement and damping coefficients obtained from theory were used to predict the journal vibration. Validity of the oil-film coefficients was inferred from a satisfactory comparison between the experimental and theoretical orbits.

Recently this approach to determination of coefficients has been substantiated by Holmes (20), who argued that as long as predicted synchronous responses have been seen to be adequate over a sufficiently large range of test conditions, some uncertainty in the coefficients is unimportant. This is due to the fact that the equations from which the stiffness and damping coefficients are deduced, tend to be ill-conditioned, whilst the reverse process is well-conditioned.

6.4 Modelling the Bearing Fluid-Film

A mechanical representation of the bearing system is illustrated in figure (6.1). Preliminary experimental tests carried out on the test-rig, indicated that the assumption of a rigid shaft is not justified. (See Chapter 8). Hence, the flexibility of the shaft has to be considered. This would require a knowledge of the test-shaft's flexibility (stiffness). A method for determining the stiffness of the test-shaft is presented in Appendix IX. The analysis showed that
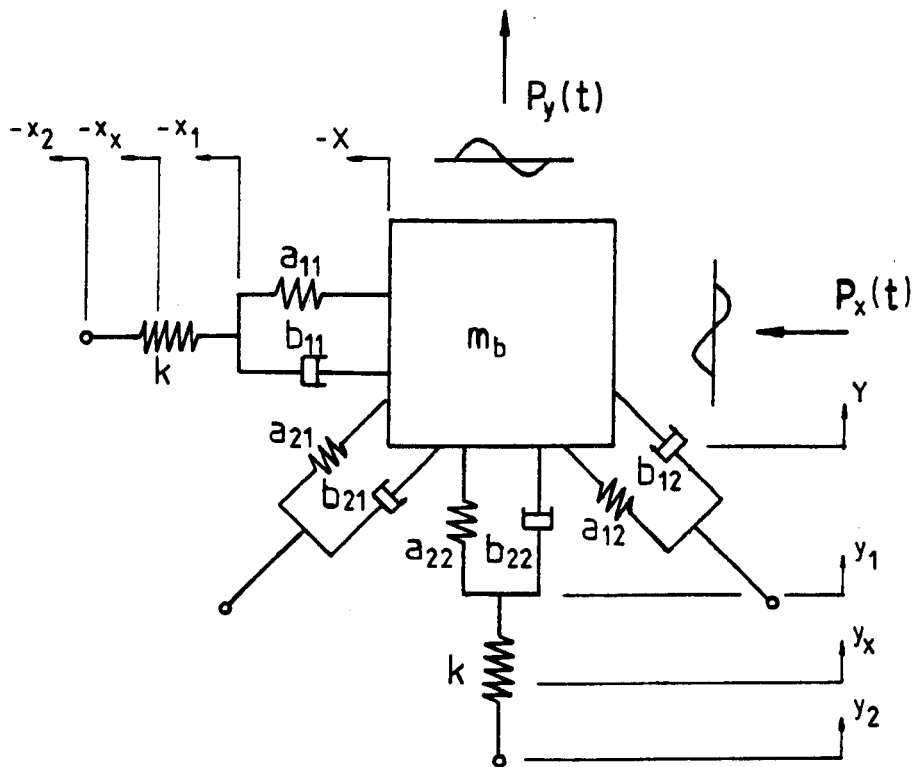
Fig. 6.1 : Mechanical Representation Of The Bearing System.
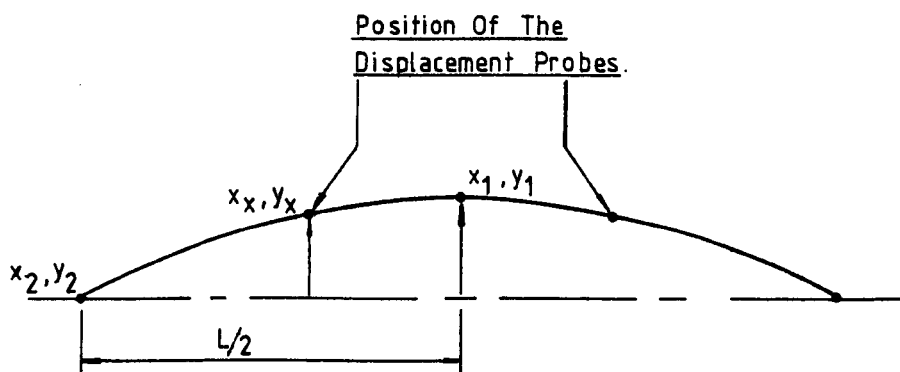
Fig. 6.2 : The Deflected Shaft.

a stiffness of 73.20 MN-m^{-1} may be assigned to the test-shaft.

With the system at equilibrium the equations of motion for

excitation by forces $P_x(t)$ and $P_y(t)$, may be written as:

$$-\delta F_x(t) = - a_{11}\, x_f - b_{11}\, \dot{x}_f + a_{12}\, y_f + b_{12}\, \dot{y}_f \;\ldots \qquad (6.1)$$

$$\delta F_x(t) = k\,(x_s + (x_x - x_2)) \;\ldots \qquad (6.2)$$

$$\delta F_y(t) = -a_{21}\, x_f - b_{21}\, \dot{x}_f + a_{22}\, y_f + b_{22}\, \dot{y}_f \;\ldots \qquad (6.3)$$

$$\delta F_y(t) = k\,(y_s + (y_x - y_2)) \qquad (6.4)$$

where:

$$\delta F_x(t) = P_x(t) - m_b\, \ddot{X} \quad ; \quad \delta F_y(t) = P_y(t) - m_b\, \ddot{Y}$$

$$x_s = (x_1 - x_x) \qquad ; \qquad x_f = (X - x_1)$$

$$y_s = (y_1 - y_x) \qquad ; \qquad y_f = (Y - y_1) \qquad (6.5)$$

$$\dot{x}_f = (\dot{X} - \dot{x}_1) \qquad ; \qquad \dot{y}_f = (\dot{Y} - \dot{y}_1)$$

Expressions governing the relationship between $(x_x - x_2)$ and x_x,

or $(y_x - y_2)$ and y_x, may be derived. The derivation is presented in

Appendix IX. By substituting equations (AIX-13) and (AIX-14) into

equations (6.2) and (6.4), the following equations are formed:

$$\delta F_x(t) = k\,(4.5044)\, x_s \qquad (6.6)$$

$$\delta F_y(t) = k\,(4.5044)\, y_s \qquad (6.7)$$

As the test-shaft is, in fact flexible, the displacement recorded by

the transducers (see figure (6.1) and (6.2)), will consist of:

(i) the displacement of the fluid-film, x_f or y_f, and

(ii) the deflection of the shaft, x_s or y_s.

So that,

$$x = x_s + x_f$$
$$y = y_s + y_f \qquad (6.8)$$

Substituting equations (6.8) into equations (6.6) and (6.7), and re-

arranging yields:

$$x_f = x - \frac{\delta F_x(t)}{k'} \qquad (6.9)$$

$$y_f = y - \frac{\delta F_y(t)}{k'} \qquad (6.10)$$

where:

$$k' = k \ (4.5044) \qquad (6.11)$$

Laplace transforming equations (6.1), (6.3), (6.9) and (6.10), with

zero initial conditions yields:

$$-\delta F_x(s) = - (a_{11} + sb_{11}) \ x_f(s) + (a_{12} + sb_{12}) \ y_f(s) \qquad (6.12)$$

$$\delta F_y(s) = - (a_{21} + sb_{21}) \ x_f(s) + (a_{22} + sb_{22}) \ y_f(s) \qquad (6.13)$$

$$x_f(s) = x(s) - \frac{\delta F_x(s)}{k'} \qquad (6.14)$$

$$y_f(s) = y(s) - \frac{\delta F_y(s)}{k'} \qquad (6.15)$$

Substituting the expressions for $x_f(s)$ and $y_f(s)$ into equations (6.12)

and (6.13), will yield the appropriate form of the equations of motion,

that take into account the deflected shaft. Hence:

$$-\delta F_x(s) = - (a_{11} + sb_{11}) \quad x(s) - \frac{\delta F_x(s)}{k'} \quad \ldots$$

$$\ldots + (a_{12} + sb_{12}) \quad y(s) - \frac{\delta F_y(s)}{k'} \qquad (6.16)$$

$$\delta F_y(s) = - (a_{21} + sb_{21}) \quad x(s) - \frac{\delta F_x(s)}{k'} \quad \ldots$$

$$\ldots + (a_{22} + sb_{22}) \quad y(s) - \frac{\delta F_y(s)}{k'} \qquad (6.17)$$

Rearranging the above equations, and writing in matrix notation yields:

$$\begin{bmatrix} (a_{11} + sb_{11}) & - (a_{12} + sb_{12}) \\ -(a_{21} + sb_{21}) & (a_{22} + sb_{22}) \end{bmatrix} \begin{bmatrix} x(s) \\ y(s) \end{bmatrix} = \ldots$$

$$\ldots \begin{bmatrix} \dfrac{k' + (a_{11} + sb_{11})}{k'} & \dfrac{-(a_{12} + sb_{12})}{k'} \\ -\dfrac{(a_{21} + sb_{21})}{k'} & \dfrac{k' + (a_{22} + sb_{22})}{k'} \end{bmatrix} \begin{bmatrix} \delta F_x(s) \\ \delta F_y(s) \end{bmatrix} \qquad (6.18)$$
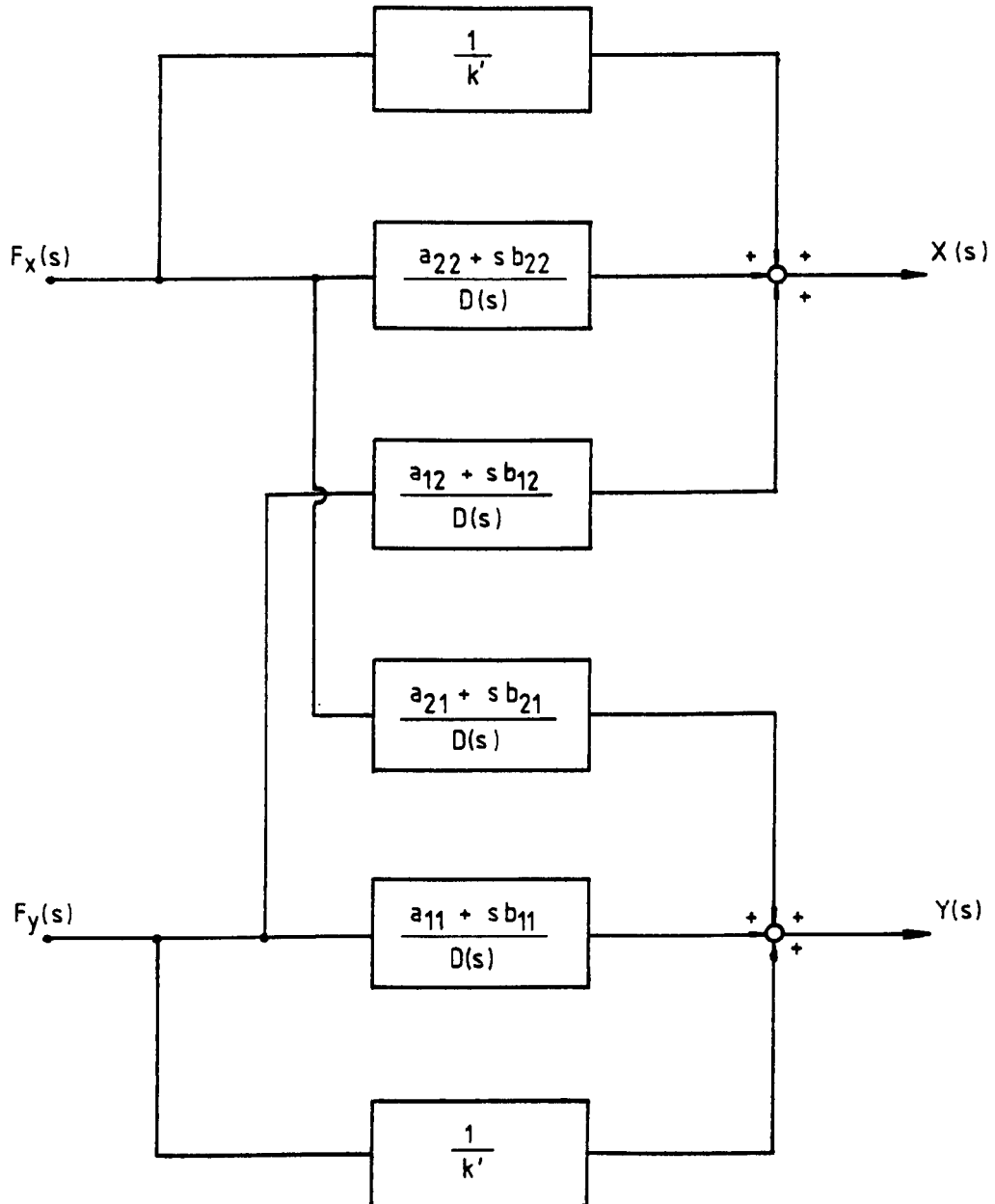
Fig. 6.3 : Block Diagram Model Of The Bearing Fluid-
Film Taking Into Account Shaft's Flexibility.

The expressions for x(s) and y(s) may be derived from the above equations and expressed in the form:

$$
\begin{bmatrix} x(s) \\ \\ y(s) \end{bmatrix}
=
\begin{bmatrix} G_{11}(s) & G_{12}(s) \\ \\ G_{21}(s) & G_{22}(s) \end{bmatrix}
\begin{bmatrix} \delta F_x(s) \\ \\ \delta F_y(s) \end{bmatrix}
\tag{6.19}
$$

where the transfer function matrix is:

$$
\begin{bmatrix} G_{11}(s) & G_{12}(s) \\ \\ G_{21}(s) & G_{22}(s) \end{bmatrix}
=
\begin{bmatrix} \left(\dfrac{(a_{22} + sb_{22})}{D(s)} + \dfrac{1}{k'}\right) & \dfrac{(a_{12} + sb_{12})}{D(s)} \\ \\ \dfrac{(a_{21} + sb_{21})}{D(s)} & \left(\dfrac{(a_{11} + sb_{11})}{D(s)} + \dfrac{1}{k'}\right) \end{bmatrix}
\tag{6.20}
$$

and

$$
D(s) = (a_{22} + sb_{22})(a_{11} + sb_{11}) - (a_{12} + sb_{12})(a_{21} + sb_{21}) \tag{6.21}
$$

The block diagram representation of equation (6.19) is illustrated in figure (6.3). It can be seen that the direct-coupled responses are functions of 3 parameters, namely:

(i)   the characteristics of the fluid-film

(ii)   the flexibility of the shaft, and

(iii)   the position where the responses are measured.

$G_{ij}(s)$ may be represented in the complex form by the frequency response function $G_{ij}(j\omega)$, obtained by replacing s by $j\omega$ in equation (6.20), that is:

$$
G_{ij}(j\omega) = R_{e\ i,j}(\omega) + I_{m\ i,j}(\omega) \tag{6.22}
$$

where,

$R_{e\ i,j}$ = Real part of $G_{i,j}$

$I_{m\ i,j}$ = Imaginary part of G_{ij}

The theoretical frequency response characteristics are then given by:

$$\left| G_{i,j} \ (j\omega) \right| \quad \text{and} \quad \phi_{i,j} \ (j\omega), \quad \text{where:}$$

$$\left| G_{i,j} \ (j\omega) \right| \quad = \quad \left[\ (R_{e \ i,j} \ (\omega))^2 + (I_{m \ i,j} \ (\omega))^2 \right]^{\frac{1}{2}}$$

$$\phi_{i,j} \ (j\omega) \quad = \quad \tan^{-1} \left(\frac{I_{m \ i,j} \ (\omega)}{R_{e \ i,j} \ (\omega)} \right)$$

(6.23)

By substituting the appropriate values of the coefficients into the expressions of G_{ij} $(j\omega)$, the complete set of frequency response characteristics may be generated. A computer program (FRP.FOR) based on equations (6.23), was written to handle this task.

6.5 Identification of the Bearing Fluid-Film Transfer Functions

The transfer functions $G_{ij}(s)$ may be determined from two experiments as follows. Due to cross-coupling effects two sets of experiments are required. In each experiment one of the input forces is arranged to be zero and the other input force and the corresponding outputs x and y are measured. If $P_y(t)$ is zero, then:

$$G_{11}(s) \quad = \quad \frac{x(s)}{\delta F_x(s)}$$

and

(6.24)

$$G_{21}(s) \quad = \quad \frac{y(s)}{\delta F_x(s)}$$

Similarly when $P_x(t)$ is zero,

$$G_{12}(s) \quad = \quad \frac{x(s)}{\delta F_y(s)}$$

and

(6.25)

$$G_{22}(s) \quad = \quad \frac{y(s)}{\delta F_y(s)}$$

An electronic circuit may be constructed to isolate the mechanics of the fluid-film from the inertia of the bearing mass, hence yielding the signals δF_x and δF_y directly. (See Chapter 7).

Any of the identification methods described in Sections 6.2 and

6.3, may be used to identify the transfer functions G_{11}, G_{12}, G_{21} and G_{22}. In this investigation, the sinusoidal testing technique was selected. Although the problems associated with sinusoidal testing are well known, it was felt that with modern instrumentation and the incorporation of a desk-top computer acting as the main controller, some of these problems may be eliminated. Human intervention is kept to a minimum, as once the initial conditions are set, the entire operation will be controlled by the computer, resulting in a full scale automatic testing routine. (See Chapters 7 and 8). The technique involves the application of sinusoidal signals in turn in the X and Y directions, at a frequency non-synchronous with the journal rotational frequency. In each case the complex responses, G_{ij} ($j\omega$), are measured for both directions.

6.6 Technique for Determination of Bearing Coefficients from the Frequency Responses

Once the frequency response functions, G_{ij} ($j\omega$), of the bearing have been found, the bearing coefficients may be determined using any of the methods described in Section 6.3. In this investigation, the direct method (a method used by Morton (5)), was used to determine the bearing coefficients. Ideally, a minimization routine, such as the least squares method, which minimizes the difference between the theoretical and experimental transfer function matrix, should be incorporated into the bearing coefficient evaluation routine.

Using the term receptance to define the complex quotient of a displacement vector and a force vector of a linear system, vibrating sinusoidally, the following equations of motion may be written:

$$\begin{bmatrix} x \\ \\ y \end{bmatrix} = \begin{bmatrix} R_{11} & R_{12} \\ \\ R_{21} & R_{22} \end{bmatrix} \begin{bmatrix} \delta F_x \\ \\ \delta F_y \end{bmatrix} \qquad (6.26)$$

where the receptance matrix is:

$$\begin{bmatrix} R_{11} & R_{12} \\ R_{21} & R_{22} \end{bmatrix} = \quad \ldots$$

$$\ldots \begin{bmatrix} \left|\dfrac{x}{\delta F_x}\right| (\cos\phi_{11} + j\sin\phi_{11}) & \left|\dfrac{x}{\delta F_y}\right| (\cos\phi_{12} + j\sin\phi_{12}) \\ \\ \left|\dfrac{y}{\delta F_x}\right| (\cos\phi_{21} + j\sin\phi_{21}) & \left|\dfrac{y}{\delta F_y}\right| (\cos\phi_{22} + j\sin\phi_{22}) \end{bmatrix} \quad (6.27)$$

or,

$$R_{i,j}(\omega) = \left| G_{i,j}(j\omega) \right| (\cos\phi_{i,j} + j\sin\phi_{i,j}) \qquad (6.28)$$

Comparing equation (6.26) with equations (6.19) and (6.20), the following relationships may be written:

$$\begin{bmatrix} R_{11}(\omega) & R_{12}(\omega) \\ \\ R_{21}(\omega) & R_{22}(\omega) \end{bmatrix} = \begin{bmatrix} \left(\dfrac{(a_{22} + j\omega b_{22})}{D(j\omega)} + \dfrac{1}{k'}\right) & \dfrac{(a_{12} + j\omega b_{12})}{D(j\omega)} \\ \\ \dfrac{(a_{21} + j\omega b_{21})}{D(j\omega)} & \left(\dfrac{(a_{11} + j\omega b_{11})}{D(j\omega)} + \dfrac{1}{k'}\right) \end{bmatrix} \quad (6.29)$$

Equation (6.29) may be rewritten as:

$$\begin{bmatrix} R_{11}^{*}(\omega) & R_{12}(\omega) \\ \\ R_{21}(\omega) & R_{22}^{*}(\omega) \end{bmatrix} = \dfrac{1}{D(j\omega)} \begin{bmatrix} (a_{22} + j\omega b_{22}) & (a_{12} + j\omega b_{12}) \\ \\ (a_{21} + j\omega b_{21}) & (a_{11} + j\omega b_{11}) \end{bmatrix} \quad (6.30)$$

where.

$$R_{11}^{*}(\omega) = \left| G_{11}(j\omega) \right| \left(\left(\cos\phi_{11} - \dfrac{1}{k'}\right) + j\sin\phi_{11}\right)$$

$$\qquad (6.31)$$

$$R_{22}^{*}(\omega) = \left| G_{22}(j\omega) \right| \left(\left(\cos\phi_{22} - \dfrac{1}{k'}\right) + j\sin\phi_{22}\right)$$

An inversion of the matrix equation (6.30) may be carried out, giving:

$$\begin{bmatrix} (a_{11} + j\omega b_{11}) & -(a_{12} + j\omega b_{12}) \\ \\ -(a_{21} + j\omega b_{21}) & (a_{22} + j\omega b_{22}) \end{bmatrix} = \begin{bmatrix} R_{11}^{*}(\omega) & R_{12}(\omega) \\ \\ R_{21}(\omega) & R_{22}^{*}(\omega) \end{bmatrix}^{-1} \quad (6.32)$$

Thus the real part of the inverted receptances lead to the stiffness

coefficients and the imaginary parts to the damping coefficients,

that is:

$$a_{i,j} \Big|_{i=j} \quad = \quad \text{Real} \left[R^*_{i,j}(\omega) \right]^{-1}$$

$$a_{i,j} \Big|_{i \neq j} \quad = \quad \text{Real} \left[R_{i,j}(\omega) \right]^{-1}$$

$$b_{i,j} \Big|_{i=j} \quad = \quad \frac{1}{\omega} \left(\text{Imag.} \left[R^*_{i,j}(\omega) \right]^{-1} \right)$$

$$b_{i,j} \Big|_{i \neq j} \quad = \quad \frac{1}{\omega} \left(\text{Imag.} \left[R_{i,j}(\omega) \right]^{-1} \right)$$

(6.33)

A program based on equations (6.33), was developed and implemented

on the desk-top computer. (See Chapter 7), Since, the values of $a_{i,j}$

and $b_{i,j}$ are determined at a single frequency, the accuracy of the

coefficients depends on the accuracy of the measurements at the part-

icular frequency. This method, therefore, requires a careful selection

of the test frequencies. By performing a sensitivity analysis, Burrows

and Turkey (21) indicated that at certain frequency bands, the phase

characteristics may be in error, whilst at some other frequency bands,

the amplitude characteristics may be in error.

REFERENCES

1. Mitchell, J.R., Holmes, R., and Van Ballegooyen, H. 'Experimental determination of a bearing oil-film stiffness.' Proc. I.Mech.Engrs., 1965-66, 180 (pt. 3k), 90.

2. Glienicke, J. 'Experimental investigation of the stiffness and damping coefficients of turbine bearings. Proc. Instn. Mech. Engrs., Vol. 181, Pt. 3B, 1966-67, pp, 116-129.

3. Orcutt, F.K., and Arwas, E.B., 'The steady-state and dynamic characteristics of a full circular bearing and a partial arc bearing in the laminar and turbulent regimes.' ASME Journal of Lub. Tech., April, 1967.

4. Woodcock, J.S., and Holmes, R. 'The determination and application of the dynamic properties of a turbo-rotor bearing oil-film.' Proc. Instn. Mech. Engrs., Vol. 184, Pt. 3L (1969-70), pp. 111-119.

5. Morton, P.G., 'Measurements of the dynamic characteristics of large sleeve bearings.' Trans. ASME, Jnl. of Lub. Tech., 1971, Vol. 193, pp. 143-150.

6. Graupe, D. 'Identification of Systems.' Van Nostraud Reinhold, 1972.

7. Harris, R.W., and Ledwidge. T.J. 'Introduction to noise analysis.' Pion Limited, 1974.

8. Morton, P.G. 'The derivation of bearing characteristics by means of transient excitation applied directly to a rotating shaft.' Proceedings of the IUTAM Symposium on Dynamics of Rotors, Copenhagen, 1974, pp. 350-379.

9.   Newland, D.E.   'Random Vibrations and Spectral Analysis.'

        Longman, 1975.

10. Burrows, C.R., and Stanway, R.   'Identification of Journal

        Bearing Characteristics.'   ASME Jnl. of Dynamic Systems,

        Measurement and Control, Sept. 1977, pp. 167-173.

11. Stanway, R., Burrows, C.R., and Holmes, R.   'Pseudo-Randon Binary

        Sequence Forcing in Journal Squeeze-Film Bearings.'   Trans.

        ASLE, Vol. 22, No. 4, 1979, pp.1-8.

12. Stanway, R., Burrows, C.R., and Holmes, R.   'Discrete-Time

        Modelling of a Squeeze-Film Bearing.'   Jml. of Mech. Eng.

        Science, I.Mech.E., Vol. 21, No. 6, 1979, pp. 419-427.

13. Stanway, R., Burrows, C.R., and Holmes, R.   'Parametric Estimation

        of a Squeeze-Film Bearing.'   5th IFAC Symposium on Ident-

        ification and Parametric Estimation, Darmstadt, Sept. 24 -

        28, 1979.

14. Burrows, C.R., and Stanway, R.   'A Coherent Strategy for Estimating

        Linearized Oil-Film Coefficient.'   Proc. Royal Soc.,

        London, Vol. A370, 1980, pp. 89-105.

15. Dogan, I.U., Burdess, J.S. and Hewit, J.R., 'Identification of

        Journal Bearing Coefficients using a Pseudo-Random Binary

        Sequence.'   2nd. International Conference on Vibrations in

        Rotating Machinery, I.Mech.E., Cambridge, Sept. 1980,

        pp. 277-281.

16. Nordmann, R. and Schollhorn, K.   'Identification of Stiffness and

        Damping Coefficients of Journal Bearings by means of the

        Impact Method.'   2nd. Int. Conf. on Vibrations in Rotating

        Machinery, I.Mech.E., Cambridge, Sept. 1980, pp. 231-238.

17. Hisa, S., Matsuura, T., and Someya, T., 'Experiments on the Dynamic Characteristics of Large Scale Journal Bearings.' 2nd. Int. Conf. on Vibrations in Rotating Machinery, I.Mech.E., Cambridge, Sept. 1980, pp. 223-230.

18. Burrows, C.R., Sayed-Esfahani, R., and Stanway, R., 'A Comparison of Multi-frequency Techniques for Measuring the Dynamics of Squeeze-Film Bearings.' ASME Jnl. of Lub. Tech., Jan. 1981, Vol. 103, pp. 137-143.

19. Burrows, C.R., and Sahinkaya, M.N. 'Frequency-Domain Estimation of Linearized Oil-Film Coefficients.' Trans. ASME, April 1982, Vol. 104, pp. 210-215.

20. Holmes, R., 'The measurement of Oil-Film Stiffness and Damping.' Seminar on Journal Bearing Dynamics, I.Mech.E. Engineering Sciences Division, Stafford, Nov. 1982.

21. Burrows C.R. and Turkay O.S., 'A Sensitivity Analysis of Squeeze-Film Bearings.' Trans. ASME, Vol. 104, Oct. 1982, pp. 516-522.

22. Sahinkaya M.N. and Burrows C.R., 'Estimation of Linearized Oil-Film parameters from the out-of-balance response.' Proc. Instn. Mech. Engrs., Vol. 198C, No. 8, 1984, pp. 131-135.

23. Sahinkaya, M.N., and Burrows, C.R., 'Kalman filters applied to time-domain estimation of linearized oil-film coefficients.' 3rd. Int. Conf. on Vib. in Rotating Machinery. I.Mech.E., York, Sept. 1984, pp. 109-118.

ADDITIONAL REFERENCES

1. Parkins, D.W., 'Theoretical and experimental determination of the dynamic characteristics of a hydrodynamic journal bearing.'

ASME Jnl. of Lub. Tech., April 1979, Vol. 101, pp. 129-139.

2. Nordmann, R., and Massman H. 'Identification of stiffness, damping and mass coefficients for annular seals.' 3rd Int. Conf. on Vib. in Rotating Machinery, I.Mech.E., York, Sept., 1984, pp. 167-182.

3. Yi L.Y., Kong, F.R., and Chang, Y.S. 'Vibration modal analysis by means of impulse excitation and measurement using strain gauges.' 3rd. Int. Conf. on Vib. in Rotating Machinery, I.Mech.E., York, Sept. 1984, pp. 391-396.

CHAPTER 7

EXPERIMENTAL RIG MODIFICATION AND

INSTRUMENTATION AND TEST SOFTWARE DEVELOPMENT

7.1 Introduction

The general purpose test rig was designed and manufactured by

Koshal (4) for carrying out experimental studies on the static charac-

teristics of slot-entry bearings. A full description of this rig was

presented in reference (4). This chapter is concerned with the mod-

ification of the existing rig, to enable the dynamic characteristics

of the slot-entry bearing to be conveniently determined, using the

identification technique (sinusoidal testing) described in the previous

chapter.

7:2 Brief Description of the Previous Rig.

The test rig was based on an arrangement where the test shaft was

allowed to rotate but could also be translated axially, while the non-

rotating bearing bush was free to float in a radial direction.

The journal was based on a 40 mm (2.57 in.) nominal diameter,

nitride-hardened EN40A chrome molybdenum steel spindle which housed an

inductive displacement transducer and a strain gauge bonded diaphragm

pressure transducer. The shaft was supported between two support blocks

employing slot-entry bearings operating at much higher supply pressures

than the test-bearing (4.48 MN/m^2 (650 lbf/in^2)).

Separate hydraulic power units were used to supply oil to the

test and support bearings. A thermostatically controlled air cooled

gear pump supplies oil to the test bearing. Air seals were installed

at both ends of the support blocks to ensure that the oil escaping

out of the support bearings was directed back into the oil tank. A

feature of this arrangement is, two different oils may be employed for

the test and support bearings, if required.
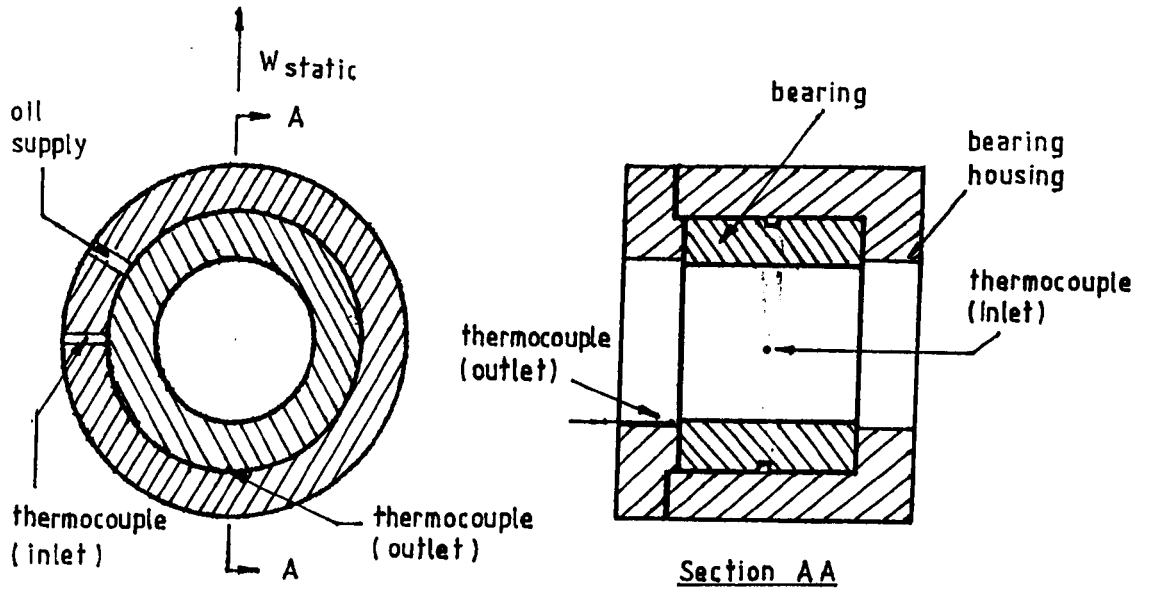
Fig. 7.1a : Test Bearing Showing Position Of Thermocouples.
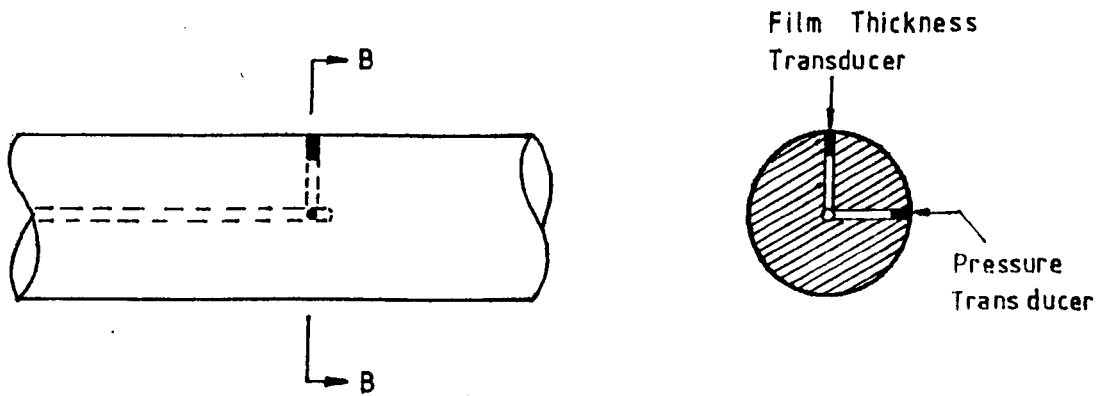
Fig. 7.1b : Test Shaft Showing Position Of Transducers.

A d.c. 3.73 kw (5 HP) thyristor controlled motor, mounted on a carriage drives the test-shaft at continuously variable speeds, from zero to 50 rev/sec. Silver-graphite to silver-graphite connection slip rings were used to direct the signals from the rotating shaft to the stationary signal conditioning equipment.

A misalignment jig was employed to align or misalign the test bearing. The misalignment jig used employed the principle that a taut wire has low lateral stiffness compared to the longitudinal stiffness.

To ensure structural rigidity and to prevent vibrations, the entire test-rig was mounted on a heavy concrete block. With this test-rig, it is possible to measure the following variables: (Figs. 7.1a and 7.1b)

(1) Film Thickness - An inductive displacement transducer mounted in the test shaft, was used to measure the film thickness in the bearing. To measure the displacement of any position in the bearing the test shaft could be rotated and moved axially. The signals from the inductive transducer were fed into a half-bridge circuit and the output was recorded on a u-v recorder or a digital volt meter. The accuracy of the film thickness measurement was $\pm$ 1 μm ($\pm$ 40 μin.) in the range of 0 to 0.7mm.

(2) Pressure - A strain gauge bonded diaphragm transducer mounted in the test shaft, was used to measure the film pressure in the bearing. The pressure at any position in the bearing may be measured. The signals from the transducer were fed into a half-bridge circuit and the output was recorded on a u-v recorder. The accuracy of the pressure measurement was $\pm$ 34.5 kPa ($\pm$ 5 p.s.i.) up to the range of 1000 p.s.i.

(3) Load - The load was applied in the upwards direction. A steel rod was screwed vertically into the bearing housing and was connected to a load cell through a decoupling spring, which allowed the bearing to take up its own attitude angle without constraint. The output from the load cell was recorded on a digital volt meter. The accuracy of the

load measurement was ± 0.5 kg (± 1.1 lb.) in the range of 1 to 125 kg.

(4) <u>Attitude Angle</u> - An inductive transducer was rigidly fixed to the stationary slip ring flange so that it was pointing vertically down-wards onto the test shaft. A fine edge pointer was screwed into the shaft in line with the sensing area of the film thickness transducer. The attitude angle measuring transducer and the pointer in the shaft were adjusted so that a pulse was obtained on the u-v recorder when the displacement transducer in the shaft was pointing vertically upwards. Hence, under rotating conditions the point of maximum film thickness on the output recording will be linearly displaced from the stationary transducer output and the attitude angle was obtained by measurement of the output trace. A sample of the output trace is shown in figure (7.1).

(5) <u>Speed</u> - The rotational speed of the test shaft was measured using a photo-electric transducer which had the light source and detector housed coaxially in a cylindrical body. The motor spindle was painted with black and white stripes (2 white and 2 black stripes). The signals from the photo-electric transducer were fed into a digital frequency counter. The speed in r.p.s. is obtained by dividing the reading shown on the frequency counter by 2. The accuracy of the speed measurement was ± 0.01 r/s within the speed range of 2.5 to 50 r.p.s.

(6) <u>Temperature</u> - Copper-constantan thermocouples were used to measure the temperatures. For the purpose of calculations, the viscosity based on the average of the inlet and outlet temperatures was used. The temperature was measured to an accuracy of ± 0.5°C in the range of 0 to 110°C.

(7) <u>Flow-Rate</u> - The bearing flow-rate may be measured by collecting oil from the test bearing in a container for a timed period. The accuracy of the flow measurement was ± 0.5 cc/min. within the range of 5 cc/min. to 50 cc/min.

(8) <u>Friction Torque</u> - The horizontal arms on each side of the bearing were used to hang pans for weights. The loading arrangement was dis-

connected from the bearing. At each speed setting, the vertical arm was brought back to the null position by adding weights to the appropriate pan. This arrangement for the measurement of torque is limited to low eccentricity-ratios.

(9) <u>Pressure Ratio (β)</u> - The pressure ratio for a hybrid journal bearing may be determined experimentally by measuring the flow-rate through the bearing without the shaft, and again with the shaft in the concentric position. The actual pressure ratio taking into account the errors of manufacture, is given by:

$$\beta = 1 - \frac{q \text{ with shaft}}{q \text{ without shaft}} \qquad (7.1)$$

7.3 Design Requirement

The following design criteria were applied, when carrying out the modifications to the previously existing rig:

(1) The journal speed, the oil supply pressure and the bearing steady load should be adjustable and easily measurable within the bearing operating range.

(2) The steady loading should be applied in such a manner that it would not over constrain the bearing.

(3) A suitable arrangement should be available for correcting any misalignments between the bearing bush and the test shaft.

(4) Provision should be made for the measurments of the eccentricity, oil-film pressure, static load and oil temperature.

(5) The bearing bush should be capable of being excited by sinusoidal excitations in two perpendicular directions over the frequency range of interest.

(6) To ensure rigidity, that is, to eliminate secondary resonance problems, the main mechanical parts of the dynamic loading system should have natural frequencies that are much higher than the

rotational and vibrational frequencies of the bearing assembly.

(7) Provision should be made for the measurements of the excitation force, the dynamic response (displacement signals) and the acceleration of the bearing bush assembly, in two perpendicular directions, and

(8) Provision should be made to facilitate data collection and recording of a large amount of experimental data, and to reduce the time spent on experimentation, as frequency response testing over a wide frequency spectrum is a time-consuming process.

7.4 Modifications Carried Out on The Test Bearing Rig

As the previous test rig was designed to meet the requirements of (1) to (4), of Section 7.3, it was only necessary to carry out work on the test rig, so that the remaining design requirements might be fulfilled. Hence, the work was mainly associated with the mechanical components and instrumentation for dynamic loading, and the development of the test-software, so that a full scale automatic testing routine was achieved.

7.4.1 Dyamic Loading System

Dynamic loads were applied in the horizontal and vertical directions using two electro-magnetic vibrators (Derritron Vibrators VP4 and VP3), which gave a sinusoidal force amplitude of approximately 230 N peak to peak, and a frequency range of 5 Hz to 10,000 Hz. Figure (7.2) shows the arrangement of the dynamic loading system. The connecting link that connected the vibrator to the bearing housing consisted of a small diameter spring steel wire, which functions to protect the vibrator from misalignment. In order that the identification problem, may be treated as a 'black-box', the force transducers were situated as close to the bearing housing as possible.

7.4.2 Bearing Housing

The bearing housing is an important part of the rig as it accommodates the eddy current probes (displacement transducers), accelerometers, force transducers, thermocouples and pressurized oil-supply. Modifications carried out on the bearing housing were as follows (See Plate 3):

(1)   End plates to accommodate the eddy-current probes at both ends of the bearing housing were manufactured. Care was taken to ensure that the end plates have sufficient rigidity.

(2)   The force transducers and the accelerometers were attached to the bearing housing in the appropriate position to ensure that a 'black-box' approach might be used. Great care was taken to ensure that the transducers were located squarely onto the bearing housing.

7.4.3 Misalignment Jig

Although the disign requirements of the existing misalignment jig were adequately met, it was modified to allow the setting up time to be reduced and make the operation of the rig easier.

The misalignment jig was lifted by a height of 60 mm to ensure that the eddy current probes could be accurately positioned and to allow adjustments to be easily carried out. A base plate was introduced into the jig assembly so that the adjustments in the lateral direction were more easily carried out. In the previous design, lateral adjustment was carried out by altering the position of the two horizontal arms that were screwed onto the bearing housing. This was a very tedious operation. In the present system the lateral adjustments may be achieved by loosening the locking screws at the base plate of the misalignment jig, and the entire jig assembly may be moved transversely. Once the correct position has been obtained, the base

plate may be locked into position. A picture of the misalignment jig is illustrated in Plate 4.

7.4.4 Support Blocks

The support bearing blocks were moved apart by 20 mm, on each side. In order that the modified test bearing housing assembly could be located in the appropriate position, care was taken to ensure that the distance moved was a minimum, so that shaft bending was not excessive. However, experimental tests showed that shaft bending did occur. (See Chapter 8).

7.5 The Bearing Test Rig and Instrumentation

A full view of the experimental rig is shown in Plate 5 and Plate 6 illustrates the instrumentation system.

The bearing housing which housed the test bearing was aligned and allowed to move axially by means of the misalignment jig. Four eddy current probes and two accelerometers were located parallel and perpendicular to the vertical axis, and two thermocouples were mounted in the bearing housing.

The steady load was transmitted to the bearing housing in an upwards direction, as described in Section 7.2.

The two vibrators were driven by the Derritron TA300 power amplifier. Input to the power amplifier was supplied from the HP9825A desk-top computer via the Solartron 1172 frequency response analyser. Dynamic force, acceleration and displacement signals from the bearing were measured and analysed by the instrumentation system which consisted of the amplifier, analogue circuits, frequency response analyser and recording and displaying instruments, as illustrated in Plate 6. The HP9825A desk-top computer was used as the active controller. Measurements were initiated and analysed, with the resultant data routed to the desired output device (tape, printer or plotter). The software

for achieving the above operations is discussed in Section 7.8, whilst Section 7.6, discusses the measurement system and the development of the analogue circuits.

7.6 Measurements and Circuit Development

A pictorial representation of the dynamic measurements system is illustrated in figure (7.3). Three electronic circuits were constructed and they formed part of the instrumentation system.

7.6.1 Circuit Development

(1) Summing Circuit for the Displacement Signals

The responses (displacement signals) were monitored at both ends of the bearing. Provided misalignment and conical mode vibrations of the bearing housing are small, a more representative displacement signal may be achieved by averaging the signals. This objective was accomplished by the circuit, illustrated in figure (7.4).

(2) Circuit for Isolating the Mechanics of the Fluid-Film from the Inertia of the Bearing Mass

The object of the experimentation was to measure the fluid-film transfer functions $(G_{i,j})$, hence, a method of extracting the signals that represent the bearing reaction forces $(\delta F_x$ or $\delta F_y)$, from the overall force signals $(P_x$ or $P_y)$, was required. The circuit illustrated in figure (7.5), was constructed to meet this requirement by subtracting inertia forces calculated from the measured values of bearing housing acceleration.

(3) Multiplexer Circuit

Direct and cross responses were required for each of the two directions of excitation. A multiplexer circuit was constructed to direct and switch between the cross and direct coupled signals to the frequency response analyser, automatically upon receiving the instructions from the active controller. The Hewlet Packard 98032A,

16-bit Interface Card (ref. 2), was used to interface the multiplexer circuit to the active controller. The multiplexer circuit is illustrated in figure (7.6).

7.6.2 Measurement of Parameters

The measurement of the following parameters is briefly discussed in Section 7.2, and a detailed description can be found in reference (4):

(1)   Eccentricity-Ratio

(2)   Pressure

(3)   Static Load

(4)   Attitude angle

(5)   Speed

(6)   Temperature

(7)   Flow-Rate

(8)   Friction Torque, and

(9)   Pressure-Ratio (β)

Attention, therefore, needs to be focussed on the dynamic measurements.

7.6.2.1 Displacement Measurements

Eddy current probes (type 250-x, manufactured by Distec, and supplied by Graham & White Instruments Ltd.) were employed to measure the displacement of the bearing bush, relative to the test shaft. Some features of the eddy current probe which made it a suitable choice for the dynamic response measurements are:

(i)   The measurement is not affected by the presence of non-conducting material, such as oil.

(ii)   The output is linear over the desired displacement range (See figure 7.9).

(iii)   It has a high voltage sensitivity of approximately 7.8 mV/μm or
198 mV/0.001 in. (To avoid violating the assumption of linear-
ity, the maximum relative motion between the bearing bush and
the test shaft was limited to 10% of the radial clearance, that
is, 3.14 μm or 125 μin.)

(iv)   It has a flat frequency response characteristic of 0-50 kHz,
which is well within the frequency range of interest.

The measurement system comprises the probes (2 probes for each
direction of excitation), signal conditioning unit (type 915, manu-
factured by Distec), the analogue circuits and the frequency response
analyser. The mounting of 2 eddy current probes, one at each end of
the bearing housing to monitor the dynamic displacement has several
advantages:

(i)   The ideal condition, that is, plane motion between the bearing
bush and test shaft may not necessarily take place, hence, as
long as the error is within the specified range (± 10%), an
averaged reading of the 2 probes would provide a satisfactory
result.

(ii)   It provides a means of checking for vibrations of the conical
mode. By feeding the outputs of the probes at each end of the
bearing directly to the frequency response analyser, the Gain and
Phase characteristics of the displacement signals at each end of
the bearing may be known.

The displacements were measured to an accuracy of ± 0.25 μm
(± 10 μin.)

7.6.2.2   Force Measurements

The dynamic forces were measured using piezo-electric transducers.
A Kistler piezo-electric transducer, type 9031 was employed to measure
the dynamic force in the vertical Y-direction. The unit had a sens-

itivity of 4.42 pC/N, an adequate frequency range (50 kHz resonant
frequency) and can measure forces up to 6 kN to within ± 0.02 N. The
transducer was connected to a Kistler type 5001, charge amplifier by
means of a low noise cable.

The dynamic force in the X-direction was measured using the
B & K piezo-electric transducer, type 8200. This unit has a sens-
itivity of 4 pC/N, a flat frequency response characteristics of 0-20
kHz and can measure forces up to 5 kN to within ± 0.01 N. The trans-
ducer was connected to a Flyde, type 128 CA charge amplifier.

The dynamic force measurement system, therefore, comprised the
load cell, the amplifier, the analogue circuits and the frequency
response analyser.

7.6.2.3 Acceleration Measurements

The accelerations of the bearing housing assembly in the vertical
and horizontal directions, were measured using Endevco type accelero-
meters. The measurement system consisted of the accelerometer, the
Flyde charge amplifier, type 128 CA and the analogue circuit. This
measurement set up was capable of measuring bearing accelerations down
to 0.1 mg.

7.7 Calibration of the Measuring Instruments

In order to establish confidence in any subsequent measurements,
it was necessary to calibrate the various measuring instruments. The
calibrations of the film thickness inductive transducer, the eddy
current probes, static load cell and the dynamic force transducers were
carried out as follows:

A method of calibrating the film thickness inductive transducer
that is dependent upon the bearing geometry was adopted. The attractive
feature of this method is that the calibration may be carried out with
the bearing in situ. Oil was pumped into the bearing and the bearing

was loaded until the bearing bush was in contact with the test shaft, that is, $\varepsilon = 1$. Then by rotating the test shaft such that the inductive transducer was at the position of zero gap, the datum was established. The test shaft was rotated in increments of 10° for a complete revolution and the output was recorded on a u-v recorder and a digital voltmeter. The obtained outputs were matched with the corresponding calculated film thickness around the bearing, at $\varepsilon = 1$. The calibration is presented in figure (7.7). A full description of this method of calibration has been presented in Ref. (4).

The calibration of the static load cell was carried out by using a set of mechanical weights. A sample of the calibrated results is shown in figure (7.8).

The eddy current probes were calibrated with the bearing in situ, that is, the calibration was carried out with the transducers mounted in their measuring positions. The gap between the transducer and the test shaft was set from 0.254 mm (0.010 in) to 1.016 mm (0.040 in), in steps of 0.126 mm (0.005 in), with a feeler gauge. The output voltage against the gap length was plotted and the gradient of the resulting line calculated. This gradient gives the actual voltage sensitivity of the eddy current probe. A sample of the calibration graph is presented in figure (7.9). As the eddy current probes, were employed to monitor the dynamic displacements, it was required to perform a dynamic calibration of the eddy current probe. The probe was removed from the bearing housing and mounted adjacent to a vibrating plate. The Endevco accelerometer was employed as the standard. The calibration set-up is illustrated in figure (7.10). The results of the calibration showed that good frequency response characteristics was observed, within the frequency range of interest. (5 Hz to 100 Hz).

Calibrations were carried out on the dynamic force transducers to

verify the accuracy of the charge output and the frequency response

characteristics of the transducers. In each case, the transducers were

dismantled from the bearing housing and mounted on an independent vib-

rator. The Endevco accelerometer was chosen as the standard. To check

the accuracy of the charge output of the transducer, a known mass was

mounted on top of the force transducer. The accelerometer was then

mounted on top of the known mass. The calibration set-up is illustrated

in figure (7.11). The accuracy of the charge output was determined by

comparing the values of the force measured by the force transducer with

the values of the force obtained by considering the known mass and the

measured acceleration, for a wide range of frequencies. The calibration

showed that the readings of the Kistler transducer has to be corrected

by a factor of 1.55, while the outputs of the B & K transducer has to

be corrected by a factor of 0.86. A calibration set-up, which is

similar to the above, was used to check the frequency response charac-

teristics of the force transducers. The results of the calibration

indicated, that there were some errors in the phase characteristics for

frequencies below 12 Hz, and these were corrected in the analysis.

The viscosity temperature relationship of the oil (Shell Tellus 27)

is presented in figure (7.12). The electronic circuits (force and dis-

placement) were calibrated by introducing voltages which were within the

range of interest, into the circuits, and noting the resulting outputs.

The errors between the theoretical and the actual output voltages were

found to be negligible (± 2%).

7.8 Software Development

Computer programs were written to provide software control over the

entire operation of the Solartron 1172 frequency response analyser

(1172 FRA), and to process the experimental data. Computing was carried

out using the Hewlett Packard 9825A Desk-Top Computer, which has a 24K

byte memory and was fitted with a general and extended input/output ROM,

advanced programing ROM, string programing ROM and matrix ROM. The software consisted of 3 files written onto magnetic tape. The programs were written in Basic. File 0, gives full control of the 1172 FRA and the dynamic measurement system. It also sets up the routine for recording the frequency response data onto magnetic tape. A graphical display of the frequency response data on hard-copy via the HP9872A graph plotter was carried out by file 1. The routine for extracting the bearing coefficients from the frequency response data based on the method described in Section 6.6, was carried out by file 2. Least squares curve fitting was performed on the experimental data, before the coefficients were computed. The listings of the programs are provided in the supplement of this thesis, therefore, in the following paragraphs, the discussion is centered on file 0.

The basic requirement of file 0, is to set up a communication network between the 1172 FRA, the multiplexer circuit and the HP9825A desktop computer, with the computer as the active controller. In order to achieve the above requirement, it is necessary to have a technical understanding of the 1172 FRA as well as the concepts of interfacing. However, dwelling on the subject of interfacing would be outside the scope of this thesis, hence, only the basic principles are discussed, and relevant references are mentioned.

Modern day computers adopt a 'bus-centred' structure, where a common 'bus' (the system's data exchange centre) is used to connect the various devices. The bus consists of address lines, data lines and control lines. All devices that are connected to the bus have a unique address. A sending device puts the address of the receiver on the address lines, and the data for it on the data lines. Devices accept the data from the bus only, when the address bus indicates that they are the intended recipients. Connections between a device and the bus or rather the computer, should ideally be plug to plug compatible, how-

ever, incompatibility of data, electrical and timing characteristics between the devices made this task impossible. It is therefore the duty of the interface to provide the necessary campatibility so that communications between the various devices may be achieved. A good introduction to this subject may be found in references (5), (6), etc.

The operational principle of the 1172 FRA is presented in Appendix X. As the purpose of this section is to describe the control of the 1172 FRA through software, attention is focussed on the programable features of the 1172 FRA. The 1172 FRA is a fully programable instrument, and consists of 2 sets of storage locations - the Latch Store and the Mos Store. The settings of all the front panel touch buttons are held in the Latch Store and each setting has a unique address. All the numerical information, including programmed information such as frequency, integration time, and also the results of measurements, are located in their designated addresses in the Mos Store. Hence, programming of the 1172 and reading of the results of measurements are accomplished by writing data into or reading data from a number of storage locations in the Latch and Mos Stores. The interface functions diagram of the above measurement system is illustrated in figure (7.13).

Data transmissions between the 1172 FRA and the computer, at 'bus' level was accomplished via the 1183-C and 98034A interfaces, and consisted of either a 'T message' or an 'S message'. The 'T message' contains the instructions for reading the data from a specified store and from a specified address or that the measurement status character (one way of detecting the end of a measurement) is to be made available. The 'S message' is to provide control of the measurement suspend facility, which ensures safety of transference of data, and the interrupt facility, which automatically signals the end of a measurement. Therefore, the programming statements consist of 'write' statements to transfer data to the 1183-C interface, by means of the 'T' and 'S' messages, or 'read'

statements to transfer data from the 1183-C interface to the active controller. Details and specifications concerning the programming of the interface are given in ref. (3).

Similarly, software control of the multiplexer circuit was achieved via the 98032-16 bit interface. Details concerning the programming of this interface are given in reference (2).

Thus the file 0 program sets up the remote control of the dynamic measurements with interrups facility, that is, the active controller is automatically interrupted at a measurement end, even though it is busy with something else and has not asked for information from the 1183-C. An interrupt will cause the active controller to output the results of the measurement to its memory store and to set up the interrupt facility for the next measurement. The program enables the 1172 FRA to execute a frequency sweep with the sweep parameters, drive level and all the settings of the front panel touch buttons, chosen and set by the operator. Measurements are point to point with the multiplexer automatically switching between the direct and cross-coupled signals, as instructed by the program. At the end of the frequency sweep, the frequency response data are stored on magnetic tape.
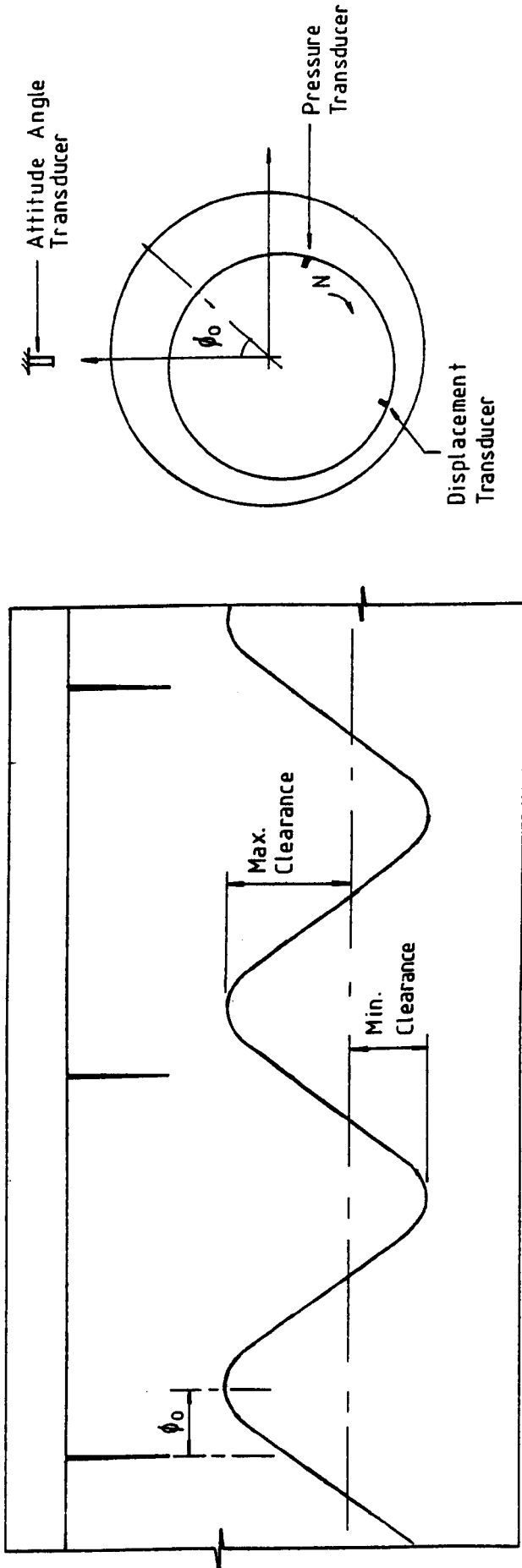
Fig. 7.1 : Output Trace From U-V Recorder.
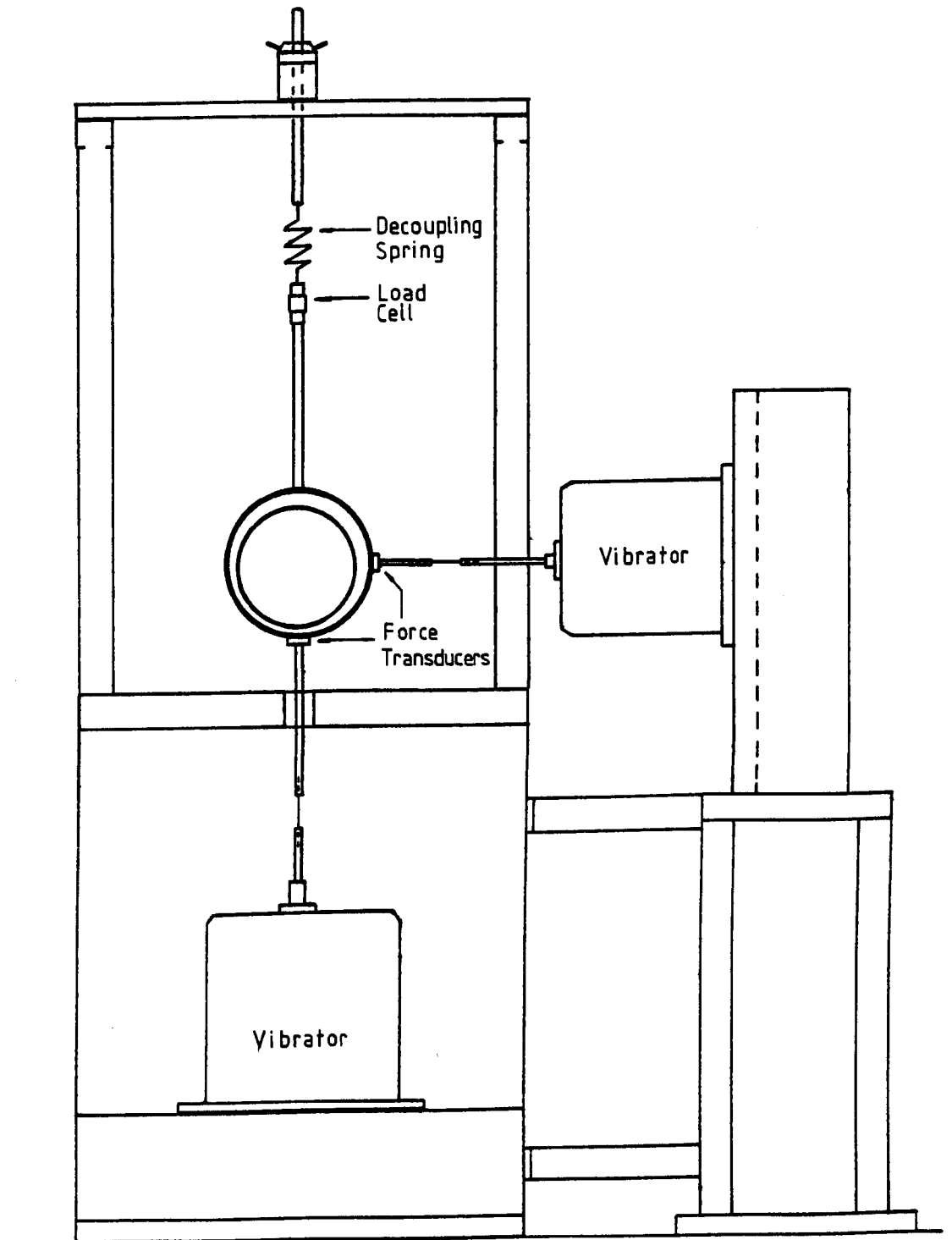
Fig. 7.2 Dynamic Loading System
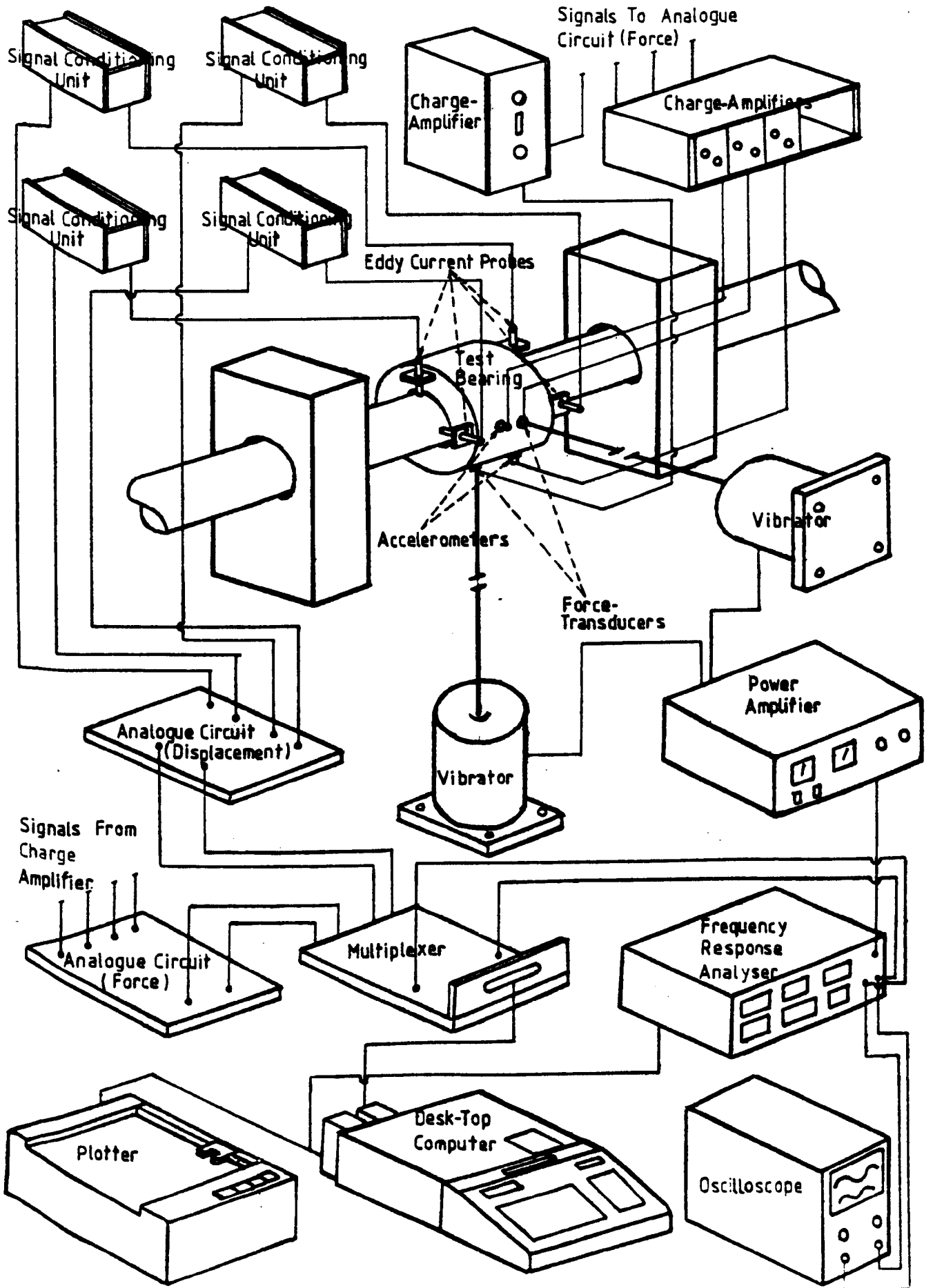
Fig.(7.3) : Instrumentation Pictorial View
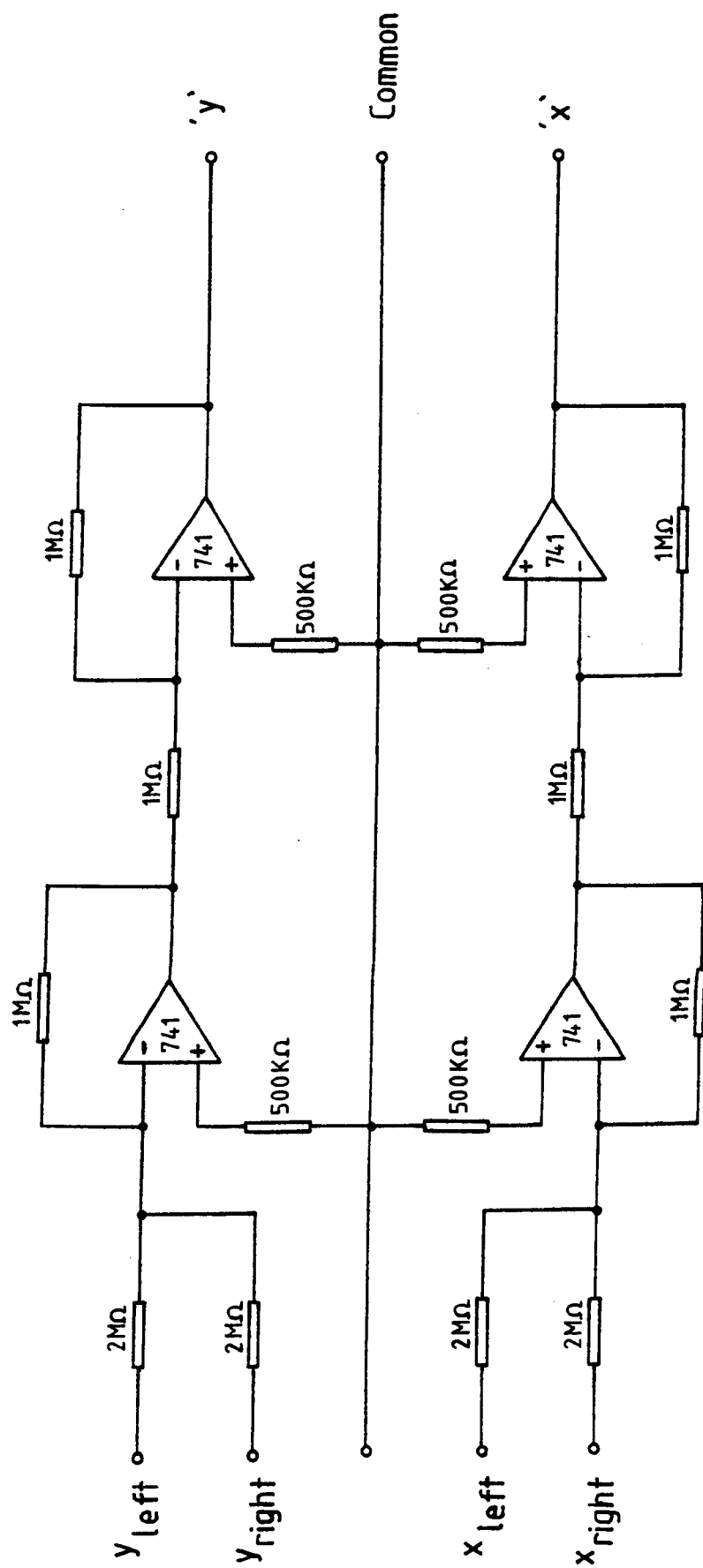
Fig.(7.4) : Summing Circuit For Displacement Signals.
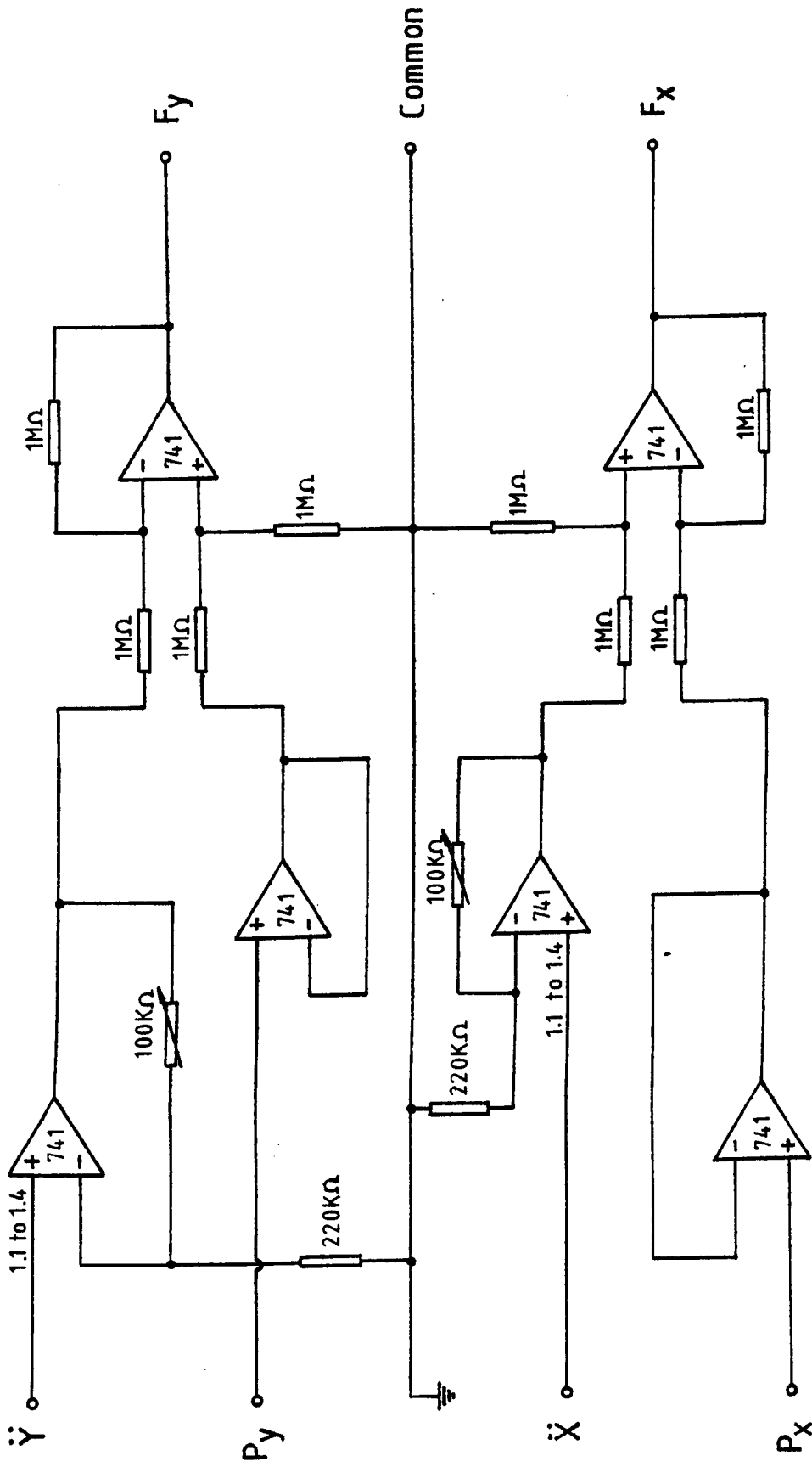
Fig.(7.5) : Circuit For Isolating The Mechanics Of The Fluid-Film From The Inertia Of The Bearing Mass.
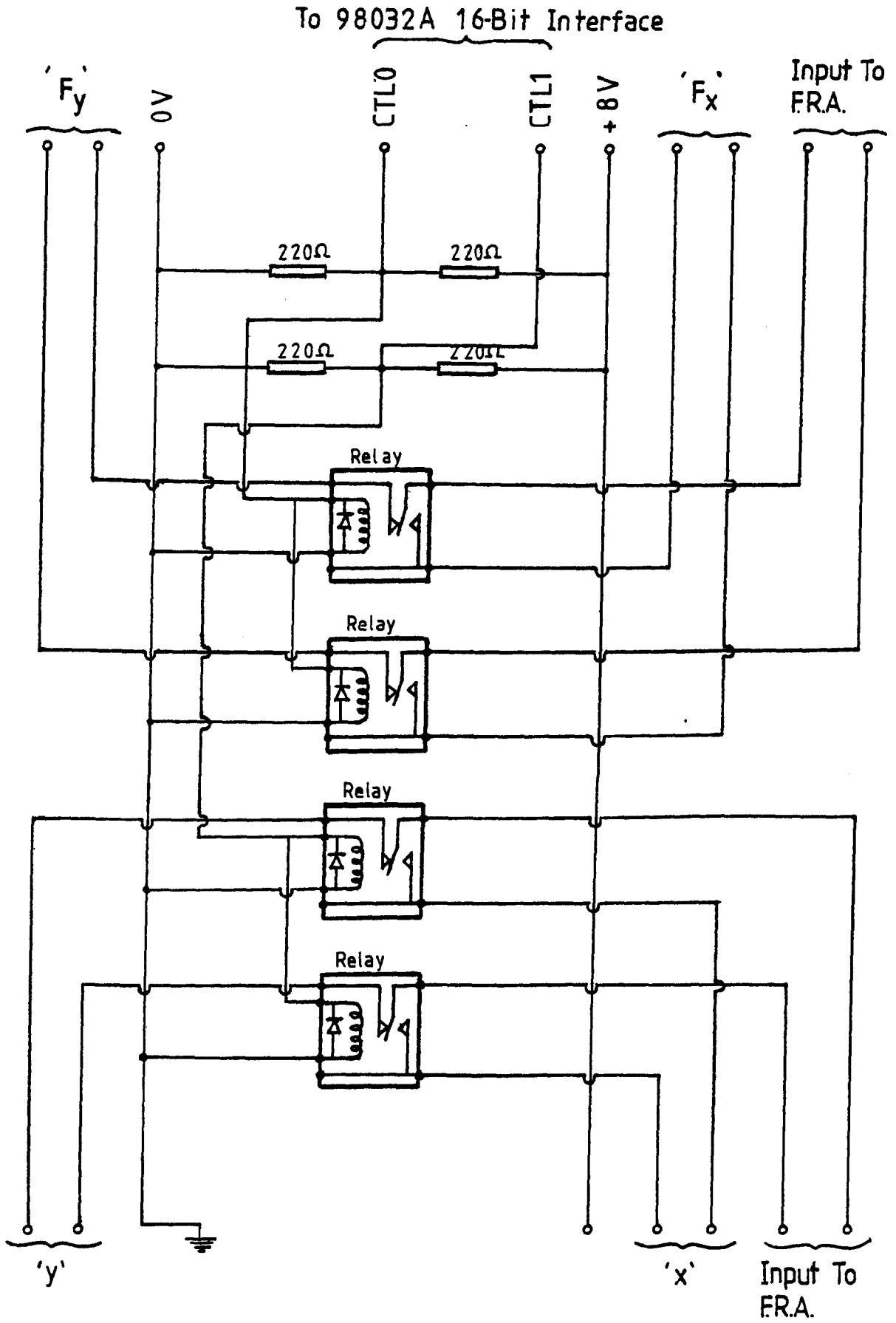
Fig. (7. 6) : Multiplexer Circuit.
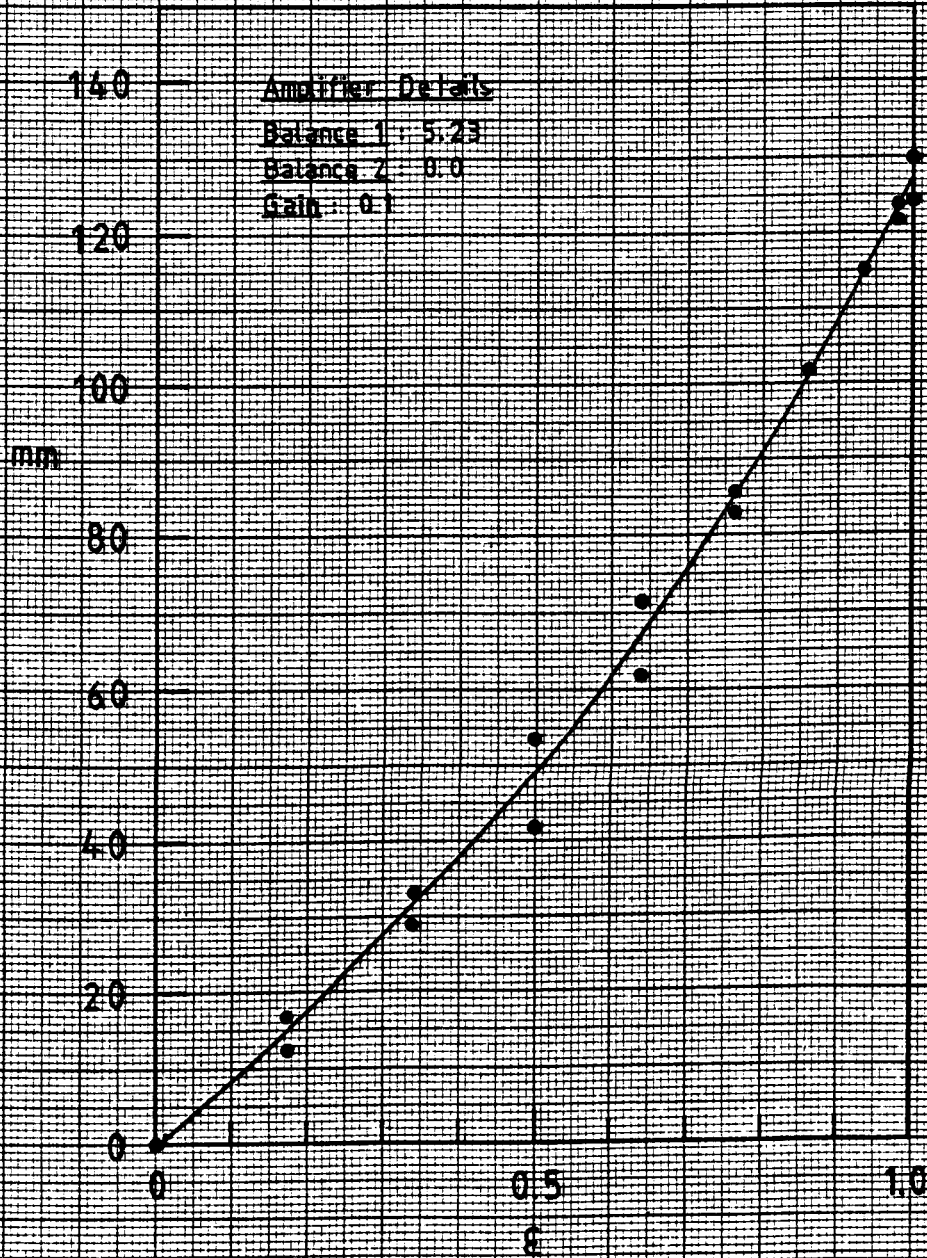
Fig.(7.7): Calibration Graph Of Film Thickness Transducer
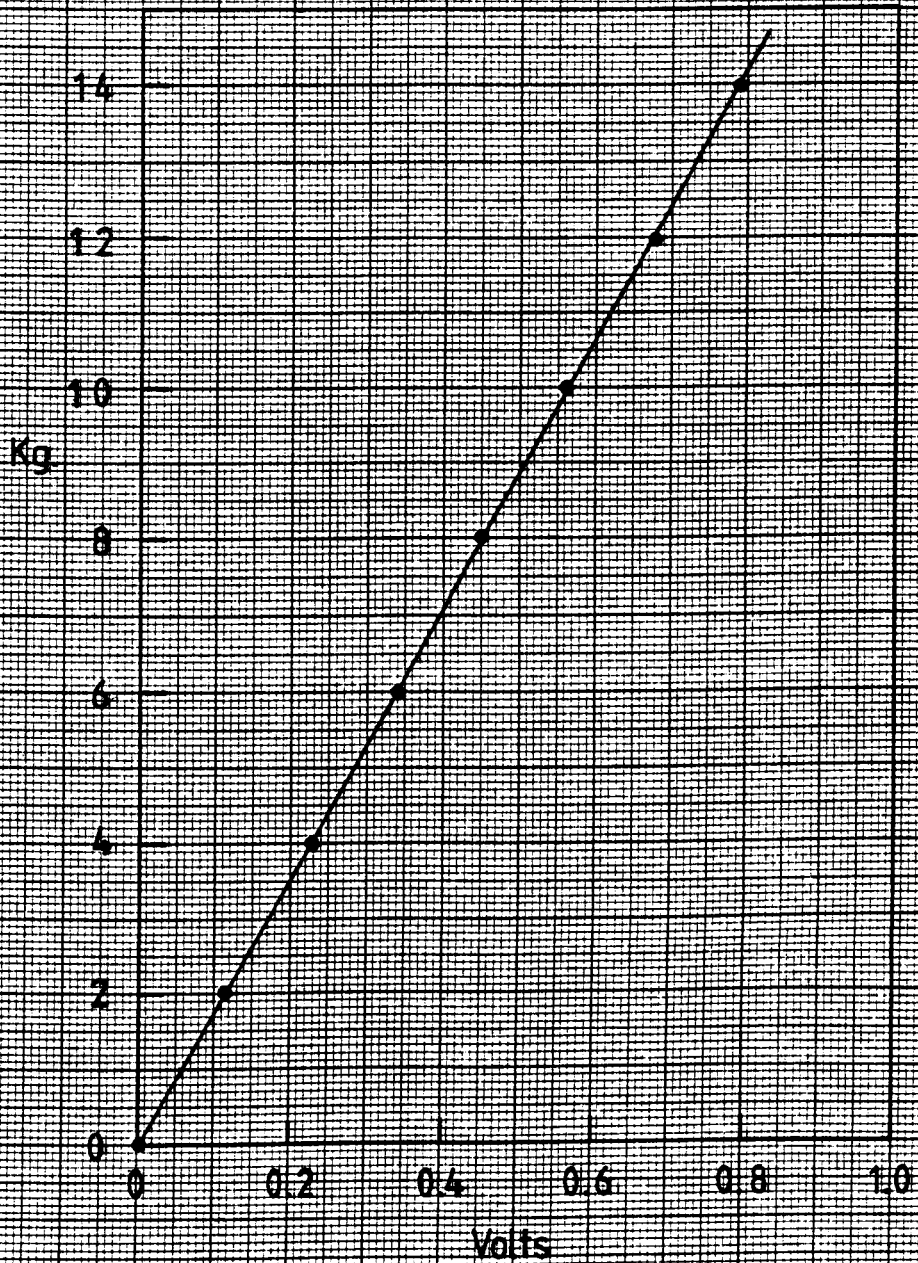
Fig.(7.8) : Calibration Graph Of Force Transducer (Static Load)
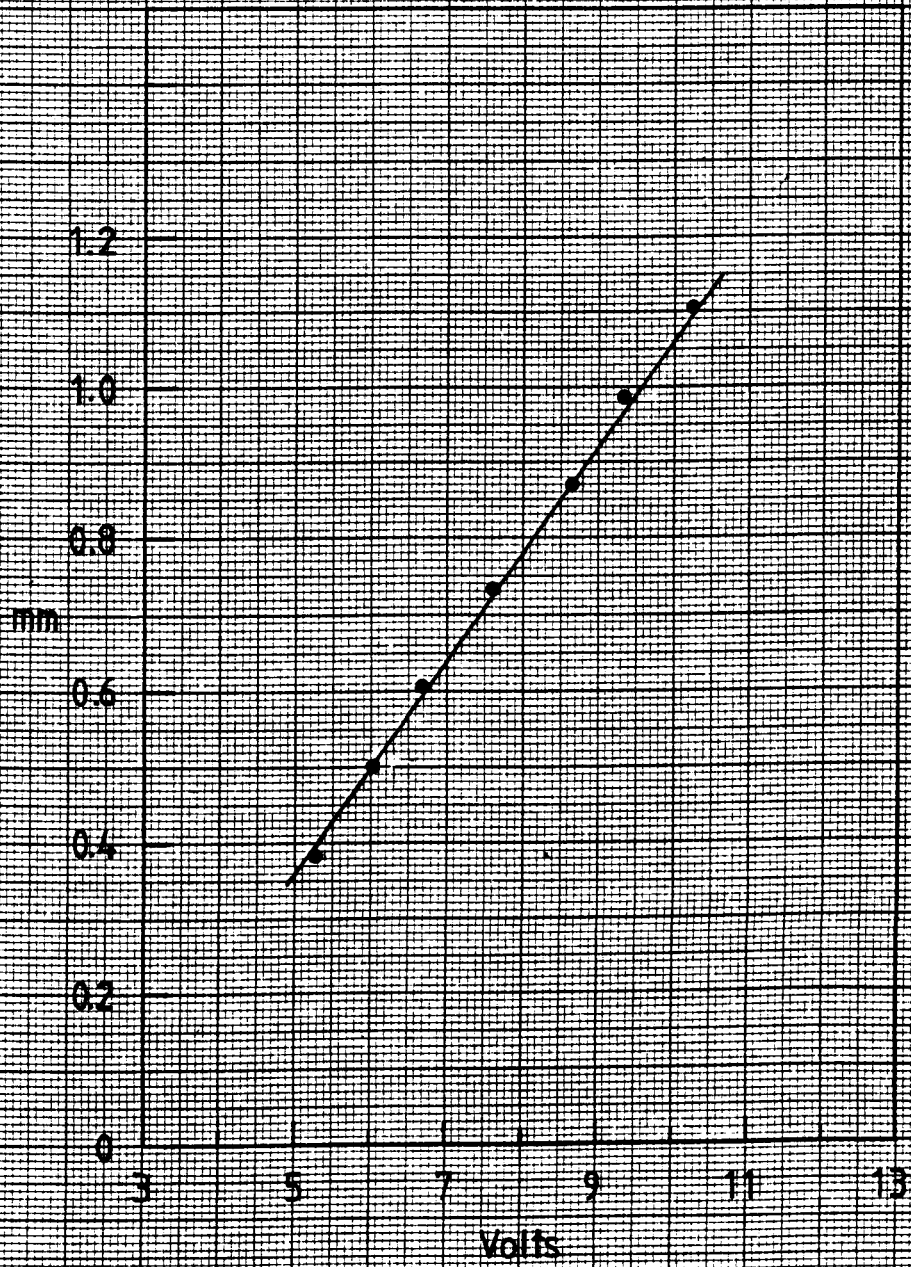
Fig.(7.9) : Calibration Graph Of Eddy Current Probe (Y_{left})
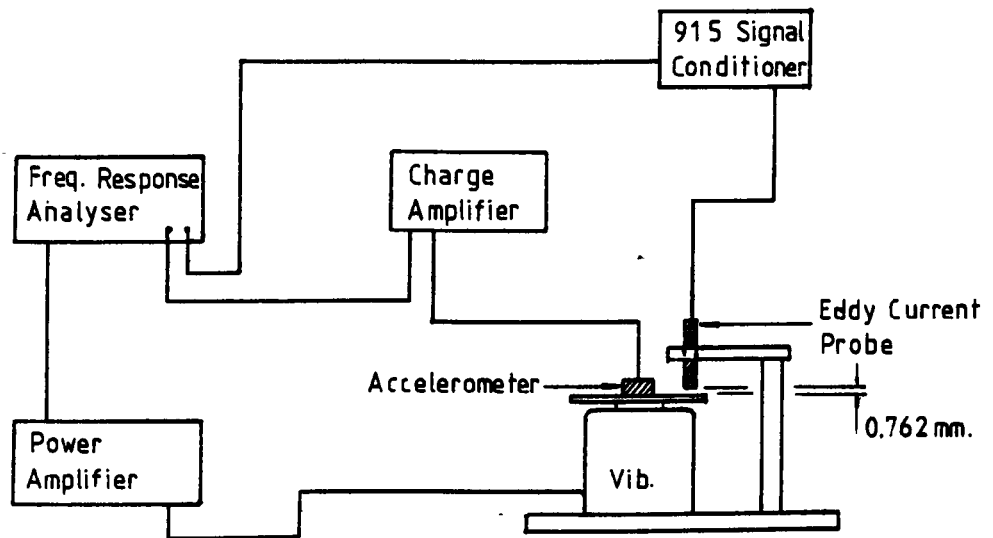
Fig. 7.10 : Dynamic Calibration — Eddy Current Probe.
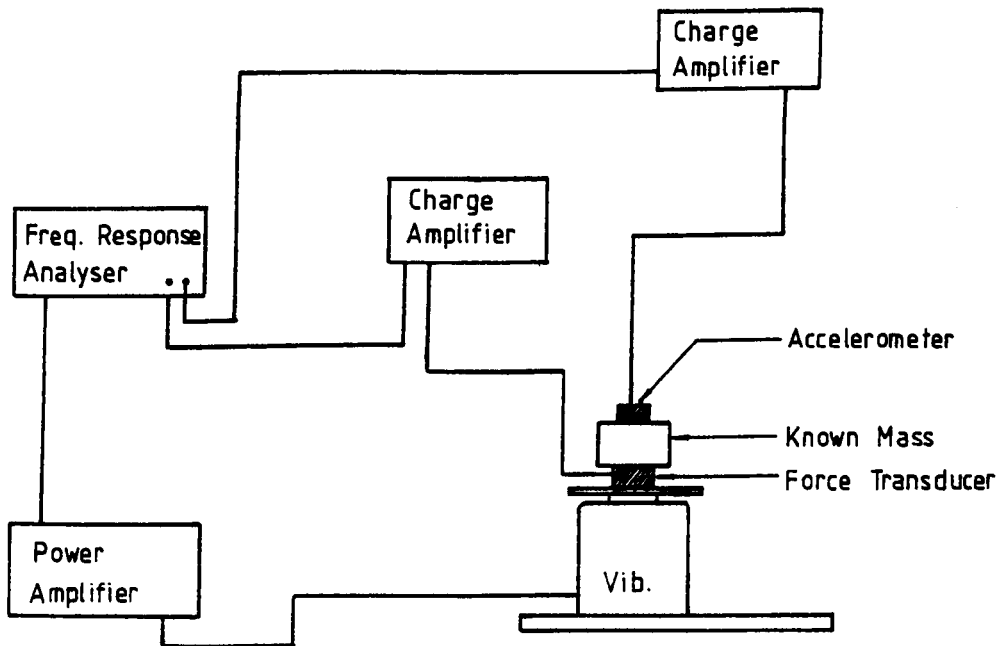
Fig. 7.11 : Dynamic Calibration — Force Transducer.
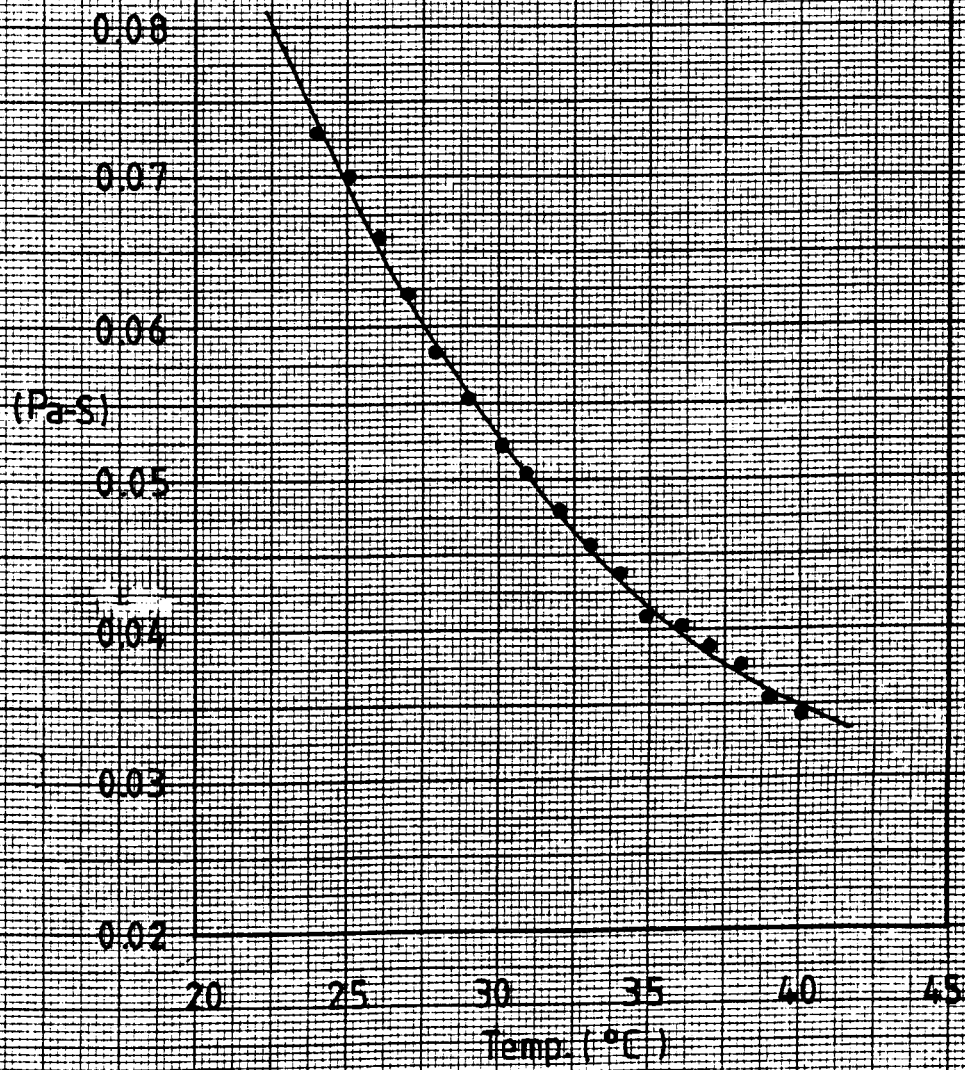
Fig. (7.12) - Calibration Graph Of Test Oil (Shell Tellus 27)
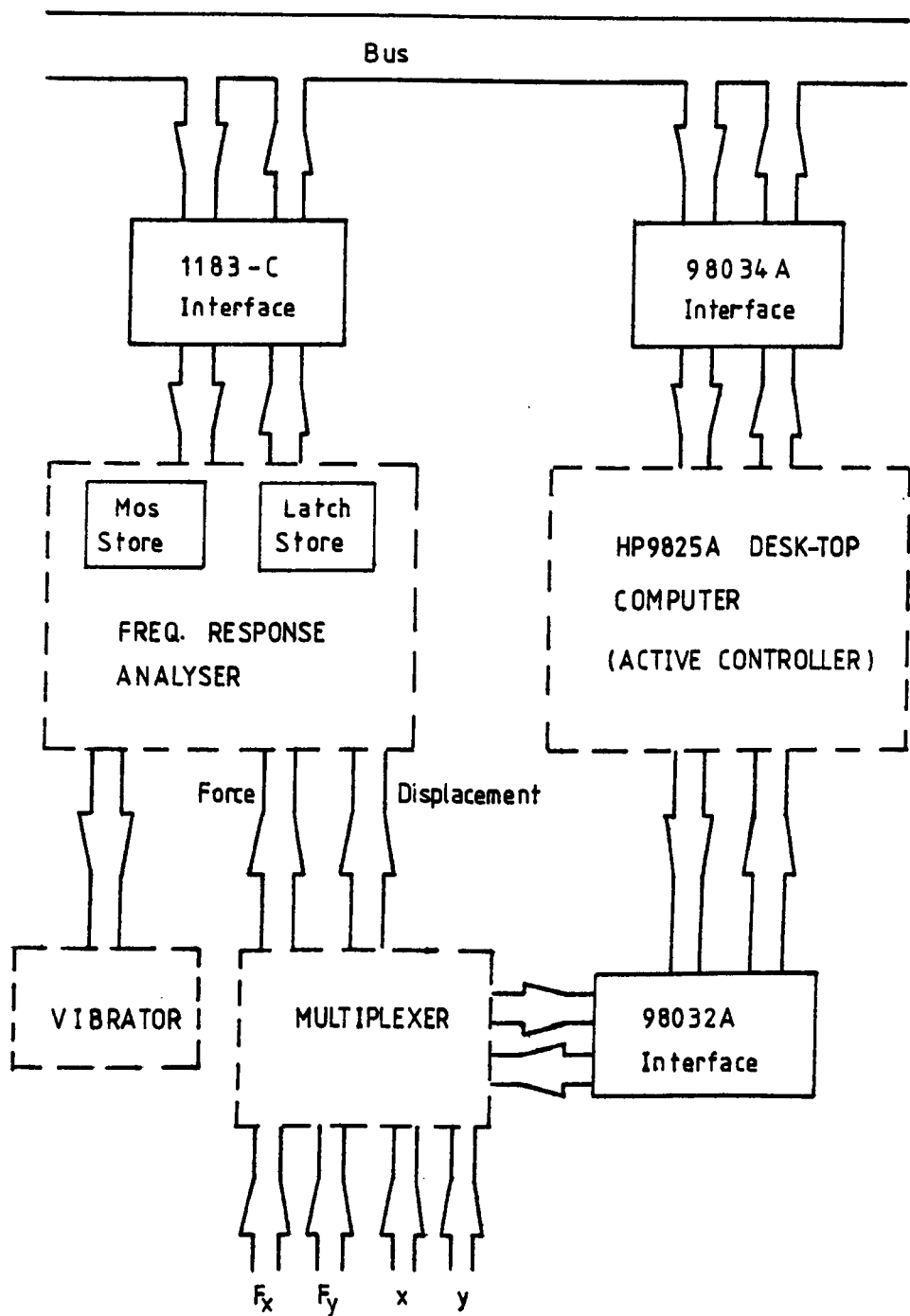
Fig. 7.13 : Interface Functional Diagram Of The
Dynamic Measurement System.
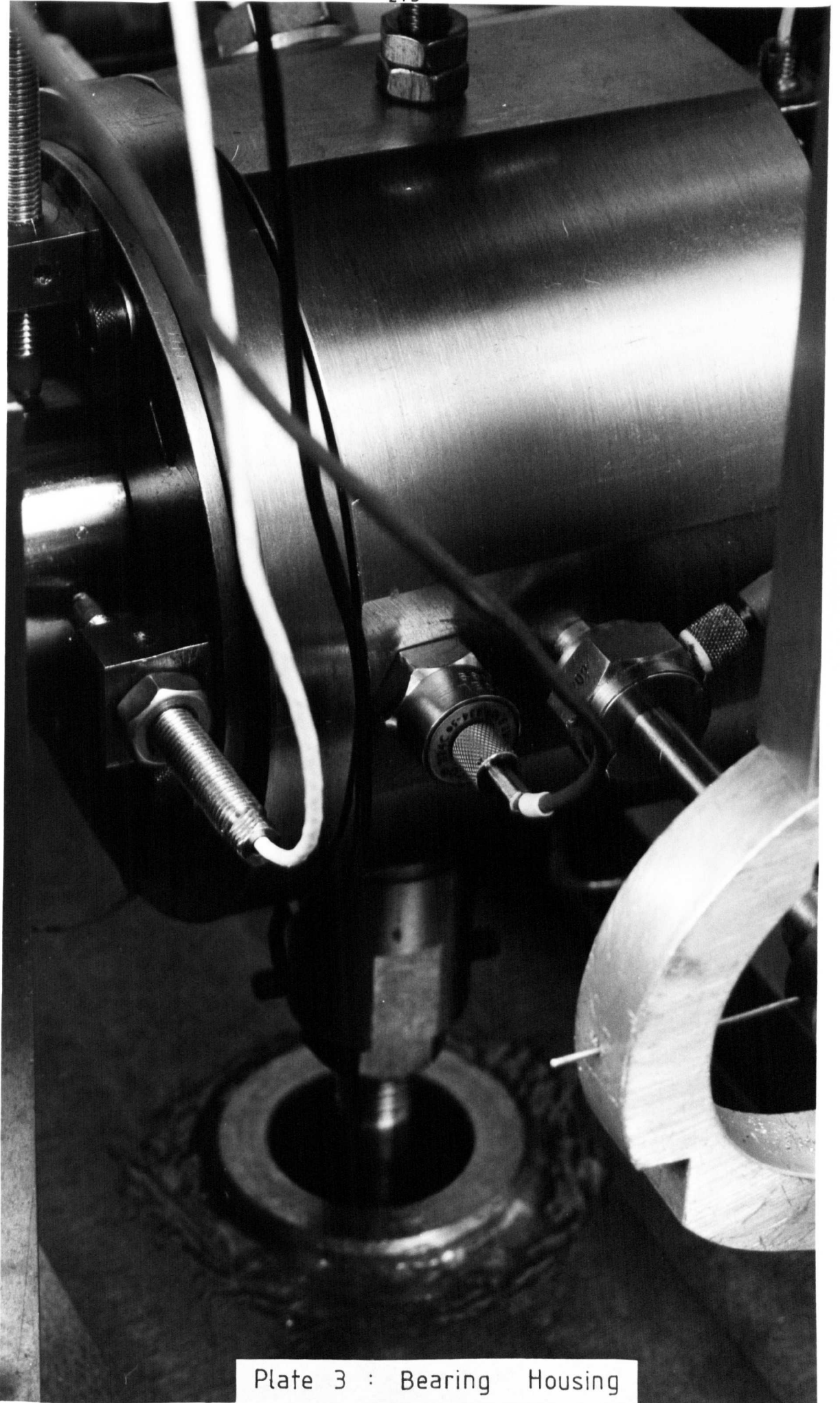
Plate 3 : Bearing Housing
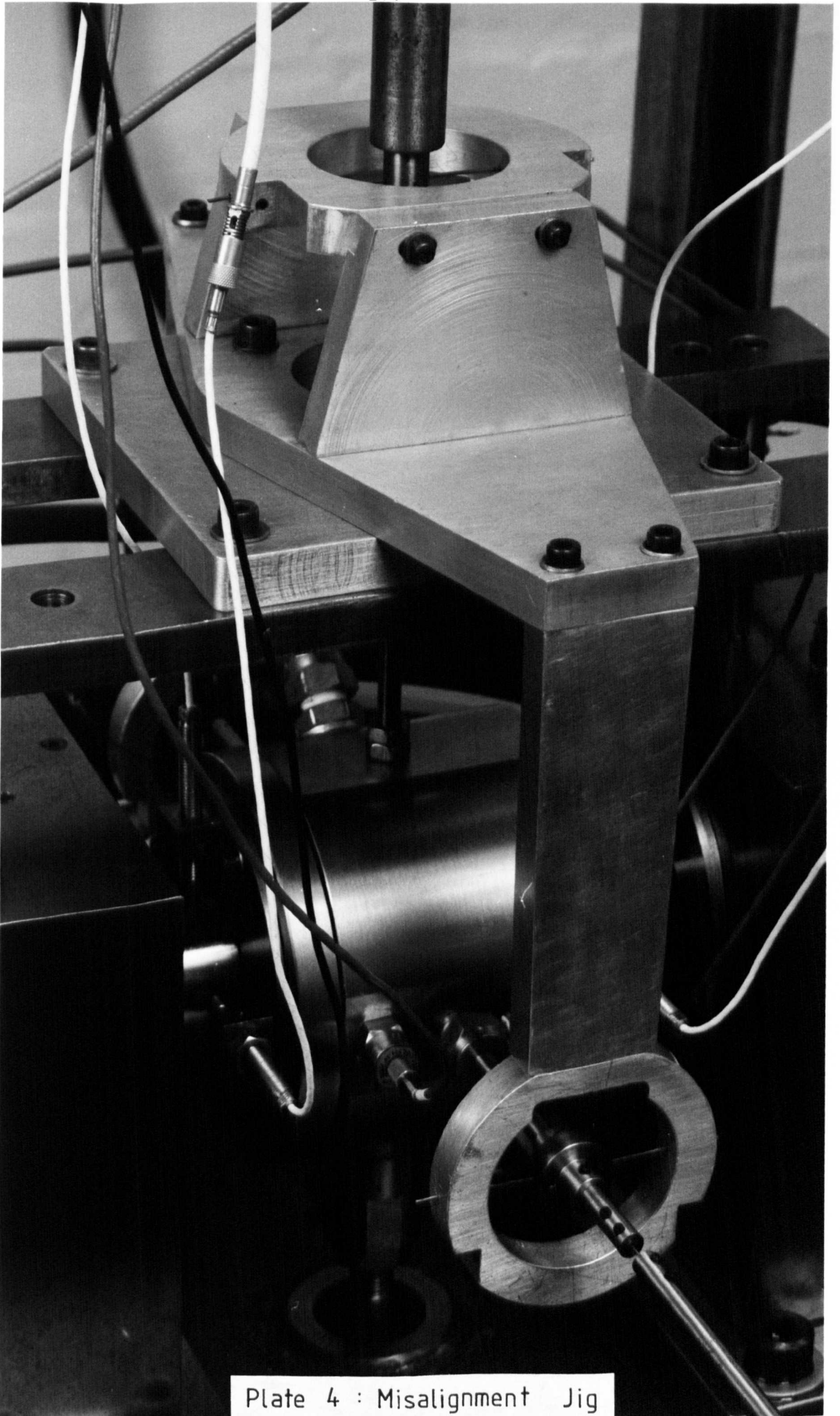
Plate 4 : Misalignment Jig
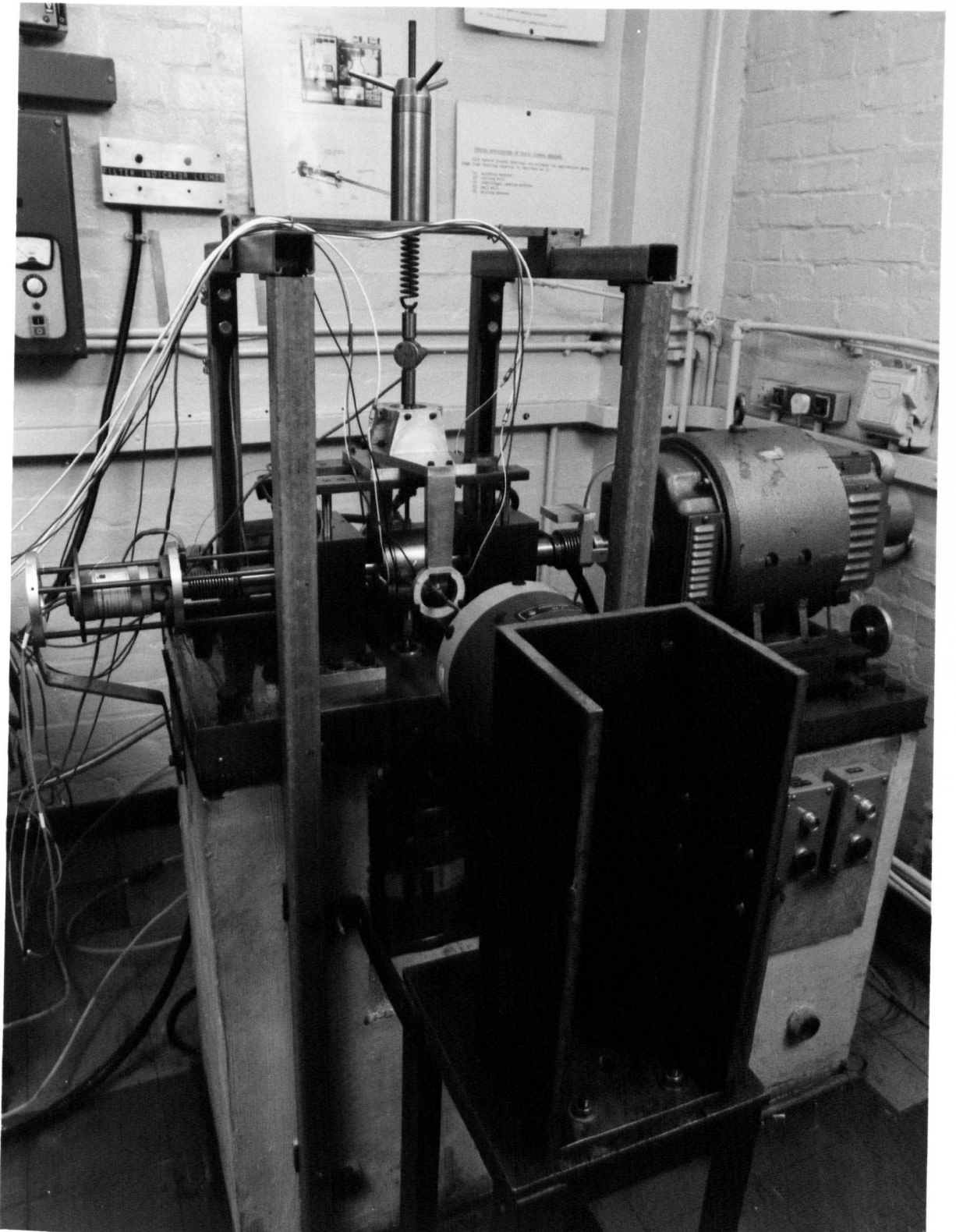
Plate 5 : A General View Of The Test Rig

216
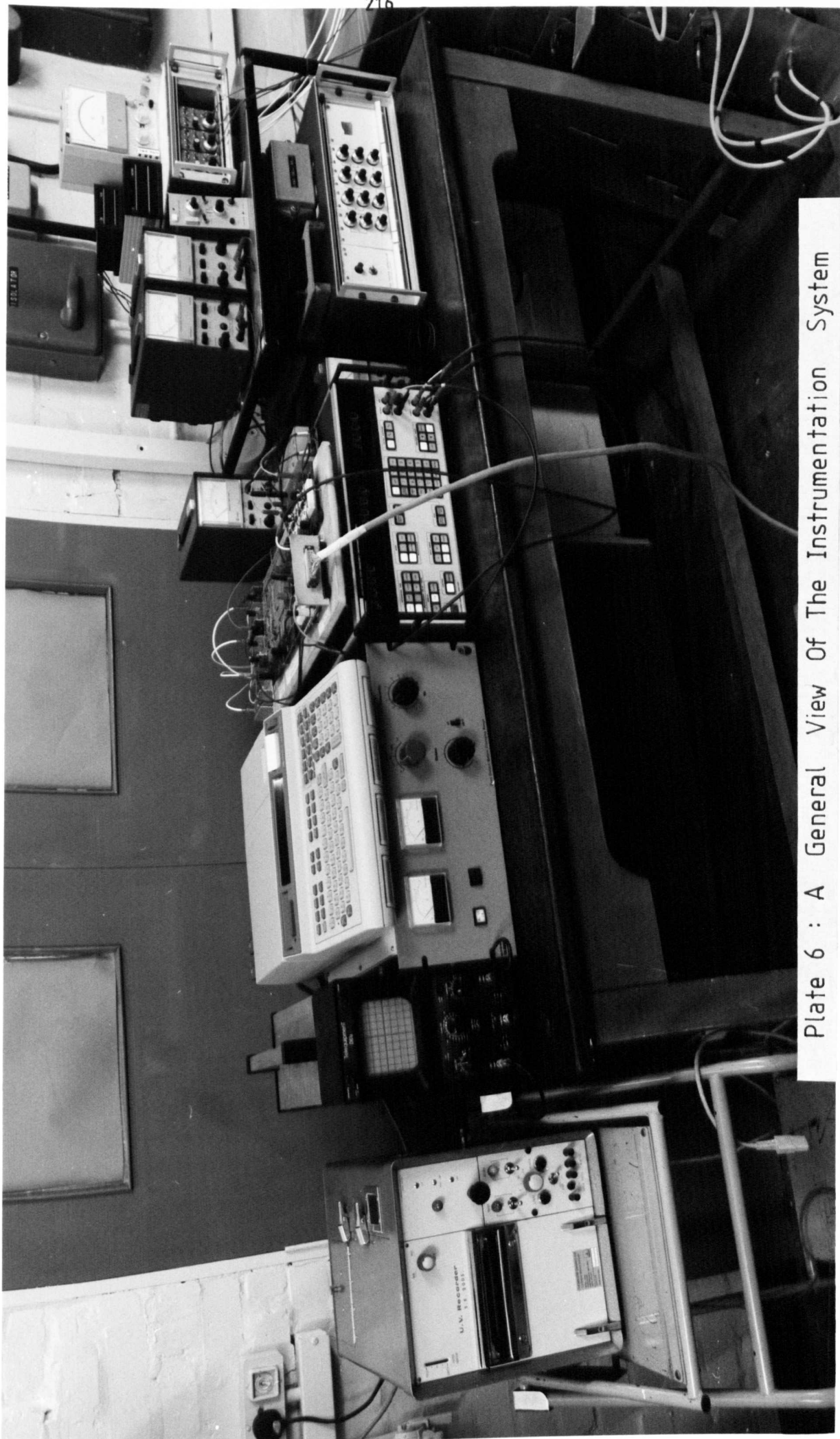
Plate 6 : A General View Of The Instrumentation System

REFERENCES

1. '98034A HP-IB Interface Installation and Service Manual', Hewlett
    Packard Computer Division, 1976.

2. '98032A Bit Parallel Interface Installation and Service Manual',
    Hewlett Packard, 1976.

3. 'GP-IB Interface 1183-C Operating Manual', The Solartron Electronic
    Group Ltd., 1977.

4. Koshal, D. 'The design and optimisation of slot hybrid journal
    bearings', Ph.D. thesis, Liverpool Polytechnic,
    1978.

5. 'Interfacing Concepts and the 9825A', Hewlett Packard, U.S.A.

6. Loveday, G. 'Practical Interface Circuits for Micros'.

CHAPTER 8

EXPERIMENTAL INVESTIGATIONS

8.1 Introduction

The main objective of the experimental work was to identify the bearing film characteristics using the sinusoidal testing technique. The experimental procedures leading to the determination of the relevant bearing data sets and the processing of the data to obtain the bearing coefficients, are presented in this chapter. The results of the experimentation are also discussed.

8.2 Test Bearing

A double-entry slot bearing with the following details was employed throughout the experimental investigations.

$$L/D = 1.0$$

$$a/L = 0.25$$

$$L = 40 \text{ mm}$$

$$C_d = 0.0627 \text{ mm}$$

$$\beta = 0.44$$

8.3 Static Tests

Before commencing with the dynamic tests, experiments were carried out to determine the static load performance of the bearing. This was necessary, because the eccentricity-ratio, ε, can only be used as a common variable in the dynamic tests, if its relationship with the steady state parameters, such as, static load, attitude angle and journal speed, is verified experimentally. The experimental procedures leading to the determination of the steady-state characteristics of the bearing are outlined in the following paragraphs.

The hydraulic power units and the instrumentation circuits were switched on and the test rig was run for approximately 45 minutes to

allow the oil temperature to stabilise. The loading arrangement was adjusted until the bearing was operating at approximately the concentric position with the shaft at zero speed. The bearing was then checked for misalignment in the horizontal and vertical axes, and adjustments were carried out, if required, by adjusting the position of the misalignment jig. Static tests were carried out for 3 values of power ratio.

These were K = 0, 13.4 and 31.0. The value of power ratio was adjusted to the required value by setting the journal rotational speed. The rotational speed was evaluated using the expressions for S_h and S_{ho}, as defined in Chapter 4. A knowledge of the oil supply pressure, viscosity of the oil and bearing dimensions is required for the speed evaluation, as

$$S_h = S_{ho} \sqrt{K} \qquad , \text{ and}$$

$$S_h = \frac{\eta N}{P_s} \left(\frac{D}{C_d}\right)^2$$

Therefore, the journal rotational speed in rev/sec may be evaluated as follows:

$$N \text{ (rev/sec)} = S_{ho} \sqrt{K} \left(\frac{C_d}{D}\right)^2 \frac{P_s}{\eta} \qquad (8.1)$$

Substituting the values of S_{ho} and bearing dimensions into equation (8.1), and multiplying by the appropriate factors, to account for the dimensional units employed in the experimentation, results in:

$$N \text{ (rev/sec)} = 7.2938 \times 10^{-4} \sqrt{K \frac{P_s \text{ (lbf/in}^2)}{\eta \ (P_a - s)}} \qquad (8.2)$$

A supply pressure of 100 lbf/in^2 was employed throughout the experimental investigations. The viscosity of the oil was evaluated based on the average of the inlet and outlet temperatures. (See figure 7.12).

The rotational speed was set and a steady load was applied in the upwards direction, through a screw arrangement via a decoupling spring

and a load cell. A further period of 5 minutes was allowed for the
bearing to reach steady running conditions. The signals from the
inductive displacement and 'attitude-angle' transducers were recorded
on the u-v recorder. The eccentricity-ratio and the attitude angle
were determined using the traces from the u-v recorder and the cali-
bration graph of figure 7.7. The above procedures were repeated for a
number of steady loads. At each loading, the inlet and outlet temper-
atures and rotational speed were checked to ensure that the correct
value of power-ratio was maintained.

The entire procedure was then repeated for the next value of
power-ratio. Experimental and theoretical plots of the dimensional
load, W, against eccentricity-ratio, ε, are presented in figures (8.1)
to (8.3). Figures (8.4a) and (8.4b), show the experimental and theo-
retical plots of the eccentricity-ratio against the bearing centre loci.
Full discussion of these results are presented in Section 8.7.

8.4 General Preparation for The Dynamic Tests

1) The bearing operating parameters, such as, the oil supply pressure,
    the steady load and the rotational speed were set approximately
    for the particular value of power-ratio. Dynamic tests were
    carried out for the three values of power-ratio, K = 0, 13.4 and
    31.0. The oil supply pressure was maintained at 100 lbf/in^2.

2) The alignments between the bearing bush and the test shaft, in
    the horizontal and vergical axes were checked, and corrected, if
    necessary. The eccentricity-ratio was then measured. If the
    eccentricity-ratio was different from the selected value, the
    bearing load was adjusted until the desired value was obtained,
    and sufficient time was allowed for the bearing to reach the
    steady running conditions.

3) In order to ensure the dynamic force was applied in one direction

at a time and the validity of the 'black-box' approach, only one vibrator was connected to the bearing housing at any one time. If the non-operating vibrator was connected to the bearing, it would produce a force due to its dynamic characteristics and the present model would be in error.

4)   The vibrator in the Y-direction was connected to the bearing housing. This was a very delicate operation and had to be carried out with care and patience. Connecting the vibrator to the bearing housing, should not alter the eccentricity-ratio and the alignment of the bearing bush. The use of the spring steel wire to link up the bearing and the vibrator helped to keep the errors down to a minimum.

5)   The eccentricity-ratio and alignment of the bearing bush were checked again. If any of these parameters were in error, the vibrator was disconnected from the bearing housing and the process of applying static load and unloading the bearing, until the selected eccentricity-ratio was achieved, had to be repeated.

6)   The correct implementation of the procedures described in the above paragraphs, ensure that the steady state conditions, such as, eccentricity-ratio and alignment of the bearing bush, remain approximately the same, before and after the vibrator was connected. The second important requirement was to guard against vibrations of the conical mode.

7)   Sinusoidal excitation was applied over the frequency range 5-60 Hz increasing in steps of 2 Hz. The four output signals from the eddy current probes were fed to the frequency response analyser via the multiplexer circuit, such that, at each frequency, the Gain and Phase relationships between the left side and right side transducers for the direct and cross-coupled signals were analysed.

If the errors were within ± 10% it was considered acceptable.

8) It was considered to be good practice however, to recheck the eccentricity-ratio and alignment of the bearing bush before proceeding to the experimentation of the bearing fluid-film transfer functions. In certain cases, it was discovered that the alignment had altered and the procedures starting from procedure (5) had to be repeated. The experimental procedures leading to the determination of the bearing fluid-film transfer functions are described in Section 8.5.

9) Since the excitation was in the Y-direction, the results of the experimentation provide information on the transfer functions, G_{12} (s) and G_{22} (s), for the selected values of eccentricity-ratio and power-ratio. The vibrator in the Y-direction, was disconnected from the bearing housing, on completion of the frequency sweep.

10) A check of the eccentricity-ratio was carried out to ensure that it had not altered. Also, the alignment between the bearing bush and test shaft was checked, and corrected, if necessary. The vibrator in the X-direction was then connected to the bearing housing and the procedures described in steps (5) to (8) were repeated. The results of this experimentation provide information on the transfer functions, G_{11} (s) and G_{21} (s), for the selected values of eccentricity-ratio and power-ratio.

11) The above procedures were repeated for several values of eccentricity-ratios, hence, providing information on the transfer functions, G_{12} (s) and G_{22} (s) or G_{11} (s) and G_{21} (s), for a range of eccentricity-ratios. The power-ratio, K, was maintained at a constant value. It was important that the temperatures and rotational speed were continuously monitored to ensure the proper value of power-ratio was maintained throughout the experimentation.

These requirements were more critical in the dynamic tests as the time involved was considerably greater than an equivalent static test, and may give rise to parameter drift.

12) A new value of power-ratio was selected and the entire procedures, starting from paragraph 1, were repeated. The experimental and theoretical plots of the bearing fluid-film transfer functions, for K = 0, are presented in figures (8.7a) to (8.11b), whilst, figures (8.12a) to 8.14d), illustrate the results for K = 13.4 and figures (8.15a) to (8.17d), illustrate the results for K = 31.0. Full discussions of these results are presented in Section 8.7.

13) Once information concerning the transfer functions, G_{11} (s), G_{12} (s), G_{21} (s) and G_{22} (s), relating to a selected value of eccentricity-ratio and power-ratio are available, the bearing coefficients pertaining to the stated value of eccentricity-ratio and power-ratio may be evaluated. The experimental procedures leading to the evaluation of the bearing coefficients from the transfer functions data are described in Section 8.6. Figures (8.18a) to (8.20c) show the experimental and theoretical plots of the dimensional stiffness and damping coefficients, against eccentricity-ratio, for values of K = 0 and 31.0. A full discussion of these results is presented in Section 8.7.

14) A summary of the procedures involved in conducting the dynamic tests is presented in the algorithm of figure (8.1).

8.5   Determination of Bearing Fluid-Film Transfer Functions by Sinusoidal Testing

With the journal bearing running at steady conditions and the vibrator correctly aligned and connected to the bearing housing, the bearing is ready to be perturbed from its static equilibrium position. The experimental procedures leading to the determination of the bearing

transfer functions are as follows:

1) Check that the instrumentation circuits are properly wired up.

2) Set the voltage sensitivity of the force amplifiers to 50 N/volt and the accelerometer amplifiers to 1 g/volt.

3) Insert the magnetic tape into the cartridge compartment of the HP9825A computer.

4) Type 'ldf 0' and press 'Execute'.

5) Eject tape from cartridge compartment and store in a safe place

6) Press 'RUN' and the computer will display the message 'Enter New Set Of Data Now'.

7) A series of interactive questions relating to the selection of the front panel settings of the frequency response analyser and the direction of loading will follow. The user is expected to input the data for each of the parameters on display. Some of the questions are straightforward and only require a 'yes' or 'no' answer. To represent a 'yes' type '1' and if 'no', type '0'. At the end of each data entry, press 'continue' to proceed to the next instruction. The experimental investigations described in the previous section was based on the following parameter settings:

       (i) Desired Integration Time - 100 sec.

       (ii) Measurement Delay - 10 sec.

       (iii) Output Volts - 0.5 volts.

       (iv) Calibration Factor - 2.5

       (v) Fmin - 5 Hz

       (vi) Fmax - 60 Hz

       (vii) Linear Increment - 2 Hz

8) On completion of the questionnaire a slow discrete sine frequency sweep with linear variation of frequency from 5 Hz to 60 Hz

proceeds automatically. The results of the experimentation (direct and cross-coupled frequency response data) for each frequency of excitation are stored in the memory of the computer.

9) When the frequency sweep is completed, the experimental data may be recorded on magnetic tape, or, if the results are not satisfactory a second test run may be carried out. If a second test run is required, proceed to step 6, or else proceed to step 10.

10) Insert the data tape into the cartridge compartment. Questions are then displayed concerning the addresses of the file, where the experimental data are to be recorded.

11) The experimental data are stored in 3 files. One file records the frequency details, the second file records the direct coupled responses. The cross-coupled responses are recorded on the third file. It is therefore necessary for the appropriate addresses of the data files to be typed and entered in response to the questionnaire. The result is the creation of frequency response files on tape.

12) The next requirement is to obtain a hard-copy of the frequency response plots via the HP9872 graph plotter.

13) Remove the data tape and insert the master tape. Then type 'ldf 1' and press 'Execute'.

14) Remove the master tape and insert the data tape in the cartridge compartment.

15) The plotting routine may be started by pressing 'Run'. Again the program responds by displaying some interactive questions, such as, the address of the data file to be plotted, the scaling of the axes, etc.

16) Procedures (12) to (15) are repeated until the direct and cross-

coupled frequency response plots are obtained.

17) Finally, the experimentation for a new set of condition as described in the previous section, is carried out, and the procedures from steps (1) to (16) are repeated.

8.6 Processing of the Bearing Coefficients from the Frequency Response Data

The experimental procedures adopted for evaluating the bearing coefficients is such that the direct and cross-coupled frequency response data for both directions of excitation (X and Y) and belonging to the same steady state conditions must be available. The program, file 2 was developed to evaluate the stiffness and damping coefficients from the experimental frequency response functions by the direct method of Chapter 6. The experimental procedures are as follows:

1) Insert the master tape, and type 'ldf 2', and press 'Execute'.

2) Remove the master tape and insert the data tape (tape where the frequency response data are stored).

3) Press 'Run' to start the computation.

4) As usual, the program responses by asking questions, like, which data files are to be processed, the number of data points, etc.

5) Upon receiving the information from the user, the appropriate files were loaded into memory and the evaluation of the bearing coefficients from the frequency response data are carried out.

6) At the end of the computation, a listing of the bearing coefficients was obtained through the HP9825 internal printer. Also, the bearing coefficients may be stored on tape.

7) The procedures starting from step (1), are repeated for the next set of steady state conditions.

8) The evaluation of the bearing coefficients were carried out at each excitational frequency. However, the coefficients were only presented in the range ω = 10 Hz to 30 Hz. The best correlation between the experimental and theoretical frequency responses occurred in this frequency range. (See figures 8.7a to 8.17d).

8.7 Discussion of Results

The steady-state performance of the slot-entry bearing was assessed by experimentally determining the bearing centre loci and the relationships between eccentricity-ratio and bearing static load for power-ratios of K = 0, 13.4 and 31. The range of power-ratios selected was such that a wide range of characteristics were covered. The results were compared with a finite difference solution, program PFD.FOR.

The load-eccentricity relationships of the slot-entry bearing for K = 0, 13.4 and 31 are shown in figures 8.2, 8.3 and 8.4, whilst, the bearing centre loci plots are presented in figures 8.5a and 8.5b. The experimental tests carried out for power-ratios of 13.4 and 31 would have been more informative if higher values of eccentricity-ratios had been investigated. Due to the high supply pressure (100 lbf/in^2) being employed and the relatively high values of power-ratios involved, it was decided to limit the eccentricity-ratios to below 0.5 to prevent over-loading the static loading arrangement. Nevertheless, this range of eccentricity-ratios, $0 < \varepsilon > 0.5$ for K > 0, were adequate for the present investigation, in view of the difficulties in achieving accurate dynamic results, even at low values of eccentricities, and the assumptions that were employed in the analysis (See Section 4.4).

The load-eccentricity-ratio plots showed that within the eccentricity-ratios range of interest, the measured characteristics agreed reasonably well with the finite difference solution. However, some scatter was observed in the bearing centre loci plots. The scatter

may be partly attributed to the design of the attitude angle measurement system. Moving the 'attitude angle' transducer and the marker to the position shown, may help to reduce the error, as the flexible coupling, as it was previously installed, may have allowed some torsional distortions, and yield a false reading.
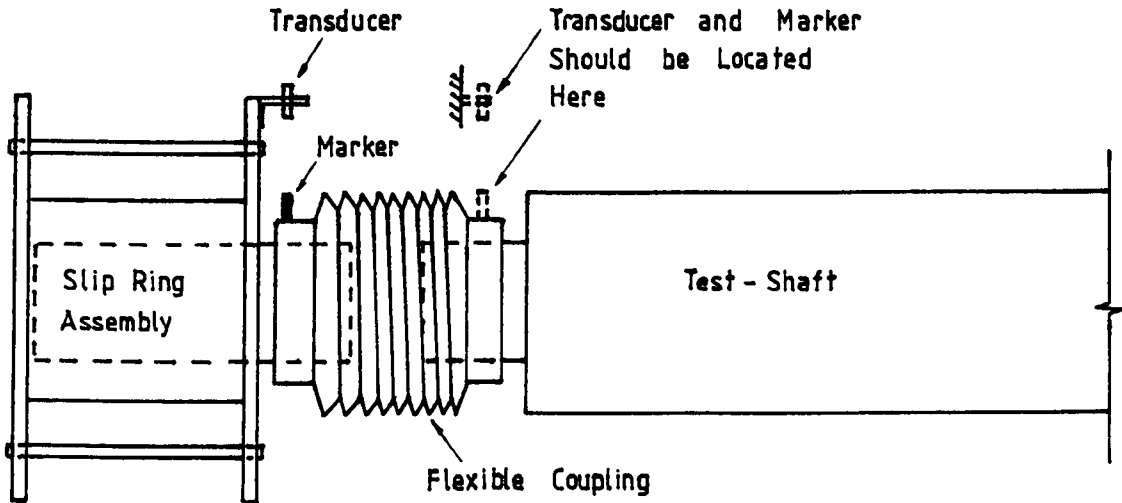
Also, the method employed to determine the attitude angle from the u-v trace should be improved. The output of the transducers should be fed into a programmable data-logger so that it can be readily analysed by computer.

There was sufficient evidence in the load-eccentricity plots of figures 8.2 to 8.4, to suggest that a reasonable degree of accuracy was achieved in the determination of eccentricity-ratio. Therefore, within the limits of experimental errors and the eccentricity-ratio range of interest, it may be concluded that the steady-state performance of the slot entry bearing was successfully determined and form a sensible basis for the dynamic tests.

The initial investigations were carried out, based on the assumption that the shaft was rigid. A comparison of the experimental and predicted transfer functions based on this assumption, for $K = 0$ and the bearing operating at the concentric condition, are illustrated in figures (8.7a) and (8.7b). There was poor correlation between the

predicted and the measured responses. It can be seen from the figures that the experimental points, in fact, follow a similar trend as predicted by the theory, but with an offset which increases with frequency. The theory under-estimates the gain characteristics and over-estimates the phase characteristics. Initially, it was thought that the errors could be traced down to the dynamic measurement system, such as, the amplifiers and transducers. Therefore, a check on the dynamic measurement system was carried out. Dynamic calibrations of the force transducers and eddy current probes were carried out. However, these investigations did not help in explaining the discrepancies between the predicted and measured responses.

The effects of shaft bending were then investigated. Instead of the eddy current probes, the shaft inductive displacement transducer, was used to monitor the dynamic displacements. The investigation was carried out at K = 0 and the bearing operating at approximately the concentric condition. Frequency response measurements for excitations in the Y-direction were obtained for 3 positions of the shaft displacement transducer. (See figure 8.6). The measured phase characteristics for the 3 positions are illustrated in figure 8.6. The results showed that the response measurements were dependent on the position where the displacements were monitored. The results where the displacement transducer was located at the centre of the bearing, agreed reasonably well with the results predicted by the rigid shaft assumption. Moving the displacement transducer to a position on the left or right of the bearing, produced results that were more representative of the responses measured by the eddy current probes. This investigation, therefore, suggested that the effects of shaft bending cannot be neglected. Hence, the method of predicting the bearing fluid-film transfer functions taking into account the effects of shaft bending as presented in Section 6.4, was employed in the present in-

vestigation.

Figures (8.7a) to (8.11b), illustrate the measured and predicted frequency response characteristics of the bearing fluid-film (G_{11} (s) and G_{22} (s)), at K = 0, for values of eccentricity-ratios ranging from ε = 0 to 0.8. Good correlation between the predicted and measured gain characteristics were obtained for eccentricity-ratios up to ε = 0.6. At ε = 0.8, the theory tended to under-estimate the gain characteristics. The discrepancy may be related back to the steady state characteristics, as correlation between the predicted and measured static characteristic was poor at this value of eccentricity. The figures also indicated that better agreement between the experimental and theoretical gain charac-teristics were obtained in the X-direction. The measured gain for the Y-direction was always larger than the predicted gain. This discrep-ancy could possibly be attributed to the inertia effect of the decoup-ling spring and suggests that this effect may be important. The phase characteristics were less accurately predicted. Good correlation between the predicted and measured phase characteristics occurred at frequencies below 30 Hz. The discrepancy increases with frequency. Structural damping or the dynamics of the bending shaft could be responsible for the larger phase lag experienced in the measured char-acteristics. It is possible that the latter effect is significant, although this was not considered in the analysis.

The frequency response characteristics of the bearing fluid-film (G_{11} (s), G_{12} (s), G_{21} (s) and G_{22} (s)), for K = 13.4 and 31 at various values of eccentricity-ratios are presented in figures (8.12a) to (8.17d). Good agreement between the predicted and measured direct coupled responses (G_{11}, ϕ_{11} and G_{22}, ϕ_{22}) can be observed. However, correlation between the predicted and measured phase lags of the cross-coupled responses (ϕ_{12} and ϕ_{21}) was poor, especially at the low amplitude region. At low values of eccentricity-ratios, the experi-

mental points were very scattered. As the eccentricity-ratio increases, the experimental points tend to follow the same trend as the theoretical predictions and the scatter was less. The ability to obtain good cross-coupled responses is limited by the present dynamic measurement system, where facilities apart from the correlator in the frequency response analyser for the analysis of noise, such as, filters had not been implemented. The introduction of filters may create more problems, as the filter characteristics cannot always be neglected, and the transfer functions associated with the filters have to be included in the overall system. Due to the low-signal to noise ratios of the cross-couples signals, the correlator in the frequency response analyser, was not able to perform the noise rejection efficiently.

The cross-coupled dynamic forces increase with eccentricity, therefore, improvements in the cross-coupled signal to noise ratios, may be expected at higher values of eccentricity-ratios. This point is reflected in the graphs of G_{12} (s) and G_{21} (s), as the scatter in the cross-coupled responses diminished with eccentricity. Therefore, this investigation suggests that in the absence of proper facilities for noise analysis, it may be more appropriate to conduct dynamic tests at high values of eccentricity-ratios, at least up to the eccentricity where the steady state performance had been verified. Although a high signal to noise ratio may be achieved by increasing the excitational force, this is not always helpful, in view of the fact that the investigation was based on a linear analysis.

Compared with the non-rotating test (K = 0), the results of the rotating tests (K = 13.4 and 31), showed up one or two doubtful experimental points, which may seem to be a system resonance. In fact, this is more likely due to the effect of noise corruption, as repeating the experimentation may fail to pick up the peak or it may be picked up at a different frequency. Periodic noise may be generated

by the rotational motion of the journal due to non-circularity of the journal or bearing. This may produce large peaks at frequencies, which are multiples of the running frequency. Electronic noise which is mainly random and mains noise (50 Hz and multipled of 50 Hz) may be generated by the measuring system and the surrounding electrical equipment. Unless, the analysis of noise is included in the investigation the source and nature of each peak cannot be accurately accounted for.

The results of the phase measurements again, reinforce the point that it was essential that the dynamic characteristics of the shaft were included in the analysis. An interesting point arising from the experimentation is that the responses were more highly damped than the theory predicts, although what proportions of the damping was due to the structure was not investigated. Hence, the theoretical predictions would be expected to be conservative. Certainly, this investigation would have been more informative, had the dynamic measurement system been capable of performing accuratley below 5 Hz. Therefore, there is a need for a dynamic measurement system, that is capable of performing well at the low frequency spectrum, perhaps, as low as 0.1 Hz.

A comparison of the experimental and theoretical stiffness and damping coefficients for K = 0 and 31, are illustrated in figures (8.18a) to (8.20c). The theoretical coefficients were obtained from the perturbed finite difference program, PFD.FOR, whilst, the experimental coefficients were determined from the measured frequency response functions by the direct method, described in Chapter 6. There is a lot of scatter and alarming discrepancies in the stiffness coefficients. This is mainly due to the problem of ill conditioning. Small errors in the frequency response functions can cause large errors in the bearing coefficients. The stiffness coefficients for K = 0, were checked with those obtained from the experimental static load locus. The results showed that the theory tends to under-

estimate the stiffness. (See figures 8.18a and 8.18b). It is interesting to note that the experimentally determined cross-coupled stiffness coefficients were lower than the predicted values. (See figures 8.19b and 8.19c). This would mean that theoretical stability studies would be conservative.

For most of the graphs, less scatter was observed in the damping coefficients, and the experimental points follow the general trend as predicted by theory. Although the cross-coupled damping coefficients showed more signs of scatter, in general the trend of the damping results were within the same order as the theoretical values, and the equality of the b_{12} and b_{21} coefficients is demonstrated (Figure 8.20b).

This investigation showed that the direct method of evaluating the bearing coefficients from frequency response functions is not adequate. A curve-fitting routine using the least squares criterion to minimize the errors between the predicted and measured frequency response functions, should be incorporated into the bearing coefficients extraction routine.

Within the limits of experimental errors, it may be concluded that the bearing fluid-film transfer functions were adequately determined, but, the accuracy of the bearing coefficients was difficult to assess. The determination of the bearing coefficients was not only subject to the problems associated with a set of ill-conditioned equations, but was strongly dictated by experimental errors, such as, the ability to maintain the selected value of eccentricity for both directions of excitation.
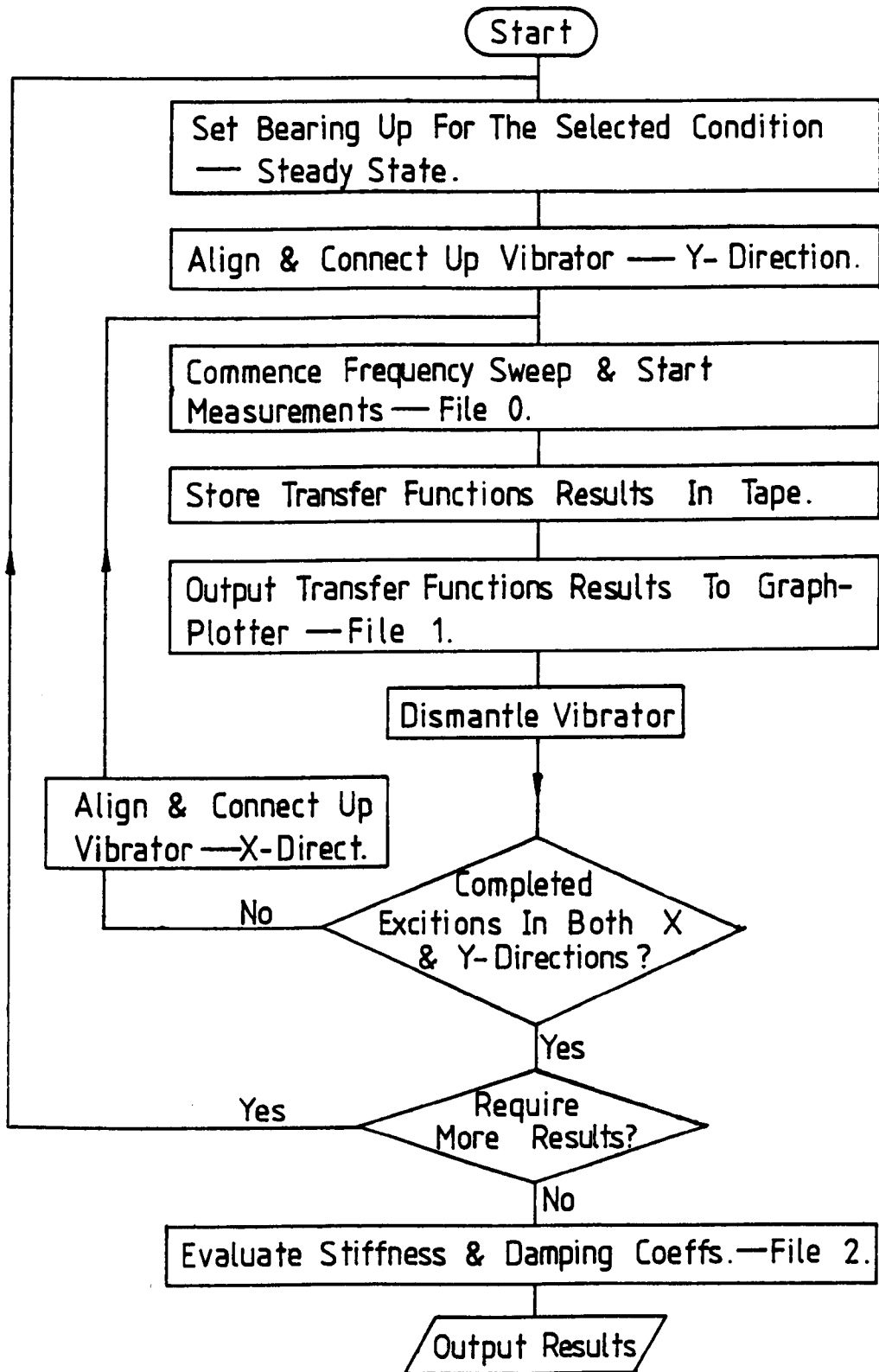
Fig.(8.1) : Algorithm For Obtaining The Experimental Transfer
Functions And The Eight Dynamic Coefficients
Of The Bearing Fluid-Film.

Fig. 8.2: Variation Of Static Load With
Eccentricity-Ratio. (K = 0.0)

a/L = 0.25 ——— Theory
L/D = 1.0 ● ● ● Exp.
β = 0.44
S_{ho} = 0.043
P_S = 689.48 KPa.

Fig. 8.3 : Variation Of Static Load With
Eccentricity-Ratio. (K = 13.4)

a/L = 0.25   —— Theory

L/D = 1.0   • • • Exp.

β = 0.44

S_{ho} = 0.043

P_S = 689.48 KPa.

Fig. 8.4: Variation Of Static Load With
Eccentricity-Ratio. (K = 31.0)

$a/L = 0.25$ —— Theory

$L/D = 1.0$ ● ● ● Exp.

$\beta = 0.44$

$S_{ho} = 0.043$

$P_s = 689.48\,KPa.$
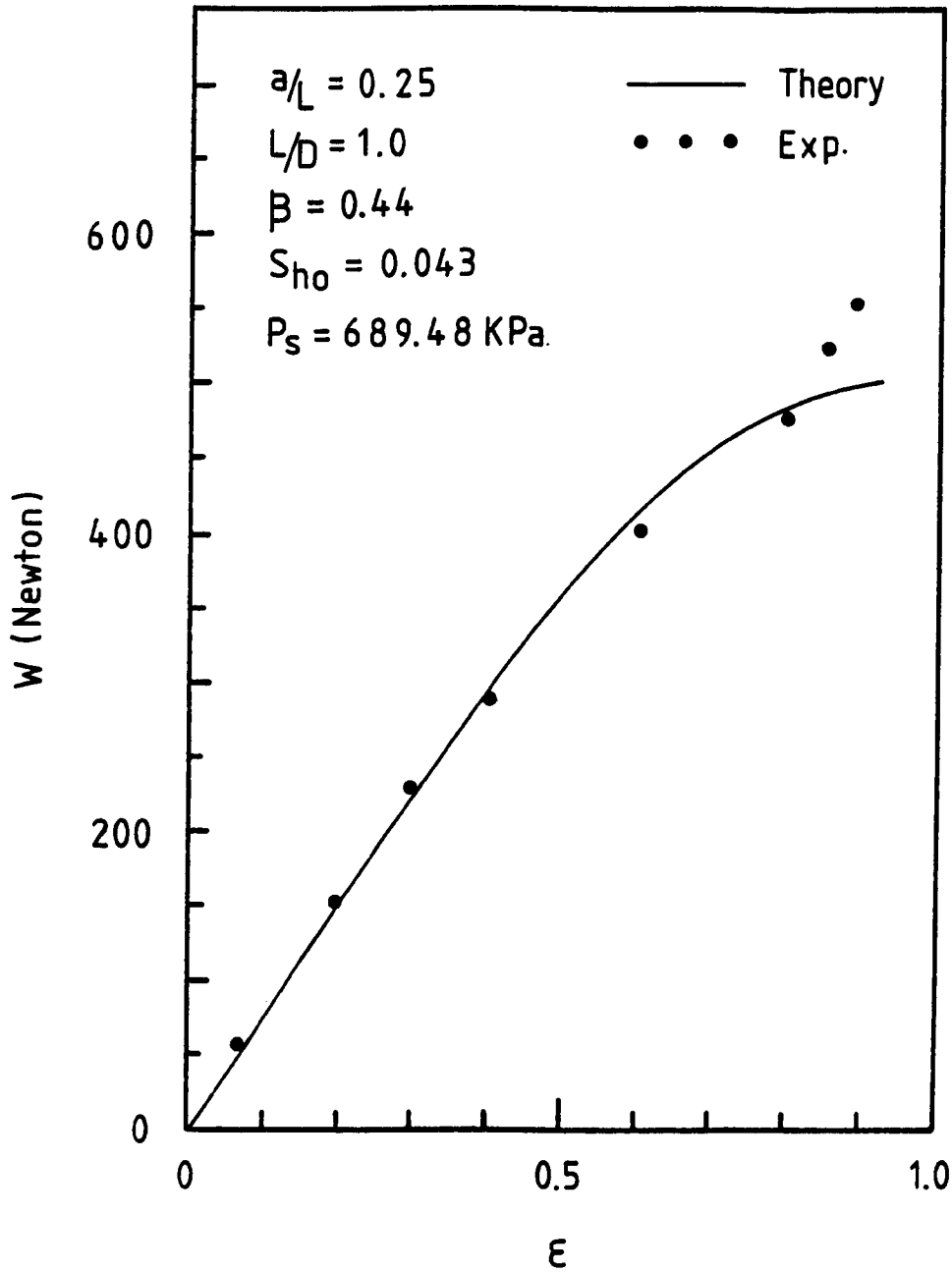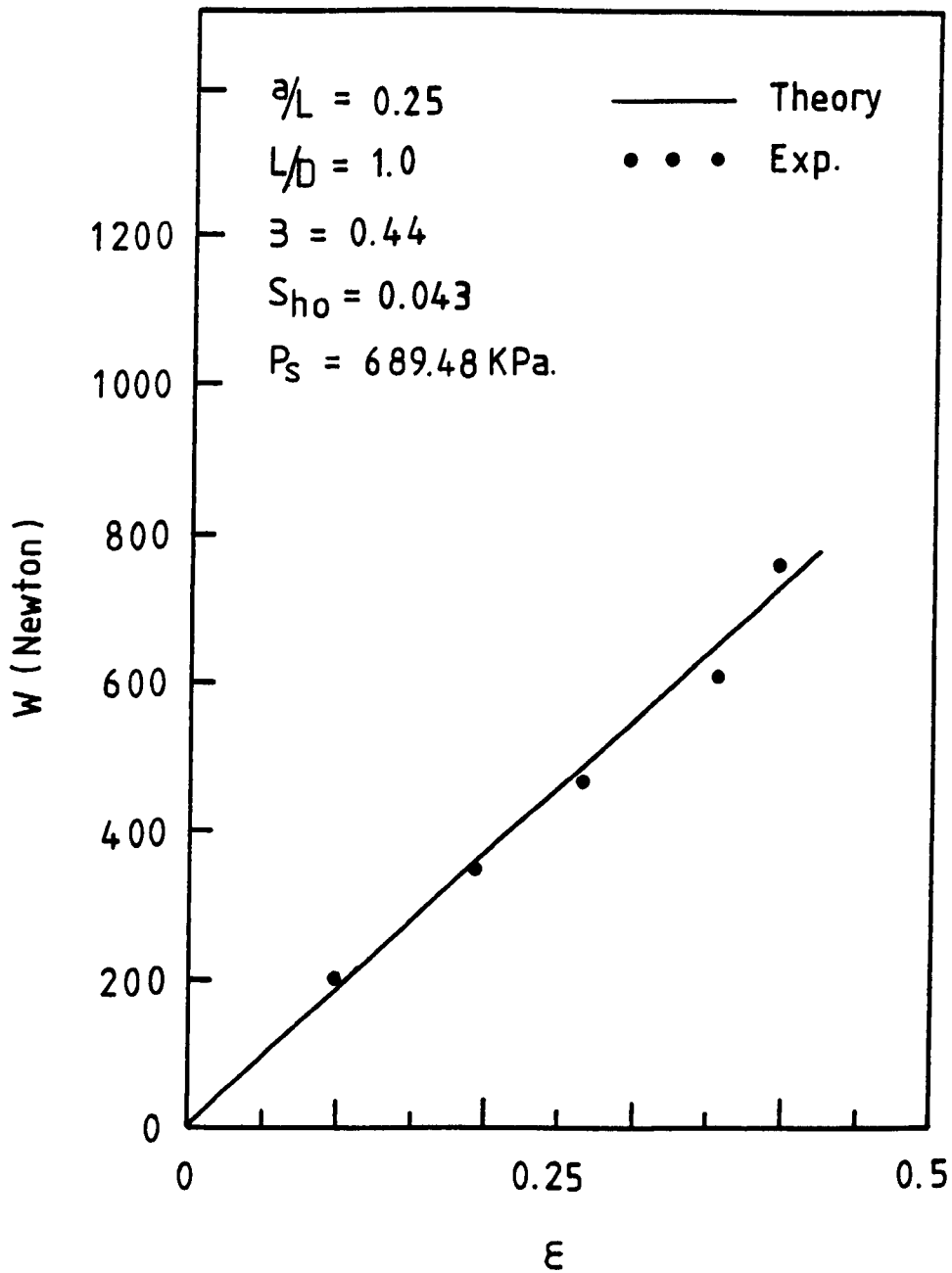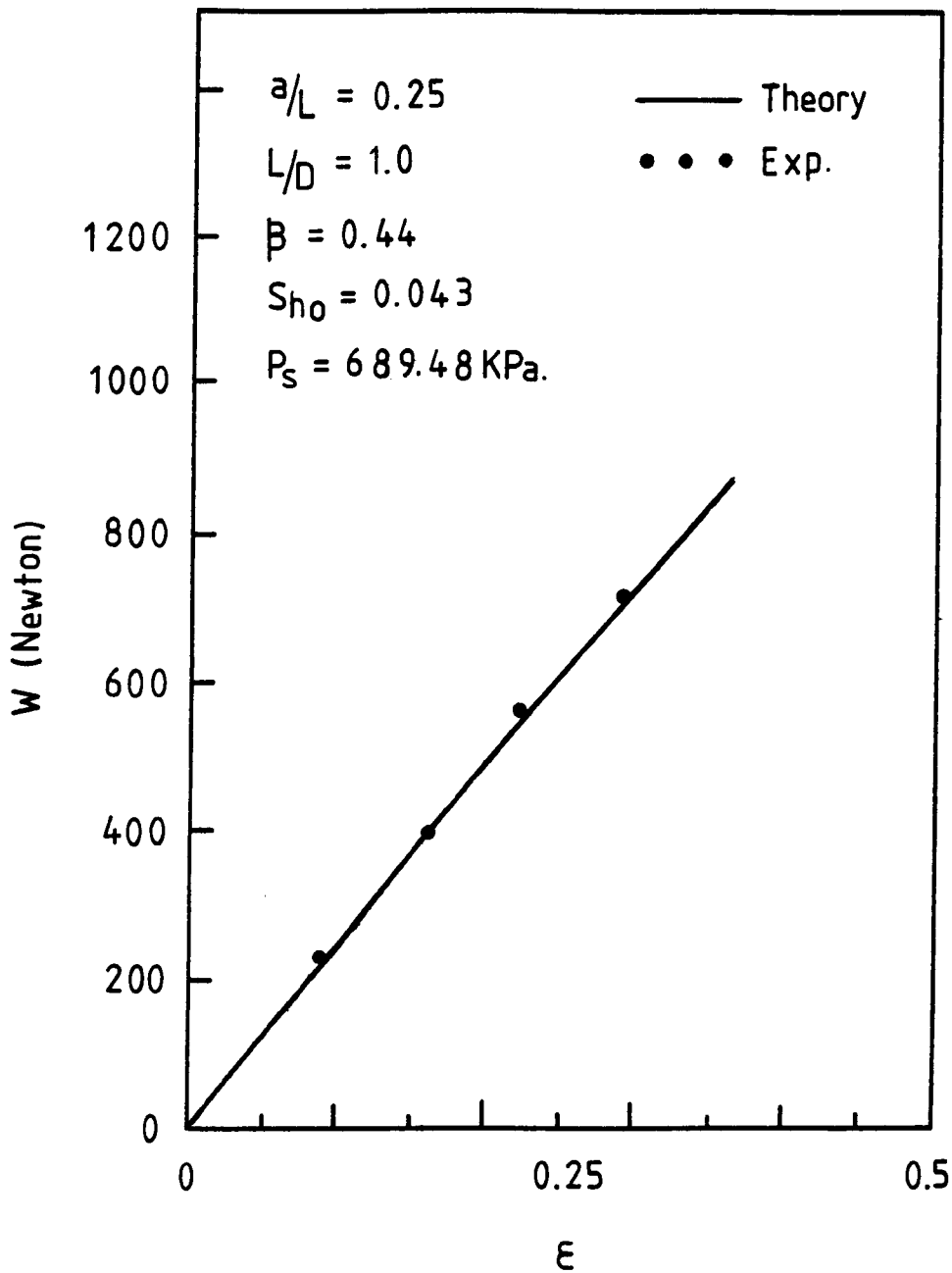
Fig. 8.5a:Variation Of Attitude-Angle With Eccentricity-Ratio. (K = 13.4)
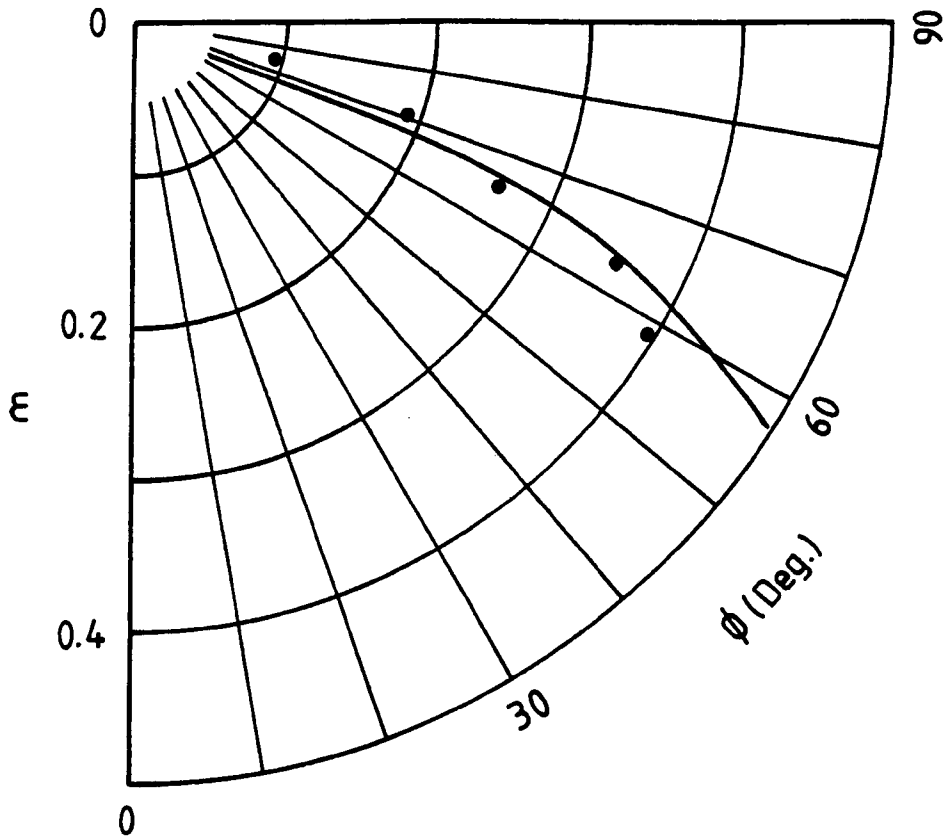
Fig. 8.5b:Variation Of Attitude-Angle With Eccentricity Ratio. (K = 31.0)
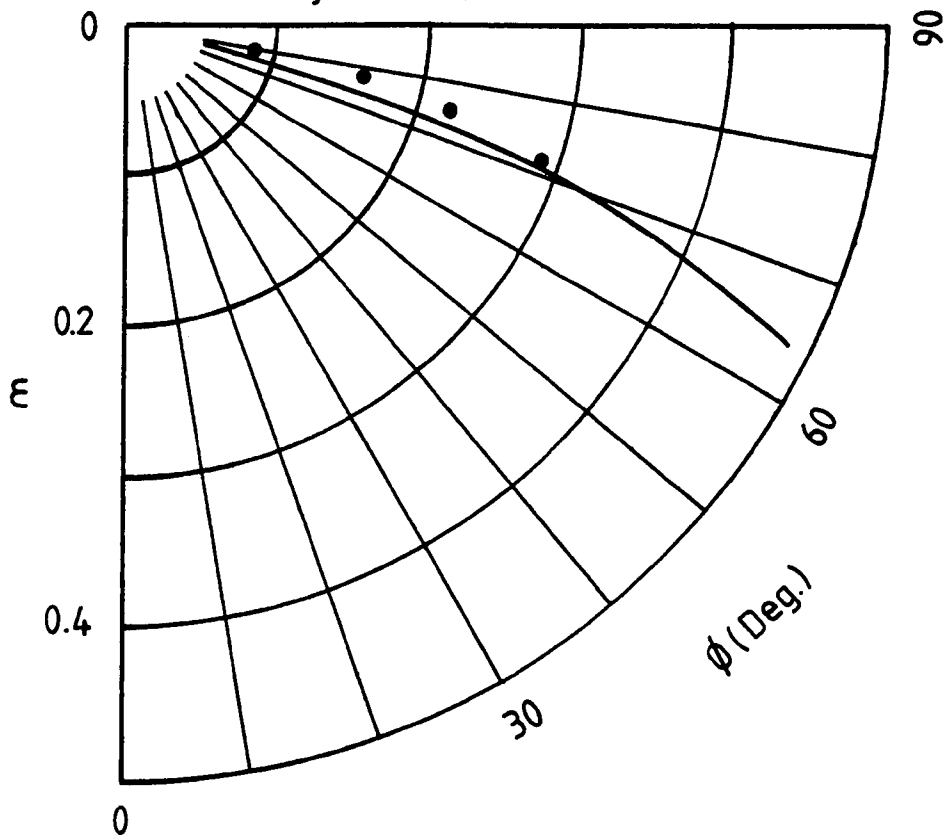
Fig. 8.6 : Graph Illustrating The Effects Of Shaft Bending On The Dynamic Response.
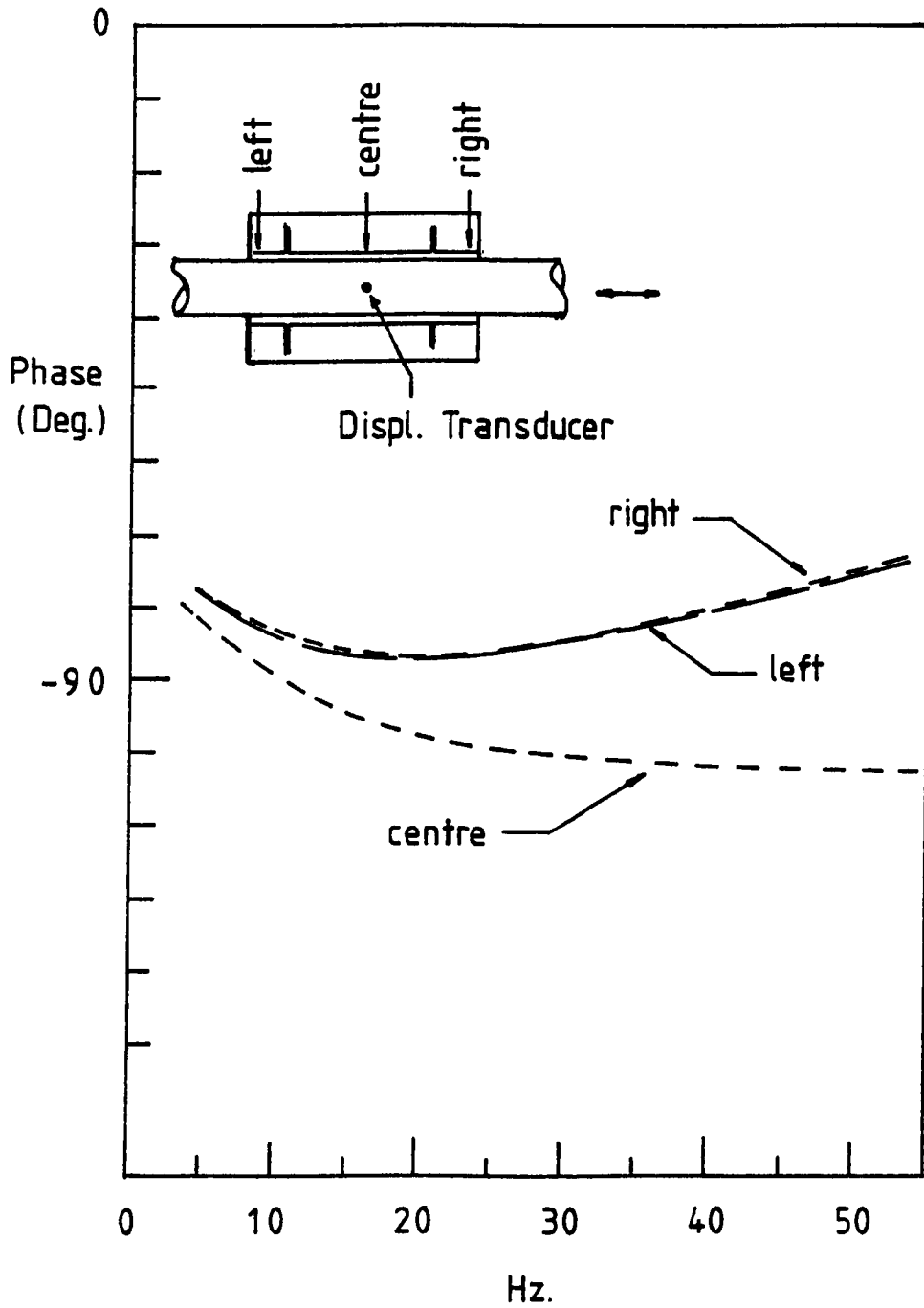
Fig. 8.7a :   Frequency Response of Plain Line-Entry (Slot)
Hybrid Journal Bearing. [E=0.0]

$a/L = 0.25$

$L/D = 1.0$

$Sho = 0.043$

$K = 0.0$
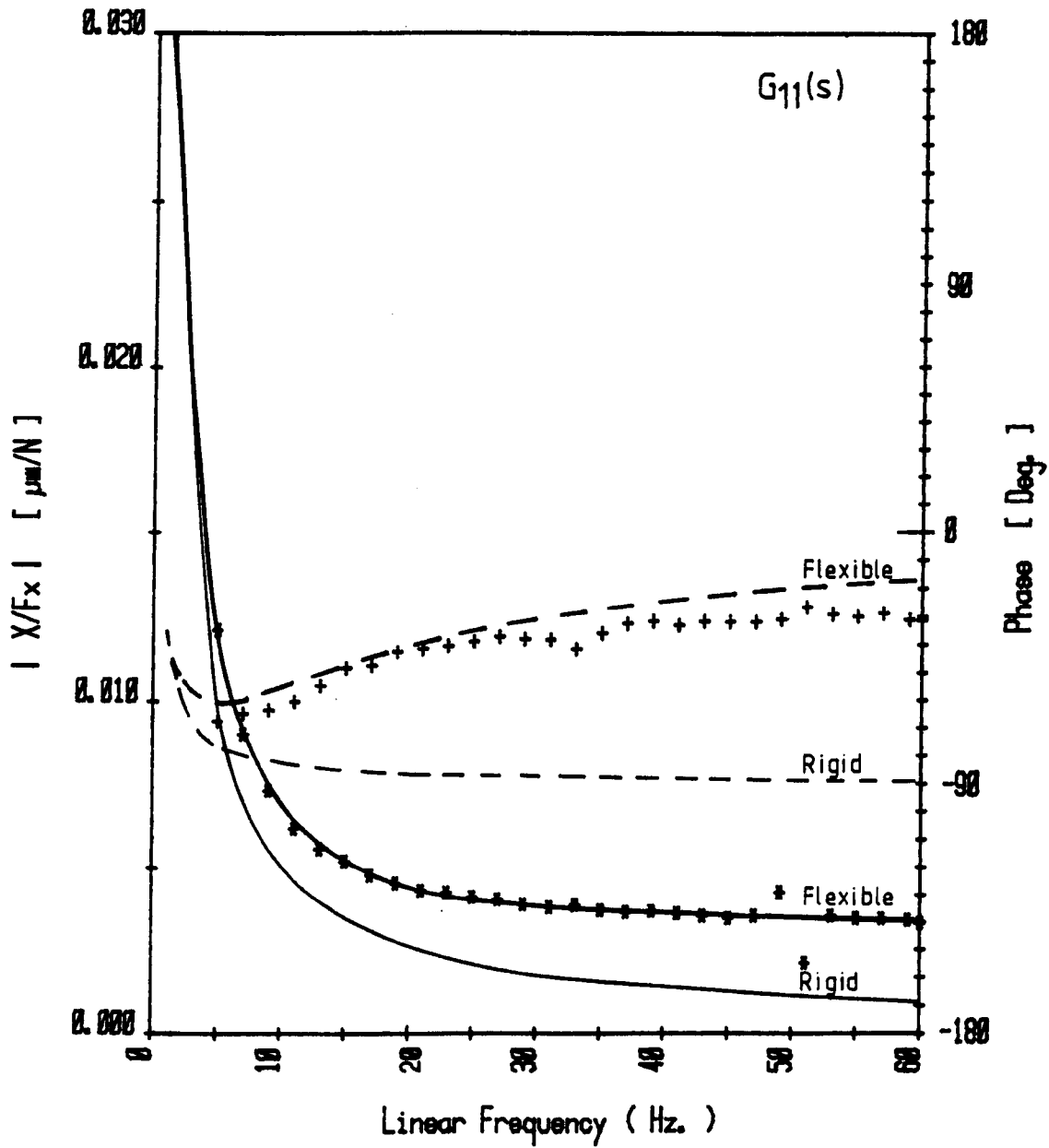
$Beta = 0.44$

$Ps = 689,476$ KPa

$Tm = 33.5°C$

	Exp.	Theory
Gain	* * * * *	————
Phase	+ + + + +	— — — —

Fig. 8.7b: Frequency Response of Plain Line-Entry (Slot)
Hybrid Journal Bearing. [E=0.0]

a/L = 0.25

L/D = 1.0

Sho = 0.043

K = 0.0
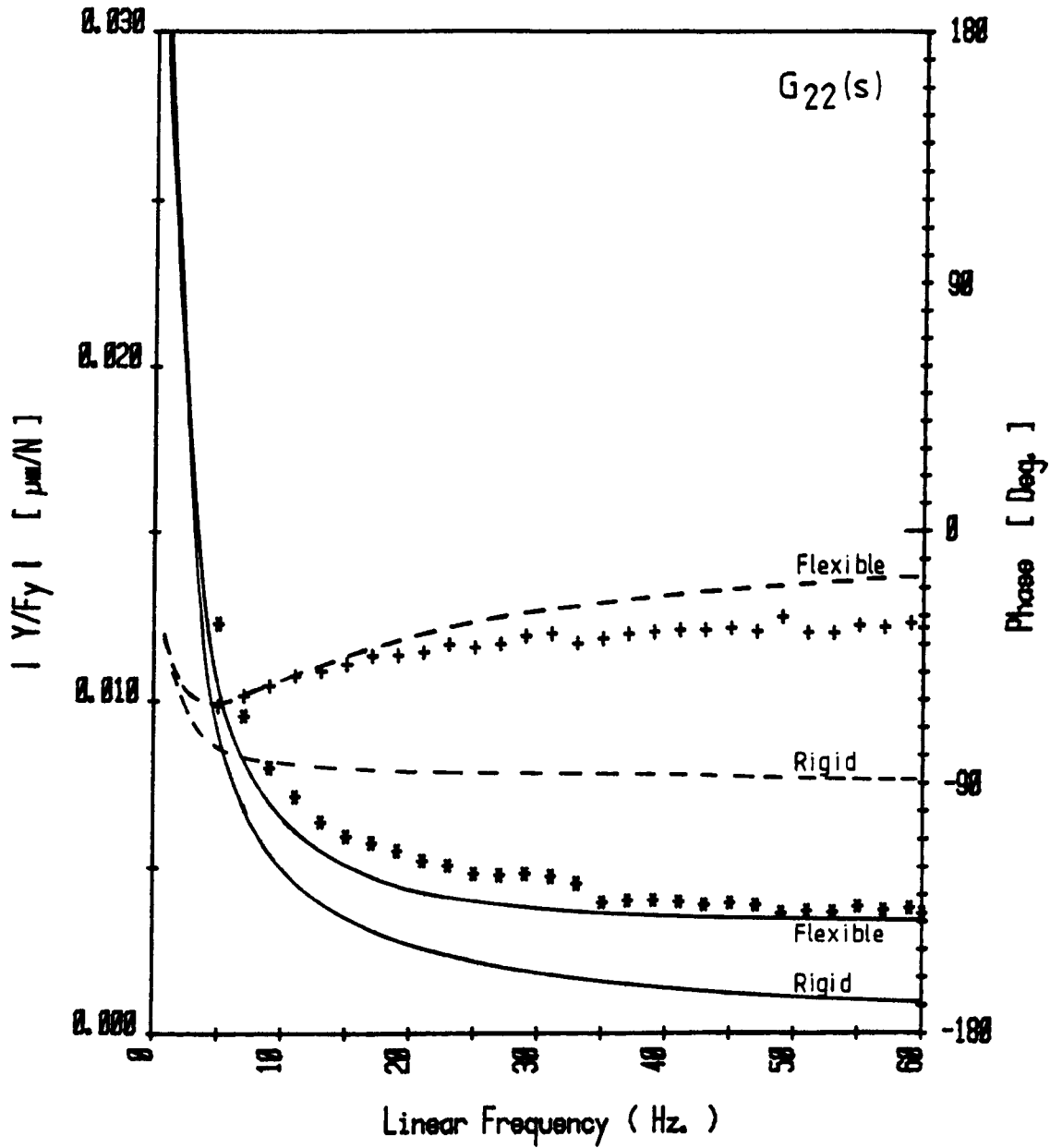
Beta = 0.44

Ps = 689,476 KPa

Tm. = 30.35°C

	Exp.	Theory
Gain	* * * * *	——————
Phase	+ + + + +	— — — —

Fig. 8.8a : Frequency Response of Plain Line-Entry (Slot)
            Hybrid Journal Bearing. [E=0.2]
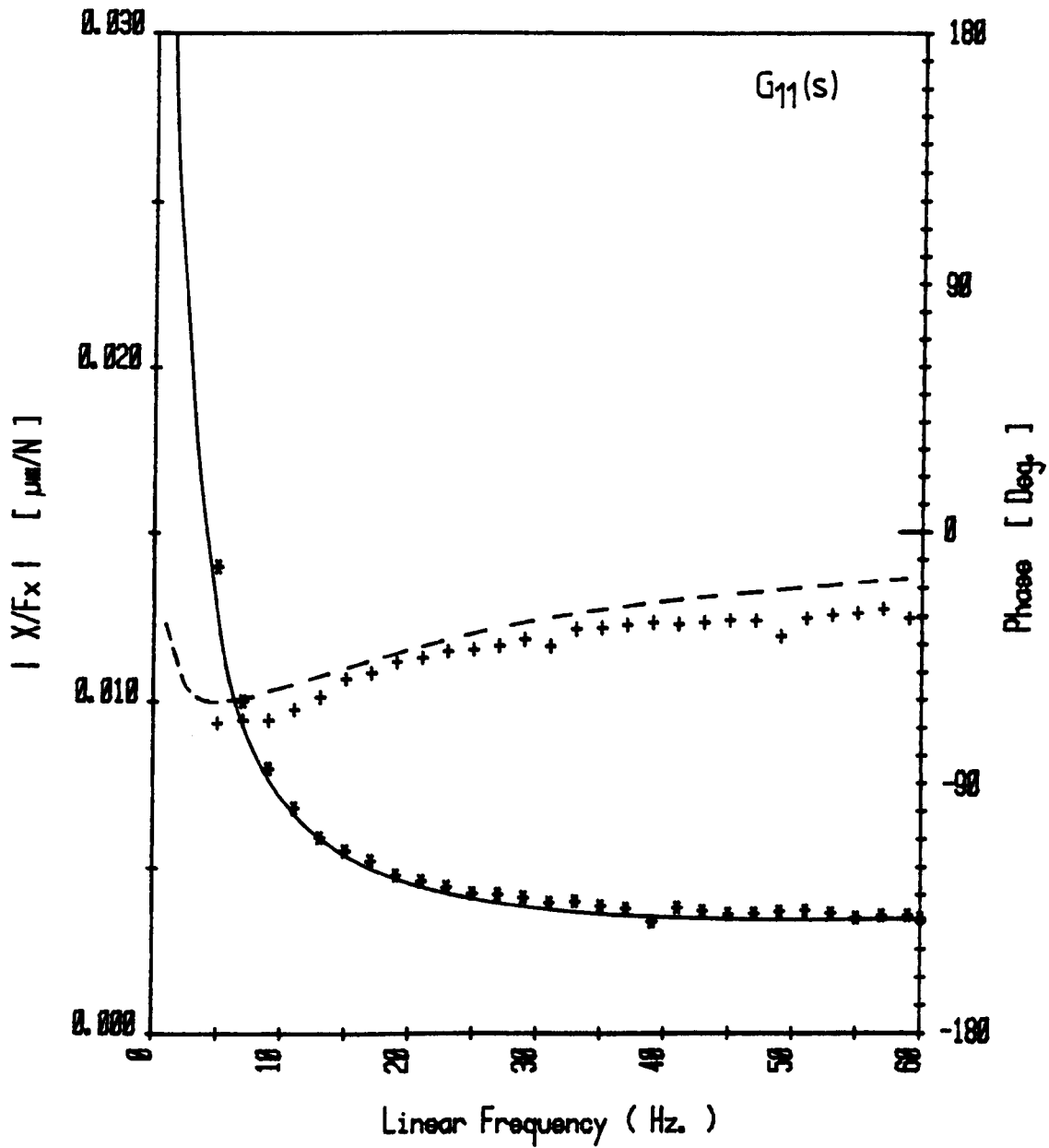
a/L = 0.25

L/D = 1.0

Sho = 0.043

K = 0.0

Beta = 0.44

Ps = 689,476 KPa

Tm = 34.5°C

	Exp.	Theory
Gain	* * * *	————
Phase	+ + + +	— — — —

Fig. 8.8b: Frequency Response of Plain Line-Entry (Slot)
            Hybrid Journal Bearing. [E=0.2]

Linear Frequency (Hz.)

a/L = 0.25   Exp.   Theory

L/D = 1.0

Sho = 0.043   Gain   * * * * *   ─────────

K = 0.0

Beta = 0.44   Phase   + + + + +   — — — —

Ps = 689,476 KPa

Tm. = 29.7°C

Fig. 8.9a :   Frequency Response of Plain Line-Entry (Slot)
              Hybrid Journal Bearing. [E=0.4]

a/L = 0.25

L/D = 1.0

Sho = 0.043

K = 0.0

Beta = 0.44

Ps = 689,476 KPa

Tm = 35.1°C

	Exp.	Theory
Gain	* * * *	———
Phase	+ + + +	— — — —

Fig. 8.9b : Frequency Response of Plain Line-Entry (Slot) Hybrid Journal Bearing. [E=0.4]

a/L = 0.25

L/D = 1.0

Sho = 0.043

K = 0.0

Beta = 0.44

Ps = 689,476 KPa

Tm = 30.7°C

	Exp.	Theory
Gain	* * * * *	————
Phase	+ + + + +	— — — —

Fig. 8.10a: Frequency Response of Plain Line-Entry (Slot)
Hybrid Journal Bearing. [E=0.6]
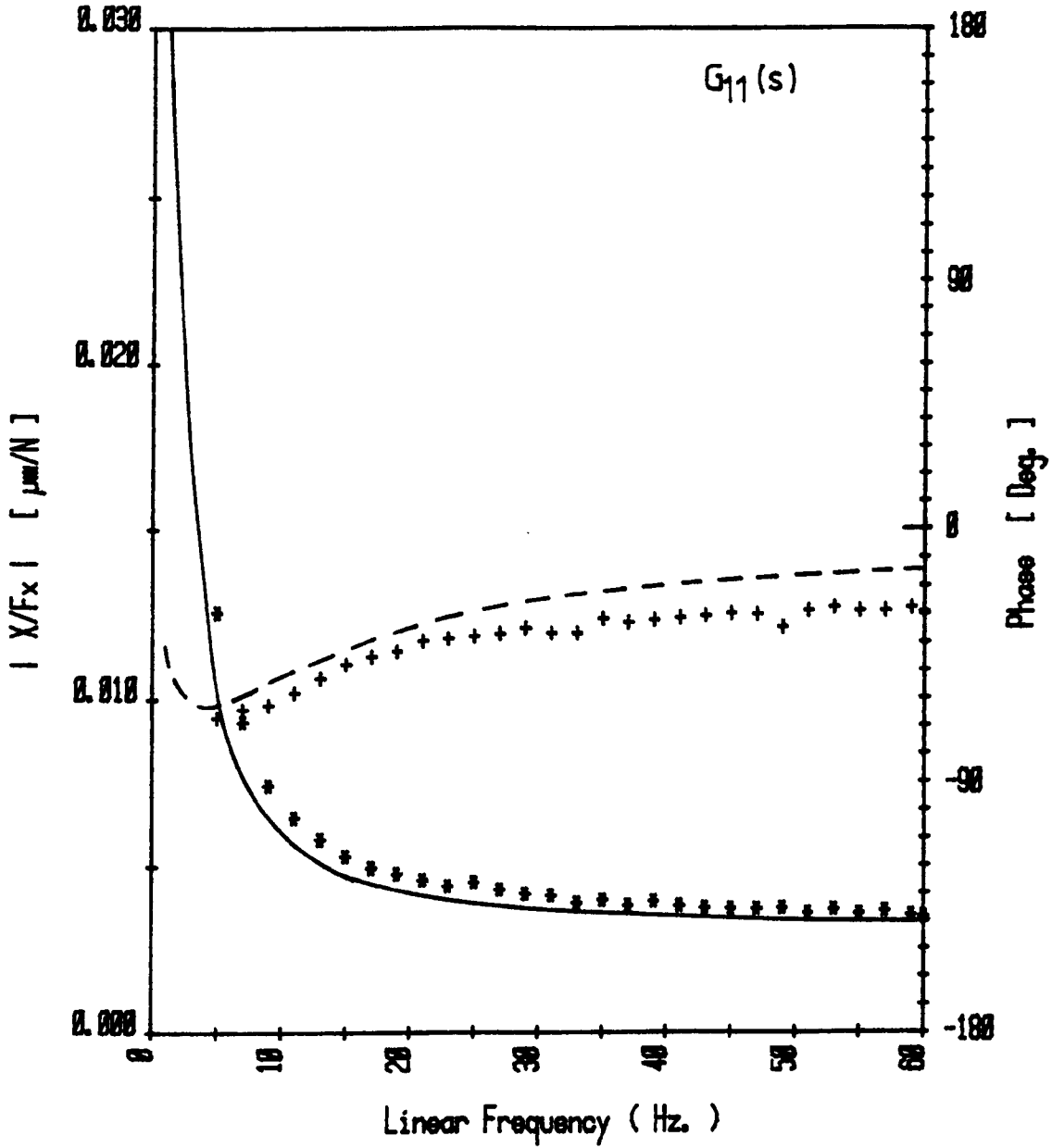
	a/L = 0.25	Exp.	Theory
	L/D = 1.0		
	Sho = 0.043		
	K = 0.0		
	Beta = 0.44		
	Ps = 689,476 KPa		
	Tm = 33.6°C		

Gain ***** ———

Phase +++++ — — — —

Fig. 8.10b: Frequency Response of Plain Line-Entry (Slot)
              Hybrid Journal Bearing. [E=0.6]
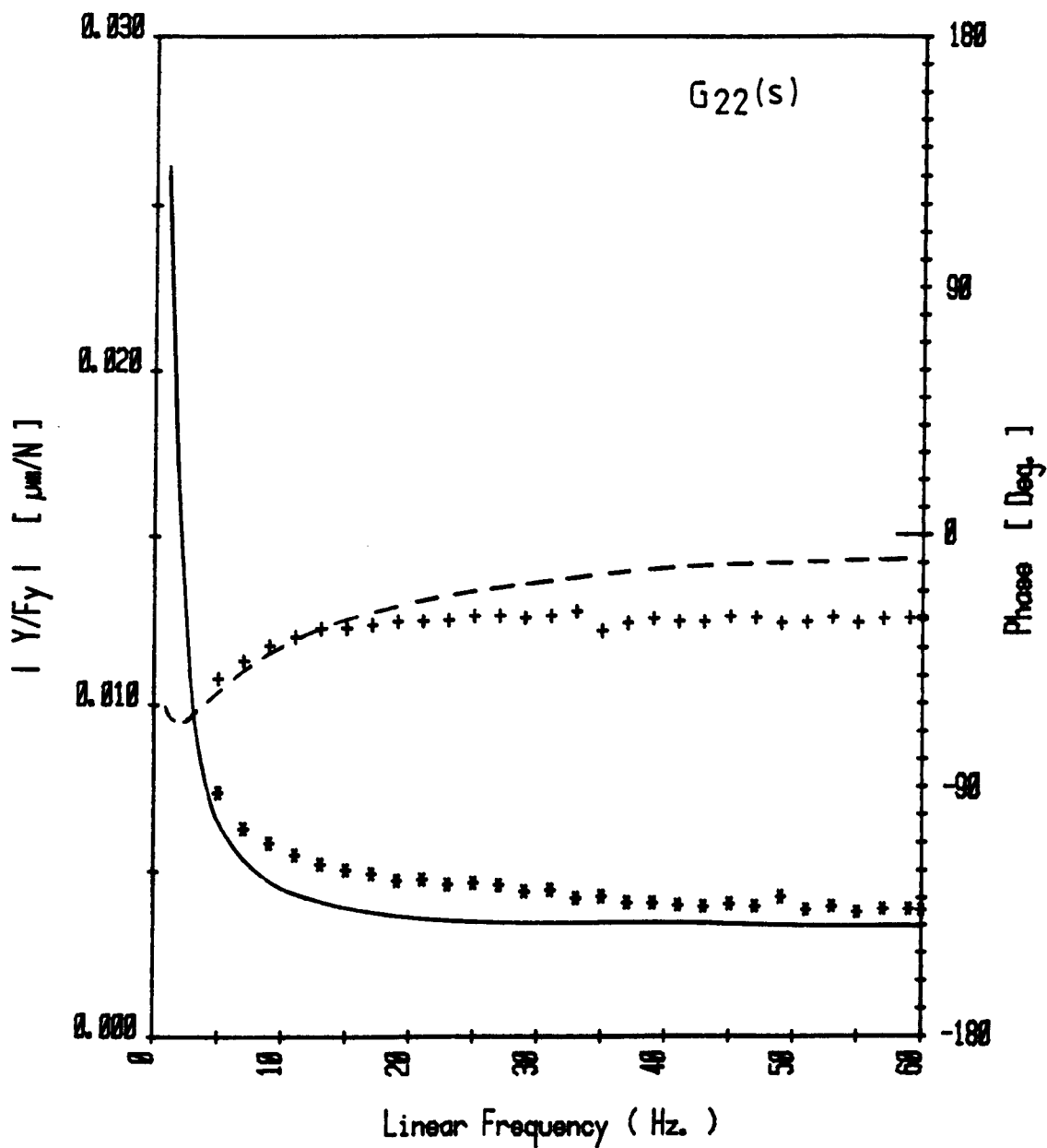
Fig. 8.11a: Frequency Response of Plain Line-Entry (Slot)
             Hybrid Journal Bearing. [E=0.8]
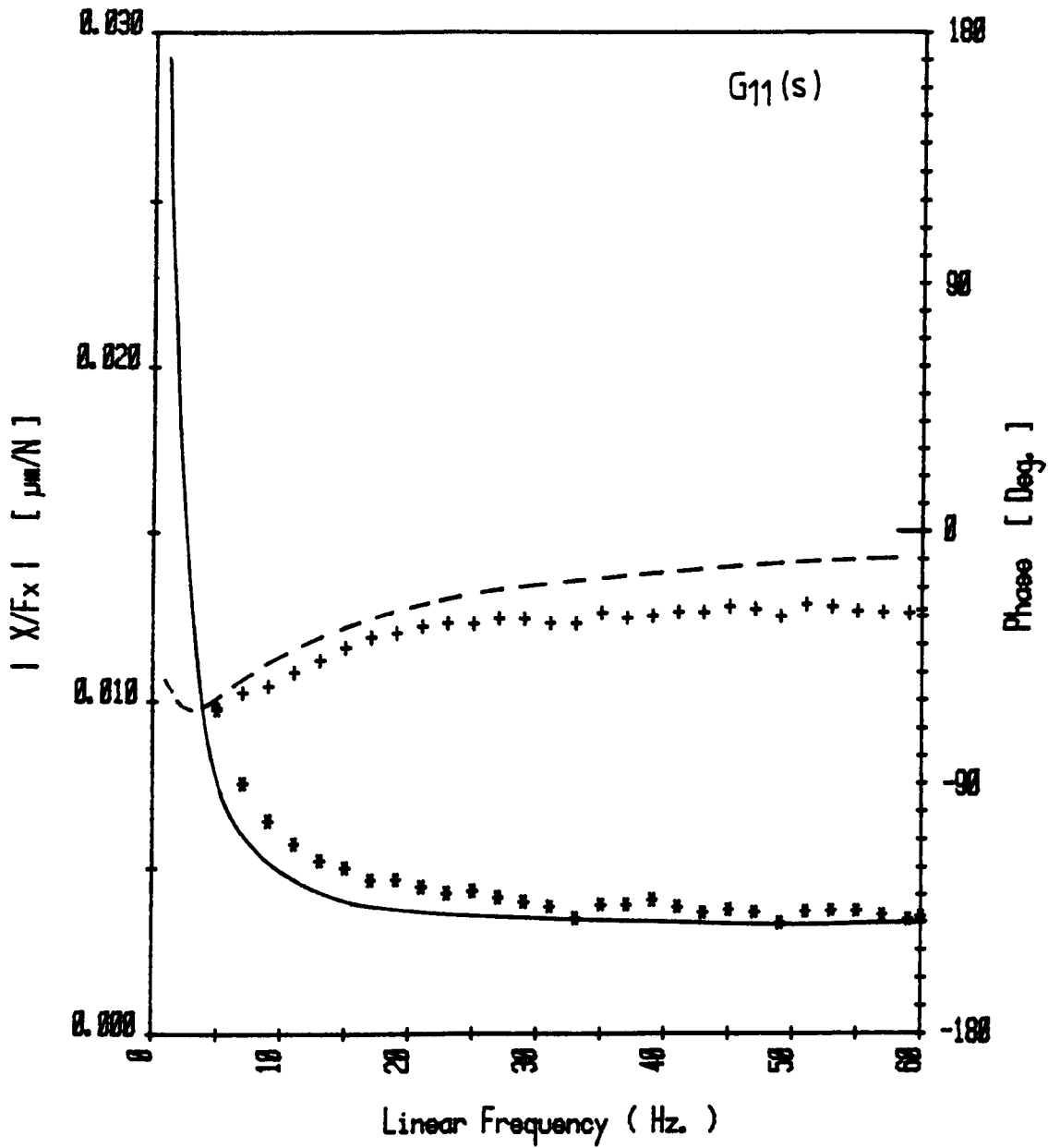
a/L = 0.25
L/D = 1.0
Sho = 0.043
K = 0.0
Beta = 0.44
Ps = 689,476 KPa
Tm = 32.6°C

	Exp.	Theory
Gain	* * * *	————
Phase	+ + + +	— — — —

Fig. 8.11b : Frequency Response of Plain Line-Entry (Slot)
Hybrid Journal Bearing. [E=0.8]
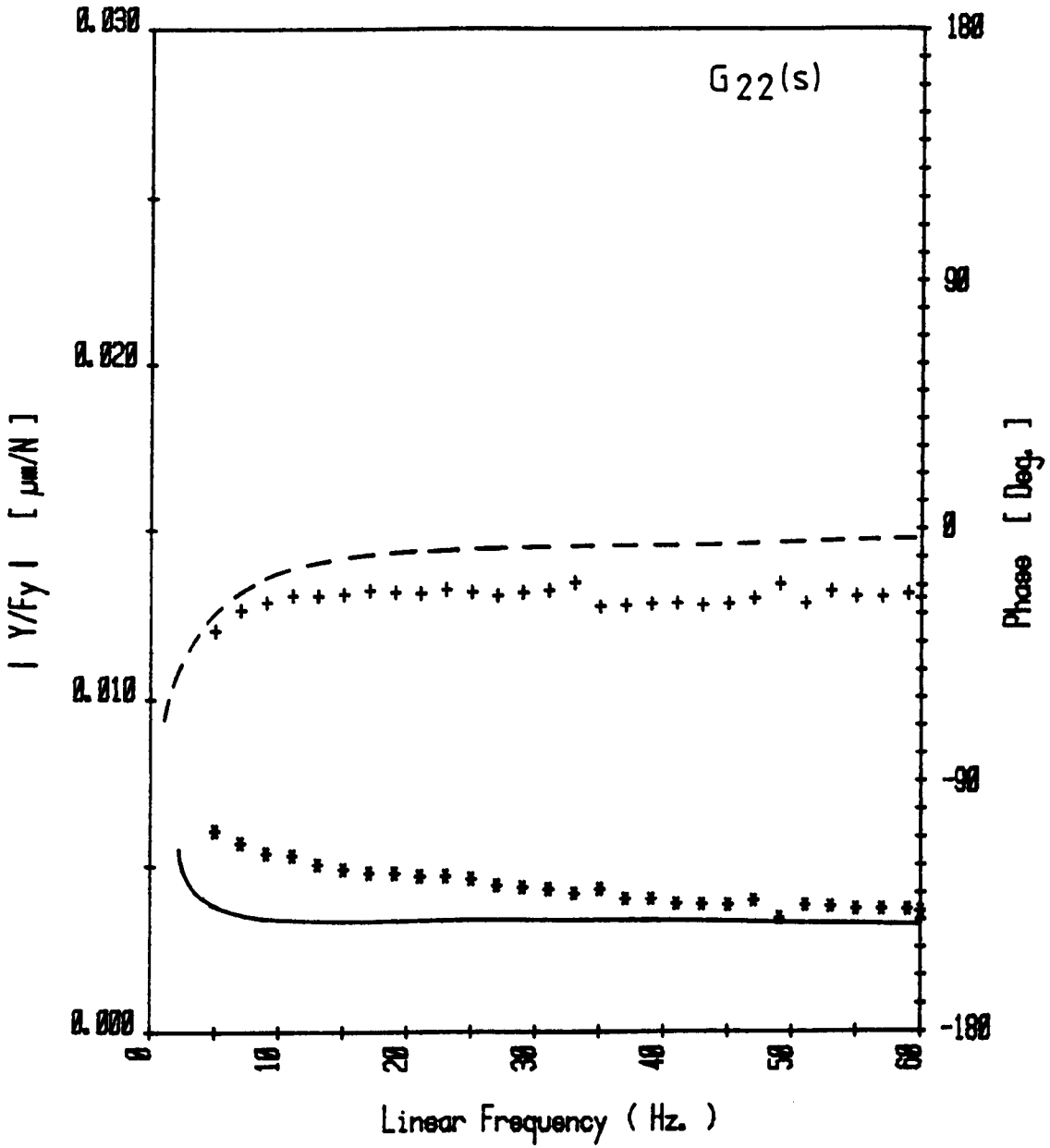
$G_{22}(s)$

| Y/Fy | [μm/N]

Phase [Deg.]

Linear Frequency (Hz.)

a/L = 0.25

L/D = 1.0

Sho = 0.043

K = 0.0

Beta = 0.44

Ps = 689,476 KPa

Tm. = 32.7°C

	Exp.	Theory
Gain	* * * * *	——
Phase	+ + + + +	— — —

Fig. 8.12a: Frequency Response of Plain Line-Entry (Slot)
Hybrid Journal Bearing. [E=0.19]
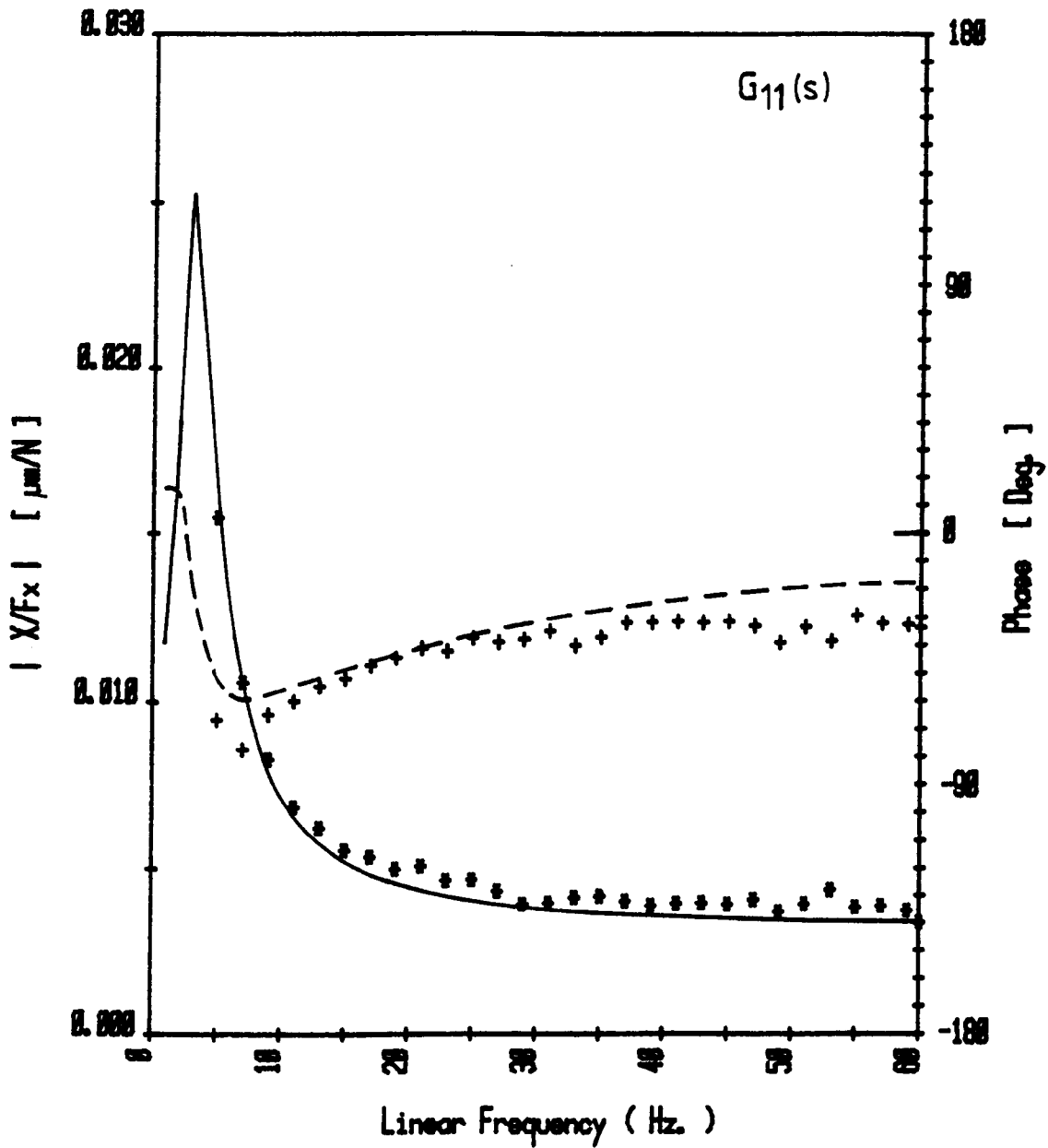
a/L = 0.25
L/D = 1.0
Sho = 0.043
K = 13.4
Beta = 0.44
Ps = 689,476 K Pa
Tm = 33.2°C

Fig. 8.12b: Frequency Response of Plain Line-Entry (Slot)
Hybrid Journal Bearing. [E=0.19]
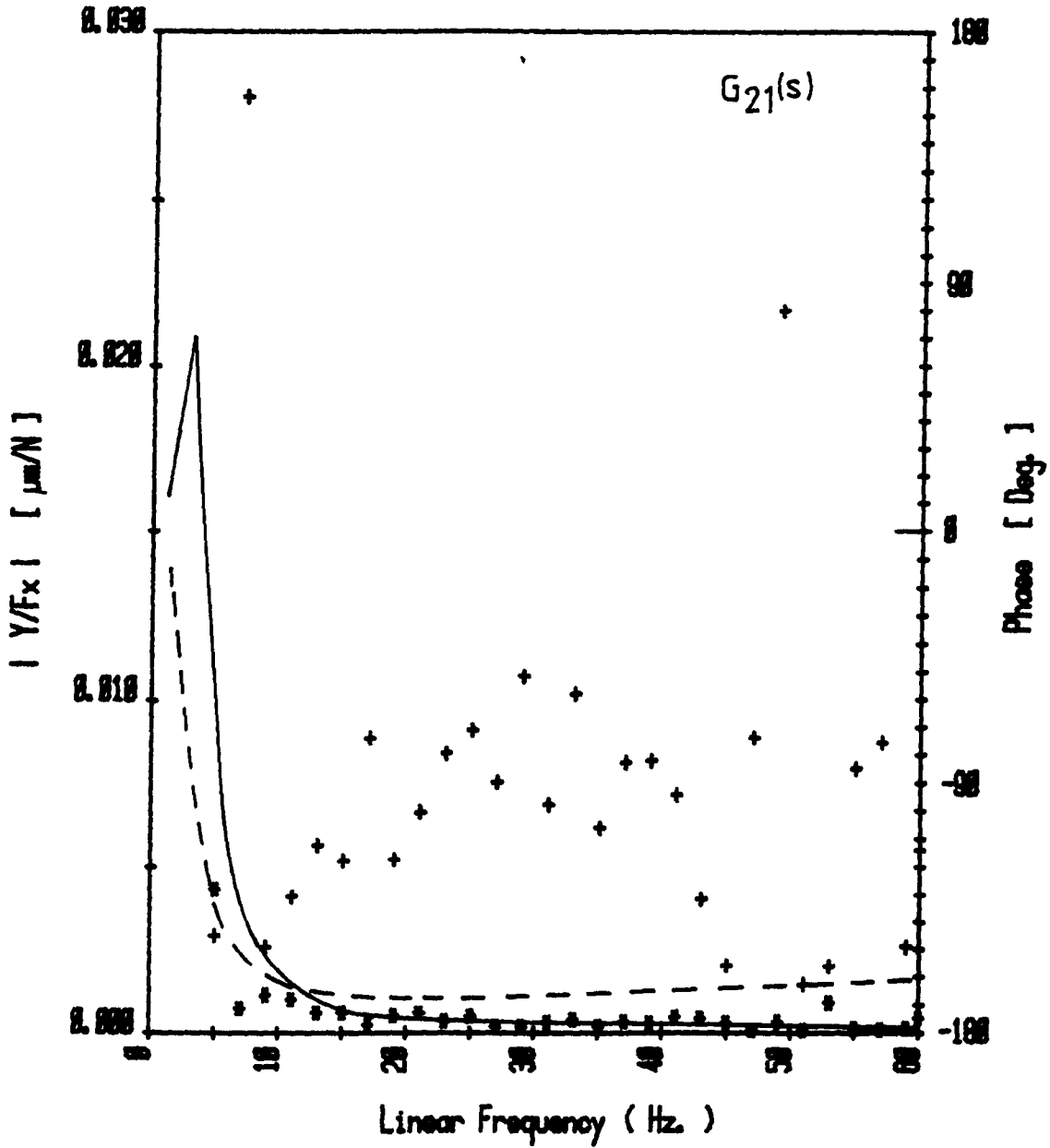
	Exp.	Theory
a/L = 0.25		
L/D = 1.0		
Sho = 0.043		
K = 13.4	Gain *****	———
Beta = 0.44	Phase +++++	— — —
Ps = 689,476 KPa		
Tm = 33.2°C		

Fig. 8.12c: Frequency Response of Plain Line-Entry (Slot)
Hybrid Journal Bearing. [E=0.19]
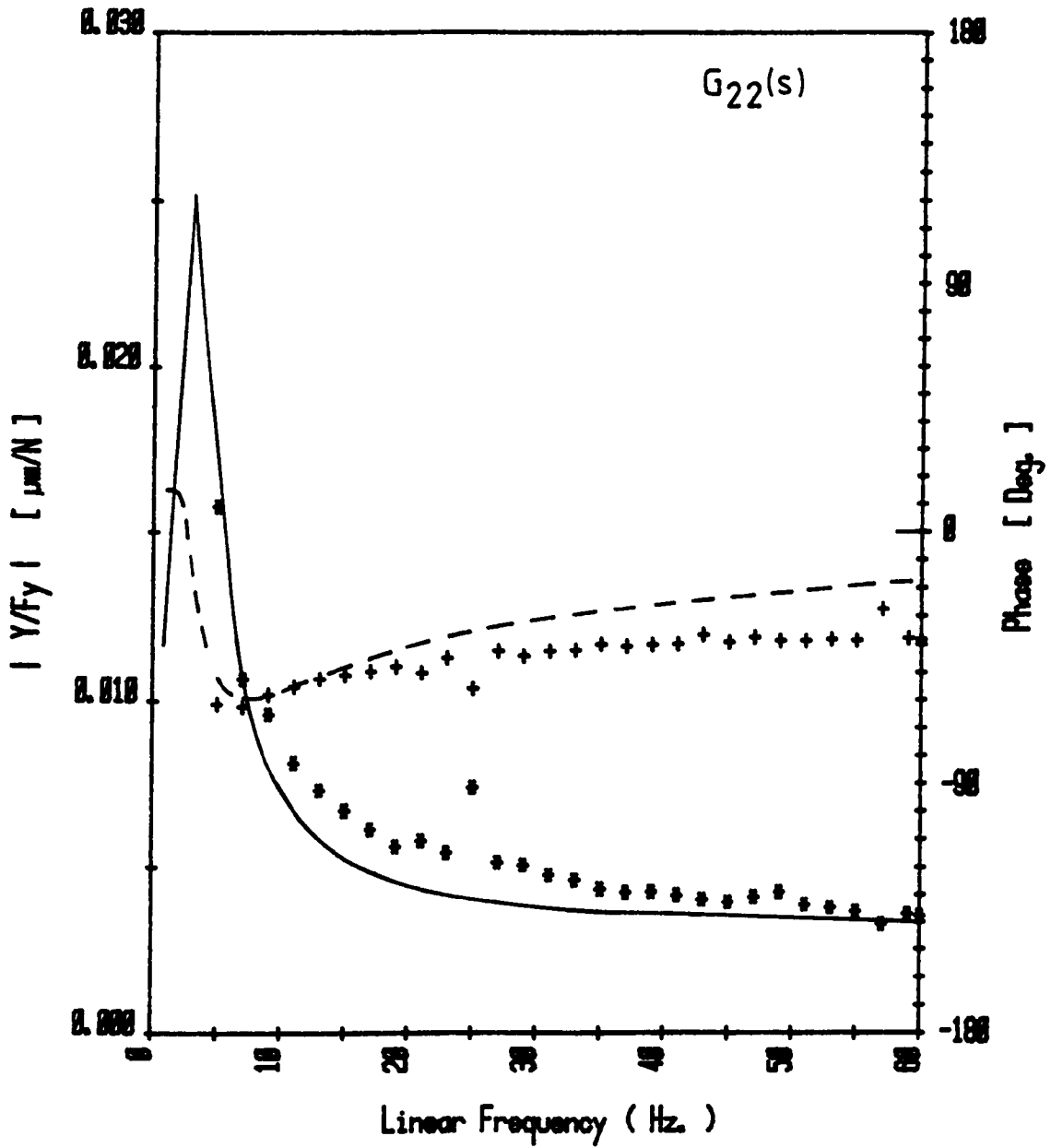
$G_{22}(s)$

| Y/Fy | [μm/N]

Phase [Deg.]

Linear Frequency (Hz.)

a/L = 0.25

L/D = 1.0

Sho = 0.043

K = 13.4

Beta = 0.44

P_s = 689,476 KPa

T_m = 33.6°C

	Exp.	Theory
Gain	* * * * *	———
Phase	+ + + + +	— — —

Fig. 8.12d: Frequency Response of Plain Line-Entry (Slot)
Hybrid Journal Bearing. [E=0.19]
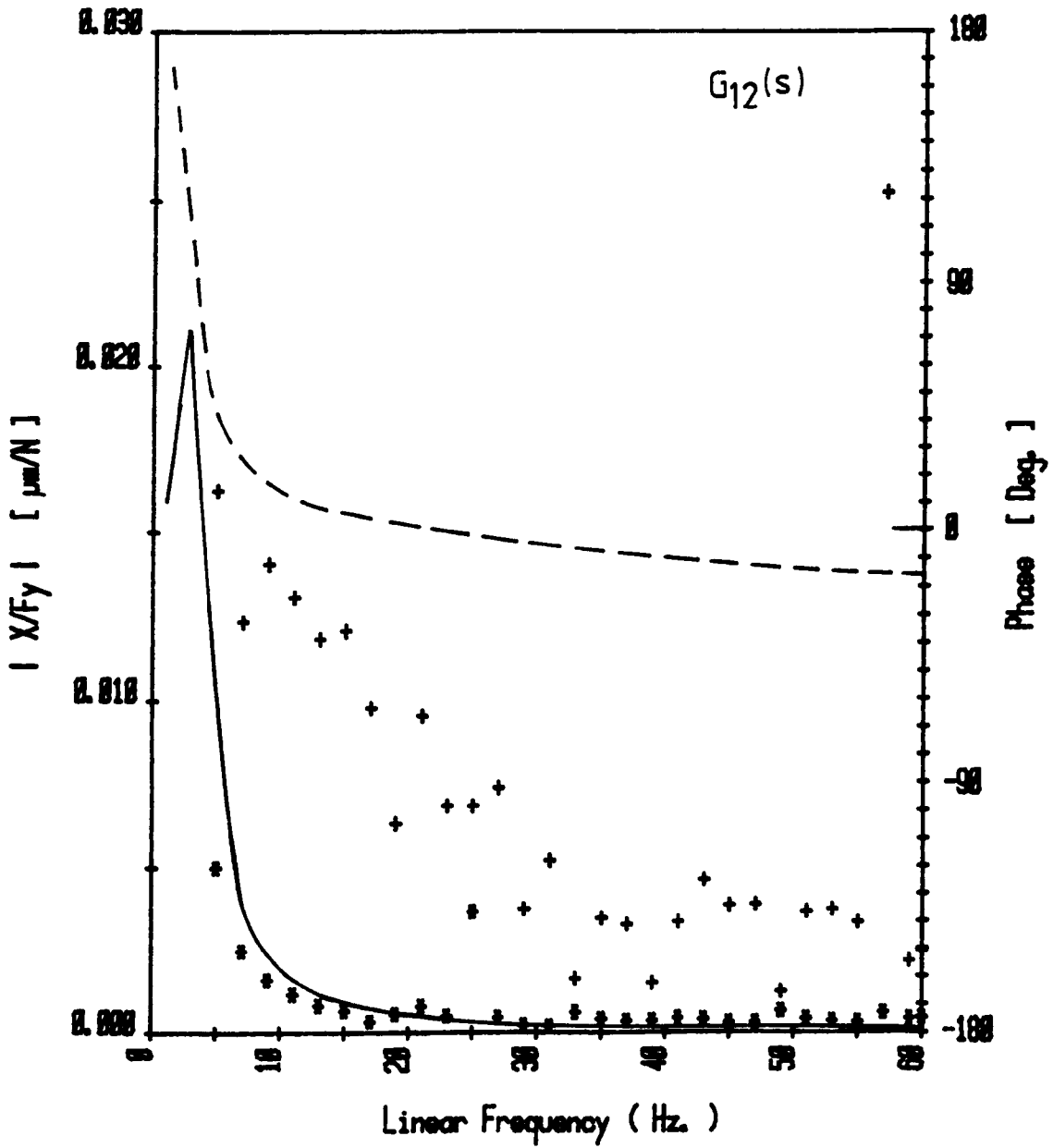
Fig. 8.13a: Frequency Response of Plain Line-Entry (Slot) Hybrid Journal Bearing. [E=0.355]
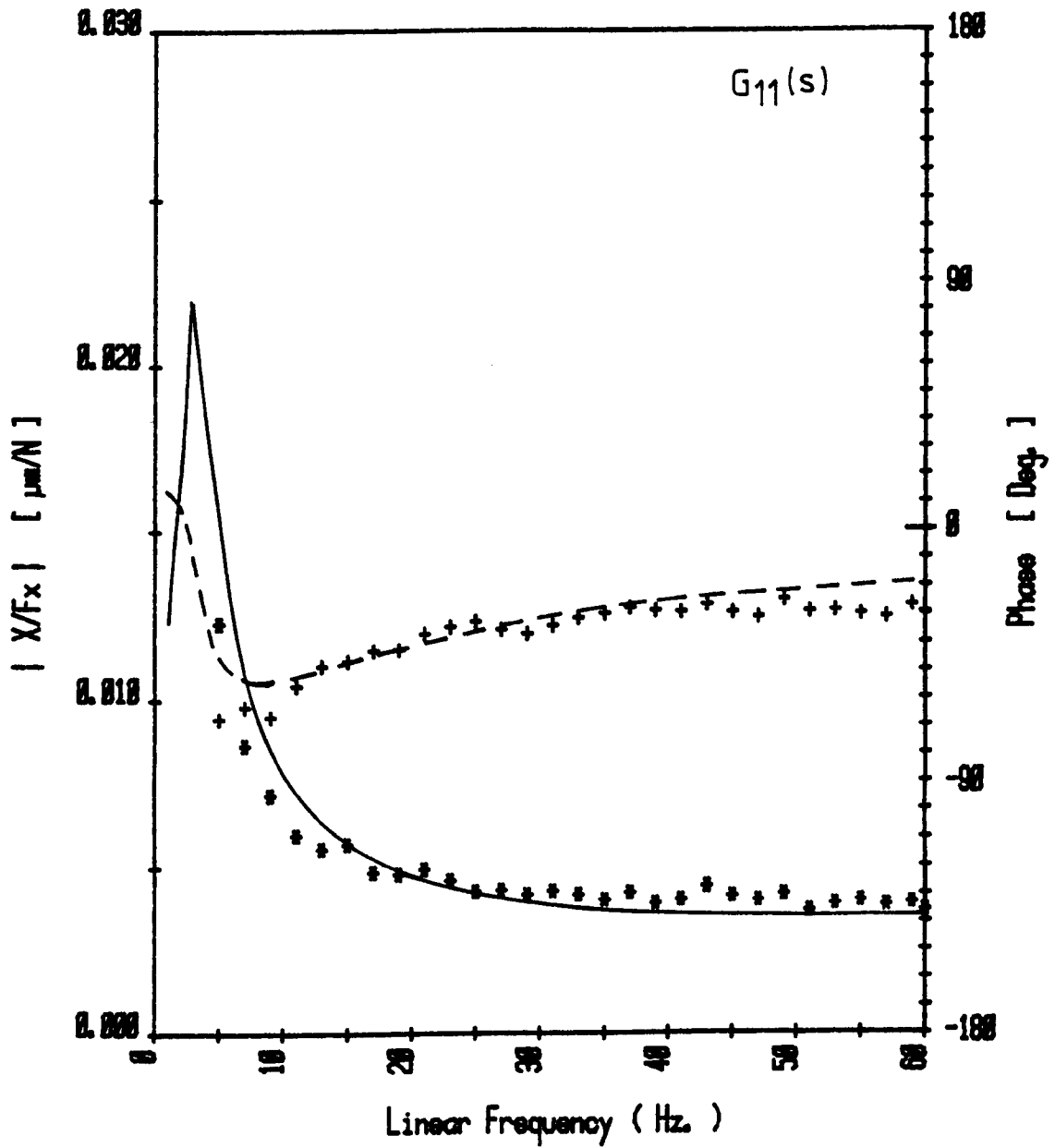
a/L = 0.25

L/D = 1.0

Sho = 0.043

K = 13.4

Beta = 0.44

Po = 689,476 KPa

Tm = 32.2°C

	Exp.	Theory
Gain	* * * * *	———
Phase	+ + + + +	— — — —

Fig. 8.13b: Frequency Response of Plain Line-Entry (Slot) Hybrid Journal Bearing. [E=0.355]
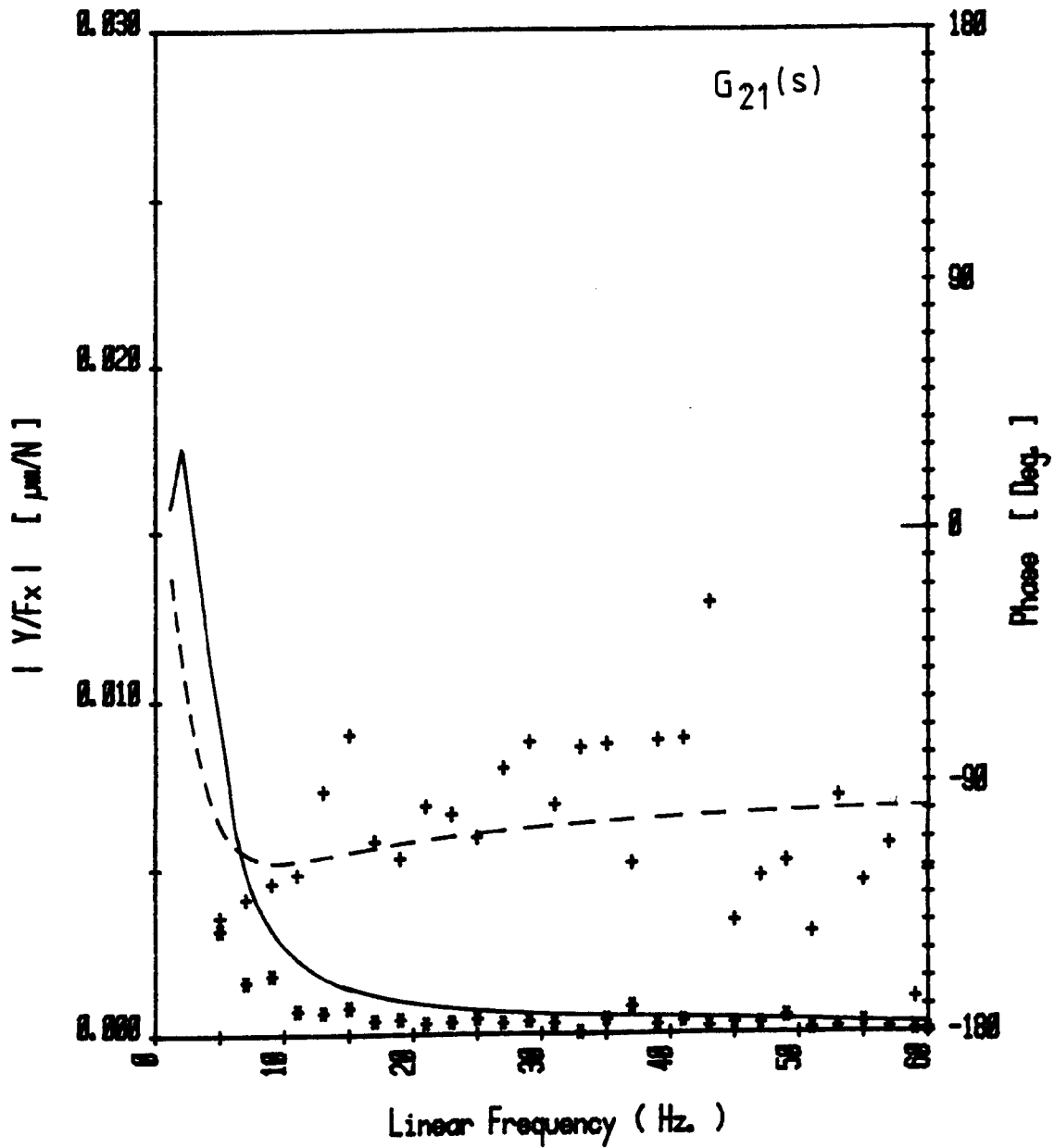
256

Fig. 8.13c: Frequency Response of Plain Line-Entry (Slot) Hybrid Journal Bearing. [E=0.355]
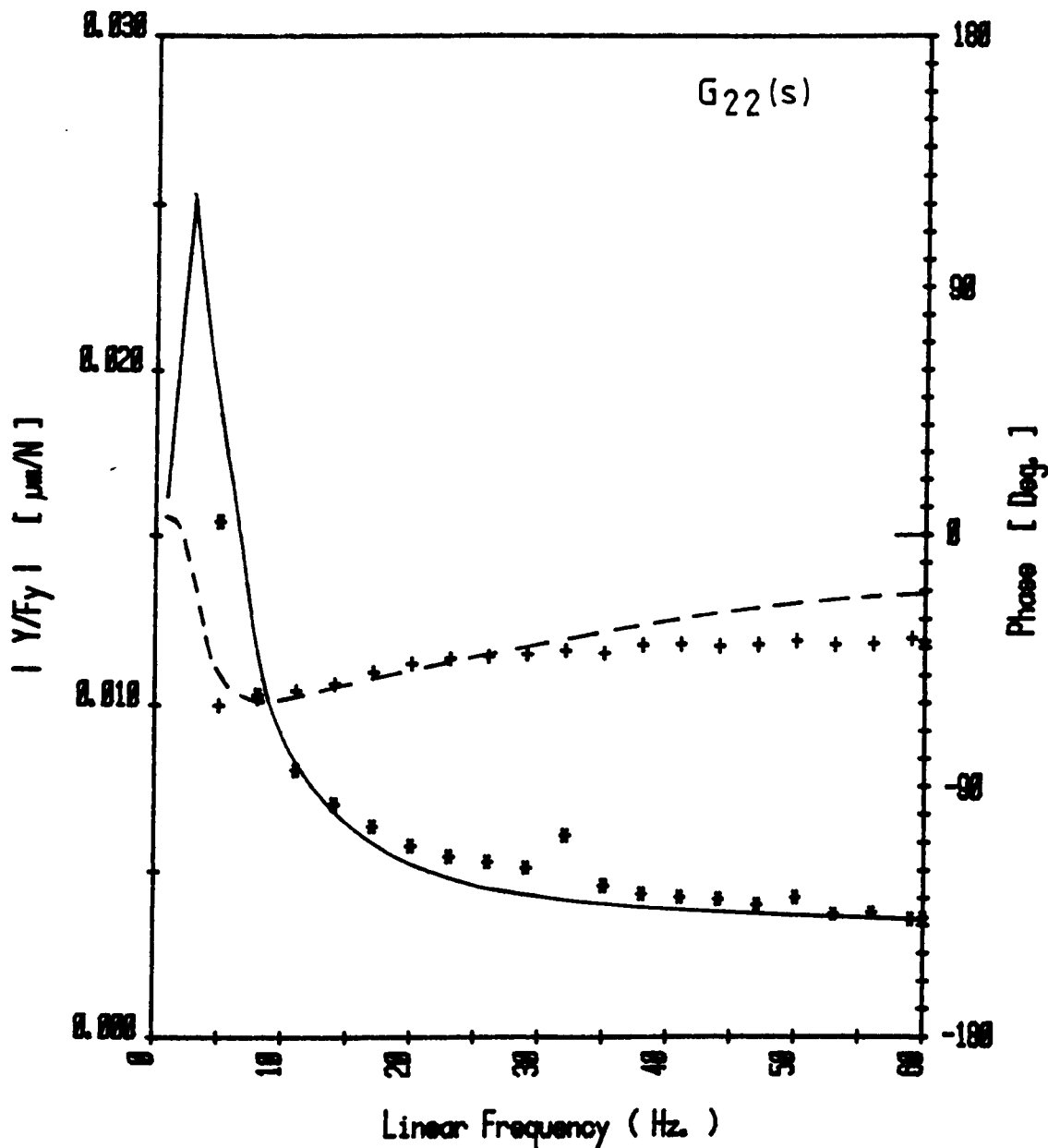
Fig. 8.13d: Frequency Response of Plain Line-Entry (Slot)
Hybrid Journal Bearing. [E=0.355]

a/L = 0.25

L/D = 1.0

Sho = 0.043

K = 13.4

Beta = 0.44

Ps = 689,476 KPa

Tm = 34°C

Fig.8.14a : Frequency Response of Plain Line-Entry (Slot) Hybrid Journal Bearing. [E=0.395]
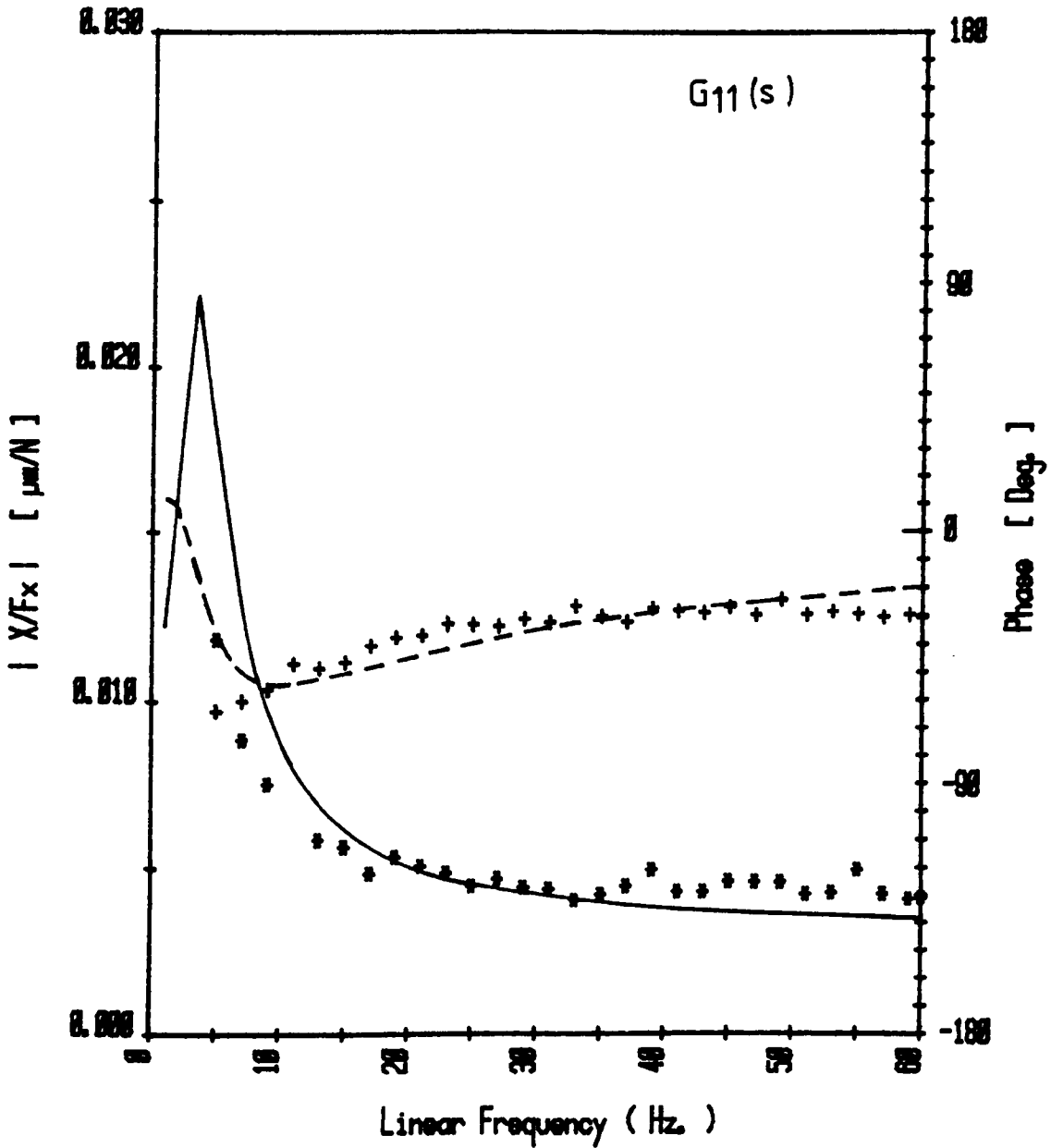
Fig. 8.14 b : Frequency Response of Plain Line-Entry (Slot)
Hybrid Journal Bearing. [E=0.395]
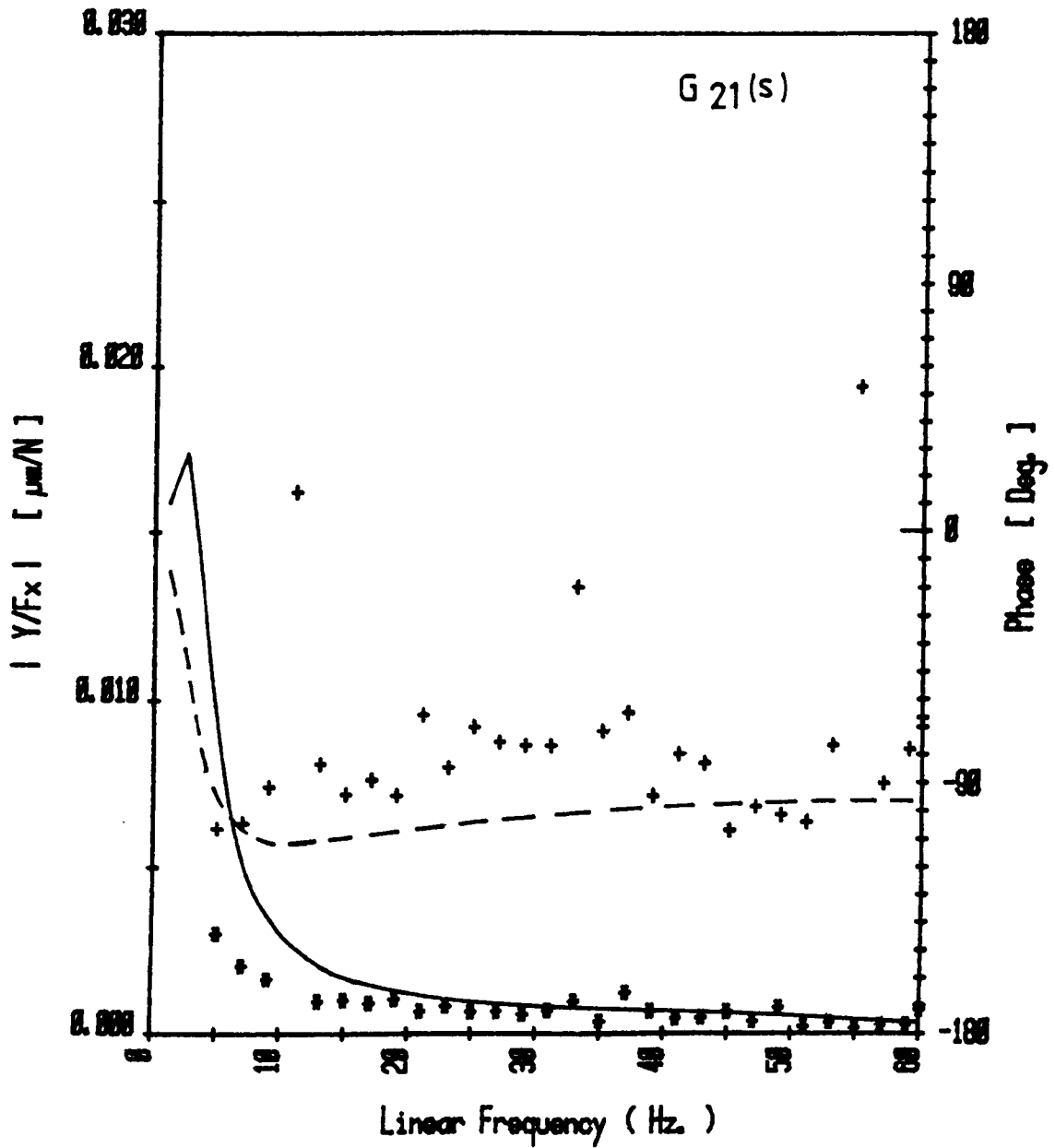
a/L = 0.25

L/D = 1.0

Sho = 0.043

K = 13.4

Beta = 0.44

Po = 689,476 KPa

Tm = 33.5°C

	Exp.	Theory
Gain	* * * * *	————
Phase	+ + + + +	— — — —

Fig. 8.14c : Frequency Response of Plain Line-Entry (Slot)
Hybrid Journal Bearing. [E=0.395]

a/L = 0.25

L/D = 1.0

Sho = 0.043

K = 13.4

Beta = 0.44

Po = 699,476 KPa

Tм = 34°C

Fig. 8.14d: Frequency Response of Plain Line-Entry (Slot) Hybrid Journal Bearing. [E=0.395]
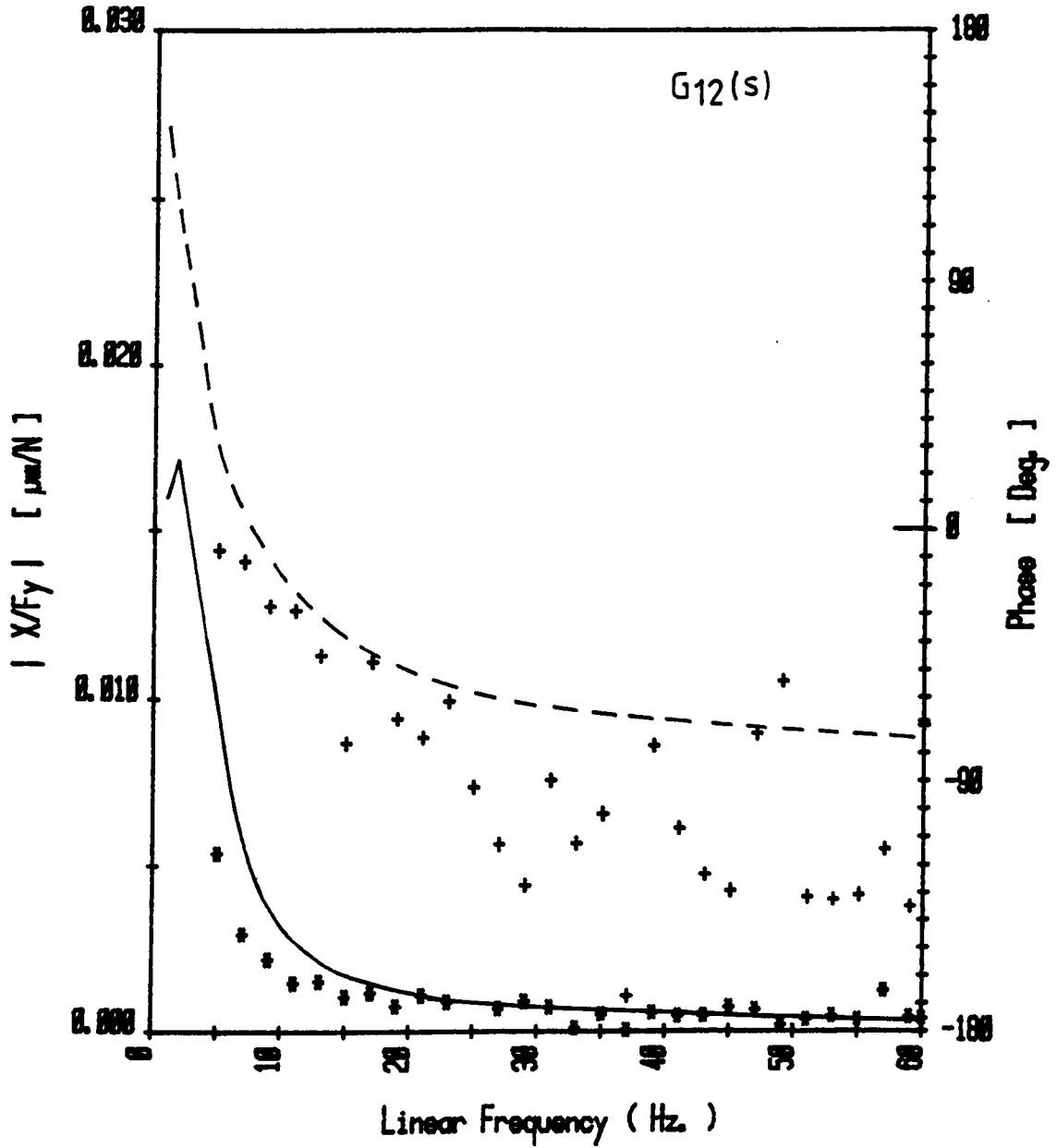
a/L = 0.25

L/D = 1.0

Sho = 0.043

K = 13.4

Beta = 0.44

Pe = 689,476 KPa

Tm = 34°C

	Exp.	Theory
Gain	* * * *	——————
Phase	+ + + + +	— — — —

Fig. 8.15a : Frequency Response of Plain Line-Entry (Slot)
Hybrid Journal Bearing. [E=0.16]
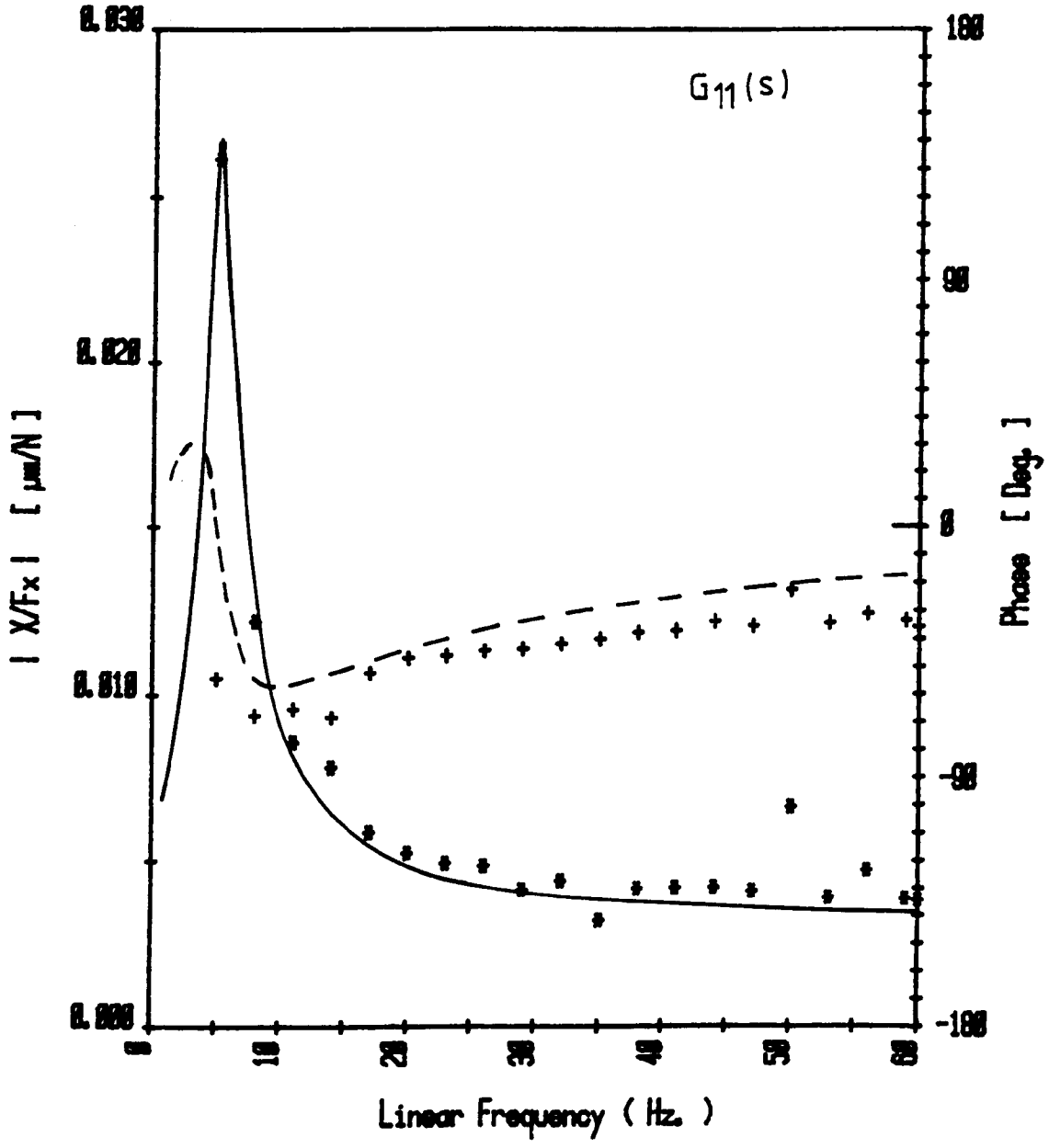
a/L = 0.25	
L/D = 1.0	
Sho = 0.043	
K = 31.0	
Beta = 0.44	
Ps = 689,476 KPa	
Ta = 35.9°C	

Exp.   Theory

Gain   * * * * *   ————

Phase   + + + + +   — — — —

Fig. 8.15b : Frequency Response of Plain Line-Entry (Slot)
          Hybrid Journal Bearing. [E=0.16]
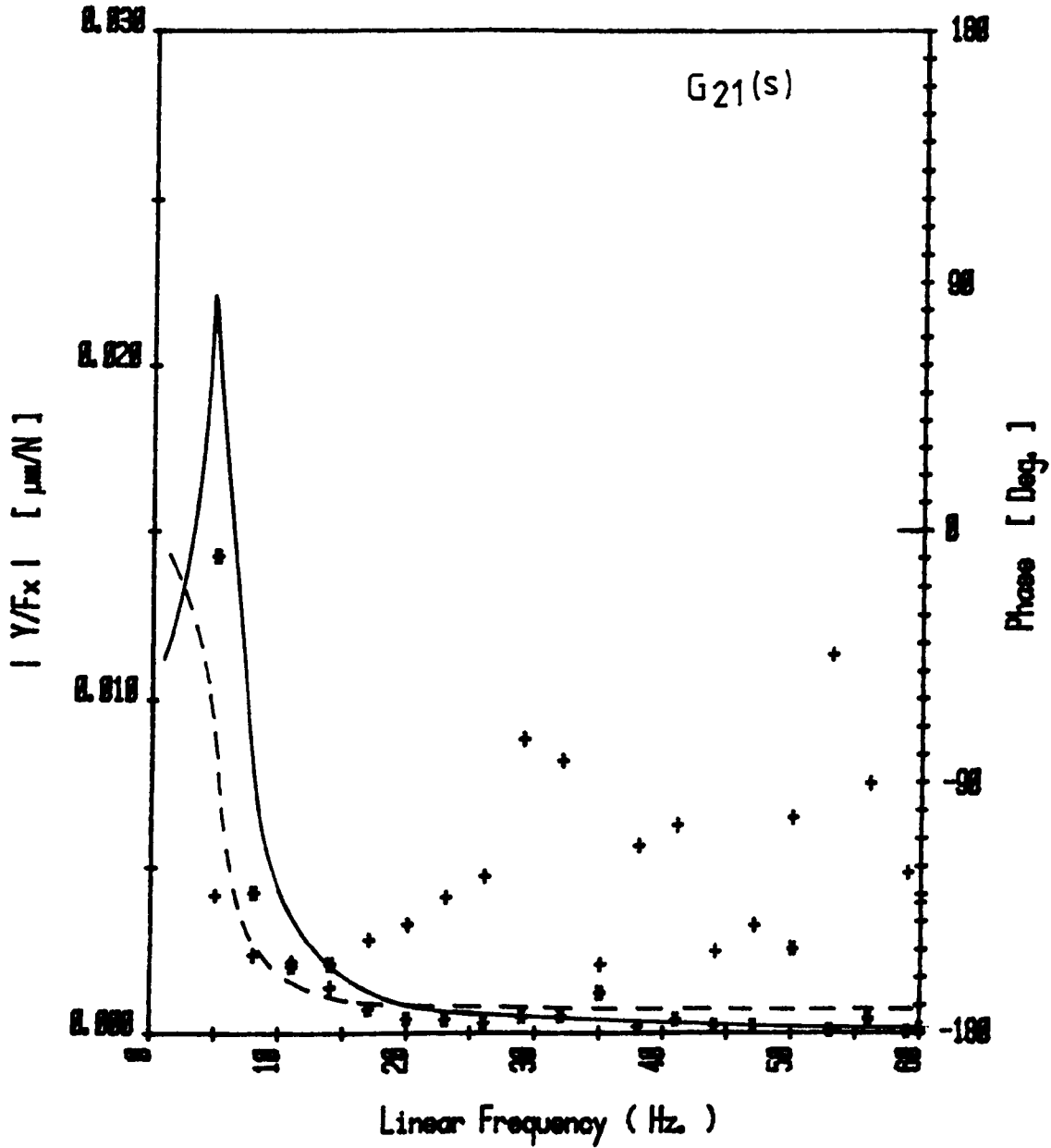
a/L = 0.25

L/D = 1.0

Sho = 0.043

K = 31.0

Beta = 0.44

Pₒ = 689,476 KPa

Tₘ = 35.9°C

	Exp.	Theory
Gain	* * * * *	———
Phase	+ + + + +	— — —

264

Fig. 8.15c : Frequency Response of Plain Line-Entry (Slot) Hybrid Journal Bearing. [E=0.16]
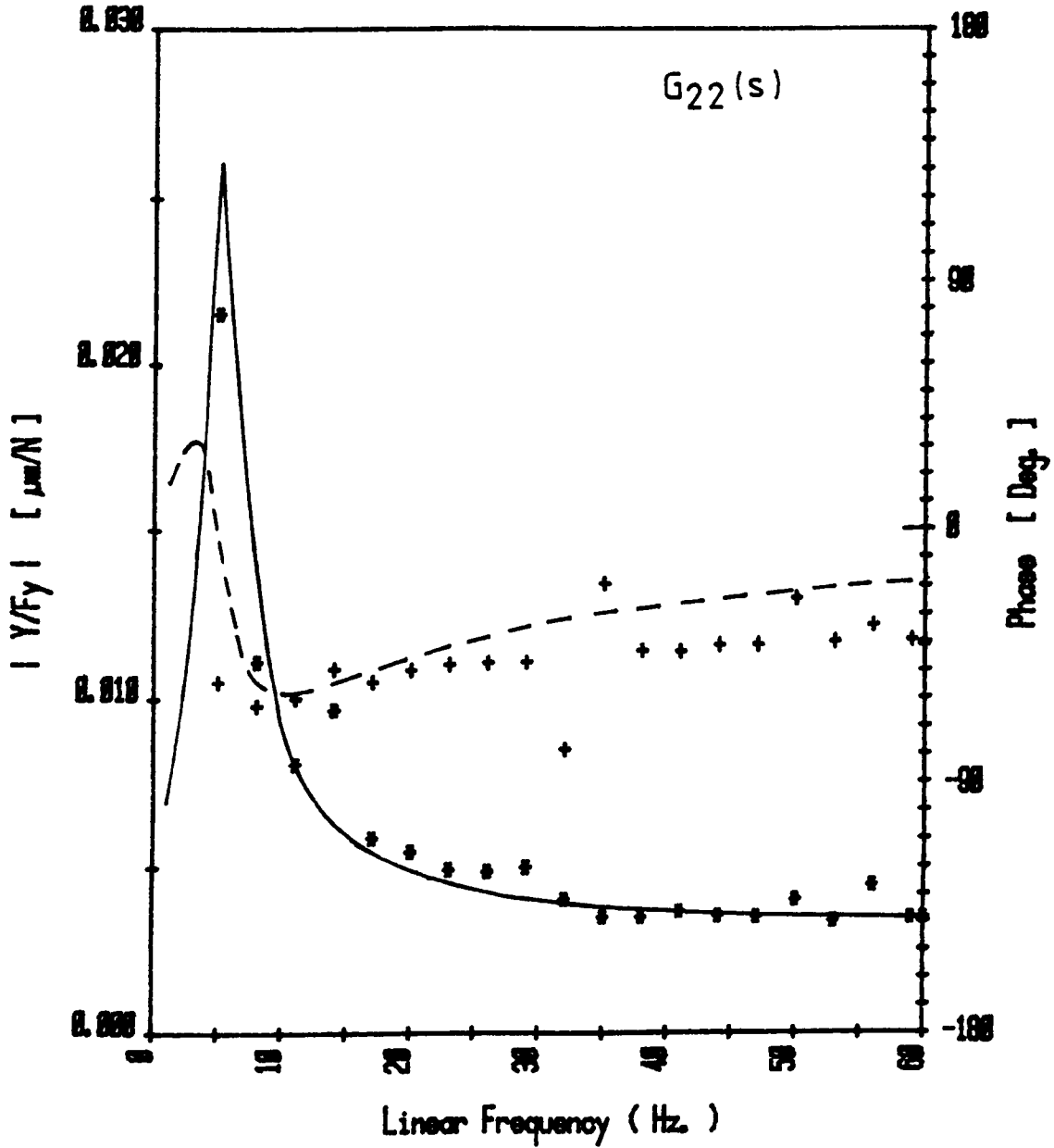
Fig. 8.15d : Frequency Response of Plain Line-Entry (Slot) Hybrid Journal Bearing. [E=0.16]

a/L = 0.25

L/D = 1.0

Sho = 0.043

K = 31.0

Beta = 0.44

Po = 689,476 KPa

Tm = 35.9 °C

	Exp.	Theory
Gain	+ + + +	———
Phase	+ + + + +	— — —
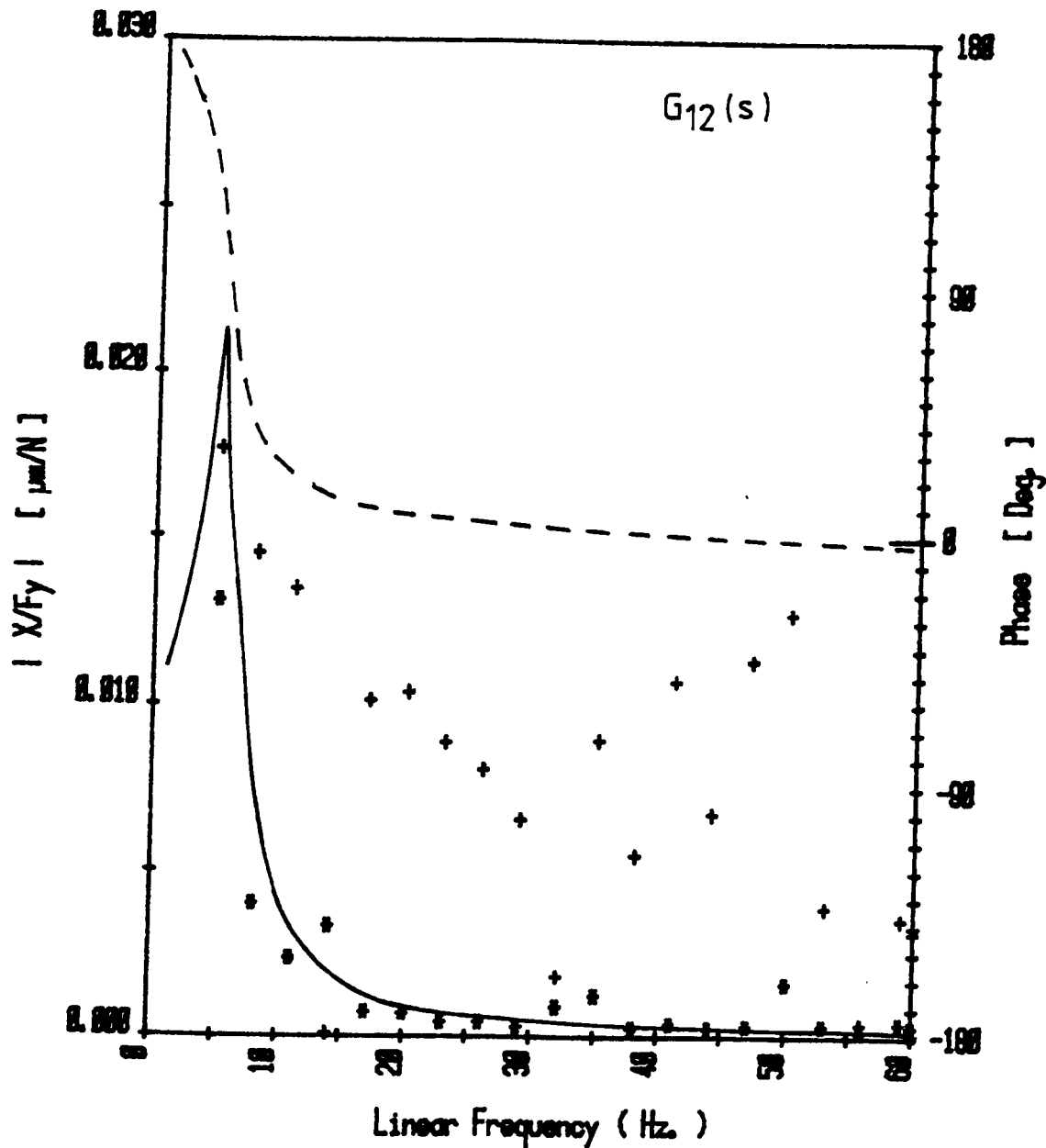
Fig. 8.16a : Frequency Response of Plain Line-Entry (Slot)
Hybrid Journal Bearing. [E=0.22]
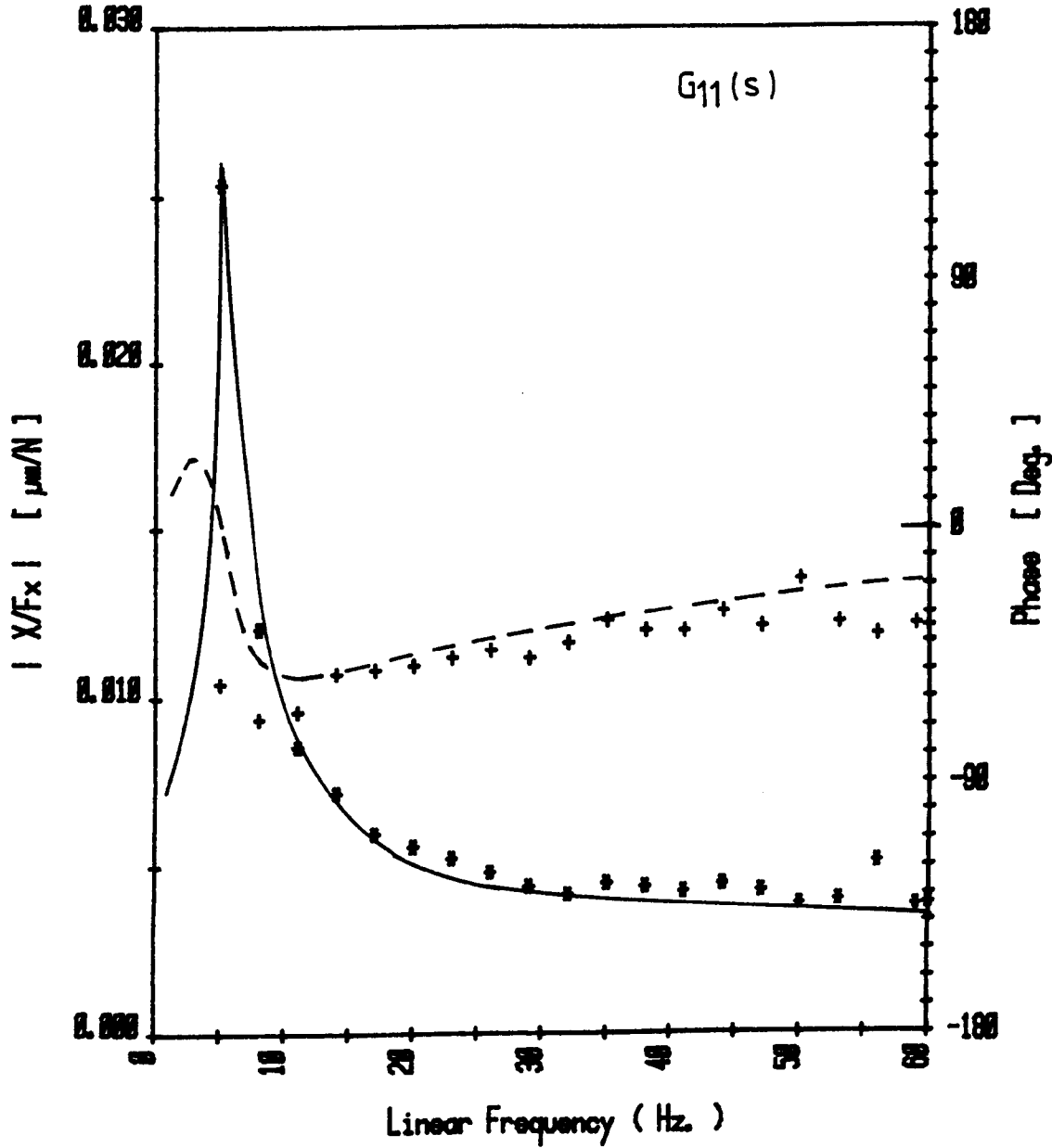
$G_{11}(s)$

a/L = 0.25

L/D = 1.0

Sho = 0.043

K = 31.0

Beta = 0.44

P_s = 689,476 KPa

T_{in} = 36.1°C

	Exp.	Theory
Gain	* * * * *	———
Phase	+ + + + +	— — —

Fig. 8.16b: Frequency Response of Plain Line-Entry (Slot)
Hybrid Journal Bearing. [E=0.22]
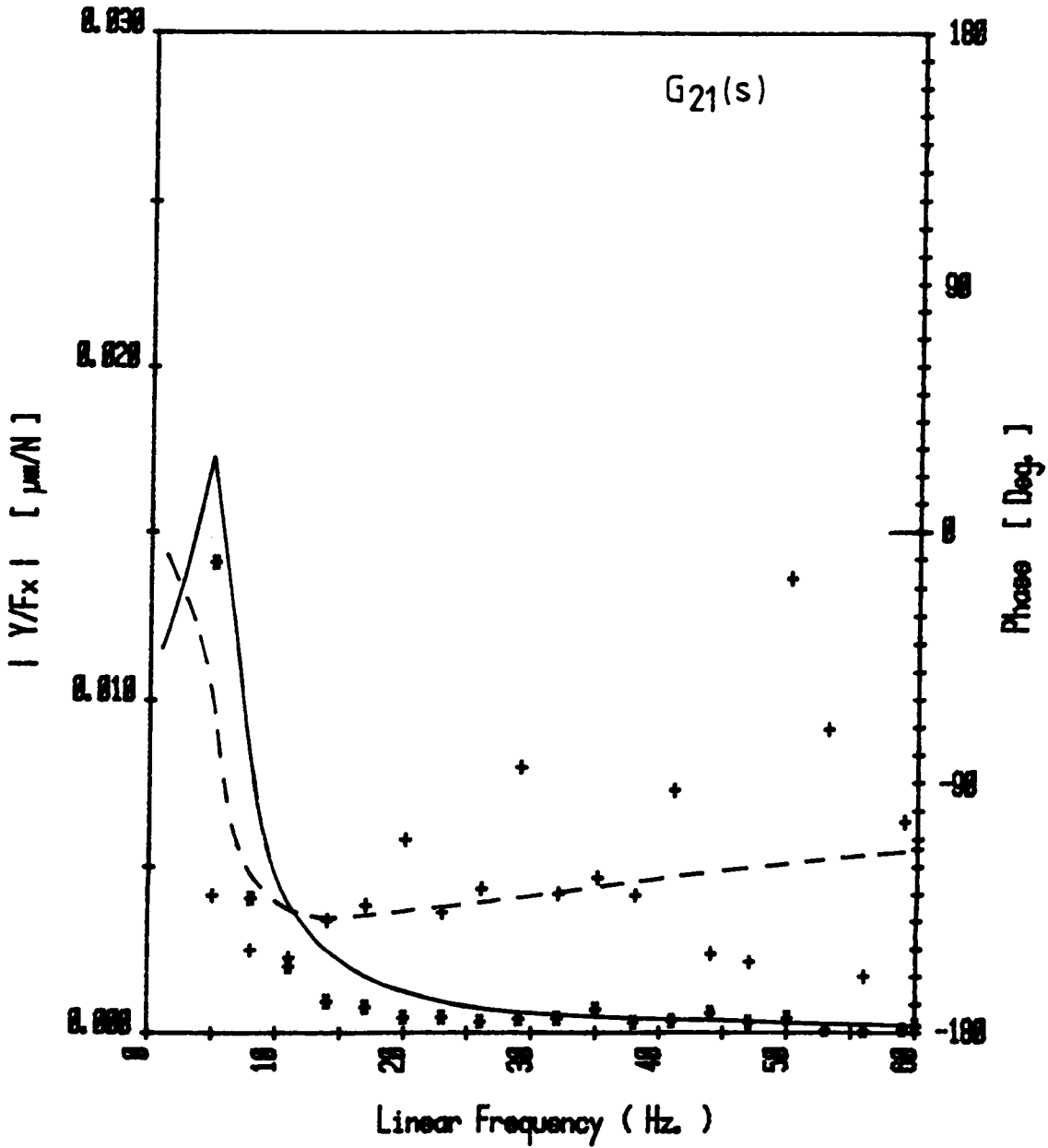
Fig. 8.16c : Frequency Response of Plain Line-Entry (Slot)
Hybrid Journal Bearing. [E=0.22]
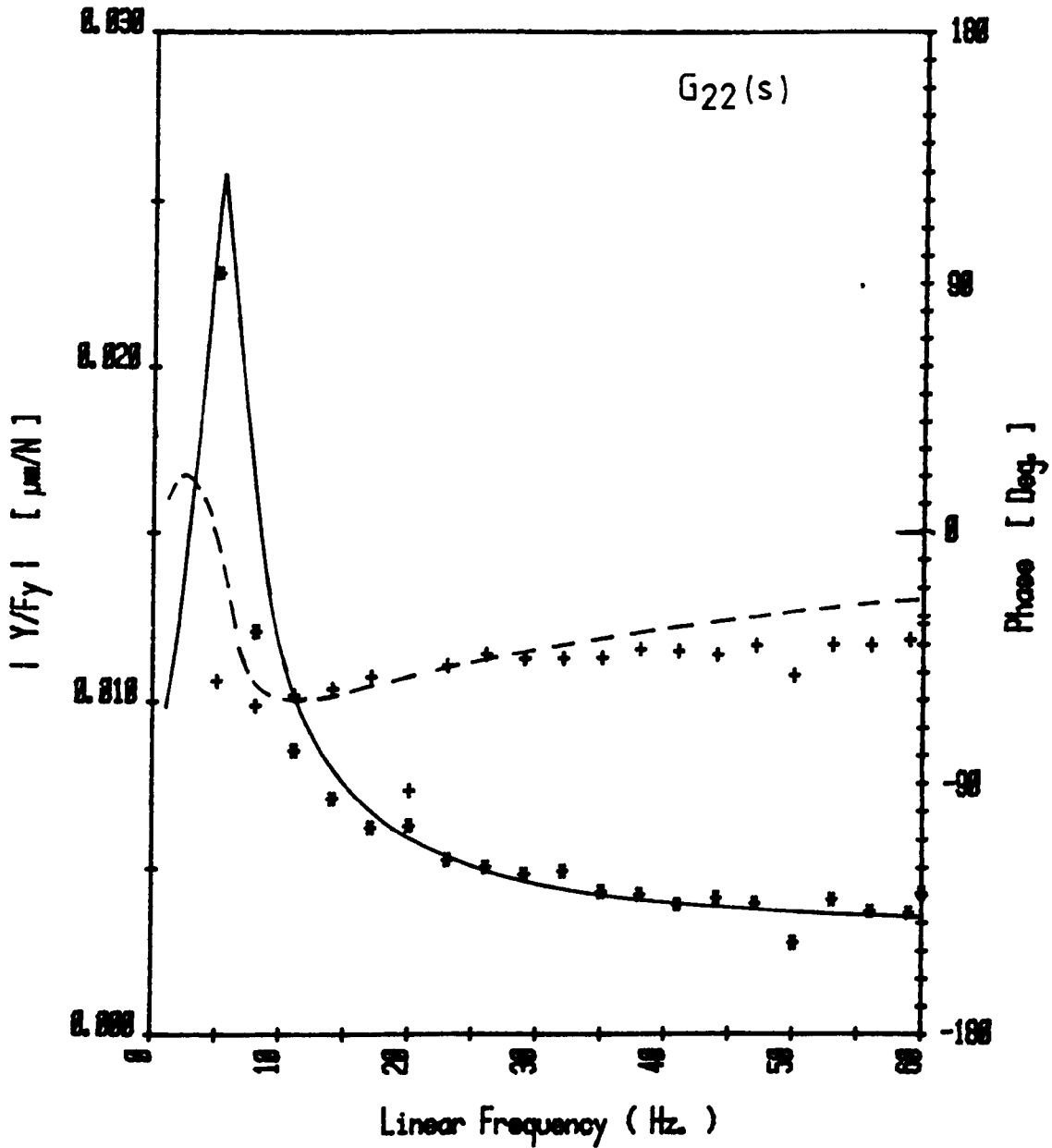
$a/L = 0.25$

$L/D = 1.0$

$Sho = 0.043$

$K = 31.0$

$Beta = 0.44$

$P_s = 689,476$ KPa

$T_m = 36.3°C$

	Exp.	Theory
Gain	* * * * *	————
Phase	+ + + + +	— — — —

Fig. 8.16d: Frequency Response of Plain Line-Entry (Slot)
Hybrid Journal Bearing. [E=0.22]

a/L = 0.25

L/D = 1.0

Sho = 0.043

K = 31.0

Beta = 0.44

Pe = 689,476 KPa

Tm = 36.3°C

	Exp.	Theory
Gain	* * * * *	————
Phase	+ + + + +	— — — —

Fig. 8.17a: Frequency Response of Plain Line-Entry (Slot)
Hybrid Journal Bearing. [E=0.29]

$G_{11}(s)$
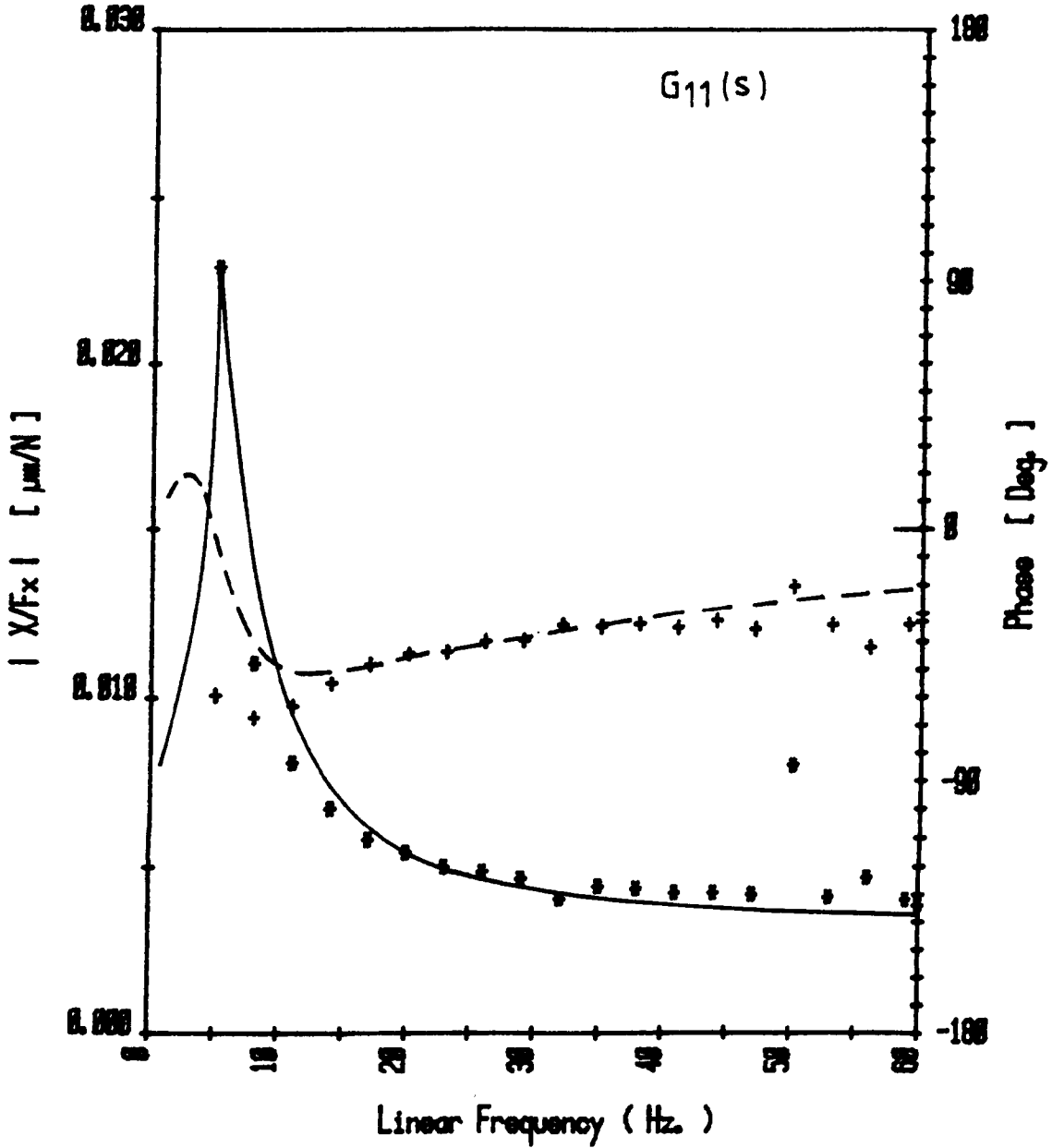
a/L = 0.25		Exp.	Theory
L/D = 1.0			
Sho = 0.043	Gain	* * * * *	————
K = 31.0			
Beta = 0.44	Phase	+ + + + +	— — — — —
Pe = 689,476 KPa			
Tm = 36.1°C			

Fig. 8.17b : Frequency Response of Plain Line-Entry (Slot) Hybrid Journal Bearing. [E=0.29]
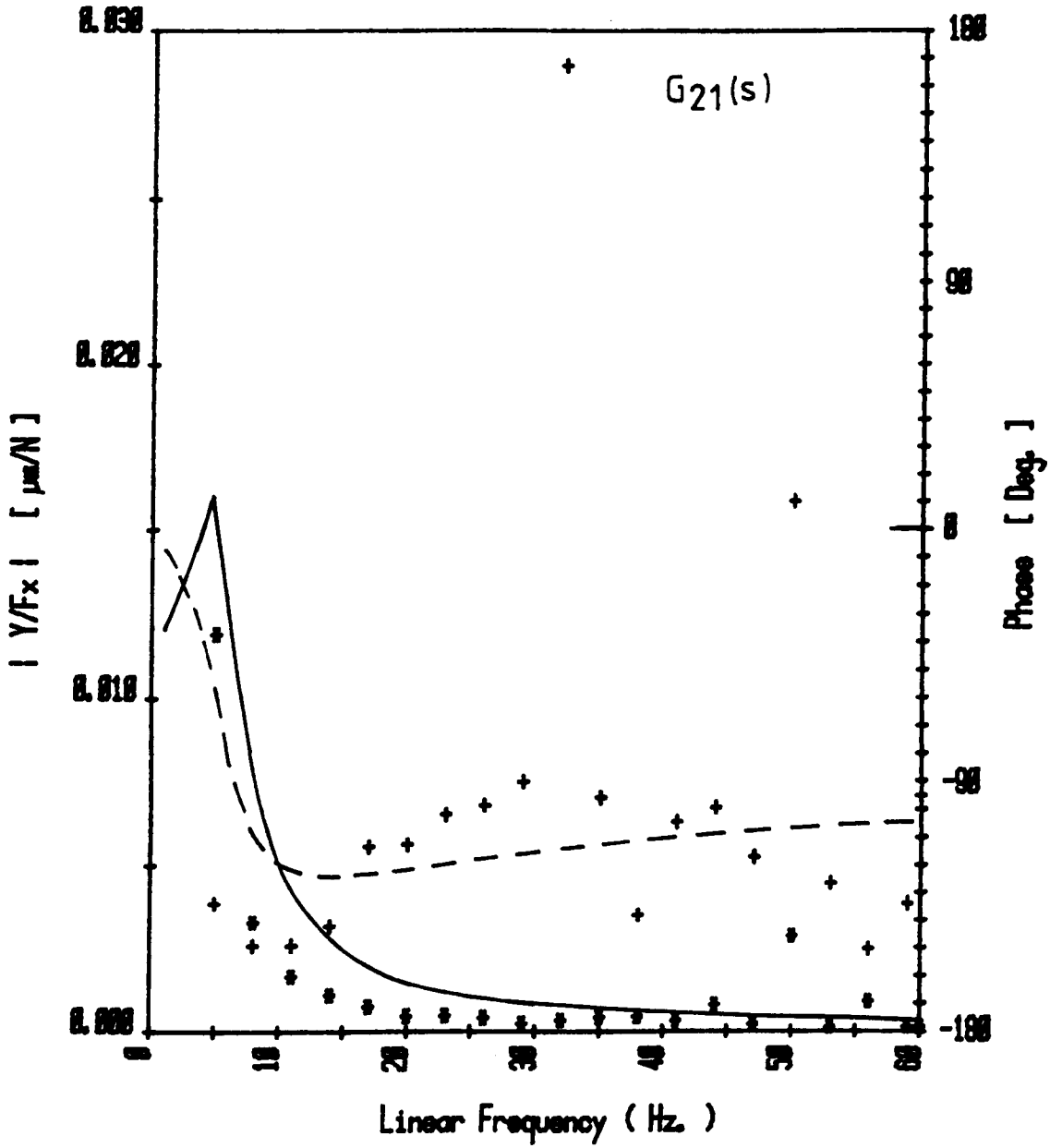
a/L = 0.25

L/D = 1.0

Sho = 0.043

K = 31.0

Beta = 0.44

Ps = 689,476 KPa

Tm = 36.1 °C

	Exp.	Theory
Gain	* * * *	———
Phase	+ + + +	— — — —

Fig. 8.17c : Frequency Response of Plain Line-Entry (Slot)
Hybrid Journal Bearing. [E=0.29]
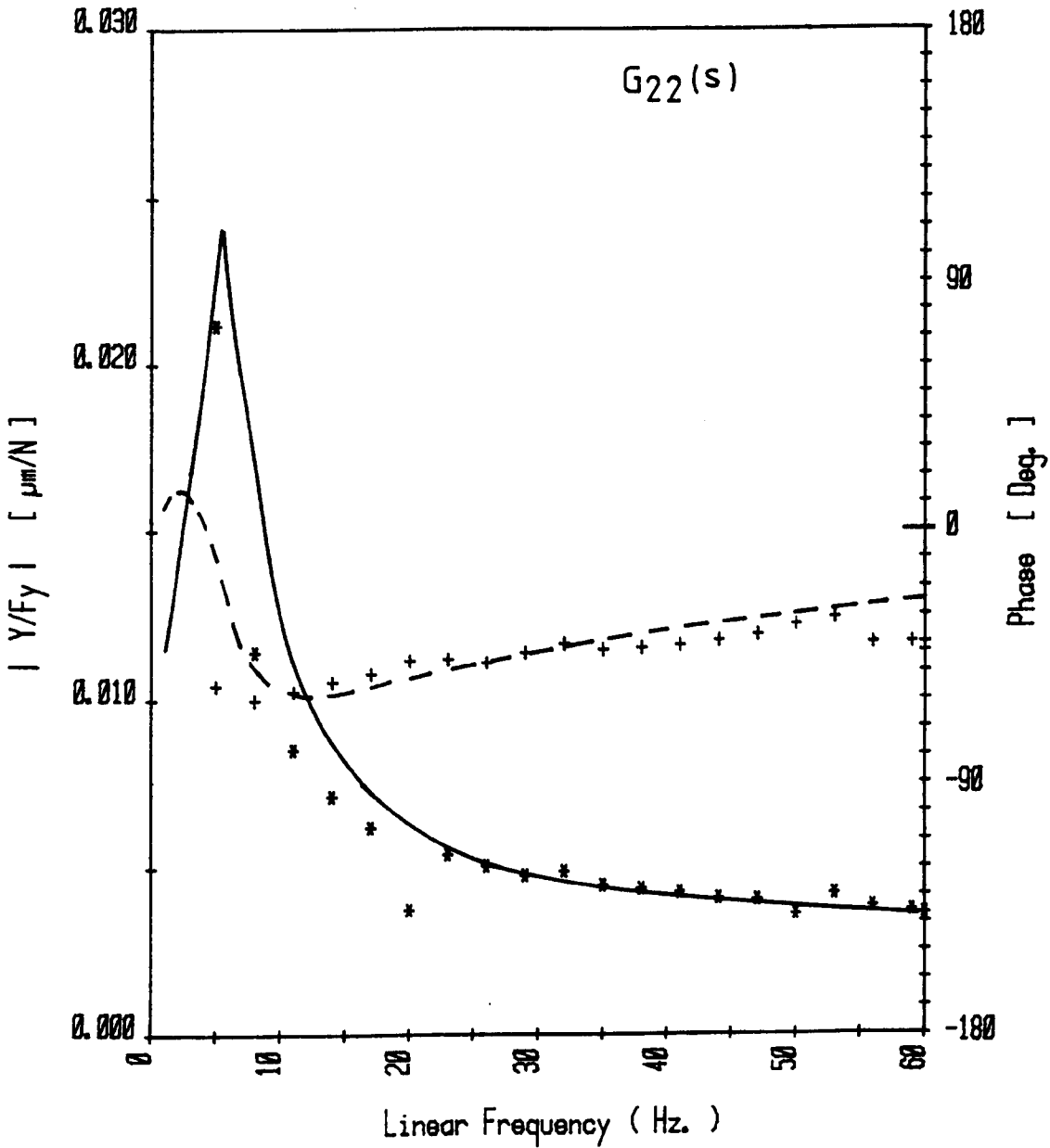
a/L = 0.25

L/D = 1.0

Sho = 0.043

K = 31.0

Beta = 0.44

Ps = 689,476 KPa

Tm. = 36.1°C

Fig. 8·17d: Frequency Response of Plain Line-Entry (Slot)
Hybrid Journal Bearing. [E=0.29]
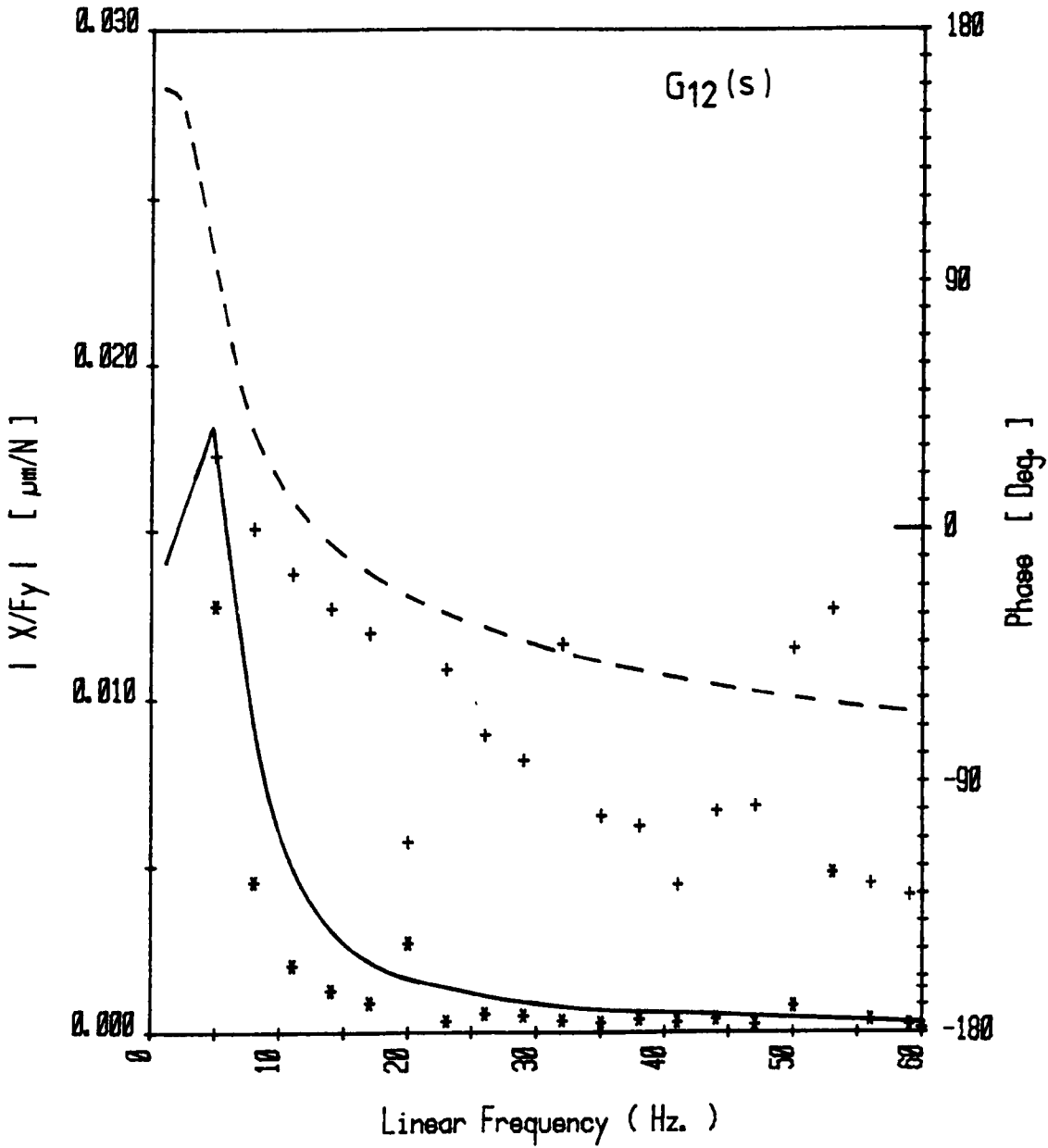
$G_{12}(s)$

a/L = 0.25

L/D = 1.0

Sho = 0.043

K = 31.0

Beta = 0.44

Ps = 689,476 KPa

Tm. = 36.1 °C

	Exp.	Theory
Gain	* * * * *	———
Phase	+ + + + +	— — — —

Fig. 8.18a:Graph Comparing Theoretical And Experimental Direct Stiffness Coeffs. (K = 0.0)

a_{11}
(N/μm)

Theory

• • • Exp.(Dyn.)

o o o Exp.(Static)

ϵ

$a/L = 0.25$ $S_{ho} = 0.043$

$L/D = 1.0$ $P_s = 689.48$ KPa.

$\beta = 0.44$
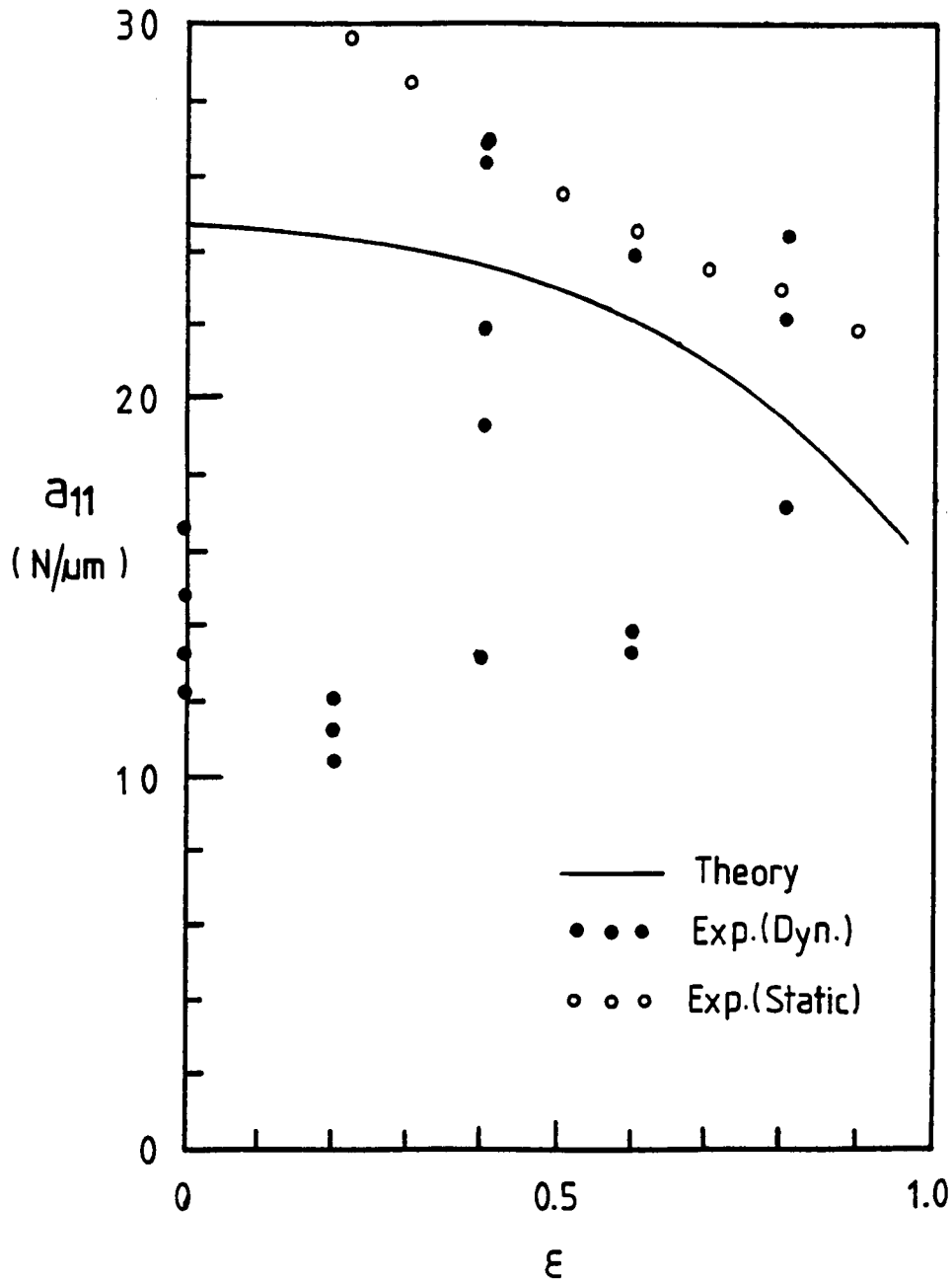
Fig.8.18b:Graph Comparing Theoretical And Experimental
Direct Stiffness Coeffs. (K = 0.0)

a_{22}

$(N/\mu m)$

100

50

0

0   0.5   1.0

ε

$a/L = 0.25$ $Sh_o = 0.043$

$L/D = 1.0$ $P_s = 689.48 KPa.$

$\beta = 0.44$

Legend:
— Theory
• • • Exp.(Dyn.)
∘ ∘ ∘ Exp.(Static)
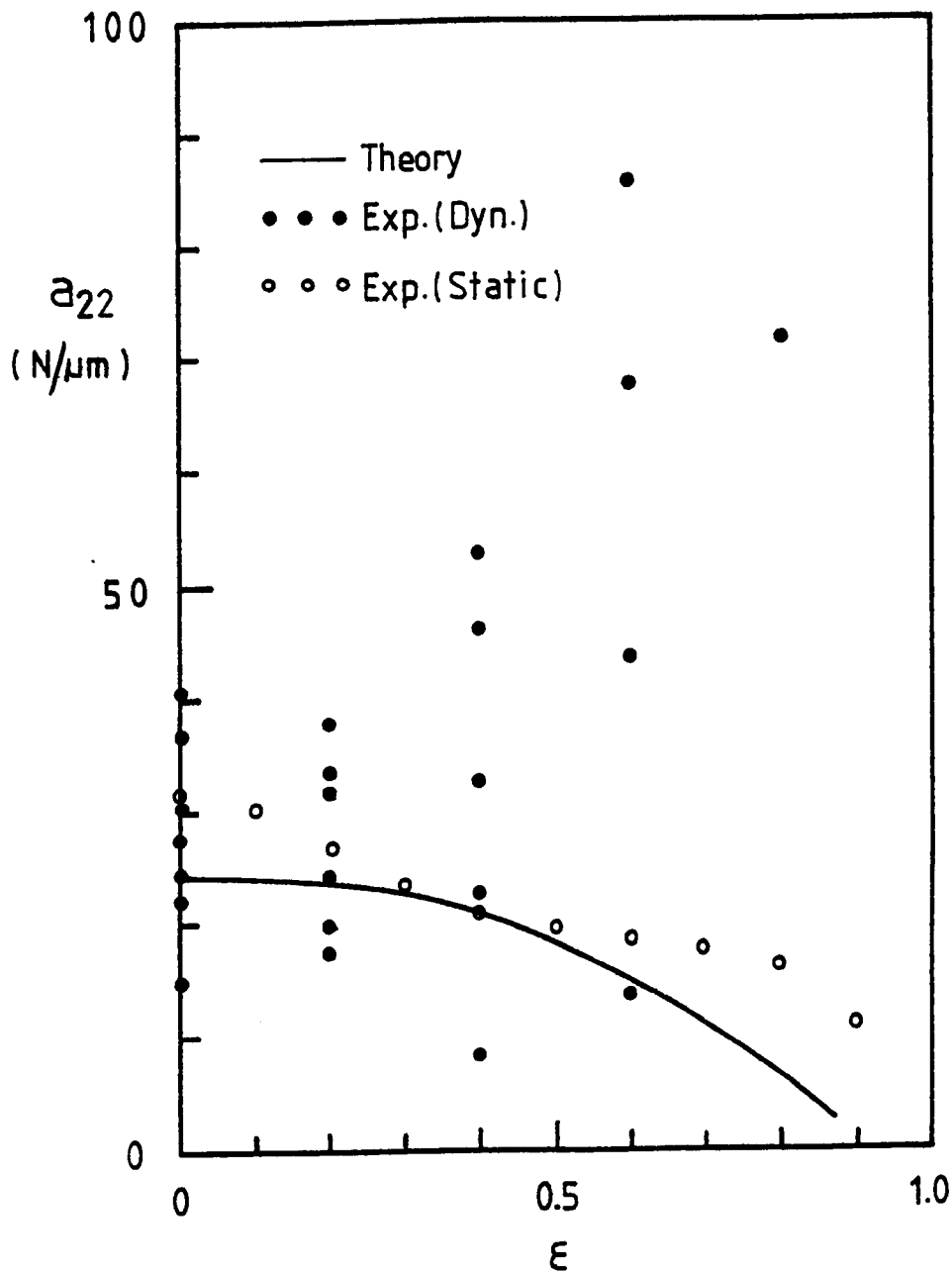
Fig.8.18c : Graph Comparing Theoretical And Experimental
Direct Damping Coeffs. (K = 0.0)

$a/L = 0.25$ $S_{ho} = 0.043$

$L/D = 1.0$ $P_s = 689.48$ KPa.

$\beta = 0.44$
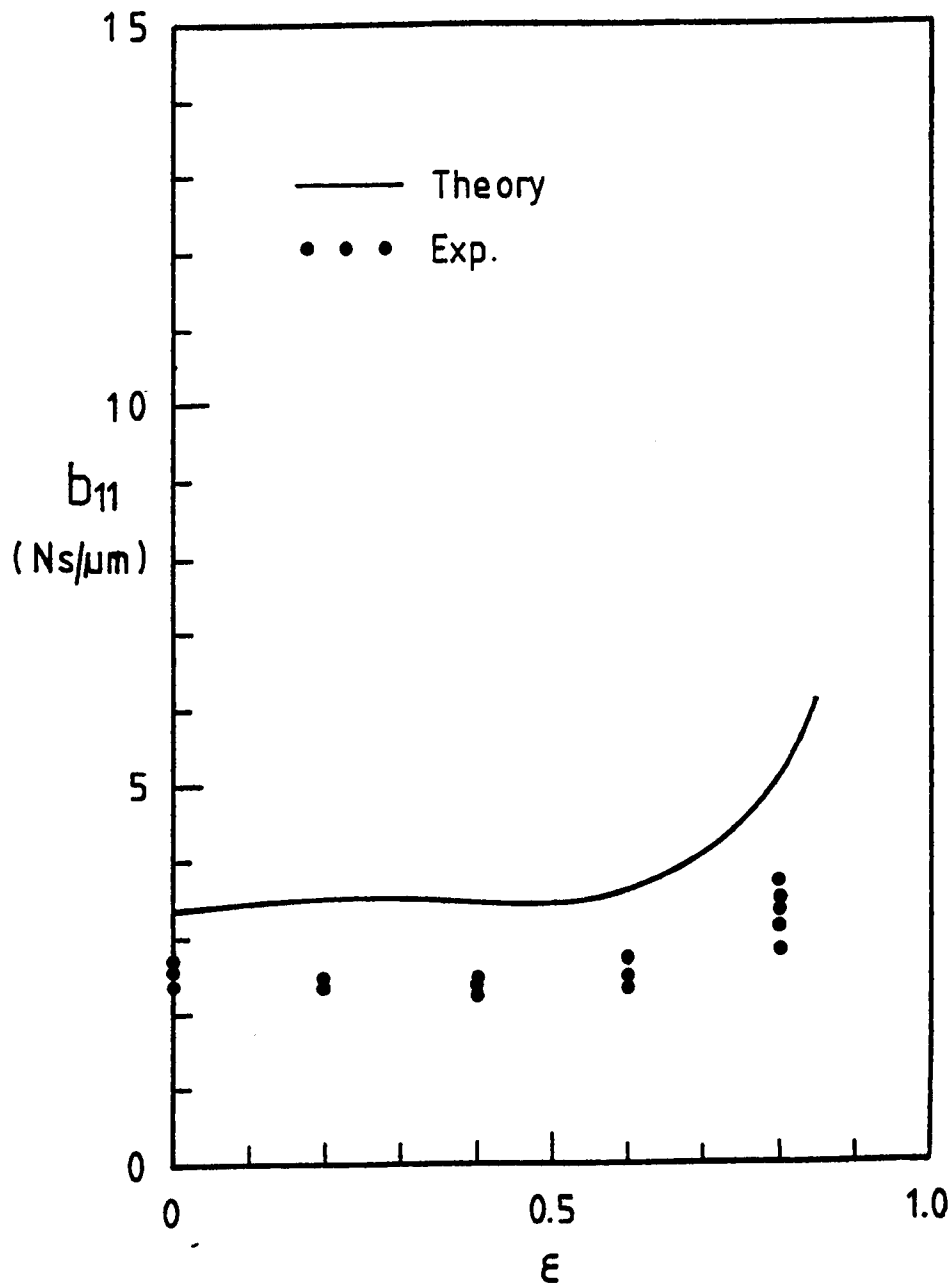
Fig.8.18d : Graph Comparing Theoretical And Experimental Direct Damping Coeffs. (K = 0.0)
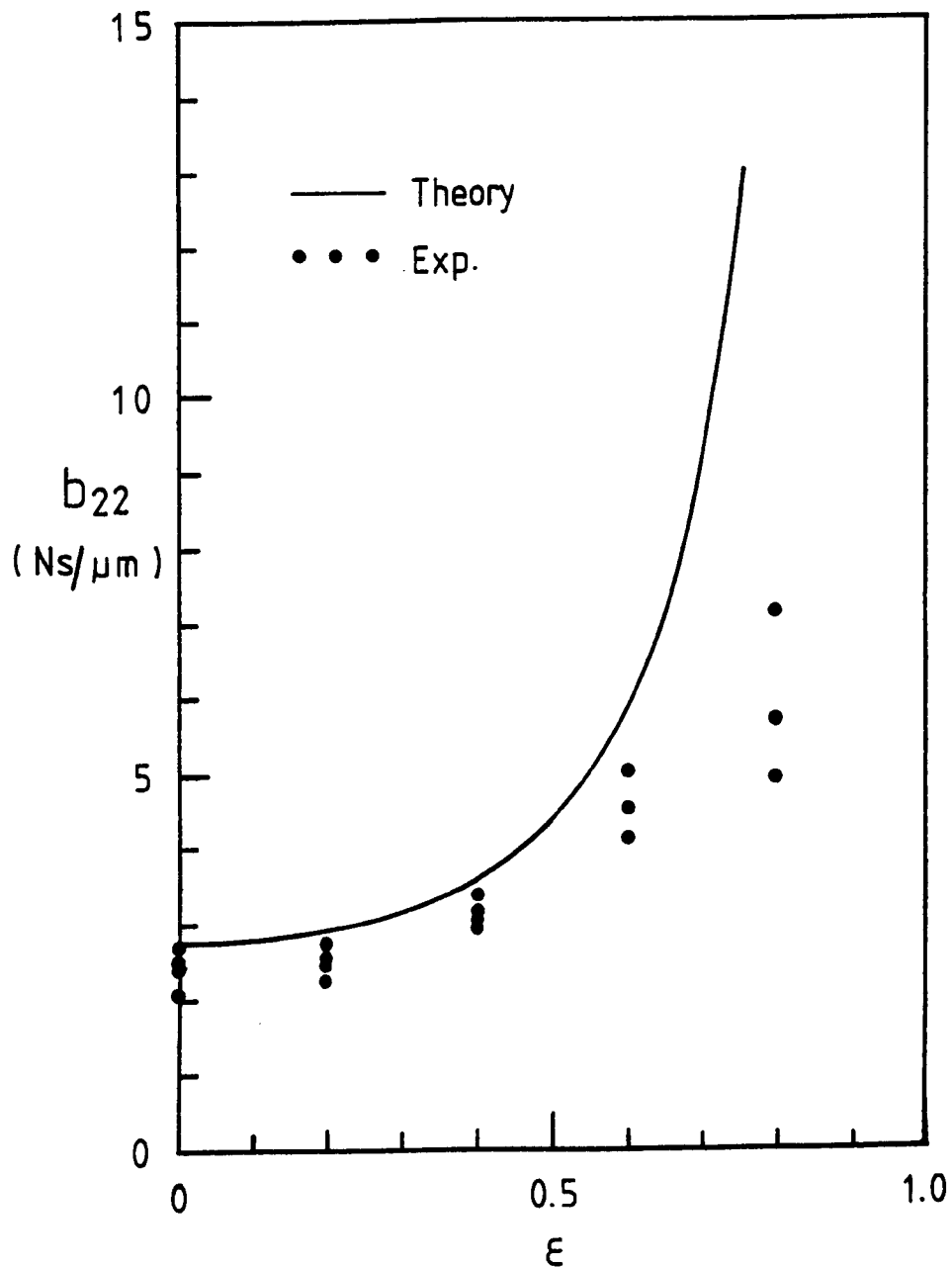
$a/L = 0.25$ $S_{ho} = 0.043$

$L/D = 1.0$ $P_s = 689.48$ KPa.

$\beta = 0.44$

Fig.8.19a:Graph   Comparing   Theoretical   And   Experimental
Direct   Stiffness   Coeffs. (K = 31.0)
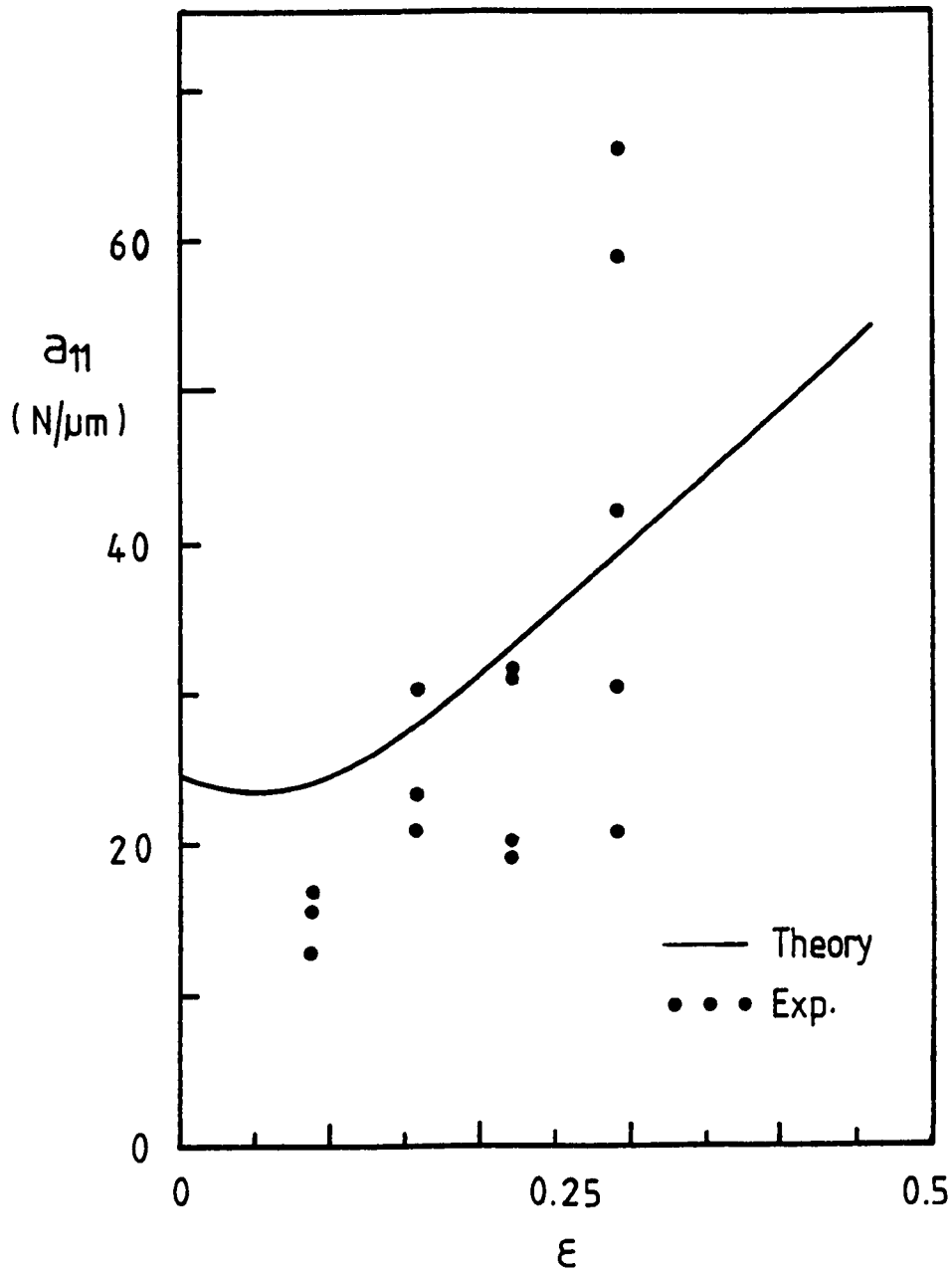
a/L = 0.25 S_{ho} = 0.043

L/D = 1.0 P_s = 689.48 KPa.

β = 0.44

Fig.8.19b:Graph Comparing Theoretical And Experimental X-Coupled Stiffness Coeffs. (K = 31.0)
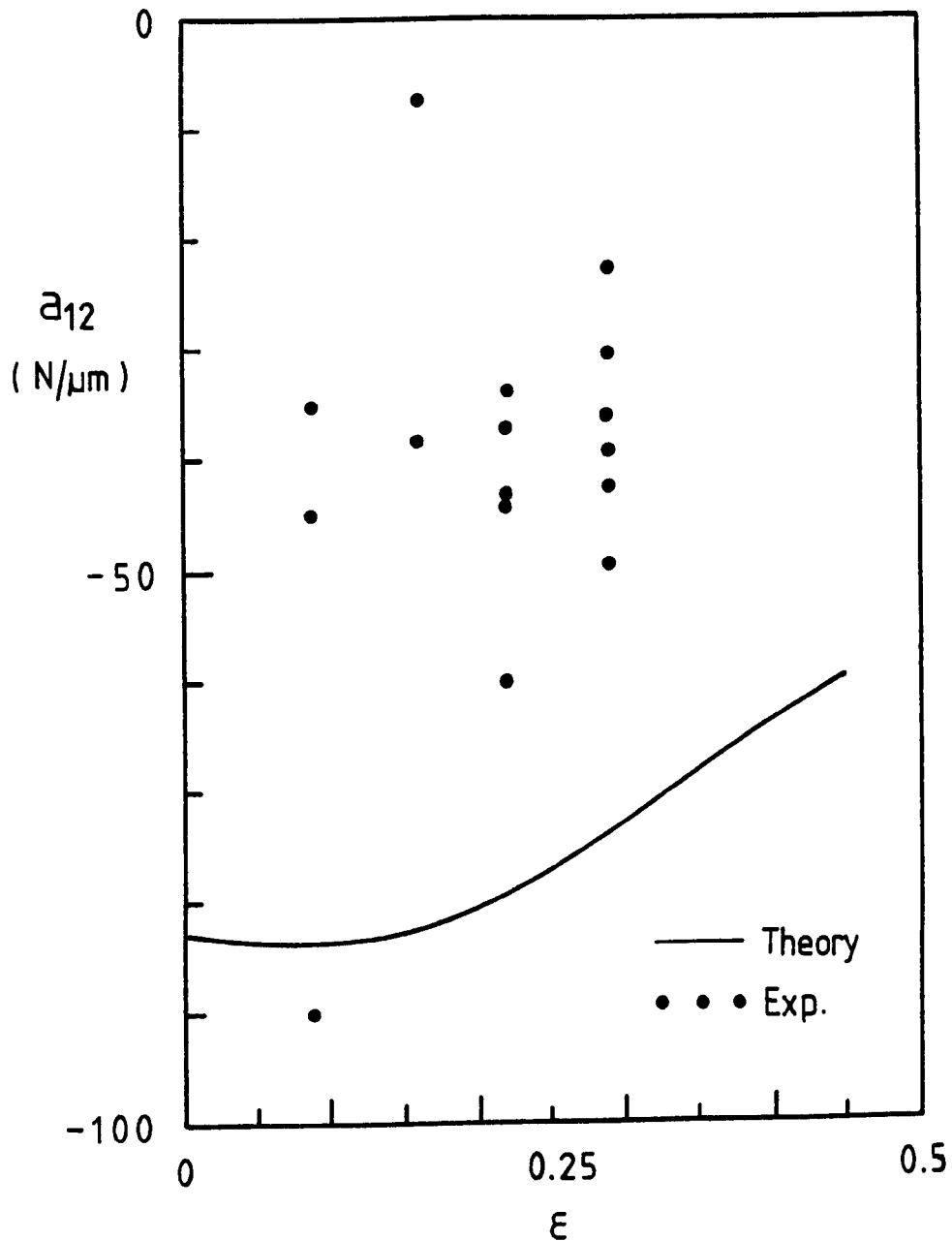
a/L = 0.25 S_{ho} = 0.043

L/D = 1.0 P_s = 689.48 KPa.

β = 0.44

Fig. 8.19c : Graph Comparing Theoretical And Experimental
X-Coupled Stiffness Coeffs. (K = 31.0)
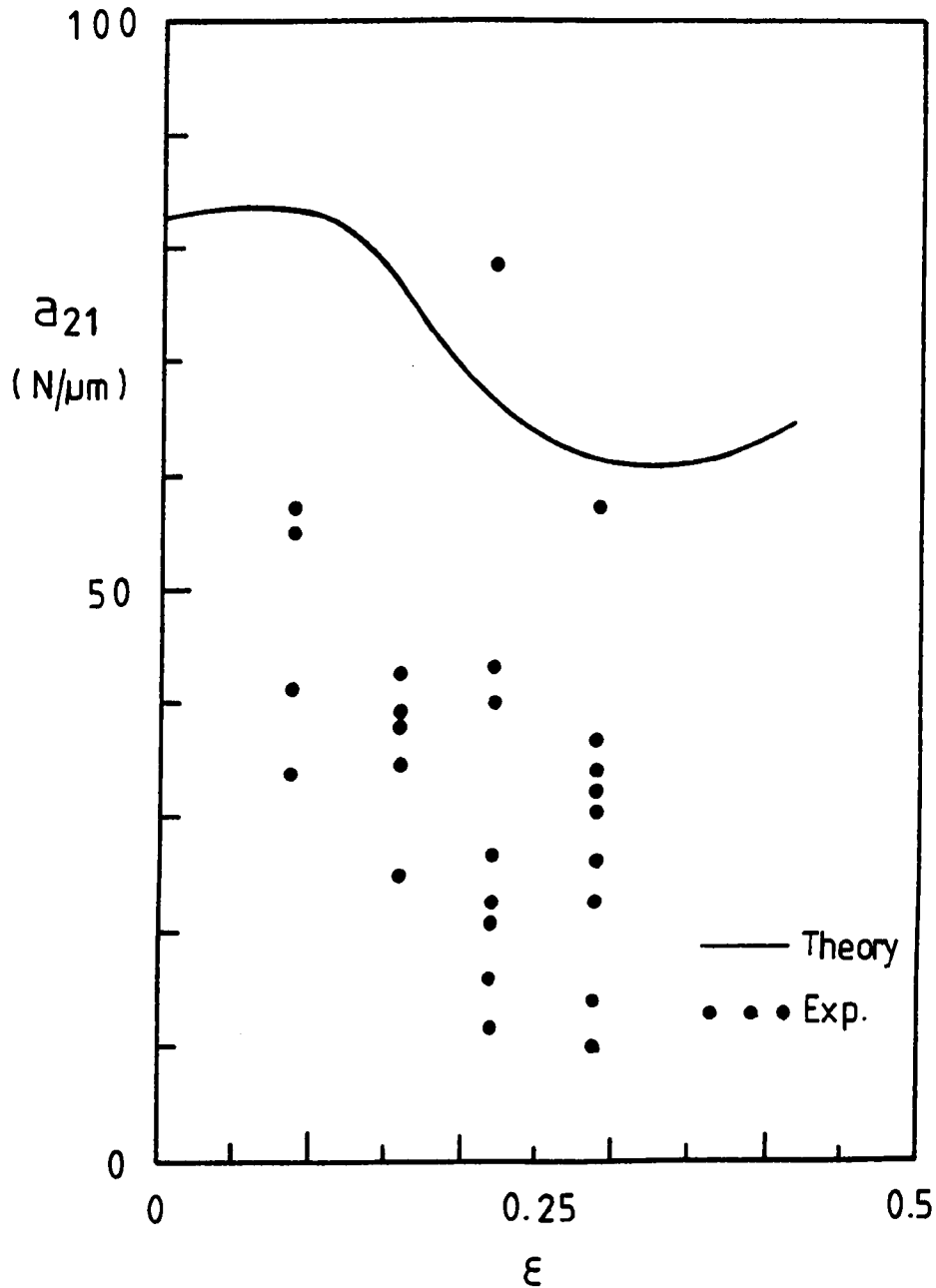
$a/L = 0.25$ $S_{ho} = 0.043$

$L/D = 1.0$ $F_s = 689.48$ KPa.

$\beta = 0.44$

Fig.8.19d: Graph Comparing Theoretical And Experimental Direct Stiffness Coeffs. (K = 31.0)
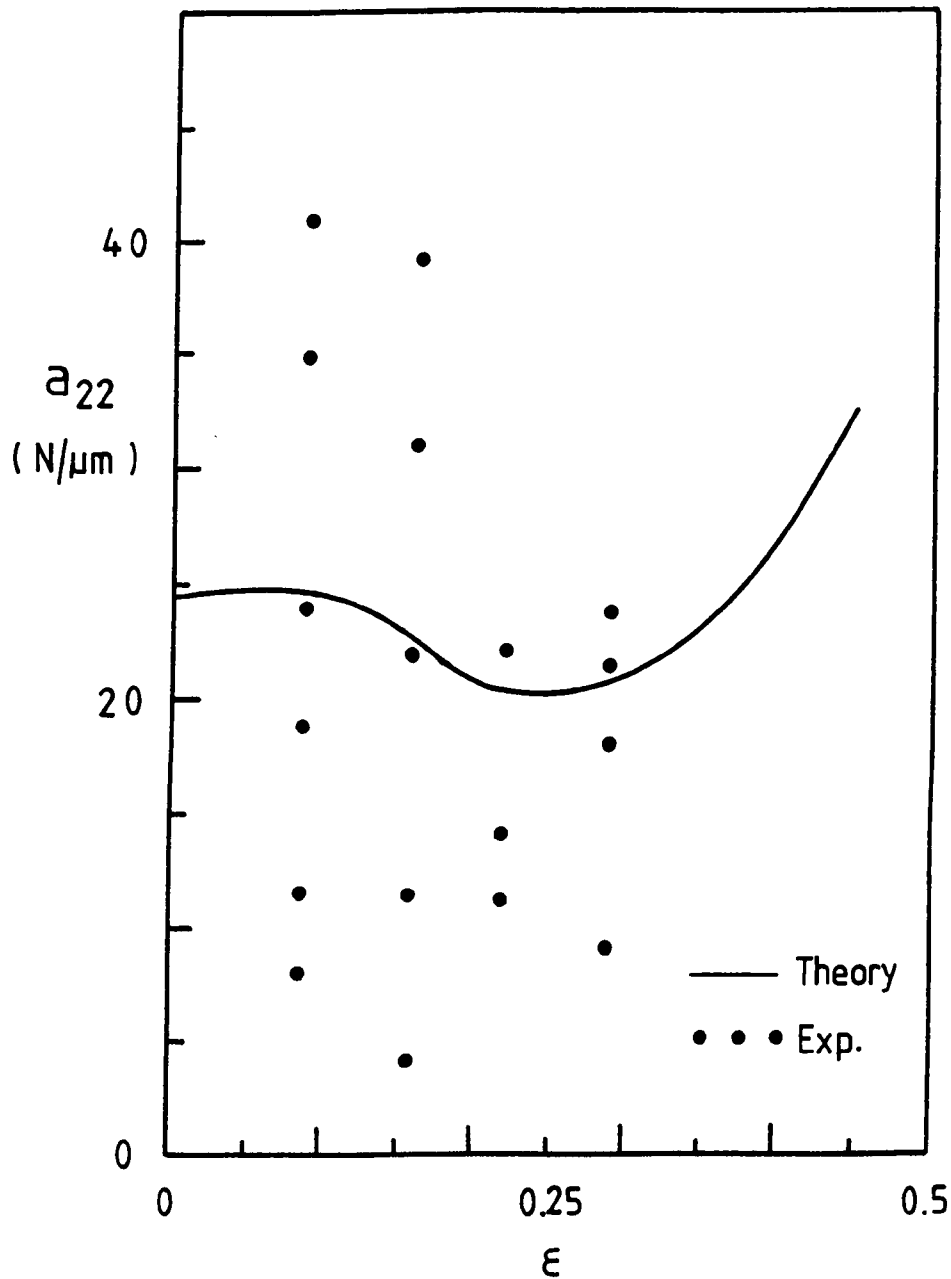
a/L = 0.25 S_{ho} = 0.043

L/D = 1.0 P_s = 689.48 KPa.

β = 0.44

Fig.8.20a: Graph Comparing Theoretical And Experimental Direct Damping Coeffs. (K = 31.0)
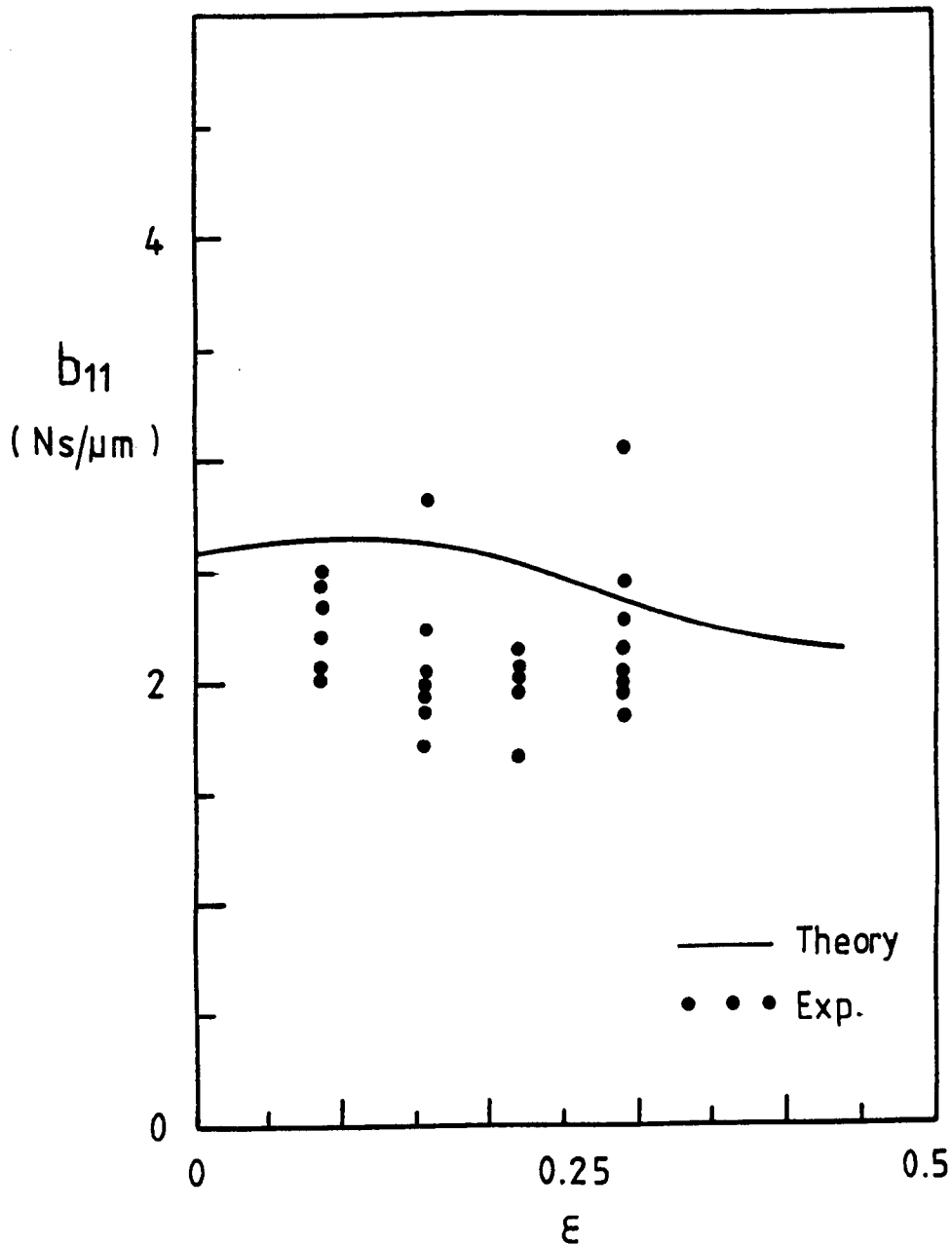
a/L = 0.25   Sho = 0.043

L/D = 1.0 P_S = 689.48 KPa.

β = 0.44

Fig.8.20b:Graph Comparing Theoretical And Experimental X-Coupled Damping Coeffs. (K = 31.0)
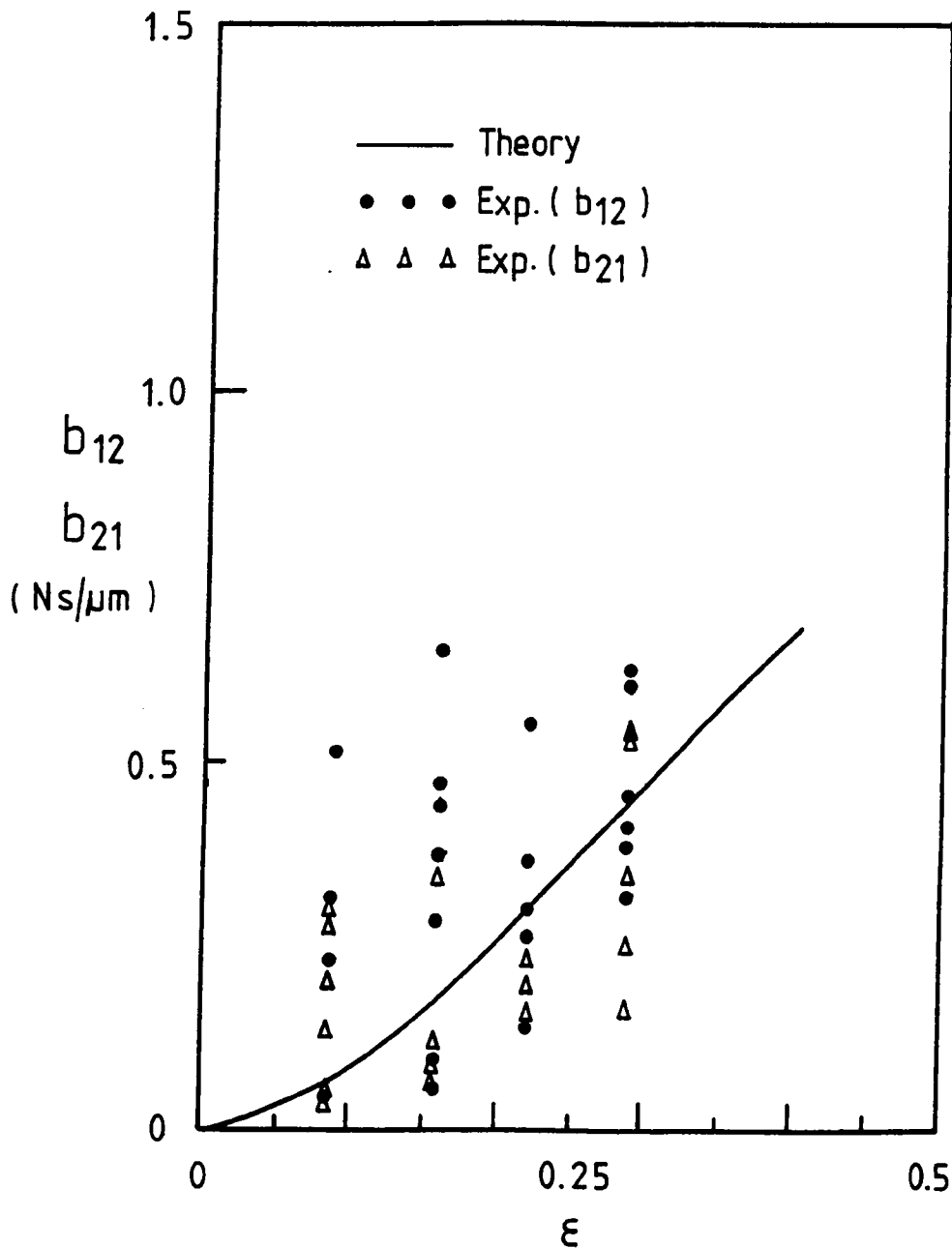
Fig.8.20c:Graph Comparing Theoretical And Experimental Direct Damping Coeffs.(K = 31.0)
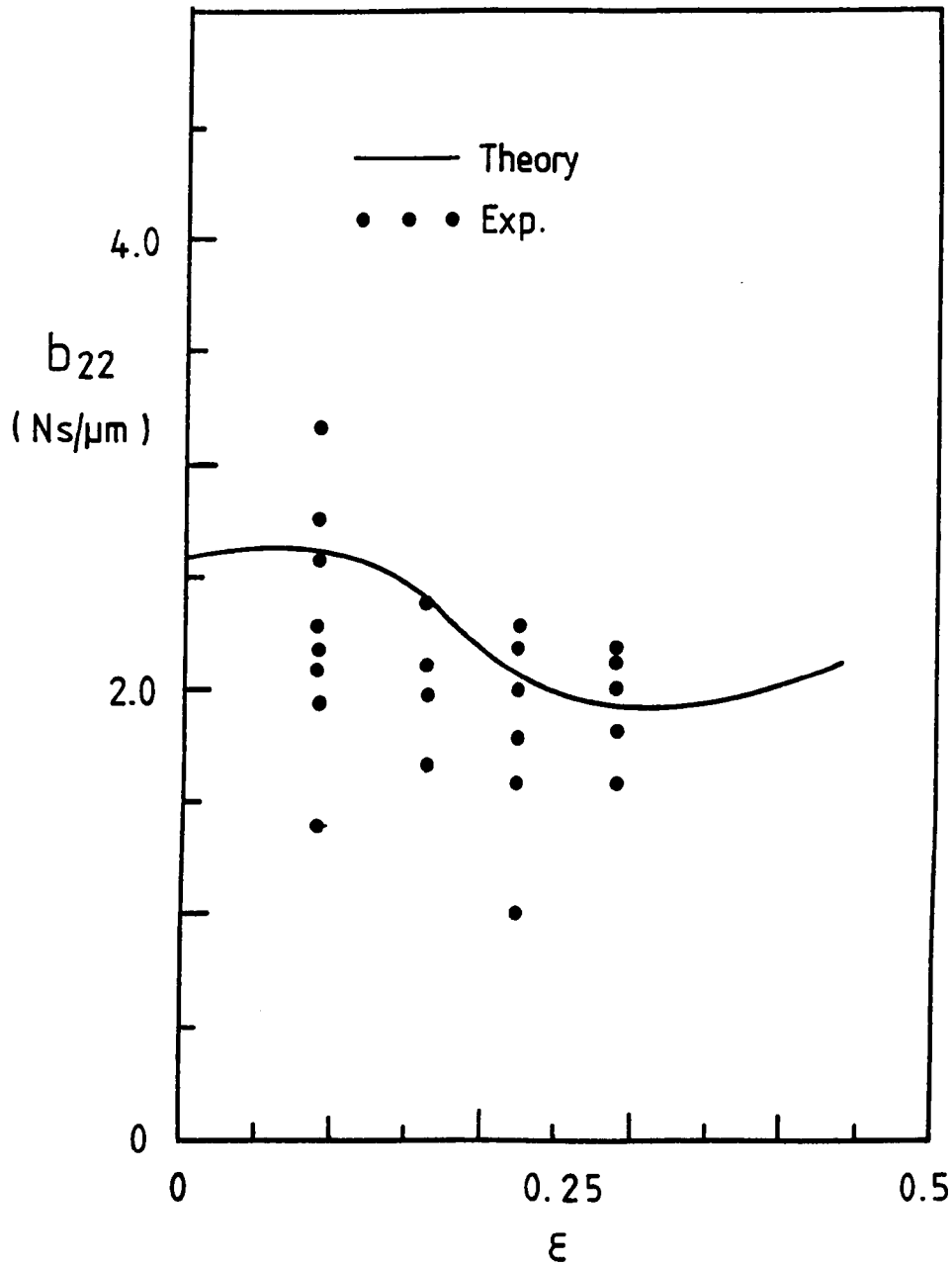
CHAPTER 9

LINEARIZED STABILITY ANALYSIS

9.1 Introduction

The work carried out in this investigation is partly an attempt to tackle the problem of integrating the subject of rotor dynamics and bearing lubrication studies into a single general approach, and, also to set the ground-work for the standardisation of the parameters employed in bearing dynamic analysis, so that comparisons between hydrostatic and hydrodynamic bearings may be carried out on an equivalent basis. It is hoped that this investigation will generate interest to stimulate the development of the subject of rotor-bearing dynamics to include externally pressurized bearings as available elements for the design of rotating machines. This would give the designer a wider range of bearings to choose from, which at the moment is practically limited to the hydrodynamic mode of lubrication.

Non-synchronous whirl (instability), synchronous whirl and critical speeds are the three main areas of rotor-bearing dynamics studies. This investigation is only concerned with non-synchronous whirl. The investigations of synchronous whirl and critical speeds should be the subject of future investigation. The stability limits for a linearized model of a simple symmetric rotor in two similar slot-entry bearings was investigated, and a comparison with other bearing configurations was carried out.

9.2 Bearing Types

Figure (9.2) illustrates the various types of bearings employed in the present investigation. The bearings were:

(i)   slot-entry

(ii)   elliptical hydrodynamic

(iii) two-axial groove hydrodynamic

(iv)   three-lobe hydrodynamic, and

(v)   offset hydrodyamic

9.3 Dimensionless Parameters

(i) Dimensionless Speed Parameter, ν

A new parameter was defined for convenience in the analysis of hybrid externally pressurised bearings.

This was $\nu = \omega \sqrt{\dfrac{m.C}{P_s\,LD}}$ $\qquad\qquad$ (9.1)

This parameter defines the stable or unstable condition of the rotor-bearing system. If the threshold of stability is denoted by ν_s, instability would be represented by values of $\nu > \nu_s$, whilst, stability would be indicated by values of $\nu < \nu_s$. In the hydrodynamic mode of lubrication, the dimensionless speed parameter, $\nu_{hyd.}$ is normally defined as:

$$\nu_{hyd.} = \omega \sqrt{\frac{m.C}{W}} \qquad\qquad (9.2)$$

or,

$$\nu_{hyd.} = \frac{\nu}{(\overline{W})^{\frac{1}{2}}} \qquad\qquad (9.3)$$

(ii) Instability whirl frequency ratio, $\overline{\omega}_s$

$$\overline{\omega}_s = \frac{\omega_s}{\omega} \qquad\qquad (9.4)$$

The instability whirl frequency ratio, $\overline{\omega}_s$ defines the ratio of the whirling frequency over the journal rotational frequency, at the threshold of instability. This value is approximately equal to 0.5, at half speed whirl. (See Chapter 3).

(iii) Flexibility parameter, F

It was convenient to define a new flexibility parameter for use with hybrid externally pressurised bearings. This was:

$$F = \frac{P_s\,LD}{C.k} \qquad\qquad (9.5)$$

The flexibility parameter, F, defines the non-dimensional stiffness of the rotor. In the hydrodynamic mode of lubrication, the flexibility parameter, $F_{hyd.}$ is usually expressed as:

$$F_{hyd.} = \frac{W}{C.k} \qquad (9.6)$$

or,

$$F = \frac{F_{hyd}}{\underline{W}} \qquad (9.7)$$

9.4 The Basis of the Theoretical Analysis

Figure (9.1), illustrates a rotor of mass 2 m and stiffness 2 k, supported by two similar hybrid journal bearings. The rotor is acted upon by a static load 2 W, in the negative direction of Y, and a general excitation force, 2 P, may act in any direction.

The theoretical analysis is based on the investigation of the system behaviour about its equilibrium position. The following assumptions were made:

(i)   system perturbations are sufficiently small to allow linearization of bearing fluid-film forces.

(ii)   the rotor may be represented with its mass lumped centrally between the bearings and supported by a massless shaft, of stiffness 2 k.

(iii)   gyroscopic effects are negligible.

(iv)   rotor motion is symmetric, and

(v)   the lubricant may be treated as an incompressible, isoviscous fluid.

This model is similar to that used by Hahn (1). The difference is that Hahn's model is derived from considerations of a rotor rotating in hydrodynamic bearings, while, th e present analysis applies to rotors rotating in externally pressurized bearings. The linearized stiffness

and damping coefficients for this analysis were obtained from a finite difference solution, program PFD.FOR. The linearized coefficients for the other bearing configurations were obtained from data computed by Lund et. al. (2).

9.5 Equations of Motion

With the system at equilibrium, at time $t \leqslant 0$, the equations of motion for excitation by forces P_x (t) and P_y (t) may be expressed by equations (9.8) to (9.11) as:

$$m.\ddot{x}_r + k (x_r - x) = P_x (t) \tag{9.8}$$

$$\delta F_x (t) = k (x_r - x) = a_{11} x + b_{11} \dot{x} + a_{12} y + b_{12} \dot{y} \tag{9.9}$$

$$m.\ddot{y}_r + k (y_r - y) = P_y (t) \tag{9.10}$$

$$\delta F_y (t) = k (y_r - y) = a_{21} x + b_{21} \dot{x} + a_{22} y + b_{22} \dot{y} \tag{9.11}$$

Introducing the following non-dimensional parameters:

$$\nu = \omega \sqrt{\frac{m.C}{P_s LD}} \qquad i.e. \qquad \nu = \omega_o \sqrt{\frac{K.m.C}{P_s LD}}$$

$$a_{i,j} = \bar{a}_{i,j} \frac{P_s LD}{C} \qquad ; \qquad b_{i,j} = \bar{b}_{i,j} \frac{P_s LD}{\omega_o C}$$

$$\tag{9.12}$$

$$F = \frac{P_s LD}{C.k} \qquad ; \qquad \tau = \omega_o t$$

$$x (t) = \bar{x} (t).C \qquad ; \qquad P_i (t) = \bar{P}_i (t) P_s LD$$

Equations (9.8) to (9.11) may be written non-dimensionally as:

$$\left(\frac{\nu^2}{K}\right) \ddot{\bar{x}}_r + \frac{1}{F} (\bar{x}_r - \bar{x}) = \bar{P}_x (t) \tag{9.13}$$

$$\delta \bar{F}_x (t) = \frac{1}{F} (\bar{x}_r - \bar{x}) = \bar{a}_{11} \bar{x} + \bar{b}_{11} \dot{\bar{x}} + \bar{a}_{12} \bar{x} + \bar{b}_{12} \dot{\bar{y}} \tag{9.14}$$

$$\left(\frac{\nu^2}{K}\right) \ddot{\bar{y}}_r + \frac{1}{F} (\bar{y}_r - \bar{y}) = \bar{P}_y (t) \tag{9.15}$$

$$\delta \bar{F}_y (t) = \frac{1}{F} (\bar{y}_r - \bar{y}) = \bar{a}_{21} \bar{x} + \bar{b}_{21} \dot{\bar{x}} + \bar{a}_{22} \bar{y} + \bar{b}_{22} \dot{\bar{y}} \tag{9.16}$$

Applying the Laplace transformation to equations (9.13 - 9.16) and re-

arranging terms yields:

$$(\frac{s^2 \nu^2}{K} + \frac{1}{F}) X_r(s) - (\frac{1}{F}) X(s) = \bar{P}_x(s) \tag{9.17}$$

$$F\{(\bar{a}_{11} + \frac{1}{F} + s \bar{b}_{11}) X(s) + (\bar{a}_{12} + s \bar{b}_{12}) Y(s)\} = X_r(s) \tag{9.18}$$

$$(\frac{s^2 \nu^2}{K} + \frac{1}{F}) Y_r(s) - (\frac{1}{F}) Y(s) = \bar{P}_y(s) \tag{9.19}$$

$$F\{(\bar{a}_{22} + \frac{1}{F} + s \bar{b}_{22}) Y(s) + (\bar{a}_{21} + s \bar{b}_{21}) X(s)\} = Y_r(s) \tag{9.20}$$

where:

$$X(s) = \int_0^\infty \bar{x}(\tau) e^{-\sigma\tau} d\tau$$

$$s = \sigma + j \Omega \tag{9.21}$$

Substituting equations (9.18) and (9.20) into equations (9.17) and (9.19) respectively yields:

$$F(\frac{s^2 \nu^2}{K} + \frac{1}{F})\{(\bar{a}_{11} + \frac{1}{F} + s\bar{b}_{11})X(s) + (\bar{a}_{12} + s\bar{b}_{12})Y(s)\} - (\frac{1}{F})X(s) = \bar{P}_x(s)$$
$$\ldots(9.22)$$

$$F(\frac{s^2 \nu^2}{K} + \frac{1}{F})\{(\bar{a}_{22} + \frac{1}{F} + s\bar{b}_{22})Y(s) + (\bar{a}_{21} + s\bar{b}_{21})X(s)\} - (\frac{1}{F})Y(s) = \bar{P}_y(s)$$
$$\ldots(9.23)$$

Simplifying and rearranging terms in equations (9.22) and (9.23) and writing in matrix notation yields:

$$\begin{bmatrix} (\frac{F\nu^2 s^2}{K} + 1)(\bar{a}_{11} + s\bar{b}_{11}) + \frac{s^2 \nu^2}{K} & (\frac{F\nu^2 s^2}{K} + 1)(\bar{a}_{12} + s\bar{b}_{12}) \\ (\frac{F\nu^2 s^2}{K} + 1)(\bar{a}_{21} + s\bar{b}_{21}) & (\frac{F\nu^2 s^2}{K} + 1)(\bar{a}_{22} + s\bar{b}_{22}) + \frac{s^2 \nu^2}{K} \end{bmatrix} \begin{bmatrix} X(s) \\ Y(s) \end{bmatrix} = \begin{bmatrix} \bar{P}_x(s) \\ \bar{P}_y(s) \end{bmatrix}$$
$$\ldots(9.24)$$

or:

$$\begin{bmatrix} X(s) \\ Y(s) \end{bmatrix} = \frac{1}{C(s)} \begin{bmatrix} (\frac{F\nu^2 s^2}{K} + 1)(\bar{a}_{22} + s\bar{b}_{22}) + \frac{s^2 \nu^2}{K} & -(\frac{F\nu^2 s^2}{K} + 1)(\bar{a}_{12} + s\bar{b}_{12}) \\ -(\frac{F\nu^2 s^2}{K} + 1)(\bar{a}_{21} + s\bar{b}_{21}) & (\frac{F\nu^2 s^2}{K} + 1)(\bar{a}_{11} + s\bar{b}_{11}) + \frac{s^2 \nu^2}{K} \end{bmatrix} \begin{bmatrix} \bar{P}_x(s) \\ \bar{P}_y(s) \end{bmatrix}$$
$$\ldots(9.25)$$

where:

$$C(s) = (\frac{Fv^2s^2}{K} + 1)(\bar{a}_{11}+s\bar{b}_{11})(\bar{a}_{22}+s\bar{b}_{22}) - (\bar{a}_{21}+s\bar{b}_{21})(\bar{a}_{12}+s\bar{b}_{12}) \dots$$

$$\dots + \frac{s^4v^4}{K^2} + \frac{s^2v^2}{K}(\frac{Fv^2s^2}{K} + 1)\{\bar{a}_{11}+\bar{a}_{22}+s(\bar{b}_{11}+\bar{b}_{22})\}\dots \quad (9.26)$$

Hence, the rotor-bearing system's transfer functions of figure (9.1) are as follows:

$$\frac{X(s)}{\bar{P}_x(s)} = \frac{(\frac{Fv^2s^2}{K} + 1)(\bar{a}_{22} + s\bar{b}_{22}) + \frac{s^2v^2}{K}}{C(s)}$$

$$\frac{X(s)}{\bar{P}_y(s)} = \frac{-(\frac{Fv^2s^2}{K} + 1)(\bar{a}_{12} + s\bar{b}_{12})}{C(s)}$$

$$\frac{Y(s)}{\bar{P}_x(s)} = \frac{-(\frac{Fv^2s^2}{K} + 1)(\bar{a}_{21} + s\bar{b}_{21})}{C(s)}$$

$$\frac{Y(s)}{\bar{P}_y(s)} = \frac{(\frac{Fv^2s^2}{K} + 1)(\bar{a}_{11} + s\bar{b}_{11}) + \frac{s^2v^2}{K}}{C(s)}$$

$$(9.27)$$

The characteristics function, $C(s)$, yields a 6th-degree polynomial, which is equivalent to a 3 degree of freedom system, and may be represented as:

$$C(s) = A_0 s^6 + A_1 s^5 + A_2 s^4 + A_3 s^3 + A_4 s^2 + A_5 s + A_6 \quad (9.28)$$

where:

$$A_0 = \frac{F^2v^4}{K^2} B_3$$

$$A_1 = \frac{v^4}{K^2}(F^2 B_4 + F.B_2)$$

$$A_2 = \frac{v^2}{K}(\frac{F^2v^2}{K} B_1 + \frac{Fv^2}{K} B_0 + 2.F.B_3 + \frac{v^2}{K})$$

$$A_3 = \frac{v^2}{K}(2.F.B_4 + B_2)$$

$$A_4 = 2.F.\frac{v^2}{K} B_1 + \frac{v^2}{K} B_0 + B_3$$

$$A_5 = B_4$$

$$A_6 = B_1$$

$$B_0 = \bar{a}_{11} + \bar{a}_{22}$$

$$B_1 = \bar{a}_{11}\,\bar{a}_{22} - \bar{a}_{12}\,\bar{a}_{21}$$

$$B_2 = \bar{b}_{11} + \bar{b}_{22}$$

$$B_3 = \bar{b}_{11}\,\bar{b}_{22} - \bar{b}_{12}\,\bar{b}_{21}, \text{ and}$$

$$B_4 = \bar{a}_{11}\,\bar{b}_{22} + \bar{a}_{22}\,\bar{b}_{11} - \bar{a}_{12}\,\bar{b}_{21} - \bar{a}_{21}\,\bar{b}_{12}$$

9.6 Rotor-Bearing Stabiligy Analysis

The stability of the rotor-bearing system depicted in figure (9.1) may be predicted by investigating the behaviour of the roots of the characteristic function, C(s), that is, if the characteristic equation has been solved and its roots are known. The stability of a linearized system depends only on the system and not on the driving function, hence, if a system is unstable any excitation will cause the system to oscillate. However, if the actual response of the rotor-bearing system is required the transfer functions given by equations (9.27) have to be considered.

The question of stability in linear systems can be resolved without solving the characteristic equation. The stability of the system is governed by the sign of the real components of the roots to the characteristic equation. If all the roots of the characteristic equation have negative real parts (i.e. the roots are located in the left hand side of the complex S-plane), the system will be stable and non-oscillatory. It will be stable but oscillatory if the conjugate imaginary roots are all different. If the roots have positive real terms, or if there are repeated zeros, or conjugate imaginary roots, the system will be unstable. Routh (3) presented a method to determine whether any root contains a real positive term by examination of the coefficients of the characteristic equation. This procedure is adopted in the present investigation. The method is outlined as follows:

The coefficients of equation (9.28) may be arranged in an array (9.29).

$$
\begin{array}{c|cccc}
s^6 & A_0 & A_2 & A_4 & A_6 \\
s^5 & A_1 & A_3 & A_5 \\
s^4 & C_1 & C_2 & C_3 \\
s^3 & D_1 & D_2 \\
s^2 & E_1 & E_2 \\
s^1 & F_1 \\
s^0 & G_1
\end{array}
\qquad (9.29)
$$

where:

$$C_1 = A_2 - A_0 A_3 / A_1 \quad ; \quad C_2 = A_4 - A_0 A_5 / A_1$$

$$C_3 = A_6$$

$$D_1 = A_3 - A_1 C_2 / C_1 \quad ; \quad D_2 = A_5 - A_1 C_3 / C_1$$

$$E_1 = C_2 - C_1 D_2 / D_1 \quad ; \quad E_2 = C_3$$

$$F_1 = D_2 - D_1 E_2 / E_1$$

$$G_1 = E_2$$

The necessary and sufficient condition of stability is that all of the coefficients of the 1st column of the array must be positive.

A program, LSA.FOR was written to compute the stability limits. Equation (9.28) shows that the system behavious is governed by the speed parameter, ν, the flexibility parameter, F, and the eight non-dimensional coefficients, $\bar{a}_{ij}$, $\bar{b}_{ij}$. An iterative approach was employed to obtain the threshold speed, ν_s. The method consists of assuming an initial value of ν, and calculating the coefficients A_0 to A_6, for the selected value of eccentricity and power-ratio. If these are all positive, the program continues and calculates the Routh coefficients and tests to see if any coefficient in the 1st column is negative. The initial value of ν, is incremented to a new value, if no negative coefficient appears.

The process is repeated until a negative coefficient appears. If a negative coefficient appears, the next value of ν, is obtained by averaging the unstable speed value with the previous stable value. This procedure is continued until a convergence criterion of $\pm$ 0.001 is satisfied. Figures (9.3) to (9.8) illustrate the stability limits of the slot-entry bearing for various values of $^a/L$, $^L/D$ and β at F = 0 and 5.

The program also performs the iterative solution of the characteristic equation, using the modified Bairstow's technique (4), in order to obtain information on the whirling frequency. A convergence criterion of 10^{-8} was employed. Using the expressions defined in Section 9.3, for relating the dimensionless parameters between the hydrostatic and hydrodynamic modes of lubrication, it was possible to compare the stability limits of the slot-entry bearing with those for hydrodynamic bearings. Such comparisons are illustrated in figures (9.9a) and (9.10a).

9.7 Discussion of Results

9.7.1 Parametric Studies of Slot-Bearing Designs

(i) The effect of varying the $^a/L$ ratio.

The effect of varying the $^a/L$ ratio, on the stability threshold speed for a rigid rotor is illustrated in figure (9.3). It can be seen that for $0 < \epsilon \leqslant 0.5$, large values of $^a/L$ ratio are required to ensure good stability. For operation within this region, an $^a/L$ of 0.25, would provide the best compromise between load capacity and stability. Although, choosing an $^a/L$ ratio of 0.4 would marginally improve the stability characteristics, the load carrying capacity would be reduced considerably. For $0.5 < \epsilon < 1.0$, small values of $^a/L$ are essential to ensure good stability.

Figure (9.4) shows that the introduction of shaft flexibility

(F = 5) into the system, has the effect of reducing the stability thres-
hold speed, as well as altering the general pattern of the stability
curve. It can be observed that to ensure good stability, large values
of $^a/L$ ratios are required. This criterion applies up to an eccentricity-
ratio as high as 0.7. For values of $\varepsilon > 0.7$, small values of $^a/L$ ratio
are desirable.

(ii) **Effect of varying the concentric pressure-ratio, β**

Figure (9.5), illustrates the effect of varying the concentric
pressure-ratio, β, on the stability threshold speed, for the case of a
rigid rotor. It can be observed that there is a large difference in
stability characteristics between a bearing with β = 0.1 and one with
β = 0.9. However, for values of β near to 0,5, it can be observed that
the influence of β, on stability characteristics is minimum. Three
operating regions may be cited here:

(a) For $0 < \varepsilon \leqslant 0.3$ — β = 0.5 should be used.

(b) For $0.3 < \varepsilon \leqslant 0.7$ — small values of β should be chosen.

(c) For $\varepsilon > 0.7$ — a large β value is desirable.

Introducing shaft flexibility into the system lowers the stability
threshold speed and alters the pattern of the stability curve, as
illustrated in figure (9.6). It is observed that β, should be designed
as far away from 0.5 as possible, for $0 < \varepsilon \leqslant 0.7$. A value of 0.1 is
preferred. It should be pointed out that β = 0.5, yields the worst
stability characteristics. For $\varepsilon > 0.7$, large values of β, should be
used to ensure good stability.

(iii) **Effect of varying the $^L/D$ ratio**

The effect of variation of $^L/D$ ratio on stability for the case of
a rigid shaft, is illustrated in figure (9.7), while figure (9.8)
illustrates the case where shaft flexibility is introduced. For both
cases, it can be observed that for $\varepsilon \leqslant 0.6$, a short bearing, that is,

a small value of $^L/D$ is essential to ensure good stability. For operation at high values of eccentricity-ratio, $^L/D$ should be designed to be as close to 1.0 as possible.

9.7.2 Comparison with other bearing types

The stability threshold speed plotted against Sommerfeld Number for the six bearing types shown in figure (9.2), are illustrated in figures (9.9a) and (9.10a). Figure (9.9a) represents the case where the shaft is rigid, while shaft flexibility is introduced in figure (9.10a). Each of the diagonal lines are lines of constant ψ, and gives the locus of the operation of a bearing with a fixed geometry as it is brought up or down in speed. The bearing parameter ψ, has been defined by Allaire (5) as:

$$\psi = \frac{S}{\nu_{hyd}}$$

i.e. $\quad \psi = \frac{\eta \, L \, D}{8 \, \pi \, W} \, (\frac{D}{C})^2 \, (\frac{W}{C.m})^{\frac{1}{2}}$

The bearing parameter ψ, is independent of the rotor speed. ψ, by itself is sufficient to describe the behaviour of a certain bearing geometry on a stability graph. As a bearing increases in speed, it will proceed along a line of constant ψ, and becomes unstable as it enters the unstable region by crossing the stability curve from below.

From the graph of figure (9.9a), it can be observed that the offset bearing is the most stable at light-load (ψ = 0.1 to 1.0), followed by the slot-entry bearing at K = 1. However, at heavy load (ψ = 0.001 to 0.1), the slot-entry bearing at K = 1 is less stable than the plain cylindrical bearing, but comparable to the two-axial groove bearings. Increasing the value of K (K = 9 and 90) results in the slot-entry bearing being the most stable at heavy loads, but less stable at light loads. For moderate loads (ψ = 0.01 to 0.1), the slot-entry bearing seems to be poor in stability. This could be improved by designing for

a small value of concentric pressure-ratio, say, $\beta = 0.1$ (See figure 9.5).

Introduction of shaft flexibility ($F_{hyd} = 5$), tends to have a drastic effect on the three-lobe and elliptical bearings at the light load region. For high values of K, the stability threshold speed of the slot-entry bearings is reduced considerably. At a Sommerfeld No. of 0.1 to 0.3 (still at light load region), the slot-entry bearing with K = 1, is the most stable, while at the moderate load region, the slot-entry bearing with K = 90, is the most stable.

Figures (9.9b) and (9.10b) illustrate the whirl speed ratio for the six bearing types plotted against Sommerfeld Number. In general, it can be observed that the most stable bearing whirls at the lowest frequency.

The relationship between Sommerfeld Number and the minimum clearance for the six bearing types are presented in figure (9.11). For the same Sommerfeld number, the slot-entry bearing (K = 1) can be observed to operate with the largest minimum film thickness. At a Sommerfeld number of 0.5, the operating minimum film thickness of the slot-entry bearing is about twice that of non-circular bearings. Therefore, the improvement in stability characteristics (by proper selection of design parameters) offered by the slot-entry bearings coupled with a larger operating minimum film thickness would lead to low friction power loss and make the bearing less sensitive to impurities in the lubricant. Also a cooler bearing is observed.

9.8 Conclusions

(1) The stability behaviour of hybrid bearings is a complex subject. Improvements can sometimes be obtained by going away from the optimum design for static loading, particularly where shaft flexibility is involved. Design predictions need to be substantiated

by experimental work.

(2) With the proper selection of design parameters, such as, the $^a/L$ ratio, the concentric pressure-ratio, β, and the power-ratio, K, the circular plain line-entry (slot) hybrid journal bearing may be designed to match the improved stability limits offered by the non-circular bearing configurations.

(3) Introduction of shaft flexibility into the system does not only lower the stability threshold speed, but, may also alter the general pattern of the stability curve.

(4) To ensure good stability for a rigid shaft, the following design parameters are recommended:

Operating Eccentricity-Ratio	β	K	$^a/L$	$^L/D$
$0 < \epsilon \leqslant 0.3$	0.5	1	0.25	Small values of $^L/D$
$0.3 < \epsilon \leqslant 0.7$	0.1	Moderate values of K	Small values of $^a/L$	Small values of $^L/D$
$0.7 < \epsilon < 1.0$	0.9	Large values of K	Small values of $^a/L$	1.0

(5) To ensure good stability for a system with shaft flexibility, the following design parameters are recommended:

Operating Eccentricity-Ratio	β	K	$^a/L$	$^L/D$
$0 < \epsilon \leqslant 0.25$	0.1 or 0.9	1	0.4	Small values of $^L/D$
$0.25 < \epsilon \leqslant 0.7$	0.1	Moderate values of K	0.4	Small values of $^L/D$
$0.7 < \epsilon < 1.0$	0.9	Large values of K	Small values of $^a/L$	1.0
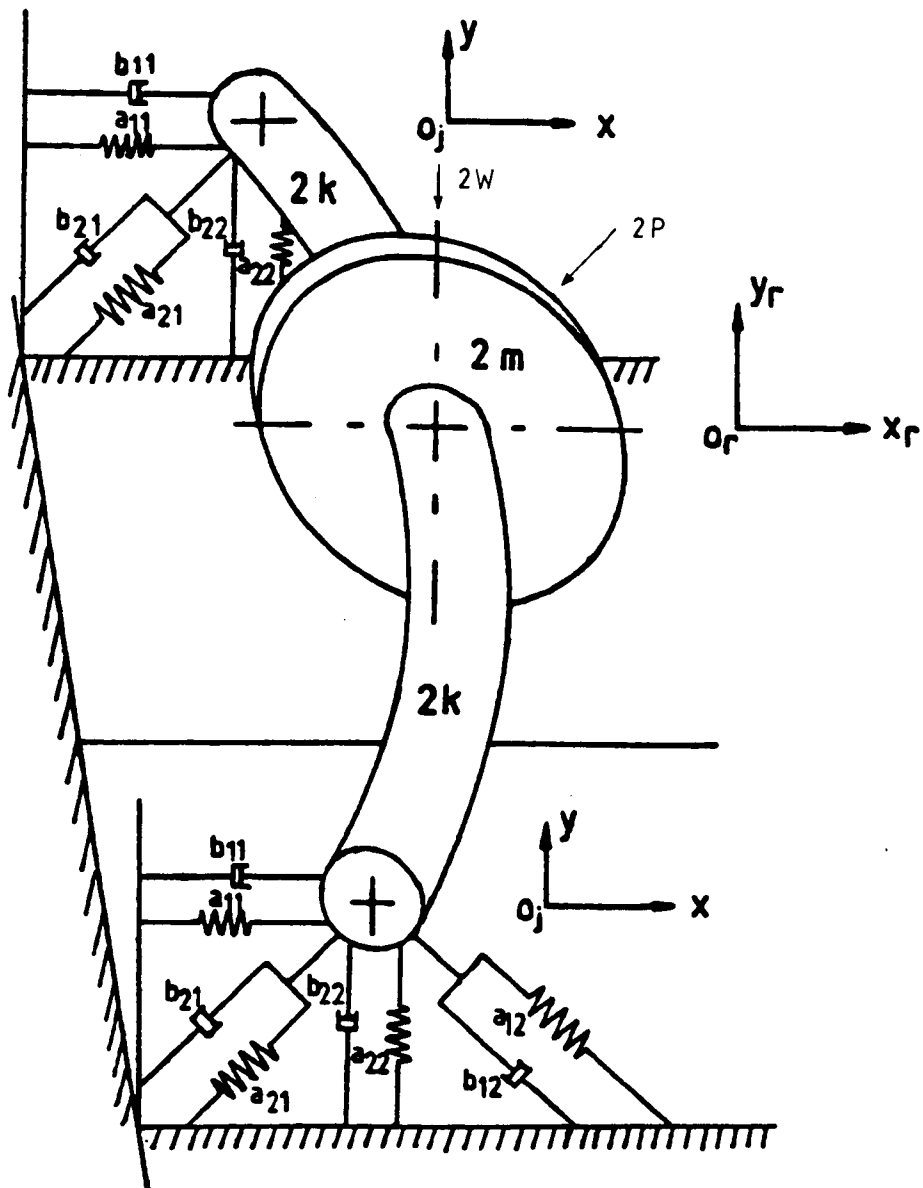
Fig.(9.1) : Single Mass Rotor Bearing System.
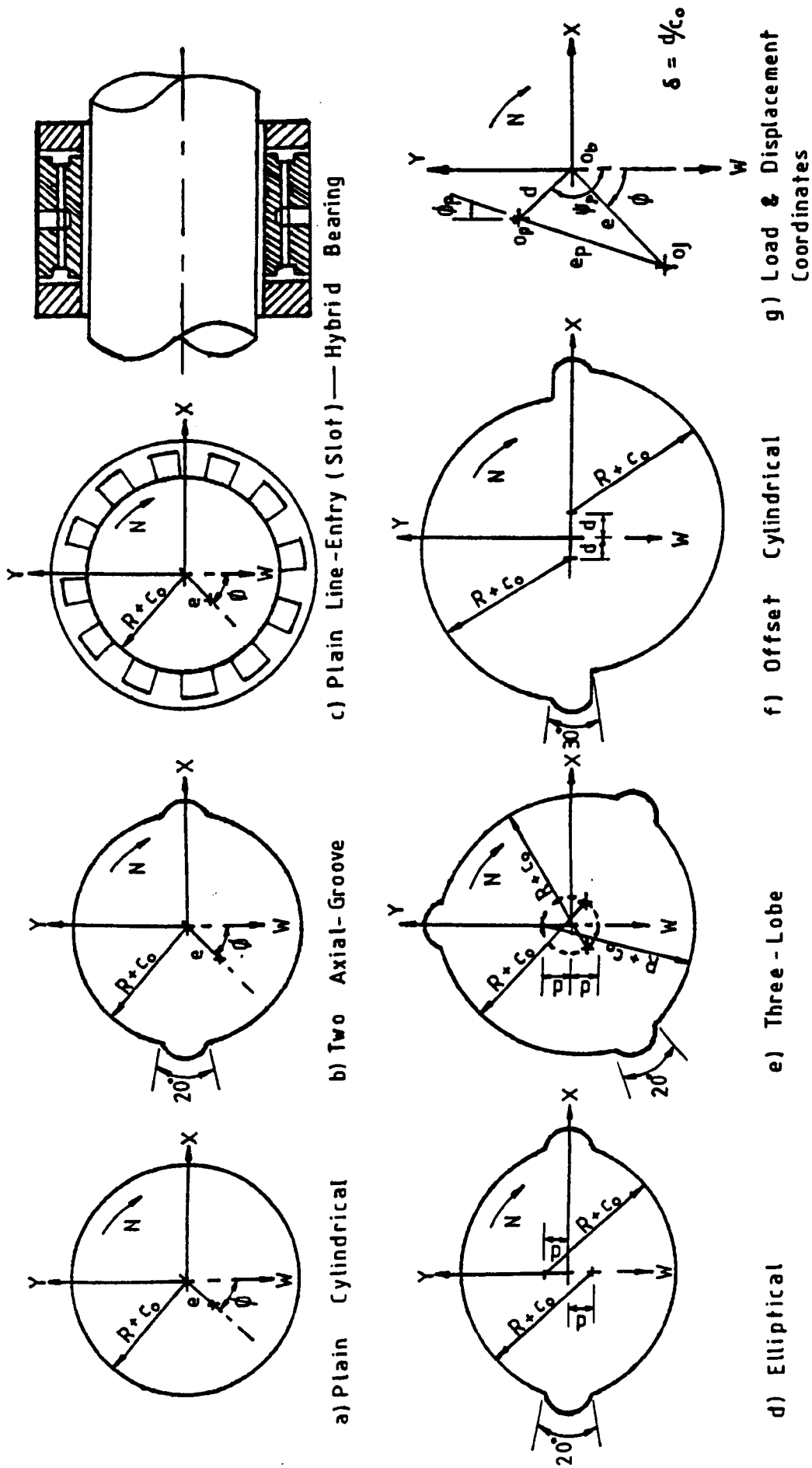
Fig.(9.2) : Geometry For Various Bearing Types

a) Plain Cylindrical

b) Two Axial-Groove

c) Plain Line-Entry (Slot) — Hybrid Bearing

d) Elliptical

e) Three-Lobe

f) Offset Cylindrical

g) Load & Displacement Coordinates

$\delta = e/c_0$

Fig.(9.3): Linearized Stability Map Of Slot-Entry Bearings Showing The Effect Of Varying The a/L Ratio. (F = 0)
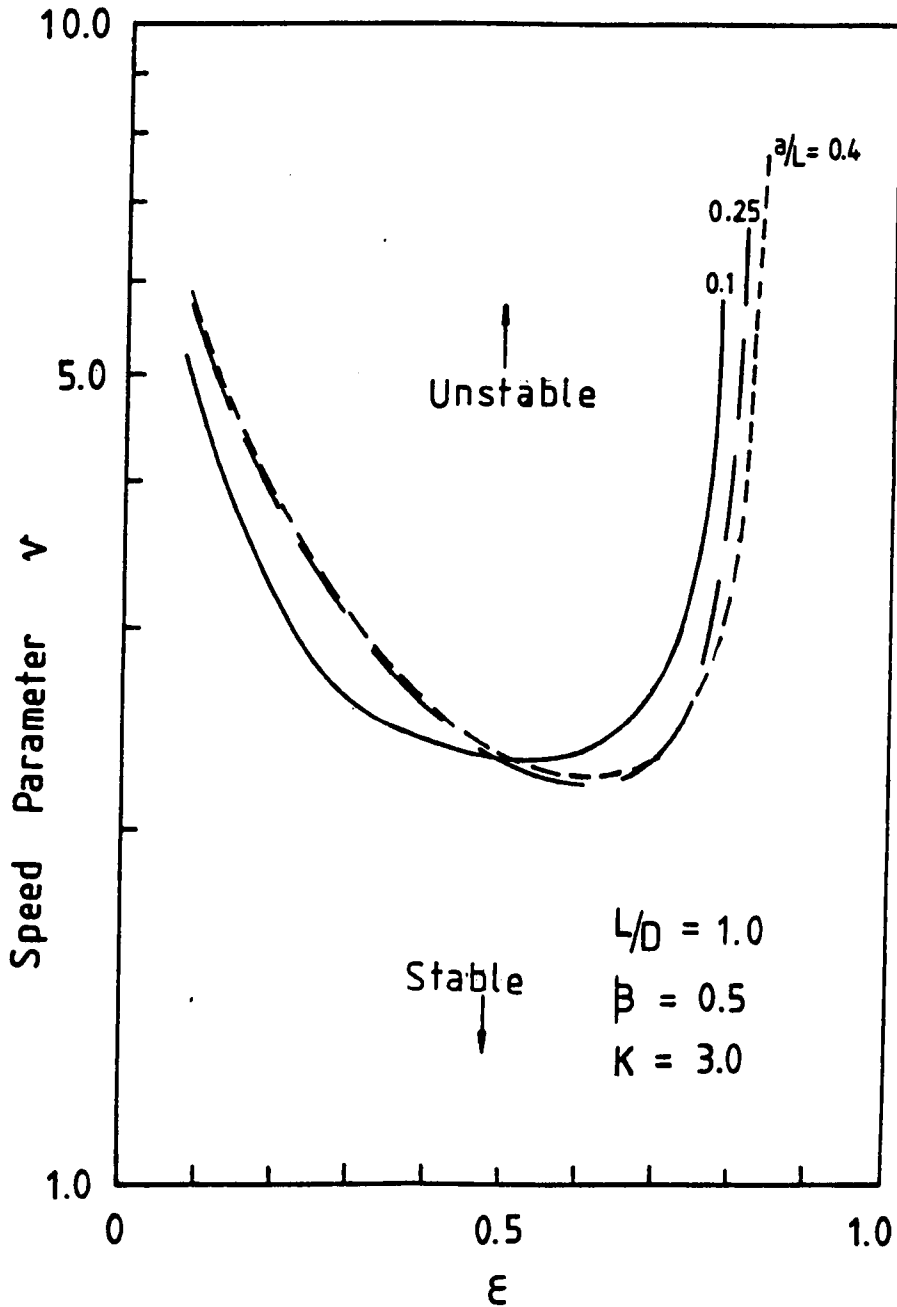
L/D = 1.0

β = 0.5

K = 3.0

Fig.(9.4): Linearized Stability Map Of Slot-Entry Bearings Showing The Effect Of Varying The a/L Ratio.
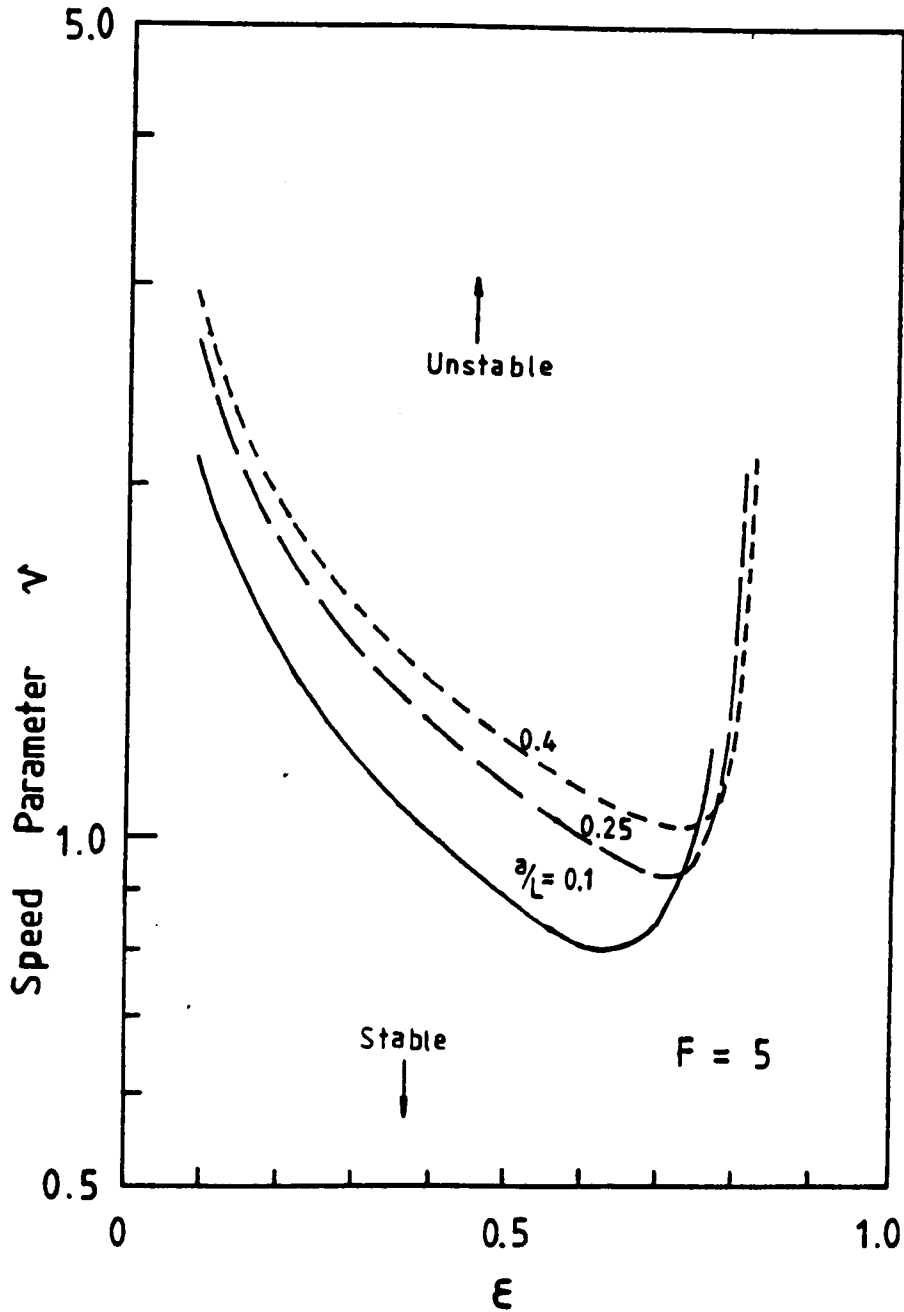
$L/D = 1.0$

$\beta = 0.5$

$K = 3.0$

Fig.(9.5): Linearized Stability Map Of Slot-Entry Bearings Showing The Effect Of Varying The Concentric Pressure-Ratio, β.
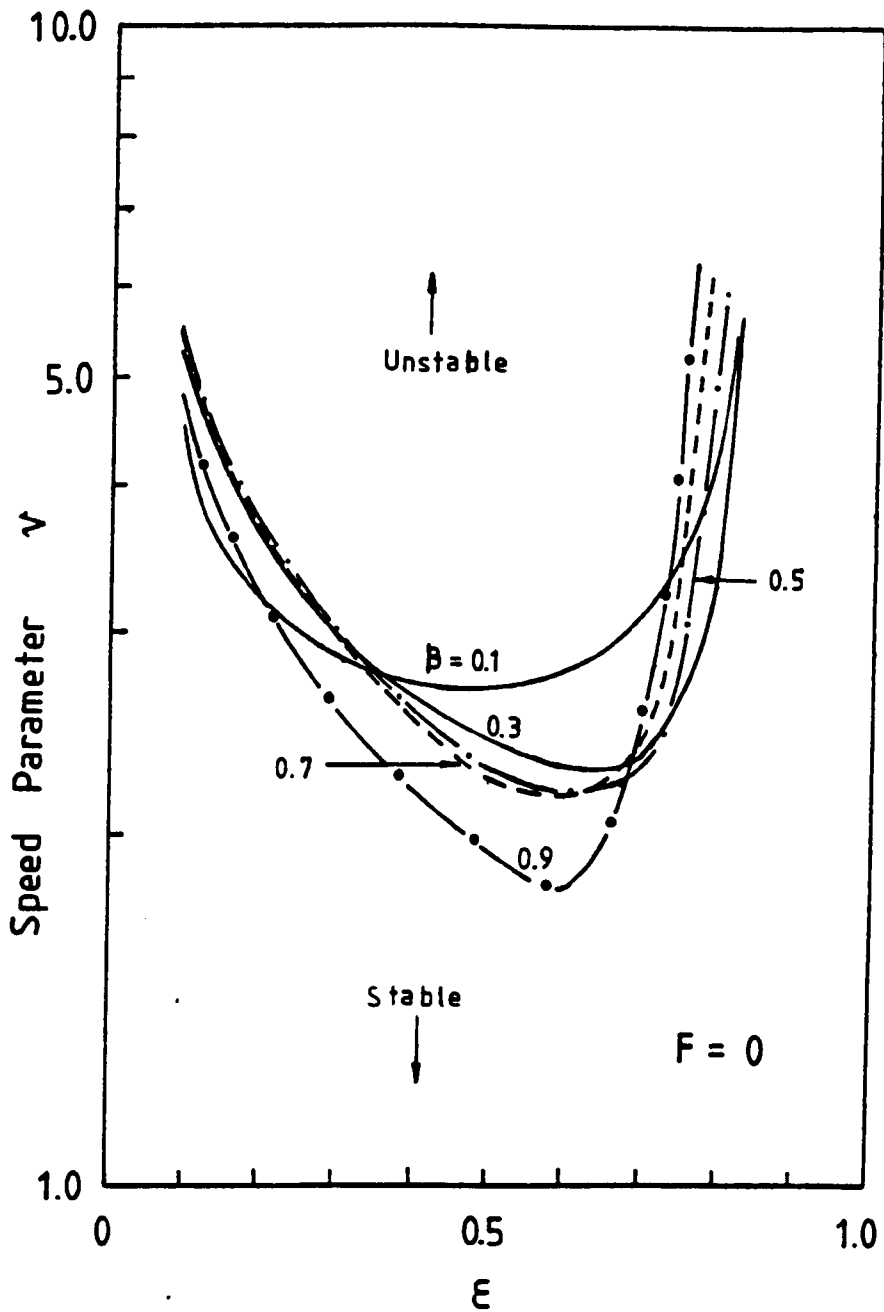
$$\frac{a}{L} = 0.25$$

$$\frac{L}{D} = 1.0$$

$$K = 3.0$$

Fig.(9.6): Linearized Stability Map Of Slot-Entry
Bearings Showing The Effect Of Varying
The Concentric Pressure-Ratio, β.
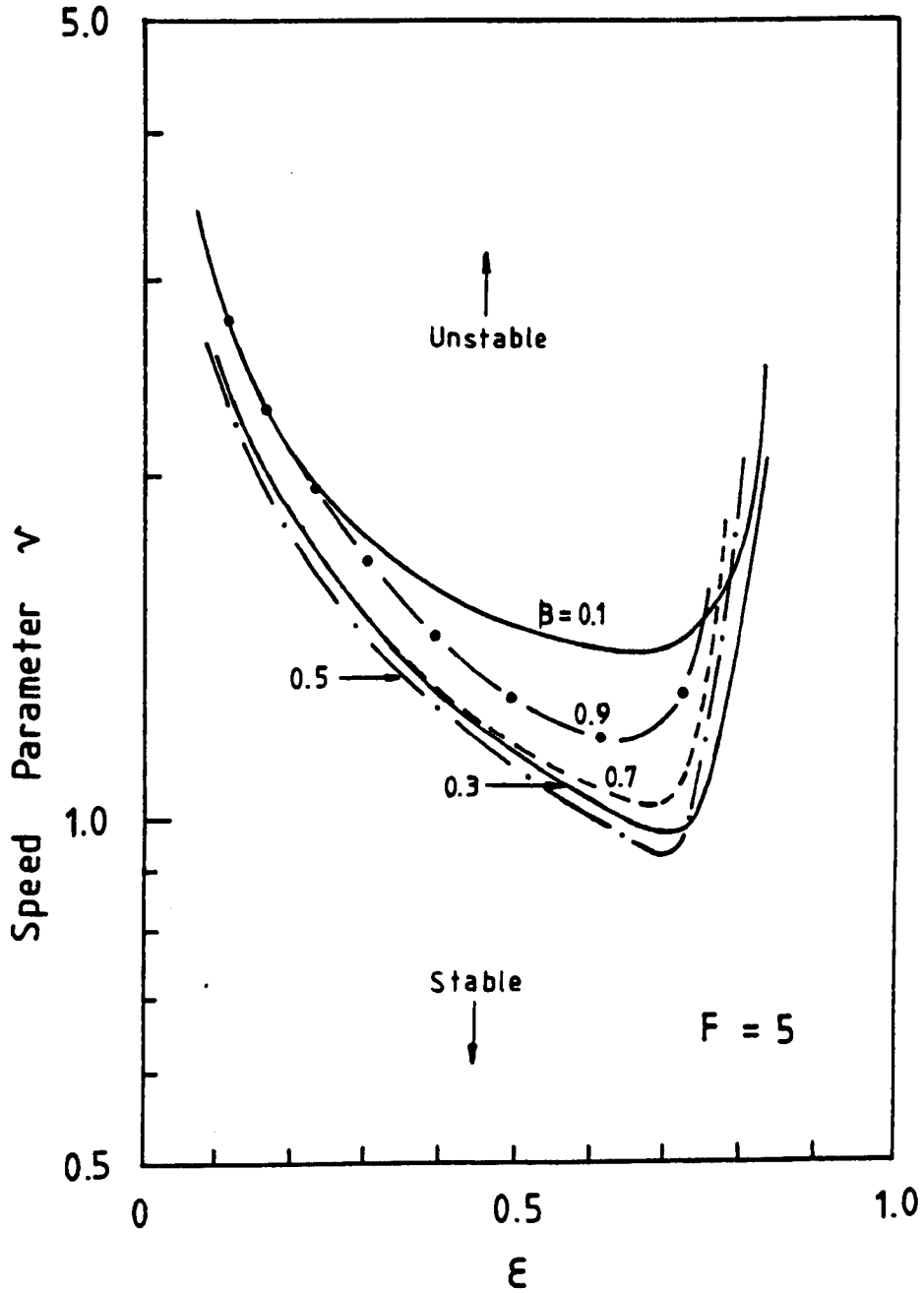
a/L = 0.25

L/D = 1.0

K = 3.0

Fig.(9.7): Linearized Stability Map Of Slot-Entry Bearings Showing The Effect Of Varying The L/D Ratio.
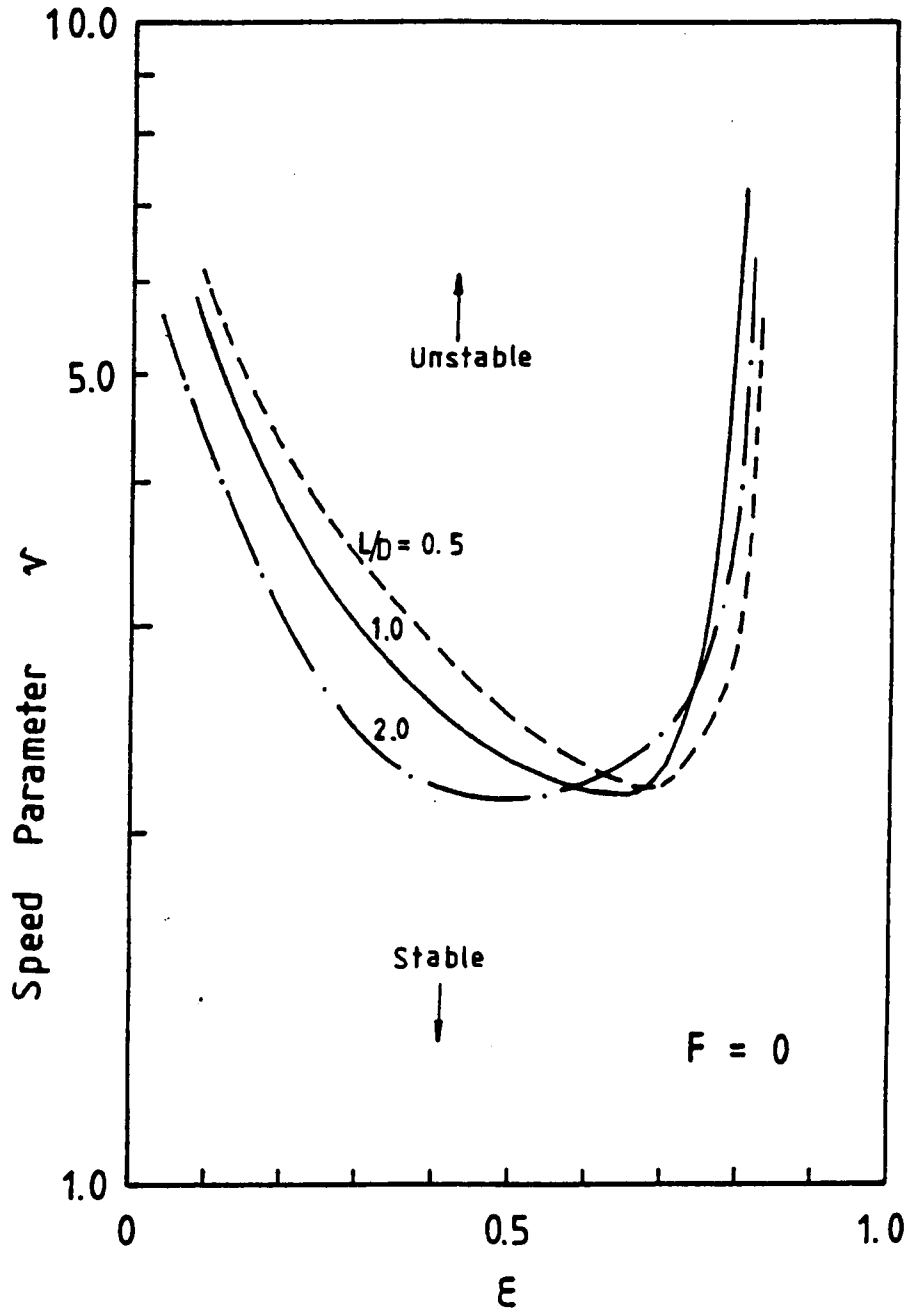
a/L = 0.25

β = 0.5

K = 3.0

Fig.(9.8) : Linearized Stability Map Of Slot-Entry
Bearings Showing The Effect Of Varying
The L/D Ratio.
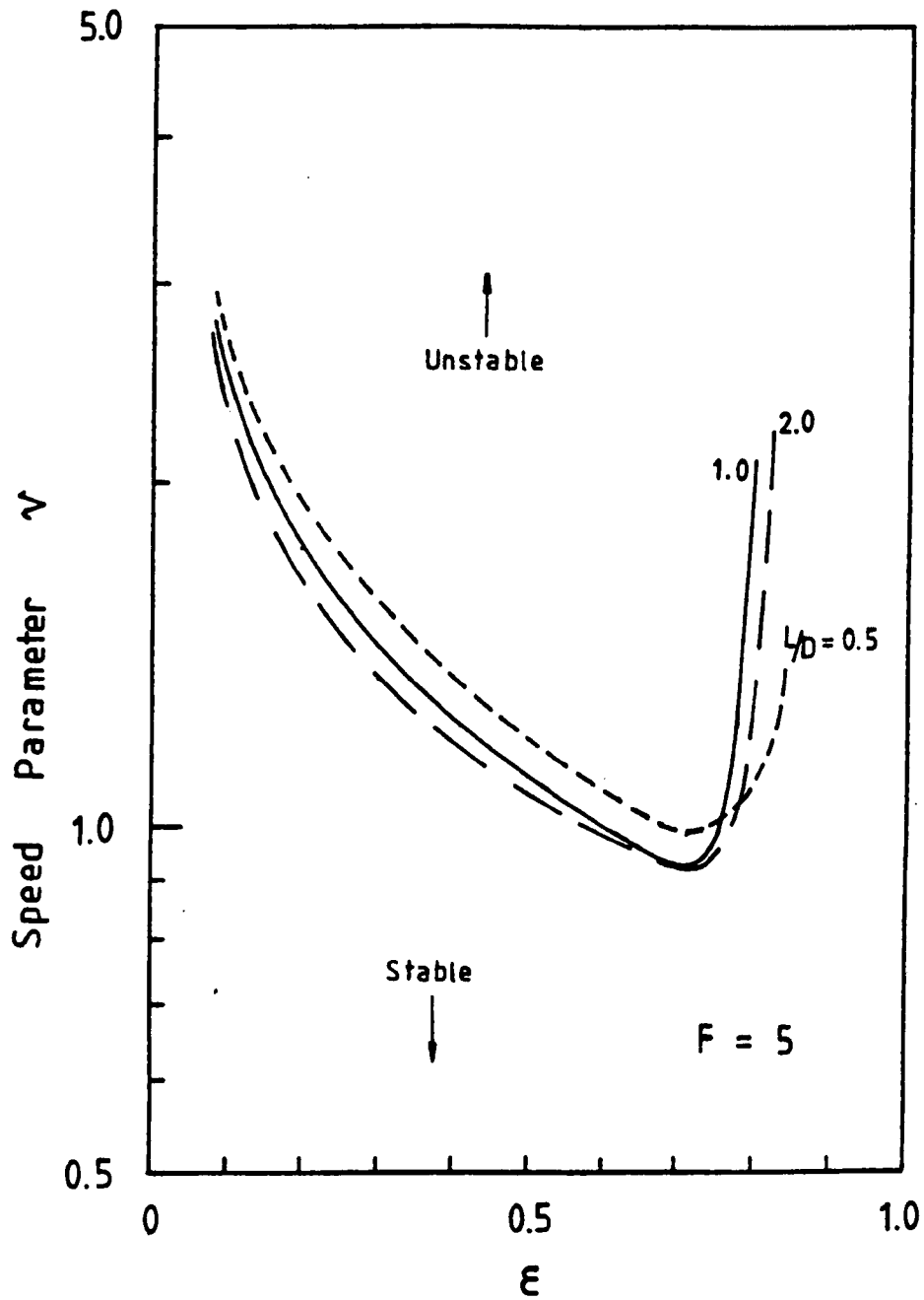
a/L = 0.25

β = 0.5

K = 3.0

Fig.(9.9a): Linearized Stability Map Comparing Plain
Hybrid (Slot-Entry) Bearings To Other
Bearing Configurations. (L/D = 1.0)
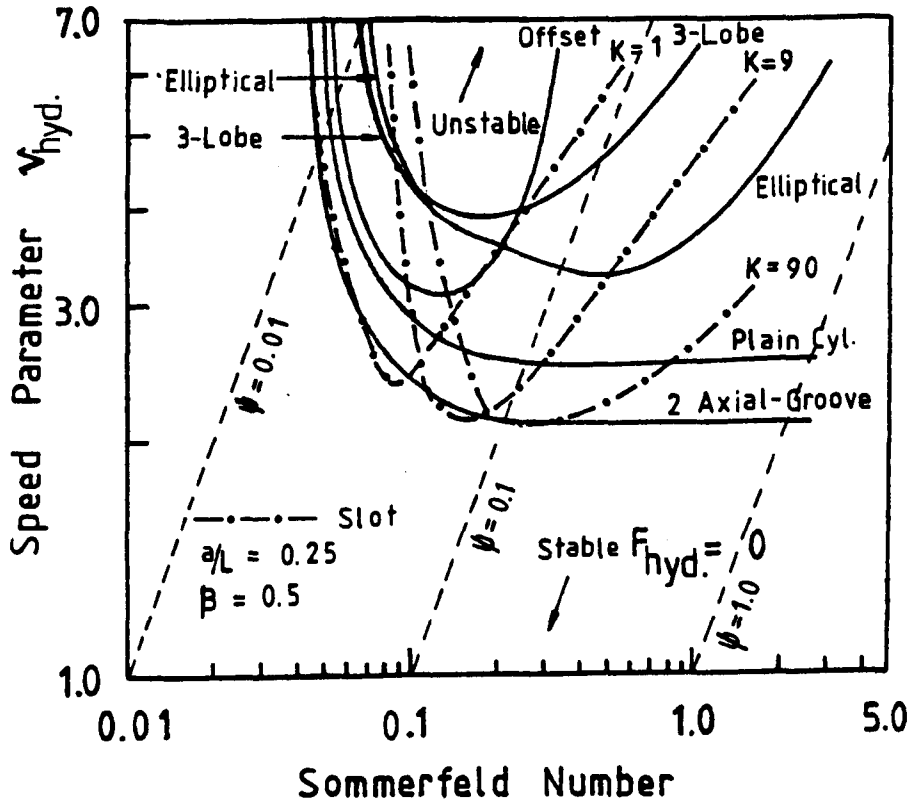
Fig.(9.9b) : Whirl Speed Ratio Versus Sommerfeld
Number. (L/D = 1.0)
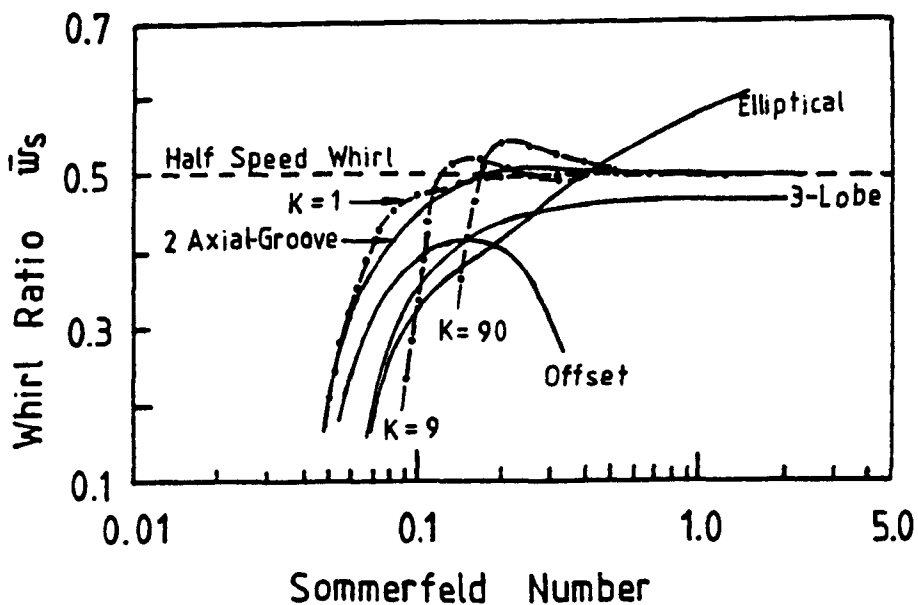
Fig.(9.10a): Linearized Stability Map Comparing Plain
Hybrid (Slot-Entry) Bearings To Other
Bearing Configurations. (L/D = 1.0)
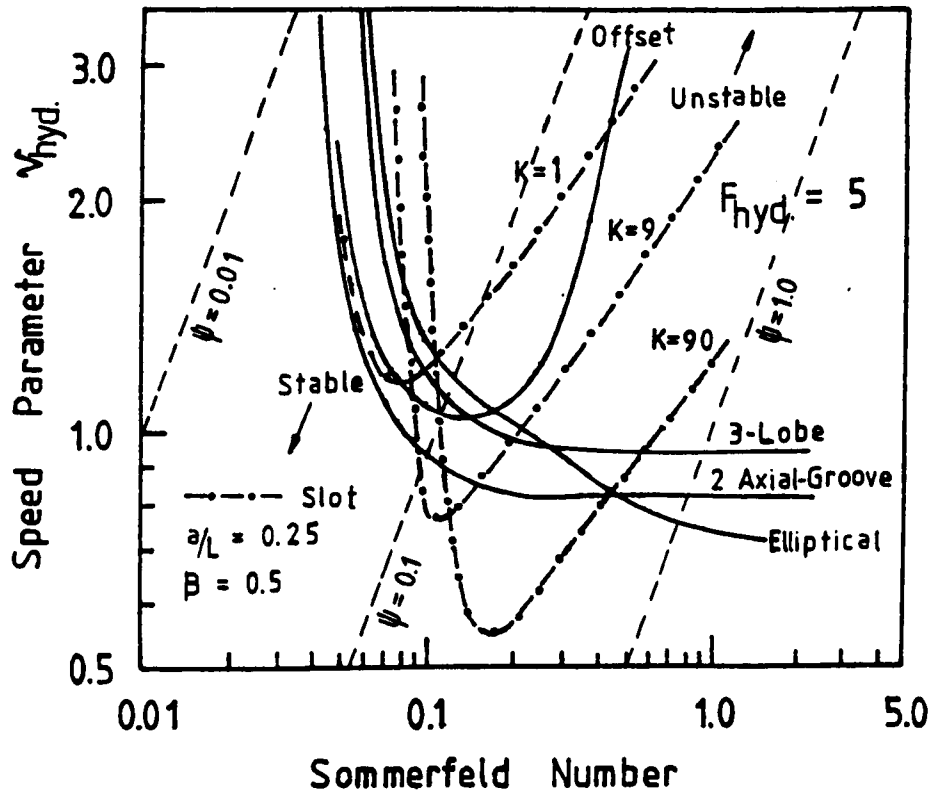
Fig.(9.10b): Whirl Speed Ratio Versus Sommerfeld
Number. (L/D = 1.0)
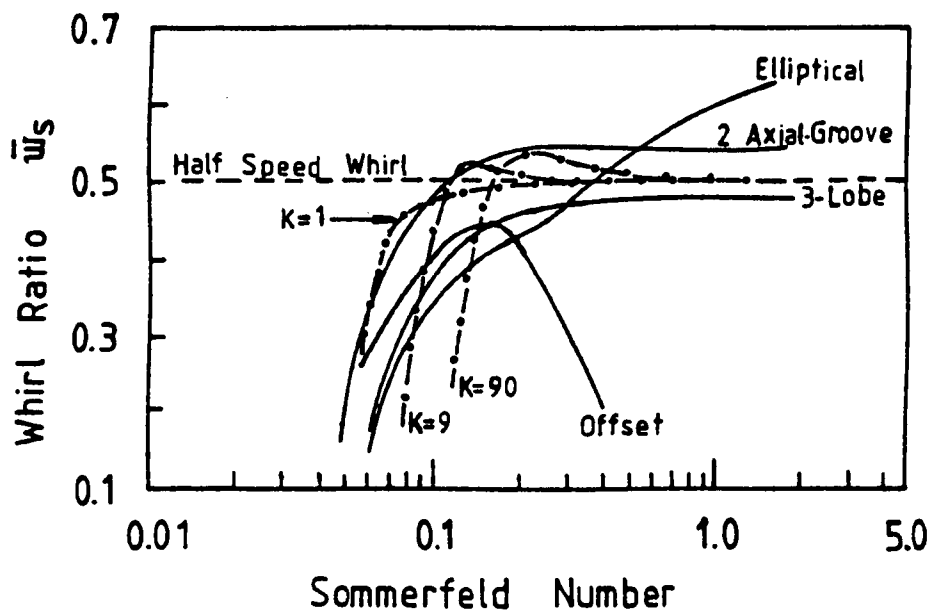
Fig.(9.11): Variation Of Minimum Film Thickness With Sommerfeld Number For Various Bearing Configurations. (L/D = 1.0)
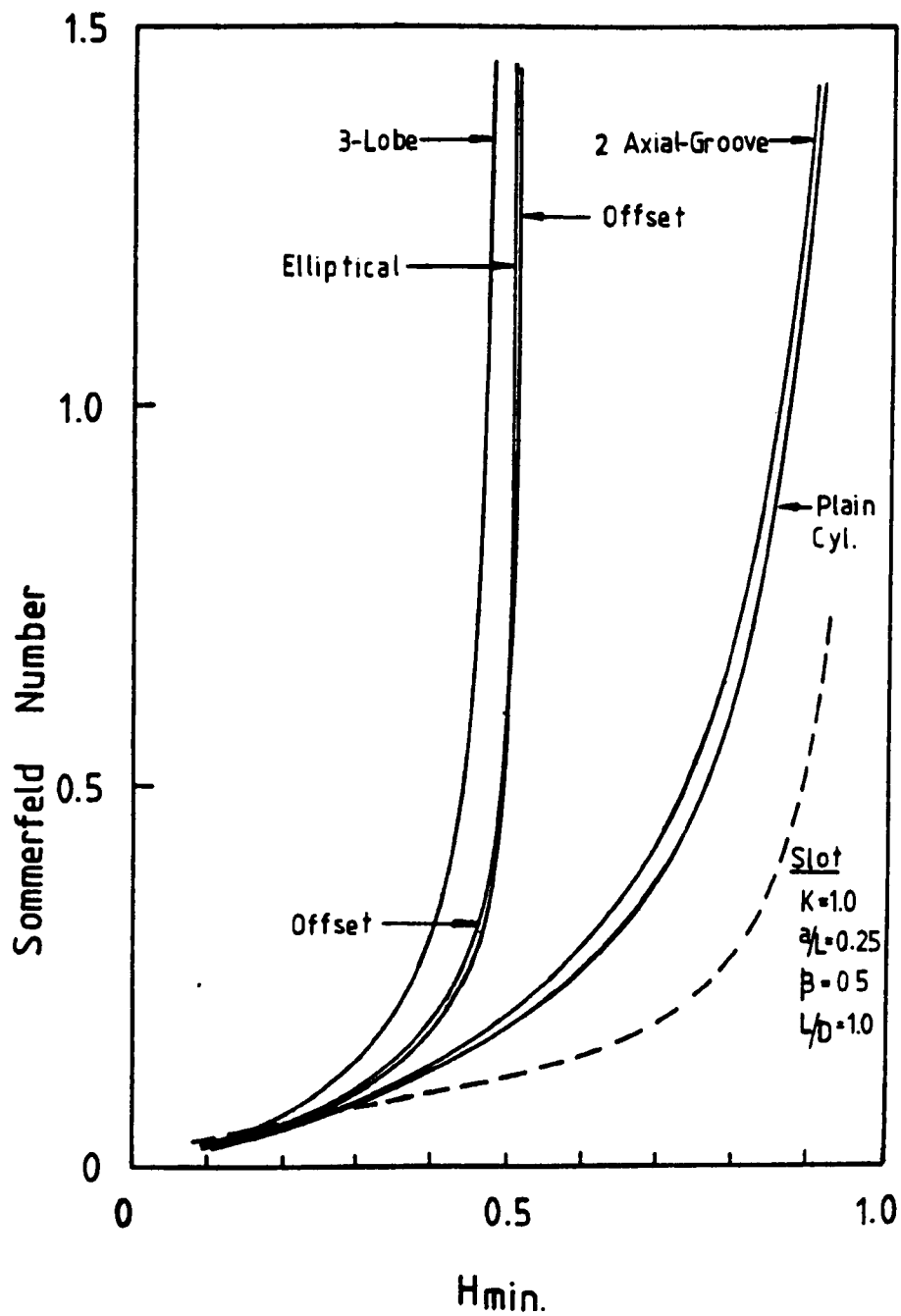
REFERENCES

1. Hahn, E. J.   'The excitability of flexible rotors in short sleeve bearings', Jnl. of Lub. Tech. Jan. 1975, pp 105 - 115.

2. Lund, J. W. and Thomsen, K. K.   'A calculation method and data for the dynamic coefficients of oil lubricated journal bearings', Topics in Fluid-film bearings and rotor bearing system design and optimization, The American Soc. of Mech. Engrs., 1978.

3. Routh, E. J.   'A treatise on the stability of a given state of motion', Macmillan Co.

4. Hamming, R. W.   'Numerical methods for Scientist and Engineers', McGraw-Hill, N.Y., 1962.

5. Allaire, P. E.   'Design of journal bearings for high speed rotating machinery', Fundamentals of the Design of fluid-film bearings. The American Soc. of Mech. Engrs., 1979.

CHAPTER 10

CONCLUSIONS AND SUGGESTIONS FOR FUTURE RESEARCH

10.1 Summary of Major Results and Conclusions

This research has developed and presented results for the stiffness and damping coefficients of slot-entry bearings, theoretical and experimental frequency responses of the bearing fluid-film and stability of rigid and flexible rotors in slot-entry bearings. An experimental technique, employing data-logging and computer processing has been incorporated into the dynamic measurement system, resulting in an automatic testing procedure. The results and conclusions may be summarized as follows:

1) A general form of the differential equation governing the pressure distribution in a bearing has been presented and may be used in the analysis of hydrostatic, hydrodynamic or hybrid bearings, thus paving the way to a unifying approach in the study of thin-film lubrication.

2) A Perturbation technique and also a Finite-Disturbance technique of predicting the dynamic force coefficients for slot-entry hybrid journal bearings have been presented. The two techniques serve to provide a cross-check on the correctness of the results and this has proved valuable in refining the computations. Hence, two finite difference programs, PFD.FOR and FFD.FOR were developed.

3) A lumped parameter technique, which is as accurate as the finite difference solutions but much faster has been presented. However, the lumped parameter results for values $^a/L \geqslant 0.4$, should be used with caution, as the lumped parameter method tended to underestimate the bearing reaction forces in this region.

4) Stability limits have been presented for rigid and flexible rotors in externally pressurized bearings using a single mass rotor model.

5) Non-dimensional parameters governing the relationship between the hydrostatic and hydrodynamic modes of lubrication have been defined, and provide a basis for comparing the performance characteristics of hydrostatic bearings with hydrodynamic bearings.

6) It has been demonstrated that it is feasible to design the circular plain line-entry (slot) hybrid journal bearing to match the stability limits offered by the non-circular bearing configurations.

7) The stability analysis of slot-entry bearings, suggests that, where shaft flexibility is involved, it may be advantageous to move away from the optimum design for static loading.

8) Although, there were reasonable correlations between the theoretical and experimental direct-coupled fluid-film frequency responses, the investigation suggested that the dynamic characteristics of the test shaft and the inertia of the decoupling spring may not be neglected in the analysis.

9) The experimental cross-coupled fluid-film frequency responses could not be accurately determined, due to the low signal to noise ratios.

10) The direct method of extracting the bearing coefficients from the frequency response functions of the fluid-film is inadequate and should be discarded in favour of more refined techniques which can give better accuracy.

10.2 Suggestions for Future Research

The potential of the test rig used in this research work is by no means exhausted. Further investigations into the effects of misalignment, oil supply pressure and other bearing configurations can be carried out with little or no modifications to the rig. It is possible that the present results could be greatly improved if:

(i)   The inertia of the decoupling spring and the dynamic charact-
        eristics of the test shaft were included in the analysis.

(ii)   Better instrumentation providing larger signal to noise ratios
        were used. Such instrumentation should include low frequency,
        low level vibration measuring transducers and filters, and the
        analysis of noise.

(iii)   An identification procedure employing the least squares cri-
        terion be used to determine the bearing coefficients using a
        large volume of data over a range of frequencies.

This research has attempted to integrate the study of rotor dy-
namics and bearing lubrication into a single discipline and explored
the common ground between hydrostatic and hydrodynamic modes of lubri-
cation. Additional data for other bearing configurations can be
produced with some modifications to the computer programs.

APPENDIX I

1. Influence of Bearing Cross-Coupling Coefficients on Stability

For the purpose of demonstrating the effect of bearing cross-coupling characteristics on stability, we shall restrict our analysis to a single mass (2 m) rigid rotor, supported on two equivalent fluid-film bearings, with plane motion and no misalignment, as illustrated in the figure below.
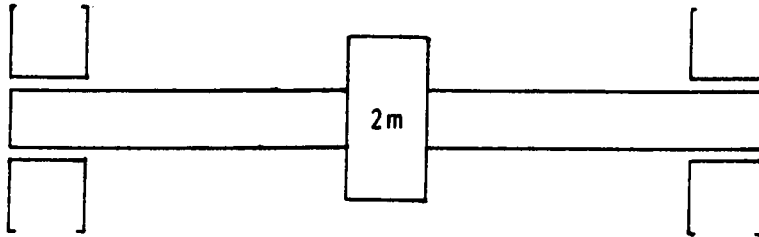
The equations of motion of the single mass rotor are:

$$a_{11}x + a_{12}y + b_{11}\dot{x} + b_{12}\dot{y} + m\ddot{x} = P_x(t)$$
$$a_{21}x + a_{22}y + b_{21}\dot{x} + b_{22}\dot{y} + m\ddot{y} = P_y(t)$$

$$\text{AI-1}$$

Restricting our analysis to the concentric condition yields:

$$a_{11}x + a_{12}y + b_{11}\dot{x} + m\ddot{x} = P_x(t)$$
$$a_{21}x + a_{22}y + b_{22}\dot{y} + m\ddot{y} = P_y(t)$$

$$\text{AI-2}$$

Now at the concentric condition:

$$a_{21} = -a_{12} \qquad\qquad \text{AI-3}$$

Equation AI-2 reduces to:

$$m\ddot{x} + b_{11}\dot{x} + a_{11}x + a_{12}y = P_x(t)$$
$$m\ddot{y} + b_{22}\dot{y} + a_{22}y - a_{12}x = P_y(t)$$

$$\text{AI-4}$$

Equation AI-4 is similar to that derived by Rowe (1), which is:

$$m\ddot{x} + C\dot{x} + \lambda_o x + \lambda_{hd}y = W_o\cos\omega t$$
$$m\ddot{y} + C\dot{y} + \lambda_o y - \lambda_{hd}x = 0$$

$$\text{AI-4a}$$

Taking the laplace transform of equation AI-4 and writing in matrix form yields:

$$\begin{bmatrix} (s^2 + sb'_{11} + a'_{11}) & a'_{12} \\ - a'_{12} & (s^2 + sb'_{22} + a'_{22}) \end{bmatrix} \begin{bmatrix} x(s) \\ y(s) \end{bmatrix} = \begin{bmatrix} P_x(s) \\ P_y(s) \end{bmatrix} \qquad \text{AI-5}$$

where: $\qquad a'_{ij} = \dfrac{a_{ij}}{m}$

$$b'_{ij} = \dfrac{b_{ij}}{m}$$

or:

$$\begin{bmatrix} \dfrac{(s^2 + sb'_{22} + a'_{22})}{D(s)} & \dfrac{-a'_{12}}{D(s)} \\ \dfrac{a'_{12}}{D(s)} & \dfrac{(s^2 + sb'_{11} + a'_{11})}{D(s)} \end{bmatrix} \begin{bmatrix} P_x(s) \\ P_y(s) \end{bmatrix} = \begin{bmatrix} x(s) \\ y(s) \end{bmatrix} \qquad \text{AI-6}$$

Hence, with force excitation in the x-direction only, one obtains for motion in the x-direction, the transfer function:

$$\frac{x(s)}{P_x(s)} = \frac{(s^2 + sb'_{22} + a'_{22})}{D(s)} \qquad \text{AI-7}$$

where: D(s), the characteristic function of the system is the fourth

degree polynomial.

$$D(s) = s^4 + s^3 (b'_{11} + b'_{22}) + s^2 (a'_{11} + a'_{22} + b'_{11} b'_{22}) \dots$$

$$\dots + s(a'_{11} b'_{22} + a'_{22} b'_{11}) + (a'_{11} a'_{22} + a'^2_{12}) \qquad \text{AI-8}$$

The stability of the governing equation of motion of the system as represented by equation AI-4, is obtained by examination of the characteristic equation denoted in equation AI-8. Whereas transfer functions such as equation AI-7 need to be considered, if the actual response of the system is desired, it is sufficient to examine the roots D(s), if the stability of the system be of interest.

Let equation AI-8 be represented by:

$$D(s) = \sum_{i=o}^{n} A^{n-i} s^{i} \qquad \text{AI-9}$$

Applying the Routh-Hurwitz stability criteria:

$$\left. \begin{aligned} D_0 &= A_1 > 0 \\ D_1 &= A_1 A_2 - A_0 A_3 > 0 \\ D_2 &= A_3 D_1 - A_4 A_1^{2} > 0 \end{aligned} \right\} \qquad \text{AI-10}$$

Expanding D_2 yields:

$$A_1 A_2 A_3 > A_4 A_1^{2} + A_0 A_3^{2} \qquad \text{AI-11}$$

.. For stability:

$$(a'_{11} b'_{22} + a'_{22} b'_{11})(a'_{11} + a'_{22} + b'_{11} b'_{22})(b'_{11} + b'_{22}) \ldots$$

$$\ldots > (a'_{11} b'_{22} + a'_{22} b'_{11})^{2} + (a'_{11} a'_{22} + a'_{12}^{2})(b'_{11} + b'_{22}) \qquad \text{AI-12}$$

Expanding and rearranging yields:

$$(a'_{11} - a'_{22})^{2} + (b'_{11} + b'_{22})(a'_{11} b'_{22} + a'_{22} b'_{11}) \ldots$$

$$\ldots > a'_{12}^{2} \frac{(b'_{11} + b'_{22})^{2}}{b'_{11} b'_{22}} \qquad \text{AI-13}$$

Therefore equation AI-13 represents the necessary condition for stability.

The above analysis clearly shows that:

1) If the cross-coupling coefficients (a_{12} and a_{21}) are zero, the system is completely stable, since the right hand side vanishes.

2) Bearing asymmetry ($a_{11} \neq a_{22}$) will raise the stability limit, hence the threshold speed of instability will increase.

Reference

1. Rowe, W. B., Weston, W. and Koshal, D. 'Static and dynamic properties of concentric hydrostatic journal bearings', The Euromech Colloquim No.124, Orbassano, Italy, Oct. 1979.

APPENDIX II

Derivation of the Optimization Parameter for Hybrid Bearings

The parameter S_h, is fundamental to bearings which involve both pressure and velocity induced flows. As evidenced from rearrangement of the non-dimensional form of the Reynolds equation, as shown below:

$$\frac{\partial}{\partial X}\left(H_o^3 \frac{\partial \bar{P}_o}{\partial X} \right) + \left(\frac{D}{L}\right)^2 \frac{\partial}{\partial Z}\left(H_o^3 \frac{\partial \bar{P}_o}{\partial Z} \right)$$

$$= 24 \pi S_h \frac{\partial H_o}{\partial X} - \frac{12 \eta D^2}{P_s C^3} \frac{S_{fo}}{\rho} \qquad \text{AII-1}$$

The group $\dfrac{\eta N}{P_s} \left(\dfrac{D}{C_d} \right)^2$ is termed S_h \qquad AII-2

The optimum value is determined by minimizing the total power dissipation at the concentric condition, as follows:

Total power = friction power + pumping power

i.e. $H_t = H_f + H_p$ \qquad AII-3

The friction power H_f, depends on the geometry of the bearing (the wetted area). For non-recessed bearings, the Petroff value is used, while for recessed bearings, the friction area, A_f, is modified to take approximate account of the recess recirculation effect. Therefore, for both recessed and plain bearings, H_f, has the same form, although the values will be different.

$$H_f = \frac{\eta A_f U^2}{C_c} \qquad \text{AII-4}$$

where: $A_f = \dfrac{A_R}{4} + A_L$ (for a 4-recessed journal bearing)

$A_f = \pi L D$ (for plain journal bearings).

The pumping power depends on the geometry of the bearing too. A non-dimensional flow factor, $\bar{B}$, is introduced into the expression for pumping power which varies with different types of bearings.

$$H_p = P_s \, q$$

For the double slot-entry bearing:

$$H_p = P_s \left(2 \, P_{i,d} \; \frac{\pi \, D \, C^3}{12 \, \eta \, a} \right)$$

$$\text{i.e} \quad H_P = \frac{P_s^2 \, \beta \, B \, C^3}{\eta} \qquad\qquad \text{AII-5}$$

where:

$$\bar{B} = \frac{\pi D}{6a}$$

The minimum power conditions (ignoring the constraints which must be built into design procedures) is achieved with the minimum clearance consistent with tolerancing and varying viscosity. Alternatively, the clearance may be varied.

Differentiating total power with respect to viscosity and equating to zero yields:

$$\frac{d \, H_t}{d \, \eta} = \frac{d \, H_f}{d \, \eta} + \frac{d \, H_p}{d \, \eta} = 0$$

$$= \frac{A_f \, U^2}{C} - \frac{P_s^2 \, \beta \, \bar{B} \, C^3}{\eta^2} = 0$$

$$= \frac{H_f}{\eta} - \frac{H_p}{\eta} = 0$$

Hence, $H_f = H_p$ \qquad\qquad AII-6

Or in general, $H_f = K \, H_p$, where K must be equal to 1, in this case. If the clearance is the varying factor, K will be equal to 3. Thus:

$$\frac{\eta \, A_f \, U^2}{C} = \frac{K \, P_s^2 \, \beta \, \bar{B} \, C^3}{\eta}$$

$$\frac{\eta \, A_f \, (\pi D N)^2}{C} = \frac{K \, P_s^2 \, \beta \, \bar{B} \, C^3}{\eta}$$

$$\left(\frac{\eta \, N}{P_s} \right)^2 \left(\frac{D}{C_d} \right)^4 = \frac{K \, \beta \, \bar{B} \, D^2}{16 \, \pi^2 \, A_f}$$

Therefore, $\quad S_h = \frac{1}{4\pi} \sqrt{\dfrac{K \, \beta \, \bar{B}}{\bar{A}_f}}$ \qquad\qquad AII-7

The optimum value of S_h corresponds to K = 1, so that:

$$S_{ho} = \frac{1}{4\pi} \sqrt{\frac{\beta \bar{B}}{\bar{A}_f}}$$ AII-8

and, $$S_h = S_{ho} \sqrt{K}$$ AII-9

The value of S_{ho} is unique for a given bearing geometry and concentric pressure ratio, β for a purely hydrodynamic bearing β = 1.

It can also be shown that the maximum temperature rise across an optimized bearing is only dependent on the supply pressure. The adiabatic temperature rise may be expressed as:

$$\Delta T = \frac{H_t}{\rho \, q \, C_v}$$

At the optimized condition, $H_f = H_p$.

$\therefore$ $$H_t = 2 \, H_p \text{ or } 2 \, H_f$$

Hence, $$\Delta T = \frac{2 \, H_p}{\rho \, q \, C_v}$$

Therefore, $$\Delta T = \frac{2 \, P_s}{\rho \, C_v}$$ AII-10

Also, it can be shown that the power ratio, K, has an additional significance for maximum temperature rise.

$$\Delta T = \frac{H_f + H_p}{\rho \, q \, C_v}$$

$$= \frac{\left(\dfrac{H_f}{H_p} + 1\right)}{\rho \, C_v \, \dfrac{q}{H_p}}$$

Thus, $$\Delta T = \frac{P_s \, (K+1)}{\rho \, C_v}$$ AII-11

APPENDIX III

Evaluation of the Source Flow Term

The source flow may be expressed as:

$$q_{si} = q_{soi} + \delta q_{si} \qquad \text{AIII-1}$$

(1) At the static equilibrium position,

$$q_{si} = q_{soi}$$

Let, n_s, be the number of feed-slots in the bearing, and, let the feed-slots be located at $j = d$. The flow through the ith feed-slot may be expressed as:

$$q_{soi} = (P_s - P_{oi,d}) \frac{a_s \ z_s^3}{12 \ \eta \ y_s} \qquad \text{AIII-2}$$

For concentric flow, q_{soi}, is equal to the flow through the ith outer land, that is:

$$q_{soi} = P_{oi,d} \frac{\pi \ D}{a \ n} \frac{h_{oi}^3}{12 \ \eta} \qquad \text{AIII-3}$$

Non-dimensionally:

Equation AIII-2 may be expressed as:

$$\frac{12 \ \eta}{P_s \ C^3} \ q_{soi} = (1 - \bar{P}_{oi,d}) \frac{a_s \ Z_s^3}{y_s} \qquad \text{AIII-4}$$

where:

$$z_s^3 = Z_s^3 \ C^3$$

and equation AIII-3 may be expressed as:

$$\frac{12 \ \eta}{P_s \ C^3} \ q_{soi} = \bar{P}_{oi,d} \frac{\pi \ D}{a \ n_s} \ H_{oi}^3 \qquad \text{AIII-5}$$

Equating equations AIII-4 and AIII-5, yields:

$$\frac{a_s \ Z_s^3}{y_s} = \frac{\bar{P}_{oi,d}}{(1 - \bar{P}_{oi,d})} \frac{\pi \ D}{a \ n_s} \ H_{oi}^3$$

At the concentric condition:

$$\bar{P}_{oi,d} = \beta$$

$$H_{oi} = H_{oi}^3 = 1$$

Therefore,
$$\frac{a_s \, z_s^{\,3}}{y_s} = \frac{\beta}{(1 - \beta)} \left(\frac{\pi \, D}{a \, n_s} \right) \qquad \text{AIII-6}$$

Hence, the source flow term is expressed as:

$$\frac{12 \, \eta}{P_s \, C^3} \, q_{soi} = (1 - \bar{P}_{oi,d}) \, \frac{\beta}{(1 - \beta)} \left(\frac{\pi \, D}{a \, n_s} \right) \qquad \text{AIII-7}$$

In equation AIII-7, it has been assumed that there is one element per slot. Let n_e, be the number of elements per slot, and within the limits of assumption (9), as outlined in Section 4.4, a general equation for the source term to include any arbitrary number of elements per slot may be expressed as:

$$\frac{12 \, \eta}{P_s \, C^3} \, q_{soi} = (1 - \bar{P}_{oi,d}) \left(\frac{\beta}{1 - \beta} \right)\left(\frac{\pi \, D}{a \, n_s} \right)\left(\frac{n_s}{n_e} \right) \qquad \text{AIII-8}$$

(2)   At the dynamic condition:

$$\delta q_{si} = q_{si} - q_{soi} \qquad \text{AIII-9}$$

Therefore, non-dimensionally equation AIII-9 may be expressed as:

$$\frac{12 \, \eta}{P_s \, C^3} \, \delta q_{si} = \frac{12 \, \eta}{P_s \, C^3} \, q_{si} - \frac{12 \, \eta}{P_s \, C^3} \, q_{soi}$$

$$= \left(\frac{\beta}{1 - \beta} \right)\left(\frac{\pi \, D}{a \, n_s} \right)\left(\frac{n_s}{n_e} \right)\left[\left(1 - \bar{P}_{i,d} \right) - \left(1 - \bar{P}_{oi,d} \right) \right]$$

Now, $\bar{P}_{i,d} = \bar{P}_{oi,d} + \delta \bar{P}_{i,d}$

Hence:

$$\frac{12 \, \eta}{P_s \, C^3} \, \delta q_{si} = - \left(\frac{\beta}{1 - \beta} \right) \left(\frac{\pi \, D}{a \, n_s} \right)\left(\frac{n_s}{n_e} \right) \delta \bar{P}_{i,d} \qquad \text{AIII-10}$$

APPENDIX IV

Derivation of the Lumped Flow Terms for the Lumped Parameter Theory

The expressions for the lumped flow terms are derived and presented below. The flows corresponding to each control volume are illustrated in Figure (4.5)

1.   Derivation of the Expressions Governing the Pressure Induced Flows

The pressure induced flows may be expressed as:

$$q^P_i = - \frac{dP_i}{dx} \frac{bh_i^3}{12\eta}$$

where: b, is the width of the lumped section,

x, is the length of the lumped section.

Substituting the expressions for $\frac{dP_i}{dx}$, as derived in Appendix V, the pressure induced flows are thus established.

Hence, the expressions for the pressure induced flows at control volume 'OUTER', may be expressed as:

$$q^P_{1i} = - \left.\frac{dP_i}{dx}\right|_{x=a} \frac{\pi D}{n_e} \frac{h_i^3}{12\eta}$$

$$= (4 P_{ai} - P_i) \left(\frac{\pi D}{a \, n_e} \right) \frac{h_i^3}{12\eta}$$

Non-dimensionally, q^P_{1i}, may be expressed as:

$$\bar{q}^P_{1i} = (4 \bar{P}_{ai} - \bar{P}_i) \left(\frac{\pi D}{a \, n_e} \right) H_i^3 \qquad\qquad \text{AIV-1}$$

where: $$\bar{q}^P_{1i} = \frac{12 \, \eta}{P_s \, C_o^3} \, q^P_{1i}$$

$$q^P_{2i} = - \left.\frac{dP_i}{dx}\right|_{x=\frac{a}{2}} \frac{\pi D}{n_e} \frac{h_i^3}{12 \, \eta}$$

$$= P_i \left(\frac{\pi D}{a \, n_e} \right) \frac{h_i^3}{12 \, \eta}$$

Or, $$\bar{q}^P_{2i} = \bar{P}_i \left(\frac{\pi D}{a \, n_e} \right) H_i^3 \qquad\qquad \text{AIV-2}$$

$$q^p_{5i} = - \frac{dP_i}{dx} \left(\frac{a}{2} \right) \frac{h_i^3 - \frac{1}{2}}{12 \, \eta}$$

$$= \left[\left(\frac{2}{3} P_{ai-1} - \frac{1}{12} P_{i-1} \right) - \left(\frac{2}{3} P_{ai} - \frac{1}{12} P_i \right) \right] \left(\frac{a}{2} \right) \left(\frac{n_e}{\pi \, D} \right) \frac{h_i^3 - \frac{1}{2}}{12 \, \eta}$$

Or, $$\bar{q}^p_{5i} = \left[\left(\frac{2}{3} \bar{P}_{ai-1} - \frac{1}{12} \bar{P}_{i-1} \right) - \left(\frac{2}{3} \bar{P}_{ai} - \frac{1}{12} \bar{P}_i \right) \right] \frac{1}{2} \left(\frac{a \, n_e}{\pi \, D} \right) H_i^3 - \frac{1}{2}$$

$$\ldots \quad \text{AIV-3}$$

Similarly,

$$\bar{q}'^p_{5i} = \left[\left(\frac{2}{3} \bar{P}_{ai} - \frac{1}{12} \bar{P}_i \right) - \left(\frac{2}{3} \bar{P}_{ai+1} - \frac{1}{12} P_{i+1} \right) \right] \frac{1}{2} \left(\frac{a \, n_e}{\pi \, D} \right) H_{i+\frac{1}{2}}$$

$$\ldots \quad \text{AIV-4}$$

The expressions for the pressure induced flows at control volume 'SOURCE', are as follows:

$$q^p_{3i} = - \frac{dP_i}{dx} \bigg|_{x=\frac{L'}{4}} \frac{\pi \, D}{n_e} \frac{h_i^3}{12 \, \eta}$$

$$= 2 \, (P_{ci} - P_i) \frac{\pi \, D}{n_e} \frac{h_i^3}{(L - 2a) \, 12 \, \eta}$$

Or, $$\bar{q}^p_{3i} = 2 \, (\bar{P}_{ci} - \bar{P}_i) \left(\frac{\pi \, D}{n_e} \right) \frac{H_i^3}{(L - 2a)} \qquad \text{AIV-5}$$

$$q^p_{6i} = - \frac{dP_i}{dx} \left(\frac{a}{2} \right) \frac{h_i^3 - \frac{1}{2}}{12 \, \eta}$$

$$= \left[\left(\frac{5}{12} P_{i-1} + \frac{2}{3} P_{ai-1} \right) - \left(\frac{5}{12} P_i + \frac{2}{3} P_{ai} \right) \right] \left(\frac{a}{2} \right) \left(\frac{n_e}{\pi D} \right) \frac{h_i^3 - \frac{1}{2}}{12 \, \eta}$$

Or, $$\bar{q}^p_{6i} = \left[\left(\frac{5}{12} \bar{P}_{i-1} + \frac{2}{3} \bar{P}_{ai-1} \right) - \left(\frac{5}{12} \bar{P}_i + \frac{2}{3} \bar{P}_{ai} \right) \right] \frac{1}{2} \left(\frac{a \, n_e}{\pi \, D} \right) H_i^3 - \frac{1}{2}$$

$$\ldots \quad \text{AIV-6}$$

Similarly,

$$\bar{q}'^p_{6i} = \left[\left(\frac{5}{12} P_i + \frac{2}{3} P_{ai} \right) - \left(\frac{5}{12} P_{i+1} + \frac{2}{3} P_{ai+1} \right) \right] \frac{1}{2} \left(\frac{a \, n_e}{\pi \, D} \right) H_i^3 + \frac{1}{2}$$

$$\ldots \quad \text{AIV-7}$$

$$q^p_{7i} = - \frac{dP_i}{dx} \frac{(L - 2a)}{4} \frac{h_i^3 - \frac{1}{2}}{12 \, \eta}$$

$$= \left[\left(\frac{1}{4}\, P_{ci-1} + \frac{3}{4}\, P_{i-1}\right) - \left(\frac{1}{4}\, P_{ci} + \frac{3}{4}\, P_i\right)\right] \frac{(L-2a)}{4} \left(\frac{n_e}{\pi D}\right) \frac{h_i^{\,3}}{12\,\eta} {}_{-\frac{1}{2}}$$

Or, $\quad \bar{q}^p_{\;71} = \left[\left(\frac{1}{4}\, \bar{P}_{ci-1} + \frac{3}{4}\, \bar{P}_{i-1}\right) - \left(\frac{1}{4}\, \bar{P}_{ci} + \frac{3}{4}\, \bar{P}_i\right)\right] \frac{(L-2a)}{4} \left(\frac{n_e}{\pi D}\right) H_i^{\,3} {}_{-\frac{1}{2}}$

$$\text{... AIV-8}$$

Similarly,

$$\bar{q}^{\prime p}_{\;\;71} = \left[\left(\frac{1}{4}\, \bar{P}_{ci} + \frac{3}{4}\, \bar{P}_i\right) - \left(\frac{1}{4}\, \bar{P}_{ci+1} + \frac{3}{4}\, \bar{P}_{i+1}\right)\right] \frac{(L-2a)}{4} \left(\frac{n_e}{\pi D}\right) H_i^{\,3} {}_{+\frac{1}{2}}$$

$$\text{... AIV-9}$$

The source flow, $\bar{q}_{si}$, is as evaluated in Appendix III.

The expressions for the pressure induced flows at control volume 'CENTRAL', are:

$$q^p_{\;4i} = -\left.\frac{dP_i}{dx}\right|_{x=0} \frac{\pi\, D}{n_e} \frac{h_i^{\,3}}{12\eta}$$

$$= 0$$

Thus, $\bar{q}^p_{\;4i} = 0$ $\hspace{4cm}$ AIV-10

$$q^p_{\;8i} = -\frac{dP_i}{dx} \frac{(L-2a)}{4} \frac{h_i^{\,3}}{12\,\eta} {}_{-\frac{1}{2}}$$

$$= \left[\left(\frac{1}{12}\, P_{i-1} + \frac{11}{12}\, P_{ci-1}\right) - \left(\frac{1}{12}\, P_i + \frac{11}{12}\, P_{ci}\right)\right] \frac{(L-2a)}{4} \left(\frac{n_e}{\pi D}\right) \frac{h_i^{\,3}}{12\,\eta} {}_{-\frac{1}{2}}$$

Or, $\quad \bar{q}^p_{\;8i} = \left[\left(\frac{1}{12}\, P_{i-1} + \frac{11}{12}\, P_{ci-1}\right) - \left(\frac{1}{12}\, P_i + \frac{11}{12}\, P_{ci}\right)\right] \frac{(L-2a)}{4} \left(\frac{n_e}{\pi D}\right) H_i^{\,3} {}_{-\frac{1}{2}}$

$$\text{... AIV-11}$$

Similarly,

$$\bar{q}^{\prime p}_{\;\;8i} = \left[\left(\frac{1}{12}\, \bar{P}_i + \frac{11}{12}\, \bar{P}_{ci}\right) - \left(\frac{1}{12}\, \bar{P}_{i+1} + \frac{11}{12}\, \bar{P}_{ci+1}\right)\right] \frac{(L-2a)}{4} \left(\frac{n_e}{\pi D}\right) H_i^{\,3} {}_{+\frac{1}{2}}$$

$$\text{... AIV-12}$$

2. __Derivation of the Expressions Governing the Velocity Induced Flows__

The velocity induced flows may be expressed as:

$$q^v_{\;i} = \frac{\pi\, D\, N}{2} \times (\text{Cross-Sectional Area})$$

Therefore, the expressions for the velocity induced flows at control

volume 'OUTER', are as follows:

$$q^v_{51} = \frac{\pi \, D \, N}{2} \left(\frac{a}{2} \right) h_{i-\frac{1}{2}}$$

Non-dimensionally, q^v_{51}, may be expressed as:

$$\bar{q}^{-v}_{51} = \frac{12 \, \eta}{P_s \, C} \frac{\pi \, D \, N}{2} \left(\frac{a}{2} \right) H_{i-\frac{1}{2}}$$

$$= 12 \frac{\eta \, N}{P_s} \left(\frac{D}{C_d} \right)^2 \pi \left(\frac{a}{L} \right) \left(\frac{L}{D} \right) H_{i-\frac{1}{2}}$$

Or, $\bar{q}^{-v}_{51} = 12 \, \pi \, S_h \left(\frac{a}{L} \right) \left(\frac{L}{D} \right) H_{i-\frac{1}{2}}$ AIV-13

Similarly,

$$\bar{q}^{-'v}_{51} = 12 \, \pi \, S_h \left(\frac{a}{L} \right) \left(\frac{L}{D} \right) H_{i+\frac{1}{2}}$$ AIV-14

At control volume 'SOURCE' the expressions for the velocity induced flows are, thus, expressed as:

$$q^v_{61} = \frac{\pi \, D \, N}{2} \left(\frac{a}{2} \right) h_{i-\frac{1}{2}}$$

Or, $\bar{q}^{-v}_{61} = 12 \, \pi \, S_h \left(\frac{a}{L} \right) \left(\frac{L}{D} \right) H_{i-\frac{1}{2}}$ AIV-15

Similarly,

$$\bar{q}^{-'v}_{61} = 12 \, \pi \, S_h \left(\frac{a}{L} \right) \left(\frac{L}{D} \right) H_{i+\frac{1}{2}}$$ AIV-16

$$q^v_{71} = \frac{\pi \, D \, N}{2} \frac{(L-2a)}{4} h_{i-\frac{1}{2}}$$

Non-dimensionally, q^v_{71}, may be expressed as:

$$\bar{q}^{-v}_{71} = 6 \frac{\eta \, N}{P_s} \left(\frac{D}{C_d} \right)^2 \pi \left(\frac{L}{D} \right) \left(1 - \frac{2a}{L} \right) H_{i-\frac{1}{2}}$$

Or, $\bar{q}^{-v}_{71} = 6 \, \pi \, S_h \left(1 - \frac{2a}{L} \right) \left(\frac{L}{D} \right) H_{i-\frac{1}{2}}$ AIV-17

Similarly,

$$\bar{q}^{-'v}_{71} = 6 \, \pi \, S_h \left(1 - \frac{2a}{L} \right) \left(\frac{L}{D} \right) H_{i+\frac{1}{2}}$$ AIV-18

The velocity induced flows at control volume 'CENTRAL', are, thus, as follows:

$$q^v_{81} = \frac{\pi \, D \, N}{2} \frac{(L-2a)}{4} h_{i-\frac{1}{2}}$$

that is, $\bar{q}^{v}_{81} = 6 \pi S_h \left(1 - \frac{2a}{L}\right)\left(\frac{L}{D}\right) H_{i-\frac{1}{2}}$

<div align="right">AIV-19</div>

Similarly,

$$\bar{q}'^{v}_{81} = 6 \quad S_h \left(1 - \frac{2a}{L}\right)\left(\frac{L}{D}\right) H_{i+\frac{1}{2}}$$

<div align="right">AIV-20</div>

3. Derivation of the Expressions Governing the Squeeze Induced Flows

The squeeze induced flows may be evaluated as follows:

$$q^{sq}_i = - \frac{dh_i}{dt} \quad x \quad (\text{Projected Area})$$

Thus, the expression for the squeeze induced flow at control volume 'OUTER', is:

$$q^{sq}_{5i} = - \frac{dh_i}{dt}\left(\frac{a}{2}\right) D \, \text{Sin} \left(\frac{\pi}{n_e}\right)$$

Non-dimensionally, q^{sq}_{5i}, may be expressed as:

$$\bar{q}^{sq}_{5i} = - \frac{dH_i}{dt}\left(\frac{a}{2}\right) D.\text{Sin}\left(\frac{\pi}{n_e}\right) \frac{12 \, \eta}{P_s \, C^2}$$

$$= - \frac{dH_i}{dt} \quad 24 \quad \frac{\eta}{P_s} \left(\frac{D}{C_d}\right)^2 \left(\frac{a}{L}\right)\left(\frac{L}{D}\right) \quad \text{Sin} \left(\frac{\pi}{n_e}\right)$$

Now, $\dfrac{dH_i}{dt} = \dot{\varepsilon} \, \text{Cos}\left[\theta_i - (\alpha - \phi_o)\right]$

<div align="right">AIV-21</div>

Hence,

$$\bar{q}^{sq}_{5i} = - 24 \frac{\eta \dot{\varepsilon}}{P_s} \left(\frac{D}{C_d}\right)^2 \left(\frac{a}{L}\right)\left(\frac{L}{D}\right) \text{Sin}\left(\frac{\pi}{n_e}\right) \text{Cos}\left[\theta_i - (\alpha - \phi_o)\right]$$

Or,

$$\bar{q}^{sq}_{5i} = - 24 \, S_s \left(\frac{a}{L}\right)\left(\frac{L}{D}\right) \text{Sin}\left(\frac{\pi}{n_e}\right) \text{Cos}\left[\theta_i - (\alpha - \phi_o)\right]$$

<div align="right">AIV-22</div>

where: $S_s = \dfrac{\eta \dot{\varepsilon}}{P_s} \left(\dfrac{D}{C_d}\right)^2$

The expressions for the squeeze induced flows at control volume 'SOURCE' are, thus:

$$q^{sq}_{6i} = - \frac{dh_i}{dt} \left(\frac{a}{2}\right) D \, \text{Sin}\left(\frac{\pi}{n_e}\right)$$

Non-dimensionally, q^{sq}_{6i}, may be expressed as:

$$\bar{q}^{-sq}_{61} = - 24 \, S_s \left(\frac{a}{L} \right) \left(\frac{L}{D} \right) \, Sin \left(\frac{\pi}{n_e} \right) \, Cos \left[\theta_i - (\alpha - \phi_o) \right] \qquad \text{AIV-23}$$

$$q^{sq}_{71} = - \frac{dh_i}{dt} \left(\frac{L-2a}{4} \right) \, D \, Sin \left(\frac{\pi}{n_e} \right)$$

It can also be shown that, non-dimensionally, q^{sq}_{71}, may be expressed as:

$$\bar{q}^{-sq}_{71} = - 12 \, S_s \left(1 - \frac{2a}{L} \right) \left(\frac{L}{D} \right) \, Sin \left(\frac{\pi}{n_e} \right) \, Cos \left[\theta_i - (\alpha - \phi_o) \right] \qquad \text{AIV-24}$$

At control volume 'CENTRAL', the expression for the squeeze induced flow is as follows:

$$q^{sq}_{81} = - \frac{dh_i}{dt} \left(\frac{L-2a}{4} \right) \, D \, Sin \left(\frac{\pi}{n_e} \right)$$

Non-dimensionally, q^{sq}_{81}, may be expressed as:

$$\bar{q}^{-sq}_{81} = - 12 \, S_s \left(1 - \frac{2a}{L} \right) \left(\frac{L}{D} \right) \, Sin \left(\frac{\pi}{n_e} \right) \, Cos \left[\theta_i - (\alpha - \phi_o) \right] \qquad \text{AIV-25}$$

APPENDIX V

Derivation of the Expressions Governing the Axial Pressure

Distribution at the Outer and Central Lands

1. **The Outer Land**

The assumed axial pressure distribution (quadratic pressure pro-file) of the outer land and the co-ordinate system used in the subsequent analysis, is illustrated below:
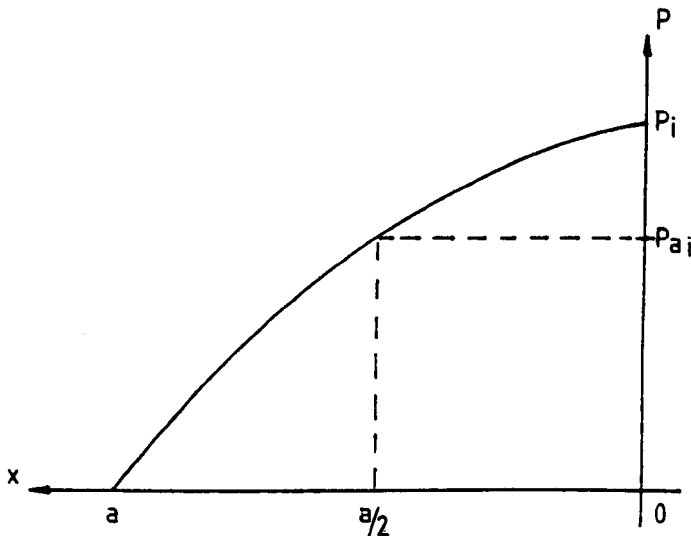
Figure illustrating the quadratic pressure profile

and the corresponding co-ordinate system

(a) **The Expression Governing the Axial Pressure Distribution**

The governing equation may be expressed as:

$$P = Ax^2 + Bx + C \qquad\qquad AV-1$$

The boundary conditions are:

(i) $\qquad\qquad$ At $x = 0$; $P = P_i$

Therefore, $\qquad C = P_i$

(ii) $\qquad\qquad$ At $x = {}^a/2$; $P = P_{ai}$

Hence, $\qquad P_{ai} = A \, ({}^a/2)^2 + B \, ({}^a/2) + P_i$

Therefore, $\qquad A = \left[P_{ai} - P_i - B \, ({}^a/2) \right] \, ({}^2/a)^2 \qquad\qquad AV-2$

(iii)   At $x = a$; $P = 0$

Hence, $0 = A\ a^2 + B\ a + P_i$

Therefore, $A = -\ (B\ a + P_i)\Big/\ a$ AV-3

Equating equations AV-2 and AV-3, yields:

$$B = (4\ P_{ai} - 3\ P_i)\Big/\ a$$

$$A = (2\ P_i - 4\ P_{ai})\Big/\ a^2$$

Therefore, the equation governing the axial pressure distribution of

the outer land may be expressed as:

$$P = (2\ P_i - 4\ P_{ai})\left(\frac{x}{a}\right)^2 + (4\ P_{ai} - 3\ P_i)\left(\frac{x}{a}\right) + P_i \qquad \text{AV-4}$$

(b)   <u>The Expression Governing the Variation of the Axial Pressure along</u>
      <u>the Outer Land $\left(\frac{dp}{dx}\right)$</u>

      The term, $\left(\frac{dp}{dx}\right)$ may be evaluated by differentiating equation,

AV-4, with respect to x.

Therefore,

$$\frac{dP}{dx} = (4\ P_i - 8\ P_{ai})\left(\frac{x}{a^2}\right) + (4\ P_{ai} - 3\ P_i)\left(\frac{1}{a}\right) \qquad \text{AV-5}$$

(i)   At $x = 0$; $\frac{dP}{dx}$, may be expressed as:

$$\left.\frac{dP}{dx}\right|_{x\ =\ 0} = (4\ P_{ai} - 3\ P_i)\left(\frac{1}{a}\right) \qquad \text{AV-6}$$

(ii)   At $x = \frac{a}{2}$; $\frac{dP}{dx}$, may be expressed as:

$$\left.\frac{dP}{dx}\right|_{x\ =\ a/2} = -\ \frac{P_i}{a} \qquad \text{AV-7}$$

(iii)   At $x = a$; $\frac{dP}{dx}$, may be expressed as:

$$\left.\frac{dP}{dx}\right|_{x\ =\ a} = (P_i - 4\ P_{ai})\left(\frac{1}{a}\right) \qquad \text{AV-8}$$

(c)   <u>Derivation of the Expression Governing the Resultant Pressure,</u>
      <u>Pm, of the Outer Land</u>

      The resultant pressure, Pm, may be expressed by the following

relationship:

$$Pm = \frac{1}{dx} \int_{x_1}^{x_2} P\ dx$$

and, substituting the expression for, P, from equation AV-4, yields:

$$Pm = \frac{1}{dx} \int_{x_1}^{x_2} \left[(2 P_i - 4 P_{ai}) \left(\frac{x}{a}\right)^2 + (4 P_{ai} - 3 P_i)\left(\frac{x}{a}\right) + P_i \right] dx$$

or,
$$Pm = \frac{1}{dx} \left[(2 P_i - 4 P_{ai}) \frac{x^3}{3 a^2} + (4 P_{ai} - 3 P_i) \frac{x^2}{2 a} + P_i x + D \right]_{x_1}^{x_2}$$

$$\ldots \text{AV-9}$$

(i) At $0 < x < \frac{a}{2}$

$$Pm = \frac{2}{a} \left[(2 P_i - 4 P_{ai}) \frac{a}{24} + (4 P_{ai} - 3 P_i) \frac{a}{8} + P_i \frac{a}{2} \right]$$

that is:
$$Pm = \frac{5}{12} P_i + \frac{2}{3} P_{ai} \qquad\qquad \text{AV-10}$$

(ii) At $\frac{a}{2} < x < a$

$$Pm = \frac{2}{a} \left[\left((2 P_i - 4 P_{ai}) \frac{a}{3} + (4 P_{ai} - 3 P_i) \frac{a}{2} + P_i a + D \right) \ldots \right.$$

$$\left. \ldots - \left((2 P_i - 4 P_{ai}) \frac{a}{24} + (4 P_{ai} - 3 P_i) \frac{a}{8} + P_i \frac{a}{2} + D \right) \right]$$

that is:
$$Pm = \frac{2}{3} P_{ai} - \frac{1}{12} P_i \qquad\qquad \text{AV-11}$$

2. The Central Land

The assumed axial pressure distribution (parabolic pressure profile) of the central land and the co-ordinate system used in the subsequent analysis, is illustrated below.
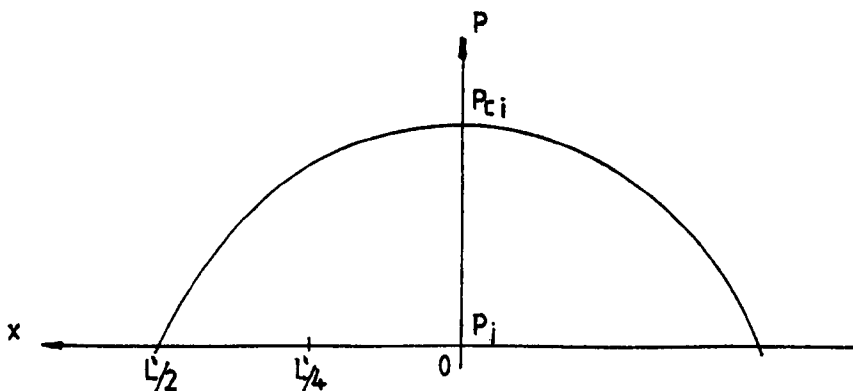
Figure illustrating the parabolic pressure profile

and the corresponding co-ordinate system

(a) The Expression Governing the Axial Pressure Distribution

The equation governing the pressure distribution at the central

land is the equation of a parabola, and may be expressed as:

$$P = P_i + (P_{ci} - P_i)(1 - (\frac{2x}{L'})^2)$$ AV-12

where: $L' = (L-2a)$

(b) The Expression Governing the Variation of the Axial Pressure

Along the Central Land ($^{dP}/dx$)

The term, $^{dP}/dx$, may be evaluated by differentiating equation,

AV-12, with respect to x.

Therefore:

$$\frac{dP}{dx} = 8 \left(\frac{x}{L'^2}\right)\left(P_i - P_{ci}\right)$$ AV-13

(i) At $x = 0$; $\frac{dP}{dx}$, may be expressed as:

$$\frac{dP}{dx}\bigg|_{x = 0} = 0$$ AV-14

(ii) At $x = \frac{L'}{4}$; $\frac{dP}{dx}$, may be expressed as:

$$\frac{dP}{dx}\bigg|_{x = \frac{L'}{4}} = 2\left(P_i - P_{ci}\right)\bigg/L'$$ AV-15

(iii) At $x = \frac{L'}{2}$; $\frac{dP}{dx}$, may be expressed as:

$$\frac{dP}{dx}\bigg|_{x = \frac{L'}{2}} = 4\left(P_i - P_{ci}\right)\bigg/L'$$ AV-16

(c) Derivation of the Expression Governing the Resultant Pressure,

Pm, of the Central Land

The resultant pressure, Pm, may be expressed by the following

relationship:

$$Pm = \frac{1}{dx} \int_{x_1}^{x_2} P \, dx$$

and, substituting the expression for, P, from equation AV-12, yields:

$$Pm = \frac{1}{dx} \int_{x_1}^{x_2} \left[P_i + (P_{ci} - P_i)(1 - (\frac{2x}{L'})^2) \right] dx$$

$$\text{or,} \quad Pm = \frac{1}{dx} \left[P_i \, x + (P_{ci} - P_i) \, x - \frac{4}{3}(P_{ci} - P_i) \frac{x^3}{L'^2} + D \right]_{x_1}^{x_2}$$

$$\dots \text{ AV-17}$$

(i) At $0 < x < \frac{L'}{4}$;

$$Pm = \frac{4}{L} \left[P_i \left(\frac{L'}{4} \right) + (P_{ci} - P_i) \frac{L'}{4} - \frac{4}{3}(P_{ci} - P_i) \frac{L'^3}{64 \, L'^2} \right]$$

$$\text{or,} \quad Pm = \frac{1}{12} P_i + \frac{11}{12} P_{ci} \qquad\qquad \text{AV-18}$$

(ii) At $\frac{L'}{4} < x < \frac{L'}{2}$;

$$Pm = \frac{4}{L'} \left[\left(P_i \left(\frac{L'}{2} \right) + (P_{ci} - P_i) \frac{L'}{2} - \frac{4}{3}(P_{ci} - P_i) \frac{L'^3}{8 \, L'^2} + D \right) \dots \right.$$

$$\left. \dots \left(- P_i \left(\frac{L'}{4} \right) + (P_{ci} - P_i) \frac{L'}{4} - \frac{4}{3}(P_{ci} - P_i) \frac{L'^3}{64 \, L'^2} + D \right) \right]$$

$$\text{or,} \quad Pm = \frac{1}{4} P_{ci} + \frac{3}{4} P_i \qquad\qquad \text{AV-19}$$

Appendix VI

Analytical Method in Bearing Coefficients

Evaluation - A Review

The computation of the bearing dynamic coefficients, requires the calculation of a pressure field and a summation of the pressures to produce the bearing reaction forces. The pressure field is normally determined from Reynolds equation, which is insoluble in closed form and only amenable to approximate numerical solutions via the use of specific boundary conditions. (See Section 2.1). The evaluation of the bearing dynamic coefficients, therefore, involves:

(1) deriving analytical approximations for the relationship between the fluid-film force and the position and velocity of the journal centre, and

(2) solving the lubrication equation in conjunction with specific boundary conditions, to obtain the bearing reaction forces.

Various analytical approximations governing the relationship between the fluid-film force and the journal centre displacement and velocity vectors have been used by bearing researchers. They may be grouped into two categories, namely, the finite disturbance or perturbation techniques.

By applying a finite displacement and a finite velocity to the journal centre, the change in fluid-film forces at each static-equilibrium position may be computed. This is the basis of the finite disturbance technique. References on this technique can be seen in the papers by Sternlicht (1), Woodcock and Holmes (4), Singh D.V., et. al (6), Craighead I.A., et.al (10) and many others. The approach, and hence, the procedures employed in the analysis differs between investigators. In general, 3 types of approaches may be distinguished.

(1) Direct Approach

This approach requires the bearing reaction forces for each direction of disturbance to be computed directly from the lubrication equation. A minimum of 5 sets of computations are required. Basically, bearing reaction forces and attitude angles are computed for each of the following:

(a) $\delta x = \delta y = \delta \dot{x} = \delta \dot{y} = 0$; and $\varepsilon = \varepsilon_o$

(b) $\delta y = \delta \dot{x} = \delta \dot{y} = 0$; $\delta x \neq 0$ and $\varepsilon = \varepsilon_x$

(c) $\delta x = \delta \dot{x} = \delta \dot{y} = 0$; $\delta y \neq 0$ and $\varepsilon = \varepsilon_y$

(d) $\delta x = \delta y = \delta \dot{y} = 0$; $\delta \dot{x} \neq 0$ and $\varepsilon = \varepsilon_o$, and

(e) $\delta x = \delta y = \delta \dot{x} = 0$; $\delta \dot{y} \neq 0$ and $\varepsilon = \varepsilon_o$.

Computations (a), (b) and (c), will yield information on the stiffness coefficients, while, computations (a), (d) and (e), will provide information on the damping coefficients. Examples of such an analysis, can be seen in the work of Woodcock and Holmes (4), Craighead I. A., et.al. (10) and others.

(2) Indirect Approach

This approach requires four sets of computations, in contrast, to the direct approach, which requires a minimum of 5. A dynamic condition is defined, at $\varepsilon = \varepsilon_d$ and $\phi = \phi_d$, using trigonometric relationships, relating small displacements, δx and δy to the static equilibrium position, ε_o. Another set of dynamical condition, involving the journal centre's whirl velocity, $\dot{\phi}$ and squeeze velocity, $\dot{\varepsilon}$ is also defined. Computations are then carried out for the following conditions:

(a) $\delta x = \delta y = \delta \dot{x} = \delta \dot{y} = 0$; $\varepsilon = \varepsilon_o$

(b) $\delta \dot{x} = \delta \dot{y} = 0$; $\delta x \neq 0$; $\delta y \neq 0$; $\varepsilon = \varepsilon_d$

(c) $\delta x = \delta y = \delta \dot{y} = 0$; $\delta \dot{x} = \varepsilon \, \dot{\phi} \cos \phi_o + \dot{\varepsilon} \sin \phi_o$; $\varepsilon = \varepsilon_o$, and

(d) $\delta x = \delta y = \delta \dot{x} = 0$; $\delta \dot{y} = -\varepsilon \, \dot{\phi} \sin \phi_o + \dot{\varepsilon} \cos \phi_o$; $\varepsilon = \varepsilon_o$.

Computations (a) and (b) in conjunction with the following partial derivations, will provide information on the stiffness coefficients, that is:

$$a_{11} = - \frac{\partial F_x}{\partial x} = - \left(\frac{\partial F_x}{\partial \varepsilon_d} \frac{\partial \varepsilon d}{\partial x} + \frac{\partial F_x}{\partial \phi d} \frac{\partial \phi d}{\partial x} \right)$$

$$a_{12} = - \frac{\partial F_x}{\partial y} = - \left(\frac{\partial F_x}{\partial \varepsilon_d} \frac{\partial \varepsilon d}{\partial y} + \frac{\partial F_x}{\partial \phi d} \frac{\partial \phi d}{\partial y} \right)$$

$$a_{21} = - \frac{\partial F_y}{\partial x} = - \left(\frac{\partial F_y}{\partial \varepsilon_d} \frac{\partial \varepsilon d}{\partial x} + \frac{\partial F_y}{\partial \phi d} \frac{\partial \phi d}{\partial x} \right)$$

$$a_{22} = - \frac{\partial F_y}{\partial y} = - \left(\frac{\partial F_y}{\partial \varepsilon_d} \frac{\partial \varepsilon d}{\partial y} + \frac{\partial F_y}{\partial \phi d} \frac{\partial \phi d}{\partial y} \right)$$

The damping coefficients are obtained from computations (d) and (e). Hence, this method is similar to the direct approach. The difference is in the specification of the journal centre velocity. Examples of such an analysis can be seen in references (6) and (7).

(3) Static Load Locus

This method is only used to evaluate the stiffness coefficients. By writing analytical approximations for small variations about the static equilibrium position and interpreting them in terms of the static characteristics, the stiffness coefficients may be determined.

In contrast to the finite disturbance technique which requires the numerical values of the disturbances (the finite displacements and finite velocities) to be specified, the perturbation technique does not require such specifications. The starting point for the perturbation technique is the formulation of a first order perturbed Reynolds (lubrication) equation. Again, two approaches may be distinguished here – the small amplitude motion approach and the harmonic vibration approach.

The small amplitude motion approach is a technique developed by

Lund (8) to compute the coefficients of hydrodynamic bearings. It is the author's opinion that this technique is currently the best technique available for evaluating the linearized bearing dynamic coefficients. It requires no superfluous assumptions regarding the nature of the vibration. The only requirement is the vibration amplitude should be sufficiently small so as not to invalidate the principles of linearity. Furthermore, complex mathematics is avoided. Two variables, the film thickness, h, and the film-pressure, P, are used to describe the dynamic condition. Hence, at the dynamic condition:

$$h = h_o + \delta h$$

$$P = P_o + \delta P$$

$$(VI-1)$$

where:

$$\delta h = \delta x \cos \theta + \delta y \sin \theta$$

$$\delta P = Px \, \delta x + Py \, \delta y + P\dot{x} \, \delta \dot{x} + P\dot{y} \, \delta \dot{y}$$

By substituting equations (VI-1) into the lubrication equation and collecting terms of zero and first order, results in five equations. One of the equations will give the static equilibrium solution and the remaining four equations will provide the solution for the bearing coefficients. An account of this work can be seen in reference (14), and Chapter 5 of this thesis.

The harmonic vibration approach, assumes that at the dynamic condition, the journal centre is performing a harmonic vibration of frequency, υ. Investigators, such as Chandra, et.al. (13), Malik, et.al. (11) and others, have used an approach similar to that of Lund (8), that is, a first order perturbation with respect to the vibration amplitudes, X and Y are carried out. Hence, the dynamic condition is described by:

$$h = h_o + \delta h = h_o + X \cos \theta + Y \sin \theta$$

$$P = P_o + \delta P = P_o + P_x X + P_y Y$$

$$(VI-2)$$

where:

$$X = R_e \left(|X| \ e^{j \upsilon t} \right)$$

$$Y = R_e \left(|Y| \ e^{j \upsilon t} \right)$$

υ = whirl frequency.

Substituting equations (VI-2) into the lubrication equation and collecting terms of zero and first order, results in three equations. One of the equations will give the static equilibrium solution, while the remaining two equations, which are in complex form will provide information on the bearing coefficients. The stiffness coefficients will be defined by the real part of the solution, while the damping coefficients are defined by the imaginary parts.

Other investigators, such as Wadhwa, et.al. (15) and Singh et.al. (12) performed a first order perturbation with respect to the eccentricity-ratio, ε, and the attitude angle, ϕ. Hence, the dynamic condition is described by:

$$h = h_o + \delta h = h_o + \varepsilon_1 \cos \theta + \varepsilon_o \phi_1 \sin \theta$$

$$P = P_o + \delta P = P_o + \varepsilon_1 P_1 + \varepsilon_o \phi_1 P_2$$

(VI-3)

where:

$$\varepsilon = \varepsilon_o + \varepsilon_1$$

$$\phi = \phi_o + \phi_1$$

$$\varepsilon_1 = R_e \left(|\varepsilon_1| \ e^{j \upsilon t} \right)$$

$$\phi_1 = R_e \left(|\phi_1| \ e^{j \upsilon t} \right)$$

Again, the bearing coefficients are obtained, as outlined in the previous paragraph.

Other authors, such as Childs et.al. (5) have derived 'Impedance' descriptions for deriving the stiffness and damping coefficients. Flexibility influence coefficients (inversions of the stiffness coefficients) have been considered by Holmes (9), who proposed that

the inversions of the corresponding stiffness coefficients should be checked against the flexibility influence coefficients.

Finally, it is appropriate to briefly mention the types of boundary conditions employed in dynamic analysis. A number of investigators, such as Holmes (2) and others, have employed the short bearing approximation in conjunction with the Half-Sommerfeld condition to determine the 8-coefficients analytically. Numerical solutions using finite difference and finite element methods in conjunction with the Reynolds boundary conditions form the bulk of the work on bearing co-efficients evaluation. Examples of such work are those of Woodcock and Holmes (4), Lund (8), Craighead (10) and many others. The Jakobsson-Floberg boundary conditions (film reformation) are not usually employed in bearing dynamic analysis. So far, and to the knowledge of the author, only one report of bearing coefficients evaluation, employing the Jakobsson-Floberg boundary conditions, has appeared in the literature. This was reported by Lundholm (3), who computed the 8-coefficients for the circumferential groove hydrodynamic bearing.

REFERENCES

1.   Sternlicht, B. 'Elastic and damping properties of cylindrical journal bearings', Journal of Basic Engrng., June 1959, pp. 101-108.

2.   Holmes, R. 'The vibration of a rigid shaft on short sleeve bearings', Jnl. of Mech. Engrng. Science., Vol. 2, Vo. 4, 1960, pp. 337-341.

3.   Lundholm, G. 'The circumferential groove journal bearing considering cavitation and dynamic stability', Acta Polytechnica Scandinavica, Mech. Engrng. Series No. 42, 1969.

4. Woodcock, J.S. and Holmes, R. 'Determination and application of the dynamic properties of a turbo-rotor bearing oil film', Proc. Instn. Mech. Engrs., Vol. 184, Pt. 3L, 1969-70, pp. 111-119.

5. Childs, D., Moes, H. and Leeuwen, H. 'Journal bearing impedance descriptions for rotordynamic applications', Jnl. of Lub. Tech., Trans. ASME, April 1977, pp. 198-214.

6. Singh, D.V., Sinhasan, R. and Ghai, R.C. 'Performance characteristics of hydrostatic journal bearings with journal rotation by a finite element method', Wear, 44 (1977), pp. 41-55.

7. Singh, D.V., Sinhasan, R. and Ghai, R.C. 'Static and dynamic analysis of capillary compensated hydrostatic journal bearings by fintie element method', Jnl. of Lub. Tech., Trans. ASME, Oct. 1977, pp. 476-484.

8. Lund, J.W. amd Thomsen, K.K.   'A calculation method and data for the dynamic coefficients of oil lubricated journal bearings', Topics in Fluid-Film Bearing and Rotor Bearing-System Design and Optimisation, The Am. Soc. of Mech. Engrs., New York, 1978.

9. Holmes, R.   'Consistency tests for published data on the stiffness characteristics of journal bearings', Tribology International, Dec. 1978, pp. 325-329.

10. Craighead, I.A., Dowson, D., Sharp, R.S. and Taylor, C.M.   'The influence of thermal effects and shaft mis-alignment on the dynamic behavious of fluid-film bearings', Proceds. of the 6th Leeds-Lyon Symp. on Tribology, Sept. 1979, pp. 47-55.

11. Malik, M., Chandra, M. and Sinhasan, R.   'Performance character-istics of 3-lobe journal bearing configurations', Tribology Int., Vol. 14, No. 6, Dec. 1981, pp. 345-349.

12. Singh, D.V., Sinhasan, R. and Wadhwa, S.S.   'Dynamic performance of plain cylindrical bearings with compressible fluid', Tribology Int., Vol. 15, No. 6, Dec. 1982.

13. Chandra, M., Malik, M. and Sinhasan, R.   'A comparative study of four gas-lubricated noncircular journal bearing configurations', Tribology Int., Vol. 16, No. 2, April 1983, pp. 103-108.

14. Rowe, W.B. and Chong, F.S.   'Computation of dynamic force co-

efficients for hybrid (hydrostatic/hydrodynamic) bearings', Presented at the 3rd. Tribology Conf., Budapest, June 1983.

15. Wadhwa, S.S., Sinhasan, R. and Singh, D.V. 'Analysis of orifice compensated externally pressurized gas bearings', Tribology Int., Vol. 16, No. 4, August 1983, pp. 203-211.

Appendix VII

Derivation of the Perturbed Slot-Entry Bearing Equation

A form of the dynamic state lubrication equation applied to a bearing with source flow is:

$$\frac{\partial}{\partial x}\left((h_o + \delta h)^3 \frac{\partial(P_o + \delta P)}{\partial x}\right) + \frac{\partial}{\partial z}\left((h_o + \delta h)^3 \frac{\partial(P_o + \delta P)}{\partial z}\right) \ldots$$

$$\ldots = 6\,\eta\,U\,\frac{\partial(h_o + \delta h)}{\partial x} + 12\eta\,\frac{\partial(h_o + \delta h)}{\partial t} - \frac{12\eta}{\rho}(S_{fo} + \delta S_f) \quad \text{(AVII-1)}$$

By considering terms of zero and first order only, equation (AVII-1), may be expressed as:

$$\frac{\partial}{\partial x}\left(h_o^3 \frac{\partial P_o}{\partial x} + h_o^3 \frac{\partial \delta P}{\partial x} + 3\,h_o^2\,\delta h\,\frac{\partial P_o}{\partial x}\right) \ldots$$

$$\ldots + \frac{\partial}{\partial z}\left(h_o^3 \frac{\partial P_o}{\partial z} + h_o^3 \frac{\partial \delta P}{\partial z} + 3\,h_o^2\,\delta h\,\frac{\partial P_o}{\partial z}\right) \ldots$$

$$\ldots = 6\,\eta\,U\,\frac{\partial h_o}{\partial x} - \frac{12\eta}{\rho}S_{fo} + 6\,\eta\,U\,\frac{\partial \delta h}{\partial x} \ldots$$

$$\ldots + 12\,\eta\,\frac{\partial \delta h}{\partial t} - \frac{12\eta}{\rho}\,\delta S_f \ldots \quad \text{(AVII-2)}$$

Equation (AVII-2) may be rewritten as:

$$\frac{\partial}{\partial x}\left(h_o^3 \frac{\partial P_o}{\partial x}\right) + \frac{\partial}{\partial z}\left(h_o^3 \frac{\partial P_o}{\partial z}\right) = 6\,\eta\,U\,\frac{\partial h_o}{\partial x} + \frac{12\eta}{\rho}\,S_{fo} \quad \text{(AVII-3)}$$

and,

$$\frac{\partial}{\partial x}\left(h_o^3 \frac{\partial \delta P}{\partial x}\right) + \frac{\partial}{\partial z}\left(h_o^3 \frac{\partial \delta P}{\partial z}\right) \ldots$$

$$\ldots = 6\,\eta\,U\,\frac{\partial \delta h}{\partial x} + 12\eta\,\frac{\partial \delta h}{\partial t} - \frac{12\eta}{\rho}\,\delta S_f \ldots$$

$$\ldots - \frac{\partial}{\partial x}\left(3\,h_o^2\,\delta h\,\frac{\partial P_o}{\partial x}\right) - \frac{\partial}{\partial z}\left(3\,h_o^2\,\delta h\,\frac{\partial P_o}{\partial z}\right) \ldots \quad \text{(AVII-4)}$$

Equation (AVII-3) gives the static equilibrium solution. The solution for the dynamic conditions is given by equation (AVII-4). Equation (AVII-4) may be simplified to yield:

$$\frac{\partial}{\partial x}\left(h_o{}^3 \frac{\partial \delta P}{\partial x}\right) + \frac{\partial}{\partial z}\left(h_o{}^3 \frac{\partial \delta P}{\partial z}\right) \dots$$

$$\dots = 6\,\eta\,U\,\frac{\partial \delta h}{\partial x} + 12\eta\,\frac{\partial \delta h}{\partial t} - \frac{12\eta}{\rho}\,\delta S_f \dots$$

$$\dots - \frac{3}{h_o}\,\delta h\left[\frac{\partial}{\partial x}\left(h_o{}^3 \frac{\partial P_o}{\partial x}\right) + \frac{\partial}{\partial z}\left(h_o{}^3 \frac{\partial P_o}{\partial z}\right)\right] \dots$$

$$\dots - h_o{}^3 \frac{\partial P_o}{\partial x}\,\frac{\partial}{\partial x}\left(3\frac{\delta h}{h_o}\right) - h_o{}^3 \frac{\partial P_o}{\partial z}\,\frac{\partial}{\partial z}\left(3\frac{\delta h}{h_o}\right)$$

Or,

$$\frac{\partial}{\partial x}\left(h_o{}^3 \frac{\partial \delta P}{\partial x}\right) + \frac{\partial}{\partial z}\left(h_o{}^3 \frac{\partial \delta P}{\partial z}\right) \dots$$

$$\dots = 6\,\eta\,U\,\frac{\partial \delta h}{\partial x} + 12\eta\,\frac{\partial \delta h}{\partial t} - \frac{12\eta}{\rho}\,\delta S_f \dots$$

$$\dots - \frac{3}{h_o}\,\delta h\left(6\,\eta\,U\,\frac{\partial h_o}{\partial x} - \frac{12\eta}{\rho}\,S_{fo}\right) \dots$$

$$\dots - 3\,h_o{}^3 \frac{\partial P_o}{\partial x}\,\frac{\partial}{\partial x}\left(\frac{\delta h}{h_o}\right)$$

that is,

$$\frac{\partial}{\partial x}\left(h_o{}^3 \frac{\partial \delta P}{\partial x}\right) + \frac{\partial}{\partial z}\left(h_o{}^3 \frac{\partial \delta P}{\partial z}\right) \dots$$

$$\dots = 6\,\eta\,U\,\frac{\partial \delta h}{\partial x} - \frac{3}{h_o}\,\delta h\,6\,\eta U\,\frac{\partial h_o}{\partial x} \dots$$

$$\dots - 3\,h_o{}^3 \frac{\partial P_o}{\partial x}\,\frac{\partial}{\partial x}\left(\frac{\delta h}{h_o}\right) + 12\eta\,\frac{\partial \delta h}{\partial t} \dots$$

$$\dots + \frac{3}{h_o}\,\delta h\left(\frac{12\eta}{\rho}\,S_{fo}\right) - \frac{12\eta}{\rho}\,\delta S_f \dots \tag{AVII-5}$$

In bearing computational analysis, it is appropriate to work with moving U - V coordinates, aligned with the eccentricity vector. The dynamic pressure, δP, arising from the excursions (δu, δv, $\delta \dot{u}$ and $\delta \dot{v}$) of the journal or bearing may be expressed as:

$$\delta P = P_u\,\delta u + P_v\,\delta v + P_{\dot{u}}\,\delta \dot{u} + P_{\dot{v}}\,\delta \dot{v} \tag{AVII-6}$$

Similarly, δh, may be expressed as:

$$\delta h = \delta u \cos\theta + \delta v \sin\theta \tag{AVII-7}$$

By substituting the expressions for P and h, into equation (AVII-5), the following equation is obtained:

$$\frac{\partial}{\partial x}\left[\left(h_o{}^3\frac{\partial P_u}{\partial x}\right) + \frac{\partial}{\partial z}\left(h_o{}^3\frac{\partial P_u}{\partial z}\right)\right]\delta u + \frac{\partial}{\partial x}\left[\left(h_o{}^3\frac{\partial P_v}{\partial x}\right) + \frac{\partial}{\partial z}\left(h_o{}^3\frac{\partial P_v}{\partial z}\right)\right]\delta v \ldots$$

$$\ldots + \frac{\partial}{\partial x}\left[\left(h_o{}^3\frac{\partial P_{\dot u}}{\partial x}\right) + \frac{\partial}{\partial z}\left(h_o{}^3\frac{\partial P_{\dot u}}{\partial z}\right)\right]\delta\dot u + \frac{\partial}{\partial x}\left[\left(h_o{}^3\frac{\partial P_{\dot v}}{\partial x}\right) + \frac{\partial}{\partial z}\left(h_o{}^3\frac{\partial P_{\dot v}}{\partial z}\right)\right]\delta\dot v \ldots$$

$$\ldots = 6\,\eta\,U\,\frac{\partial}{\partial x}\,(\delta u\sin\theta + \delta v\cos\theta) - \frac{3}{h_o}\,6\,\eta\,U\,\frac{\partial h_o}{\partial x}\,(\delta u\sin\theta + \delta v\cos\theta)\ldots$$

$$\ldots - 3\,h_o{}^3\frac{\partial P_o}{\partial x}\,\frac{\partial}{\partial x}\left(\frac{\delta u\sin\theta + \delta v\cos\theta}{h_o}\right) + 12\eta\,\frac{\partial}{\partial t}\,(\delta u\sin\theta + \delta v\cos\theta)\ \ldots$$

$$\ldots + \frac{3}{h_o}\left(\frac{12\eta}{\rho}\,S_{fo}\right)(\delta u\sin\theta + \delta v\cos\theta) - \frac{12\eta}{\rho}\,\delta S_f \qquad\text{(AVII-8)}$$

By introducing the non-dimensional terms as defined in equations (5.17) of Chapter 5, into equation (AVII-8), and multiplying through by $\frac{D^2}{C\,P_s}$, and simplifying results in equation (AVII-9):

$$\left[\frac{\partial}{\partial X}\left(H_o{}^3\frac{\partial\bar P_u}{\partial X}\right) + \left(\frac{D}{L}\right)^2\frac{\partial}{\partial Z}\left(H_o{}^3\frac{\partial\bar P_u}{\partial Z}\right)\right]\delta\bar u \ldots$$

$$\ldots + \left[\frac{\partial}{\partial X}\left(H_o{}^3\frac{\partial\bar P_v}{\partial X}\right) + \left(\frac{D}{L}\right)^2\frac{\partial}{\partial Z}\left(H_o{}^3\frac{\partial\bar P_v}{\partial Z}\right)\right]\delta\bar v \ldots$$

$$\ldots + \left[\frac{\partial}{\partial X}\left(H_o{}^3\frac{\partial\bar P_{\dot u}}{\partial X}\right) + \left(\frac{D}{L}\right)^2\frac{\partial}{\partial Z}\left(H_o{}^3\frac{\partial\bar P_{\dot u}}{\partial Z}\right)\right]\delta\bar{\dot u} \ldots$$

$$\ldots + \left[\frac{\partial}{\partial X}\left(H_o{}^3\frac{\partial\bar P_{\dot v}}{\partial X}\right) + \left(\frac{D}{L}\right)^2\frac{\partial}{\partial Z}\left(H_o{}^3\frac{\partial\bar P_{\dot v}}{\partial Z}\right)\right]\delta\bar{\dot v} \ldots$$

$$\ldots = 6\,\eta\,U\,\frac{D}{P_s\,C^3}\,\frac{\partial}{\partial X}\,(\delta\bar u\sin\theta + \delta\bar v\cos\theta)\,C \ldots$$

$$\ldots - \frac{3}{H_o}\,6\,\eta\,U\,\frac{D}{P_s\,C^3}\,\frac{\partial H_o}{\partial X}\,(\delta\bar u\sin\theta + \delta\bar v\cos\theta)\,C \ldots$$

$$\ldots - 3\,H_o{}^3\frac{\partial\bar P_o}{\partial X}\,\frac{\partial}{\partial X}\left(\frac{\delta\bar u\sin\theta + \delta\bar v\cos\theta}{H_o}\right)\ldots$$

$$\ldots + 12\,\eta\,\omega_o\,C\,\frac{\partial}{\partial\tau}\,(\delta\bar u\sin\theta + \delta\bar v\cos\theta)\,\frac{D^2}{C^3\,P_s}\ \ldots$$

$$\ldots + \frac{3}{H_o} \left(\frac{12\ \bar\eta}{P_s\ C^3} \ \frac{D^2}{\rho}\ S_{fo} \right) (\delta \bar u\ \sin\theta + \delta \bar v\ \cos\theta) \ldots$$

$$\ldots - \frac{12\ \eta}{P_s\ C^3}\ \frac{D^2}{\rho}\ \delta S_f \qquad\qquad (AVII\text{-}9)$$

Now:

$$q_{so} = \frac{D^2\ S_{fo}}{\rho} \left(\frac{L}{D} \right) \Delta X\ \Delta Z$$

Hence,

$$S_{fo} = q_{so} \left(\frac{D}{L} \right) \frac{1}{\Delta X\ \Delta Z} \qquad\qquad (AVII\text{-}10)$$

Similarly,

$$\delta S_f = \delta q_s \left(\frac{D}{L} \right) \frac{1}{\Delta X\ \Delta Z} \qquad\qquad (AVII\text{-}11)$$

By substituting the expressions for S_{fo} and δS_f, into equation (AVII-9) and simplifying, the following equation is obtained:

$$\left[\frac{\partial}{\partial X} \left(H_o^3\ \frac{\partial \bar P_u}{\partial X} \right) + \frac{\partial}{\partial Z} \left(H_o^3\ \frac{\partial \bar P_u}{\partial Z} \right) \left(\frac{D}{L} \right)^2 \right] \delta \bar u \ldots$$

$$\ldots + \left[\frac{\partial}{\partial X} \left(H_o^3\ \frac{\partial \bar P_v}{\partial X} \right) + \frac{\partial}{\partial Z} \left(H_o^3\ \frac{\partial \bar P_v}{\partial Z} \right) \left(\frac{D}{L} \right)^2 \right] \delta \bar v \ldots$$

$$\ldots + \left[\frac{\partial}{\partial X} \left(H_o^3\ \frac{\partial \bar P_{\dot u}}{\partial X} \right) + \frac{\partial}{\partial Z} \left(H_o^3\ \frac{\partial \bar P_{\dot u}}{\partial Z} \right) \left(\frac{D}{L} \right)^2 \right] \delta \bar{\dot u} \ldots$$

$$\ldots + \left[\frac{\partial}{\partial X} \left(H_o^3\ \frac{\partial \bar P_{\dot v}}{\partial X} \right) + \frac{\partial}{\partial Z} \left(H_o^3\ \frac{\partial \bar P_{\dot v}}{\partial Z} \right) \left(\frac{D}{L} \right)^2 \right] \delta \bar{\dot v} \ldots$$

$$\ldots = \left[48\ \pi\ S_h \left(\frac{3}{H_o}\ \epsilon\ \sin\theta\ \sin\theta + \cos\theta \right) \ldots \right.$$

$$\ldots - 6\ H_o\ \frac{\partial \bar P_o}{\partial X}\ (H_o\ \cos\theta + \epsilon\ \sin\theta\ \sin\theta)$$

$$\ldots + \frac{3}{H_o} \left(\frac{12\ \eta}{P_s\ C}\ q_{so} \left(\frac{D}{L} \right) \frac{1}{\Delta X\ \Delta Z} \right) \sin\theta \Big]\ \delta \bar u \ldots$$

$$\ldots + \left[48\ \pi\ S_h \left(\frac{3}{H_o}\ \epsilon\ \sin\theta\ \cos\theta - \sin\theta \right) \ldots \right.$$

$$\ldots + 6\ H_o\ \frac{\partial \bar P_o}{\partial X}\ (H_o\ \sin\theta - \epsilon\ \sin\theta\ \cos\theta) \ldots$$

$$\ldots + \frac{3}{H_o} \left(\frac{12\,\eta}{P_s\,C}\, q_{so} \left(\frac{D}{L} \right) \frac{1}{\Delta X\, \Delta Z} \right) \cos\theta \Big] \delta\bar{v} \ldots$$

$$\ldots + \Big[48\,(2\,\pi\, S_{ho})\,\sin\theta \Big]\, \delta\bar{u} \ldots$$

$$\ldots + \Big[48\,(2\,\pi\, S_{ho})\,\cos\theta \Big]\, \delta\bar{v} \ldots$$

$$\ldots - \left(\frac{12\,\eta}{P_s\,C}\, \delta qs \left(\frac{D}{L} \right) \frac{1}{\Delta X\, \Delta Z} \right) \qquad\qquad \text{(AVII-12)}$$

Substituting the expressions for source flows q_{so} and δ_{qs}, as derived in Appendix III, into equation (AVII-12) and rearranging terms results in the formation of four sets of partial differential equations. These equations, together with the steady-state equation, may be expressed in matrix form as:

$$\left[\frac{\partial}{\partial X} \left(H_o^{\,3} \frac{\partial}{\partial X} \right) + \left(\frac{D}{L} \right)^2 \frac{\partial}{\partial Z} \left(H_o^{\,3} \frac{\partial}{\partial Z} \right) - \left(\frac{\pi\, D}{a\, n_s} \right) \left(\frac{n_s}{n_e} \right). \right.$$
$$\left. \ldots \left(\frac{\beta}{1-\beta} \right) \left(\frac{D}{L} \right) \frac{1}{\Delta X\, \Delta Z}. \right]
\begin{bmatrix} \bar{P}_o \\[4pt] \bar{P}_u \\[4pt] \bar{P}_v \\[4pt] \bar{P}_{\dot{u}} \\[4pt] \bar{P}_{\dot{v}} \end{bmatrix} =$$

$$24\,\pi\, S_h\, \frac{\partial H_o}{\partial X} - \left(\frac{\pi\, D}{a\, n_s} \right) \left(\frac{n_s}{n_e} \right) \left(\frac{\beta}{1-\beta} \right) \left(\frac{D}{L} \right) \frac{1}{\Delta X\, \Delta Z}.$$

$$48\,\pi\, S_h \left(\frac{3}{H_o}\, \epsilon\, \sin\theta\sin\theta + \cos\theta \right) - 6\, H_o\, \frac{\partial \bar{P}_o}{\partial X} \left(H_o\, \cos\theta + \epsilon\sin\theta\sin\theta \right) \ldots$$

$$\ldots + \frac{3}{H_o}\,(1-\bar{P}_o) \left(\frac{\pi\, D}{a\, n_s} \right) \left(\frac{n_s}{n_e} \right) \left(\frac{\beta}{1-\beta} \right) \left(\frac{D}{L} \right) \frac{\sin\theta}{\Delta X\, \Delta Z}.$$

$$48\,\pi\, S_h \left(\frac{3}{H_o}\, \epsilon\, \sin\theta\cos\theta - \sin\theta \right) + 6\, H_o\, \frac{\partial \bar{P}_o}{\partial X} \left(H_o\, \sin\theta - \epsilon\sin\theta\cos\theta \right) \ldots$$

$$\cdots \quad + \frac{3}{H_o} \left(1-\bar{P}_o\right)\left(\frac{\pi \ D}{a \ n_s}\right) \ \left(\frac{n_s}{n_e}\right)\left(\frac{\beta}{1-\beta}\right)\left(\frac{D}{L}\right) \ \frac{\cos \ \theta}{\Delta X \ \Delta Z} \ .$$

$$48 \ (2 \ \pi \ S_{ho}) \ \sin \ \theta .$$

$$48 \ (2 \ \pi \ S_{ho}) \ \cos \ \theta .$$

(AVII-13)

The first equation is the steady-state equation. The remaining four equations, give the solution for the dynamic pressures, which can be integrated to obtain the stiffness and damping coefficients of the slot-entry bearing.

Appendix VIII

Derivation of the Frequency Response of a System

Frequency response methods enable the dynamic behaviour of a linear system to be investigated by determining the amplitude and phase of the response to a sinusoidal input of the form:

$$x_i(t) = A_i \sin \omega t \qquad \text{(AVIII-1)}$$

The relationship between the input $x_i(t)$ and the output $x_o(t)$ of a constant parameter linear system may be expressed by a differential equation of the form:

$$(a_n D^n + a_n{-1} D^{n-1} + \ldots + a_1 D + a_o) \, x_i(t) \ldots$$

$$\ldots = (b_m D^m + b_{m-1} D^{m-1} + \ldots + b_1 D + b_o) \, x_o(t)$$

$$\text{(AVIII-2)}$$

where:

the operators $D^n = \dfrac{d^n}{dt^n}$, and

$$D^m = \dfrac{d^m}{dt^m}$$

the coefficients a_i and b_i are constants.

Laplace transforming each term of equation (AVIII-2), when all initial conditions are zero, and rearranging yields:

$$x_o(s) = \left(\frac{a_n s^n + a_n{-1} s^{n-1} + \ldots a_1 s + a_o}{b_m s^m + b_{m-1} s^{m-1} + \ldots b_1 s + b_o} \right) x_i(s)$$

$$= G(s) \, x_i(s) \qquad \text{(AVIII-3)}$$

where, $G(s)$ is the system transfer function which contains basic information concerning the essential characteristics of the system.

Substituting for $x_i(s)$ the laplace transform of $(A_i \sin \omega t)$ which is equal to $\dfrac{A_i \, \omega}{s^2 + \omega^2}$ into equation (AVIII-3) and factorizing results in:

$$x_o(s) = \frac{A_i \, \omega(s-z_1) \, (s-z_2) \, \ldots \ldots \, (s-z_n)}{(s^2 + \omega^2) \, (s-p_1) \, (s-p_2) \, \ldots \ldots \, (s-p_m)} \qquad (AVIII-4)$$

This expression may be rewritten by a partial fraction expansion to give:

$$x_o(s) = A_i \left(\frac{G(s) \, \omega}{s^2 + \omega^2} \right) = A_i \left[\frac{B_1}{s-j\omega} + \frac{B_2}{s+j\omega} + \frac{C_1}{s-p_1} + \frac{C_2}{s-p_2} \, \cdots \right.$$

$$\left. \cdots + \frac{C_m}{s-p_m} \right] \qquad (AVIII-5)$$

where,

B_1, B_2, C_1, C_2 ... C_m are constants,

p_1, p_2, ... p_m are the poles of $G(s)$

Taking the Laplace inverse of equation (AVIII-5) gives the time response as:

$$x_o(t) = A_i \left[B_1 \, e^{j\omega t} + B_2 e^{-j\omega t} + C_1 \, e^{p_1 t} \, \cdots \right.$$

$$\left. \cdots + C_2 \, e^{p_2 t} + \ldots \ldots C_m \, e^{p_m t} \right] \qquad (AVIII-6)$$

The first two terms denote the particular integral component of the solution and provide the steady-state response, while the remaining terms describe the complementary function, the transient response. For the case in which the real parts of the poles are negative, the terms describing the transient part decay to zero with time.

Hence the steady-state response is:

$$x_o(t)_{ss} = A_i \left[B_1 e^{j\omega t} + B_2 \, e^{-j\omega t} \right] \qquad (AVIII-7)$$

To determine the coefficient B_1, multiply both sides of equation (AVIII-5) by $(s-j\omega)$ and then let $s = j\omega$:

$$B_1 = \left[\frac{(s-j\omega) \, G(s)\omega}{s^2 + \omega^2} \right]_{s \, = \, j\omega}$$

$$= \left[\frac{G(s) \, \omega}{s + j\omega} \right]_{s \, = \, j\omega}$$

$$= \frac{G(j\omega)}{2j}$$

i.e. $B_1 = \frac{1}{2j} \left| G(j\omega) \right| e^{j \, \angle \, G(j\omega)} \qquad (AVIII-8)$

Similarly, B_2 may be obtained by multiplying equation (AVIII-5) by $(s + j\omega)$ and let $s = -j\omega$.

$$B_2 = \left[\frac{(s + j\omega)\ G\ (s)\omega}{s^2 + \omega^2} \right]_{s = -j\omega}$$

$$= \frac{G\ (-j\omega)}{-2j}$$

i.e. $B_2 = -\frac{1}{2j} \left| G(j\omega) \right| e^{-j \angle G\ (j\omega)}$ \hfill (AVIII-9)

The steady state expression for the output is therefore:

$$x_o(t)_{ss} \left| G(j\omega) \right| \frac{1}{2j} \left[e^{j\omega t + j \angle G(j\omega)} - e^{-j\omega t - j \angle G(j\omega)} \right]$$

that is:

$$x_o(t)_{ss} = A_i \left| G(j\omega) \right| \sin (\omega t + \angle G\ (j\omega))$$

or,

$$x_o(t)_{ss} = A_o \sin (\omega t + \angle G\ (j\omega))$$ \hfill (AVIII-10)

Hence:

The amplitude ratio, $\dfrac{A_o}{A_i} = \left| G\ (j\omega) \right|$

and the phase angle, $\angle G(j\ ) = \tan^{-1} \left\{ \dfrac{I_m\ G(j\omega)}{R_e\ G(j\omega)} \right\}$ \hfill (AVIII-11)

Equation (AVIII-10), represents the frequency response of the system with transfer function $G(s)$. It is evident that, if the system is excited by a sinusoid of amplitude A_i, the steady-state system output is also a sinusoid of equal frequency with amplitute $A_o = A_i \left| G(j\omega) \right|$, and phase angle, $\arg G(j\omega)$. If $\left| G(j\omega) \right|$ and angle of arg. $G(j\omega)$, are determined, then the system is identified.

Appendix IX

A) Method to Determine the Stiffness of the Test-Shaft

A general arrangement of the test-shaft system is illustrated in figure (1). Figure (2) illustrates the dimensional details of the test-shaft. The full details of the test-shaft have been presented in Reference (1), hence, only the details that are relevant to this analysis will be mentioned. The properties of the shaft are as follows:

(i)   Material: Nitride hardened EN40A chrome molybdenum steel.

(ii)   Density, ρ: 0.7832 x 10^{-5} kg. - mm^{-3}

(iii)   Modulus of elasticity, E: 206 x 10^{-3} N - μm^{-2}

(iv)   Nominal diameter, d: 40 mm

(v)   Total length, L_t: 475 mm

(vi)   Length between supports, L: 257 mm

The following characteristics are calculated based on the above properties:

(i)   Mass of shaft, m_s: 0.7832 x 10^{-5} x $\frac{\pi}{4}$ $(40)^2$ x 475 = 4.67 kg.

(ii)   Weight of shaft, W_s: 4.67 x 9.81 = 45.86 N.

(iii)   Polar moment of Inertia, I: $\frac{\pi\ d^4}{64}$ = 1.25663 x 10^{17} μm^4

As the shaft is supported symmetrically by two highly pressurized bearings (650 p.s.i.) and the ends are connected to flexible couplings, the following assumptions were made:

(i)   the shaft may be treated as a simply supported beam with rigid supports.

(ii)   the load acting on the shaft may be treated as a concentrated load of W_s, acting at mid-span.

Such a model is illustrated in figure (3). The maximum deflection, y_{max} may be expressed as:

$$y_{max} = \frac{W_s \, a^2 \, b^2}{3 \; E \; I \; L} \qquad \text{(AIX-1)}$$

$$= \frac{W_s \, (128.5 \times 10^3)^2 \, (128.5 \times 10^3)^2}{3.(0.206)(1.25663 \times 10^{17})(257 \times 10^3)}$$

i.e. $y_{max} = 0.013661 \, W_s$ (µm) $\qquad$ (AIX-2)

The stiffness, $k = \dfrac{W_s}{y_{max}}$ $\qquad\qquad$ (AIX-3)

$$= \frac{W_s}{0.013661.W_s} \qquad (\text{N } \mu\text{m}^{-1})$$

i.e. $k = 73.20$ (MN-m^{-1}) $\qquad\qquad$ (AIX-4)

The fundamental frequency of the shaft may be approximated (reference (3)) by:

$$\omega = \sqrt{\frac{g \, \Sigma \, m_i.y_i}{\Sigma \, m_i.y_i{}^2}} \qquad\qquad \text{(AIX-4)}$$

$$= \sqrt{\frac{g \, m_s \, y_{max}}{m_s \, y_{max}{}^2}}$$

$$= \sqrt{\frac{9.81 \times 10^6 \times 4.67 \times 0.6265}{4.67 \times 0.6265^2}}$$

i.e. $\omega = 3957$ rad -s^{-1} or 630 Hz $\qquad$ (AIX-6)

B) <u>Derivation of the Expressions Governing the Deflection of the Test-Shaft in Relation to the Position where the Displacements are Measured</u>

Figure (4) illustrates the deflected shaft. Expressions are required for $(x_x - x_2)$ and $(y_x - y_2)$ in terms of x_s and y_s, respectively. From reference (2):

$$(x_1 - x_2) = \frac{W_s \, L^3}{48 \; E \; I} \qquad\qquad \text{(AIX-7)}$$

$$(x_x - x_2) = \frac{W_s \, x}{12 \, E \, I} \left(\frac{3 \, L^2}{4} - x^2\right) \qquad \text{(AIX-8)}$$

Equation (AIX-8) may be rewritten as:

$$(x_x - x_2) = \frac{W_s \, L^3}{48 \, E \, I} \left(\frac{4 \, x}{L^3}\right) \left(\frac{3 \, L^2}{4} - x^2\right) \qquad \text{(AIX-9)}$$

Substituting the expression for $\dfrac{W_s \, L^3}{48 \, E \, I}$ into equation (AIX-9) yields:

$$(x_x - x_2) = (x_1 - x_2) \left(\frac{4 \, x}{L^3}\right) \left(\frac{3 \, L^2}{4} - x^2\right) \qquad \text{(AIX-10)}$$

As, $(x_1 - x_2) = x_s + (x_x - x_2)$, equation (AIX-10) becomes:

$$(x_x - x_2) = (x_s + (x_x - x_2)) \left(\frac{4 \, x}{L^3}\right) \left(\frac{3 \, L^2}{4} - x^2\right) \qquad \text{(AIX-11)}$$

Hence,

$$(x_x - x_2) = \frac{\left(\frac{4 \, x}{L^3}\right) \left(\frac{3 \, L^2}{4} - x^2\right) x_s}{\left[1 - \left(\frac{4 \, x}{L^3}\right)\left(\frac{3 \, L^2}{4} - x^2\right)\right]} \qquad \text{(AIX-12)}$$

Substituting, x = 75.25 mm and L = 257 mm into equation (AIX-12), yields:

$$(x_x - x_2) = 3.5044 \, x_s \qquad \text{(AIX-13)}$$

Similarly, in the y - direction:

$$(y_x - y_2) = 3.5044 \, y_s \qquad \text{(AIX-14)}$$

Connected To
Flexible Coupling

Location Of
Displacement Probe

Connected To
Flexible Coupling

Test Shaft

53.25

Test
Bearing

Support
Bearing

Support
Bearing

65   89   168   89   65
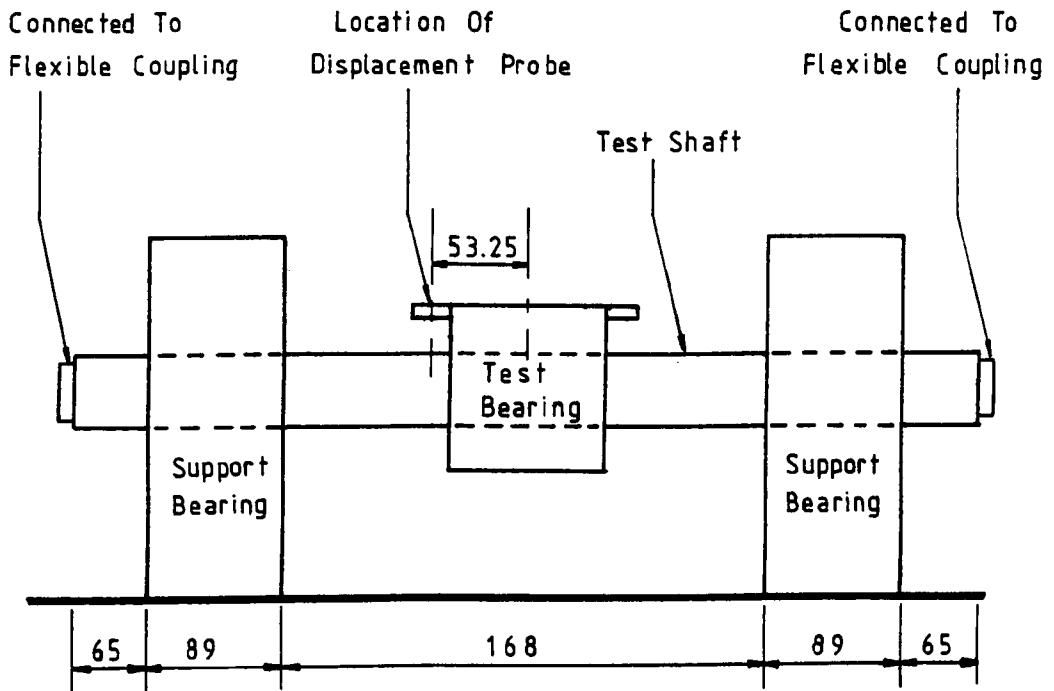
Fig.1: A General View Of The Shaft Assembly.

40ϕ

4.76ϕ

250

476
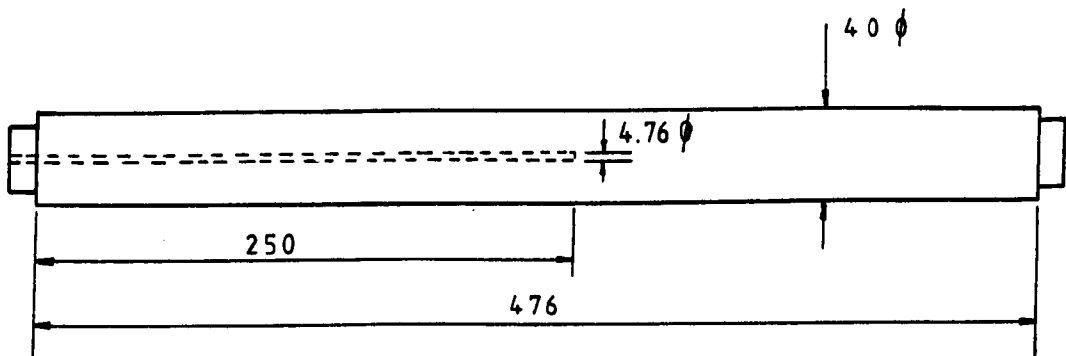
Fig.2: Test Shaft Details.

NOTE : All Dimensions In mm.
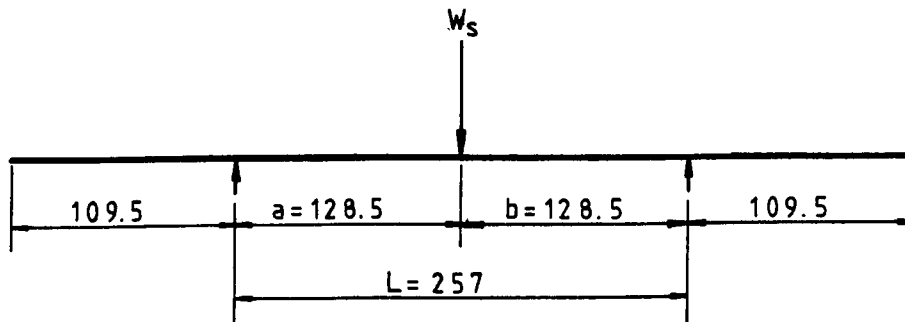
Fig. 3 : Figure Representing The Shaft By A Beam
On Rigid Supports.
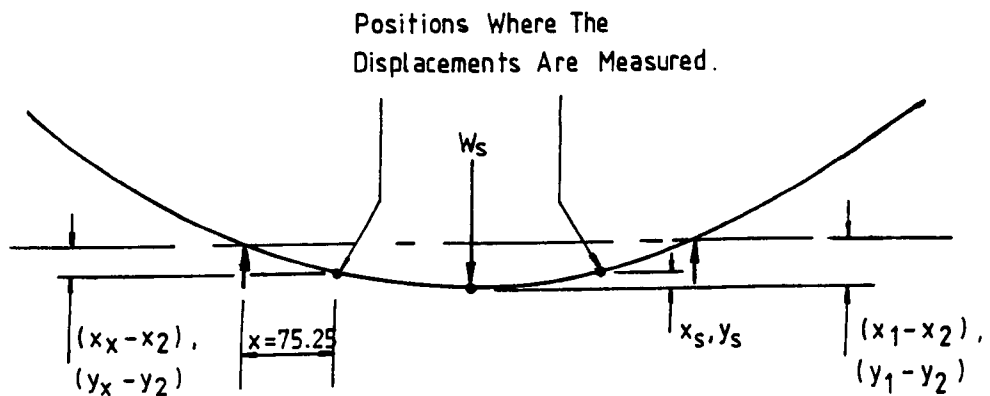
Fig. 4 : The Deflected Shaft Showing The Locations
Where The Displacements Are Measured.

REFERENCES

1. Koshal, D. 'The Design and Optimization of Slot-Hybrid Journal
    Bearings.' Ph.D. Thesis, Liverpool Polytechnic, 1978.

2. Robert L. Mott, 'Applied Strength of Materials.' Prentice Hall
    Inc.

3. William T. Thomson, 'Theory of Vibration with Applications.'

APPENDIX X

The 1172 Frequency Response Analyser

The 1172 frequency response analyser (1172 FRA) may be employed to measure a system's response to various input signals. It consists of a programmable generator to provide an excitation signal, a correlator to analyses the system's response and a display to present the results.
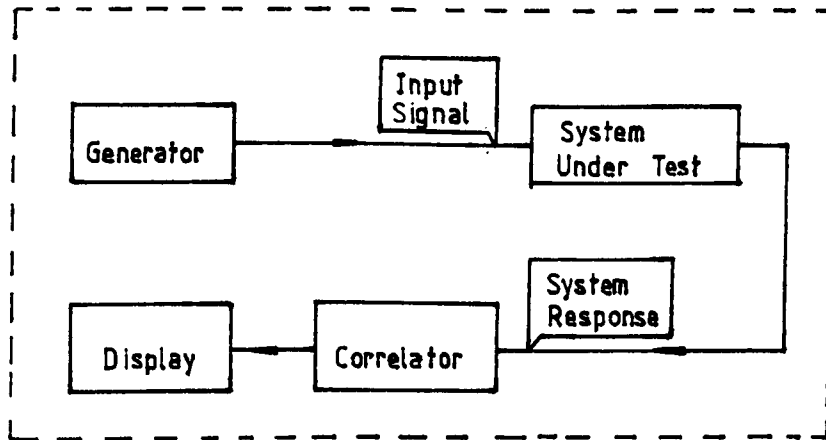
The Basic Measurement System

The generator provides an output signal of known amplitude and frequency which is in the form A sin ωt. This signal is applied to the system to be tested.

The fundamental response of a system to a sinusoidal input signal is in the form R sin (ωt + ϕ). As well as this fundamental term, higher order harmonics due to system non-linearities together with random noise will also be present in the system's output. A correlation process is used to analyse the system's response. This technique has the advantage of rejecting all harmonics present in the system's output and also minimizing the effect of random noise.

A measurement of the ratio between an amplifier output (Y input signal) and its input signal (X input signal), as illustrated below, allows a calculation of gain (Y/X) to be made.
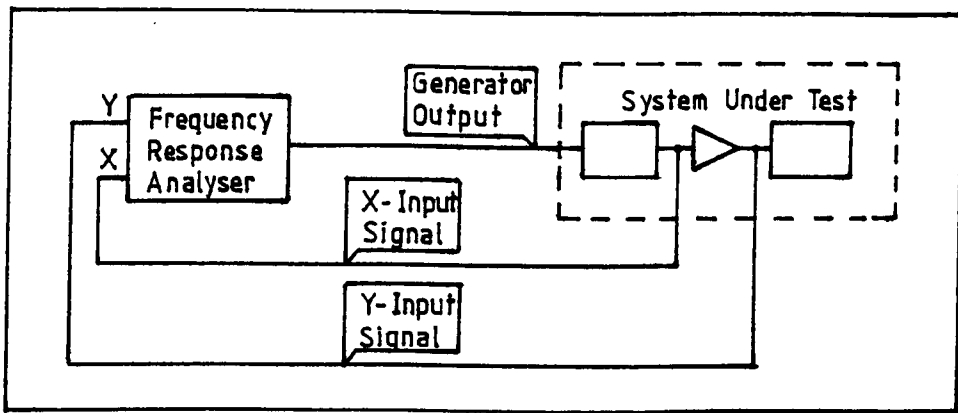
Measurement of the Ratio between Two Signals

The X and Y signals are analysed separately and the amplitude, R and phase angle, ϕ of each signal is determined.
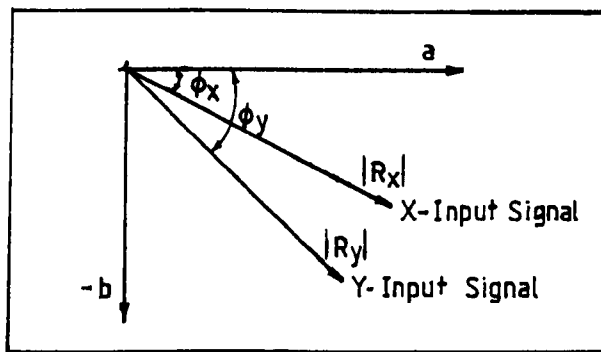
By calculating the ratio $\dfrac{|R_y|}{|R_x|}$ and the angle $(\phi_y - \phi_x)$, the transfer function between the two voltage vectors X and Y, may be determined and may be represented in cartesian, polar or log-polar form.
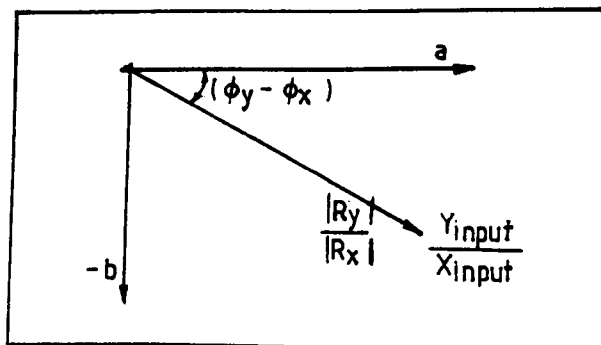
REFERENCE

1. Schlumberger Operating Manual for the 1172 Frequency Response

Analyser, Date of Issue: July, 1975.